SCALE MICROCHEMISTRY AS A NON-LETHAL ALTERNATIVE FOR TRACKING INDIVIDUALLY VARIABLE MIGRATION PATTERNS IN MOBILE FISH

A Thesis

By

ETHAN J. TAULBEE

BS, Indiana University East, 2016

Submitted in Partial Fulfillment of the Requirement for the Degree of

MASTER OF SCIENCE

In

FISHERIES AND MARICULTURE

Texas A&M University-Corpus Christi

Corpus Christi, Texas

May 2020

May 2020

SCALE MICROCHEMISTRY AS A NON-LETHAL ALTERNATIVE FOR TRACKING INDIVIDUALLY VARIABLE MIGRATION PATTERNS IN MOBILE FISH

A Thesis

by

ETHAN J. TAULBEE

This thesis meets the standards for scope and quality of

Texas A&M University-Corpus Christi and is hereby approved.

Benjamin Walther, PhD

Chair

J. Derek Hogan, PhD

Committee Member

Simon Geist, PhD

Committee Member

May 2020

ABSTRACT

Estuaries are important habitats to many coastal fishes. Some species of fish can use the low salinity and freshwater environments that estuaries provide, though the exact patterns of usage for these habitats for some species is not well understood. Stable isotope and microchemical analysis of fish otoliths and muscle tissue have been used to analyze fish migratory behavior in many studies, especially in the case of euryhaline fishes. However, removal of otoliths and muscle tissue require the sacrifice of the subject organism. Scales are another structure of fish that experience deposition of stable isotopes and elements from the environment during their formation, and the removal of scales for most species is a non-lethal process. For this study, Red Drum *Sciaenops ocellatus* were collected in bays and estuaries along coastal Texas and analyzed for a suite of chemical assays including stable isotope (δ^{13}C and δ^{15}N) and trace element (strontium and barium) composition of scales. Scale chemistry was compared among fish collected in bays that differed in their distance from freshwater inflow sources to assess divergence in terrestrial influence as well as degree of fish residency in isotopically distinct food webs. Scale stable isotopes and elements are often compared to determine if different chemical markers support comparable conclusions about movement or residency. Scale chemistry compositions were compared to prior analyses of otoliths and muscle isotope compositions to assess agreement in chemical history information between structures that can be sampled lethally and nonlethally. Stable isotope signatures of muscle tissue and scales were closely matched. Qualitative analysis of elemental profiles of scales and otoliths did not reveal any clear matching trends, though they will be further examined to determine if pattern matching is present.

DEDICATION

This work is dedicated to those who have helped me on my fisheries journey thus far. To my family and friends who kept me sane throughout the process. To Bill Benken, my high school science teacher who instilled in me a love of the scientific process and a greater appreciation of the natural world. To Dr. Neil Sabine, who has wholly supported me since my first course with him and played an integral role in my receiving internships and my admission into graduate school. And thank you so much to my partner, Kaylyn Zipp, for being a constant source of inspiration and motivation to work hard and chase my dreams.

ACKNOWLEDEMENTS

I would like to thank all of those that helped me through my time working on this project. Mike Kleine, you put in a ton of hours helping me do the tedious work of this project purely because of his interest in fish and willingness to help. Our conversations kept me sane and I learned a ton about fishing in Texas. It's a shame you're in geology, because you'd make an excellent fisheries professional. Jason Selwyn, thank you for your help and expertise with statistical analysis and data visualization. Your help saved me many hours of precious time. To Dr. Hogan and Dr. Geist, thank you both for teaching me everything you have through coursework and while serving on my committee. I've learned a ton. Thank you to the Texas Parks and Wildlife Coastal Fisheries personnel that obtained the samples that made both mine and Louisa's work possible (Brian Bartram, Justin Dunn, Stephen Hale, Jacob Harris, Moises Hinojosa, Jr., Cindy Kelly, Dr. Christopher Mace, Evan Pettis, Johnny Rios, Jason Slocum, Caleb Taylor, Luis Uballe, Jr., and Tom Wagner). To Dr. Nathaniel Miller, thank you so much for your guidance during laser ablation analysis, trusting me with the instrumentation, and sacrificing your personal time so I could get all my samples completed in a timely manner. Thank you to the sources of research funding for this project, including the TAMUCC Fisheries and Mariculture Program, the Family of Dr. Henry Hildebrand, and the TAMUCC Division of Research and Innovation. And lastly, thank you to Dr. Benjamin Walther for taking me on as a student. After a very disheartening graduate school application process, Dr. Walther was the only person willing to take a chance on me, and I appreciate it more than he can ever know. I likely would not be in the fisheries profession without his help. I could not have asked for a more patient, grounded, and supportive advisor. The Institutional Animal Care and Use Committee Protocol Number for this thesis is AUP#11-15.

TABLE OF CONTENTS

LIST OF FIGURES

FIGURES PAGE

LIST OF TABLES

TABLES PAGE

INTRODUCTION

Previous lab work explored the otolith and tissue chemistry of Red Drum (*Sciaenops ocellatus*) to determine individually variable migration patterns and freshwater usage (Torrance 2018). The fish examined in this study were from bays within the Mission-Aransas and Nueces Estuaries in southern Texas (Torrance 2018). In the work discussed in this thesis, scales from fish analyzed during Torrance's study were analyzed and individual comparisons were made to their respective otolith chemistry profiles and muscle isotope values.

The movement of organisms within or between environments is vital to the survival and long-term success of many species. Movement often has several driving factors, among those including reproduction (Thorstad et al. 2010), survival during parts of the life cycle where the organism is most vulnerable to mortality (Stewart and Scharf 2008), and pursuit of prey (Huang and Diekmann 2001). Movements can vary greatly in scope, with some organisms undergoing migrations that span thousands of miles, while others moving short distance within their own ecosystem.

Within fish populations there can be individual variation in behavior where small groups or individual organisms employ a different life history strategy than the majority of the population. These groups of individuals with alternative behaviors within a species have been deemed as "contingents" (Clark 1968; Secor 1999; Secor and Piccoli 2007; Kerr et al. 2010; Nims and Walther 2014). Understanding individual and small-scale variability in fish behavior is important because these behaviors can serve as a "bet-hedging" strategy to allow for the survival of the species in the face of perturbations that can impact the larger population (Kerr et al. 2010; Nims and Walther 2014). Also, mobile fishes with individually variable migration strategies have the potential to serve as connective vectors for nutrients between the different

areas they occupy. Transmission of nutrients occurs typically through feeding, secretion, egestion, mortality, and migrant organisms being preyed upon, creating complex webs of nutrient influx and facilitating connectivity between various environments (Secor and Rooker 2005). For example, a fish could reside within an estuary during its juvenile phase and gain mass while feeding within the estuarine food web. Soon after, the fish reaches the adult phase and moves out into the open ocean into a new food web. The biomass of the fish and the waste it produces is largely made up of estuarine derived nutrients, effectively transferring these nutrients to the marine system. Similarly, terrestrial organisms and environments can subsidize estuarine and ocean environments via riverine inputs. Nutrient subsidies from various systems increase the complexity of systems of influx and can provide important sources of unique nutrients to subsidized systems.

Importance of Estuaries and Low Salinity Habitats

The full or partial use of estuaries by many economically important fishes in the Gulf of Mexico, often as juveniles, is vital to their survival and development. Estuarine environments serve many purposes for estuarine organisms, such as serving as nursery grounds, feeding areas, or stopover areas during migrations (Elliott et al. 2007). Many of these species are euryhaline, meaning that they can tolerate a wide variety of salinities (Crocker et al. 1983; Gross et al. 1988; Watson et al. 2014). Oftentimes, euryhaline species have punctuated and well understood patterns of movement and migration, but even within those such species, individually variable movement patterns may exist that alter our understanding of the ecological role of these species. Further, some individuals may move into non-estuarine habitats briefly or extensively, thereby expanding the suite of habitats required to sustain populations. A full understanding of how euryhaline fishes

use environments of various salinities is vital in developing effective conservation strategies for these species.

All organisms that utilize estuarine environments generally fall into one of two categories; obligate or facultative. Movement across salinity gradients by obligate species are necessitated by their biology and are essential to their survival and reproduction, such as the freshwater spawning run made by anadromous salmonid species (Quinn and Myers 2004). Conversely, the movements undergone by facultative species are not vital to the survival of the species. Such is the case in the strategy of a bluefish (*Pomatomus salatrix*), a "marine estuarine-opportunist" under the Whitfield (1999) classification, which can use coastal waters as nursery areas, but regardless, still move into estuarine environments (Potter 2015).

How to Study Movement: Stable Isotopes

An indirect method of determining migration behavior is through the analysis of isotopic ratios of $\delta^{13}C$ and $\delta^{15}N$ of muscle tissue. The ratios of stable isotopes present in an environment vary due to several factors, including salinity (Qian et al. 1996; Fry 2002), terrestrial inputs (Peterson and Fry 1987; Mook and De Vries 2000) and anthropogenic impacts (Fry 2002; Mooney and McClelland 2012). These stable isotopes are taken up in the tissues of the primary producers in an environment and passed up the food chain as primary producers and subsequent consumers are preyed upon (Michener and Kaufman 2007). Muscle tissue is constantly being added through growth and reworked via metabolism in organisms, so muscle tissue stable isotope concentrations serve as a reflection of the diet of the organism over a time period of several weeks to months (Suzuki et al. 2005; Trueman et al. 2005; Mohan et al. 2016; Maruyama et al. 2017).

The Greek lowercase symbol delta, δ, is used in stable isotope notation.

$$\delta = \left[\frac{R_{sample}}{R_{standard}} - 1\right] * 1000$$

R is the fraction of the heavy isotope to the light isotope, and the equation is multiplied by 1000 to return the δ value in ‰. Therefore, a higher δ value is indicative of higher enrichment in the heavier isotope. Generally, differences in stable isotopes are very minute, so the ratio of a ratio aspect of the δ equation expands and makes these differences more pronounced (Fry 2006).

Geographic variations in δ^{13}C and δ^{15}N values of primary producers generate the distinct isotopic signatures observed in mobile individuals. These geographic variations can be used to construct isoscapes; maps reflecting the stable isotope baselines (West 2010). Because stable isotopes signatures in soft tissues are primarily diet derived and originate from uptake by primary producers, different environments have unique isotopic baselines that are reflected in the tissue of their primary producers. Individuals in an environment that are non-migratory have similar isotopic signatures to one another due to residence and feeding within the same isotopic baseline. Those that are migratory or transient show unique isotopic signatures reflective of the various isotopic baselines of the different environments they are feeding in. Isotopic baselines are the result of the stable isotopes primary producers take in from particulate organic matter in the system, which is then integrated by organisms feeding on primary producers, and therefore the organisms feeding at higher levels of the food chain (Herzka 2005). As a migrant organism moves into and begins feeding in a new environment, they break down old muscle tissue via metabolic processes, and accrue new muscle tissue that dilutes and mixes their previous stable isotope signature with that of the new food web, and after a sufficient period of residence in the new environment the organism will fully equilibrate and reflect the new stable isotope signature, a process known as turnover (Herzka and Holt 2011; Fry and Arnold 2002; Bucheister and Latour 2010; Gorokhova

and Hansson 2011; Vander Zanden et al. 2015; Mohan et al. 2016). The faster growth rate of a species, the faster the dilution of existing tissue is. At the same time, older tissue is being metabolized and upon full breakdown, the new fully equilibrated isotopic signature is reflected in the tissue of the organism (Tieszen et al. 1983). Other factors influence turnover rate by influencing growth rate, such as age, but metabolic rate influences the breakdown of existing tissue and is therefore also a primary determinant of turnover rates (Hesslein et al. 1993; Herzka and Holt 2011). Turnover time increases as the fish gets older and its growth rate slows down and directs more energy away from somatic growth to other processes. If unique baselines exist for the environments being compared in a muscle tissue stable isotope study, migration behavior and food web participation will be reflected and show clear differences within muscle tissues (Fry 1983, 1999, 2002; Herkza 2005; Herzka and Holt 2011; Michener and Kaufman 2007).

Another factor that can alter isotopic signatures aside from various baselines is fractionation, the offset between diet stable isotope signatures and those of the baseline system. Fractionation in organisms is a result of chemical reactions happening during consumption, metabolic processes, and excretion. In biological reactions, heavy isotopes are typically centered around where bonds are the strongest, meaning that heavy isotopes take more energy to react than light isotopes (Fry 2002). In the context of food webs, this results in "bioaccumulation" of heavier stable isotopes as you move up the food chain. This difference is the most pronounced with $\delta^{15}N$, but trophic fractionation of $\delta^{13}C$ is also measurable (Herzka et al. 2002; Bucheister and Latour 2010; Gorokhova and Hansson 2011; Herzka and Holt 2011). Trophic fractionation magnitudes vary based on system, but on average, previous studies have found about 0-1 ‰ fractionation per trophic level for $\delta^{13}C$ and 3.4 ‰ fractionation per trophic level for $\delta^{15}N$ (Peterson and Fry 1987; Post 2002). There is, however, a growing body of work showing

different fractionation levels than this, raising doubts about the ubiquity of these values (McCutchan et al. 2003; Vanderklift and Posnard 2003; Focken 2004). Nitrogen has a higher degree of fractionation because lighter isotopic nitrogen is excreted in urine, leaving behind the heavier nitrogen isotope (Cabana and Rasmussen 1996). Carbon isotopes undergo the same selected excretion, but to a lesser degree (Peterson and Fry 1987). Because of its higher degree of fractionation, $\delta^{15}N$ is the most useful stable isotope to use in trophic position estimations if baseline environmental signatures for the subject species are known (Cabana and Rasmussen 1996, Post 2002).

$\delta^{13}C$ values in marine waters vary based on the exchange of carbon between bicarbonate in the water and atmospheric CO_2 gas (Mook et al. 1974). In freshwater systems, $\delta^{13}C$ can vary based on weathering of carbonate rocks, mineral spring inputs, atmospheric CO_2 levels, and organic matter present (Peterson and Fry 1987; Mooney and McClelland 2012). In addition, in this project's study system (Figure 2), $\delta^{13}C$ has been shown to increase with salinity (Qian et al. 1996; Fry 2002; Lebreton et al. 2016; Bishop et al. 2017). In a 2017 study, $\delta^{13}C$ values at the lowest salinities recorded in the Mission-Aransas Estuary were about -30 ‰, and the $\delta^{13}C$ values at near oceanic salinities were around -20 ‰ (Bishop et al. 2017). $\delta^{13}C$ values are also strongly affected by the photosynthetic method of the dominant primary producers. Terrestrial C_3 plants often have lower $\delta^{13}C$ values, around -26.5 ‰, and therefore so do freshwater systems subject to terrestrial influx. Terrestrial C_4 plants have average $\delta^{13}C$ value of about -12.5 ‰ (Tykot R. H. 2004). Seagrass derived $\delta^{13}C$ averages around -10 ‰ (Fry 2006). Phytoplankton derived $\delta^{13}C$ ranges typically are between -19 and -21 ‰ (Rooker et al. 2010).

$\delta^{15}N$ values are typically not as predictable as $\delta^{13}C$ regarding salinity because the freshwater endmembers of $\delta^{15}N$ can vary dramatically, though several studies have shown that

δ^{15}N decreases with salinity in our study system, with δ^{15}N values at the lowest salinities recorded in the Mission-Aransas Estuary around 12 ‰, and the δ^{15}N values at near oceanic salinities were around -2 ‰ (Lebreton et al. 2016; Bishop et al. 2017). Anthropogenically introduced nitrates can also affect δ^{15}N values (Fry 2002; Mooney and McClelland 2012). Because of the various mechanisms at play in determining a stable isotope signature, sometimes it can be hard to determine the true cause of variation of an isotopic signature in animal tissue (Post 2002). For example, a high δ^{15}N value in muscle tissue could be interpreted as residence within an environment with a high δ^{15}N baseline, or as high trophic position within their food web. It is also impossible to use stable isotopes to determine geographic migration if the isotopic baselines of the different environments are the same due to things like similar primary producers or proximity to riverine input. Such difficulties can be further exacerbated when the possibility of things like migrant predators bringing in signatures from other systems is considered, or when a diet switch of a predator occurs that isotopically looks like an indicator of migration (Herzka 2005). Because of some of these compounding difficulties, it is useful to pair tissue stable isotopes with structural hard-part microchemistry to provide a complementary assessment of habitat use patterns (Elsdon et al. 2008).

How to Study Movement: Trace Elements

Otolith chemistry is a common lethal method of determining the migratory behavior of fish that reside within estuaries during some period of their life (Campana et al. 2000; Rooker et al. 2010; Walther and Limburg 2012). Otoliths are the inner ear stones of fishes. These calcium carbonate structures assist fish with balance and hearing (Secor 1999; Payan 2004) and accrete successive layers over time, allowing them to be used to estimate the age of fishes (Pannella 1971, 1974). Otoliths are the primary structure used for natural tag trace element studies, but

other natural tags exist and are sometimes used, such as bone, fin rays and spines (Tzadik et al. 2017). Otolith trace element analysis is as a useful tool for determining migrations of diadromous euryhaline fishes (Secor 1992; Limburg 1995; Elsdon et al. 2008), and technological advancements in the field like the use of LA-ICPMS have allowed higher resolution analysis of trace element profiles and migration patterns (Thorrold et al. 1997; Nims and Walther 2014)

In addition to effectively recording age, otoliths also incorporate certain chemicals from the water in which a fish resides (Elsdon et al. 2008). Otoliths are metabolically inert, so structural components deposited into the structure of an otolith will remain there indefinitely (Campana and Neilson 1985). The ambient water chemistry of a location varies based on many factors including proximity to terrestrial environments, as indicated by presence of materials derived from rocks in rivers and waterways. (Bernat et al. 1972; Shaw et al. 1998) and salinity (Shaw et al. 1998; Walther and Nims 2015). Trace element particles from the ambient water around the fish are taken up at the gills and deposited into the blood. From the blood, these trace elements move through membrane channels within the fish into the endolymph, and subsequently the otolith (Campana 1999). Elements are also taken up in the intestinal tract after the drinking of seawater by marine fish (Olsson et al. 1998).

Many elements are present in otoliths, and the most useful elements for migration studies are those that closely match their ambient water concentrations or vary predictably in how they are regulated during uptake and deposition (Campana et al. 2000). Some trace elements, such as strontium and barium, vary predictably across estuarine salinity gradients and therefore can be effective tracers of migration between marine, estuarine and freshwater habitats. Strontium and barium appear to move through the same biological channels as calcium and are typically deposited into the calcium carbonate matrix in place of calcium. Because of this, trace elements

are reported and analyzed in ratio with calcium because barium and strontium moving through calcium channels means that they are not highly physiologically regulated and are deposited into the otolith in similar proportion to calcium ions (Campana 1999).

Ba:Ca ratios in carbonate structures are a very useful metric to analyze the movement of estuarine fishes because as water salinity increases, Ba:Ca concentrations in many systems, including our Texas study system, decrease (Walther and Nims 2015). Ba levels are usually significantly higher in freshwater and near river mouths due to weathering of rocks along the river (Bernat et al. 1972) but these ratios have also been shown to decrease with high levels of anthropogenic input and runoff into river systems (Characklis and Wisener 1997). In our study system, Ba:Ca serves as a reliable indicator of salinity, with Ba:Ca decreasing with higher levels of salinity (Walther and Nims 2015). Ba concentrations in water do decrease in a non-linear fashion, because it is non-conservatively mixed because of ionic exchange and release of particulate Ba when riverine water and estuarine water meet at areas of inflow where salt wedges are formed. When ratioed to Ca, Ba:Ca values undergo exponential decline with the highest degree of change occurred below salinities of 10 (Coffey et al. 1997; Walther and Nims 2015).

Sr:Ca ratios tend to decrease as salinity decreases (Brown and Severin 2009). Dissolved Sr:Ca ratios are typically constant in well mixed marine waters at around 8.54 mmol per mol (Bernat et al. 1972; de Villiers 1999), allowing changes in Sr:Ca ratios to be used to elucidate migrations between estuaries and open ocean for diadromous species (Secor 1992; Limburg 1995; Brown and Severin 2009). Sr uptake in fish has been shown to be influenced by factors such as temperature and variable physiology, which can skew values away from those of true ambient water conditions (Kinsman and Holland 1969). Unlike Ba, Sr is not heavily taken up in biological or geochemical reactions in seawater and has a linear increase in concentration with

salinity (Dodd and Crisp 1982). When ratioed to Ca, Sr:Ca undergoes a short exponential increase before leveling off at marine concentrations (Walther and Nims 2015). In the South Texas system this study takes place within, the ratio results in a small difference between freshwater and marine Sr:Ca endmembers due to riverine inputs weathering bedrock that is strontium rich. For this reason, Ba:Ca is regarded as a stronger indicator of salinity change than Sr:Ca.

Natural tags like otoliths and muscle tissue serve as chemical recording devices within fish. All fish have otoliths from the beginning of their life cycle, meaning that ambient water chemistry is being recorded and taken up in this metabolically inert structure, providing a complete record of exposure to chemically variable environments for some elements and isotopes (Campana and Neilson 1985). This completeness is also insured by the fact that otoliths are constantly growing and depositing material, unlike some other structures that cease to grow when somatic growth is not taking place (Maillet and Checkley, Jr. 1989).These are significant advantages over telemetry and mark-recapture studies, as no gaps in data exist from the life stage prior to capture or recapture. Otolith analysis also allows the analysis of fish at a significantly lower cost per specimen than telemetry and mark recapture work.

Muscle tissue offers a recent, diet derived isotopic signature that can be paired with trace element analysis for a complementary analysis of fish movement. This tissue is an especially powerful tool when the isoscape of an environment is known, because then isotopes can be used for a more in-depth analysis of an organism's interactions, such as using $\delta^{15}N$ fractionation to determine trophic position (Post 2002).

Though otoliths are an excellent structure to analyze regarding trace elements, they lack substantial amounts of organic material, making it difficult to use them to gain insight into trophic

dynamics or feeding behavior in order to further analyze movement behaviors. Though otolith and muscle chemistry are valuable tools in determining the environments fishes inhabit, removal of these tissues and structures requires the sacrifice of the subject organism. Due to the necessary lethality of otolith and muscle tissue extraction, it is not an ideal method for attempting to determine the habitat use patterns of fish that have a recreational catch limit or are part of catch and release fisheries.

Scales as an Alternative Structure

The lethality of otolith and muscle tissue analysis has prompted a shift toward investigating non-lethal alternative structures to otoliths that can provide migratory histories. For instance, previous work conducted in the lab of Dr. Benjamin Walther used scale chemistry as an otolith and muscle tissue analog in Atlantic Tarpon *Megalops atlanticus*, a vulnerable sport fish in the Gulf of Mexico (Woodcock et al. 2013; Woodcock and Walther 2014; Seeley and Walther 2018). To fully verify that scales provide analogous information to otoliths and muscle tissue, scale chemical profiles must be compared to those of muscle tissue and otoliths from the same individuals. This was not possible with Atlantic Tarpon as those fisheries are a catch and release fishery, preventing any otolith or muscle tissue analysis from taking place.

Scales are a bipartite structure that are typically formed in 2 distinct layers (Figure 1). The basal layer, also referred to as the fibrillar layer, is made up of collagen fibers. Overlaid above the basal layer is an external layer of calcified calcium phosphate (Fouda 1979; Zyllerberg and Nicolas 1982; Zylberberg 2004; Hutchinson and Trueman 2006). Like otoliths, scales grow in successive increments, with the external calcified layer of a typical teleost scale growing concentrically outwards from the center. In addition to the successive growth of scales, scales also deposit some of the same trace elements as otoliths, such as barium, cadmium and strontium

(Wells et al. 2000; Wells et al. 2003). Excess trace elements that are taken up by a fish are transported to the growing edge of a scale where they are then deposited into or external layer's calcified matrix (Wells et al. 2000). Barium is deposited in higher concentrations in the external layer of the scale than in otoliths (Johnson 1989; Pender and Griffin 1996; Campana and Thorrold 2001).

The underlying basal layer of a scale grows by adding collagen lamellae in layers from the growth tip of the scale to the focus. This results in an increase in thickness near the focus of the scale, and under layering deposits newly collected materials not just at the growing edge, but near the focus as well (Fouda 1979). As the basal fibers are deposited, they change directions, with the new fibers laying at a 90-degree angle from the layer above it (Zylberberg et al. 1988). The basal layer is the heavier part of the scale, comprising about 70% of the scale by weight. When sectioned vertically, the basal layer shows successive layers of growth and isotopic compositions from different stages of life, due to the makeup of collagen in the scale being largely diet derived (Hutchinson and Trueman 2006). Isotopic compositions of scale basal layers are skewed towards later growth due to under layering growth pattern of the basal plate. New collagen layers deposited at the bottom of the basal plate are larger than previous layers as the scale grows, resulting in more recent material being more abundant in the basal plate of the scale (Hutchinson and Trueman 2006; Ramsay et al. 2012). Diet derived $\delta^{13}C$ and $\delta^{15}N$ signatures can be derived from the basal layer of the scale like they can from muscle tissue. Because scales deposit diet stable isotopes as collagen layers on the basal plate of the scale that lay from the growing edge of the scale to the focus, the growing edge of the scale contains the most recent diet signature of the fish. Scales are metabolically inert, so the most recent stable isotope

signatures from the edge of the scale were determined to match the recency of stable isotope signatures of muscle tissue, which change according to the turnover rate of the fish.

Several studies have been done on the stable isotope profiles of muscle vs scales that showed a high degree of matching between the two structures (Estep and Vigg 1985; Satterfield and Finney 2002; Perga and Gerdeaux 2003; Pruell et al. 2003; Estrada et al. 2005). More specifically, studies typically report linear relationships between the two structures, but with a 2-4 ‰ offset for $\delta^{13}C$, and no significant offset for $\delta^{15}N$ (Hutchinson and Trueman 2006). This study is the first to explore movement behavior using scales in Red Drum.

This dual deposition within the bipartite structure makes scale analysis attractive as a robust method of determining habitat use. Microchemical analysis of trace elements can be done by examining the calcified external layer of the scale, while stable isotope analysis can take place by targeting and examining the basal layer of the scale. This dual deposition allows scales to serve as a potential single proxy for 2 structures, otoliths and muscle tissue.

Scale Microchemistry as a Method of Determining Migration Behavior

Previous lab work explored the otolith and tissue chemistry of Red Drum (*Sciaenops ocellatus*) to determine individually variable migration patterns, and 4-6 whole scales from each of these specimens were collected during this study (Torrance 2018). In the work discussed in this thesis, scales from Torrance's study were analyzed and individual comparisons to their respective otolith chemistry profiles and muscle isotope values were generated to conduct a robust assessment of their usefulness as a non-lethal alternative structure in this species. If scale microchemical and stable isotope analysis yield similar results as analysis of otolith and muscle tissues, this will allow for quantification of individually variable habitat use and provide an estimate of the diversity of

estuarine and freshwater habitats required to sustain this important mobile species. If scale chemistry can be further validated as a consistent and reliable method of determining habitat use, it could be a large step forward regarding the preservation and recovery of many fish species via a non-lethal assay.

Red Drum

Red Drum are a common species along the entire east coast of the United States and the Gulf of Mexico as far south as Vera Cruz, Mexico (Mercer 1984). Sizable populations are found in the Gulf of Mexico, with the largest recorded populations in the Gulf being off the coasts of Louisiana and Texas (Pattillo et al. 1997). Their coloration varies, with most being gray with darker bronze and copper colors appearing as the fish ages. The colors of the fish come from strips of pigmented tissue attached to the ends of the ctenoid scales of the fish (Mercer 1984). The recreational Red Drum fishery generates significant revenue for Gulf states. As of 2011, the recreational Red Drum fishery in the state of Texas carried an economic value of $350 million (Vega et al. 2011).

Adult Red Drum move into inlets and bay entrances during the end of summer and fall to spawn (Wilson and Nieland 1994). Red Drum are prolific spawners, and the amount of eggs a female Red Drum produces increases exponentially with length (Overstreet 1983). Larvae and eggs are carried by currents into estuaries where settlement occurs. Post-settled juveniles often settle in seagrass areas, which offer protection from water movement and predation, and offer easy access to food (Havel and Fuiman 2016). Once juveniles can freely swim, they disperse across the estuary, often residing on the edges of suitable habitat (Stunz et al. 2002). Juvenile Red Drum remain in the estuary until they migrate outwards to join the offshore spawning stock anywhere from 3-5 years of age (Holt et al. 1983). Juvenile fish that are still within the estuary

seek warmth in warmer, deeper bay waters during the winter (Osburn et al. 1982). Male Red Drum reach maturity between 411 and 791 mm (16.18 – 31.14 in) total length, and females reach maturity between 629 and 900 mm (24.76 – 35.43 in) total length (Murphy and Taylor 1986).

Red Drum are a euryhaline fish that use estuaries throughout their native range along the entire Gulf of Mexico coast of the United States and along the east coast of the U.S. north until the Gulf of Maine, Massachusetts (Mercer 1984). Larval Red Drum settle into estuaries and further develop, residing in estuaries until adulthood (Holt 1981; Rooker et al. 1999). Upon reaching maturity, the majority of Red Drum migrate offshore to reside and spawn for the rest of their life (Matlock 1987). Juvenile Red Drum disperse throughout estuaries, making use of environments with both various benthic compositions (seagrasses, oyster beds, etc) and various salinities due to their euryhaline capabilities (Peters and McMichael 1987; Stunz et al. 2002; Stewart and Scharf 2008; Havel and Fuiman 2016). When moving between areas of various salinities, the intestinal fluid volume of Red Drum changes, facilitating a physiological switch in the type of osmotic regulation the fish employs, allowing them to withstand large changes in salinities with minimal stress or detriment to the fish (Esbaugh and Cutler 2016). Because of this, and their demand as a recreational catch species, Red Drum are stocked in some freshwater bodies in Texas, such as Braunig Lake and Calveras Lake (Texas Parks and Wildlife Department).

Though Red Drum are capable of inhabiting low salinity environments, past studies have generally shown them to rarely venture into low salinity areas (Kenworthy et al. 2018; Torrance 2018). Anecdotal reports from fisherman and some select studies have yielded specimens caught upriver and in freshwater creeks connected to estuaries (Wenner 1992; Adams and Tremain 2000; Bachelor et al. 2008; Stevens et al. 2013). Though some Red Drum have been shown to move into freshwater habitats during their life cycle, it is not well understood why, or how often individuals

do so. Juvenile Red Drum serve as a useful subject species for this study due to their dispersal throughout and residence within the various salinities of estuarine systems post settlement and during early development.

Comprehensive data pertaining to current Red Drum stock assessments is not available to the public, but studies have aggregated states' data to assess populations in the Gulf. A study of Red Drum stocks in the Gulf showed that abundances are currently on the decline, suggesting an absence of young fish was to blame, potentially pointing to low levels of estuarine escapement (Hightower 2013).

Essential Fish Habitat (EFH) for Red Drum includes every bay and estuary in the Gulf of Mexico (NOAA Fisheries). The concept of Essential Fish Habitat was introduced in the 1996 Sustainable Fisheries Act and includes any environment that is necessary for fish reproduction, feeding, shelter, and growth (Baird 1999). Previous studies have found that Red Drum populations vary based on available estuarine area, a factor playing into the widespread designation of all estuarine areas as essential Red Drum habitat (Yokel 1966). Federal actions have been enacted to preserve estuarine habitat, usually through the lens of state coastal management plans, though other concerns affecting estuarine environments are prevalent still, such as nitrogen influx, pollution, dredging, and development. When it comes to habitat usage that may be atypical to a species, such as the freshwater usage of Red Drum discussed above, it is important to understand the frequency of such habitat usage to determine if EFH should consider these 'atypical' environments for managed species.

Red Drum are predatory fish, with their diet varying based on age. Juvenile Red Drum are generalist predators with diets comprised of many species, such as blue crab (*Callinectus sapidus*), white shrimp (*Penaeus setiferus*), and Gulf Menhaden (*Brevoortia patronus*) among

other (Scharf and Schlight 2000). Juvenile Red Drum with a total length of less than 25 mm (0.98 in) feed largely on copepods (Colura et al. 1976). Upon reaching a total length of 50 mm (1.96 in) fish such as other sciaenids and Mysidacea become the majority of the Red Drum's diet. At around 75 mm (2.94 in) decapods became about 20% of the fish's diet, primarily caridean shrimps (Bass and Avault 1975). Adult Red Drum feed on fish and crabs, with more of a focus on crab as a prey species as the fish grow older (Yokel 1966). Past observations of Red Drum in freshwater environments may be a function of following prey that move into low salinity environments, such as blue crab and brown shrimp which have been shown to move into river mouths and tidal creeks (Ettinger and Blye 1981; Riera et al. 2000).

Prey availability varies within the bays of this study's system, and the generalist predation strategy Red Drum employ result in varied stable isotope baselines between bays that can examined to detect movement by fish between bays. Previous studies have analyzed the stable isotope signatures of suspended particulate organic matter (SPOM), baseline organisms and prey species of Red Drum in the Nueces and Mission-Aransas Estuaries (Riera et al. 2000; Lebreton et al. 2016; Rezek et al. 2017). There is some temporal variation in signatures that can be caused by freshwater inflow, anthropogenic inputs, among other factors. It is important to have baseline information from a similar time period as any collection that occurs to account for potential temporal instability. This information was used in interpretation of scale stable isotope signatures.

If the methods applied during this study can be transferred to other species, then simply removing a scale from a specimen prior to release can provide us with comparable information to what killing the organism to extract structures would. Being able to analyze scales for this purpose offers the possibility of determining habitat use for a myriad of different species, telling us which

habitats need to be preserved the most in order to allow populations to recover or avoid further decline. With overfishing being such a prevalent problem in many commercial fisheries, insight into the habitat use of commercial species can help avoid stock crashes as newly determined Essential Fish Habitat can be protected and managed.

In summary, methodologically, trace elements can serve as a measure of the ambient water chemistry the fish is exposed to. Stable isotopes, in our case $\delta^{13}C$ and $\delta^{15}N$, serve as a reflection of the fishes diet, and thus indirectly can give insight into their location and movement behavior. The primary goal of this study was to assess the suitability of scales as a non-lethal alternative to otoliths and muscle tissue in Red Drum via these two analyses. Beyond this, we also wanted to use the information gathered from scales to independently reassess the central goals of Torrance's previous work, determining many Red Drum are entering into freshwater and how often are they doing so, and if red drum move into freshwater, if they feeding when doing so. Trace element analysis and comparisons to otolith trace element profiles were exploratory, and few predictions about the results of these analyses were made. As in previous studies of scale stable isotopes, we anticipated that stable isotope values of scales and muscle tissue would match well but with a species specific offset, assuming that similar temporal periods of each structure are analyzed (Estep and Vigg 1985; Satterfield and Finney 2002; Perga and Gerdeaux 2003; Pruell et al. 2003; Estrada et al. 2005).

METHODS

Scale Collection

Juvenile and sub-adult Red Drum were caught during Texas Parks and Wildlife Department (TPWD) gill net surveys in the Nueces and Mission-Aransas estuaries (Figure 2)

including Aransas Bay, Copano Bay, Corpus Christi Bay, St. Charles/Mesquite Bay, and Nueces Bay. The Nueces estuary includes Corpus Christi Bay and Nueces Bay. Freshwater inflow to the system comes from the Nueces River, which flows into Nueces Bay from the east, the Rincon Delta just north of the river, and from Oso Creek (Longley 1994; Chandler et al. 1981). Nueces Bay is directly connected to Corpus Christi Bay and has an average salinity of 21.4 to 25 (Longley 1994). Corpus Christi Bay is also connected to Oso Bay to the south, Redfish Bay to the north, and the Gulf of Mexico several through points of exchange on the western barrier islands (Simms et al. 2008). Corpus Christi Bay has an average salinity of 26.5 to 31.4 (Longley 1994). This Nueces estuary's primary producers are predominantly the seagrasses *Halodule wrightii* and *Thalassia testidinum* (Pulich et al. 1998). Because Corpus Christi Bay is so large and has so much water exchange with other bays, the east side of Corpus Christi Bay closest to Mustang Island was delineated as its own region when doing analysis of data by bay of capture.

The Mission-Aransas Estuary is made up of Aransas Bay, Redfish Bay, and Copano Bay. Redfish Bay is a small sub-bay south of Aransas Bay directly north of the Corpus Christi shipping channel between Port Aransas and Aransas Pass. Redfish Bay exchanges water with Aransas Bay to the North, Corpus Christi Bay to the South, and the Gulf of Mexico via the Corpus Christi shipping channel. Copano Bay is the furthest inland, and receive freshwater inflow from the Aransas and Mission Rivers and multiple smaller creeks (Chandler et al. 1981). Copano Bay only directly shares water with Aransas Bay to the east (Chen 2010). Aransas Bay is a centralized bay to the east of Copano Bay. It exchanges water with Redfish Bay to the south, Copano Bay to the east, and St. Charles and Mesquite Bay to the north. Copano Bay has an average salinity of 10.9, while Aransas Bay has an average salinity of 16.4 (Longley 1994). These systems are dominated by the seagrass *H. wrightii*, reefs made up of the oyster species

Crassostrea virginica, and the marsh grass *Spartina alterniflora* (Froeschke et al. 2013). The final study bays, St. Charles Bay and Mesquite Bay are just North of the Mission-Aransas System. Only one specimen was caught in St. Charles Bay. Mesquite Bay exchanges water with Aransas Bay to the south, the Gulf via the sometimes-open Cedar Bayou, and has freshwater inflow from the San Antonio River to the North. The known salinities of all these systems were similar to the salinities recorded at the time of specimen capture (Figure 2).

Fish age in years was estimated using annuli of otoliths during the previous study. Fish age ranged from 0-2 years old, with an average age of 0.96 years. Because otoliths were only used for laser ablation of the first 100 fish in the previous study, only 100 fish had ages estimated. A total of 203 Red Drum were captured during the surveys, and 190 of those fish were used for scale analysis (Table 1). These surveys occurred in November of 2016 and April through June of 2017. Gill nets were placed one hour prior to sunset, and then collected the next morning at sunrise. These nets were 182.9 m long, 1.2 m tall and separated into 4 equal length sections (45.7 m of various mesh sizes to allow capture of various size class fish (7.6, 10.2, 12.7, and 15.2 cm monofilament mesh sizes). At the time of capture various additional abiotic data was recorded, including date of capture, salinity, and location, among other data. Specimens were then taken to the lab and processed. Fish processing entailed weighing and measuring the fish, removal of the sagittal otolith, removal of a dorsal muscle sample, and removal of 2 to 7 scales from most specimens. Average fish length was 423 mm total length and ranged from 303 to 719 mm total length. Scales were not collected or analyzed from specimens RD-006 through RD-014, and RD-201 through RD-203

Scales were scrubbed with a toothbrush in deionized (DI) water to remove surface contaminants and excess tissue. Scales were then submerged in DI water in a Branson 200

sonicator and sonicated for 5 minutes. Each scale was then triple rinsed in DI water and placed in an open petri dish in a Supreme Air Venturi fume hood overnight to dry. After drying, scales were viewed under a microscope to identify growth increments to determine if the scale was regenerated (Figure 3) because regenerated scales can display recently generated chemical signatures rather than those reflective of the full life history of the fish (Seeley et al. 2017). All scales were then photographed using Zen 2.3 Pro software on a Zeiss Discovery V8 microscope with a Zeiss Axiocam 506 Color microscope camera and then placed into individual plastic bags. The plastic bags were then placed into scintillation values based on the fish the sample was taken from and stored.

Most of the scales collected had a diameter of about a centimeter. Scales from 6 of my fish (RD-001 – RD-005 and RD-119) were significantly larger than those of the other fish. These scales were 2-3x the diameter of the other scales, much thicker, and weighed almost 4x as much as a typical scale. This subset of scales will be hereafter referred to as large size class scales

Stable Isotope Analysis

Previous work by Torrance (2018) obtained the $\delta^{13}C$ and $\delta^{15}N$ values of muscle samples from 203 captured Red Drum. Scales from 190 of those specimens were saved and available for analysis in this study. Because of the scarcity of non-regenerated scales in our repository, regenerated scales were selectively chosen for analysis, provided that the regenerated portion of the scale was small enough that it would not make up a portion of the scale sample analyzed and result in a temporally skewed stable isotope signature (Seeley et al. 2017). Whole non-regenerated scales were reserved for later laser ablation analysis. Samples were taken from the growing edge of the scale to obtain recent basal layer material in an attempt to match the recent

diet signature of muscle tissue (Hutchinson and Trueman 2006; Ramsay et al. 2012). A 2 mm wide by 3 mm long sample portion of each scale was excised from the growing edge of the scale using a scalpel blade. The 3mm section of scale was cut from the growing edge inwards towards the focus of the scale (Figure 4). Excised samples were cut to this size to make their weight between 0.5 mg and 1.5 mg, the sample weight range required by isotope ratio mass spectrometry (IR-MS). If a sample was heavier than 1.5 mg, a very small portion was cut and removed from the inner portion of the scale fragment and it was reweighed. This process was repeated as necessary until the weight of the sample was equal to or less than 1.5 mg. The six large size class scales in our raised concern that large scales would result in more underplating effect and signature more reflective of past growth prior to the time series muscle tissue reflects. In order to examine if this was true, a small and large sample were both excised from these scales to determine which size sample returned a value closer to that of the muscle tissue. Small samples were cut to a weight of 0.5 mg, and large samples were cut to a weight close to 1.5 mg (Figure 4). Samples were then packaged into 3.5 mm tin capsules, placed into 96-well trays and sent to the University of California, Davis, Stable Isotope Facility for dual $\delta^{13}C$ $\delta^{15}N$ natural abundance analysis with IR-MS in August 2019. Analyses were conducted using a PDZ Europa ANCA-GSL elemental analyzer interfaced to a PDZ Europa 20-20 isotope ratio mass spectrometer (Sercon Ltd., Cheshire, UK). These samples were compared against 7 reference materials (Appendix 1A). The mean standard deviation for $\delta^{13}C$ was 0.07‰, and the mean absolute accuracy for calibrated reference materials was 0.03‰. The mean standard deviation for $\delta^{13}C$ was 0.08‰, and the mean absolute accuracy for calibrated reference materials was 0.03‰.

Decalcification

Inorganic carbon can skew stable isotope ratios when included for analysis of scales, resulting in a combined signature indicative of both inorganic carbon and dietary signatures (Woodcock and Walther 2014). Because of the capability of the inorganic portion of scales to house inorganic carbon, decalcification of a subset of scale portions occurred prior to primary stable isotope analysis in order to determine if decalcification of all samples was required. Scales were cut down the middle to obtain two symmetrical halves. Various scales were selected from 14 fish for the preliminary stable isotope analysis. Scales from fish with wide variety of isotopic signatures from muscle tissue were selected in order to best determine pair-wise matching of scale portions. These scales were cleaned of surface contaminants and sonicated. Selected scales were cut in half, resulting to two symmetric scale halves. One half of the scale was soaked in 1.2 M HCl for 2 minutes and then triple rinsed in DI water to decalcify it (Perga and Gerdeaux 2003). The other half of the scale was left untreated. The treated portion of the scale was dried overnight. After drying, a 2 mm wide by 3 mm long sample portion of each scale half was excised from the growing edge of the scale using a scalpel blade, with each sample portion having been adjacent to the other prior to cutting the sample (Figure 4c). This process resulted in 28 paired samples from 14 individuals, half being decalcified samples, and the other half being untreated samples for comparison. Samples were then packaged into 3.5 mm tin capsules, placed into 96-well trays and sent to the University of California, Davis, Stable Isotope Facility for dual $\delta^{13}C$ $\delta^{15}N$ natural abundance analysis with IR-MS in June 2019. These samples were compared against 4 reference (Appendix 1B). The $\delta^{13}C$ $\delta^{15}N$ values of the paired samples from each fish were then compared using linear regression.

Scale Residuals

Residuals of the scale stable isotope data were calculated to determine if there was any scale isotopic bias against muscle for any bay. Another confounding factor aside from diet could contribute to the scale stable isotope values of captured Red Drum, and confound our results in a way that differed from actual trends. For example, maybe scale values from fish caught in Nueces Bay were all skewed above the trendline. Residual analysis was done to look for these kinds of trends and further examine the viability of scales as a muscle tissue alternative. The residuals of $\delta^{13}C$ and $\delta^{15}N$ were calculated by subtracting the isotopic values of muscle tissue from the predicted values of scale signatures.

Statistical Analysis

The statistical analysis program R was used for all statistical testing. Linear regressions were used to determine linear relationships between scale and otolith stable isotope values. One-way ANOVAs were used to determine significant differences in stable isotope values of scales and residuals of fish based on bay of capture. Post hoc testing was done using the Tukey method with a Holm correction for multiple comparisons. Ward's hierarchical clustering analysis was also used to cluster individuals into distinct groups based on their $\delta^{13}C$ and $\delta^{15}N$ signatures. The Stable Isotope Bayesian Ellipses in R package was used to create a plot of the Ward's clustered values with convex hull areas and 95% confidence ellipses mapped.

Trace Element Analysis

Torrance's previous work (2018) conducted trace element analysis of otoliths from 100 of the Red Drum captured and processed. Scales from 91 of these fish were available and used to conduct comparative laser ablation analysis. One scale per specimen was chosen from the repository with non-regenerated scales selectively chosen when possible in order to obtain a

signature indicative of the entire life span of the fish (Seeley et al. 2017). In some cases, a non-regenerated scale was not available, so a regenerated scale had to be used. 25.53% of scales (n = 23) used for ablation analysis showed some signs of regeneration (Appendix Table 1).

Many of the scales in this study had a significant amount of physiographic relief. This relief made it difficult to mount the scales to glass slides, so steps were taken to flatten the scales. Scales were soaked overnight in a petri dish filled with deionized water to make the scale more pliable. After soaking, the scales were placed back into their representative plastic bag with the top of the bag open, and then placed under the outer edges of textbooks with the open top of the bag visible and uncovered by the book. The scales were pressed under several textbooks until they had fully dried.

A 5 mm wide channel of each flattened scale was cut, containing the focus of the scale at one end, and the growing edge of the scale at the other (Figure 4D). These portions were superglued to 3" x 1" glass microscope slides in the same orientation. These samples were then taken to the University of Texas at Austin Jackson School of Geosciences for laser ablation inductively coupled plasma mass spectrometry (ICP-MS) analysis with an Agilent 7500ce quadrupole ICP-MS with a 193-nm New Wave Up-193FX laser system to determine changes in the chemical composition across the surface of each scale. The concentrations of ^{43}Ca, ^{44}Ca, ^{88}Sr, and ^{137}Ba, were analyzed. Scales were first pre-ablated at 60% power at 20 Hz with a 75 μm spot size at 75 μm/s to remove any surface contaminants that were not previously removed manually. Ablation then took place from the focus of the scale to the edge to obtain Ba/Ca and Sr/Ca ratios for the calcium phosphate surface of the scale. Primary ablation was done at 55% power at 10 Hz with a spot size of 25 μm and a scan rate of 15 μm/s. Instrument drift calibration took place according to the University of Texas Jackson School of Geosciences standards (USGS MACS-3

calcium carbonate, USGS MAPS-4 synthetic modern bone and NIST 612 glass certified standards). Elemental counts were converted to concentrations (ppm) using known concentrations in the standards. Because of the laser often running off of the scale in many transects, the data was trimmed using concentrations of ^{43}Ca and ^{44}Ca to isolate data actually returned from the scale. A 15-point running mean was then applied to returned values of ^{88}Sr and ^{137}Ba to remove high frequency variability inherent to laser acquisition methods. Concentrations were then converted to molar concentrations and then ratioed against ^{44}Ca to obtain Ba:Ca and Sr:Ca molar ratios. The distance across the scale was calculated using the laser speed and the time the laser spent running.

Comparative Analysis of Both Structures

Since both trace elements and stable isotopes vary predictably with salinity, it was necessary to examine trace elements and stable isotopes in tandem to determine if they were in agreement about residency within salinity regimes. To do this, the Ba:Ca and Sr:Ca trace element profiles of each scale were averaged across the tracts of varying distances from the edge of the scale. A 3000 μm distance was included in analysis because the scale portions for stable isotopes were cut to be 3 millimeters long. The averaged Ba:Ca and Sr:Ca values were compared against the $\delta^{13}C$ and $\delta^{15}N$ values from the same scale. This allowed us to compare the values of the two analyses from the same portions of the scale.

RESULTS

Decalcification

The values of the decalcified and untreated samples did not differ significantly, so further decalcification of the remainder of the scale samples was deemed unnecessary. The regression line equation of $\delta^{13}C$ in decalcified scales vs untreated ones was y=0.98x + 0.10 with an adjusted R^2 value of 0.99 (p-value < 0.0001, n = 14)(Figure 5). The regression line equation of $\delta^{15}N$ in decalcified scales vs untreated ones was y = 0.99x - 0.24 with an adjusted R^2 value of 0.99 (p-value < 0.0001, n = 14)(Figure 6).

Small vs Large Scale Samples

In the case of large size class scales that were tested with both small and large samples, these values were very similar, with the average difference in muscle $\delta^{13}C$ and large scale samples being slightly smaller than those of small samples. In the case of $\delta^{15}N$ however, the average difference in muscle $\delta^{15}N$ and small scale samples was slightly smaller than that of the large samples (Table 3). Since no size of scale sample could be determined as the best match with this small number of samples, large scale samples were selected and used for all subsequent data analysis.

Matching of Scale and Muscle Stable Isotopes

Linear regressions were calculated comparing pairwise stable isotope values of scale samples against their respective muscle tissue values for each individual fish. Significant relationships existed between scale and muscle values for both $\delta^{13}C$ and $\delta^{15}N$. For $\delta^{13}C$, the regression line equation was y = 1.01x + 3.31 with an adjusted R^2 value of 0.79 and p = <0.001

(Figure 7). For δ^{15}N the regression line question was y = 0.97x - 1.29 with an adjusted R^2 value of 0.89 and p = <0.001 (Figure 8). Large size class scales were outliers in this regression, and removing those points yielded a linear equation of y = 1.07x + 4.38 for δ^{13}C (p = <0.001, adjusted r-squared = 0.95) and a linear equation of y = 0.98x - 1.36 for δ^{15}N (p = <0.001, adjusted r-squared = 0.91). Regressions of δ^{13}C and δ^{15}N scale values against fish total length revealed significant relationships, but low r-squared values, meaning that further size correction for isotopic values was not necessary (δ^{13}C p = <0.001, adjusted r-squared = 0.15; δ^{15}N p = < 0.001, adjusted r-squared = 0.07).

Scale Stable Isotopes by Location

To begin independently reassessing the questions about Red Drum freshwater movement of Torrance's work, a biplot of δ^{13}C and δ^{15}N scale values delineated by bay of fish capture was created and showed obvious clustering of most of individuals by bay of capture (Figure 9). Bays of capture were further delineated from the previous study. Fish captured in Aransas Bay in the previous study were further delineated into either the newly classified Redfish Bay or Aransas Bay. Boxplots were used in conjunction with one-way ANOVAs and post hoc Tukey method testing with a Holm correction for multiple comparisons to determine significant differences in δ^{13}C and δ^{15}N by bay (δ^{13}C p-value: <0.00001, δ^{15}N p-value: <0.00001). For δ^{13}C, Redfish Bay was significantly different than all other bays. Corpus Christi Bay – Mustang Island and Aransas Bay were not significantly different from one another but were significantly different from all other bays. Such was also the case for the pairs of Nueces Bay and Corpus Christi Bay, and for Copano Bay and St. Charles/Mesquite Bay (Figure 10). For δ^{15}N, Corpus Christi - Mustang Island was significantly different from all other bays. Corpus Christi Bay was not significantly

different from Nueces Bay, but was significantly different from all other bays. Nueces Bay was significantly different than all other bays except St. Charles/Mesquite Bay and Corpus Christi Bay. Copano Bay, Aransas Bay, and Redfish Bay were not significantly different from one another, but were significantly different from all other bays (Figure 11).

Ward's hierarchical clustering analysis was used to cluster individuals into distinct groups based on their $\delta^{13}C$ and $\delta^{15}N$ signatures (Figure 15). Three distinct groups were determined with the analysis. Group 1 was characterized by low $\delta^{13}C$ (15.58 ± 1‰, mean ± 1 S.D.) and low $\delta^{15}N$ (9.92 ± 0.44‰) values and was primarily comprised of individuals from Copano Bay. Group 2 was characterized by high $\delta^{13}C$ values (-10.85 ± 0.96‰) and low $\delta^{15}N$ values (10.38 ± 0.95‰), with representative individuals being mostly from Redfish Bay, Aransas Bay, and Corpus Christi Bay – Mustang Island. Group 3 individuals possessed low $\delta^{13}C$ values (-14.49 ± 0.79‰) and high $\delta^{15}N$ (13.12 ± 0.82‰) values, with fish captured typically being from St. Charles/Mesquite Bay and Nueces Bay. The Stable Isotope Bayesian Ellipses in R package was used to create a plot of the Ward's clustered values with convex hull areas and 95% confidence ellipses mapped (Figure 16).

Scale Residuals

The residuals of $\delta^{13}C$ and $\delta^{15}N$ were calculated by subtracting the isotopic values of muscle tissue from the predicted values of scale signatures. These values were biplotted and delineated by bay, with large size class scales having the highest residuals (Figure 12). Scale residuals were delineated by bay and post hoc Tukey testing with a Holm correction for multiple comparisons was done ($\delta^{13}C$ residuals p-value: <0.00001, $\delta^{15}N$ residuals p-value: <0.00001). For $\delta^{13}C$ residuals, Corpus Christi Bay had significantly higher residuals than any other bay, and no

other bays were significantly different from one another (Figure 13). For $\delta^{15}N$ residuals, there was a high degree in overlap of significance. Nueces, Copano, Redfish, and Corpus Christi Bay were not significantly different from one another. Copano, Redfish, Corpus Christi, and Aransas Bay were not significantly different. Redfish, Corpus Christi, Aransas, Mesquite/St. Charles, and Mustang Island – Corpus Christi Bay were not significantly different from each other (Figure 14). Based on these values being distributed all over the plot, no clear bias was observed.

Trace Element Scale and Otolith Matching

Precisions and accuracies were calculated based on measurements of NIST corrected by MAPS 4 (n=32) and were reported as residual standard deviations (RSD) and average limits of detection (LOD). ^{44}Ca RSD = 1.01, LOD = 207.19 ppm. ^{88}Sr RSD = 1.08, LOD = 0.15 ppm. ^{137}Ba RSD = 1.06, LOD = 0.51 ppm. Ba:Ca and Sr:Ca profiles for scales were plotted against their respective Ba:Ca and Sr:Ca profiles for otoliths do a qualitative assessment of pattern marching between the two structures (Appendix 1). Distances in the profiles were converted to proportions of distance across the structure, putting scale and otolith distance on the same temporal scale. With qualitative analysis, we were looking for general pattern matching such as spikes in Barium to calcium levels across both structures. Pattern matching seemed to follow an inverse relationship in some scales (Figure 21, 22), and some scales showed matching relationships (Figure 23, 24). The aforementioned figures are examples of these occurrences, and are not the only cases these patterns were observed in. Many scale trace element patterns while many seemed to show no matching relationship to otoliths.

Comparative Analysis of Trace Elements and Stable Isotopes

In order to determine if a significant correlation between Ba:Ca ratios, Sr:Ca ratios, and $\delta^{13}C$ values was present, averaged elemental ratio values were calculated for differing distances of the growing edge of the scale. Ba:Ca ratios and $\delta^{13}C$ values were significantly correlated at all distances calculated (1000 μm, 2000 μm, and 3000 μm), with all p values being less than 0.0001 (Figure 17). Though significant R-squared values were low at 0.20, 0.20, and 0.22, respectively. As Ba:Ca values increased, δ^{13}Carbon values decreased as well. Sr:Ca ratios and $\delta^{13}C$ values were also significantly correlated at all distances, with all p values being less than 0.001 (Figure 18). Again, although significant, R-squared values were low at 0.15, 0.14, and 0.13, respectively. As Sr:Ca values increased, δ^{13}Carbon values increased as well. It is important to note that these trendlines were largely driven by select scales on the periphery of the distributions that showed values matching salinity trends between Ba:Ca, Sr:Ca and $\delta^{13}C$. When scales had high Ba:Ca levels, they only had low $\delta^{13}C$ values, and when scales had low Sr:Ca values, they were always accompanied by low $\delta^{13}C$ values, which is in line with Ba:Ca, Sr:Ca, and $\delta^{13}C$ salinity trends in this system.

Ba:Ca and Sr:Ca values were also plotted against each other, showing weak correlation (Figure 19). Averaged Ba:Ca values from the outer 2000 μm of scales from each fish were plotted against averaged Ba:Ca values from the outer 500 μm of otoliths to determine correlation between structures. This size choice was made in an attempt to obtain a similar temporal scale for both structures, as both distances made up roughly the same proportion of growth for the two structures. No correlation was found (Figure 20).

DISCUSSION

The intention of this work was to determine if Red Drum scales are a suitable analogue to otoliths regarding the stable isotope and trace element profiles they contain. Like the previous study, an independent assessment of Red Drum usage of low-salinity environments was also conducted using data elicited from scale analysis.

Scales as a Muscle Tissue Alternative for Stable Isotopes

Our high R squared values for our scale vs muscle stable isotope regressions indicate that the sampled portion of our scales represented a time period similar to that of muscle tissue. It was fortunate to get such temporal matching, as the size of our samples was limited by the analytical capabilities of the facility conducting our stable isotope analysis, with samples only having a leeway in mass of 1 gram. Before executing a study like this determining scale stable isotope matching with that of muscle tissue for another fish species, it is advisable to test various scale sample area sizes to determine what most closely matches that of muscle tissue before committing to the preparation of multiple samples of a selected area. If scales are sufficiently large or exceptionally small, it may be impossible to match the temporal stable isotope signature of a scale with that of muscle tissue as samples within the allowable size or weight range for analysis will likely contain varied trace element signatures indicative of differing time periods.

To independently reassess questions about the freshwater use of Red Drum, stable isotope clustering was conducted and results showed that 3 major groupings of Red Drum were observed with significantly different means among groups for $\delta^{13}C$ and $\delta^{15}N$ values, likely reflecting residency within sub-bays at different distances from riverine input (Figure 16). These clusters were largely comprised of fish from a small number of bay systems, indicating that

residency within bays is the most common behavior for sub-adult Red Drum, rather that migration between bay systems (Figure 9). Group 1 was characterized by low $\delta^{13}C$ and $\delta^{15}N$ values and was mainly comprised of individuals from Copano Bay. Group 2 was characterized by high $\delta^{13}C$ values and low $\delta^{15}N$ values, with representative individuals being mostly from Redfish Bay, Aransas Bay, and Corpus Christi Bay – Mustang Island. Geographically, these bays are all quite close to one another and are also close to areas of water exchange with the ocean. Group 3 individuals possessed low $\delta^{13}C$ values and high $\delta^{15}N$ values, with fish captured typically being from St. Charles/Mesquite Bay and Nueces Bay. The low $\delta^{13}C$ values associated with fish from these bays make sense as they both experience significant freshwater inflow; Mesquite Bay from the San Antonio River and Nueces Bay from the Nueces River. When Torrance (2018) did clustering analysis using muscle stable isotope values, two primary clusters were identified. There was always a suspicion with Torrance's data that a 3rd group might exist, and that thought was validated with this clustering analysis.

This strong clustering of individuals matching to distinct bays likely indicates strong site fidelity in Red Drum (Figure 9), as stable isotope signatures from fish caught in the same bays tend to be close to one another. Such matching stable isotope signatures means that fish resided in the area of capture long enough to equilibrate to the isotopic signature of their capture site. Similar residence patterns with high site and bay fidelity have been observed in other studies of Red Drum as well (Osburn et al. 1982; Moulton et al. 2017; Nelson and Powers 2020).

In the case of Red Drum, few studies have attempted to establish the isotopic turnover rate of Red Drum tissue, but larval turnover rates have been explored in 2 studies which established turnover rates of about 10 days (Herzka et al. 2002; Herzka and Holt 2011). However, as fish age, their growth rates generally slow down, increasing muscle tissue turnover times. Because of the

lack of information about the turnover rates of stable isotope signatures in juvenile Red Drum, a controlled study of another juvenile sciaenid species was used as an estimate of juvenile Red Drum muscle turnover rate. In a controlled study of juvenile Atlantic Croaker (*Micropogonias undulatus*) the 95% turnover rate of $\delta^{13}C$ was 129 ± 47 days and for $\delta^{15}N$ was 115 ± 12 days (Mohan et al. 2016). Therefore, the scale stable isotope values obtained from the basal layer of the scale are likely indicative of approximately the most recent 4 months of dietary behavior.

Scales as an Otolith Alternative for Trace Elements

Ba:Ca ratios obtained from otolith analysis suggested that ~2-35% of individuals made use of low salinity habitats during their lifetime. Sr:Ca ratio results were less reliable given the minimal dynamic range between fresh and marine end members in Texas systems (Torrance 2018). Unlike the methods employed in the previous study, a threshold analysis was not used as an indicator of low salinity movement because the concentrations of Ba in the external layer of scales is higher than that of otoliths (Johnson 1989; Pender and Griffin 1996; Campana and Thorrold 2001). Therefore, the Ba threshold employed in the previous study could not be applied to this project.

Qualitative comparisons of Ba:Ca and Sr:Ca profiles of scales and otoliths were largely inconclusive. Some profiles seemed to show inverse relationships between scales and otoliths, such as the Ba:Ca profiles of RD-015 (Figure 21) and RD-016 (Figure 22). On the other hand, some Ba:Ca profiles seem to potentially match, such as those from RD-034 (Figure 23) and RD-062 (Figure 24). Sr:Ca pattern matching was inconclusive due to clear patterns not appearing in the profiles, likely a result of the narrow endmember range of Sr:Ca in Texas waters. The trendlines of Ba:Ca and Sr:Ca averaged values compared against $\delta^{13}C$ values showed trends in accordance with known salinity trends (Figures 17 and 18), but the slopes of the regression lines were largely

driven by several outliers in each distribution. Despite this, those outliers for both Ba:Ca and Sr:Ca adhered to expected trends with salinity, lending credence to both structures reflecting the trace element and stable isotope salinity trends of the local system.

For trace element analysis, we elected to use top down laser ablation because it was easy to set up and prepare samples for analysis, and because top down laser ablation has only been attempted for scales in a handful of studies, to varying degrees of success, and never in red drum. With this comes a few factors that might affect our results. Scales are exposed to seawater, and therefore the external layer of the scale can undergo ionic exchange with seawater. This is not a concern with otoliths, because they are completely internal structures. Other scale studies, including those on tarpon (Seeley et al. 2015), elected to use a cross sectioning approach instead, so growth layers that were never exposed to seawater could be analyzed.

High levels of precipitation or riverine input into an estuarine system can cause resident individuals to reflect a chemical signature indicative of freshwater residence as freshwater flows over organisms. This is a potential issue in any natural tag, not just scales. It is unlikely that this was the case in this study, as freshwater discharge was shown to be quite low during this time period (https://txpub.usgs.gov/txwaterdashboard/index.html). Another potential issue with the use of natural tags is the idea of migratory prey. If the prey species that Red Drum are feeding upon are moving between bay systems, Red Drum will integrate dietary stable isotope signatures that are potentially different from that of the area they are feeding within.

In this study, some fish did not have any non-regenerated scales available to use for laser ablation analysis (Appendix Table 1). For those scales, they likely show a trace element profile that is not indicative of the entire life history of the fish, but rather the time period from when the original scale was lost, and the regenerated scale began formation. In the case of Red Drum scales,

regeneration in scales is visible with minimal magnification, so any future studies involving Red Drum scales as a natural tag should take care to ensure that non-regenerated scales are removed from the fish and available for analysis.

Even though some scales used were regenerated, the distance data shown in Figures 17, 18 and 19 were most likely unaffected, as the degree of regeneration of most scales did not extend into the outer 3000 μm from the growing edge of the scale inwards. However, the comparison of averaged values of otolith Ba:Ca and scale Ba:Ca over set distances showed no correlation (Figure 20). If the sampled sections of both otoliths and scales covered the same temporal growth period, this could be an indicator of overall mismatch between scale and otolith trace element profiles.

It is also important to note that scales technically cannot contain a chemical history encompassing a red drums full life cycle, since scales do not grow until squamation occurs when the fish enters the juvenile stage, usually 3 weeks after hatching for red drum. This means that these patterns may have a very slight actual offset, where the scale elemental profile starts 3 weeks after the otolith profile begins.

Scales as a Non-Lethal Alternative Structure

Unlike otoliths, scales are a structure whose growth is often beholden to the somatic growth of the individual. While an otolith will continue growing during times of no somatic growth, a scale often will not (Campana and Thorrold 2001). Scales have also shown to have useful applications outside of trace element and stable isotopes, as several recent studies have explored the use of cortisol in fish scales as an indicator of stress (Aerts et al. 2015; Laberge et al. 2019). Like other natural tags that are chemically affected by ambient water chemistry, they can at times be misleading due to temporal changes in ambient water chemistry. In the case of

something like a flood event or heavy rains, chemically new water can move into the environment fish reside in, giving them a new chemical signature that may look like migration when that is not actually the case. Ion exchange can also occur after deposition between the external layer of the scale and the surrounding water, affecting the elemental composition of the surface of the scale (Seeley et al. 2015). The depth of the calcium phosphate layer of the scale which could be subject to this phenomenon is currently unknown and require further study.

Scales as a natural tag are most useful for juvenile and sub-adult fish due to the increased likelihood of fish losing and regenerating scales as they age. The older the fish, the more likely they are to have scales that are regenerated and not indicative of the full life profile of the fish. Scales as a natural tag are also non-viable for larval fish, as they have not undergone full scale formation.

Future Research

Historically, the use of natural tag microchemistry has proven most useful in the detection of diadromy in fishes because of punctuated microchemical signatures corresponding to movements between freshwater and marine environments (Gillanders 2005). In this study, all captured individuals were juveniles and had yet to undergo the movement to marine waters associated with Red Drum reaching spawning age. Because of this, finer scale changes in microchemical profiles are likely observed across the transect of the scale, making qualitative comparisons of scale and otolith profiles difficult. In order to further examine the viability of scale trace element profiles as an alternative to those of otoliths, a comparison study of adult Red Drum scales and otoliths or of another diadromous species would be most useful in determining if signatures indicating punctuated movements are observable in both profiles.

In addition to this, scales do not offer a trace element profile that is indicative of the entire life history of the fish, because complete scale squamation occurs after the larval phase in Red Drum (Fuiman et al. 1998). This results in a potential temporal offset in trace element signatures that results in the omittance of larval signatures in scale microchemistry. In the case of the scale and otolith profiles of this study, scale profiles are likely skewed left of their respective time period on the otolith profile. Such drawbacks and facets need to be considered when using scales as structures to study fish movement.

Ideally, controlled studies should be done exposing red drum to a set concentration of Barium and Calcium ions in order to determine uptake rate in scales. If the scale trace element uptake rate of a species can be determined, then scale concentrations can likely be more easily compared to otoliths, assuming that uptake and deposition is constant.

Fine scale otolith and scale matching hasn't been found before. Studies comparing otolith and scale trace elements have largely been limited to using bulk measures to determine natal origins. At this point, it is especially important to start determining down the physiological differences in deposition between scales and otoliths to determine if the structures can match with higher resolution. There is certainly another possibility here, that maybe this is simply not a suitable study species for using as a test species for otolith and scale matching. Historically, otolith trace element analysis has been used primarily for detecting movements of fish from fully marine areas to freshwater, and vice-versa, because in those cases you usually get large spikes of barium and strontium that are not difficult to detect. In the case of red drum, they are a fish residing in intermediate salinities that may make fine scale movements into freshwater, which has historically been difficult for a natural tag like otoliths.

Aside from the subject species potentially not being ideal from this kind of comparative analysis, the trace elements used may not be ideal as well. $\delta^{13}C$ has a linear relationship in this study system, increasing with salinity (Bishop et al. 2017). Ba:Ca undergoes a non-linear decrease as salinity increases, but it undergoes its biggest change between the salinities of 0-10. There is a much narrower change in Ba:Ca values from salinities of 20-50 (Walther and Nims 2015). So even though Barium is better than strontium for determining freshwater movement, it's not well suited and determining finer scale movements between estuarine waters of varying salinities, since none of our bays of residence was below a salinity of 13.

Despite these difficulties, the benefits of scale analysis cannot be ignored, especially the fact that they serve as a non-lethal natural tag with promise of informing movement activity of fish in low or declining populations. Also, scales have long been used to age fish, as the concentric rings of growth can often correspond to years or seasons of growth. Because of this, many large repositories of scales exist in collections across the world, and the validation of scales as a structure to study migration behavior can allow for many historical studies of fish movement using stored scales (Perga and Gerdeaux 2003; Gerdeaux and Perga 2006).

Conclusion

The results of this study indicated that Red Drum were not commonly using low salinity habitats and were remaining resident to their respective bays throughout the system. Scales were shown to be a good analog to muscle tissue, providing that the portion of scale sampled encompasses the same time frame as the muscle turnover rate of the fish. This is not a guarantee of this method working for scales from all species, as analytical limitations for stable isotope analysis may make obtaining a scale sample that encompasses the same time frame as muscle

difficult, especially for scales considerably smaller or larger than those of the Red Drum in this study. Matching of scale and muscle time periods regarding stable isotopes can be done in other species by varying scale sample size or homogenizing whole scales or scale portions if removal of samples within the weight range required for stale isotope analysis is difficult.

Because stable isotope values of both structures matched well, the study independently reached similar conclusion about Red Drum movement as the previous study, that juvenile Red Drum are largely site specific and remaining in the same bay for significant periods of the juvenile phase, and likely not moving into freshwater environments. Based on the dynamics of stable isotopes in this Texas system, changes in Red Drum scale isotope values are likely due to long-time residence of individuals in Bays with varying amounts of freshwater inflow, resulting in groups of individuals that are clearly occupying different salinity regimes than other fish (Figure 16).

This study did determine that decalcification of Red Drum scales is unnecessary for stable isotope analysis, as stable isotope signatures of decalcified scales did not differ significantly from those of untreated scales. Future studies that analyze the stable isotope signatures of Red Drum scales can forgo decalcification steps in their procedures.

Trace element analysis did not show clear pattern matching or correlation between the two structures. Some scale trace element profiles seemed to match those of otoliths well, while others showed little correlation. Further data analysis will be conducted to examine if pattern matching does exist between the structures, and under what parameters matching is present. It is possible that some factors such as reduced scale growth and regeneration, among other factors result in scale trace element profiles that differ from those of otoliths. Further analysis will be done in order to examine the influence of factors such as regeneration.

Literature Cited

Adams, D. H., and D. M. Tremain. 2000. Association of Large Juvenile Red Drum, Sciaenops ocellatus, with an Estuarine Creek on the Atlantic Coast of Florida. Environmental Biology of Fishes 58(2):183–194.

Aerts, J., J. R. Metz, B. Ampe, A. Decostere, G. Flik, and S. De Saeger. 2015. Scales Tell a Story on the Stress History of Fish. PLOS ONE 10(4):e0123411.

Bacheler, N. M., L. M. Paramore, J. A. Buckel, and F. S. Scharf. 2008. Recruitment of Juvenile Red Drum in North Carolina: Spatiotemporal Patterns of Year-Class Strength and Validation of a Seine Survey. North American Journal of Fisheries Management 28(4):1086–1098.

Baird, R. C. 1999. Part one: essential fish habitat perspective. Pages 1–2 *in* American Fisheries Society Symposium 22 - Fish Habitat: Essential Fish Habitat and Rehabilitation. Bethesda, Maryland.

Bass, R. J., and J. W. Avault, Jr. 1975. Food habit, length-weight relationship, condition factor, and growth of juvenile red drum, Sciaenops ocellatus, in Louisiana. Transactions of the American Fisheries Society. 104:35-45.

Bernat, M., T. Church, and C. J. Allegre. 1972. Barium and strontium concentrations in Pacific and Mediterranean Sea water profiles by direct isotope dilution mass spectrometry. Earth and Planetary Science Letters 16(1):75-80.

Bishop, K. A., J. W. McClelland, and K. H. Dunton. 2017. Freshwater Contributions and Nitrogen Sources in a South Texas Estuarine Ecosystem: a Time-Integrated Perspective from Stable Isotopic Ratios in the Eastern Oyster (Crassostrea virginica). Estuaries and Coasts 40(5):1314–1324.

Brown, R. J., and K. P. Severin. 2009. Otolith chemistry analyses indicate that water Sr:Ca is the primary factor influencing otolith Sr:Ca for freshwater and diadromous fish but not for marine fish. Canadian Journal of Fisheries and Aquatic Sciences 66:1790-1808.

Buchheister, A., and R. J. Latour. 2010. Turnover and fractionation of carbon and nitrogen stable isotopes in tissues of a migratory coastal predator, summer flounder (Paralichthys dentatus). Canadian Journal of Fisheries and Aquatic Sciences 67(3):445-461.

Cabana, G., and J. B. Rasmussen. 1996. Comparison of aquatic food chains using nitrogen isotopes. Proceedings of the National Academy of Sciences 93(20):10844–10847.

Campana, S. 1999. Chemistry and composition of fish otoliths:pathways, mechanisms and applications. Marine Ecology Progress Series 188:263–297.

Campana, S. E., and J. D. Neilson. 1985. Microstructure of Fish Otoliths. Canadian Journal of Fisheries and Aquatic Sciences 42(5):1014–1032.

Campana, S.E., G.A. Chouinard, J.M. Hanson, A. Frechet, and J. Brattey. 2000. Otolith elemental fingerprints as biological tracers of fish stocks. Fisheries Research 46(1): 343-357.

Campana, S. E., and S. R. Thorrold. 2001. Otoliths, increments, and elements: keys to a comprehensive understanding of fish populations? Canadian Journal of Fisheries and Aquatic Sciences 58(1):30–38.

Chandler, C., Knox, J., and Byrd, L. 1981. Nueces and Mission-Aransas estuaries; a study of influence of freshwater inflows. Limited Publication, 108. Texas Department of Water Resources, Austin, Texas, 362.

Characklis, G., and M. Wiesner. 1997. Particles, metals, and water quality in runoff from large urban watershed. Journal of Environmental Engineering 123:753–759.

Chen, G.F. 2010. Freshwater Inflow Recommendations for the Mission-Aransas Estuarine System. Texas Parks and Wildlife Department, Austin, TX. 120.

Clark, J. 1968. Seasonal movements of striped bass contingents of Long Island Sound and the New York Bight. Transactions of the American Fisheries Society 97(4):320-343.

Coffey, M., F. Dehairs, O. Collette, G. Luther, T. Church, and T. Jickells. 1997. The Behaviour of Dissolved Barium in Estuaries. Estuarine, Coastal and Shelf Science 45(1):113–121.

Colura, R. L., B. T. Hysmith, and R. E. Stevens. 1976. Fingerling production of striped bass (Morone saxatilis), spotted seat trout (Cynoscion nebulosus), and red drum (Sciaenops ocellatus) in salt-water ponds. World Mariculture Society 7: 79-92.

Crocker, P. A., C. R. Arnold, J. A. DeBoer and G. J. Holt. 1983. Blood osmolality shift in juvenile red drum, Sciaenops ocellatus L. exposed to fresh water. Journal of Fish Biology 23(3): 315-319.

de Villiers, S. 1999. Seawater strontium and Sr/Ca variability in the Atlantic and Pacific oceans. Earth and Planetary Science Letters 171:623-634.

Dodd, J. R., and E. L. Crisp. 1982. Non-linear variation with salinity of Sr/Ca and Mg/Ca ratios in water and aragonitic bivalve shells and implications for paleosalinity studies. Palaeogeography, Palaeoclimatology, Palaeoecology 38(1–2):45–56.

Elliott, M., A. K. Whitfield, I. C. Potter, S. J. M. Blaber, D. P. Cyrus, F. G. Nordlie, and T. D. Harrison. 2007. The guild approach to categorizing estuarine fish assemblages: a global review. Fish and Fisheries 8(3):241–268.

Elsdon, T. S., B. K. Wells, S. E. Campana, B. M. Gillanders, C. M. Jones, K. E. Limburg, D. H. Secor, S. R. Thorrold., and B. D. Walther. 2008. Otolith chemistry to describe movements and life-history parameters of fishes. Oceanography and Marine Biology: An Annual Review 46:297-330.

Esbaugh, A. J., and B. Cutler. 2016. Intestinal Na+, K+, 2Cl− cotransporter 2 plays a crucial role in hyperosmotic transitions of a euryhaline teleost. Physiological Reports 4(22): e13028.

Estep, M. L. F., and S. Vigg. 1985. Stable Carbon and Nitrogen Isotope Tracers of Trophic Dynamics in Natural Populations and Fisheries of the Lahontan Lake System, Nevada. Canadian Journal of Fisheries and Aquatic Sciences 42(11):1712–1719.

Estrada, J. A., M. Lutcavage, and S. R. Thorrold. 2005. Diet and trophic position of Atlantic bluefin tuna (Thunnus thynnus) inferred from stable carbon and nitrogen isotope analysis. Marine Biology 147(1):37–45.

Ettinger, W. S., and R. W. Blye. 1981. Occurrence of the Blue Crab Callinectes Sapidus in the Tidal Freshwater Reaches of the Delaware and Schuylkill Rivers in 1976. Journal of Crustacean Biology 1(2):177–182.

Focken, U. 2004. Feeding fish with diets of different ratios of C3- and C4-plant-derived ingredients: a laboratory analysis with implications for the back-calculation of diet from stable isotope data. Rapid Communications in Mass Spectrometry 18(18):2087–2092.

Fouda, M. M. 1979. Studies on scale structure in the common goby Pomatoschistus microps Kroyer. Journal of Fish Biology 15(2):173–183.

Froeschke, B. F., G. W. Stunz, M. M. R. Robillard, J. Williams, and J. T. Froeschke. 2013. A Modeling and Field Approach to Identify Essential Fish Habitat for Juvenile Bay Whiff (Citharichthys spilopterus) and Southern Flounder (Paralichthys lethostigma) Within the Aransas Bay Complex, TX. Estuaries and Coasts 36(5):881–892.

Fry, B. 1983. Fish and shrimp migrations in the northern Gulf of Mexico analyzed using stable C, N, and S isotope ratios. Fishery Bulletin 81:789- 801.

Fry, B. 1999. Using stable isotopes to monitor watershed influences on aquatic trophodynamics. Canadian Journal of Fisheries and Aquatic Sciences 56(11):2167-2171.

Fry, B. 2002. Conservative mixing of stable isotopes across estuarine salinity gradients: a conceptual framework for monitoring watershed influences on downstream fisheries production. Estuaries 25(2):264-271.

Fry, B. 2006. Stable Isotope Ecology. Springer New York, New York, NY.

Fry, B., and C. Arnold. 1982. Rapid 13C/12C turnover during growth of brown shrimp (Penaeus aztecus). Oecologia 54(2):200–204.

Fuiman, L. A., K. R. Poling, and D. M. Higgs. 1998. Quantifying Developmental Progress for Comparative Studies of Larval Fishes. Copeia 1998(3):602.

Gerdeaux, D., and M. E. Perga. 2006. Changes in whitefish scales $\delta^{13}C$ during eutrophication and reoligotrophication of subalpine lakes. Limnology and Oceanography 51(1):772–780.

Gillanders, B. M. 2005. Otolith chemistry to determine movements of diadromous and freshwater fish. Aquatic Living Resources 18(3):291–300.

Gorokhova, E., and S. Hansson. 2011. An experimental study on variations in stable carbon and nitrogen isotope fractionation during growth of Mysis mixta and Neomysis integer. Canadian Journal of Fisheries and Aquatic Sciences 56(11):2203–2210.

Gross, M. R., R. M. Coleman and R. M. McDowall, 1988. Aquatic productivity and the evolution of diadromous fish migration. Science 239(4845):1291-1293.

Havel, L. N. and L. A. Fuiman. 2016. Settlement-Size Larval Red Drum (*Sciaenops ocellatus*) Respond to Estuarine Chemical Cues. Estuaries and Coasts. 39:560-570.

Herzka, S. Z. 2005. Assessing connectivity of estuarine fishes based on stable isotope ratio analysis. Estuarine, Coastal and Shelf Science 64(1):58-69.

Herzka, S. Z., S. A. Holt, and G. J. Holt. 2002. Characterization of settlement patterns of red drum Sciaenops ocellatus larvae to estuarine nursery habitat: a stable isotope approach. Marine Ecology Progress Series 226:143–156.

Herzka, S. Z., and G. J. Holt. 2011. Changes in isotopic composition of red drum (*Sciaenops ocellatus)* larvae in response to dietary shifts: potential applications to settlement studies. Canadian Journal of Fisheries and Aquatic Sciences 57(1):137-147.

Hesslein, R. H., K. A. Hallard, and P. Ramlal. 1993. Replacement of Sulfur, Carbon, and Nitrogen in Tissue of Growing Broad Whitefish (*Coregonus nasus*) in Response to a Change in Diet Traced by $\delta^{34}S$, $\delta^{13}C$, and $\delta^{15}N$. Canadian Journal of Fisheries and Aquatic Sciences 50(10):2071–2076.

Hightower, C. L. 2013. Evaluating the current status of red drum (Sciaenops ocellatus) in offshore waters of the North Central Gulf of Mexico: age and growth, abundance, and mercury concentration. Master's thesis. The University of Southern Alabama.

Holt, J., R. Godbout and C. R. Arnold. 1981. Effects of temperature and salinity on egg hatching and larval survival of red drum, *Sciaenops ocellata*. Fishery Bulletin 79(3):569-573.

Holt, S. A., Kitting, C. L., and Arnold, C. R. 1983. Distribution of young red drums among different sea-grass meadows. Transactions of the American Fisheries Society 112:267-271.

Huang, Y., and O. Diekmann. 2001. Predator migration in response to prey density: What are the consequences? Journal of Mathematical Biology 43(6):561–581.

Hutchinson J. J., and C. N. Trueman. 2006. Stable isotope analyses of collagen in fish scales: limitations set by scale architecture. Journal of Fish Biology 69:1874-1880.

Johnson, M. G. 1989. Metals in Fish Scales Collected in Lake Opeongo, Canada, from 1939 to 1979. Transactions of the American Fisheries Society 118:331–335.

Kenworthy, M. D., J. H. Grabowski, C. A. Layman, G. D. Sherwood, S. P. Powers, C. H. Peterson, R. K. Gittman, D. A. Keller, and F. H. Fodrie. 2018. Movement ecology of a mobile predatory fish reveals limited habitat linkages within a temperate estuarine seascape. Canadian Journal of Fisheries and Aquatic Sciences 75(11):1990-1998.

Kerr, L. A., S. X. Cadrin, and D. H. Secor. 2010. The role of spatial dynamics in the stability, resilience, and productivity of an estuarine fish population. Ecological Applications 20(2):497-507.

Kinsman, D. J. J., and H. D. Holland. 1969. The co-precipitation of cations with CaCO3—IV. The co-precipitation of Sr2+ with aragonite between 16° and 96°C. Geochimica et Cosmochimica Acta 33(1):1–17.

Laberge, F., I. Yin-Liao, and N. J. Bernier. 2019. Temporal profiles of cortisol accumulation and clearance support scale cortisol content as an indicator of chronic stress in fish. Conservation Physiology 7(1):coz052.

Lebreton, B., J. Beseres Pollack, B. Blomberg, T. A. Palmer, L. Adams, G. Guillou, and P. A. Montagna. 2016. Origin, composition and quality of suspended particulate organic matter in relation to freshwater inflow in a South Texas estuary. Estuarine, Coastal and Shelf Science 170:70–82.

Limburg, K. E. 1995. Otolith strontium traces environmental history of subyearling American shad *Alosa sapidissima*. Marine Ecology Progress Series 119:25-35.

Longley, W.L. 1994. Freshwater Inflows to Texas Bays and Estuaries: Ecological Relationships and Methods for Determination of Needs. Texas Water Development Board, Austin, Texas, 386.

Maillet, G. L., and D. M. Checkley, Jr. 1989. Effects of Starvation on the Frequency of Formation and Width of Growth Increments in Sagittae of Laboratory-Reared Atlantic Menhaden Brevoortia tyrannus Larvae. Fishery Bulletin 88(1):155–165.

Maruyama, A., E. Tanahashi, T. Hirayama, and R. Yonekura. 2017. A comparison of changes in stable isotope ratios in the epidermal mucus and muscle tissue of slow-growing adult catfish. Ecology of Freshwater Fish 26(4):636-642.

Matlock, G.C. 1987. The life history of the red drum. Manual of Red Drum Aquaculture 1–47.

McCutchan, J. H., W. M. Lewis, C. Kendall, and C. C. McGrath. 2003. Variation in trophic shift for stable isotope ratios of carbon, nitrogen, and sulfur. Oikos 102(2):378–390.

Mercer, L. P. 1984. A biological and fisheries profile of red drum, *sciaenops ocellatus*. North Carolina Department of Natural Resources and Community Development Division of Marine Fisheries 41.

Michener, R. H., and L. Kaufman. 2007. Stable isotope ratios as tracers in marine food webs: an update. Stable Isotopes in Ecology and Environmental Science 2:238-282.

Mohan, J. A., S. D. Smith, T. L. Connelly, E. T. Attwood, J. W. McClelland, S. Z. Herzka, and B. D. Walther. 2016. Tissue-specific isotope turnover and discrimination factors are affected by diet quality and lipid content in an omnivorous consumer. Journal of Experimental Marine Biology and Ecology 479:35-45.

Mook, W. G., J. C. Bommerson, and W. H. Staverman. 1974. Carbon isotope fractionation between dissolved bicarbonate and gaseous carbon dioxide. Earth and Planetary Science Letters 22(2):169–176.

Mook, W. G., and J. J. De Vries. 2000. Volume I, Introduction: theory methods review. Environmental Isotopes in the Hydrological Cycle—Principles and Applications, International Hydrological Programme (IHP-V), Technical Documents in Hydrology (IAEA/UNESCO) 39:75-76.

Mooney, R. F., and J. W. McClelland. 2012. Watershed Export Events and Ecosystem Responses in the Mission–Aransas National Estuarine Research Reserve, South Texas. Estuaries and Coasts 35(6):1468-1485.

Moulton, D. L., M. A. Dance, J. A. Williams, M. Z. Sluis, G. W. Stunz, and J. R. Rooker. 2017. Habitat Partitioning and Seasonal Movement of Red Drum and Spotted Seatrout. Estuaries and Coasts 40(3):905–916.

Murphy, M. D., and R. G. Taylor. 1986. Reproduction, growth, and mortality of red drum, Sciaenops ocellatus, in Florida. Florida Department of Natural Resources.

Nelson, T. R., and S. P. Powers. 2020. Estimates of Red Drum Mortality via Acoustic Telemetry. Marine and Coastal Fisheries 12(1):78–97.

Nims, M. K., and B. D. Walther. 2014. Contingents of southern flounder from subtropical estuaries revealed by otolith chemistry. Transactions of the American Fisheries Society 143(3): 721-731.

NOAA Fisheries. Essential Fish Habitat Mapper. https://www.fisheries.noaa.gov/resource/map/essential-fish-habitat-mapper. 1/7/2020. Accessed 3/25/20.

Olsson, P.-E., P. Kling, and C. Hogstrand. 1998. Mechanisms of heavy metal accumulation and toxicity in fish. Pages 321–350 *in* W. J. Langston and M. J. Bebianno, editors. Metal Metabolism in Aquatic Environments. Springer US, Boston, MA.

Osburn, H. R., G. C. Matlock, and A. W. Green. 1982. Red drum (sciaenops ocellatus) movement in Texas bays. Contributions in Marine Science 25:85–97.

Overstreet, R. M. 1983. Aspects of the Biology of the Red Drum, Sciaenops ocellatus, in Mississippi. Gulf Research Reports 7.

Pannella, G. 1971. Fish otoliths: daily growth layers and periodic patterns. Science 173: 1124-1127.

Pannella, G. 1974. Otolith growth patterns: an aid in age determination in temperate and tropical fishes. The Ageing of Fish 28-39.

Pattillo, M. E., Czapla, T. E., Nelson, D. M., and Monaco, M. E. 1997. Distribution and abundance of fishes and invertebrates in Gulf of Mexico estuaries, Volume II: Species life history summaries. ELMR Rep. No. 11. NOAA/NOS Strategic Environmental Assessments Division, Silver Springs, MD.

Payan, P., H. De Pontual, G. Bœuf, and N. Mayer-Gostan. 2004. Endolymph chemistry and otolith growth in fish. Comptes Rendus Palevol 3(6-7):535-547.

Pender, P. J., and R. K. Griffin. 1996. Habitat History of Barramundi Lates calcarifer in a North Australian River System Based on Barium and Strontium Levels in Scales. Transactions of the American Fisheries Society (125):679–689.

Perga, M. E., D. Gerdeaux. 2003. Using the $\delta^{13}C$ and $\delta^{15}N$ of whitefish scales for retrospective ecological studies: changes in isotope signatures during the restoration of Lake Geneva, 1980–2001. Journal of Fish Biology 63(5):1197-1207.

Peters, K. M. and R. H. McMichael, Jr. 1987. Early Life History of the Red Drum, *Sciaenops ocellatus* (Pisces: Sciaenidae), in Tampa Bay, Florida. 10(2):92-107.

Peterson, B. J., and B. Fry. 1987. Stable isotopes in ecosystem studies. Annual Review of Ecology and Systematics 18(1):293-320.

Post, D. M. 2002. Using Stable Isotopes to Estimate Trophic Position: Models, Methods, and Assumptions. Ecology 83(3):703–718.

Potter, I. C., J. R. Tweedley, M. Elliott, and A. K. Whitfield. 2015. The ways in which fish use estuaries: a refinement and expansion of the guild approach. Fish and Fisheries 16(2):230–239.

Pruell, R. J., B. K. Taplin, and K. Cicchelli. 2003. Stable isotope ratios in archived striped bass scales suggest changes in trophic structure. Fisheries Management and Ecology 10(5):329–336.

Pulich, W., Dunton, K.H., Roberts, L.R., Calnan, T., Lester, J., and McKinney, L.D. 1998. Seagrass conservation plan for Texas. Texas Parks and Wildlife Department. Austin, Texas. 79.

Qian, Y., M. C. Kennicutt II, J. Svalberg, S. A. Macko, R. R. Bidigare, and J. Walker, 1996. Suspended particulate organic matter (SPOM) in Gulf of Mexico estuaries: compound specific isotope analysis and plant pigment compositions. Organic Geochemistry 24(8-9): 875-888.

Quinn, T. P., and K. W. Myers. 2004. Anadromy and the marine migrations of Pacific salmon and trout: Rounsefell revisited. Reviews in Fish Biology and Fisheries 14(4):421–442.

Ramsay, A. L., N. J. Milner, R. N. Hughes, and I. D. McCarthy. 2012. Fish scale δ15N and δ13C values provide biogeochemical tags of fish comparable in performance to element concentrations in scales and otoliths. Hydrobiologia 694(1):183–196.

Rezek, R. J., B. Lebreton, E. B. Roark, T. A. Palmer, and J. B. Pollack. 2017. How does a restored oyster reef develop? An assessment based on stable isotopes and community metrics. Marine Biology 164(3):54.

Riera, P., P. Montagna, R. Kalke, and P. Richard. 2000. Utilization of estuarine organic matter during growth and migration by juvenile brown shrimp Penaeus aztecus in a South Texas estuary. Marine Ecology Progress Series 199:205–216.

Rooker, J. R., G. W. Stunz, S. A. Holt, and T. J. Minello. 2010. Population connectivity of red drum in the northern Gulf of Mexico. Marine Ecology Progress Series 407: 187-196.

Rooker, J. R., S. A. Holt, G. J. Holt, L. A. Fuiman. 1999. Spatial and temporal variability in growth, mortality, and recruitment potential of post settlement red drum, *Sciaenops ocellatus*, in a subtropical estuary. Fishery Bulletin 97(3):581-590.

Satterfield IV, F. R., B. P. Finney. 2002. Stable isotope analysis of Pacific salmon: insight into trophic status and oceanographic conditions over the last 30 years. Progress in Oceanography 53(2-4):231-246.

Scharf, F. S., and K. K. Schlicht. 2000. Feeding Habits of Red Drum (Sciaenops ocellatus) in Galveston Bay, Texas: Seasonal Diet Variation and Predator-Prey Size Relationships. Estuaries 23(1):128.

Secor, D. H. 1992. Application of otolith microchemistry analysis to investigate anadromy in Chesapeake Bay striped bass Morone saxatilis. Fishery Bulletin 90:798–806.

Secor, D. H. 1999. Specifying divergent migrations in the concept of stock: the contingent hypothesis. Fisheries Research 43(1-3):13-34.

Secor, D. H., and J. R. Rooker. 2005. Connectivity in the life histories of fishes that use estuaries. Estuarine, Coastal and Shelf Science 64(1):1–3.

Secor, D. H., and P. M. Piccoli. 2007. Oceanic migration rates of upper Chesapeake Bay striped bass (Morone saxatilis), determined by otolith microchemical analysis. Fishery Bulletin 105(1):62-73.

Seeley, M. E, and B. D. Walther. 2018 Facultative oligohaline habitat use in a mobile fish inferred from scale chemistry. Marine Ecology Progress Series 598:233-245.

Seeley, M. E., W. K. Logan, and B. D. Walther. 2017. Consistency of elemental and isotope-ratio patterns across multiple scales from individual fish: consistent chemical patterns in scales. Journal of Fish Biology 91(3):928–946.

Seeley, M., N. Miller, and B. Walther. 2015. High resolution profiles of elements in Atlantic tarpon (Megalops atlanticus) scales obtained via cross-sectioning and laser ablation ICP-MS: a literature survey and novel approach for scale analyses. Environmental Biology of Fishes 98(11):2223–2238.

Shaw, T. J., W. S. Moore, J. Kloepfer, and M. A. Sochaski. 1998. The flux of barium to the coastal waters of the southeastern USA: the importance of submarine groundwater discharge. Geochimica et Cosmochimica Acta 62(18):3047-3054.

Simms, A. R., J. B. Anderson, A. B. Rodriguez, and M. Taviani. 2008. Mechanisms controlling environmental change within an estuary: Corpus Christi Bay, Texas, USA. Pages 121–146 Special Paper 443: Response of Upper Gulf Coast Estuaries to Holocene Climate Change and Sea-Level Rise. Geological Society of America.

Stevens, P. W., M. F. D. Greenwood, and D. A. Blewett. 2013. Fish Assemblages in the Oligohaline Stretch of a Southwest Florida River during Periods of Extreme Freshwater Inflow Variation. Transactions of the American Fisheries Society 142(6):1644–1658.

Stewart, C. B., and F. S. Scharf. 2008. Estuarine Recruitment, Growth, and First-Year Survival of Juvenile Red Drum in North Carolina. Transactions of the American Fisheries Society 137(4):1089–1103.

Stunz, G. W, T. J. Minello, P. S. Levin. 2002. A comparison of early juvenile red drum densities among various habitat types in Galveston Bay, Texas. Estuaries 25(1):76-85.

Suzuki, K. W., A. Kasai, K. Nakayama, and M. Tanaka. 2005. Differential isotopic enrichment and half-life among tissues in Japanese temperate bass (*Lateolabrax japonicus*) juveniles: implications for analyzing migration. Canadian Journal of Fisheries and Aquatic Sciences 62(3):671-678.

Texas Parks and Wildlife Department. Fish Stocking Reports. https://tpwd.texas.gov/fishboat/fish/management/stocking/fishstock_water.phtml. (Accessed 3/25/2020)

Thorrold, S. R., C. M. Jones, and S. E. Campana. 1997. Response of otolith microchemistry to environmental variations experienced by larval and juvenile Atlantic croaker (Micropogonias undulatus). Limnology and Oceanography 42(1):102–111.

Thorstad, E. B., F. Whoriskey, A. H. Rikardsen, and K. Aarestrup. 2010. Aquatic Nomads: The Life and Migrations of the Atlantic Salmon. Pages 1–32 *in* Ø. Aas, S. Einum, A. Klemetsen, and J. Skurdal, editors. Atlantic Salmon Ecology. Wiley-Blackwell, Oxford, UK.

Tieszen, L. L., T. W. Boutton, K. G. Tesdahl, and N. A. Slade. 1983. Fractionation and turnover of stable carbon isotopes in animal tissues: Implications for ?13C analysis of diet. Oecologia 57(1–2):32–37.

Torrance, L. E. 2018. The importance of low salinity habitat to red drum (Sciaenops occelatus). Master's thesis. Texas A&M University – Corpus Christi, Corpus Christi, Texas.

Trueman, C. N., R. A. McGill, and P. H. Guyard. 2005. The effect of growth rate on tissue-diet isotopic spacing in rapidly growing animals. An experimental study with Atlantic salmon (*Salmo salar*). Rapid Communications in Mass Spectrometry 19(22):3239-3247.

Tykot R. H. 2004. Stable isotopes and diet: You are what you eat. Proceedings of the International School of Physics "Enrico Fermi"; 154:433–444.

Tzadik, O. E., J. S. Curtis, J. E. Granneman, B. N. Kurth, T. J. Pusack, A. A. Wallace, D. J. Hollander, E. B. Peebles, and C. D. Stallings. 2017. Chemical archives in fishes beyond otoliths: A review on the use of other body parts as chronological recorders of microchemical constituents for expanding interpretations of environmental, ecological, and life-history changes: Chemical archives in fishes beyond otoliths. Limnology and Oceanography: Methods 15(3):238–263.

Vander Zanden, M. J., M. K. Clayton, E. K. Moody, C. T. Solomon, and B. C. Weidel. 2015. Stable Isotope Turnover and Half-Life in Animal Tissues: A Literature Synthesis. PLOS ONE 10(1):e0116182.

Vanderklift, M. A., and S. Ponsard. 2003. Sources of variation in consumer-diet ?15N enrichment: a meta-analysis. Oecologia 136(2):169–182.

Vega, R., Neill, W., Gold, J., and Ray, M. 2011. Enhancement of Texas sciaenids (red drum and spotted seatrout). Interactions of Fisheries and Fishing Communities Related to Aquaculture. Proc. 38th U.S. - Japan Aquaculture Panel Symposium. 85–92.

Walther, B. D., and K. E. Limburg. 2012. The use of otolith chemistry to characterize diadromous migrations. Journal of Fish Biology 81(2):796-825.

Walther, B. D., and M. Nims. 2015. Spatiotemporal Variation of Trace Elements and Stable Isotopes in Subtropical Estuaries: I. Freshwater Endmembers and Mixing Curves. Estuaries and Coasts 38:754-768.

Watson, C. J., M. N. Nordi, A. J. Esbaugh. 2014. Osmoregulation and branchial plasticity after acute freshwater transfer in red drum, *Sciaenops ocellatus.* Comparative Biochemistry and Physiology Part A: Molecular & Integrative Physiology 178:82-89.

Wells B. K., G. E. Bath, S. R. Thorrold, C. M. Jones. 2000. Incorporation of strontium, cadmium, and barium in juvenile spot (Leiostomus xanthurus) scales reflects water chemistry. Canadian Journal of Fisheries and Aquatic Sciences 57:2122–2129.

Wells, B., B. Rieman, J. Clayton, D. Horan, and C. Jones. 2003. Relationships between Water, Otolith, and Scale Chemistries of Westslope Cutthroat Trout from the Coeur d'Alene River, Idaho: The Potential Application of Hard-Part Chemistry to Describe Movements in Freshwater. Transactions of The American Fisheries Society – Transactions of the American Fisheries Society 132:409–424.

Wenner, C. A. 1992. Red drum : natural history and fishing techniques in South Carolina. South Carolina State Library.

West, J. B., editor. 2010. Isoscapes: understanding movement, pattern, and process on earth through isotope mapping. Springer, Dordrecht ; New York.

Whitfield, A. K. 1999. Ichthyofaunal assemblages in estuaries: A South African case study. Reviews in Fish Biology and Fisheries 9(2):151–186.

Wilson, C. A., and Nieland, D. L. 1994. Reproductive biology of red drum, *Sciaenops ocellatus*, from the neritic waters of the northern Gulf of Mexico. Fishery Bulletin, 92:841-850.

Woodcock, S. H., and B. D. Walther. 2014. Trace elements and stable isotopes in Atlantic tarpon scales reveal movement across estuarine gradients. Fisheries Research 153:9-17.

Woodcock, S. H., C. A. Grieshaber, and B. D. Walther. 2013. Dietary transfer of enriched stable isotopes to mark otoliths, fin rays, and scales. Canadian Journal of Fisheries and Aquatic Sciences 70(1):1–4.

Yokel, B. J. 1966. A contribution to the biology and distribution of the red drum, Sciaenops ocellatus. M.S. Thesis, University of Miami, Coral Gables. 160.

Zylberberg, L., and G. Nicolas. 1982. Ultrastructure of scales in a teleost (Carassius auratus L.) after use of rapid freeze-fixation and freeze-substitution. Cell and Tissue Research 223:349–367.

Zylberberg, L., J. Bereiter-Hahn, and J.-Y. Sire. 1988. Cytoskeletal organization and collagen orientation in the fish scales. Cell and Tissue Research 253:597–607.

Zylberberg, L. 2004. New data on bone matrix and its proteins. Comptes Rendus Palevol 3(6–7):591–604.

LIST OF FIGURES

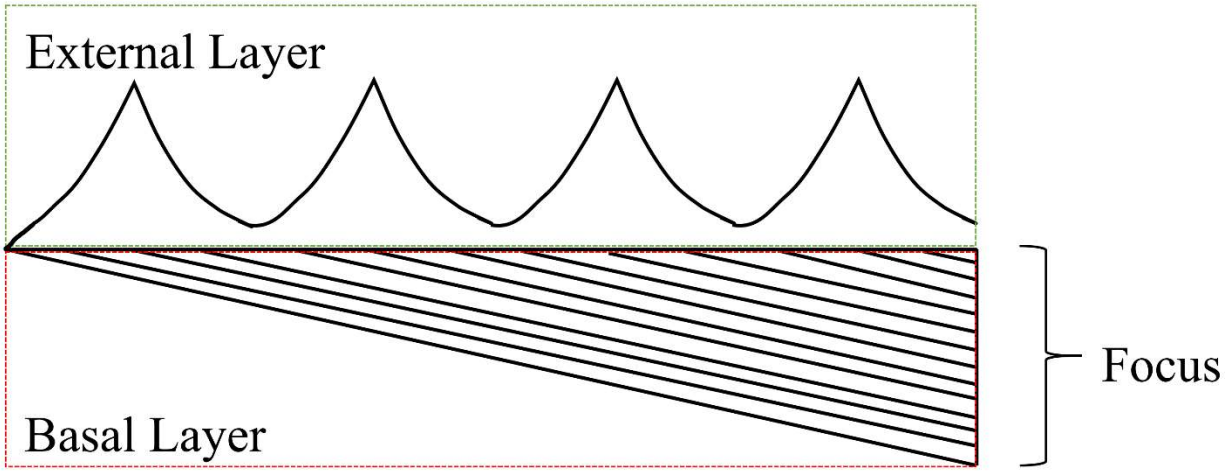

Figure 1. Architecture of a typical fish scale depicted in cross section. The external layer is comprised of the hardened calcium phosphate, hydroxyapatite. The basal layer is made up of subsequent layers of collagen that grow from the growing edge of the scale to the focus.

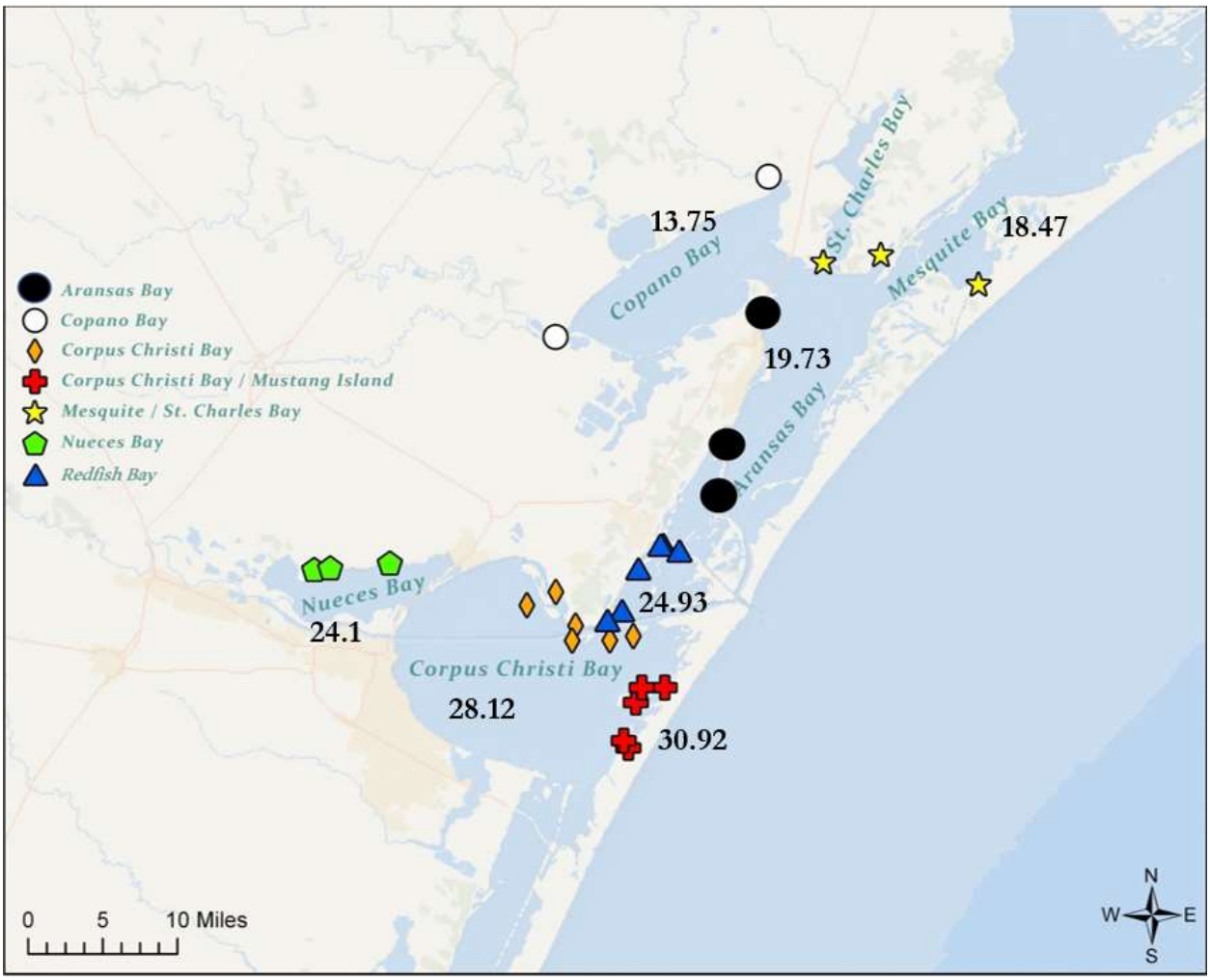

Figure 2. Sites of capture for Red Drum specimens caught during Texas Parks and Wildlife annual sampling in the Nueces and Mission-Aransas estuaries, Texas, USA. The values in black are the average salinities of each bay, taken at the time of specimen capture. Aransas Bay = Black Circle, Copano Bay = White Circle, Corpus Christi Bay = Orange Diamond, Corpus Christi Bay Mustang Island = Red Cross, St. Charles/Mesquite Bay = Yellow Star, Nueces Bay = Green Pentagon, Redfish Bay – Blue Triangle.

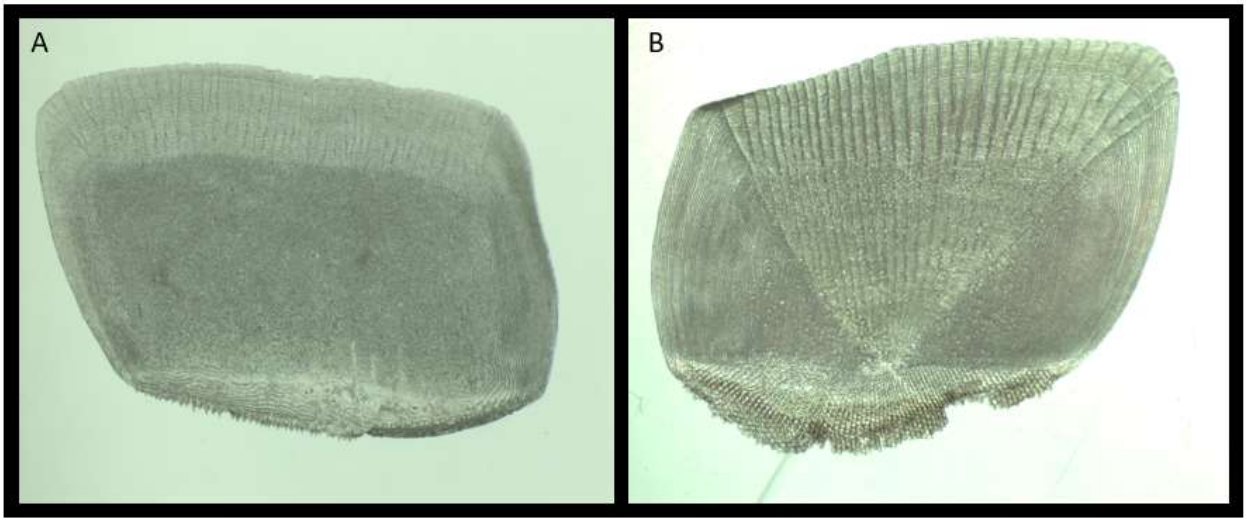

Figure 3A. Photograph of a Red Drum scale exhibiting extensive regeneration, characterized by the lack of concentric growth in the interior of the scale.
B. Photograph of a non-regenerated Red Drum scale, exhibiting concentric growth from the focus of the scale outwards.

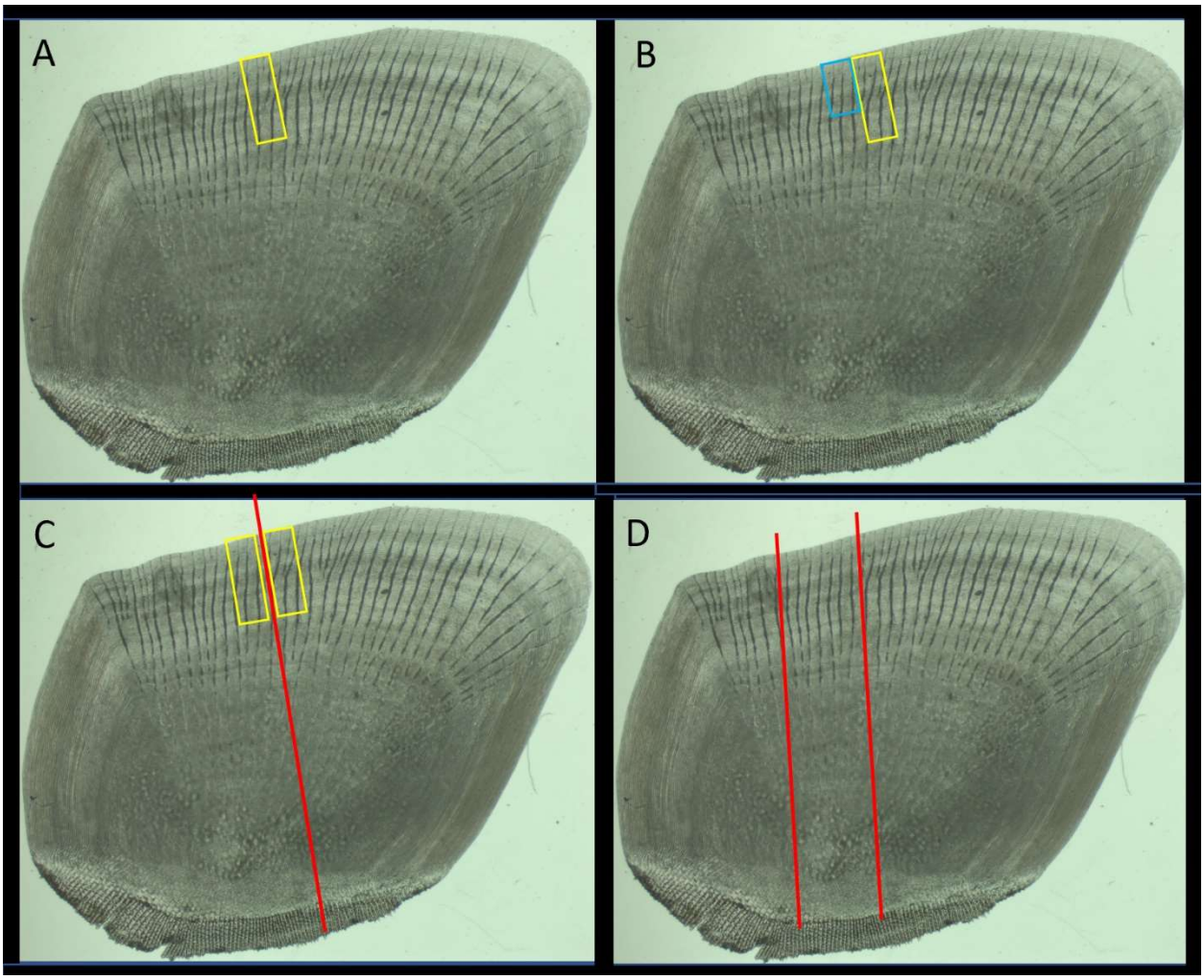

Figure 4. Scale cutting methods employed for stable isotope analyses.
A. The portion of the scale photograph heighted in yellow was the typical portion of a scale removed for primary stable isotope analysis.
B. When examining the differing signatures of large and small scales, the scale section heighted in green is indicative of the typical small portion examined, while the yellow portion like in primary analysis was cut to be indicative of a larger scale section.
C. In decalcification trials, scales were cut into two halves and a section of each scale half was removed for analysis.
D. For laser ablation analysis, a central transect of the scale was cut from focus to scale edge, shown between the red lines.

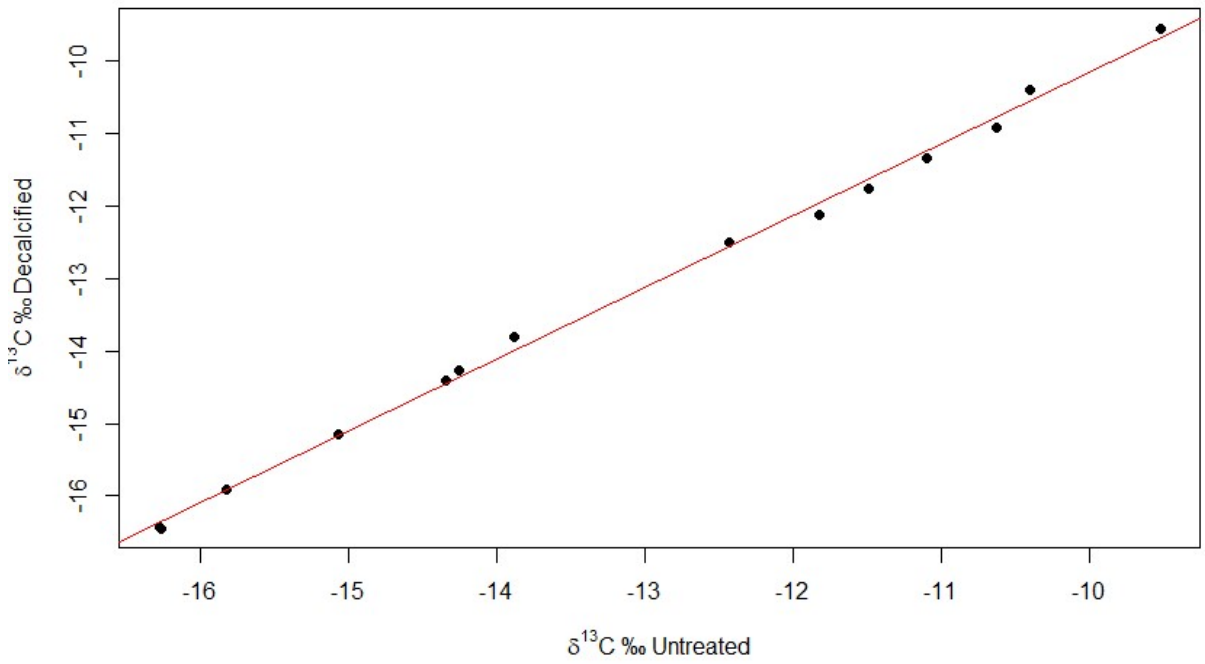

Figure 5. Regression of $\delta^{13}C$ scale values against $\delta^{13}C$ scale values from decalcified scales from the same individual. Regression line equation: $y = 0.99x - 0.24$ with an adjusted R^2 value of 0.99. $p < 0.0001$. $n = 14$.

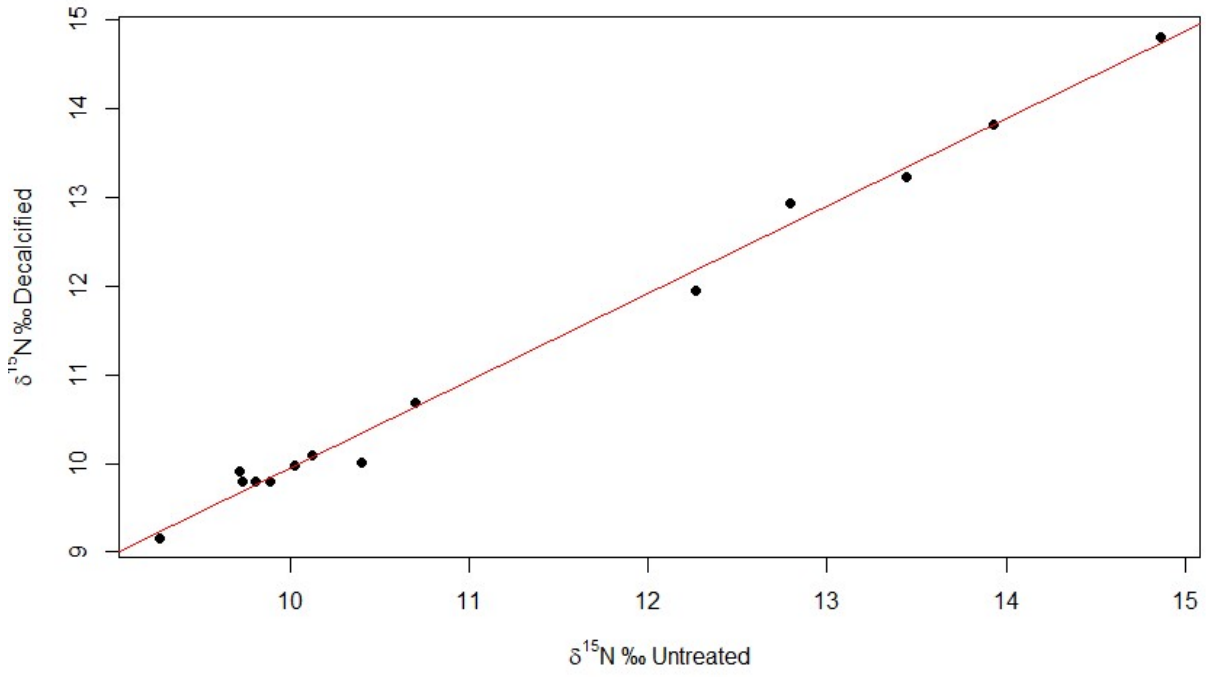

Figure 6. Regression of δ^{15}N scale values against δ^{15}N scale values from decalcified scales from the same individual. Regression line equation: $y = 0.98x + 0.10$ with an adjusted R^2 value of 0.99. $p < 0.0001$. $n = 14$.

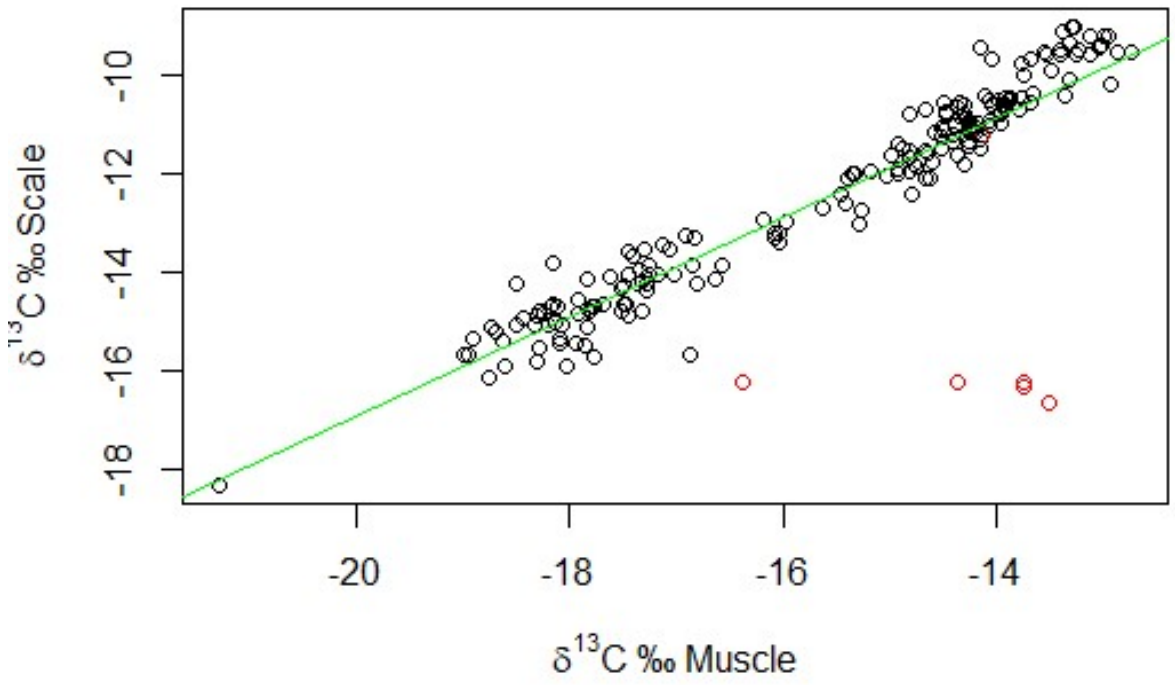

Figure 7. Regression of $\delta^{13}C$ scale values against $\delta^{13}C$ muscle values from the same individual. Red points are from individuals with large size class scales. Regression line equation (n = 191): y=1.01x + 3.31 with an adjusted R^2 value of 0.79. With large scales omitted from calculations (n = 185), the regression line equation is y = 1.07x + 4.38 with an adjusted R^2 value of 0.95. $p < 0.00001$ in both regressions.

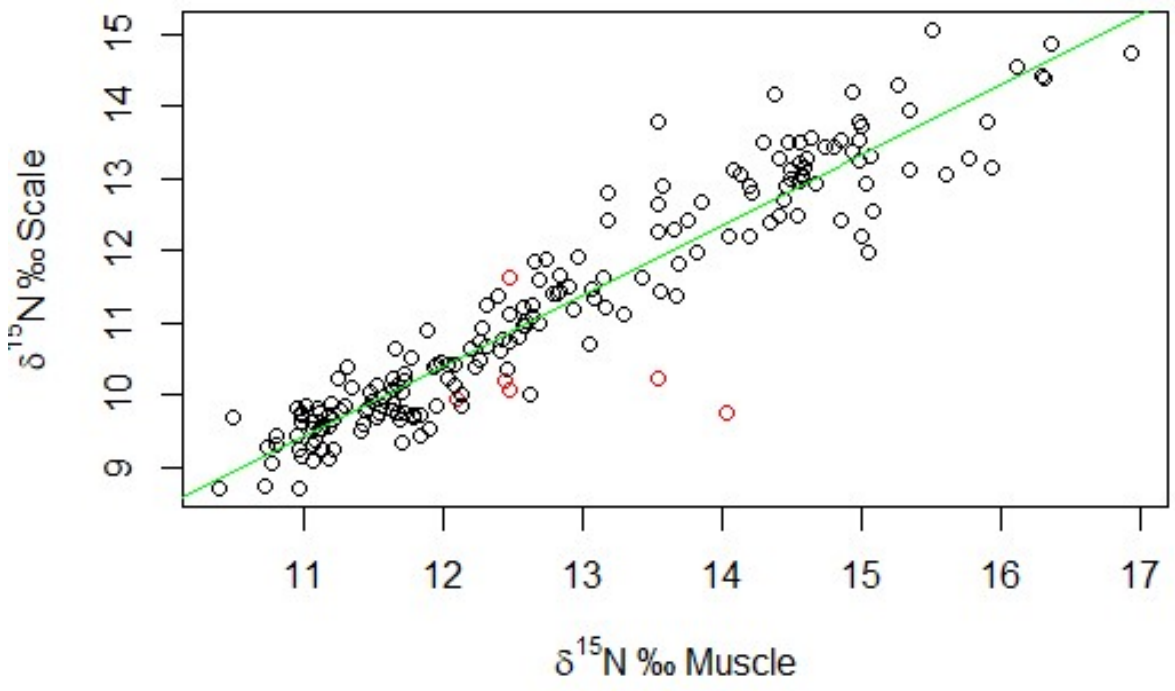

Figure 8. Regression of $\delta^{15}N$ scale values against $\delta^{15}N$ muscle values from the same individual. Red points are from individuals with large size class scales. Regression line equation (n = 191): y= 0.97x - 1.29 with an adjusted R^2 value of 0.89. With large size class scales omitted from calculations (n =185), the regression line equation is y = 0.98x - 1.36 with an adjusted R^2 value of 0.91. $p < 0.00001$ in both regressions.

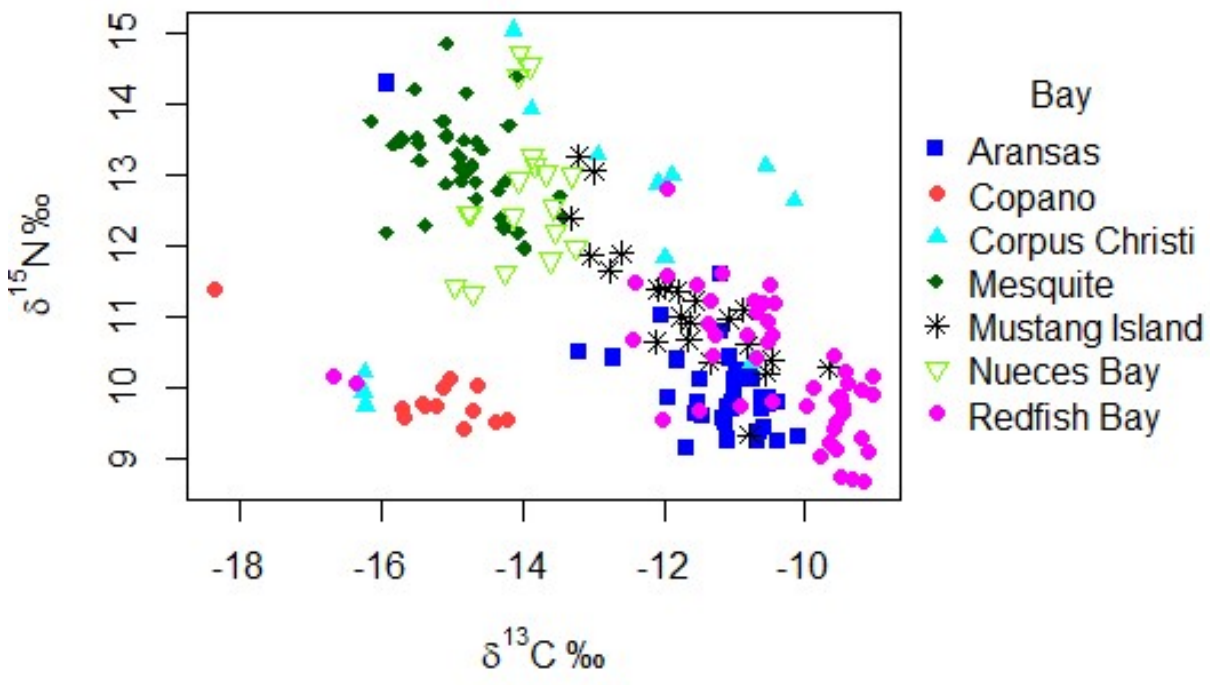

Figure 9. Biplot of $\delta^{13}C$ and $\delta^{15}N$ values of Red Drum scale portions delineated by bay of capture. *n* = 191.

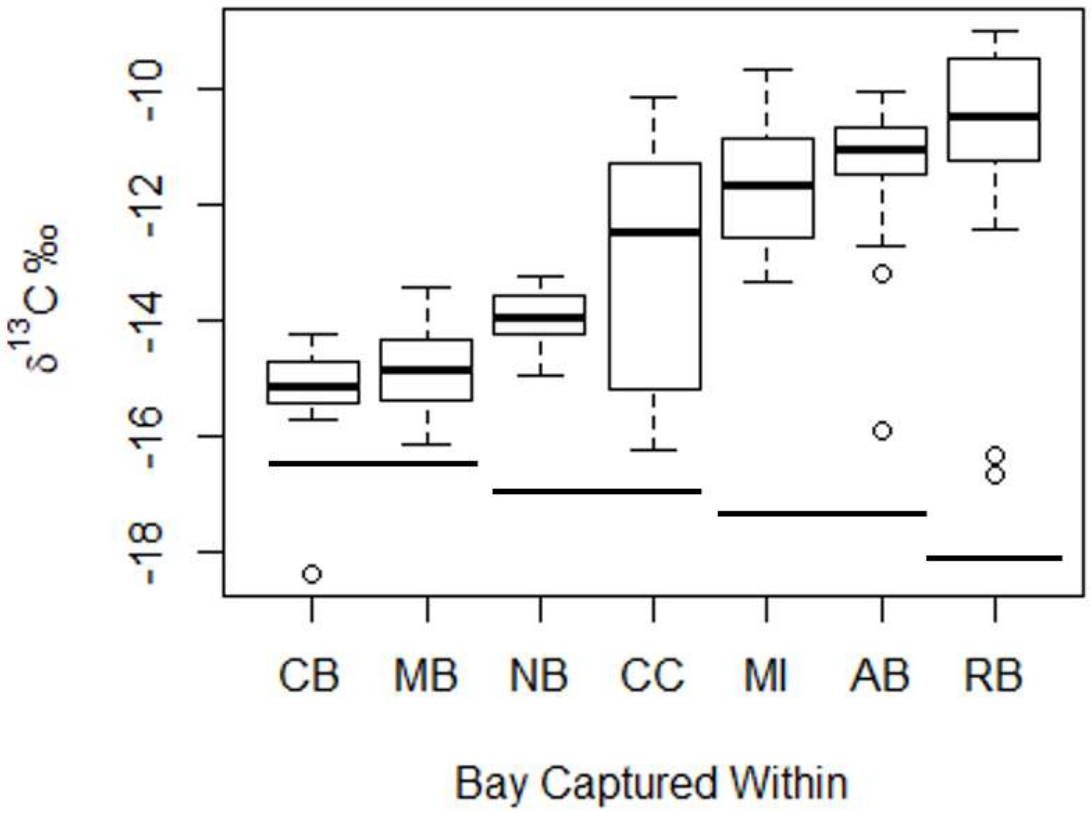

Figure 10. Boxplot of $\delta^{13}C$ values of Red Drum scale portions delineated by bay of capture. Bays sampled were CB - Copano Bay (n = 13), MB - Mesquite/St. Charles Bay (n = 38), NB - Nueces Bay (n = 18), CC - Corpus Christi Bay (n = 12), MI - Corpus Christi Bay – Mustang Island (n = 22), AB - Aransas Bay (n = 38), and RB - Redfish Bay (n = 50). Bays connected with lines are not significantly different.

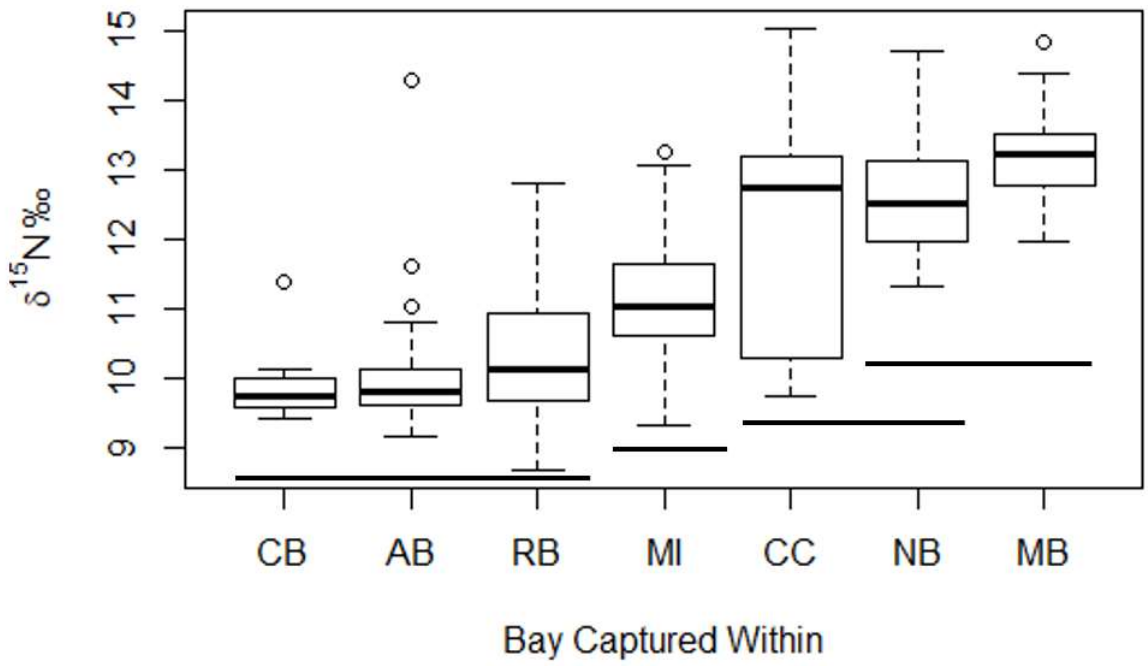

Figure 11. Boxplot of $\delta^{15}N$ values of Red Drum scale portions delineated by bay of capture. Bays sampled were CB - Copano Bay (n = 13), AB - Aransas Bay (n = 38), RB - Redfish Bay (n = 50), MI - Corpus Christi Bay – Mustang Island (n = 22), CC - Corpus Christi Bay (n = 12), NB - Nueces Bay (n = 18), and MB - Mesquite/St. Charles Bay (n = 38). Bays connected with lines are not significantly different.

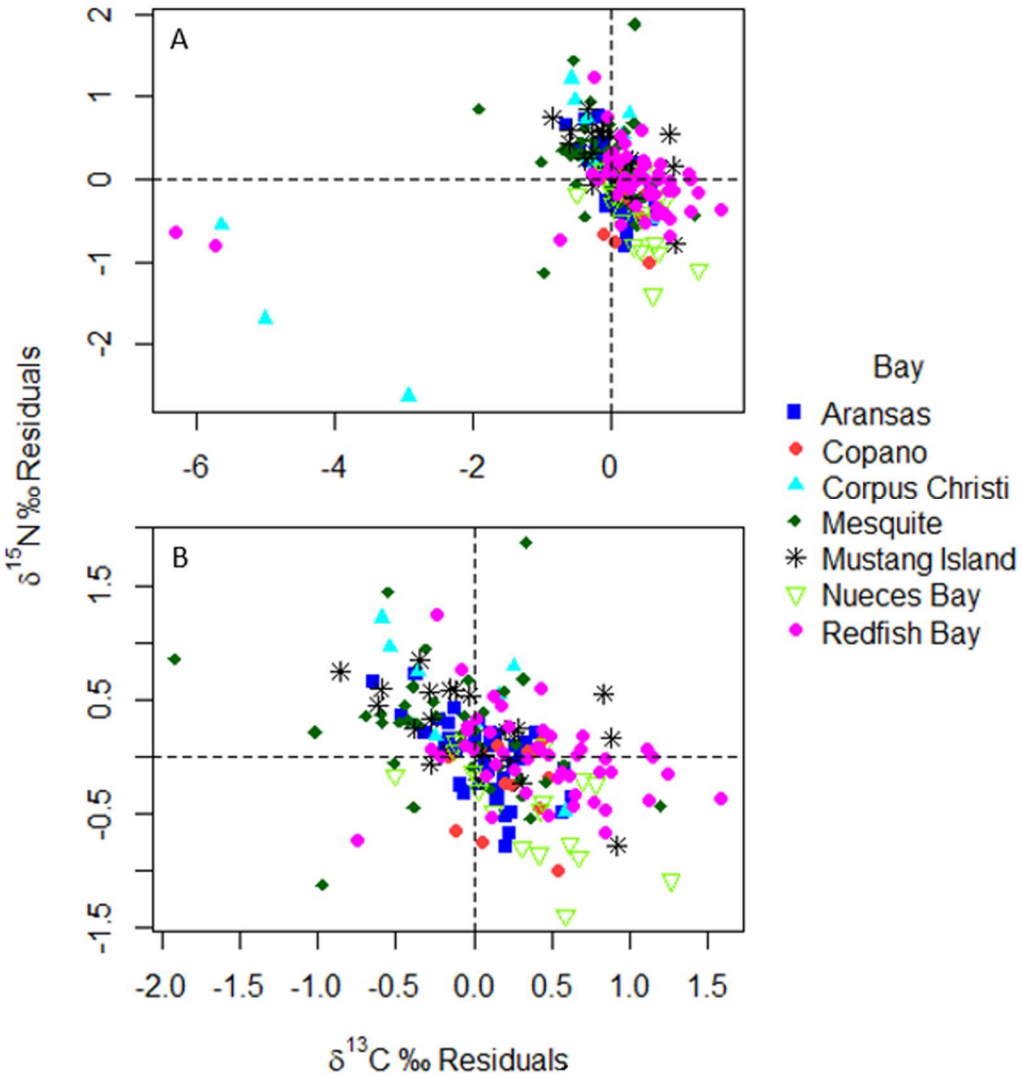

Figure 12. Biplots of scale $\delta^{13}C$ and $\delta^{15}N$ residuals of Red Drum scale portions (n = 191). Figure B has values from large size class scales omitted (n = 185).

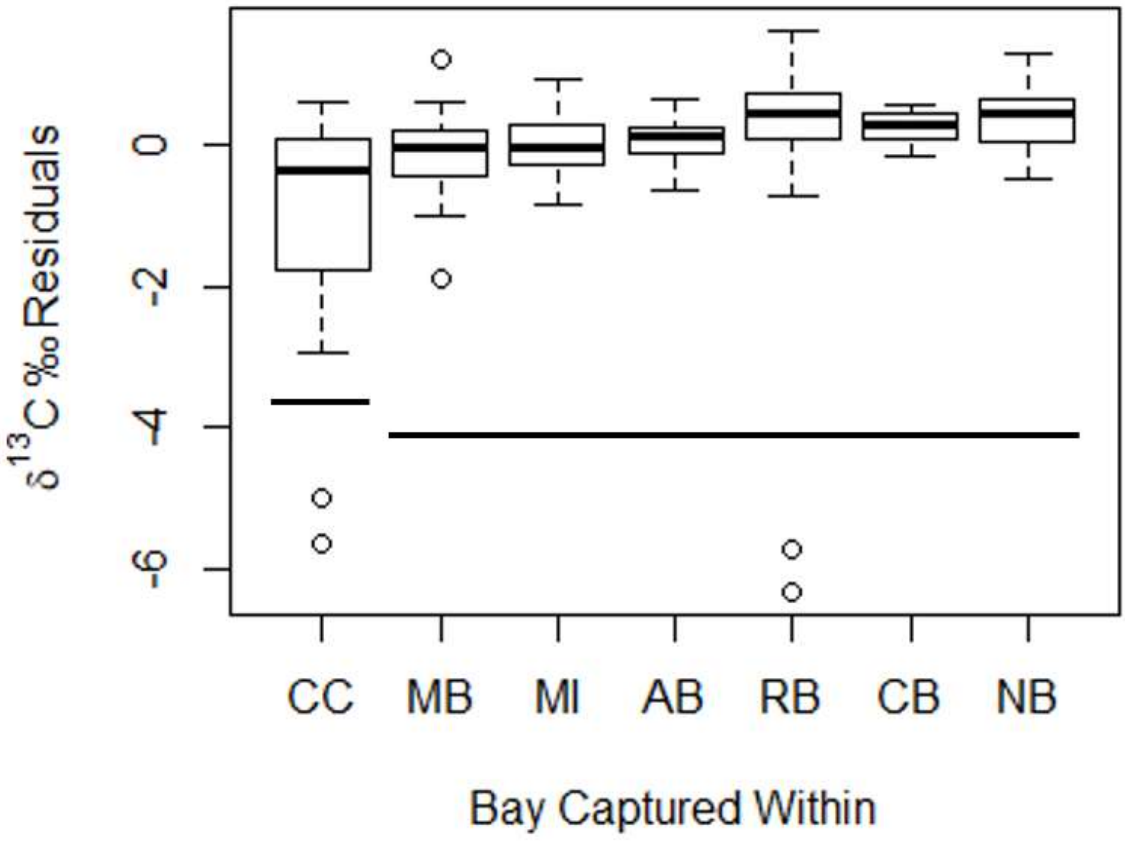

Figure 13. Boxplot of $\delta^{13}C$ residual values of Red Drum scale portions delineated by bay of capture. Bays sampled were CC - Corpus Christi Bay (*n* = 12), MB - Mesquite/St. Charles Bay (*n* = 38), MI - Corpus Christi Bay – Mustang Island (*n* = 22), AB - Aransas Bay (*n* = 38), RB - Redfish Bay (*n* = 50), CB - Copano Bay (*n* = 13), and NB - Nueces Bay (*n* = 18). Bays connected with lines are not significantly different.

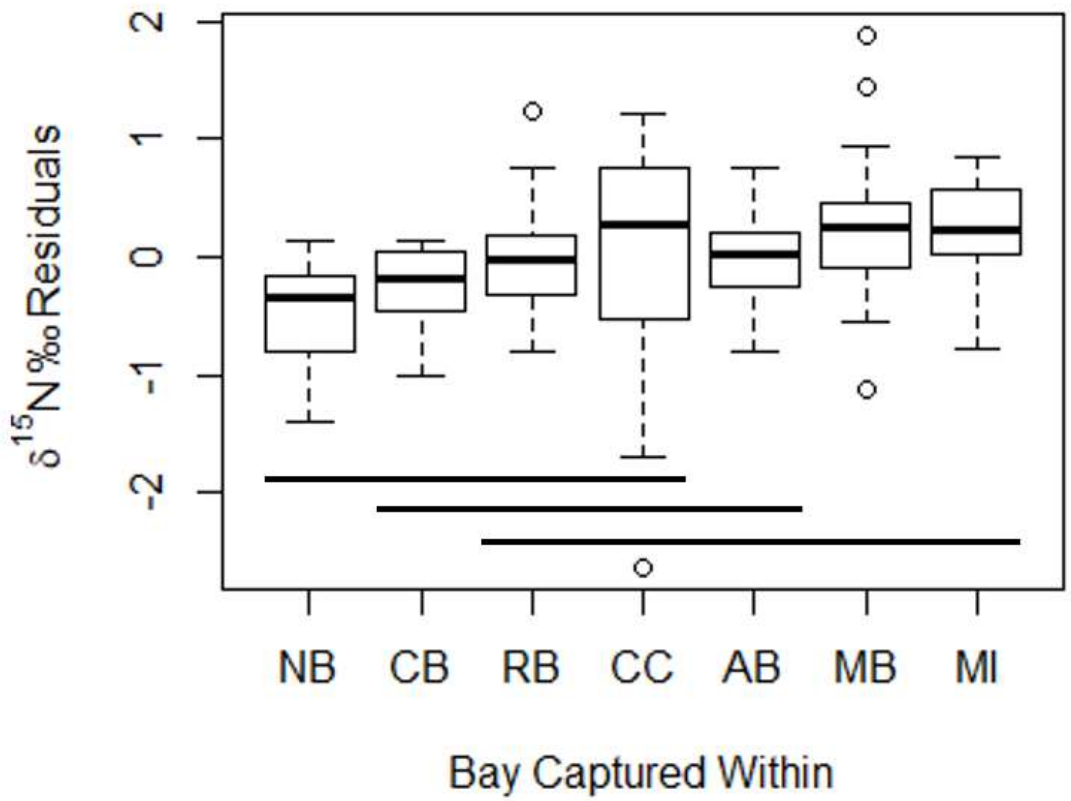

Figure 14. Boxplot of $\delta^{15}N$ residual values of Red Drum scale portions delineated by bay of capture. Bays sampled were NB - Nueces Bay (*n* = 18), CB - Copano Bay (*n* = 13), RB - Redfish Bay (*n* = 50), CC - Corpus Christi Bay (*n* = 12), AB - Aransas Bay (*n* = 38), MB - Mesquite/St. Charles Bay (*n* = 38), and MI - Corpus Christi Bay – Mustang Island (*n* = 22). Bays connected with lines are not significantly different.

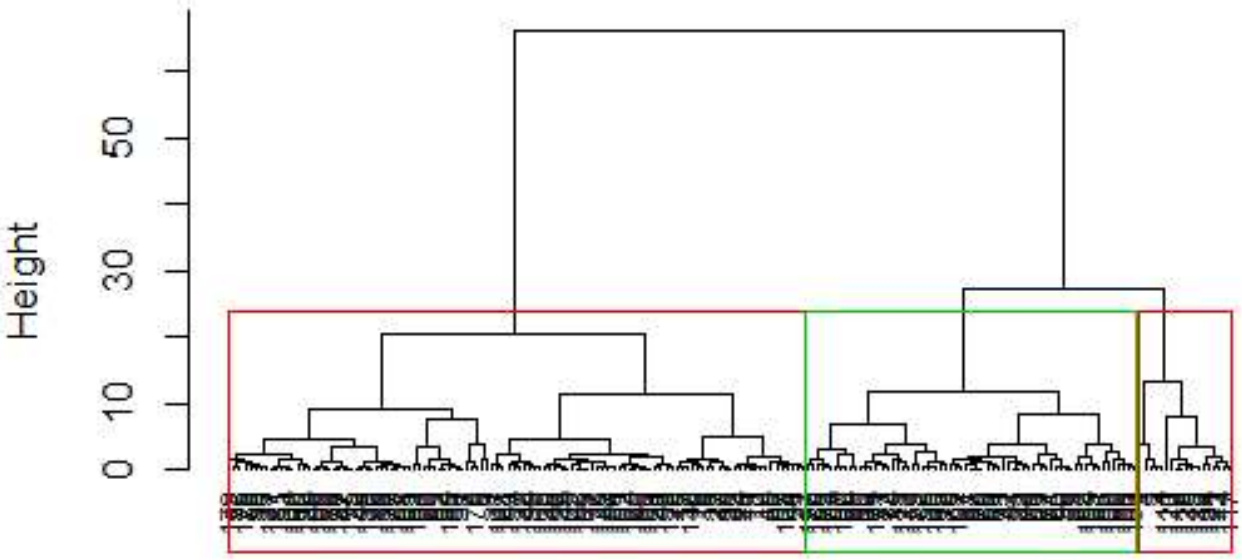

Figure 15. Cluster dendrogram generated using Ward's hierarchical clustering analysis of $\delta^{13}C$ and $\delta^{15}N$ stable isotope values from all sampled scales (n = 191). Three clusters were delineated.

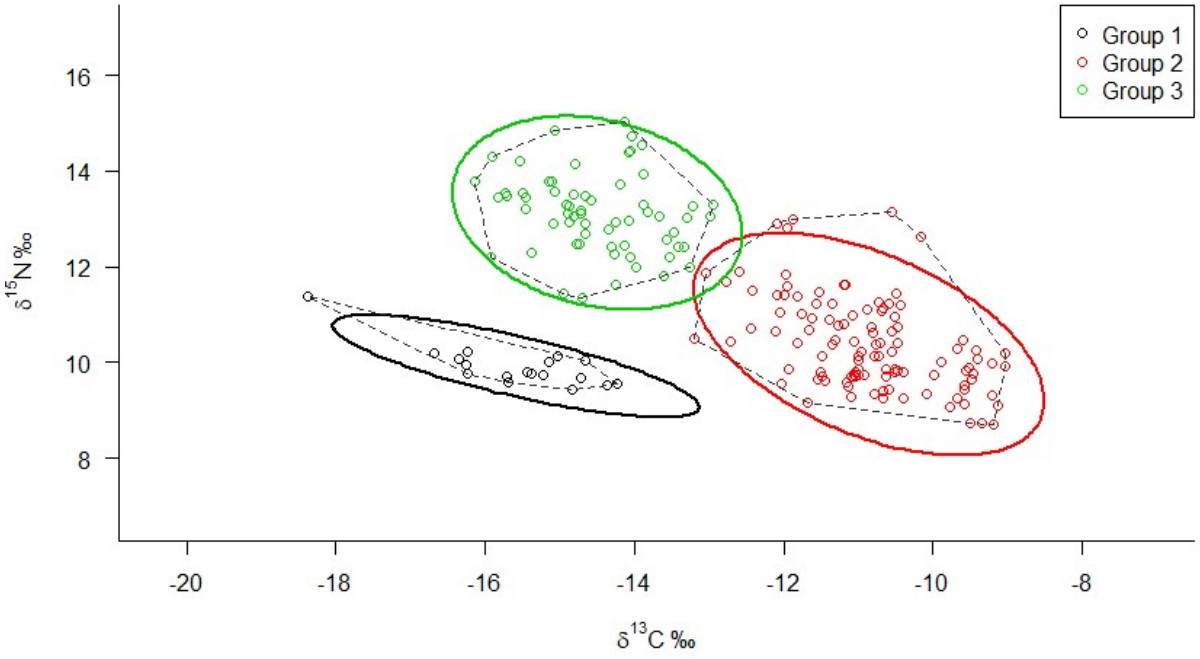

Figure 16. SIBER biplot of the clusters determined by Ward's hierarchical clustering analysis of $\delta^{13}C$ and $\delta^{15}N$ stable isotope values from all sampled scales (n= 191). Convex hull total area and standard ellipse area are shown. Three clusters were delineated, group 1 (*n* = 18), group 2 (*n* = 110), and group 3 (*n* = 63).

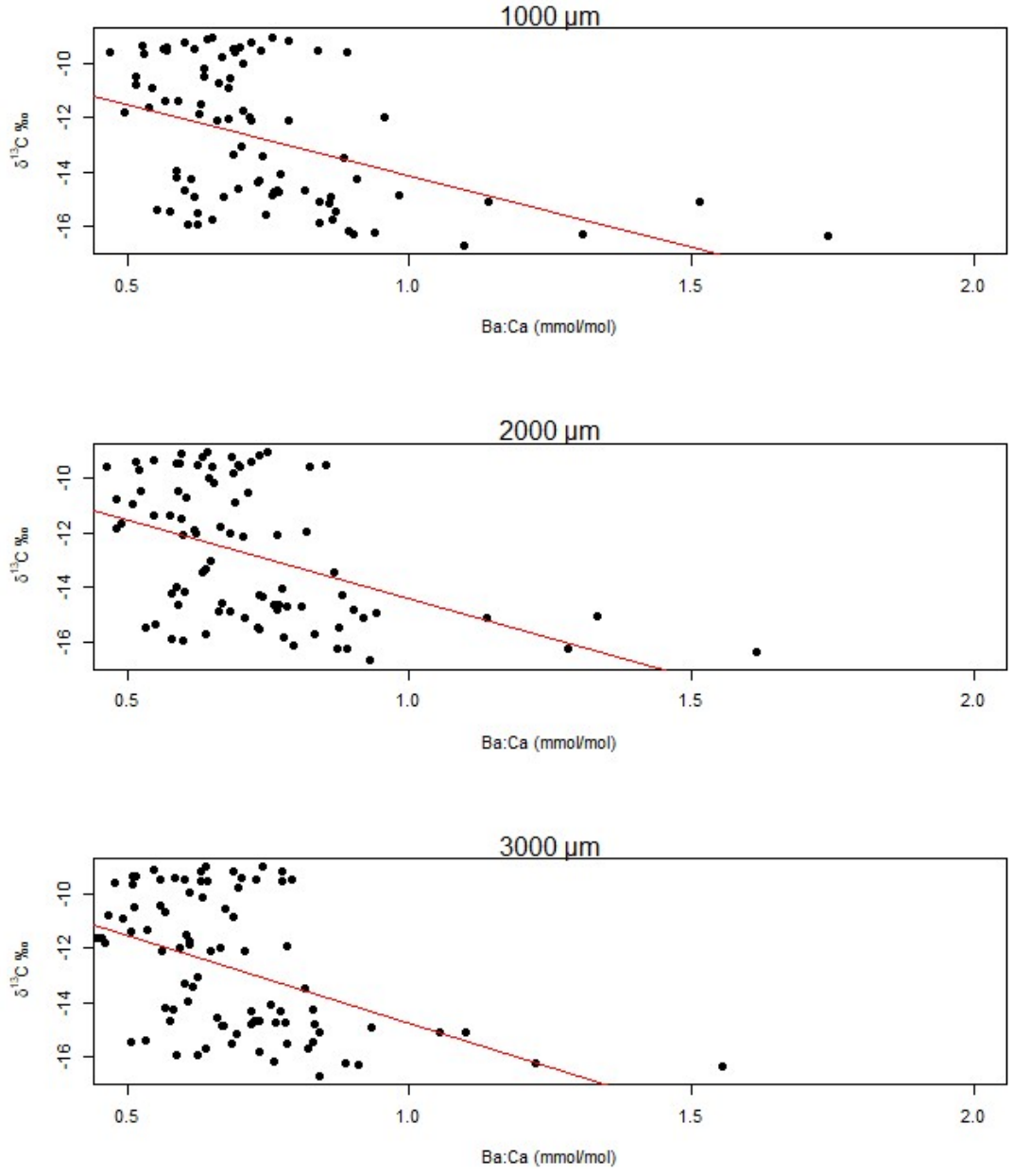

Figure 17. $\delta^{13}C$ values from Red Drum scales correlated against Ba:Ca ratios of averaged sections of exterior scale growth. For all correlations, $p < 0.0001$. Adjusted R-squared values: 1000 µm = 0.20; 2000 µm = 0.20; 3000 µm = 0.22.

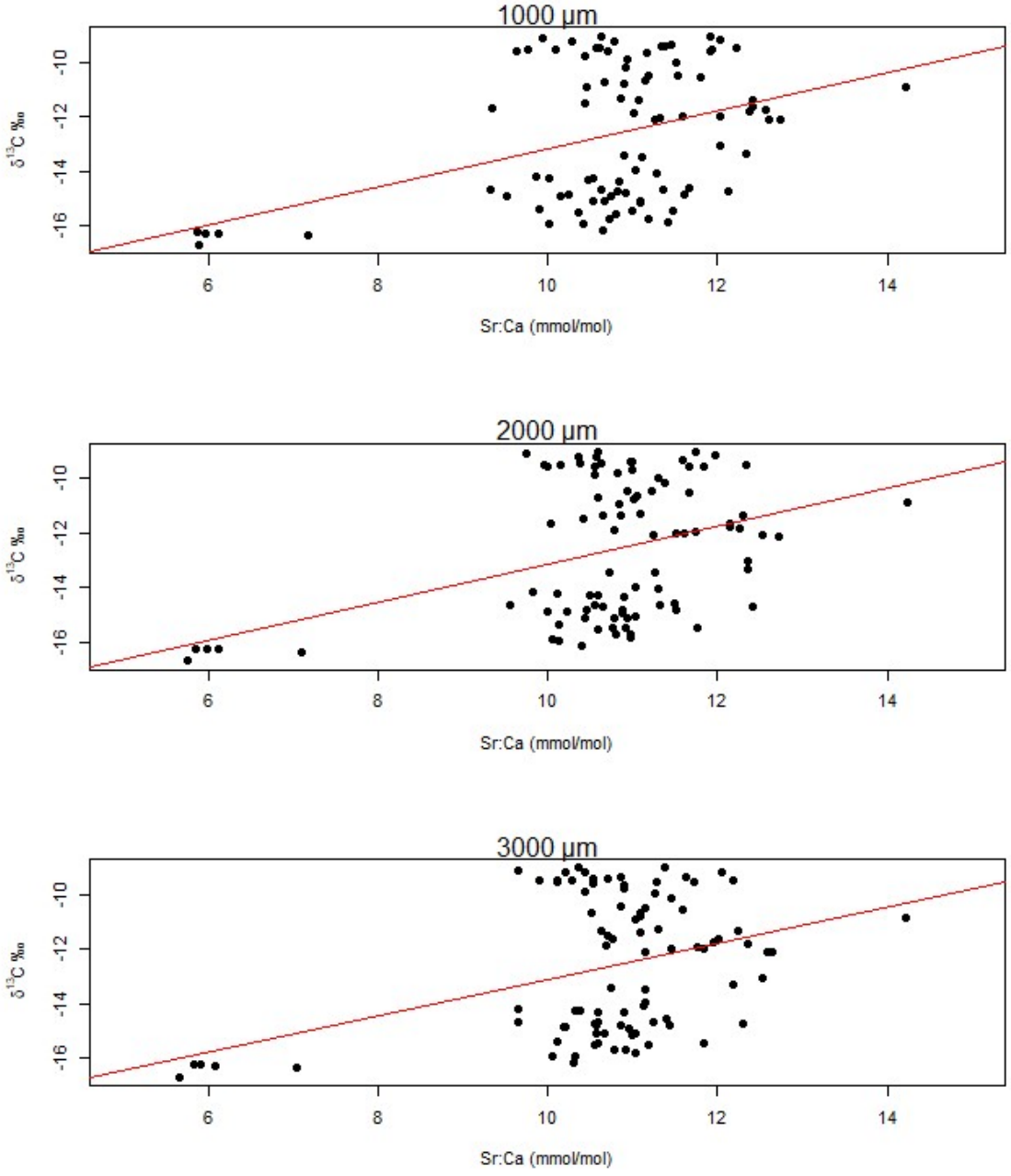

Figure 18. $\delta^{13}C$ values from Red Drum scales correlated against Sr:Ca ratios of averaged sections of exterior scale growth. For all correlations, $p < 0.001$. Adjusted R-squared values: 1000 µm = 0.15; 2000 µm = 0.14; 3000 µm = 0.13.

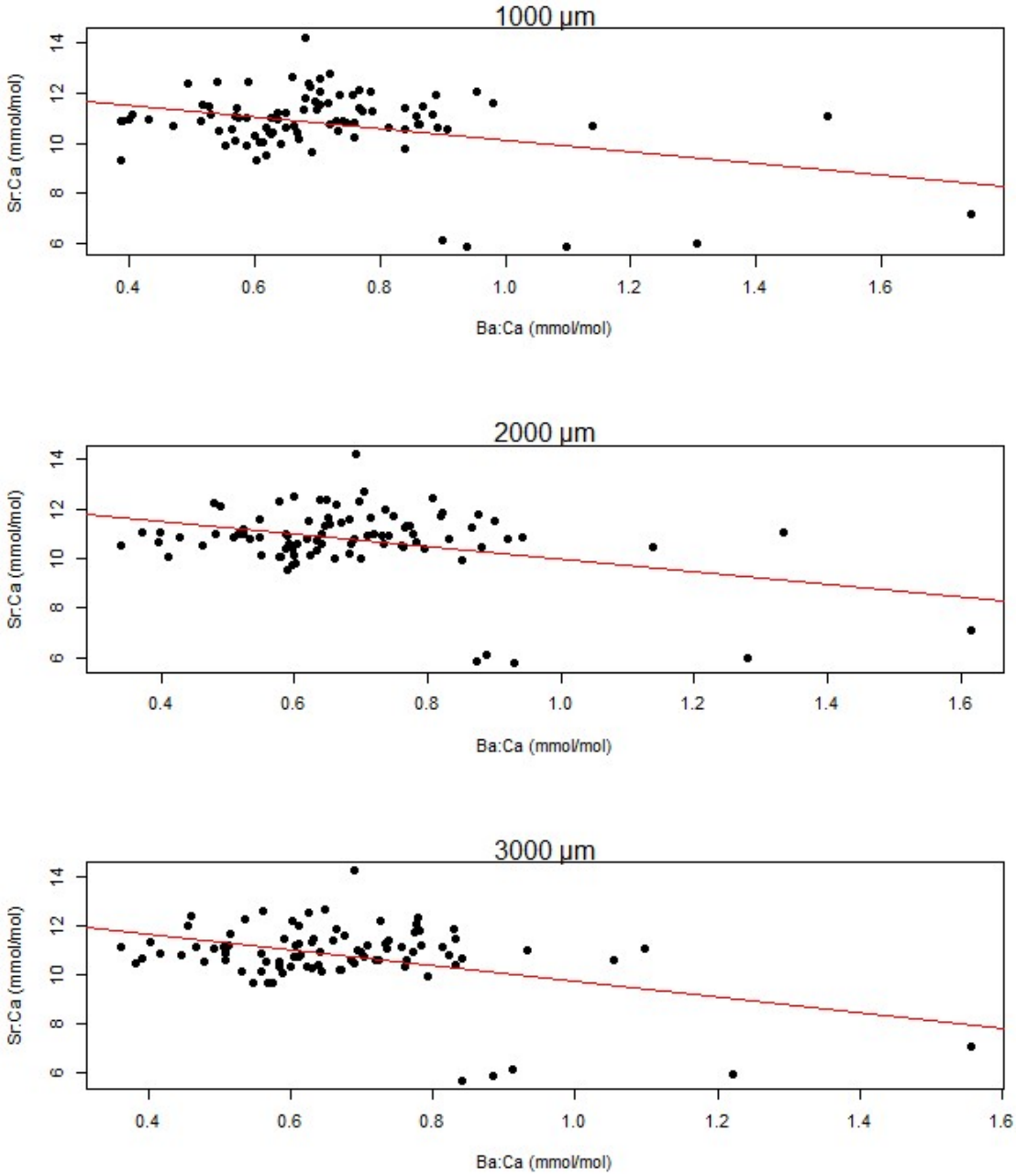

Figure 19. Averaged Sr:Ca values from Red Drum scales correlated against Ba:Ca ratios of averaged sections of exterior scale growth. For all correlations, $p < 0.001$. Adjusted R-squared values: 1000 µm = 0.12; 2000 µm = 0.13; 3000 µm = 0.16.

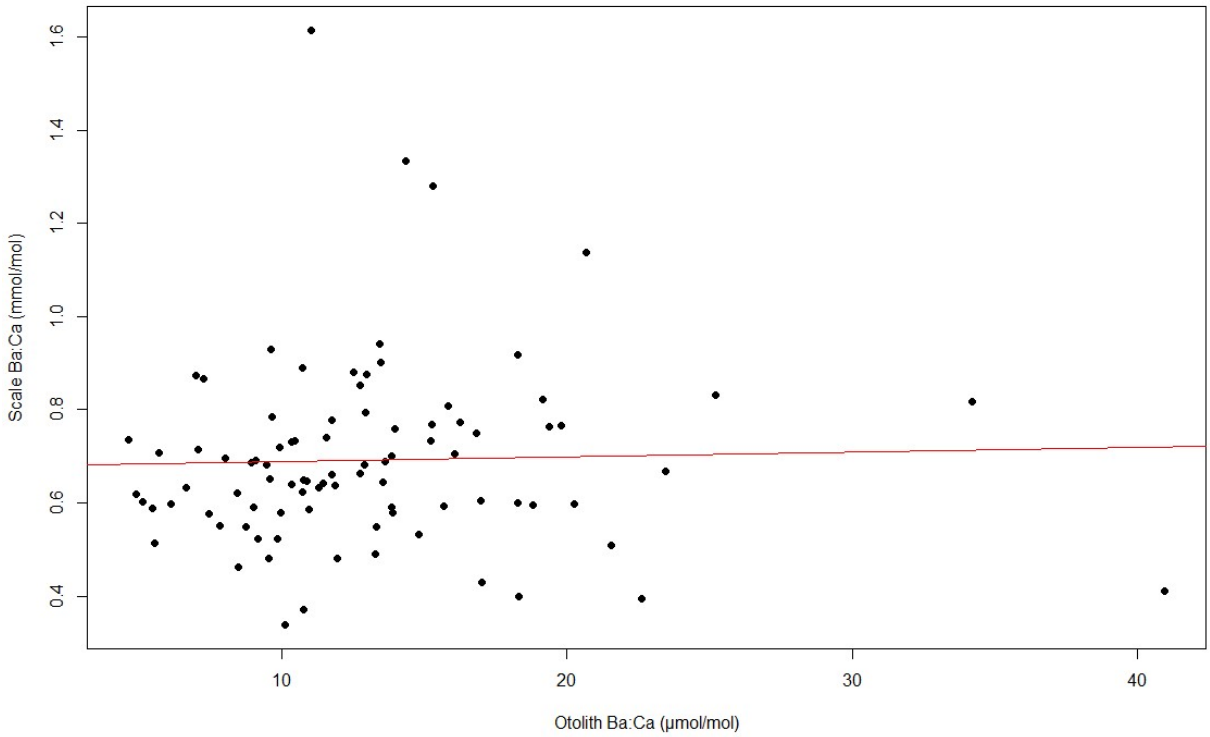

Figure 20. Averaged Ba:Ca values from Red Drum scales correlated against Ba:Ca ratios of averaged sections of exterior growth. The distance averaged for scales was 2000 μm, and the distance averaged for otoliths was 500 μm. Regression line equation: y = 0.68x + 0.001048 with a p-value of 0.77. Adjusted R-squared = -0.01

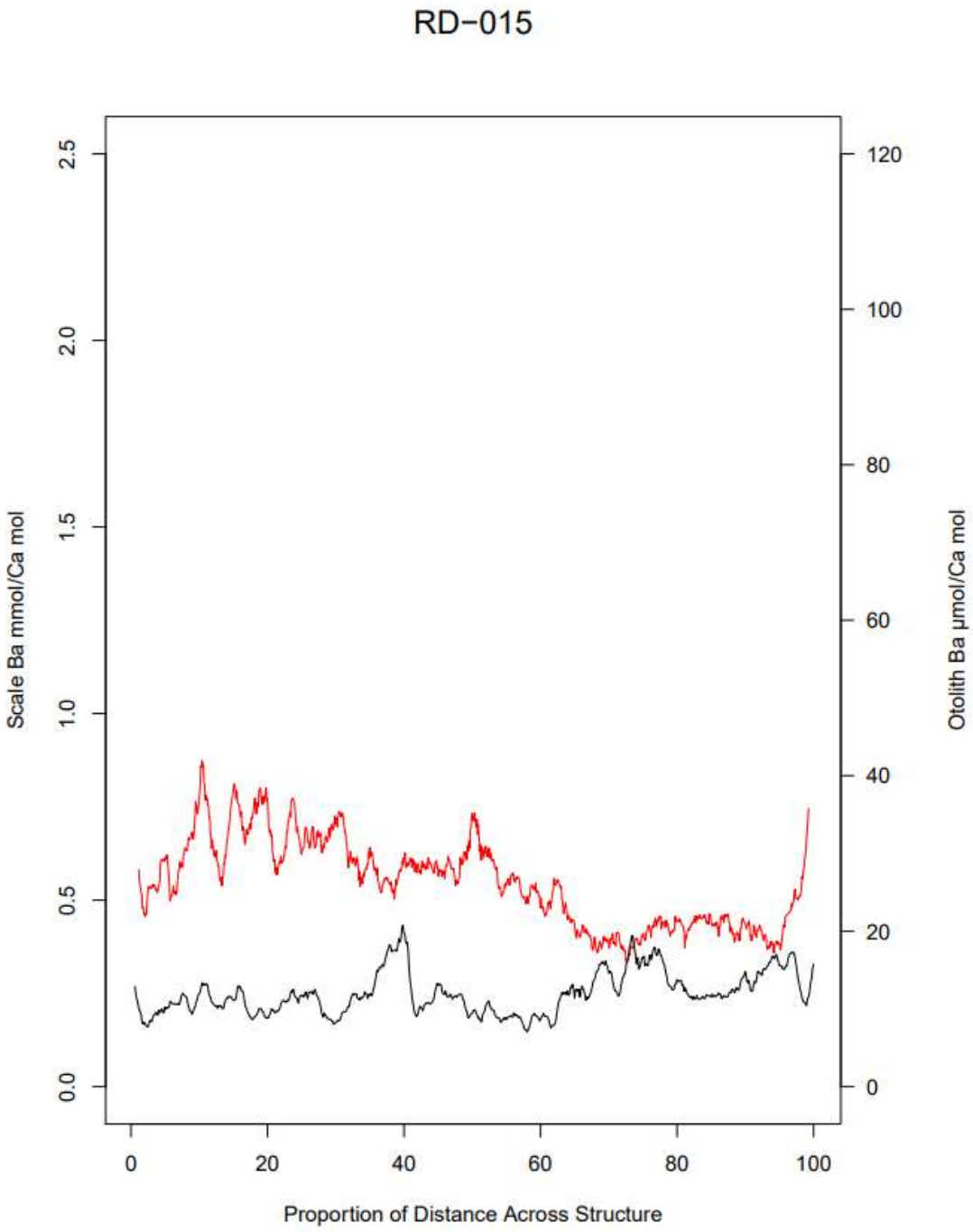

Figure 21. Scale and otolith Ba:Ca profiles for fish RD-015 showing a potential inverse relationship between scale and otolith Ba:Ca profiles (Scale data = red, otolith = black).

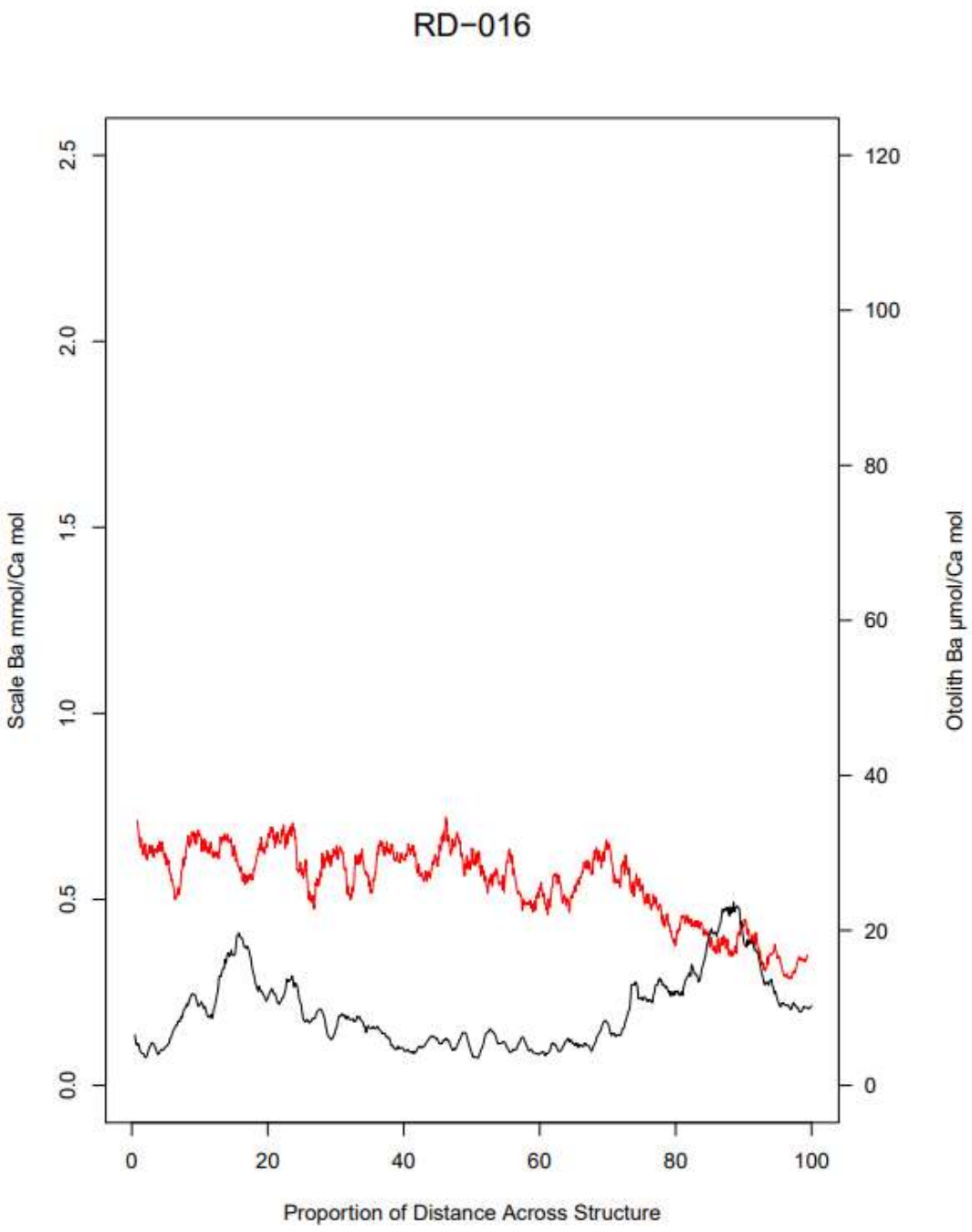

Figure 22. Scale and otolith Ba:Ca profiles for fish RD-016 showing a potential inverse relationship between scale and otolith Ba:Ca profiles (Scale data = red, otolith = black).

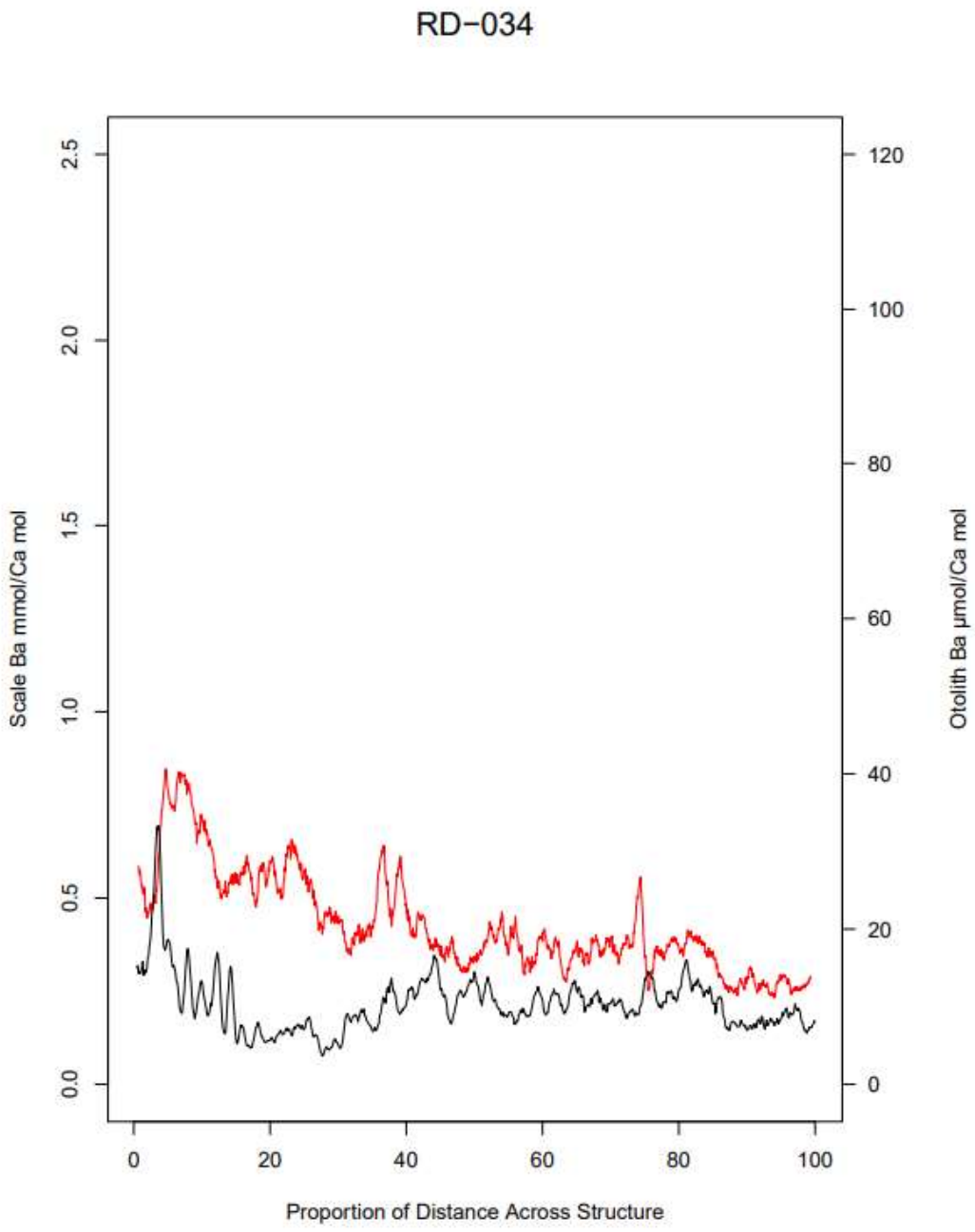

Figure 23. Scale and otolith Ba:Ca profiles for fish RD-034 showing a potential matching relationship between scale and otolith Ba:Ca profiles (Scale data = red, otolith = black).

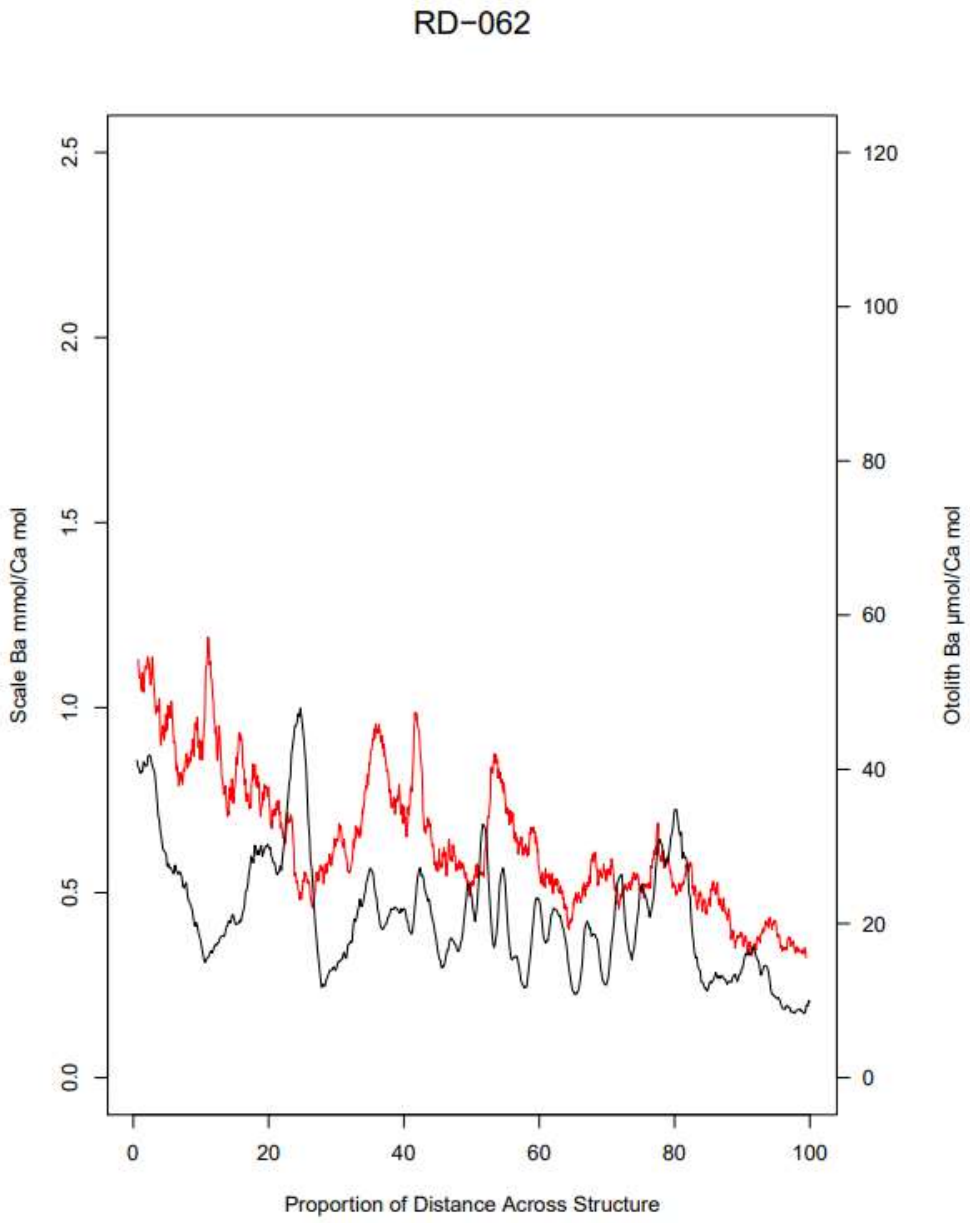

Figure 24. Scale and Otolith Ba:Ca profiles for fish RD-062 showing a potential matching relationship between scale and otolith Ba:Ca profiles (Scale data = red, otolith = black).

LIST OF TABLES

Table 1. Means and standard deviations of total length (TL), wet weight (WW), $\delta^{13}C$, and $\delta^{15}N$ of sampled individuals delineated by bay of collection. For average age, the value in parentheses is the amount of aged fish used to calculate the average. Only fish used for otolith analysis were aged, not all individuals captured. Stable isotope values are reported as mean (standard deviation). Total length (TL) and wet weight (WW) are reported as minimum values, median values, and maximum values.

Bay of Capture	***n***	**Average Age**	**$\delta^{13}C$ ‰**	**$\delta^{15}N$ ‰**	**TL (mm)**	**WW (g)**
Aransas Bay	38	1 (1)	-11.26 (0.99)	10.03 (0.88)	335 395 719	365 630 3875
Copano Bay	13	- (0)	-15.29 (1.04)	9.88 (0.50)	358 399 429	375 650 825
Corpus Christi Bay	12	0.44 (7)	-13.09 (2.25)	12.17 (1.73)	303 386 628	271 595 2580
Corpus Christi Bay Mustang Island	22	1.13 (12)	-11.73 (0.99)	11.19 (0.93)	335 382 561	365 553 1675
Mesquite Bay	38	1.13 (35)	-14.85 (0.64)	13.21 (0.65)	335 383 719	365 565 3875
Nueces Bay	18	- (0)	-14.01 (0.51)	12.75 (1.02)	321 453 573	340 935 1820
Redfish Bay	50	1.04 (35)	-10.58 (1.55)	10.27 (0.89)	309 399 719	309 660 3875

Table 2. $\delta^{13}C$ and $\delta^{15}N$ values (‰) of untreated and decalcified scale samples. Differences for both samples were calculated as the value of the untreated sample minus that of the decalcified sample.

Sample ID	$\delta^{13}C$ Untreated	$\delta^{13}C$ Decalcified	$\delta^{13}C$ Difference	$\delta^{15}N$ Untreated	$\delta^{15}N$ Decalcified	$\delta^{15}N$ Difference
RD-001	-16.28	-16.43	0.15	9.73	9.80	-0.08
RD-004	-16.27	-16.45	0.19	10.03	9.97	0.06
RD-023	-9.52	-9.55	0.02	9.89	9.79	0.10
RD-045	-14.34	-14.40	0.06	12.79	12.93	-0.14
RD-071	-14.26	-14.27	0.02	12.27	11.95	0.32
RD-074	-15.83	-15.92	0.09	13.44	13.23	0.20
RD-104	-13.88	-13.81	-0.07	13.93	13.82	0.11
RD-118	-15.07	-15.16	0.09	14.86	14.81	0.05
RD-138	-10.40	-10.39	-0.01	9.81	9.80	0.01
RD-143	-10.62	-10.91	0.30	9.72	9.91	-0.19
RD-160	-11.10	-11.34	0.24	9.27	9.16	0.10
RD-176	-11.82	-12.12	0.30	10.40	10.01	0.39
RD-177	-11.49	-11.76	0.27	10.12	10.10	0.02
RD-188	-12.43	-12.50	0.07	10.70	10.69	0.01

Table 3. $\delta^{13}C$ and $\delta^{15}N$ values (‰) for large and small scale samples and the differences between those values and those of past muscle tissue samples.

ID	$\delta^{13}C$ Large Scale Cut	$\delta^{13}C$ Small Scale Cut	$\delta^{13}C$ (Muscle - Large)	$\delta^{13}C$ (Muscle - Small)	$\delta^{15}N$ Large Scale Cut	$\delta^{15}N$ Small Scale Cut	$\delta^{15}N$ (Muscle - Large)	$\delta^{15}N$ (Muscle - Small)
RD-001	-16.23	-16.40	-0.15	0.02	9.76	10.03	4.27	4.00
RD-002	-16.26	-16.62	2.5	2.86	9.95	10.19	2.15	1.91
RD-003	-16.24	-16.64	1.88	2.27	10.23	10.36	3.32	3.20
RD-004	-16.35	-16.66	2.59	2.90	10.08	10.19	2.40	2.29
RD-005	-16.69	-17.11	3.17	3.59	10.19	10.49	2.25	1.95
RD-119	-11.20	-12.00	-2.94	-2.14	11.62	12.17	0.85	0.30

Table 4. Stable isotope values for each cluster group determined by Ward's hierarchical clustering analysis. Values are reported as mean(standard deviation).

	Cluster Group 1 n=18	**Cluster Group 2 n=110**	**Cluster Group 3 n=63**
$\delta^{13}C$	-15.58 (1.00)	-10.85 (0.96)	-14.49 (0.79)
$\delta^{15}N$	9.92 (0.44)	10.38 (0.95)	13.12 (0.82)

LIST OF APPENDICES

APPENDIX PAGE

Appendix 1. Stable Isotope Standards

Table A. UC-Davis Stable Isotope Facility reference materials for primary stable isotope analysis. $\delta^{13}C$ and $\delta^{15}N$ values reported in ‰. δ values are mean values of multiple analyses.

Standard	**$\delta^{13}C$**	**$\delta^{15}N$**	**%C**	**%N**
Amaranth Flour	-12.89	2.45	42.62	4.68
Bovine Liver	-21.69	7.72	-	-
Caffeine	-35.05	-2.80	47.64	28.35
Chitin	-19.03	2.27	44.52	6.75
Glutamic Acid	-11.07	-8.53	40.82	9.52
Keratin	-24.40	4.91	49.31	14.91
Nylon 6	-27.69	-10.54	-	-

Table B. UC-Davis Stable Isotope Facility reference materials for decalcification stable isotope analysis. $\delta^{13}C$ and $\delta^{15}N$ values reported in ‰. δ values are mean values of multiple analyses.

Standard	**$\delta^{13}C$**	**$\delta^{15}N$**	**%C**	**%N**
Bovine Liver	-21.71	7.74	-	-
Enriched Alanine	43.02	41.13	-	-
Glutamic Acid	-16.70	-6.81	40.82	9.52
Nylon 6	-27.76	-10.54	-	-

Appendix 2. Metadata for the samples of this study

Table A. Metadata for the samples of this study. Sample site (AB = Aransas Bay, CB = Copano Bay, CC = Corpus Christi Bay, MB = Mesquite Bay, MI = Corpus Christi – Mustang Island, NB = Nueces Bay), scale regeneration status and stable isotope values for all samples tested. Muscle stable isotope values determined during a previous study (Torrance 2018).

Fish ID	Sample Site	Capture Date	Total Length (mm)	Laser Ablation Scale Regenerated	$\delta^{13}C$ Scale	$\delta^{13}C$ Muscle	$\delta^{15}N$ Scale	$\delta^{15}N$ Muscle	Stable Isotope Scale Regenerated
RD-001	CC	1/18/2017	303	X	-16.23	-16.38	9.76	14.030	X
RD-002	CC	1/18/2017	327	X	-16.26	-13.76	9.95	12.100	X
RD-003	CC	2/3/2017	610	X	-16.24	-14.36	10.23	13.550	X
RD-004	AB	2/3/2017	510	X	-16.35	-13.76	10.08	12.480	X
RD-005	AB	2/3/2017	407	X	-16.69	-13.52	10.19	12.440	X
RD-015	CC	2/3/2017	311		-10.16	-12.94	12.64	13.540	
RD-016	CC	2/13/2017	341		-11.88	-14.75	13.00	14.490	
RD-017	CC	2/13/2017	309		-12.09	-14.67	12.89	13.570	
RD-018	CC	2/13/2017	473		-10.55	-13.68	13.13	14.500	
RD-019	CC	2/13/2017	491		-9.51	-12.87	9.89	11.200	
RD-020	CC	2/13/2017	497	X	-9.40	-13.02	10.07	11.650	X
RD-021	CC	3/3/2017	471		-9.42	-13.05	10.25	11.650	X
RD-022	CC	3/3/2017	500	X	-9.21	-12.96	9.31	11.060	X
RD-023	CC	3/3/2017	628		-9.52	-12.74	9.89	11.650	
RD-024	AB	3/3/2017	433		-9.67	-14.04	9.24	10.970	
RD-025	AB	3/3/2017	365		-9.58	-13.41	9.43	10.810	X
RD-026	AB	3/3/2017	355		-9.78	-13.78	9.06	10.770	
RD-027	AB	3/3/2017	465		-9.57	-13.13	9.53	11.060	
RD-028	AB	4/7/2017	445	X	-9.35	-13.32	8.73	10.975	X
RD-029	AB	4/7/2017	471		-9.57	-13.54	9.14	11.190	X
RD-030	AB	4/7/2017	460		-9.55	-13.56	9.84	11.560	X
RD-031	AB	4/7/2017	479	X	-9.47	-13.24	9.66	11.690	X
RD-032	AB	4/7/2017	509		-9.03	-13.31	9.91	11.500	
RD-033	AB	4/14/2017	591	X	-9.03	-13.27	10.19	11.720	X
RD-034	AB	4/14/2017	560	X	-9.12	-13.38	9.11	11.070	X
RD-035	AB	4/14/2017	518	X	-9.21	-13.01	9.99	11.570	X
RD-036	AB	4/14/2017	464		-9.18	-13.12	8.70	10.400	X
RD-037	AB	4/14/2017	450		-9.50	-13.40	8.75	10.720	
RD-038	AB	4/14/2017	399	X	-15.91	-18.60	14.30	15.260	X

Fish ID	Sample Site	Capture Date	Total Length (mm)	Laser Ablation Scale Regenerated	$\delta^{13}C$ Scale	$\delta^{13}C$ Muscle	$\delta^{15}N$ Scale	$\delta^{15}N$ Muscle	Stable Isotope Scale Regenerated
RD-039	MI	4/14/2017	370		-11.63	-14.37	10.92	12.280	X
RD-040	MI	4/14/2017	354	X	-12.11	-14.63	10.66	11.660	X
RD-041	MI	4/14/2017	386		-11.35	-14.27	10.38	11.940	X
RD-042	MI	4/14/2017	416		-11.76	-14.60	11.01	12.690	
RD-043	MI	4/14/2017	561		-10.88	-14.28	11.11	12.480	X
RD-044	MB	4/14/2017	345		-13.97	-17.35	11.98	13.820	
RD-045	MB	4/14/2017	383		-14.34	-17.52	12.79	14.220	X
RD-046	MB	4/14/2017	430		-14.06	-17.45	12.20	14.200	
RD-047	MB	4/24/2017	379	X	-15.49	-17.87	13.54	14.860	X
RD-048	MB	5/8/2017	335	X	-15.38	-18.09	12.30	13.655	X
RD-049	MB	5/8/2017	353		-15.72	-17.78	13.53	14.990	X
RD-050	MB	5/8/2017	381		-14.65	-17.69	13.49	14.480	
RD-051	MB	5/8/2017	369	X	-14.79	-17.32	14.16	14.380	X
RD-052	MB	5/8/2017	386		-14.58	-17.92	13.38	14.940	
RD-053	AB	5/15/2017	374	X	-11.49	-14.53	9.70	10.500	
RD-054	AB	5/15/2017	370		-10.92	-14.06	9.75	10.990	X
RD-055	AB	5/15/2017	440		-9.45	-14.16	9.77	11.730	X
RD-056	AB	5/15/2017	504		-10.48	-13.87	10.75	12.470	X
RD-057	AB	5/15/2017	536	X	-10.67	-13.91	11.13	13.300	X
RD-058	AB	5/15/2017	456		-11.30	-14.15	10.46	11.990	
RD-059	AB	5/15/2017	529		-9.59	-13.26	10.48	12.270	X
RD-060	AB	5/15/2017	398		-11.34	-14.42	11.23	12.570	
RD-061	AB	5/15/2017	395		-11.38	-14.92	10.90	11.890	X
RD-062	AB	5/16/2017	385		-11.95	-15.19	11.60	12.690	X
RD-063	AB	5/16/2017	380		-12.02	-14.92	9.55	11.130	X
RD-064	AB	5/16/2017	438		-10.70	-14.66	10.42	12.040	X
RD-065	AB	5/16/2017	397		-9.99	-13.76	9.75	11.670	
RD-066	AB	5/16/2017	445		-9.89	-13.50	10.01	12.130	
RD-067	AB	5/16/2017	337		-10.47	-13.77	9.82	10.950	
RD-068	MB	5/16/2017	370	X	-15.46	-17.94	13.45	14.745	X
RD-069	MB	5/16/2017	383	X	-15.45	-18.10	13.21	14.560	X
RD-070	MB	5/16/2017	405		-14.72	-18.11	13.12	14.090	X
RD-071	MB	5/16/2017	358		-14.26	-17.28	12.27	13.550	
RD-072	MB	5/16/2017	367		-16.14	-18.76	13.77	14.990	X
RD-073	MB	5/16/2017	355		-14.66	-17.50	12.90	14.200	X
RD-074	MB	5/16/2017	371		-15.83	-18.31	13.44	14.810	X
RD-075	MB	5/16/2017	373		-15.07	-18.33	13.56	14.650	X

Fish ID	Sample Site	Capture Date	Total Length (mm)	Laser Ablation Scale Regenerated	$\delta^{13}C$ Scale	$\delta^{13}C$ Muscle	$\delta^{15}N$ Scale	$\delta^{15}N$ Muscle	Stable Isotope Scale Regenerated
RD-076	MB	5/16/2017	391		-15.53	-18.29	14.21	14.940	X
RD-077	MB	5/17/2017	396		-14.71	-17.79	13.16	14.600	X
RD-078	MB	5/17/2017	395		-14.92	-18.15	13.31	15.075	
RD-079	MB	5/17/2017	363		-14.25	-18.51	12.92	15.030	
RD-080	MB	5/17/2017	370		-15.71	-16.88	13.49	14.290	X
RD-081	MB	5/17/2017	385		-14.31	-17.49	12.40	14.340	X
RD-082	MB	5/17/2017	384		-15.10	-18.50	13.78	13.540	X
RD-083	MB	5/17/2017	358		-15.93	-18.03	12.20	15.000	
RD-084	MI	5/17/2017	370		-11.65	-14.99	10.68	12.320	
RD-085	MI	5/17/2017	354		-11.81	-14.77	11.37	12.390	X
RD-086	MI	5/17/2017	339		-10.79	-14.82	9.34	11.710	X
RD-087	MB	5/17/2017	360		-14.88	-17.45	13.26	14.990	
RD-088	MB	5/17/2017	385		-14.81	-17.81	13.04	14.570	X
RD-089	MB	5/17/2017	348		-14.65	-17.47	12.68	13.850	X
RD-090	MB	5/17/2017	410		-15.09	-18.20	12.89	14.470	X
RD-091	MB	5/17/2017	341	X	-14.82	-17.51	13.51	14.560	X
RD-092	MB	5/17/2017	517		-14.19	-17.33	13.71	15.000	X
RD-093	MB	5/19/2017	529	X	-13.42	-16.04	12.42	13.760	X
RD-094	MB	5/19/2017	530	X	-13.47	-17.13	12.71	14.440	X
RD-095	MB	5/19/2017	405		-15.14	-17.83	13.77	15.910	
RD-096	MB	5/19/2017	405		-14.87	-17.93	12.92	14.680	
RD-097	MI	5/19/2017	401		-11.99	-15.35	11.42	12.830	X
RD-098	MI	5/19/2017	375		-13.33	-16.08	12.41	13.190	X
RD-099	MI	5/19/2017	358		-13.04	-15.29	11.87	12.740	
RD-100	MI	5/19/2017	366		-12.09	-15.40	11.40	12.790	X
RD-101	MI	5/23/2017	361		-12.77	-15.26	11.67	12.840	X
RD-102	MI	5/23/2017	364		-12.60	-15.42	11.91	12.965	X
RD-103	AB	5/23/2017	410		-11.98	-15.34	11.84	12.660	X
RD-104	AB	5/23/2017	391		-13.88	-16.58	13.93	15.340	X
RD-105	AB	5/23/2017	526		-10.77	-14.47	10.37	12.460	X
RD-106	AB	5/23/2017	380		-12.94	-16.20	13.29	14.410	X
RD-107	MI	5/23/2017	360		-10.48	-13.91	10.40	12.240	X
RD-108	MI	5/23/2017	352		-11.56	-14.65	11.24	12.310	X
RD-109	MI	5/23/2017	386		-13.21	-16.03	13.27	14.610	X
RD-110	MI	5/23/2017	356		-10.81	-13.97	10.61	12.420	X
RD-111	MI	5/23/2017	381		-11.08	-14.26	10.98	12.570	
RD-112	MI	5/24/2017	344		-9.67	-13.68	10.29	11.720	X

Fish ID	Sample Site	Capture Date	Total Length (mm)	Laser Ablation Scale Regenerated	$\delta^{13}C$ Scale	$\delta^{13}C$ Muscle	$\delta^{15}N$ Scale	$\delta^{15}N$ Muscle	Stable Isotope Scale Regenerated
RD-113	MI	5/24/2017	406		-12.99	-15.97	13.06	14.130	X
RD-114	MI	5/24/2017	361		-10.55	-14.50	10.22	11.250	
RD-115	CC	5/24/2017	398		-14.14	-16.64	15.04	15.510	X
RD-116	MB	5/25/2017	383		-14.89	-18.32	13.11	15.340	X
RD-117	MB	5/25/2017	395		-14.08	-17.62	14.39	16.320	X
RD-118	MB	5/25/2017	394		-15.07	-18.07	14.86	16.360	X
RD-119	AB	5/25/2017	719		-11.20	-14.14	11.62	12.470	
RD-120	CB	5/25/2017	358		-18.37	-21.28	11.39	13.680	X
RD-121	NB	5/25/2017	385		-14.24	-16.82	11.63	13.430	X
RD-122	NB	5/25/2017	429		-14.78	-18.29	12.48	14.540	X
RD-123	CB	5/25/2017	428		-14.65	-18.15	10.03	11.480	X
RD-124	CB	5/25/2017	395		-15.37	-18.91	9.77	11.540	X
RD-125	CB	5/25/2017	403		-15.70	-18.96	9.71	11.530	
RD-126	CB	5/25/2017	407		-15.02	-18.13	10.13	11.670	X
RD-127	CB	5/25/2017	427		-15.69	-19.00	9.60	11.430	X
RD-128	CB	6/7/2017	366		-14.37	-17.29	9.54	11.110	X
RD-129	CB	6/8/2017	368		-15.14	-18.74	10.02	12.630	X
RD-130	CB	6/8/2017	370		-14.83	-18.24	9.43	10.960	X
RD-131	CB	6/8/2017	380		-15.22	-18.70	9.74	11.785	X
RD-132	CB	6/9/2017	415		-14.71	-18.18	9.68	11.210	
RD-133	CB	6/9/2017	379		-14.23	-17.36	9.55	11.900	X
RD-134	CB	6/9/2017	399		-15.43	-18.64	9.79	11.270	
RD-135	CB	6/9/2017	424		-10.99	-13.96	9.87	11.300	X
RD-136	CB	6/9/2017	371		-11.93	-14.92	9.87	11.020	X
RD-137	CB	6/9/2017	423		-12.04	-15.04	11.04	12.590	
RD-138	CB	6/9/2017	510		-10.40	-13.37	9.81	11.100	X
RD-139	CB	6/9/2017	515		-10.62	-14.31	9.87	11.960	X
RD-140	CB	6/9/2017	452		-10.67	-13.95	9.26	11.130	X
RD-141	CB	6/9/2017	367		-13.20	-16.08	10.51	11.780	X
RD-142	CB	6/9/2017	530		-11.06	-14.25	10.43	12.080	X
RD-143	CB	6/9/2017	532		-10.62	-13.95	9.72	11.840	X
RD-144	CB	6/10/2017	484		-10.95	-14.26	10.24	12.040	
RD-145	CB	6/10/2017	518		-10.73	-14.48	10.13	12.090	X
RD-146	CB	6/10/2017	500		-11.20	-14.41	10.81	12.540	X
RD-147	CB	6/10/2017	393		-11.67	-14.82	9.16	10.980	X
RD-148	CB	6/10/2017	378		-11.54	-14.67	9.64	11.060	
RD-149	CB	6/10/2017	365		-10.09	-13.33	9.33	10.800	X

Fish ID	Sample Site	Capture Date	Total Length (mm)	Laser Ablation Scale Regenerated	$\delta^{13}C$ Scale	$\delta^{13}C$ Muscle	$\delta^{15}N$ Scale	$\delta^{15}N$ Muscle	Stable Isotope Scale Regenerated
RD-150	AB	6/10/2017	397		-11.51	-14.88	9.81	11.460	X
RD-151	AB	6/10/2017	475		-10.99	-14.18	10.04	11.715	
RD-152	AB	6/10/2017	455		-11.03	-14.07	9.80	11.640	
RD-153	AB	6/10/2017	453		-10.58	-13.91	9.45	11.840	X
RD-154	AB	6/10/2017	496		-10.99	-14.26	10.13	11.520	X
RD-155	AB	6/10/2017	558		-10.52	-13.90	9.79	11.450	X
RD-156	AB	6/10/2017	514		-11.14	-14.20	9.51	11.410	X
RD-157	AB	6/10/2017	467		-10.51	-13.87	9.86	12.140	X
RD-158	AB	6/10/2017	477		-10.39	-13.67	9.25	11.220	X
RD-159	AB	6/11/2017	478		-11.04	-14.40	9.71	11.790	X
RD-160	AB	6/11/2017	413		-11.10	-14.49	9.27	10.740	
RD-161	AB	6/11/2017	356		-10.66	-14.36	9.39	11.080	X
RD-162	AB	6/11/2017	348		-12.71	-15.63	10.43	11.950	X
RD-163	NB	6/11/2017	485		-13.82	-18.15	13.15	15.930	X
RD-164	NB	6/11/2017	540		-13.66	-17.41	13.04	15.610	X
RD-165	NB	6/11/2017	529		-13.53	-17.31	12.21	14.060	X
RD-166	NB	6/11/2017	430		-13.56	-17.06	12.56	15.090	X
RD-167	NB	6/11/2017	386		-14.07	-17.03	12.95	14.560	X
RD-168	NB	6/11/2017	411		-14.70	-17.77	11.34	13.090	X
RD-169	NB	6/11/2017	434		-13.60	-17.46	11.81	13.690	X
RD-170	NB	6/11/2017	369		-13.87	-17.26	13.29	15.780	X
RD-171	AB	6/11/2017	519		-11.00	-14.23	9.75	11.120	X
RD-172	AB	6/11/2017	514		-10.79	-14.31	10.14	11.520	X
RD-173	AB	6/11/2017	500		-11.06	-14.51	9.73	11.190	X
RD-174	AB	6/11/2017	489		-11.16	-14.58	9.58	11.180	X
RD-175	AB	6/11/2017	512		-11.45	-14.26	9.62	10.980	X
RD-176	AB	6/11/2017	462		-11.82	-14.30	10.40	11.320	X
RD-177	AB	6/11/2017	512		-11.49	-14.15	10.12	11.350	X
RD-178	AB	6/11/2017	512		-11.10	-14.26	9.72	10.980	X
RD-179	NB	6/11/2017	546		-13.25	-16.92	11.99	15.060	X
RD-180	NB	6/12/2017	520		-14.14	-17.83	12.43	14.860	X
RD-181	NB	6/12/2017	432		-14.95	-18.44	11.45	13.560	X
RD-182	NB	6/12/2017	416		-14.74	-17.84	12.47	14.420	
RD-183	NB	6/12/2017	365		-13.30	-16.84	13.01	14.570	X
RD-184	AB	6/12/2017	470		-10.52	-13.99	10.96	12.590	X
RD-185	AB	6/12/2017	345		-11.96	-14.83	12.81	13.190	X
RD-186	AB	6/12/2017	325		-10.82	-14.34	10.75	12.270	X

Fish ID	Sample Site	Capture Date	Total Length (mm)	Laser Ablation Scale Regenerated	$\delta^{13}C$ Scale	$\delta^{13}C$ Muscle	$\delta^{15}N$ Scale	$\delta^{15}N$ Muscle	Stable Isotope Scale Regenerated
RD-187	AB	6/12/2017	340		-10.68	-13.80	11.09	12.640	X
RD-188	AB	6/12/2017	321		-12.43	-14.79	10.70	13.060	X
RD-189	AB	6/12/2017	383		-11.53	-14.83	11.47	13.070	X
RD-190	AB	6/12/2017	375		-11.27	-14.53	10.76	12.430	X
RD-191	AB	6/12/2017	493		-10.54	-14.34	10.66	12.200	X
RD-192	AB	6/12/2017	334		-12.41	-15.47	11.51	12.900	X
RD-193	AB	6/13/2017	561		-11.18	-14.24	11.62	13.150	X
RD-194	AB	6/13/2017	518		-10.43	-14.12	11.19	12.940	X
RD-195	AB	6/13/2017	562		-10.50	-14.07	11.45	12.840	X
RD-196	AB	6/13/2017	573		-10.73	-13.96	11.25	12.650	X
RD-197	AB	6/13/2017	556		-10.59	-14.05	11.22	13.160	X
RD-198	NB	6/13/2017	397		-14.04	-17.25	14.73	16.940	X
RD-199	NB	6/13/2017	381		-13.89	-16.86	14.55	16.120	X
RD-200	NB	6/13/2017	401		-14.06	-17.17	14.41	16.295	X

Appendix 3: Supplemental Scale and Otolith Ba:Ca and Sr:Ca Profiles

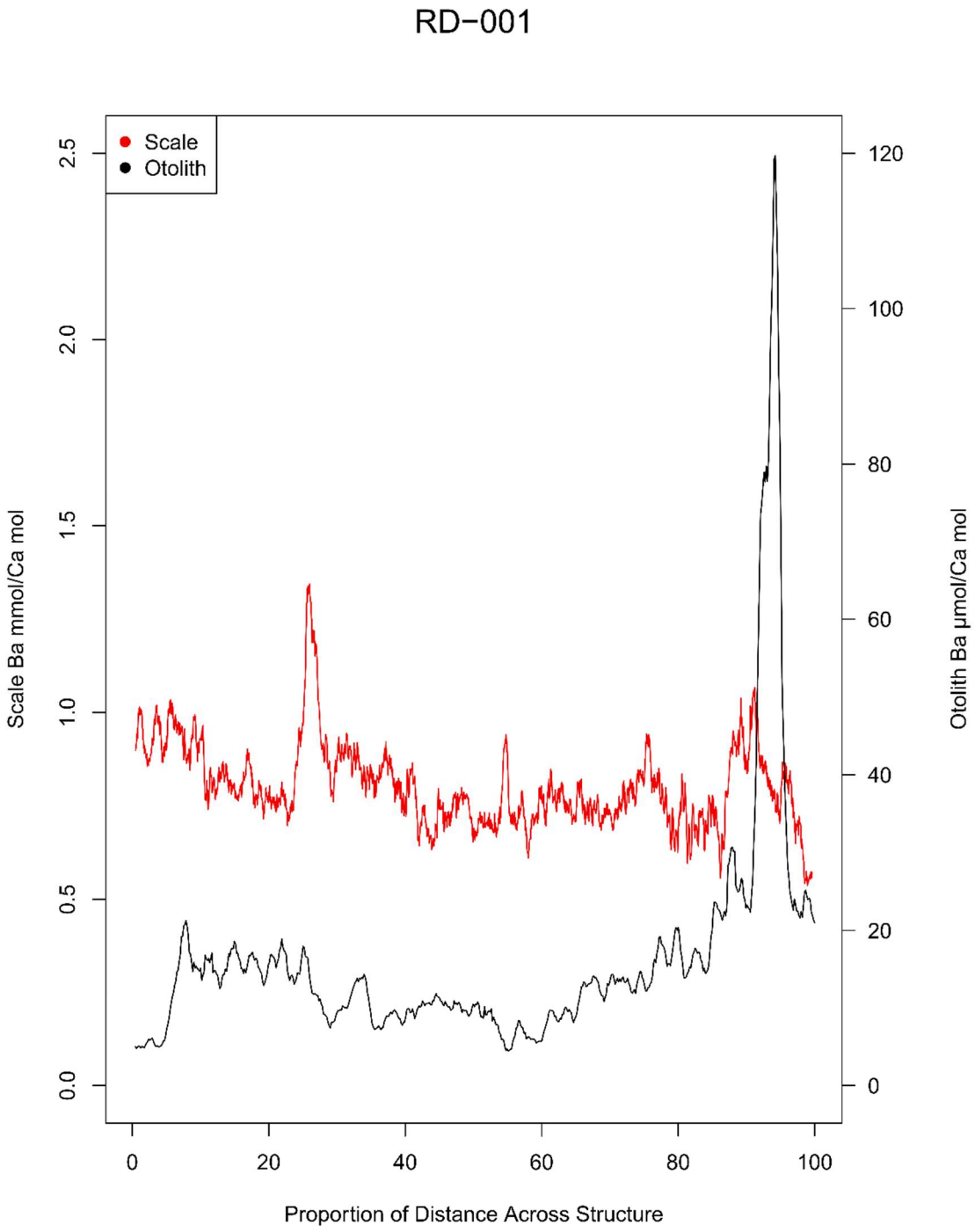

RD-001

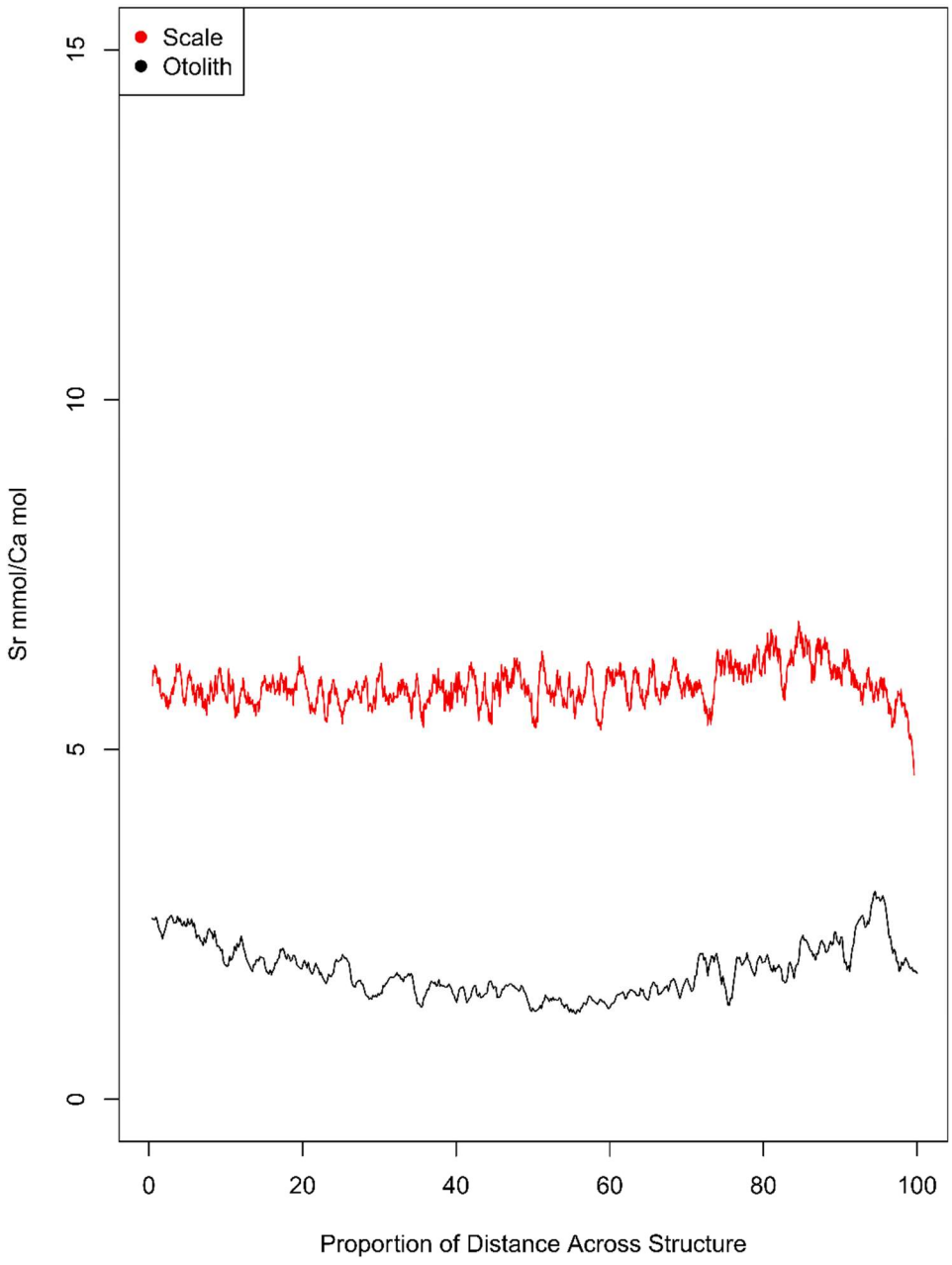
Scale
Otolith
Sr mmol/Ca mol
0
5
10
15
0
20
40
60
80
100
Proportion of Distance Across Structure

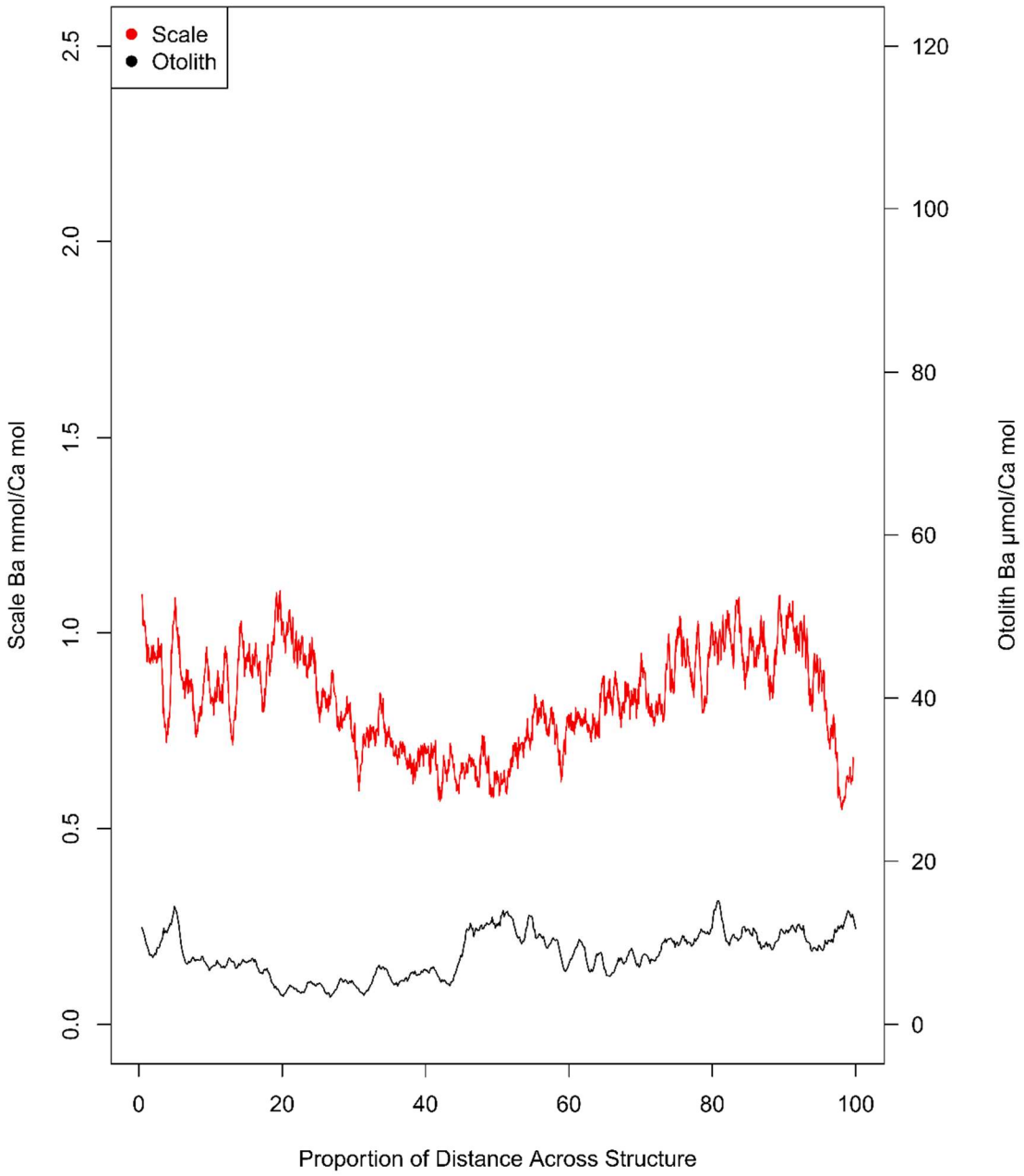
RD−002
Scale
Otolith
Scale Ba mmol/Ca mol
Otolith Ba µmol/Ca mol
Proportion of Distance Across Structure
0.0
0.5
1.0
1.5
2.0
2.5
0
20
40
60
80
100
120

RD−002

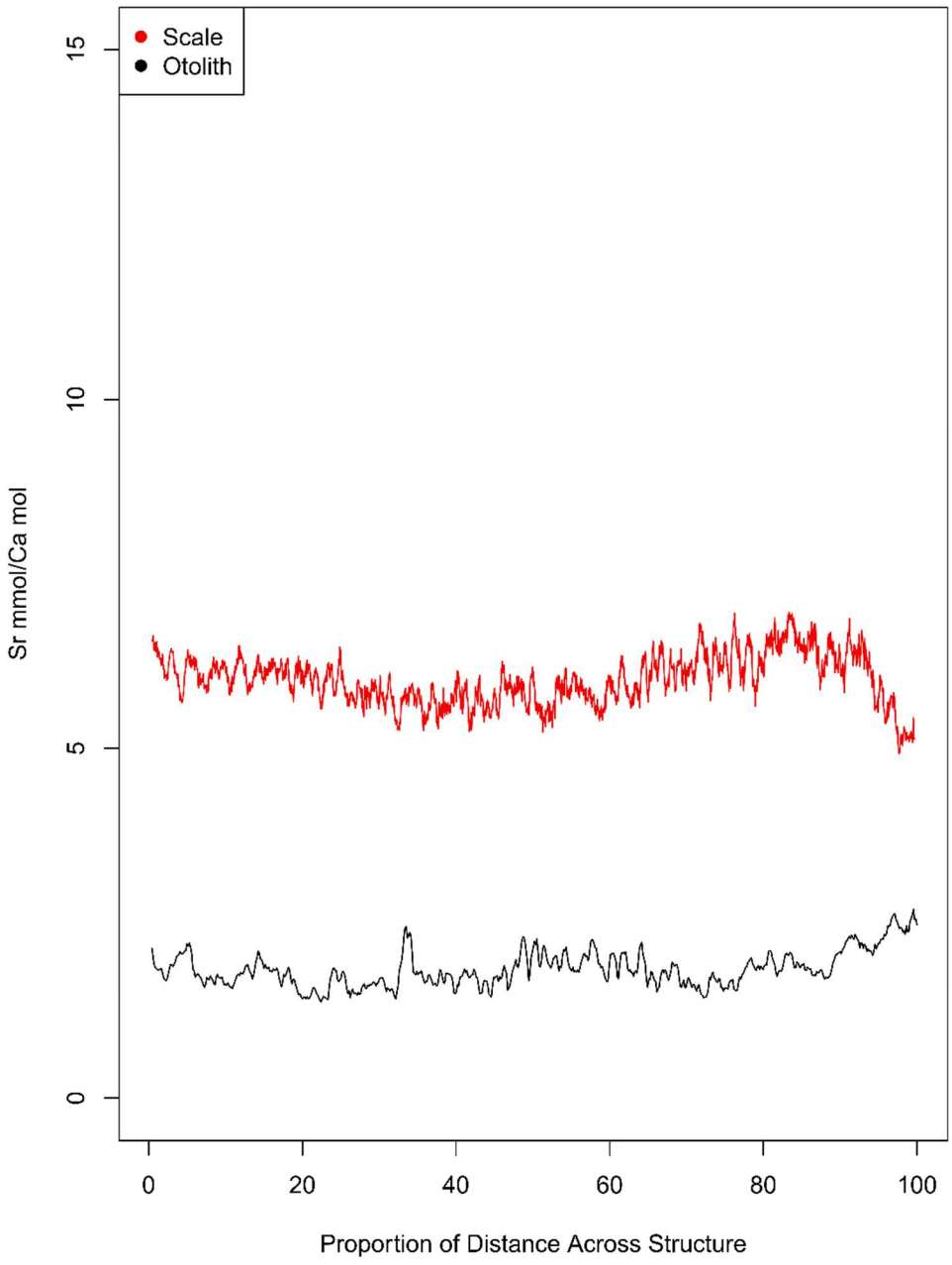
Scale
Otolith
Sr mmol/Ca mol
0
5
10
15
0
20
40
60
80
100
Proportion of Distance Across Structure

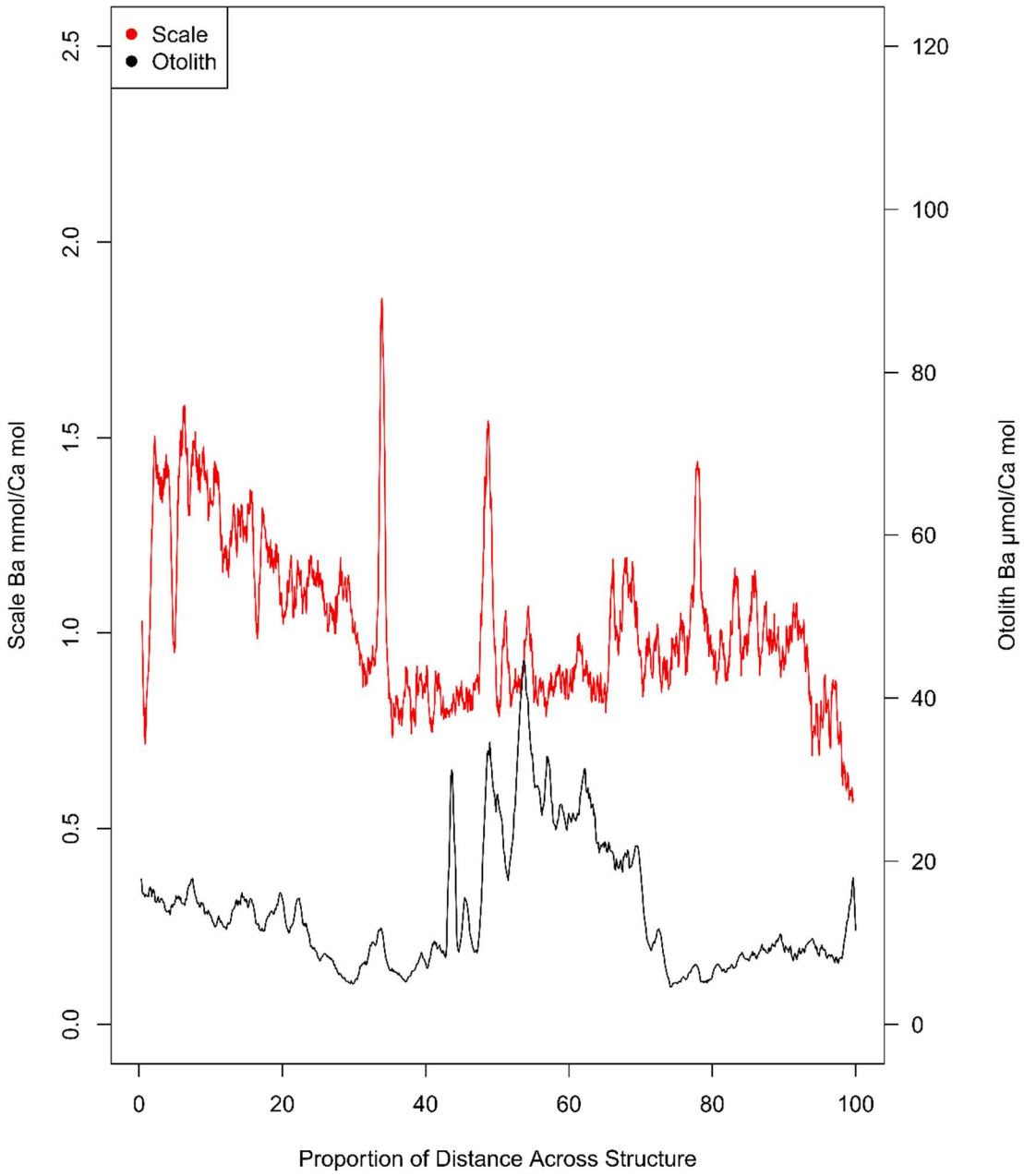
RD−003
Scale
Otolith
Scale Ba mmol/Ca mol
Otolith Ba µmol/Ca mol
Proportion of Distance Across Structure
0.0
0.5
1.0
1.5
2.0
2.5
0
20
40
60
80
100
120

RD-003

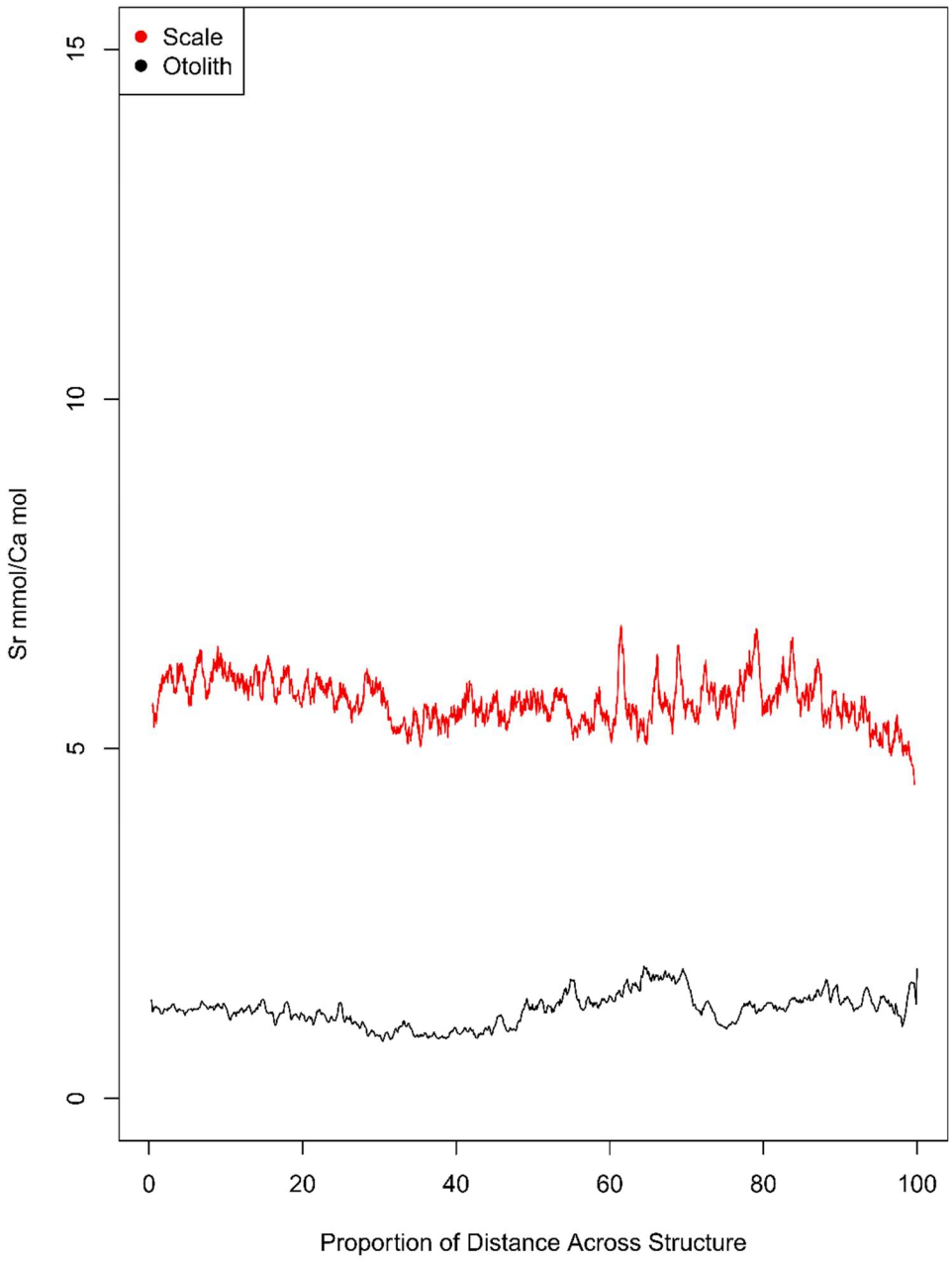
Scale
Otolith
Sr mmol/Ca mol
0
5
10
15
0
20
40
60
80
100
Proportion of Distance Across Structure

RD−004

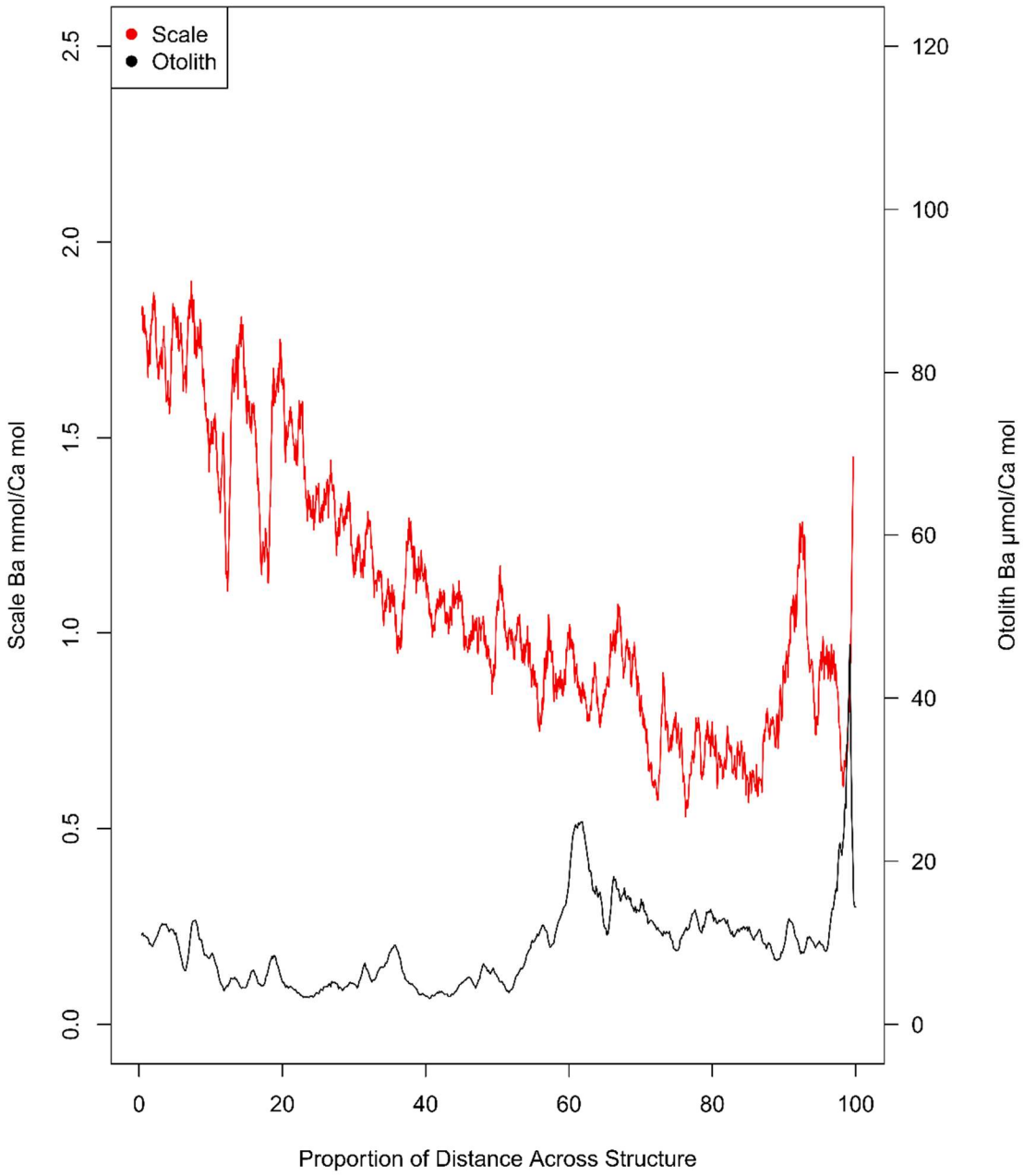
Scale
Otolith
Scale Ba mmol/Ca mol
Otolith Ba µmol/Ca mol
Proportion of Distance Across Structure
0.0
0.5
1.0
1.5
2.0
2.5
0
20
40
60
80
100
120

RD−004

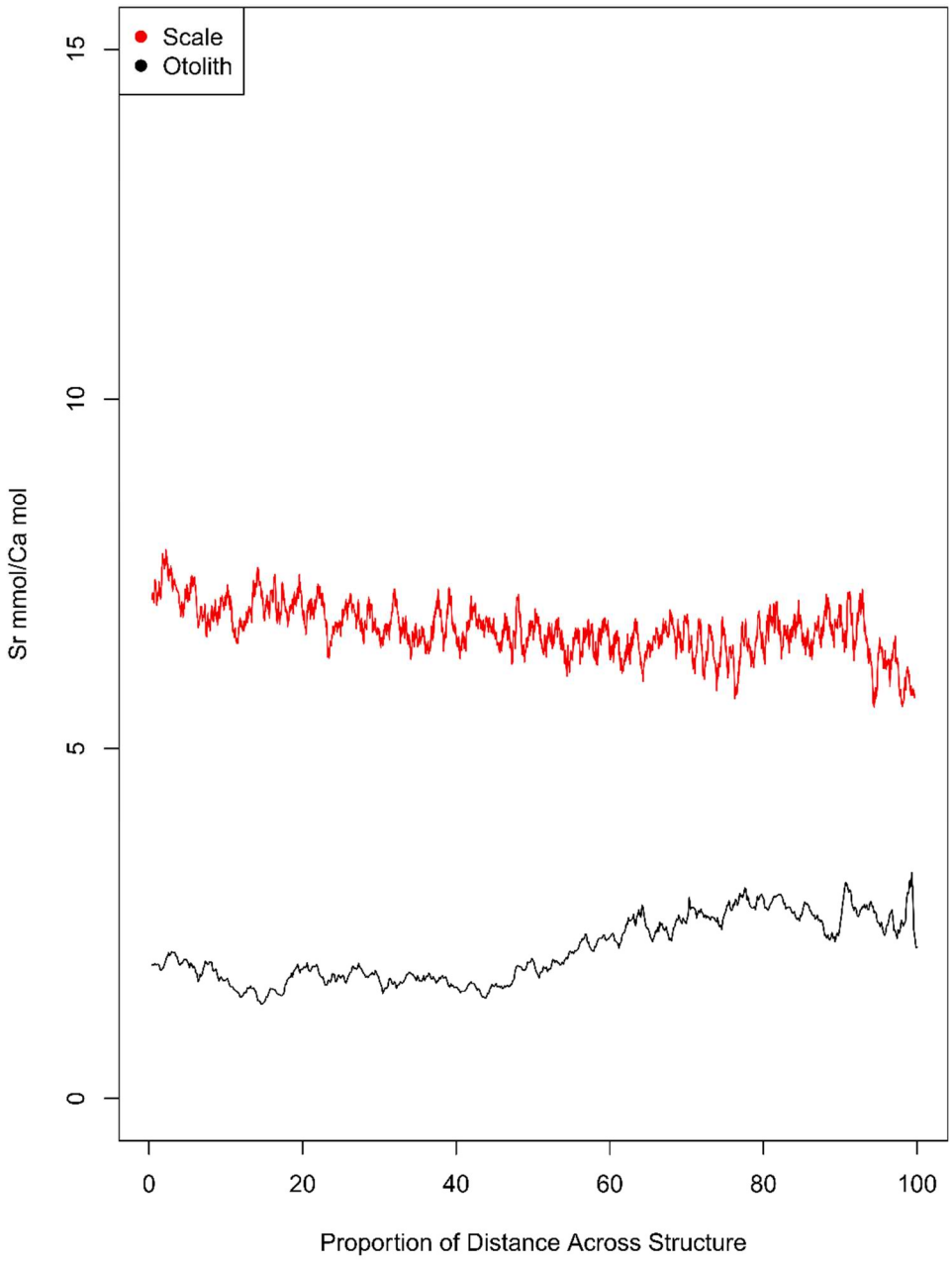
Scale
Otolith
Sr mmol/Ca mol
0
5
10
15
0
20
40
60
80
100
Proportion of Distance Across Structure

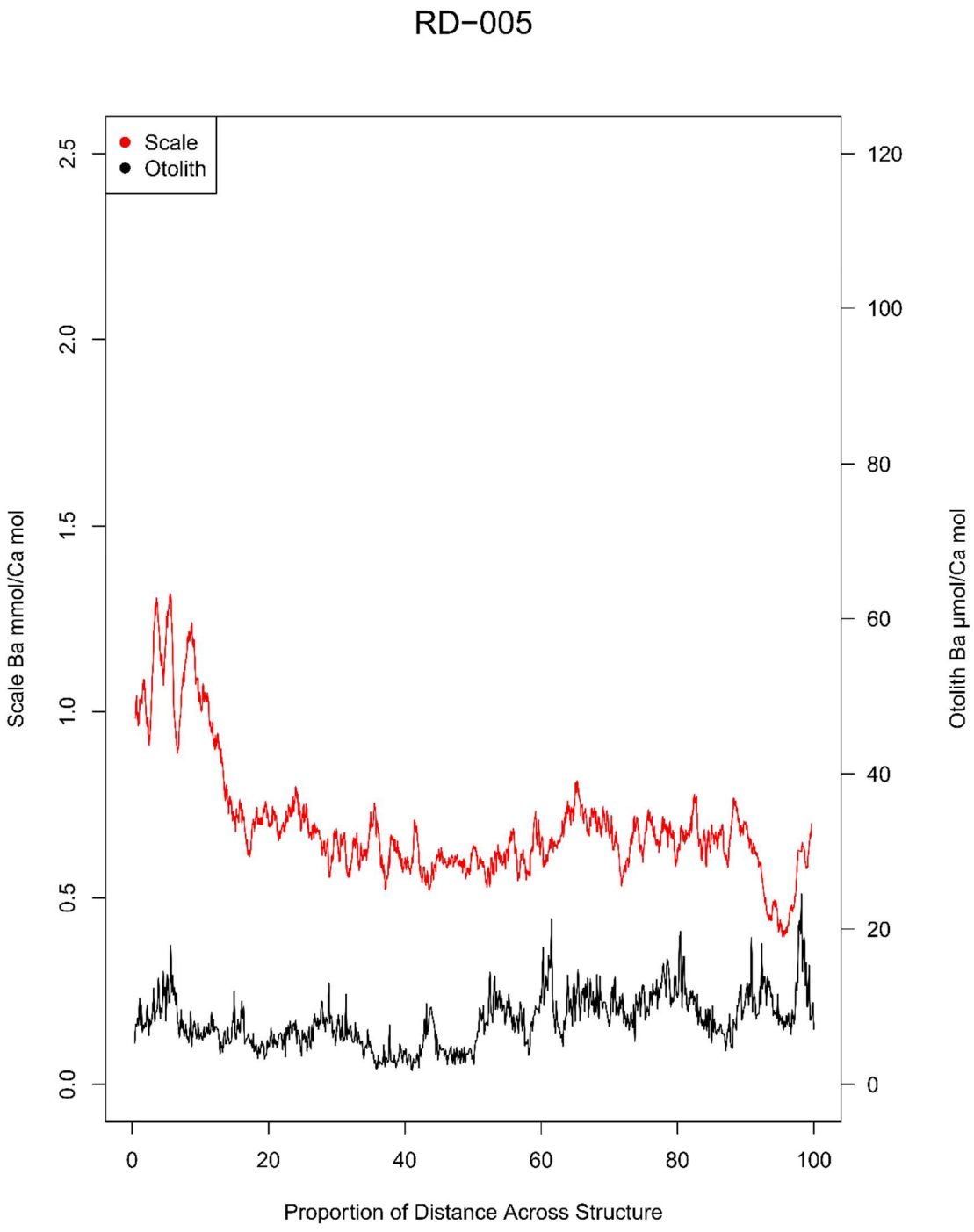
RD−005
Scale
Otolith
Scale Ba mmol/Ca mol
Otolith Ba µmol/Ca mol
Proportion of Distance Across Structure
0.0
0.5
1.0
1.5
2.0
2.5
0
20
40
60
80
100
120

RD-005

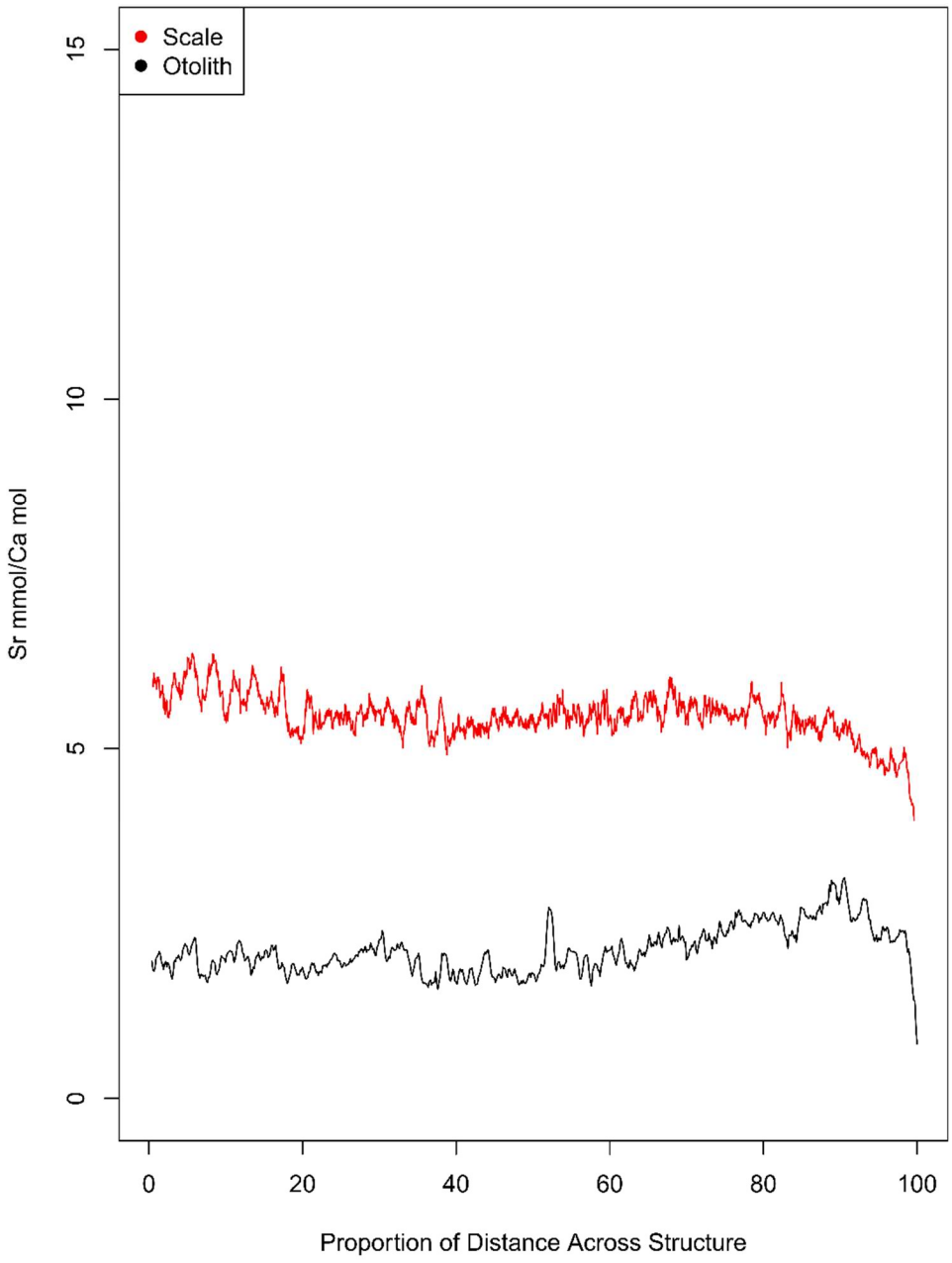
Scale
Otolith
Sr mmol/Ca mol
0
5
10
15
0
20
40
60
80
100
Proportion of Distance Across Structure

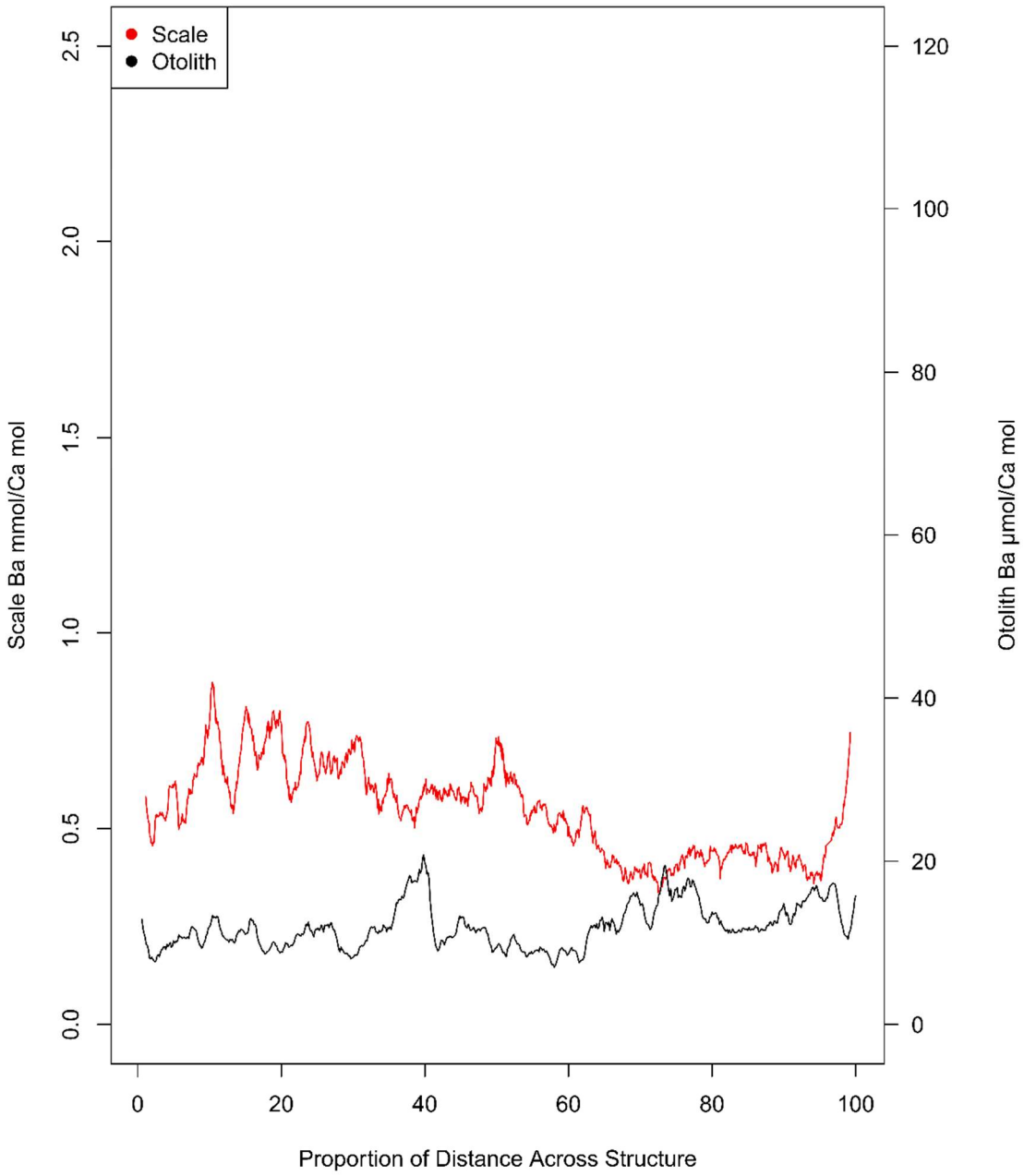
RD−015
Scale
Otolith
Scale Ba mmol/Ca mol
Otolith Ba µmol/Ca mol
Proportion of Distance Across Structure
0.0
0.5
1.0
1.5
2.0
2.5
0
20
40
60
80
100
120

RD-015

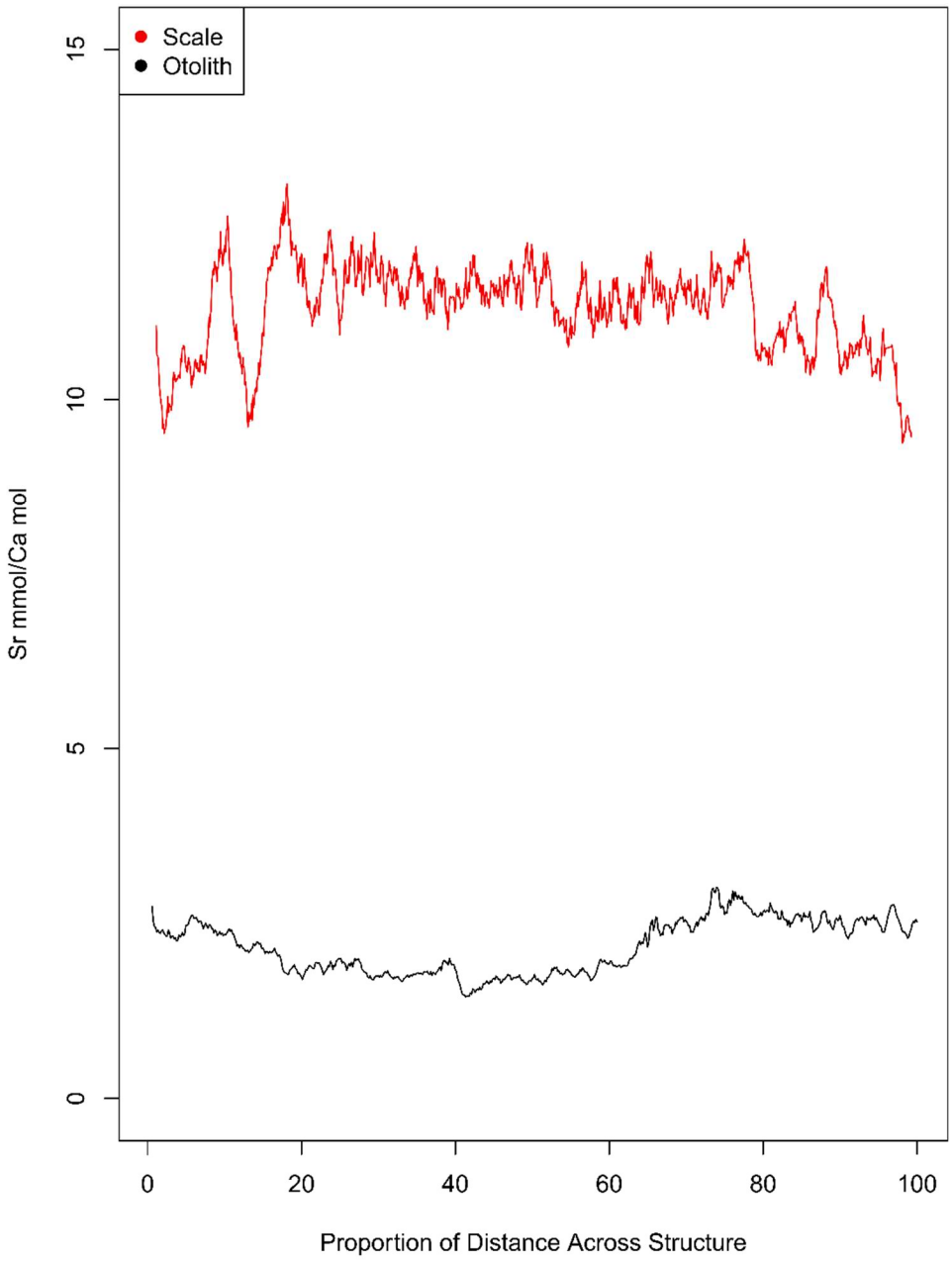
Scale
Otolith
Sr mmol/Ca mol
0
5
10
15
0
20
40
60
80
100
Proportion of Distance Across Structure

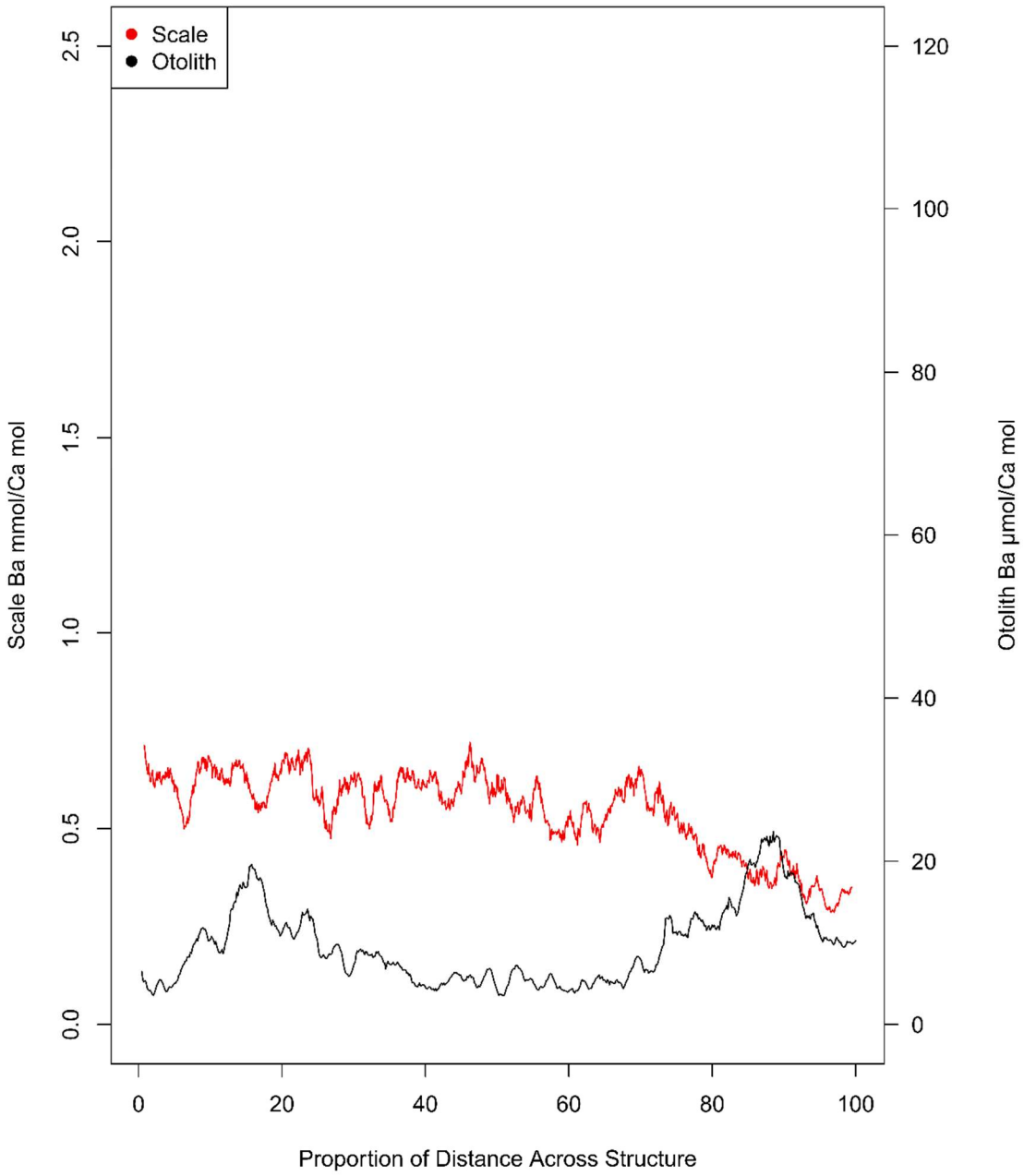
RD−016
Scale
Otolith
Scale Ba mmol/Ca mol
Otolith Ba µmol/Ca mol
Proportion of Distance Across Structure
0.0
0.5
1.0
1.5
2.0
2.5
0
20
40
60
80
100
120

RD-016

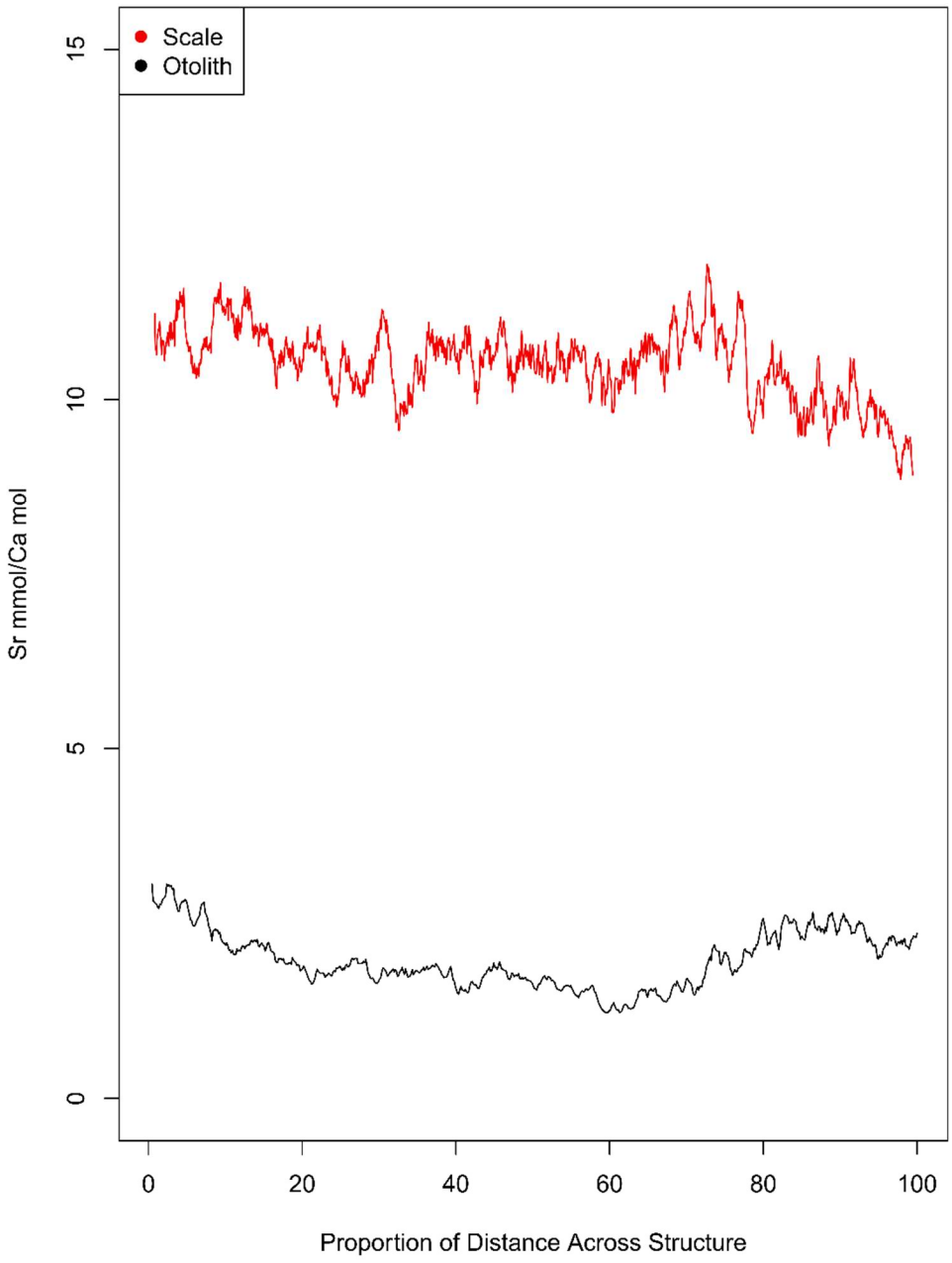
Scale
Otolith
Sr mmol/Ca mol
0
5
10
15
0
20
40
60
80
100
Proportion of Distance Across Structure

RD−017

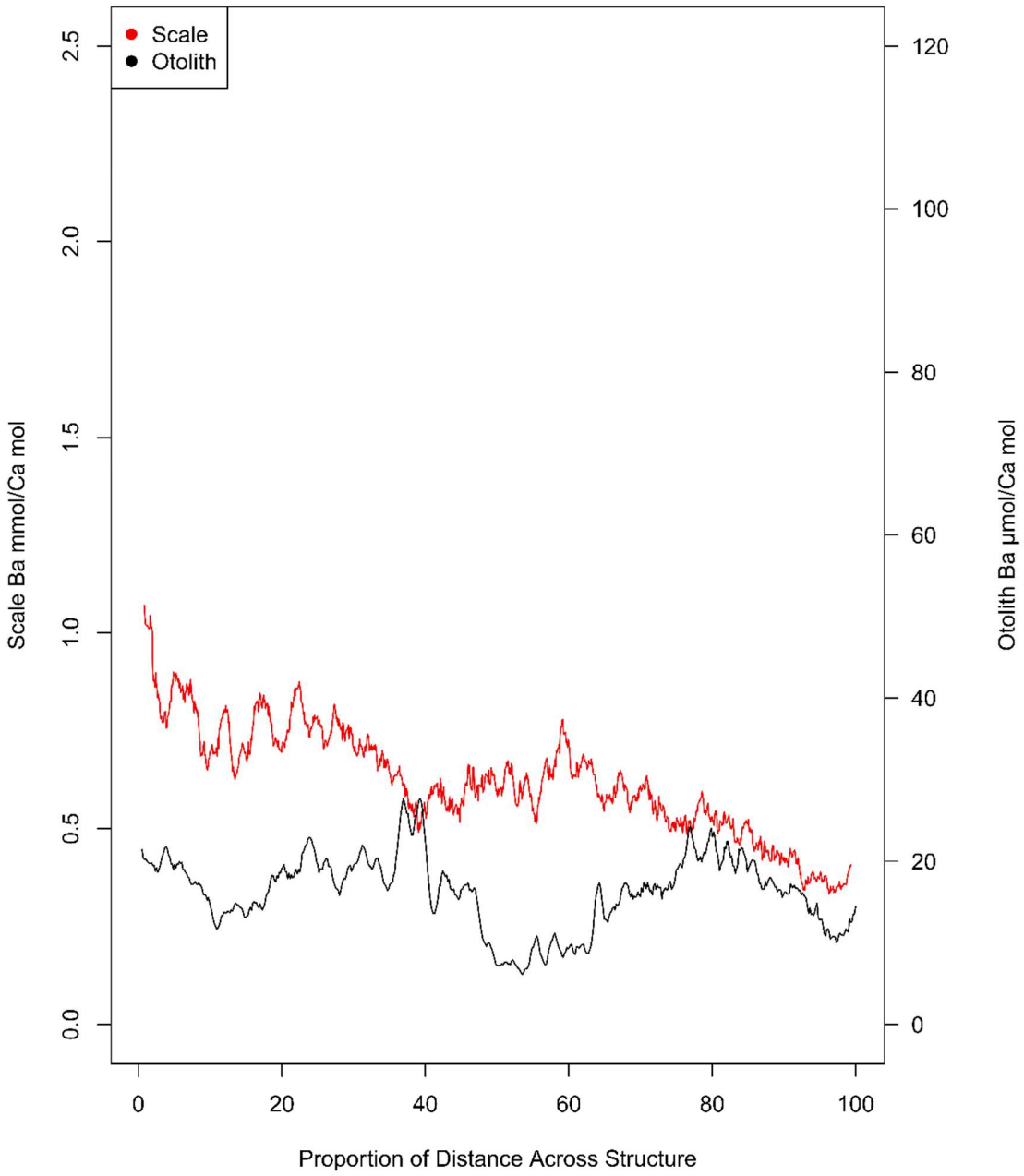
Scale
Otolith
Scale Ba mmol/Ca mol
Otolith Ba µmol/Ca mol
Proportion of Distance Across Structure
0.0
0.5
1.0
1.5
2.0
2.5
0
20
40
60
80
100
120

RD-017

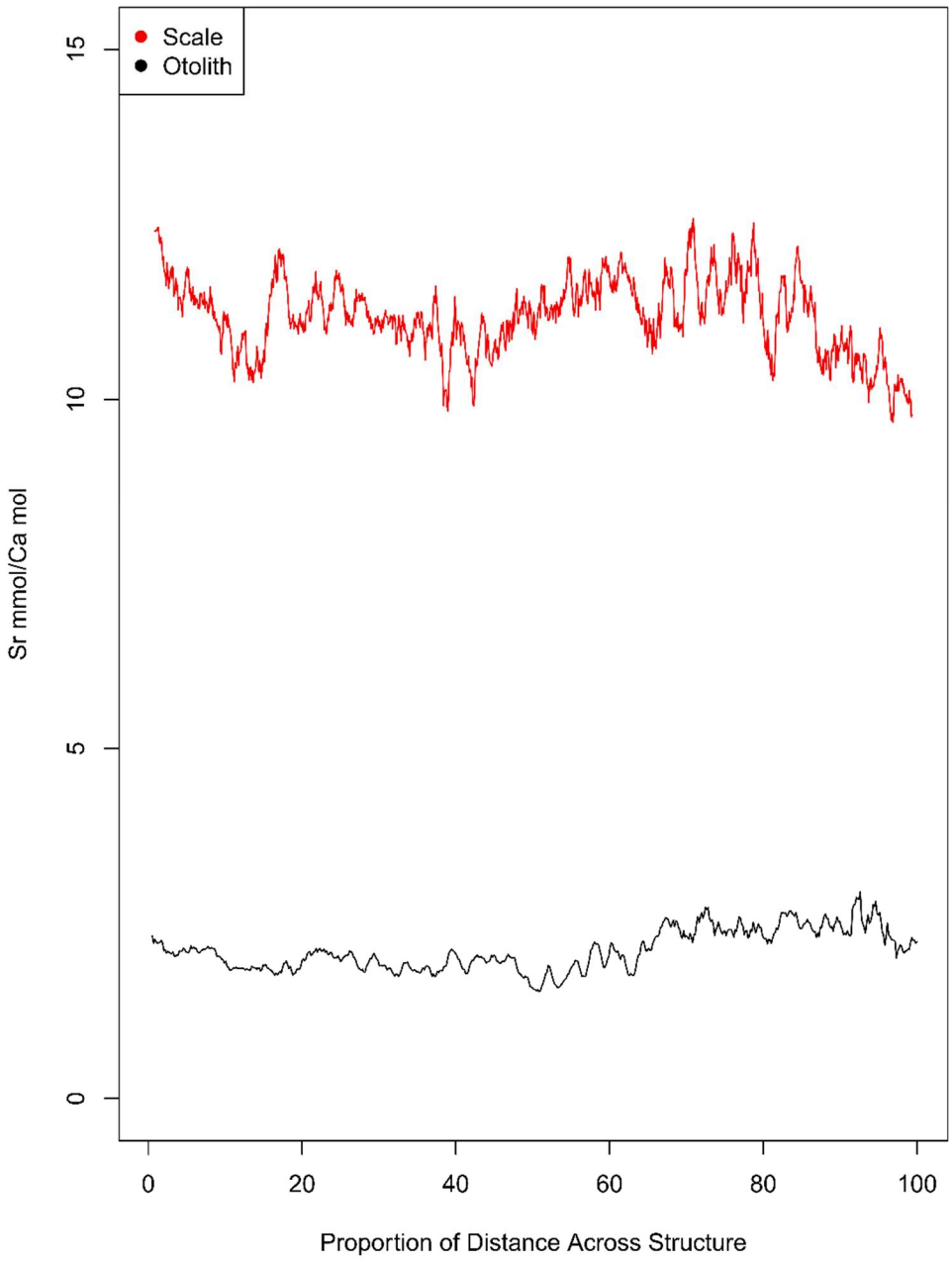
Scale
Otolith
Sr mmol/Ca mol
0
5
10
15
0
20
40
60
80
100
Proportion of Distance Across Structure

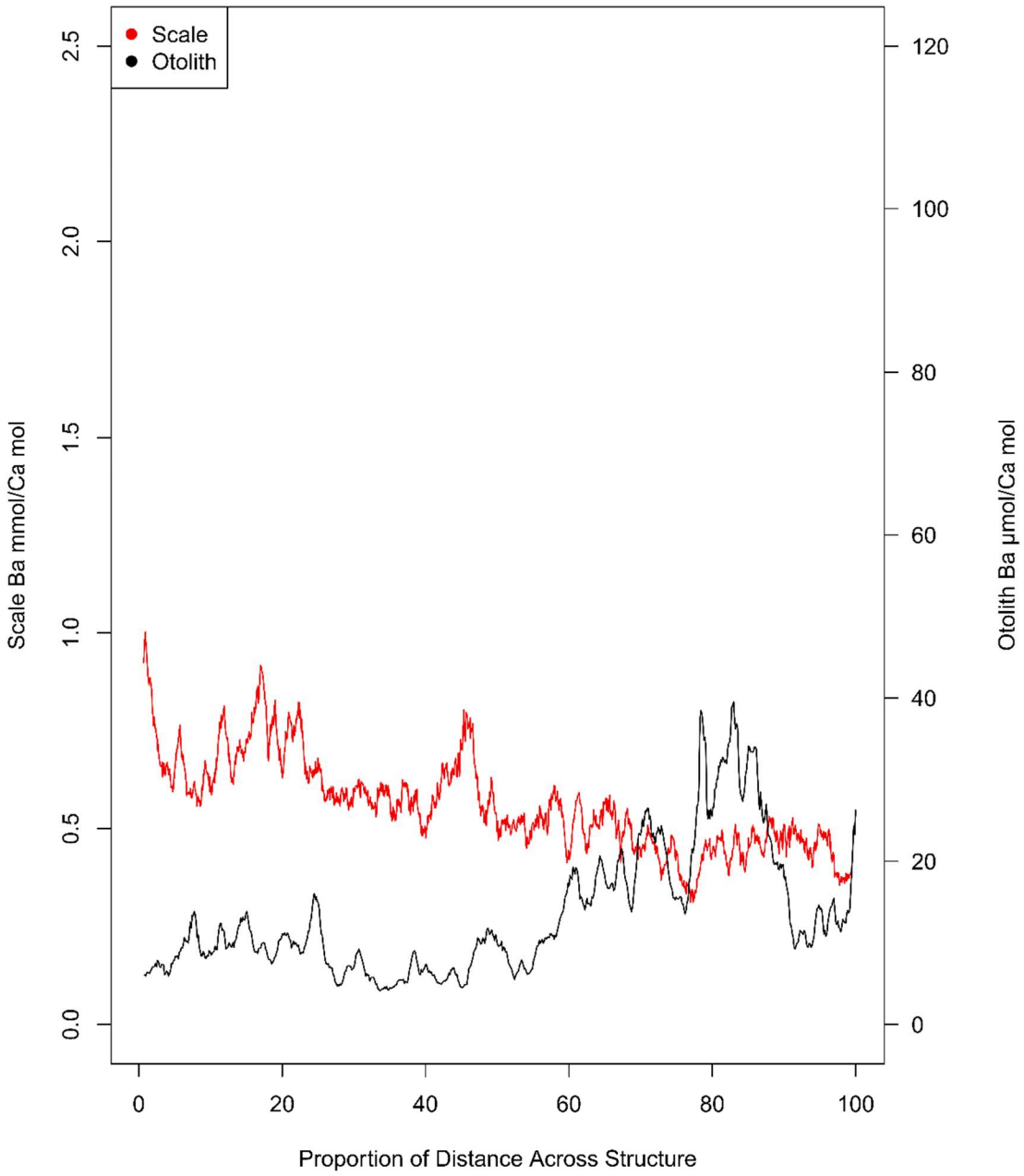
RD−018
Scale
Otolith
Scale Ba mmol/Ca mol
Otolith Ba µmol/Ca mol
Proportion of Distance Across Structure
0.0
0.5
1.0
1.5
2.0
2.5
0
20
40
60
80
100
120

RD-018

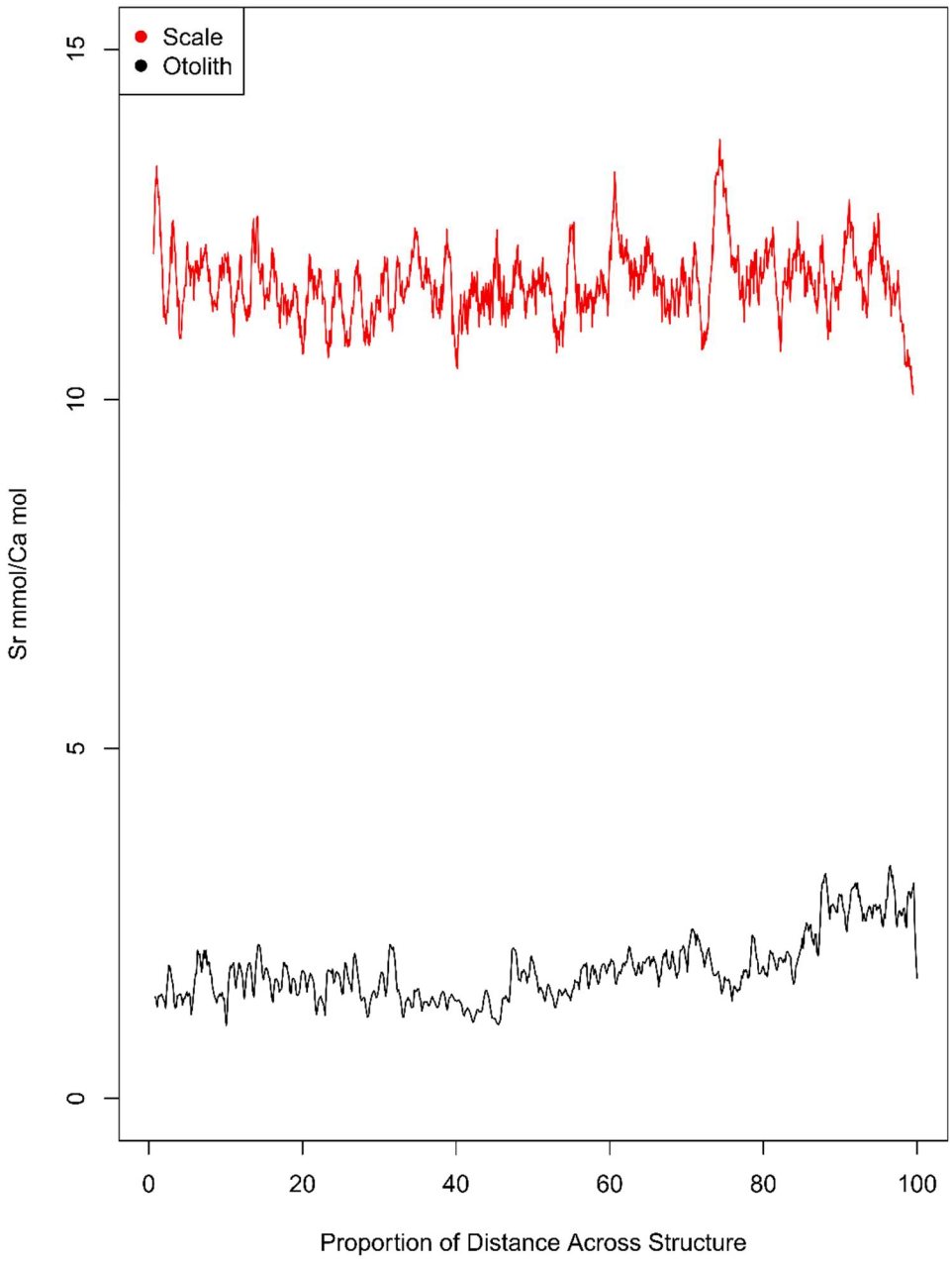
Scale
Otolith
Sr mmol/Ca mol
0
5
10
15
0
20
40
60
80
100
Proportion of Distance Across Structure

RD−019

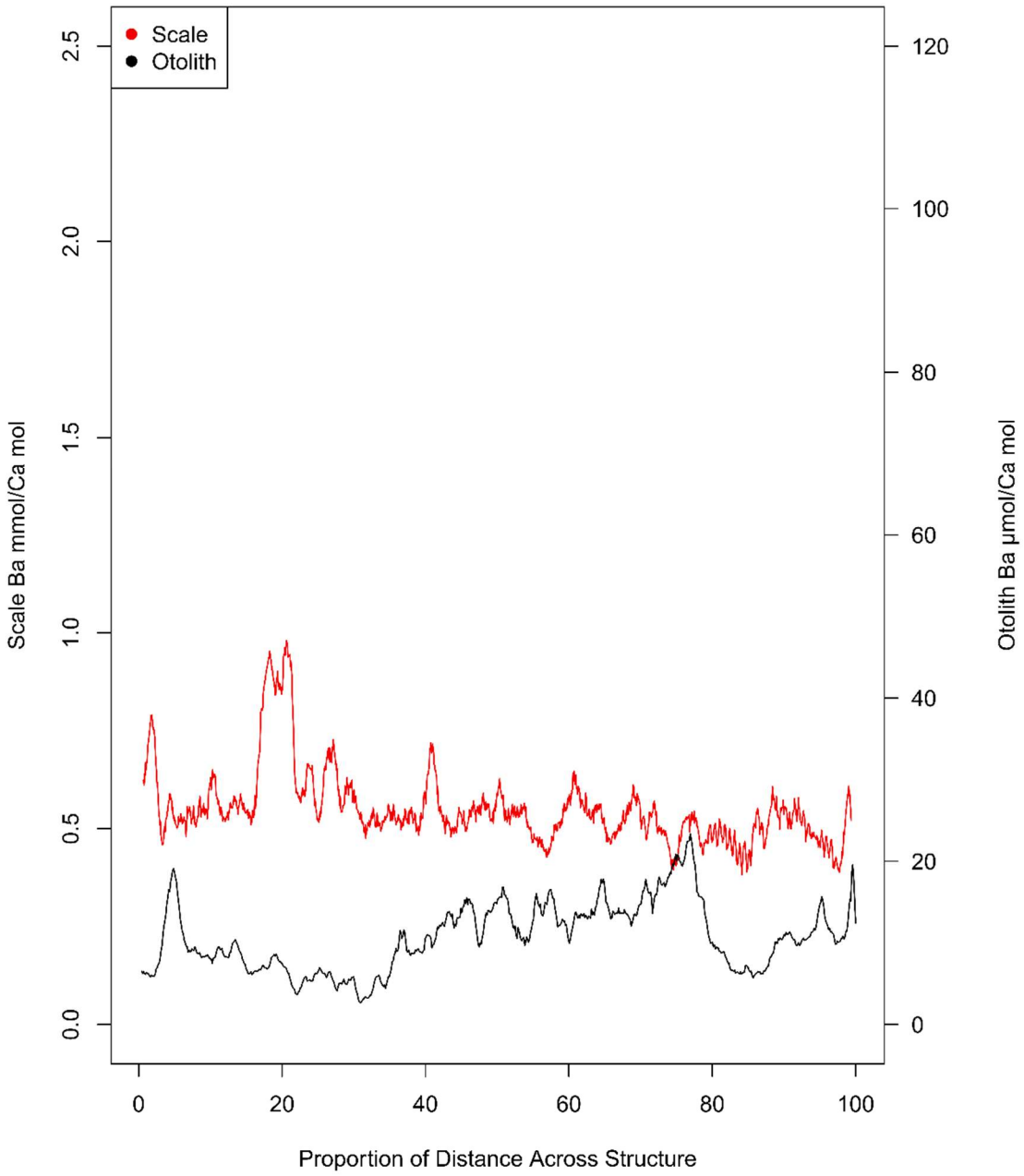
Scale
Otolith
Scale Ba mmol/Ca mol
Otolith Ba µmol/Ca mol
Proportion of Distance Across Structure
0.0
0.5
1.0
1.5
2.0
2.5
0
20
40
60
80
100
120

RD-019

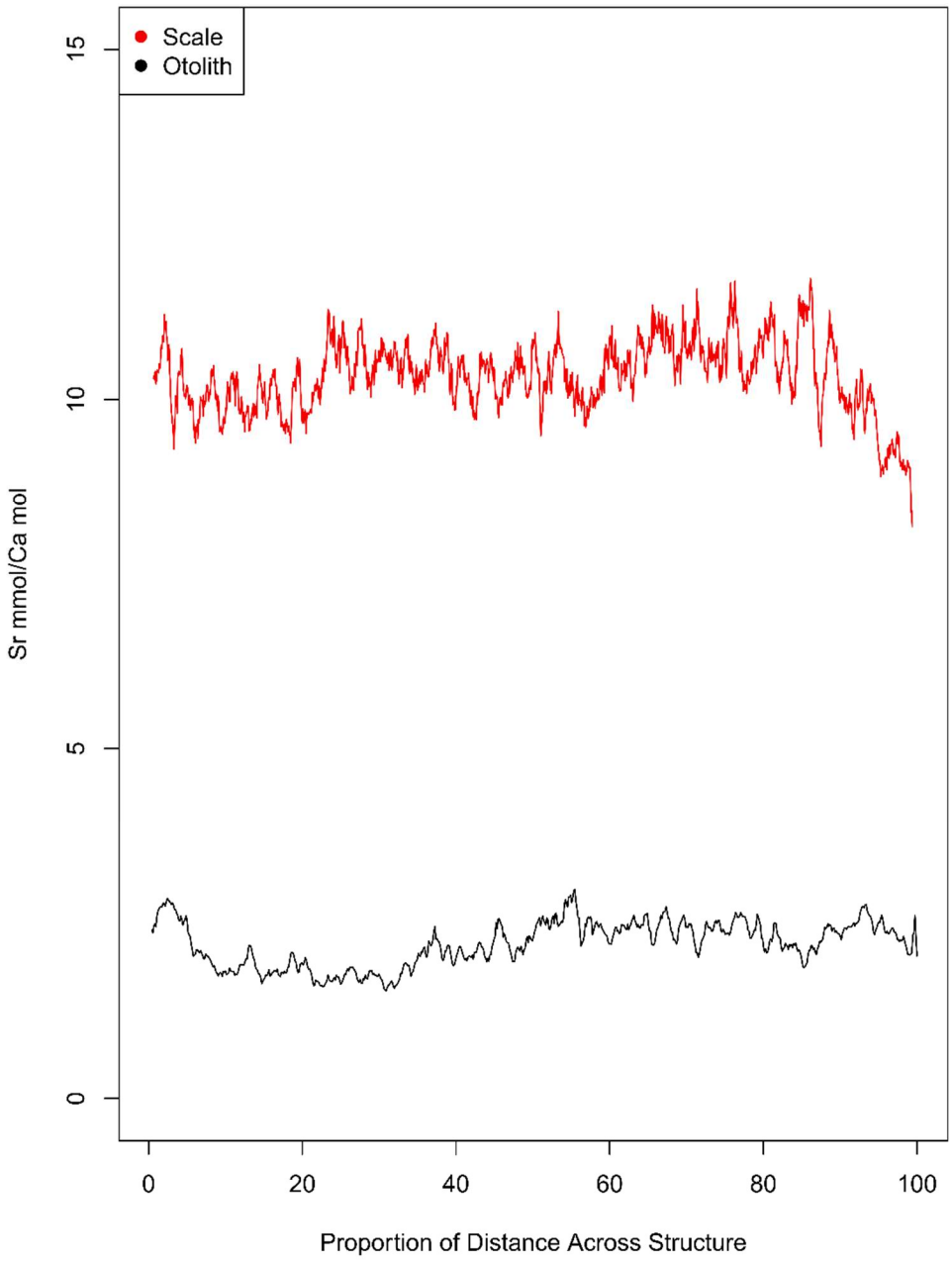
Scale
Otolith
Sr mmol/Ca mol
0
5
10
15
0
20
40
60
80
100
Proportion of Distance Across Structure

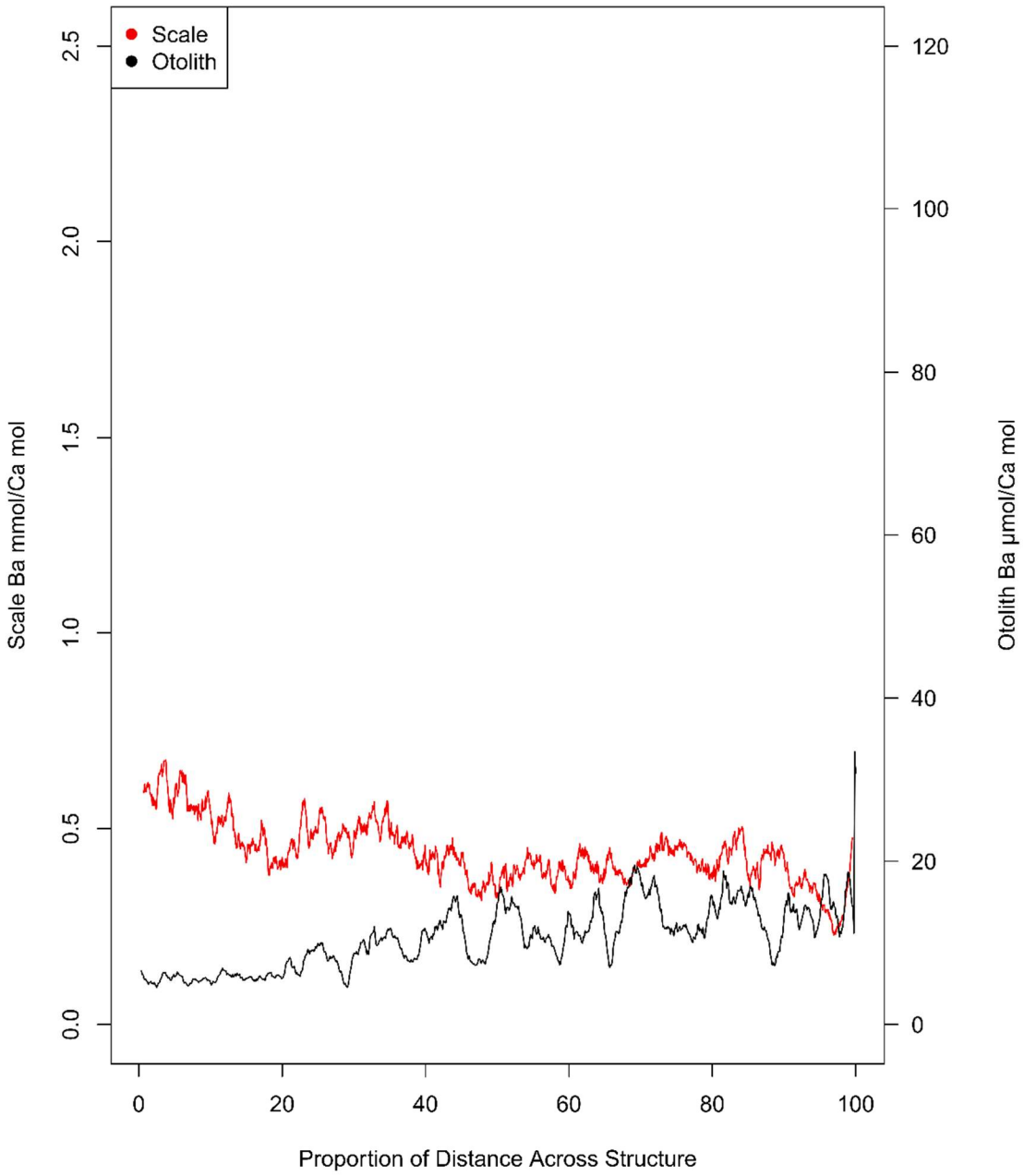
RD-020
Scale
Otolith
Scale Ba mmol/Ca mol
Otolith Ba µmol/Ca mol
Proportion of Distance Across Structure
0.0
0.5
1.0
1.5
2.0
2.5
0
20
40
60
80
100
120

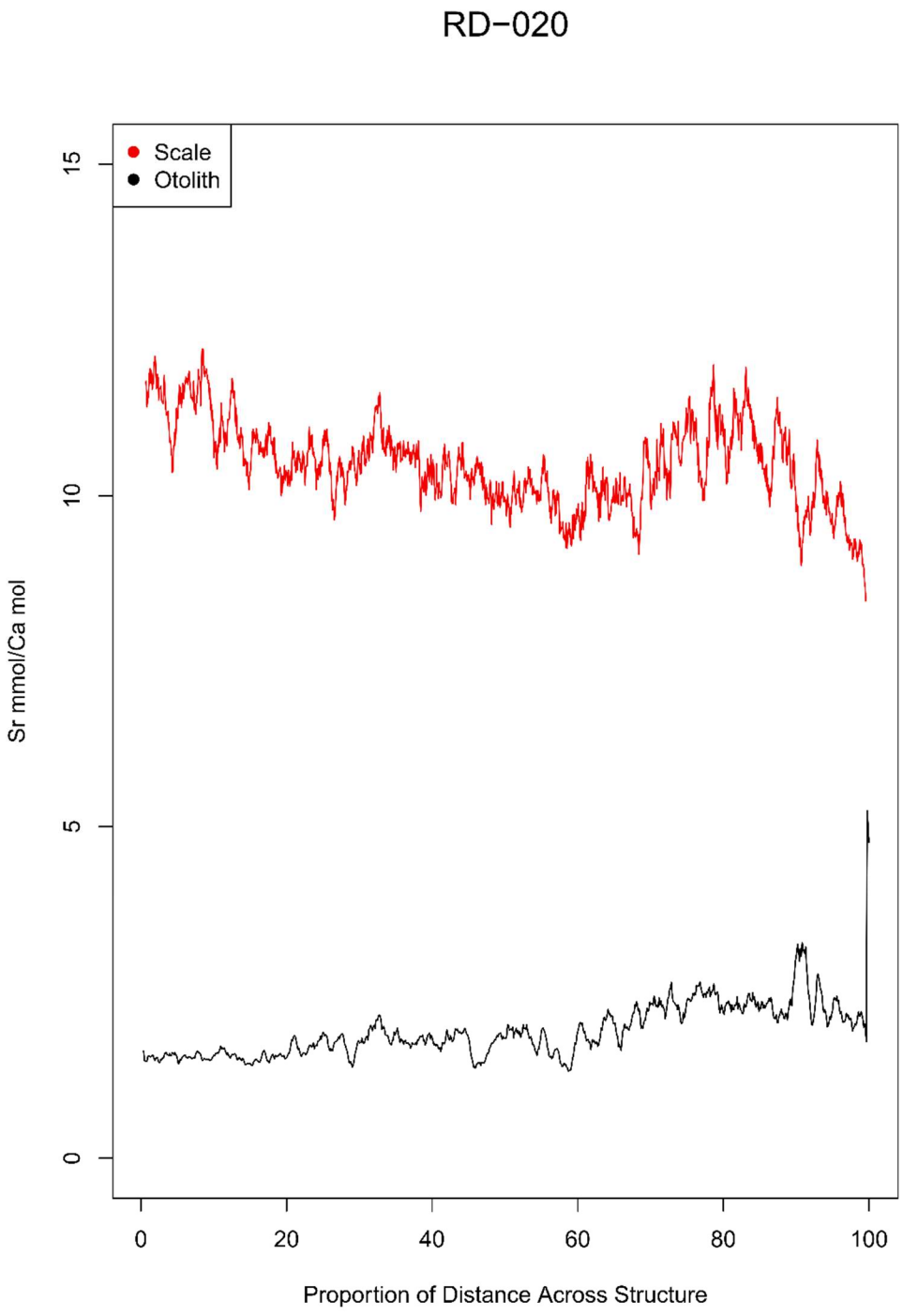
RD-020
Scale
Otolith
Sr mmol/Ca mol
0
5
10
15
0
20
40
60
80
100
Proportion of Distance Across Structure

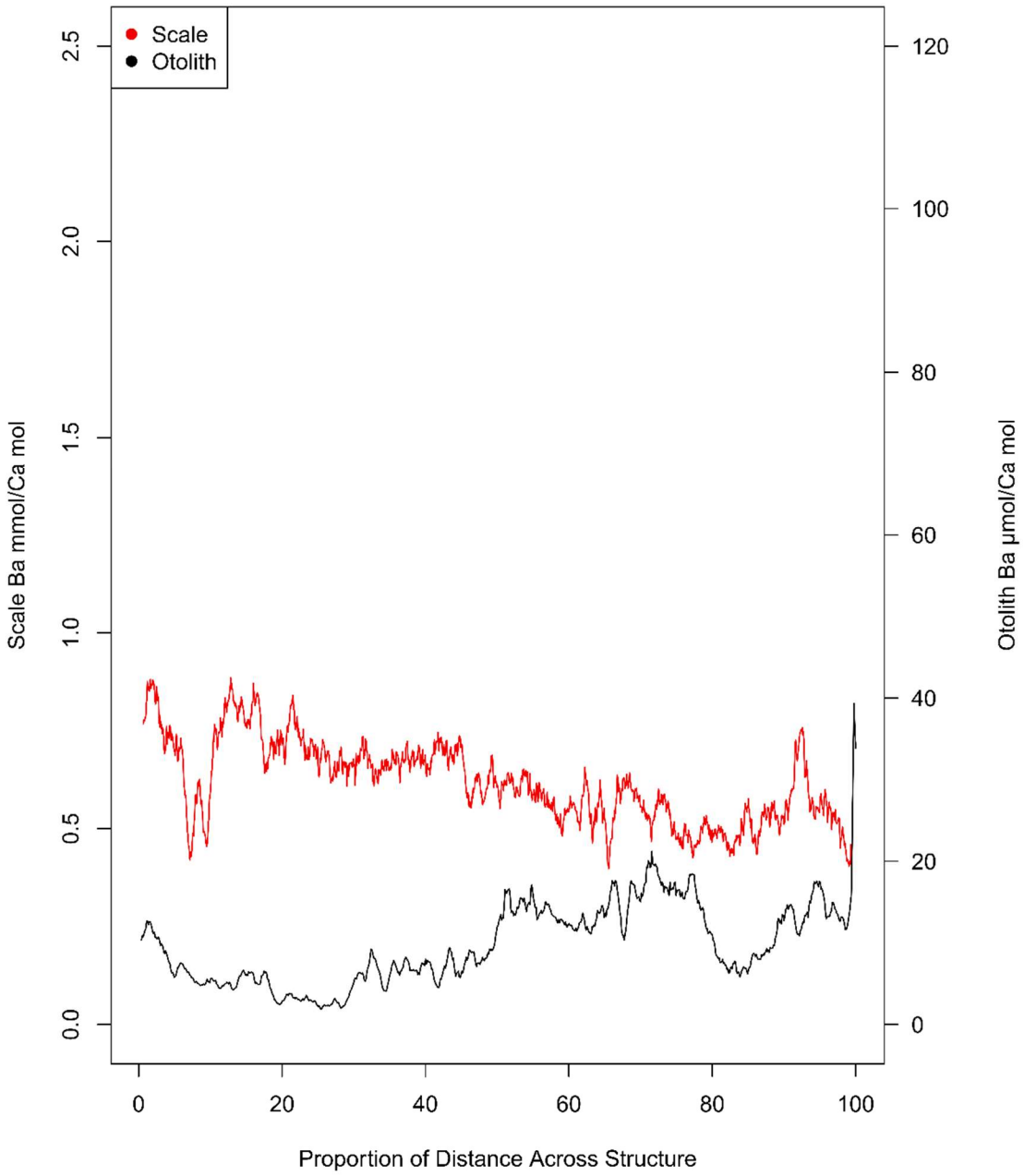
RD−021
Scale
Otolith
Scale Ba mmol/Ca mol
Otolith Ba µmol/Ca mol
Proportion of Distance Across Structure
0.0
0.5
1.0
1.5
2.0
2.5
0
20
40
60
80
100
120

RD-021

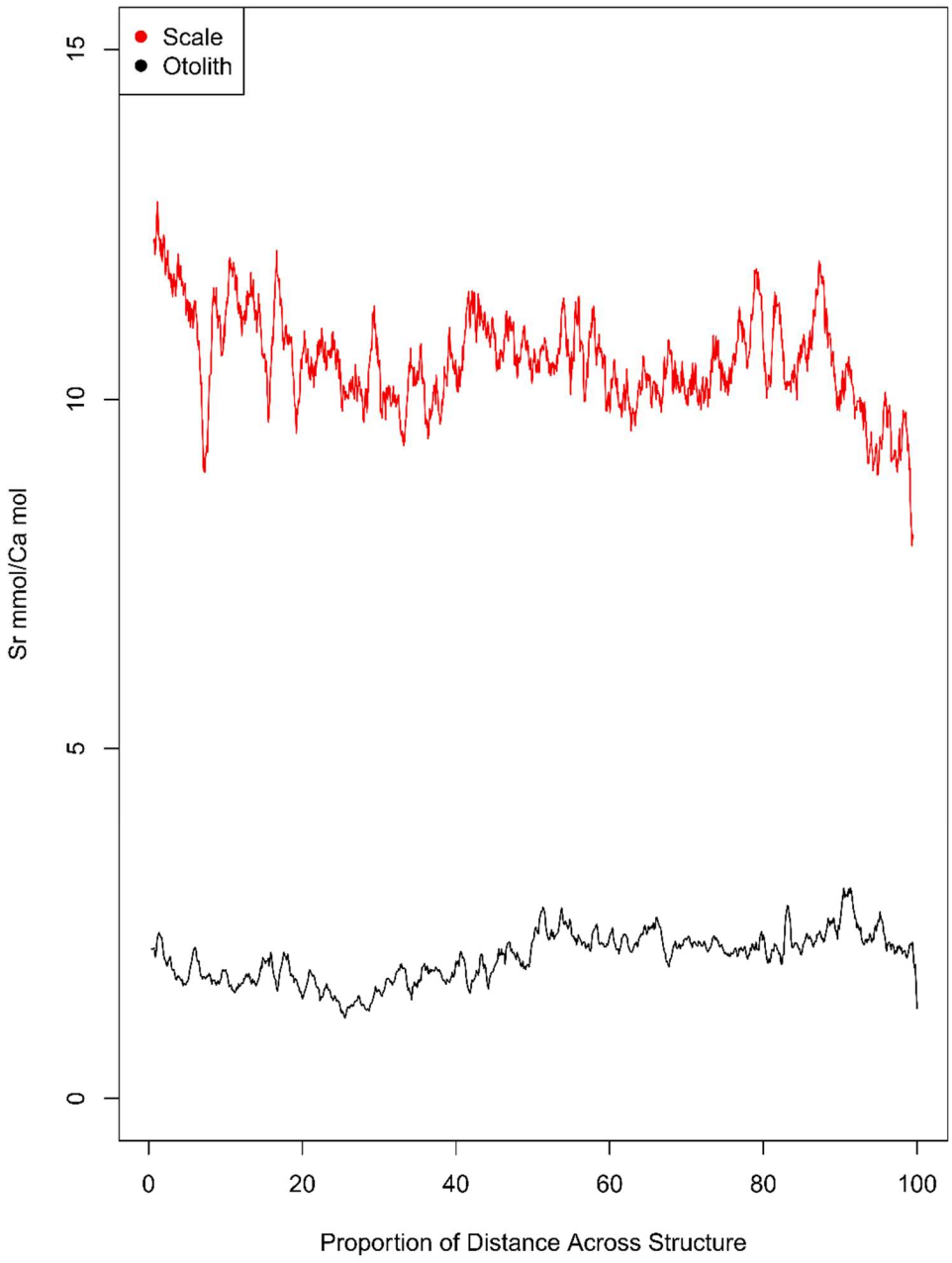
Scale
Otolith
Sr mmol/Ca mol
0
5
10
15
0
20
40
60
80
100
Proportion of Distance Across Structure

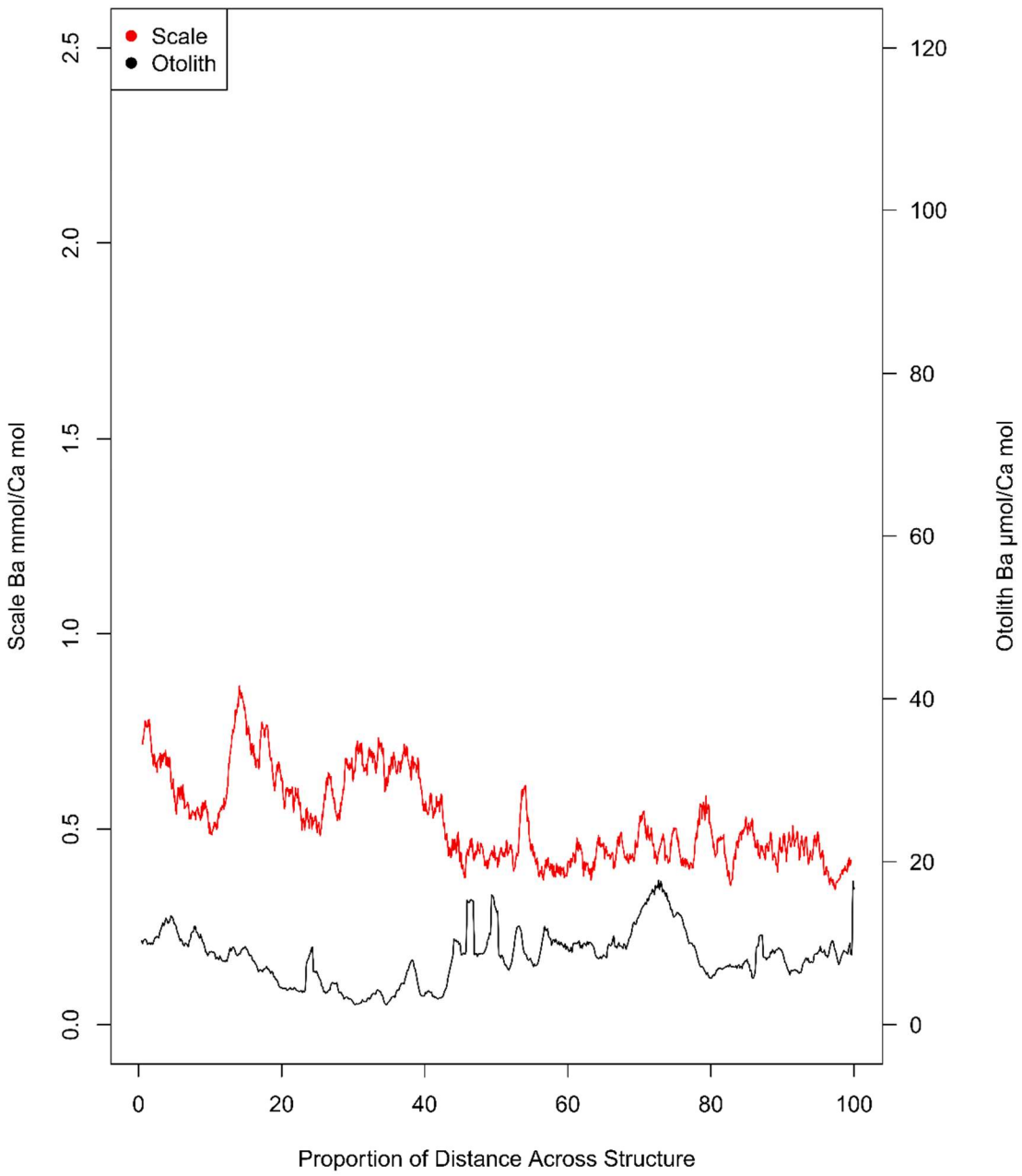
RD−022
Scale
Otolith
Scale Ba mmol/Ca mol
Otolith Ba µmol/Ca mol
Proportion of Distance Across Structure
0.0
0.5
1.0
1.5
2.0
2.5
0
20
40
60
80
100
120

RD-022

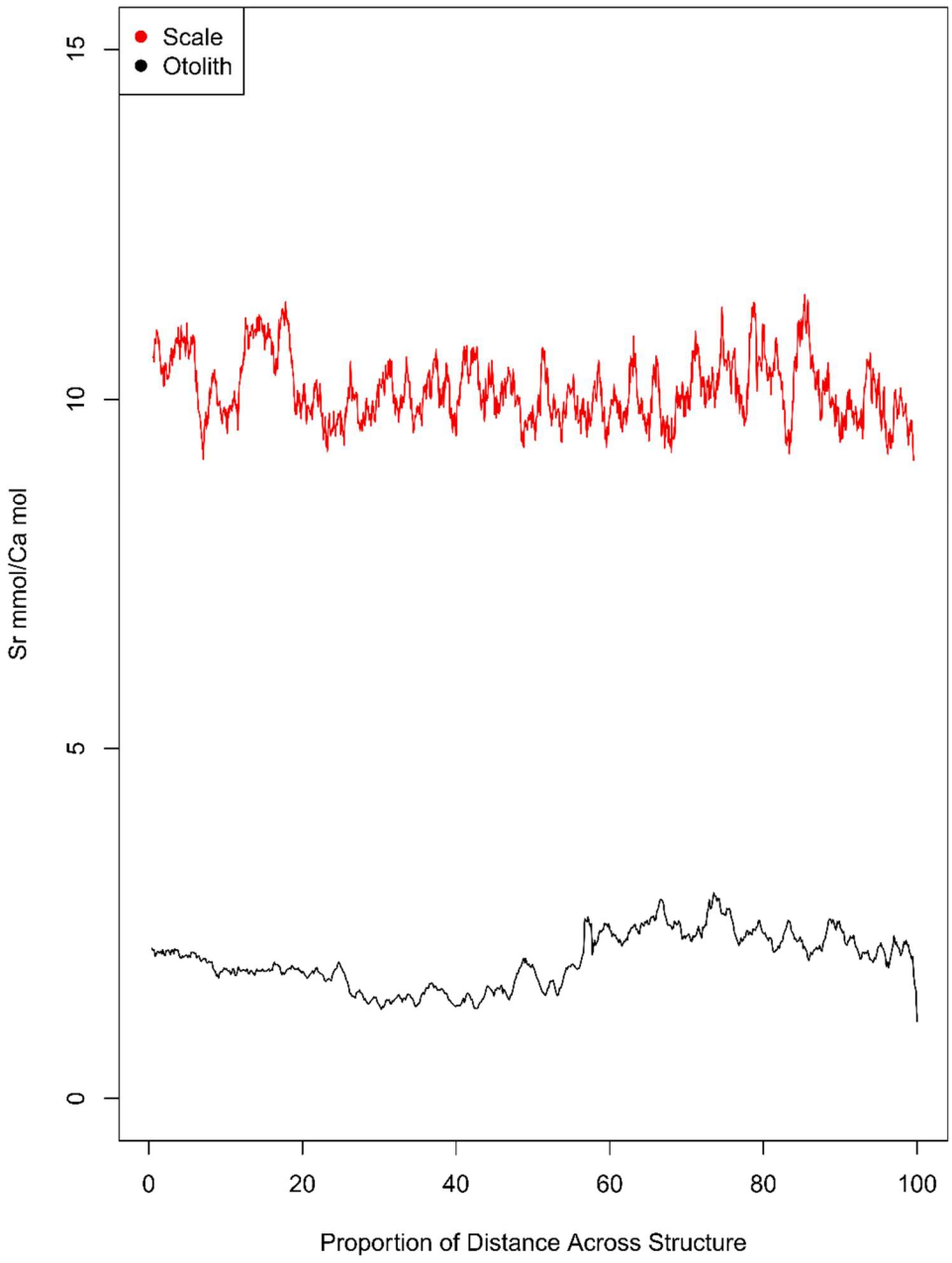
Scale
Otolith
15
10
5
0
Sr mmol/Ca mol
0
20
40
60
80
100
Proportion of Distance Across Structure

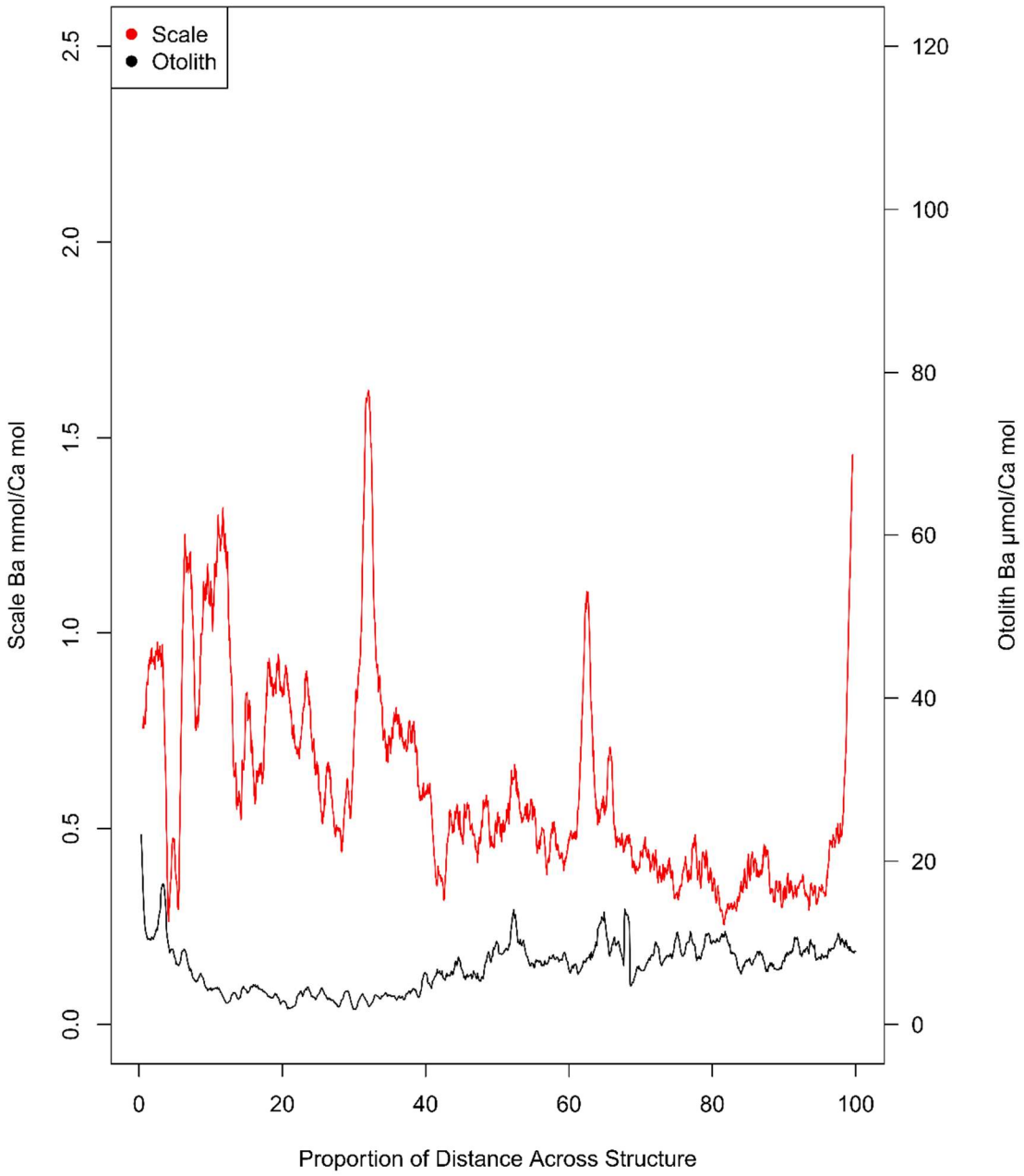
RD−023
Scale
Otolith
Scale Ba mmol/Ca mol
Otolith Ba µmol/Ca mol
Proportion of Distance Across Structure
0.0
0.5
1.0
1.5
2.0
2.5
0
20
40
60
80
100
120

RD-023

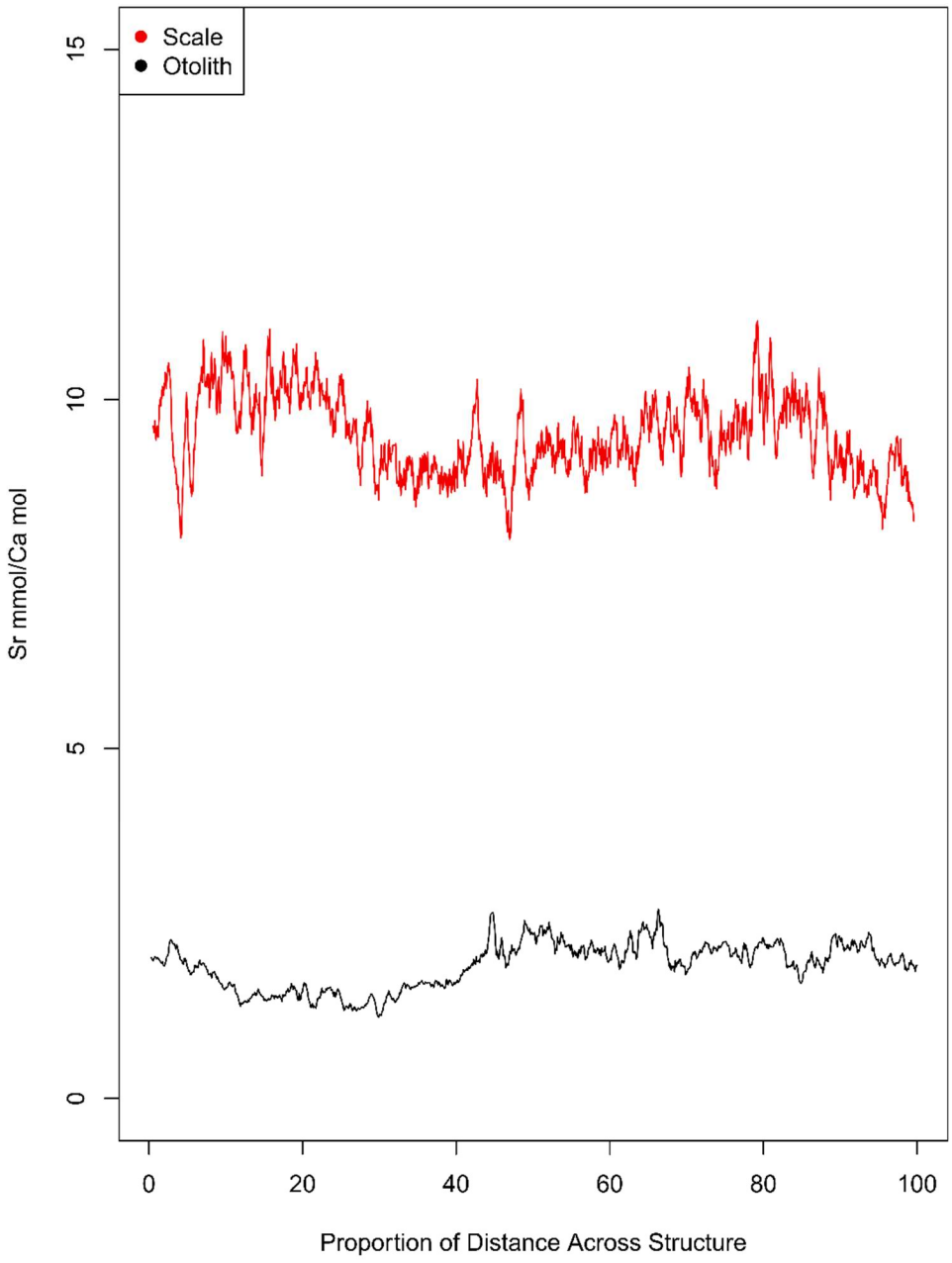
Scale
Otolith
Sr mmol/Ca mol
0
5
10
15
0
20
40
60
80
100
Proportion of Distance Across Structure

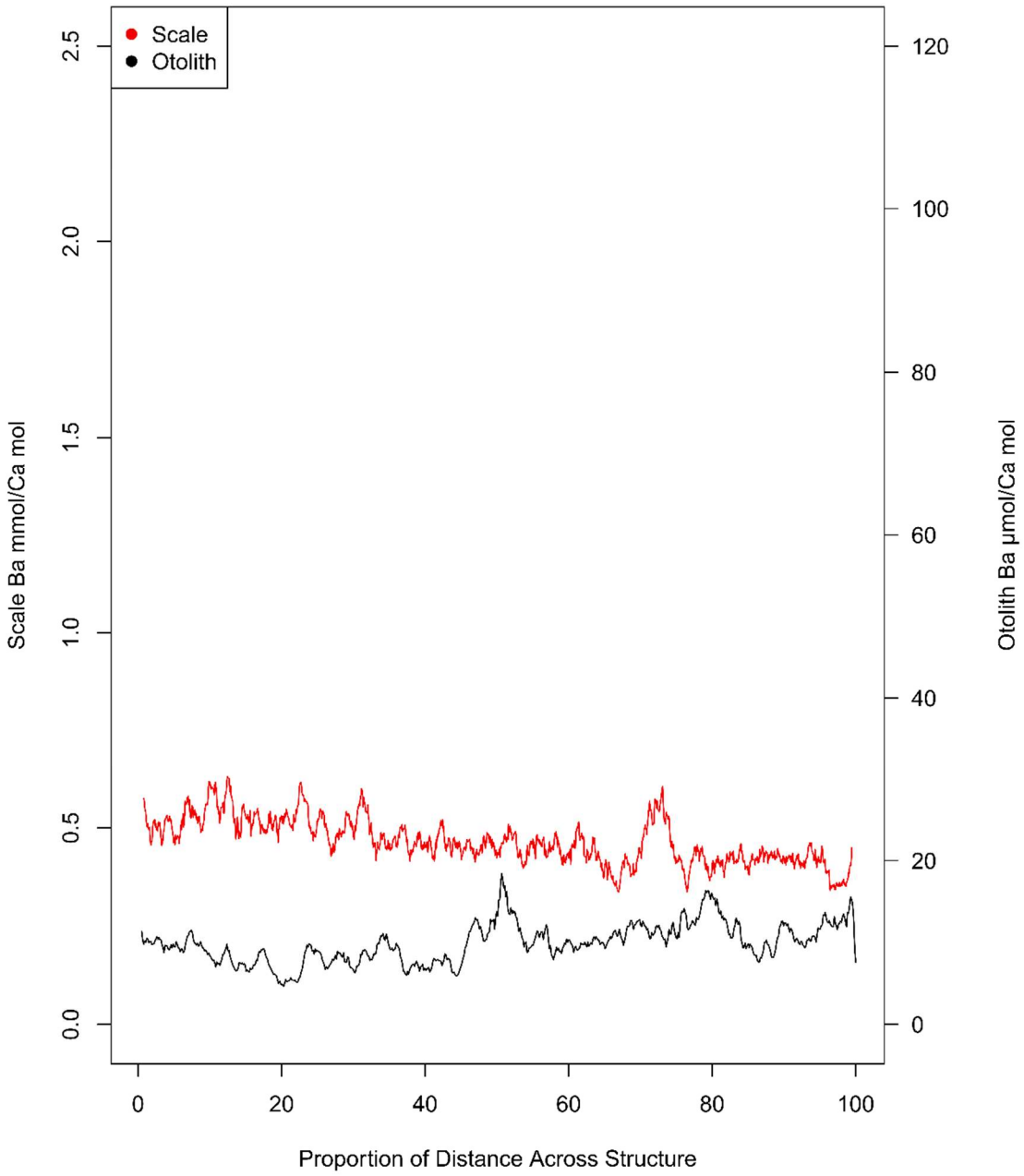
RD−024
Scale
Otolith
Scale Ba mmol/Ca mol
Otolith Ba µmol/Ca mol
Proportion of Distance Across Structure
0.0
0.5
1.0
1.5
2.0
2.5
0
20
40
60
80
100
120

RD-024

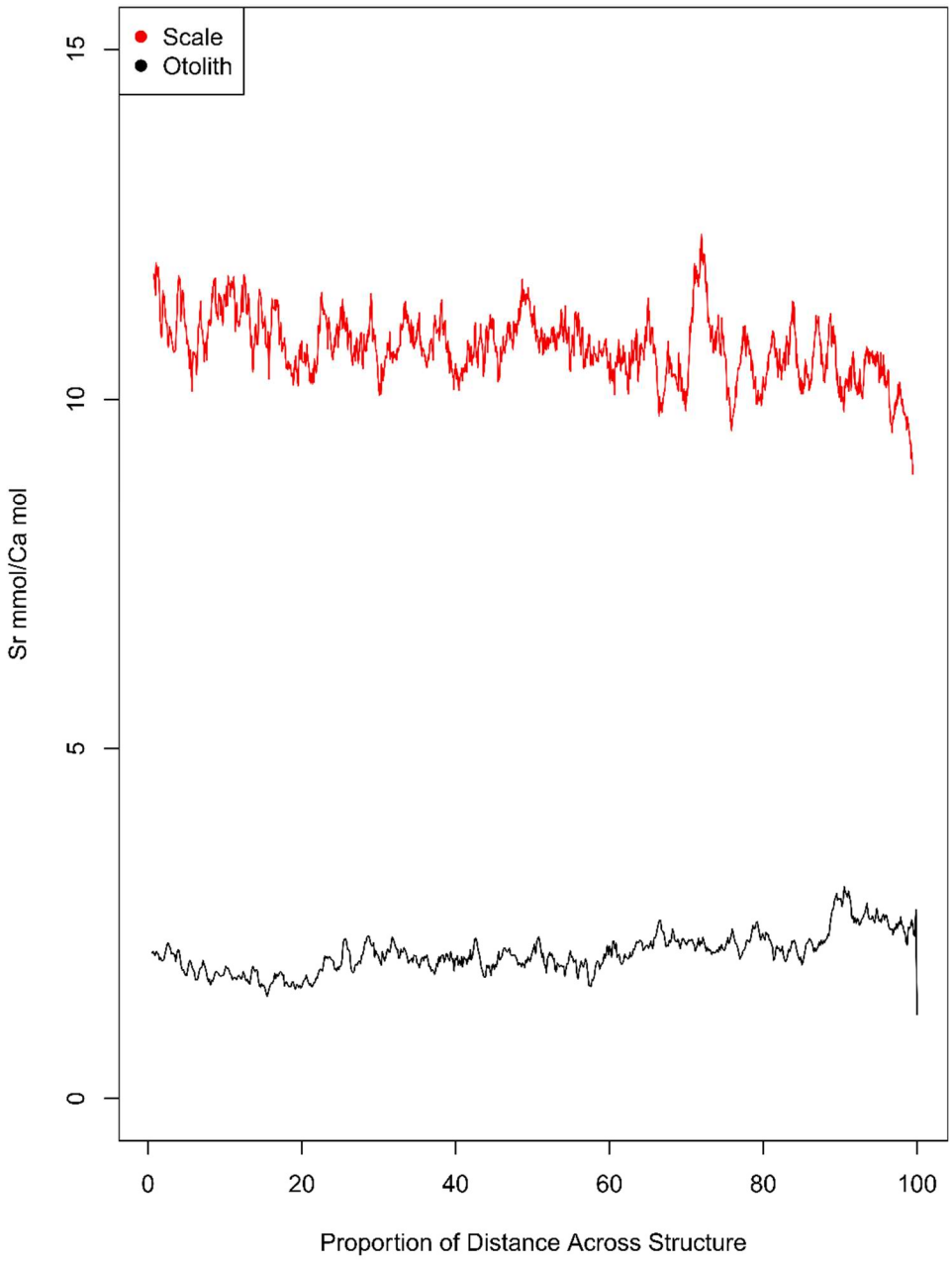
Scale
Otolith
Sr mmol/Ca mol
0
5
10
15
0
20
40
60
80
100
Proportion of Distance Across Structure

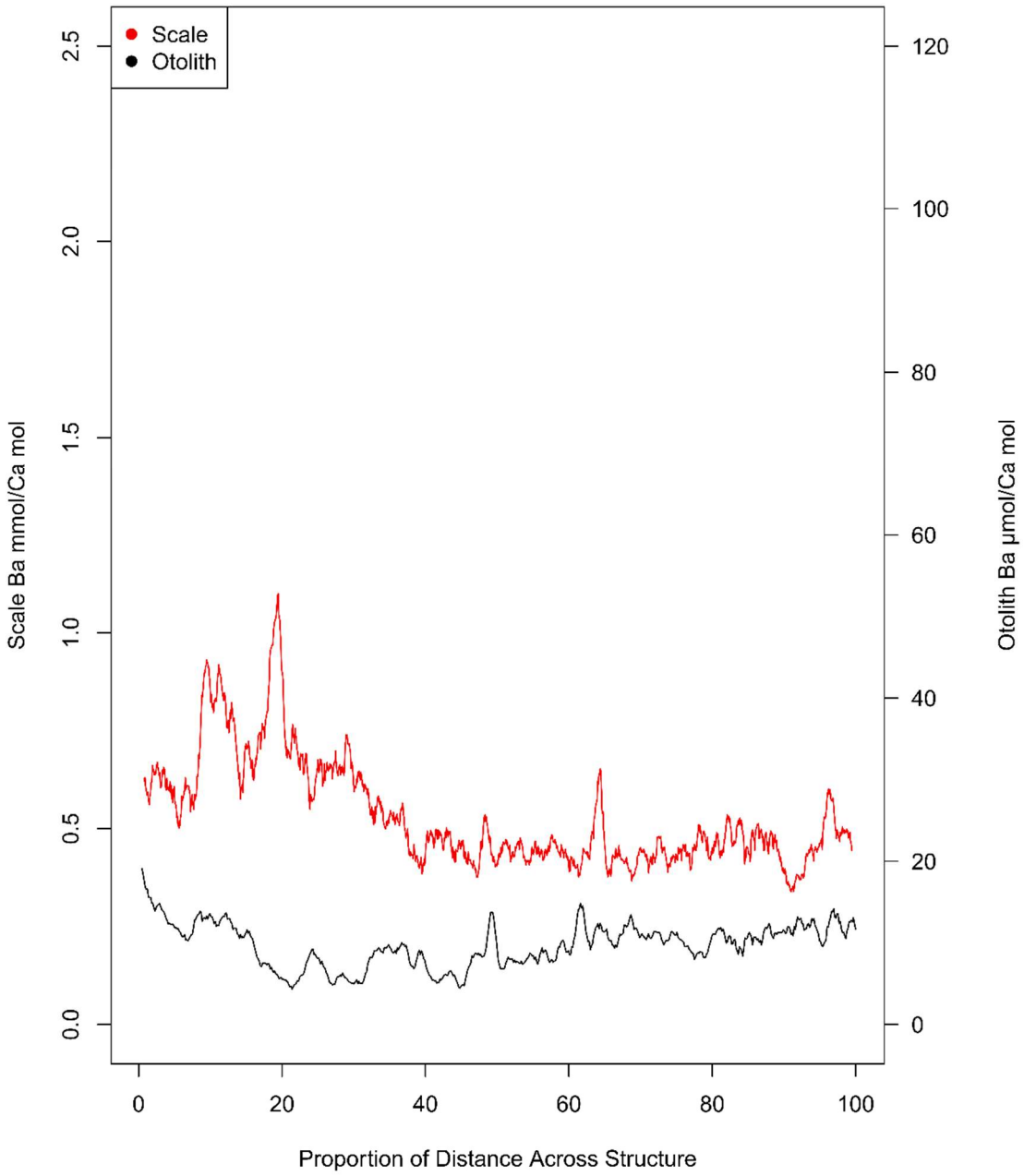
RD−025
Scale
Otolith
Scale Ba mmol/Ca mol
Otolith Ba µmol/Ca mol
Proportion of Distance Across Structure
0.0
0.5
1.0
1.5
2.0
2.5
0
20
40
60
80
100
120

RD-025

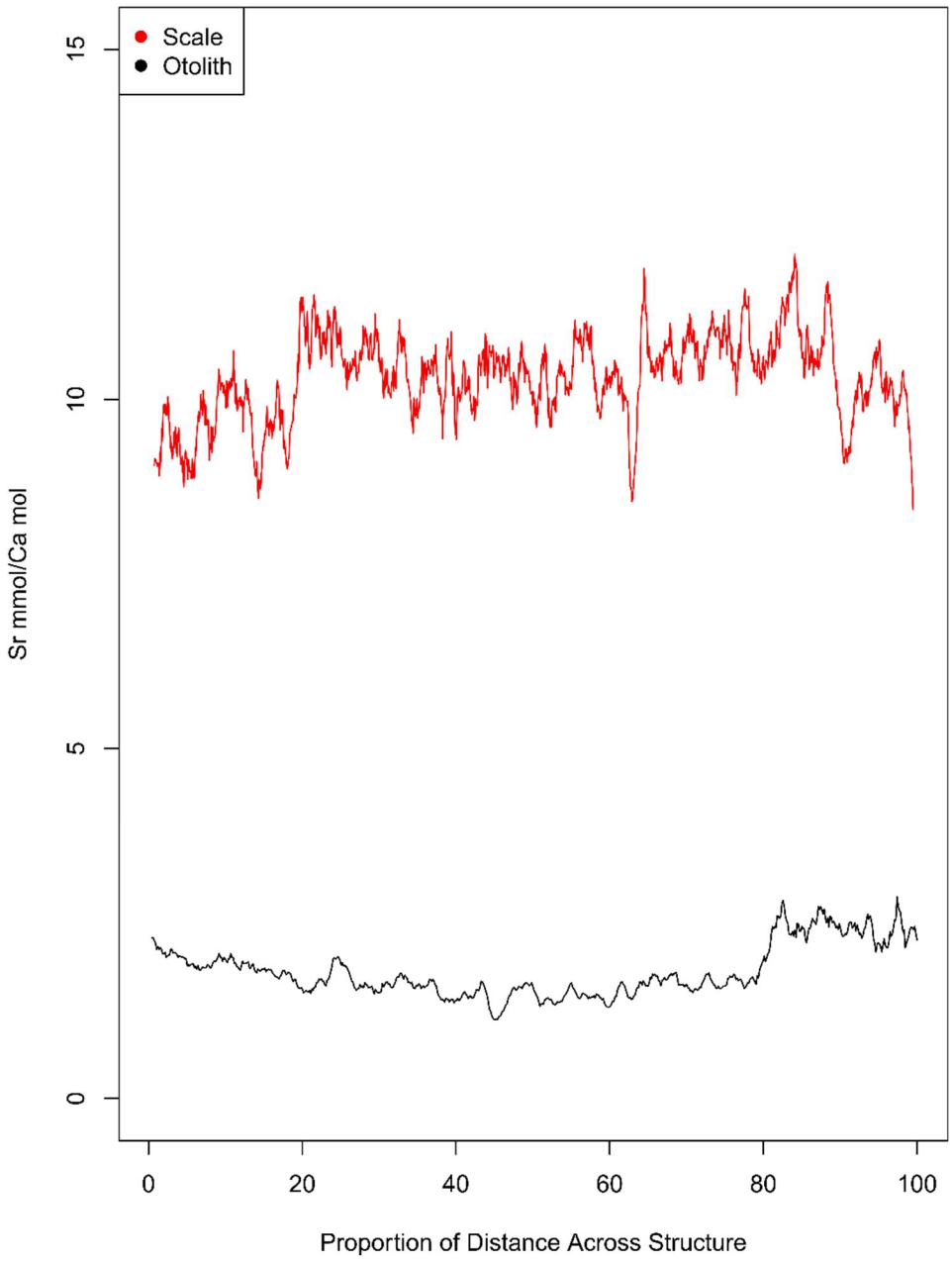
Scale
Otolith
Sr mmol/Ca mol
0
5
10
15
0
20
40
60
80
100
Proportion of Distance Across Structure

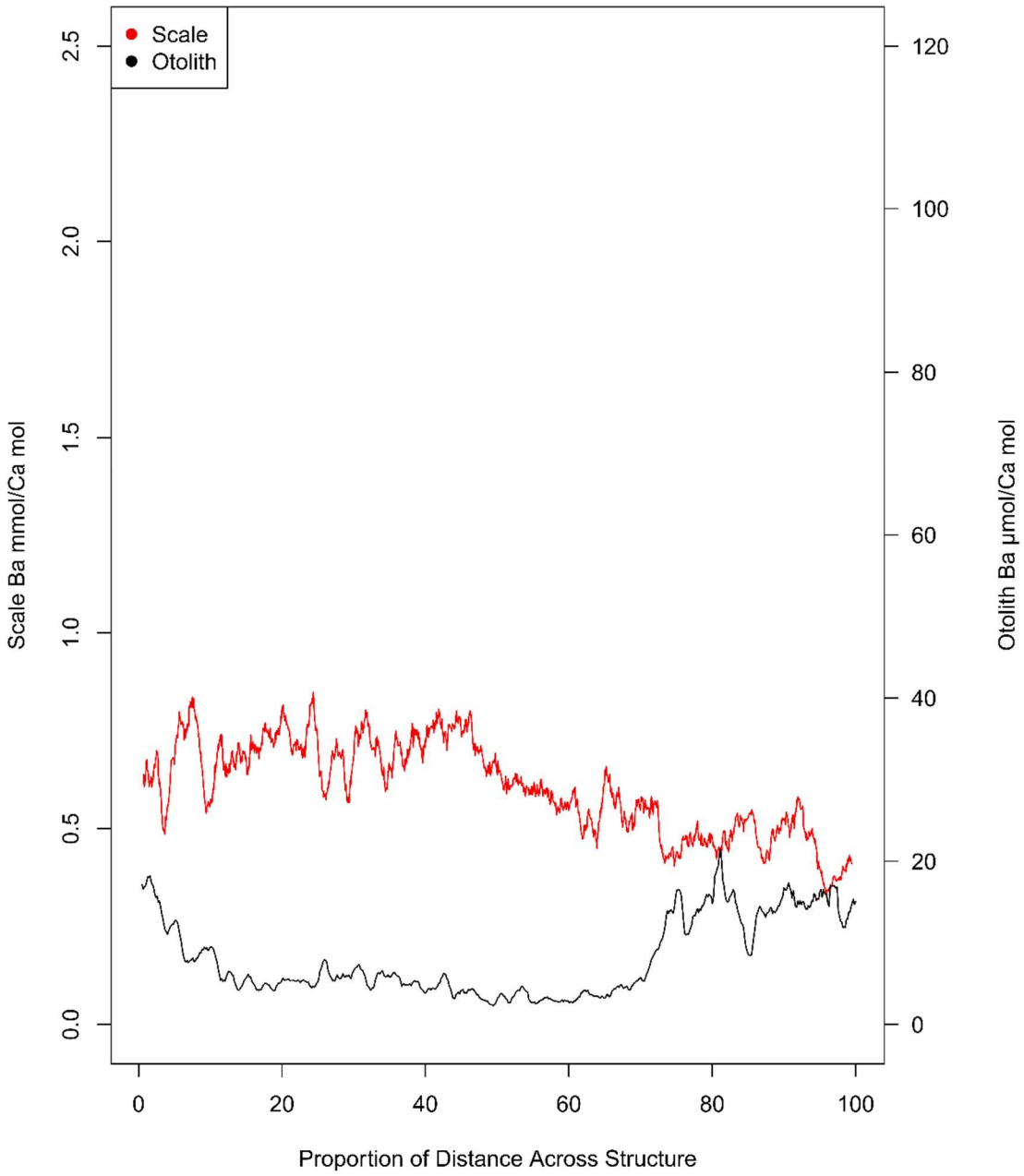
RD−026
Scale
Otolith
Scale Ba mmol/Ca mol
Otolith Ba µmol/Ca mol
Proportion of Distance Across Structure
0.0
0.5
1.0
1.5
2.0
2.5
0
20
40
60
80
100
120

RD-026

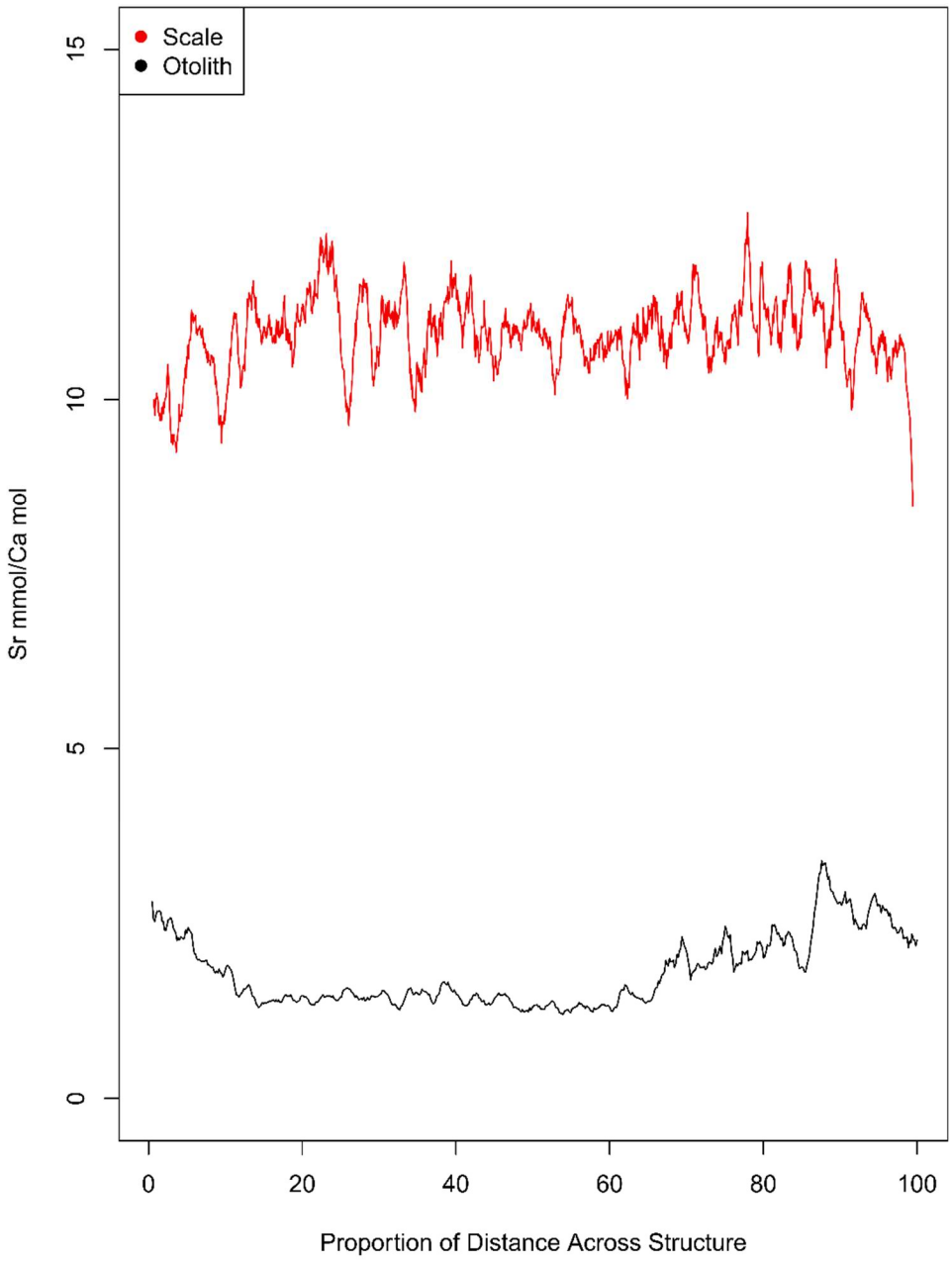
Scale
Otolith
Sr mmol/Ca mol
0
5
10
15
0
20
40
60
80
100
Proportion of Distance Across Structure

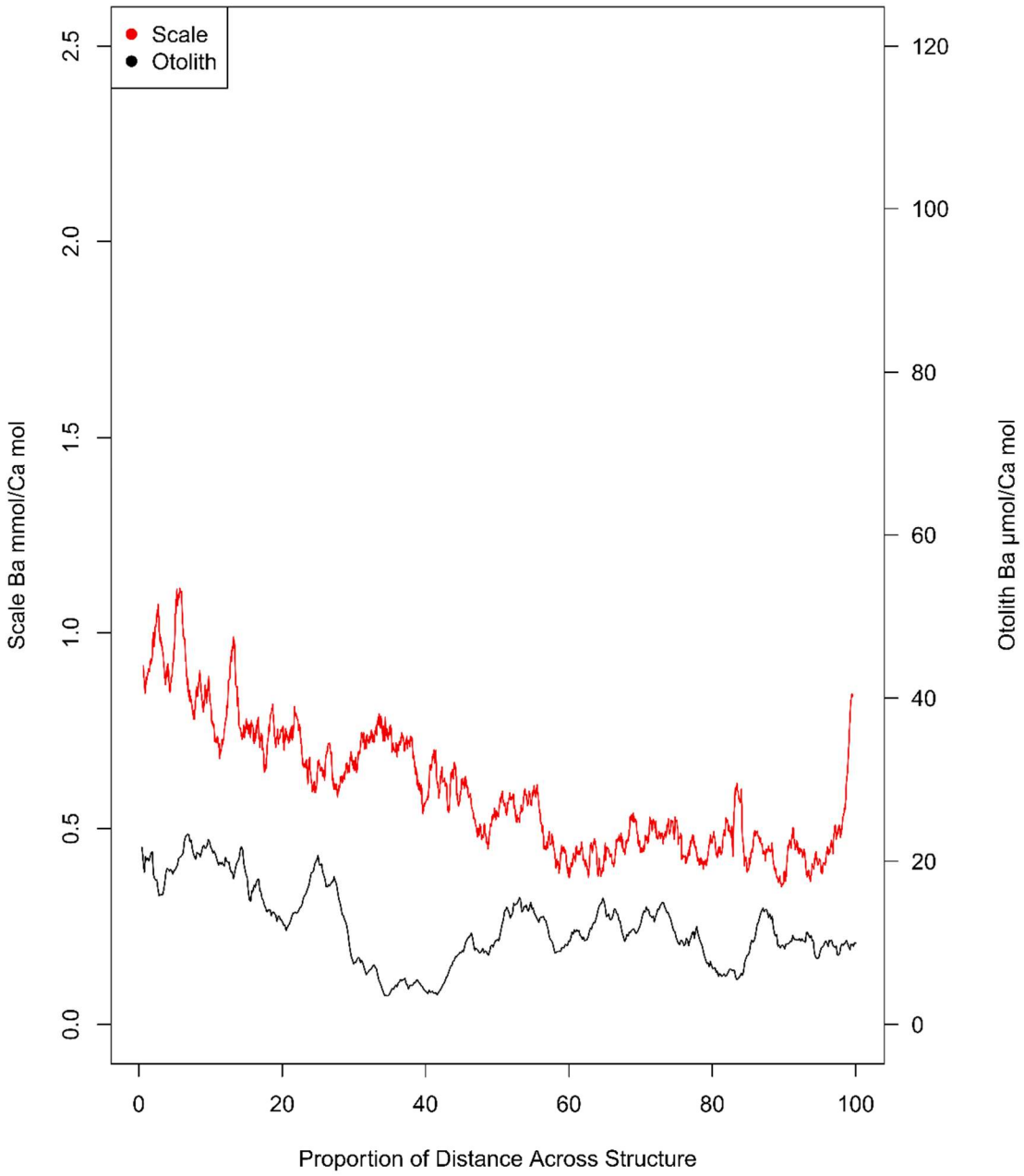
RD−027
Scale
Otolith
Scale Ba mmol/Ca mol
Otolith Ba µmol/Ca mol
Proportion of Distance Across Structure
0.0
0.5
1.0
1.5
2.0
2.5
0
20
40
60
80
100
120

RD-027

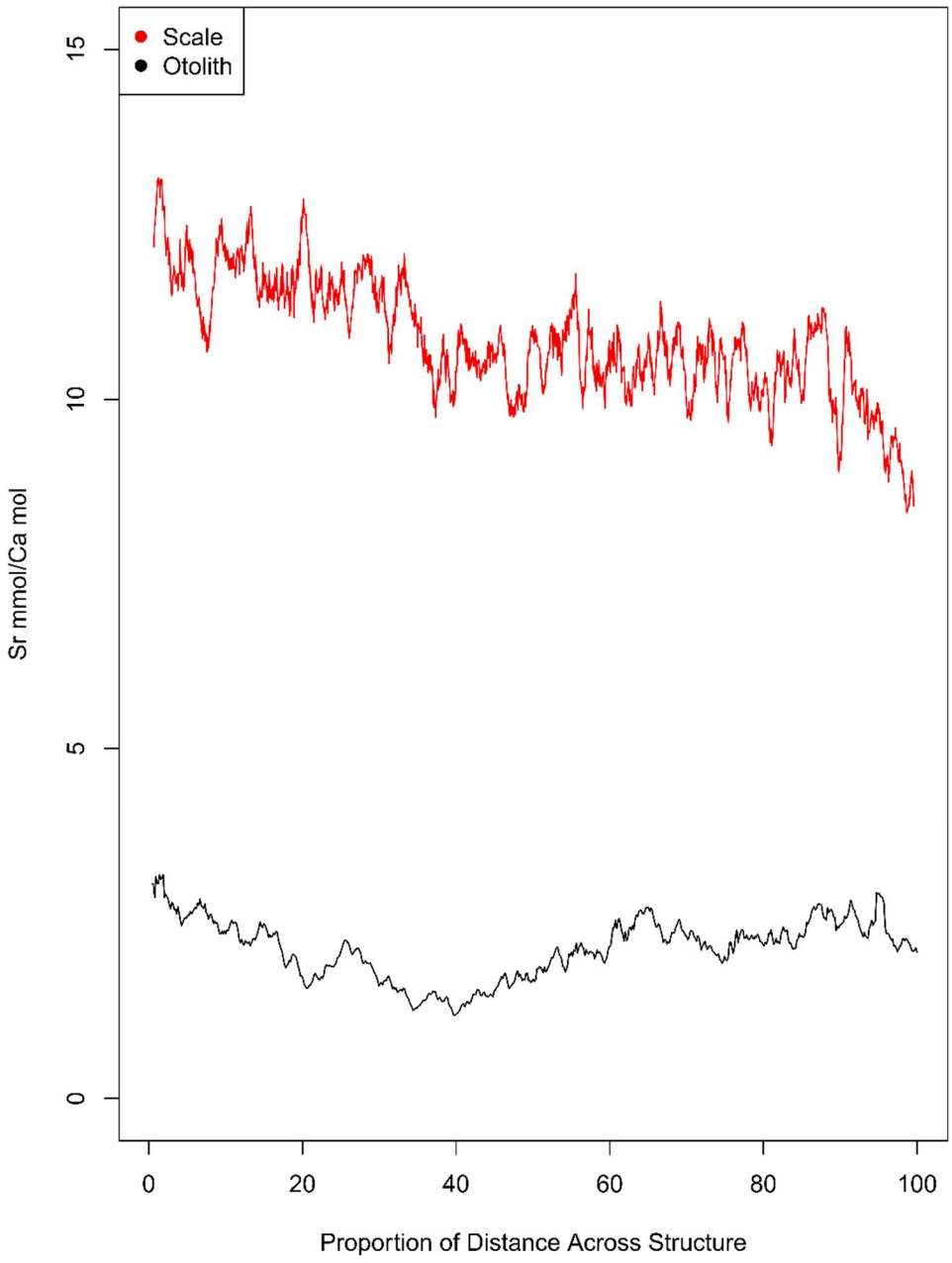
Scale
Otolith
Sr mmol/Ca mol
0
5
10
15
0
20
40
60
80
100
Proportion of Distance Across Structure

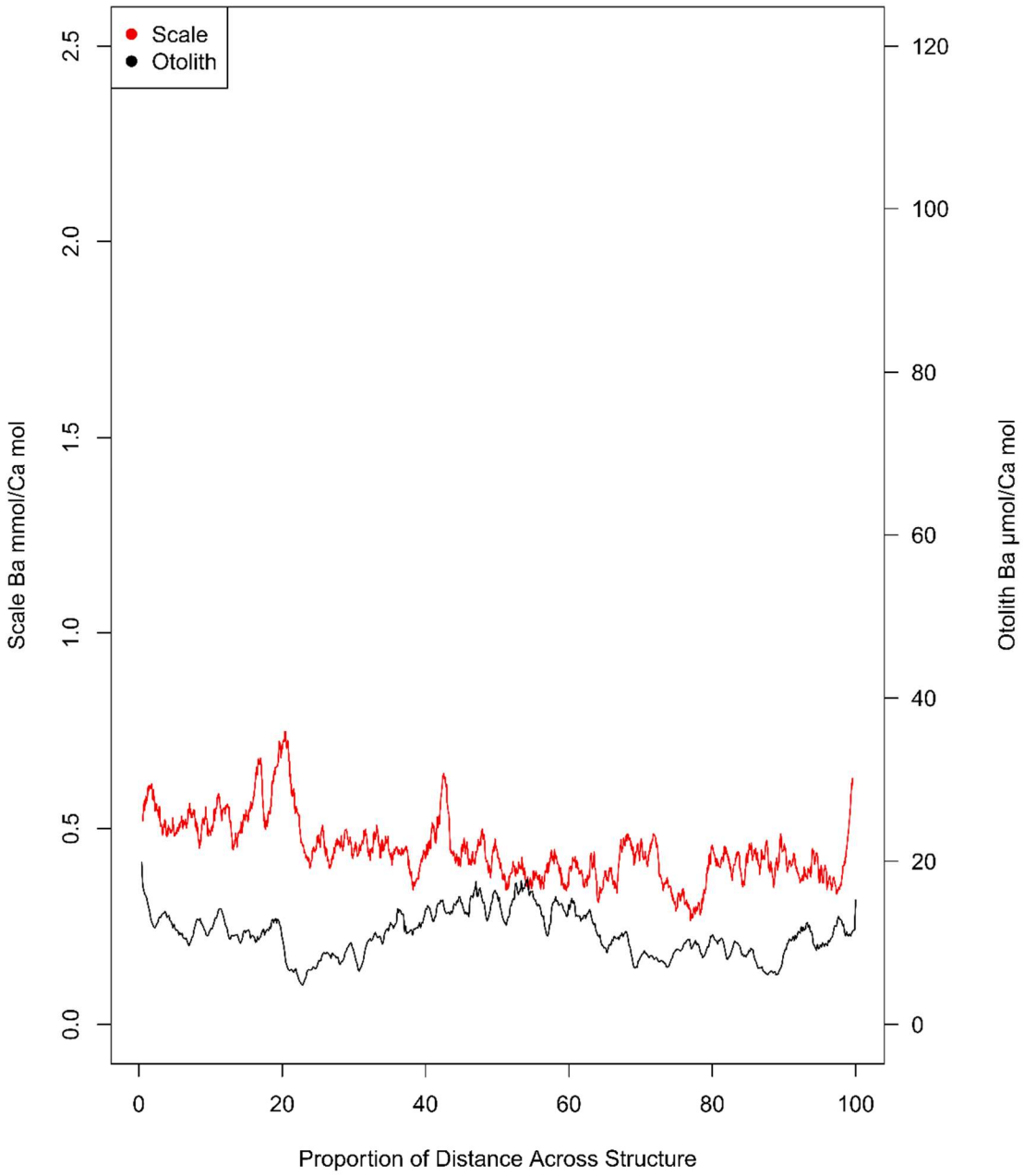
RD-028
Scale
Otolith
Scale Ba mmol/Ca mol
Otolith Ba µmol/Ca mol
Proportion of Distance Across Structure
0.0
0.5
1.0
1.5
2.0
2.5
0
20
40
60
80
100
120

RD-028

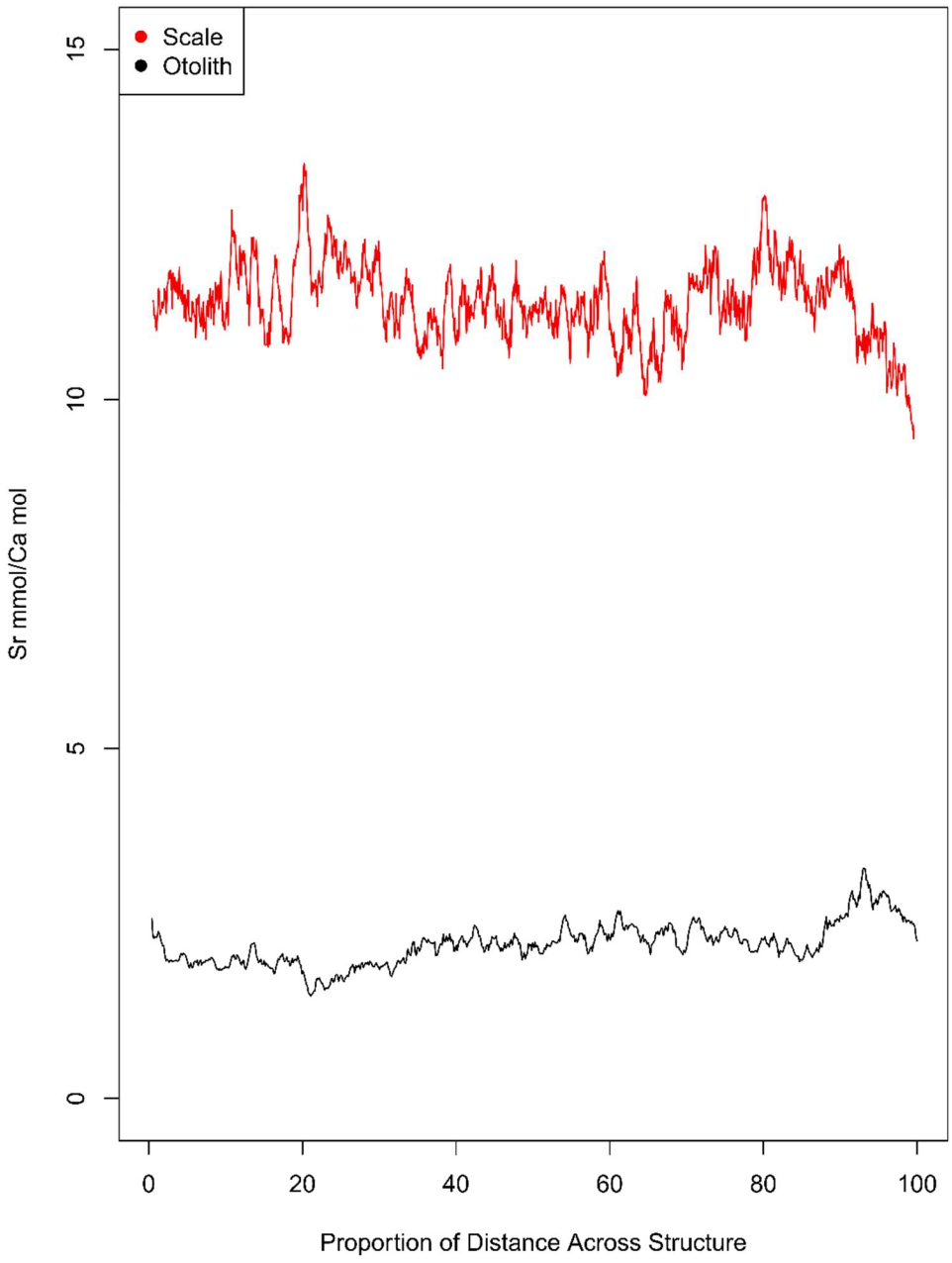
Scale
Otolith
Sr mmol/Ca mol
0
5
10
15
0
20
40
60
80
100
Proportion of Distance Across Structure

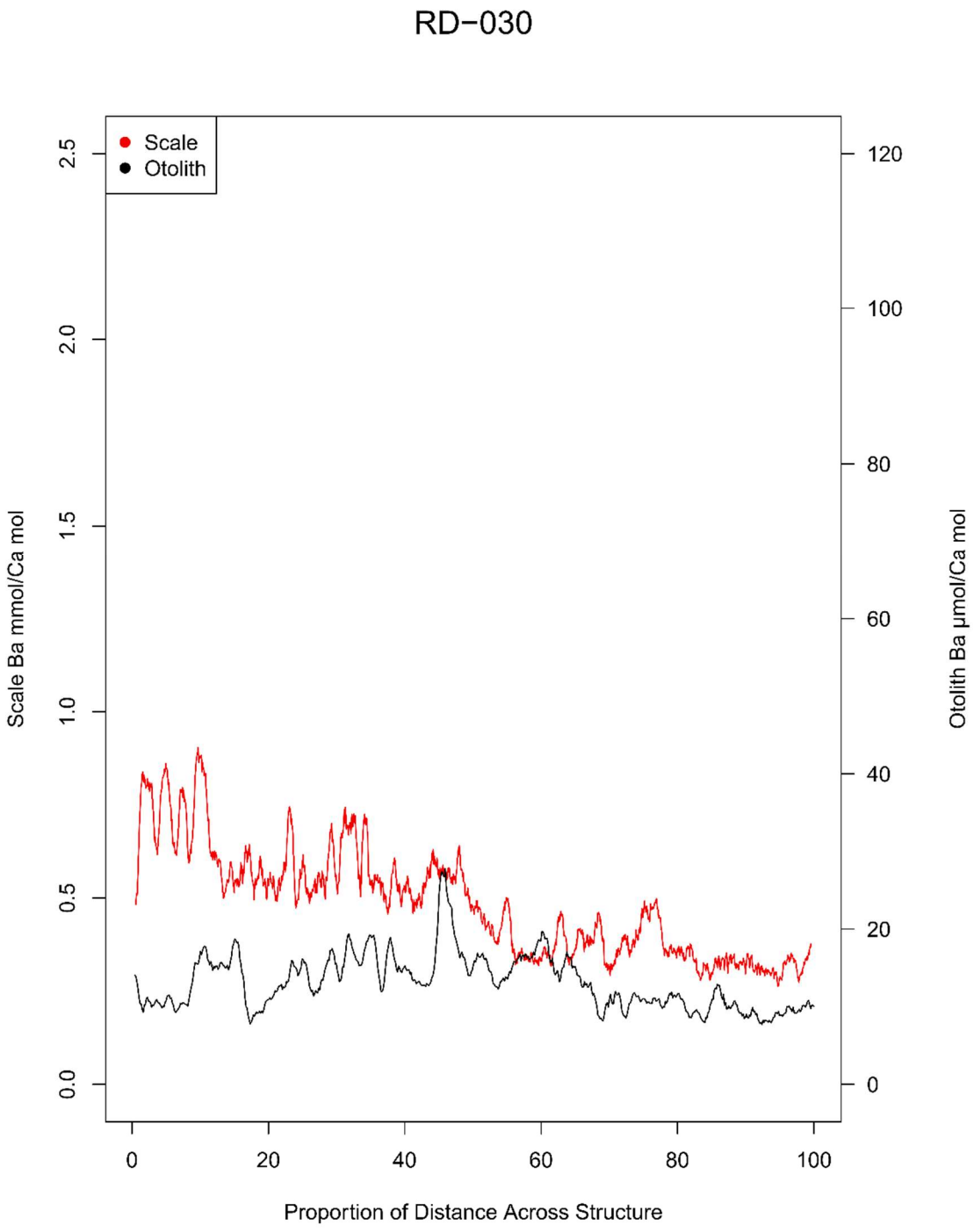
RD−030
Scale
Otolith
Scale Ba mmol/Ca mol
Otolith Ba µmol/Ca mol
Proportion of Distance Across Structure
0.0
0.5
1.0
1.5
2.0
2.5
0
20
40
60
80
100
120

RD-030

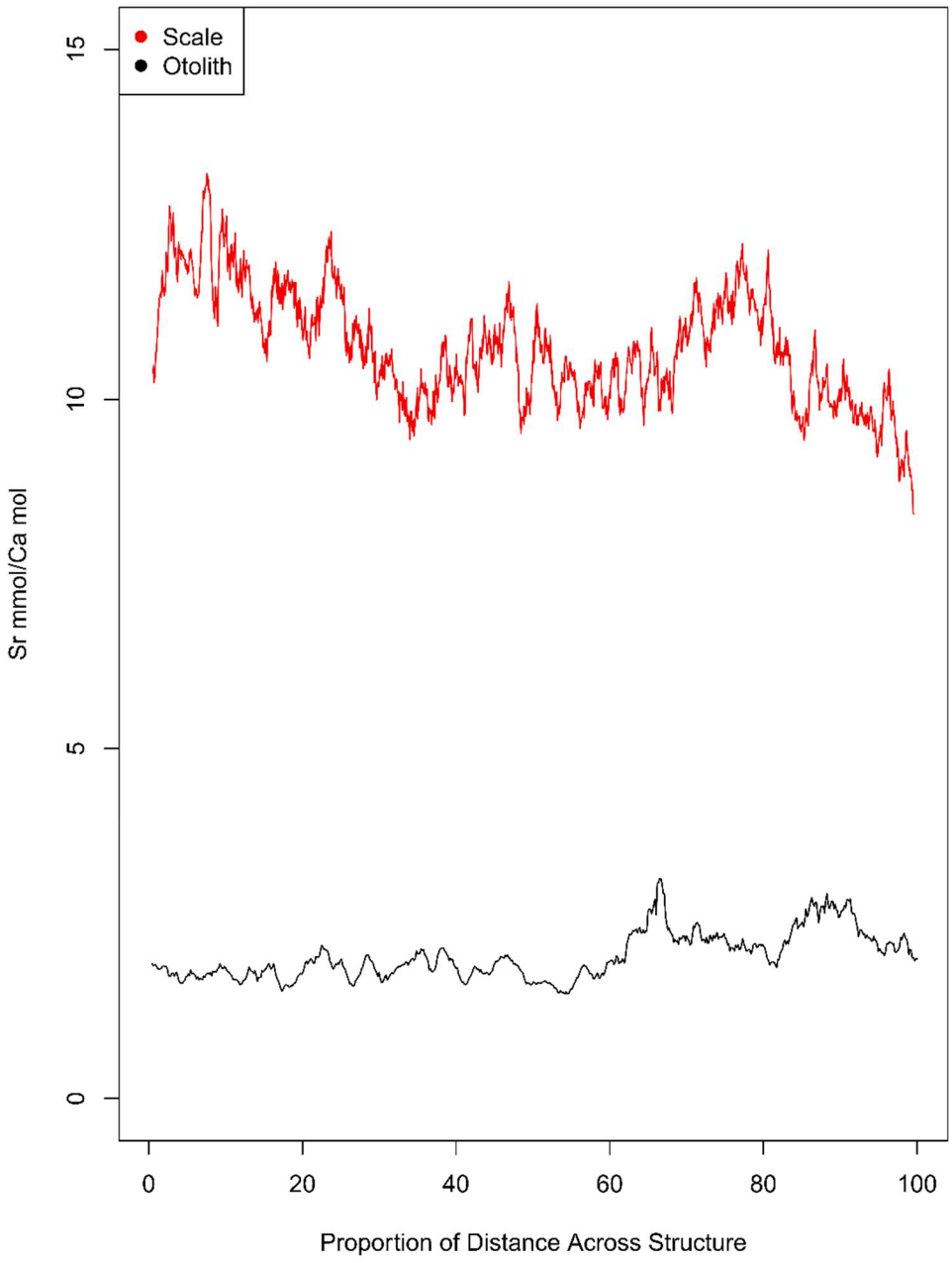
Scale
Otolith
Sr mmol/Ca mol
0
5
10
15
0
20
40
60
80
100
Proportion of Distance Across Structure

RD-031

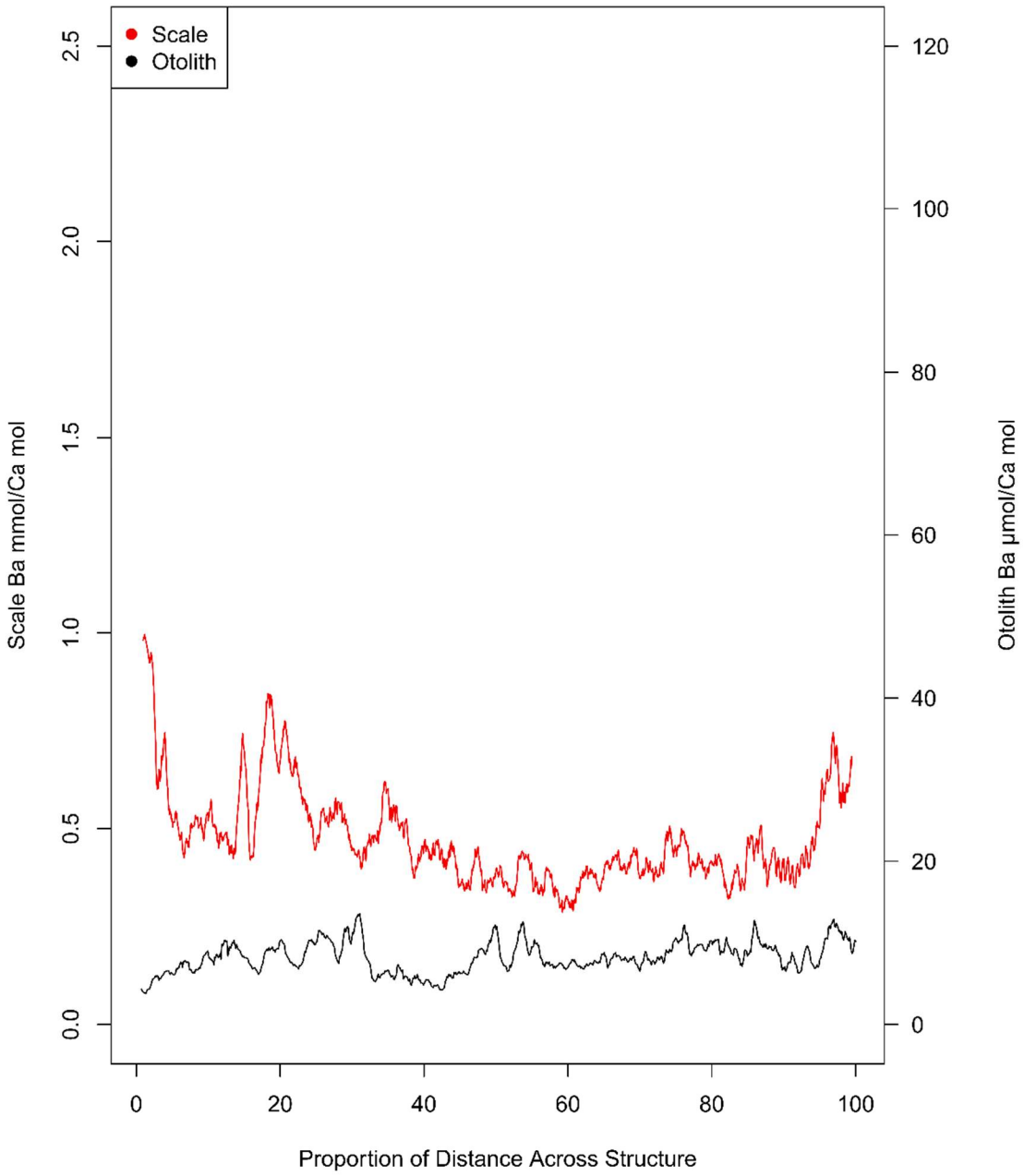
Scale
Otolith
Scale Ba mmol/Ca mol
Otolith Ba µmol/Ca mol
Proportion of Distance Across Structure
0.0
0.5
1.0
1.5
2.0
2.5
0
20
40
60
80
100
120

RD-031

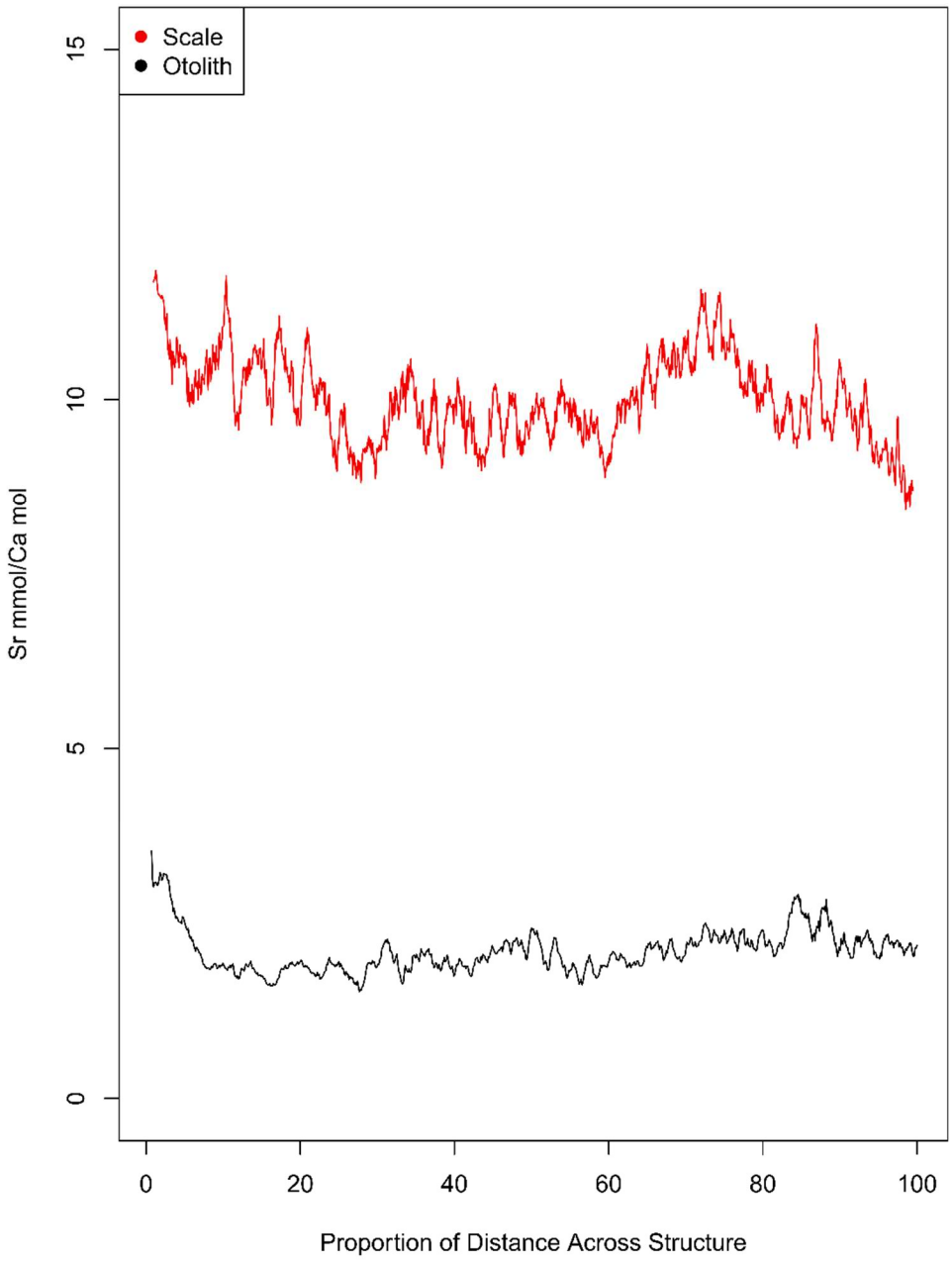
Scale
Otolith
Sr mmol/Ca mol
0
5
10
15
0
20
40
60
80
100
Proportion of Distance Across Structure

RD-032

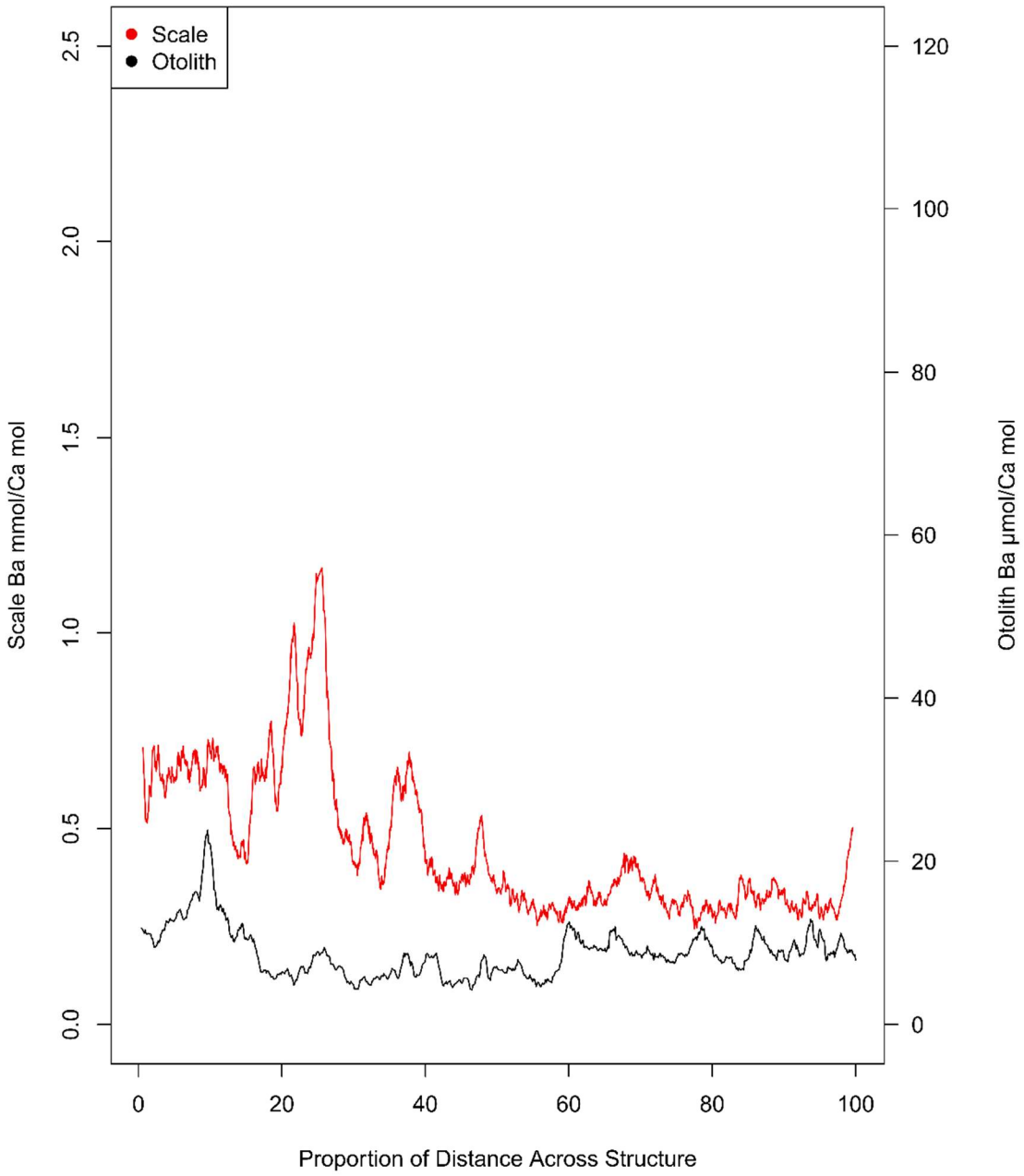
Scale
Otolith
Scale Ba mmol/Ca mol
Otolith Ba µmol/Ca mol
Proportion of Distance Across Structure
0.0
0.5
1.0
1.5
2.0
2.5
0
20
40
60
80
100
120

RD-032

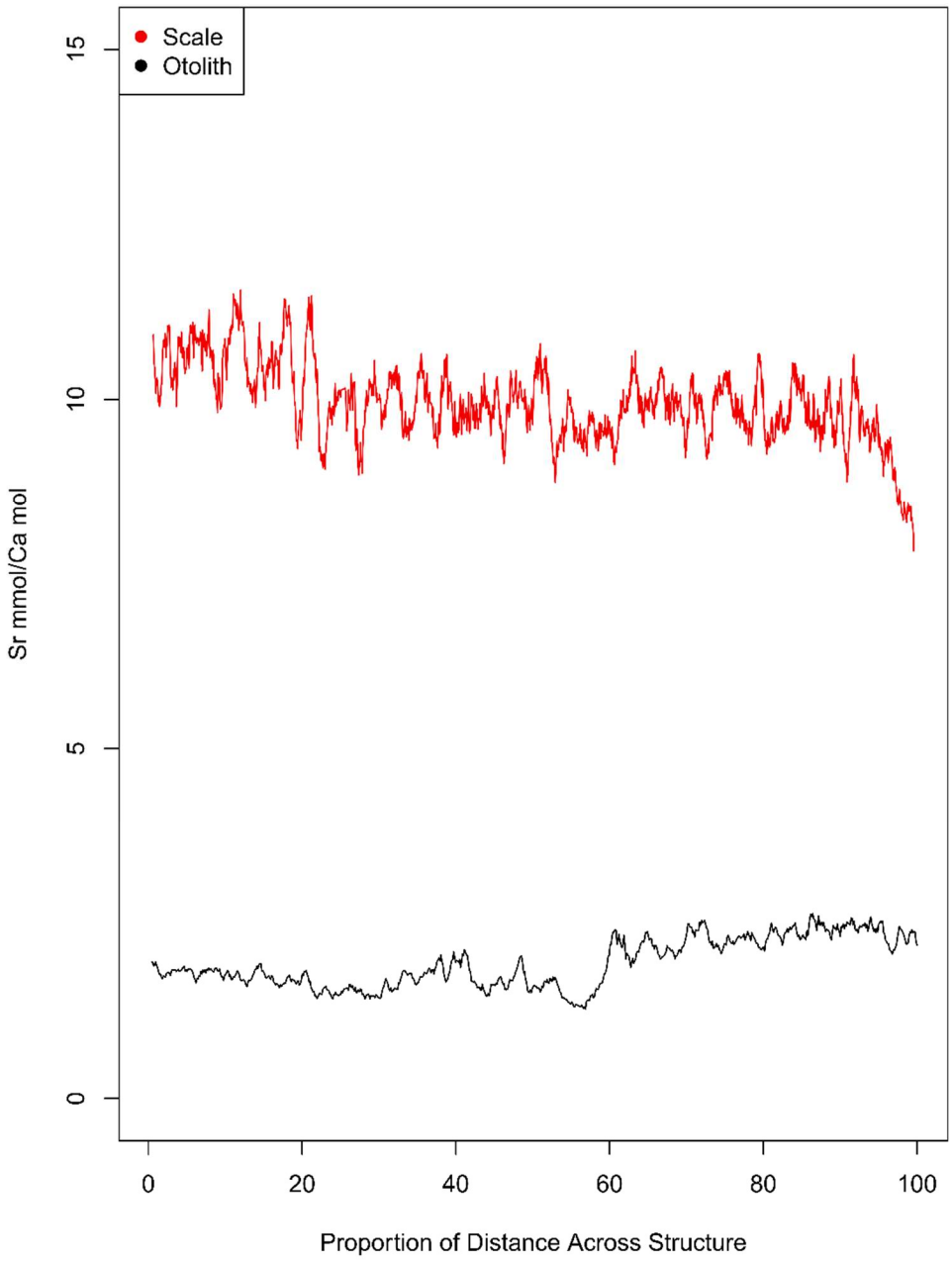
Scale
Otolith
Sr mmol/Ca mol
0
5
10
15
0
20
40
60
80
100
Proportion of Distance Across Structure

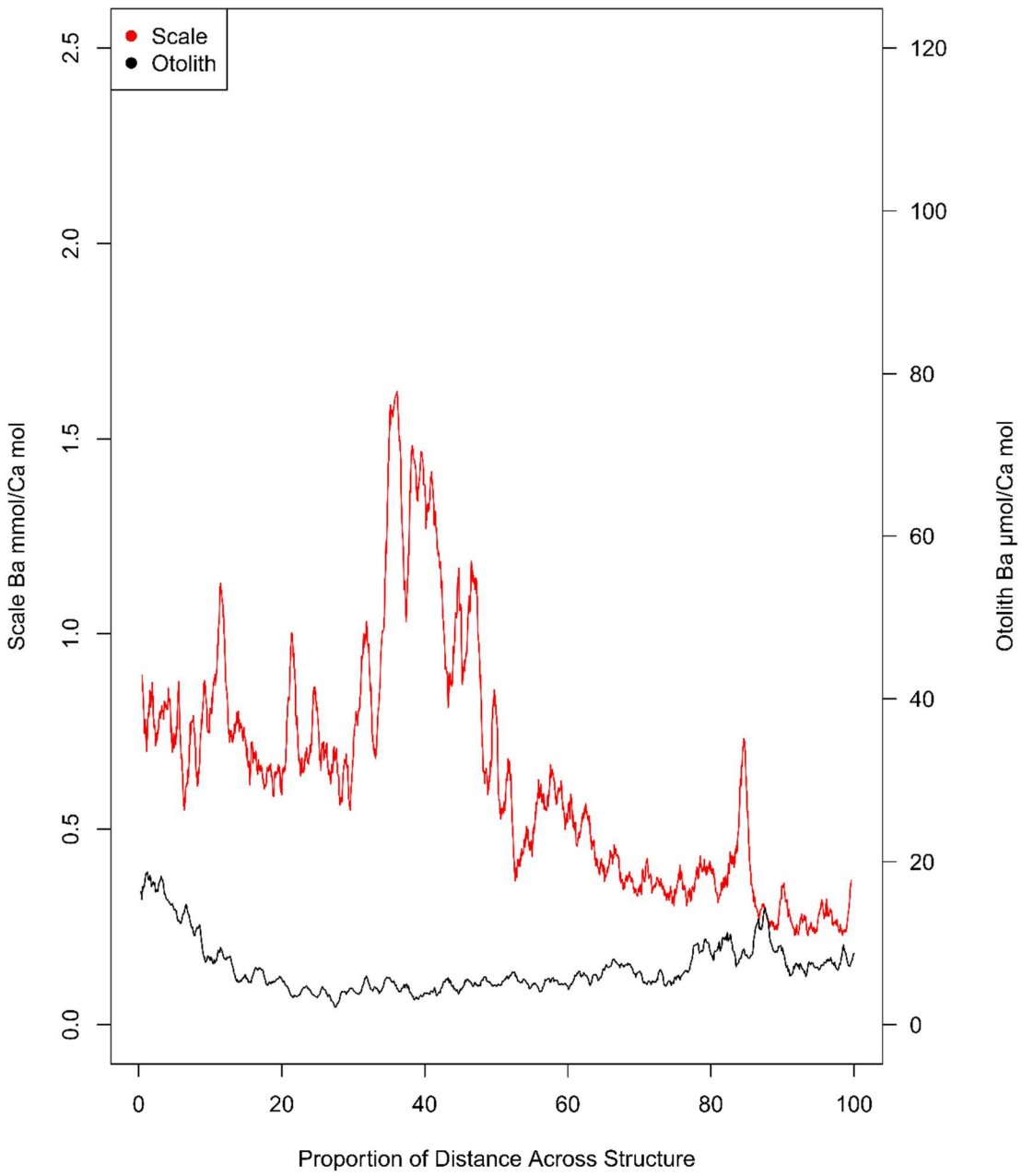
RD-033
Scale
Otolith
Scale Ba mmol/Ca mol
Otolith Ba µmol/Ca mol
Proportion of Distance Across Structure
0.0
0.5
1.0
1.5
2.0
2.5
0
20
40
60
80
100
120

RD-033

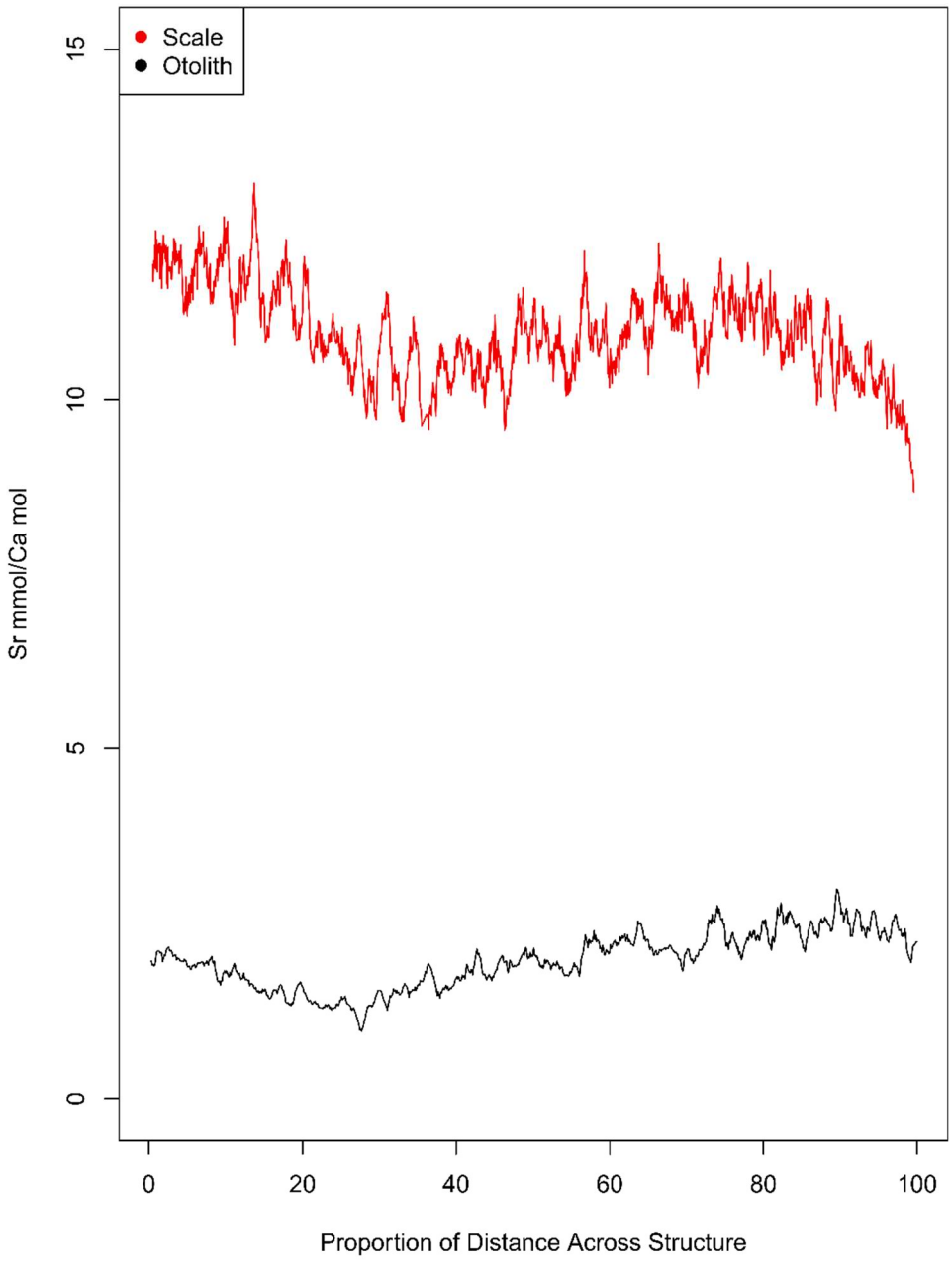
Scale
Otolith
Sr mmol/Ca mol
0
5
10
15
0
20
40
60
80
100
Proportion of Distance Across Structure

RD-034

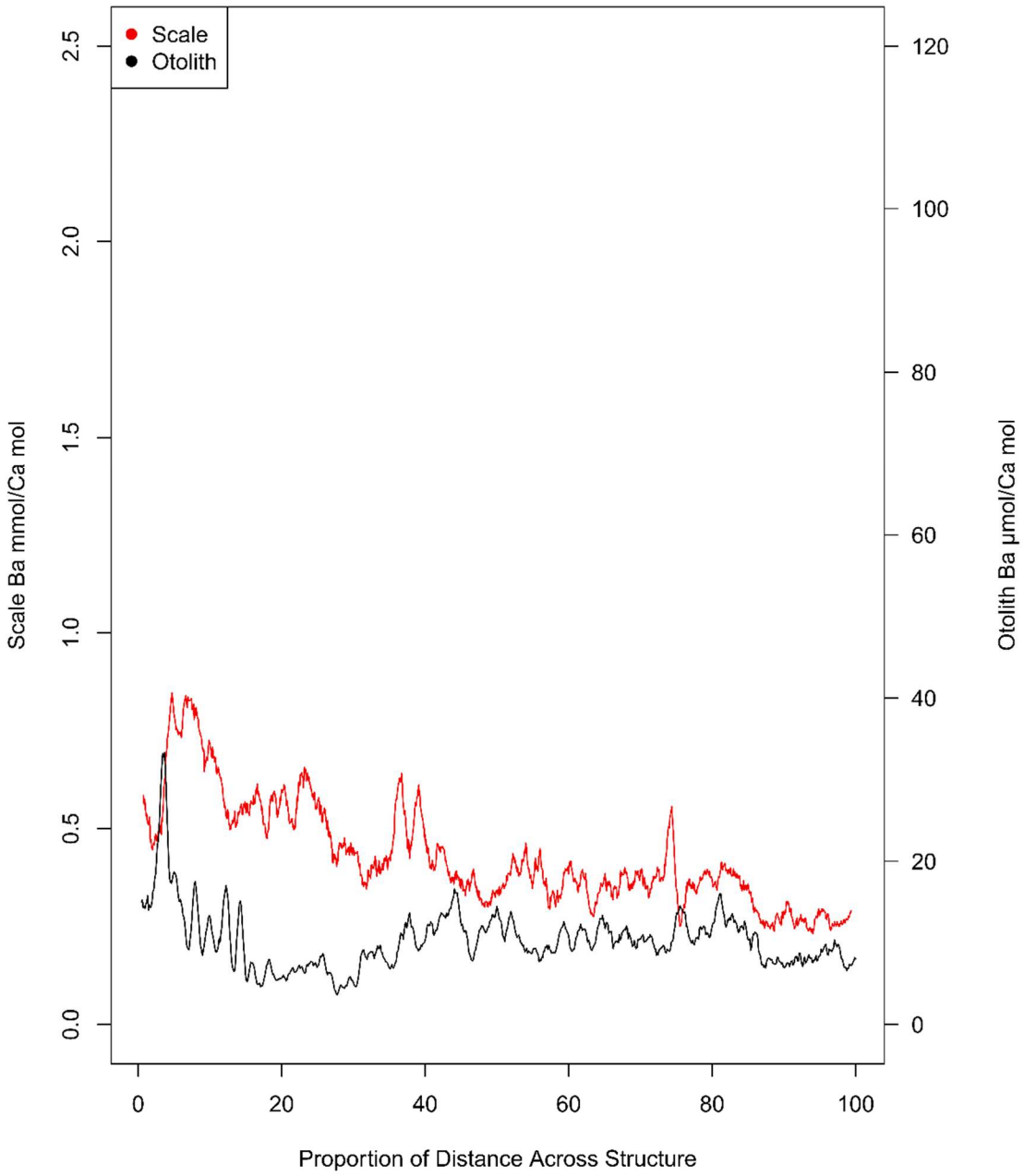
Scale
Otolith
Scale Ba mmol/Ca mol
Otolith Ba µmol/Ca mol
Proportion of Distance Across Structure
0.0
0.5
1.0
1.5
2.0
2.5
0
20
40
60
80
100
120

RD-034

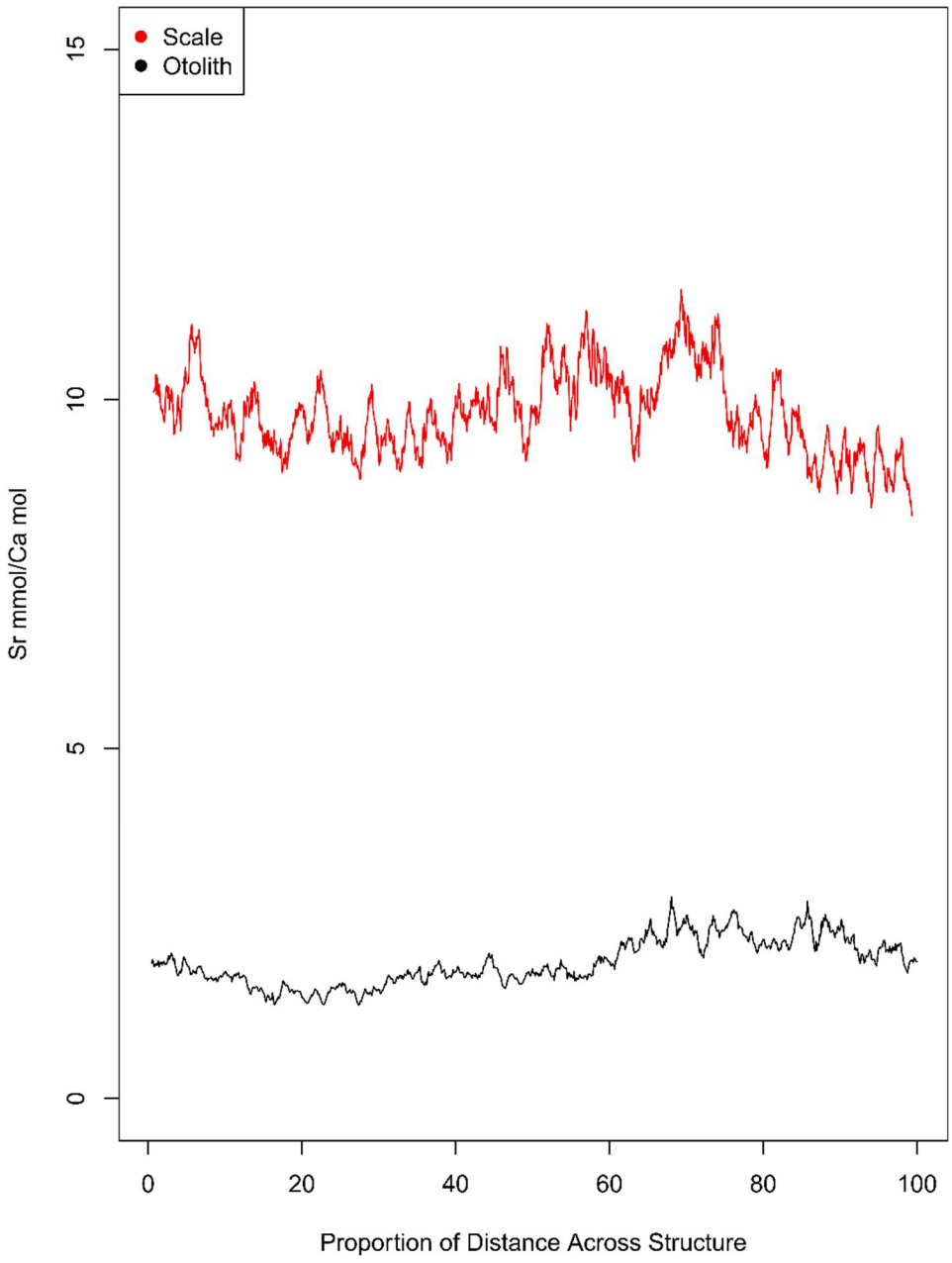
Scale
Otolith
Sr mmol/Ca mol
0
5
10
15
0
20
40
60
80
100
Proportion of Distance Across Structure

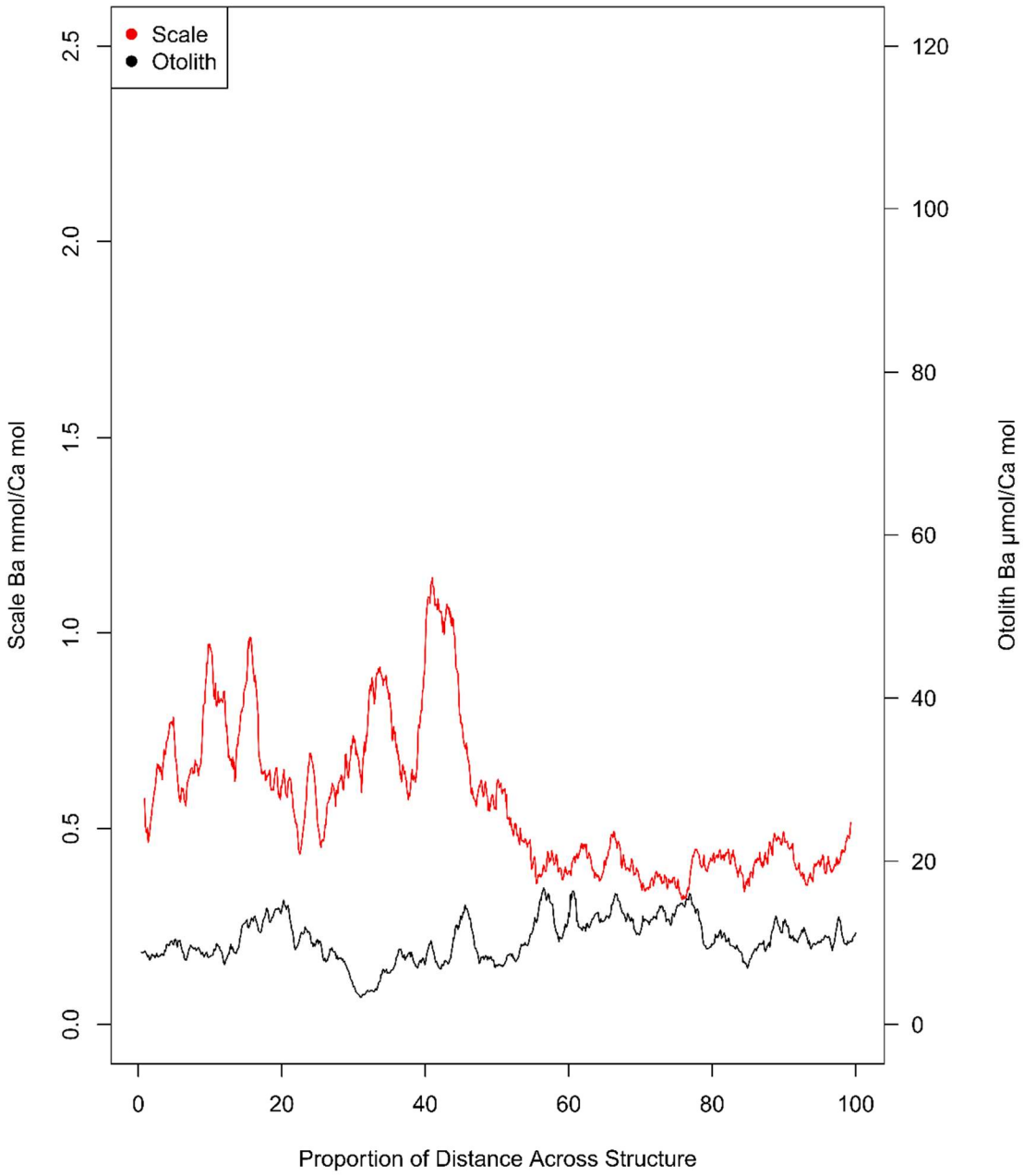
RD−035
Scale
Otolith
Scale Ba mmol/Ca mol
Otolith Ba µmol/Ca mol
Proportion of Distance Across Structure
0.0
0.5
1.0
1.5
2.0
2.5
0
20
40
60
80
100
120

RD-035

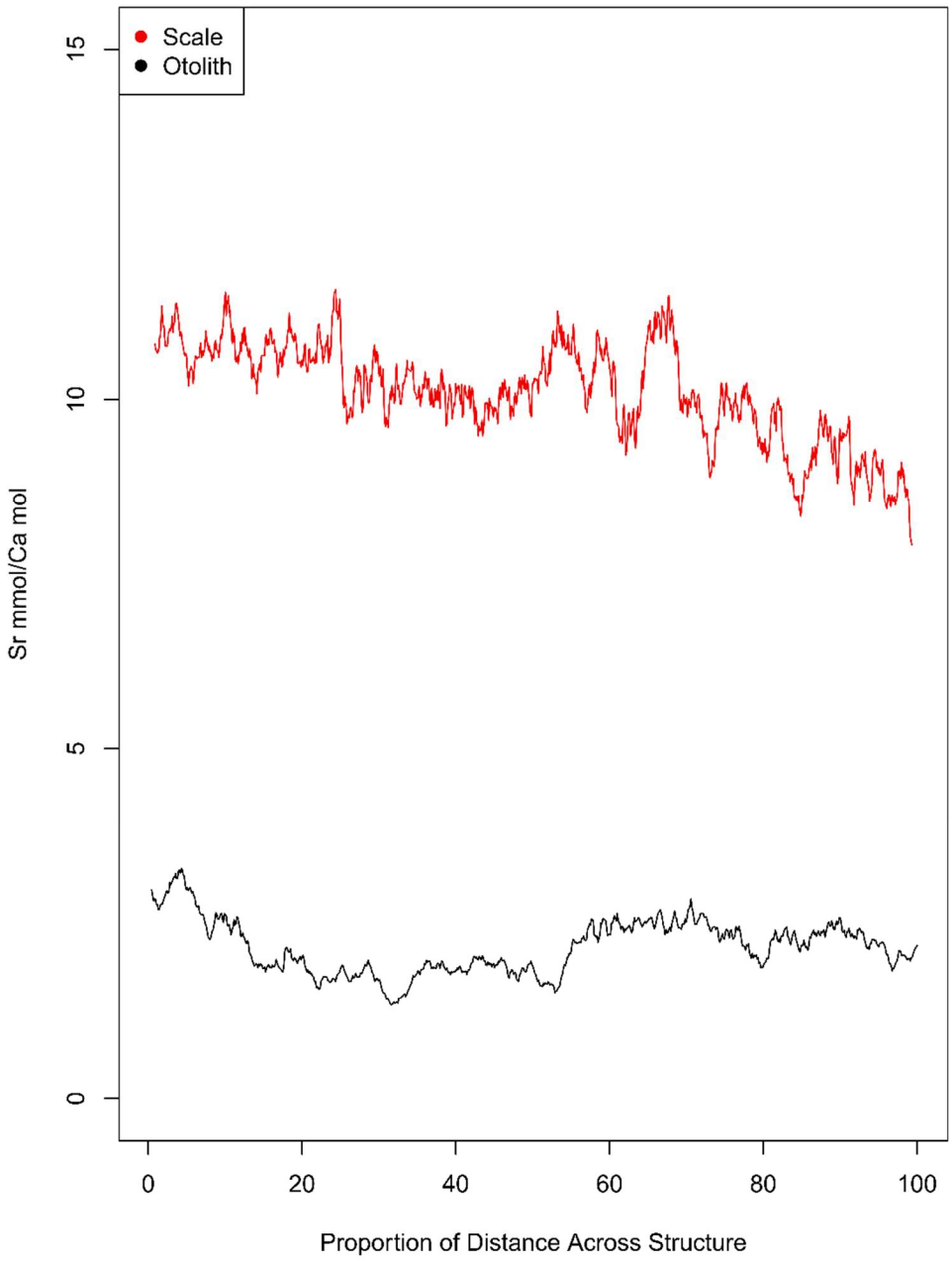
Scale
Otolith
Sr mmol/Ca mol
0
5
10
15
0
20
40
60
80
100
Proportion of Distance Across Structure

RD-036

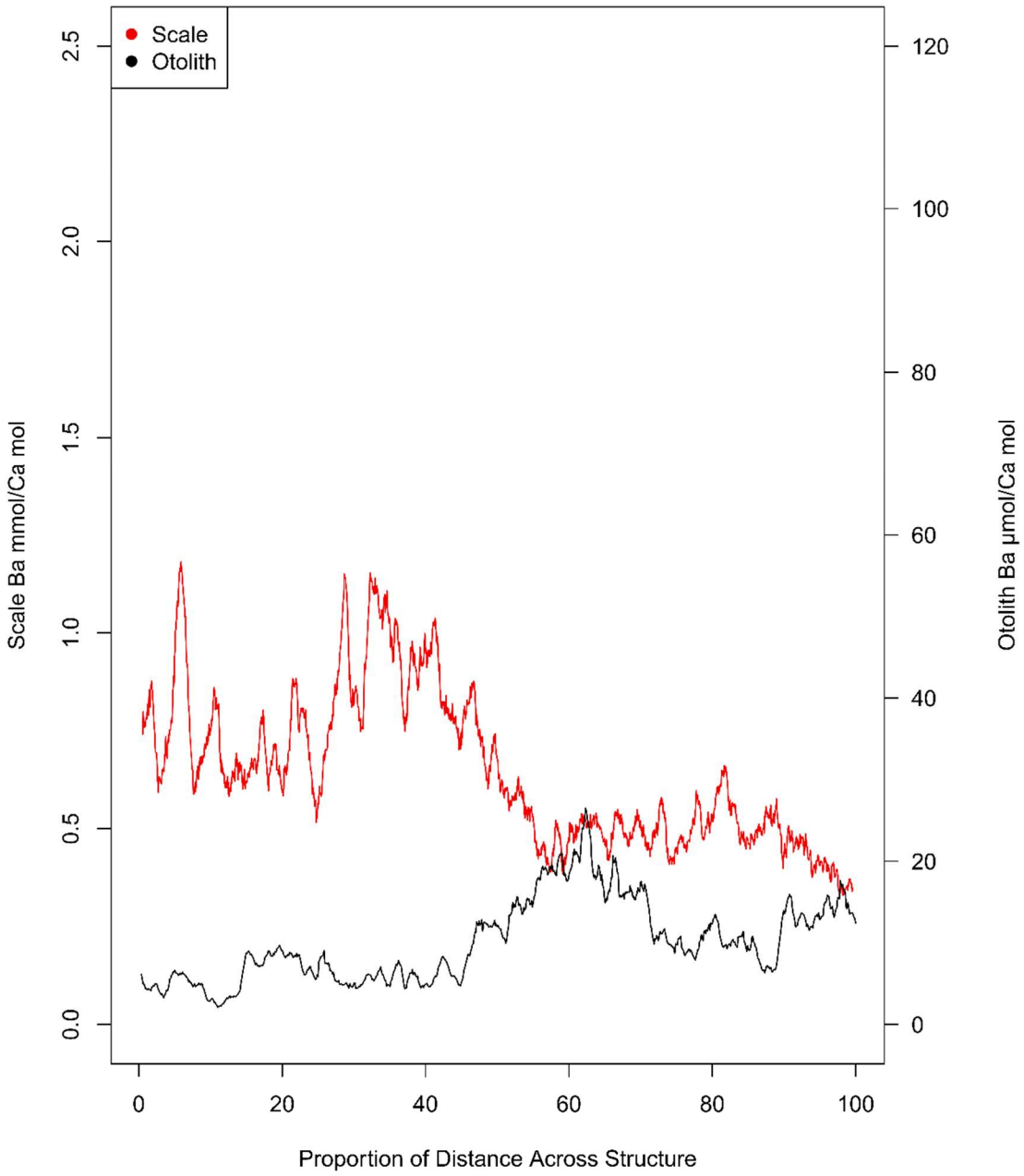
Scale
Otolith
Scale Ba mmol/Ca mol
Otolith Ba µmol/Ca mol
Proportion of Distance Across Structure
0.0
0.5
1.0
1.5
2.0
2.5
0
20
40
60
80
100
120

RD-036

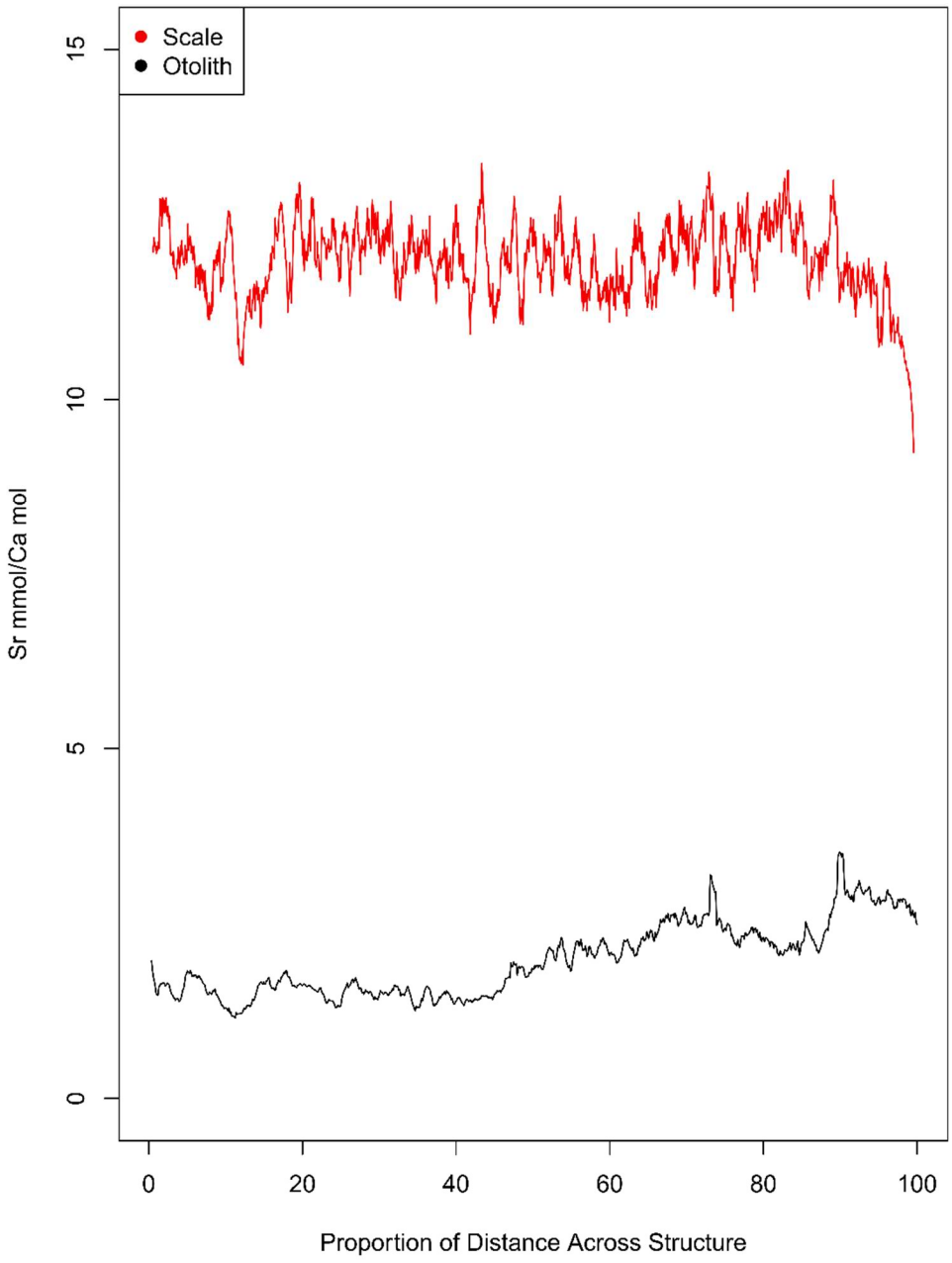
Scale
Otolith
Sr mmol/Ca mol
0
5
10
15
0
20
40
60
80
100
Proportion of Distance Across Structure

RD-037

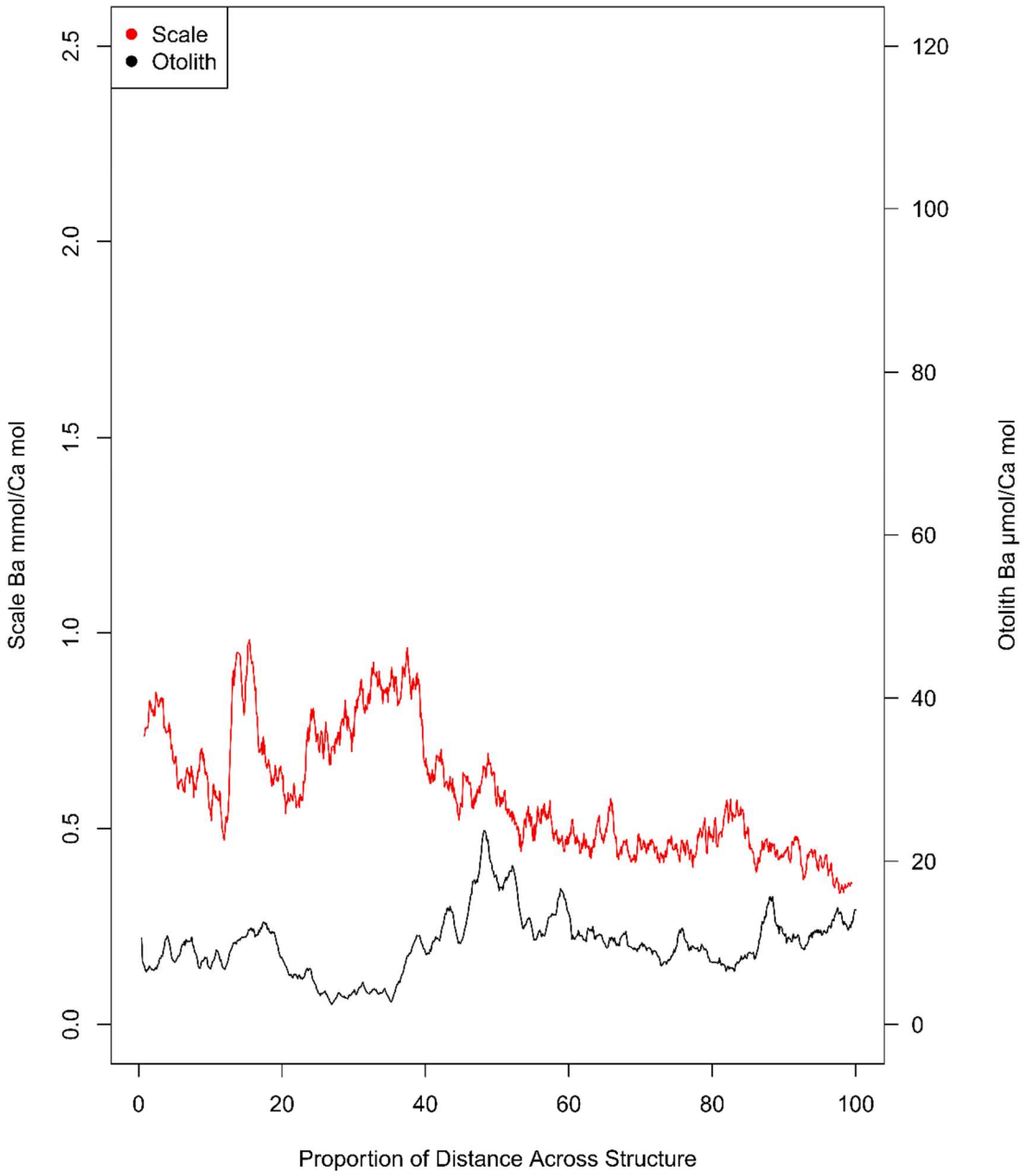
Scale
Otolith
Scale Ba mmol/Ca mol
Otolith Ba µmol/Ca mol
Proportion of Distance Across Structure
0.0
0.5
1.0
1.5
2.0
2.5
0
20
40
60
80
100
120

RD-037

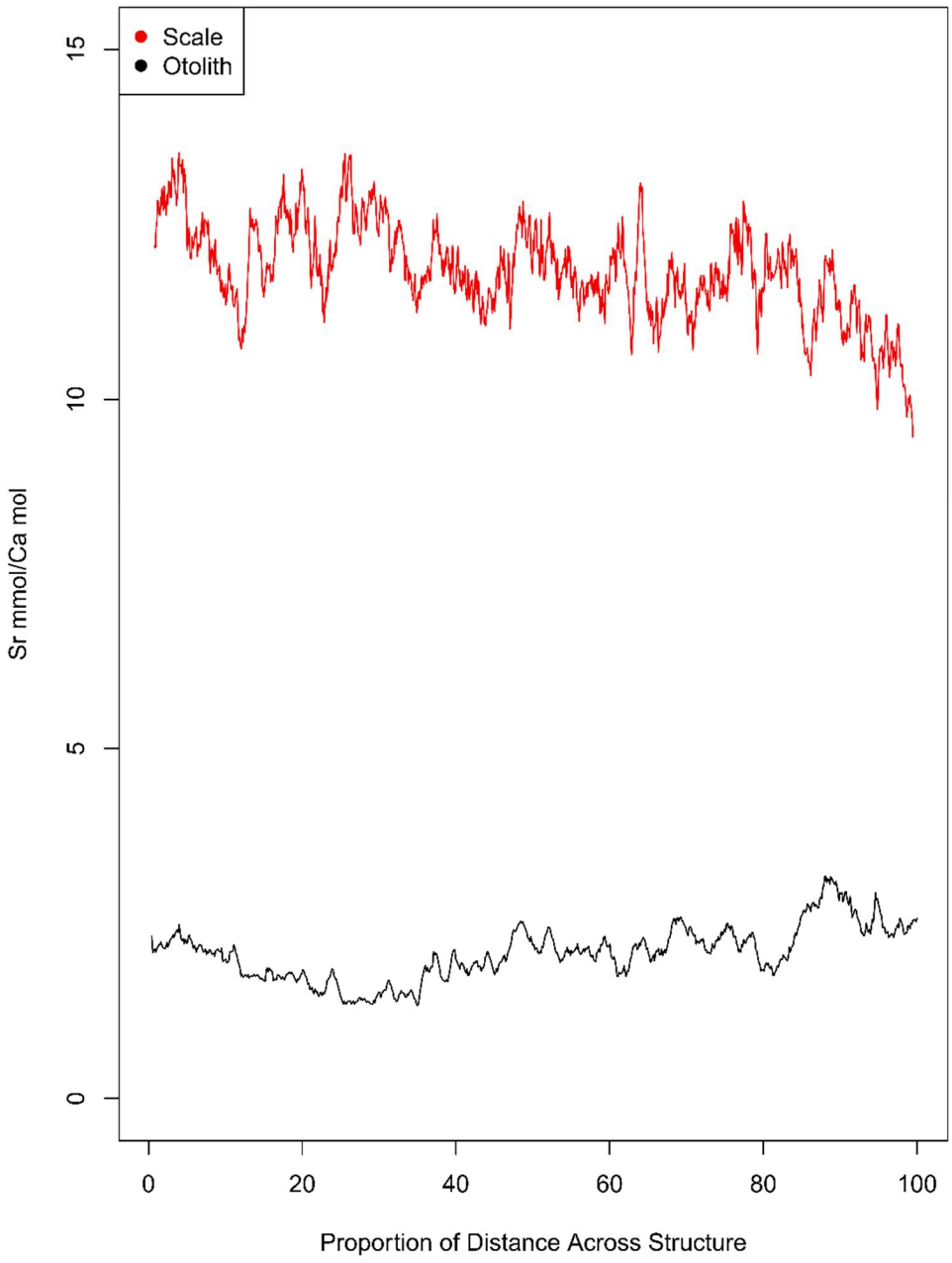
Scale
Otolith
Sr mmol/Ca mol
0
5
10
15
0
20
40
60
80
100
Proportion of Distance Across Structure

RD-038

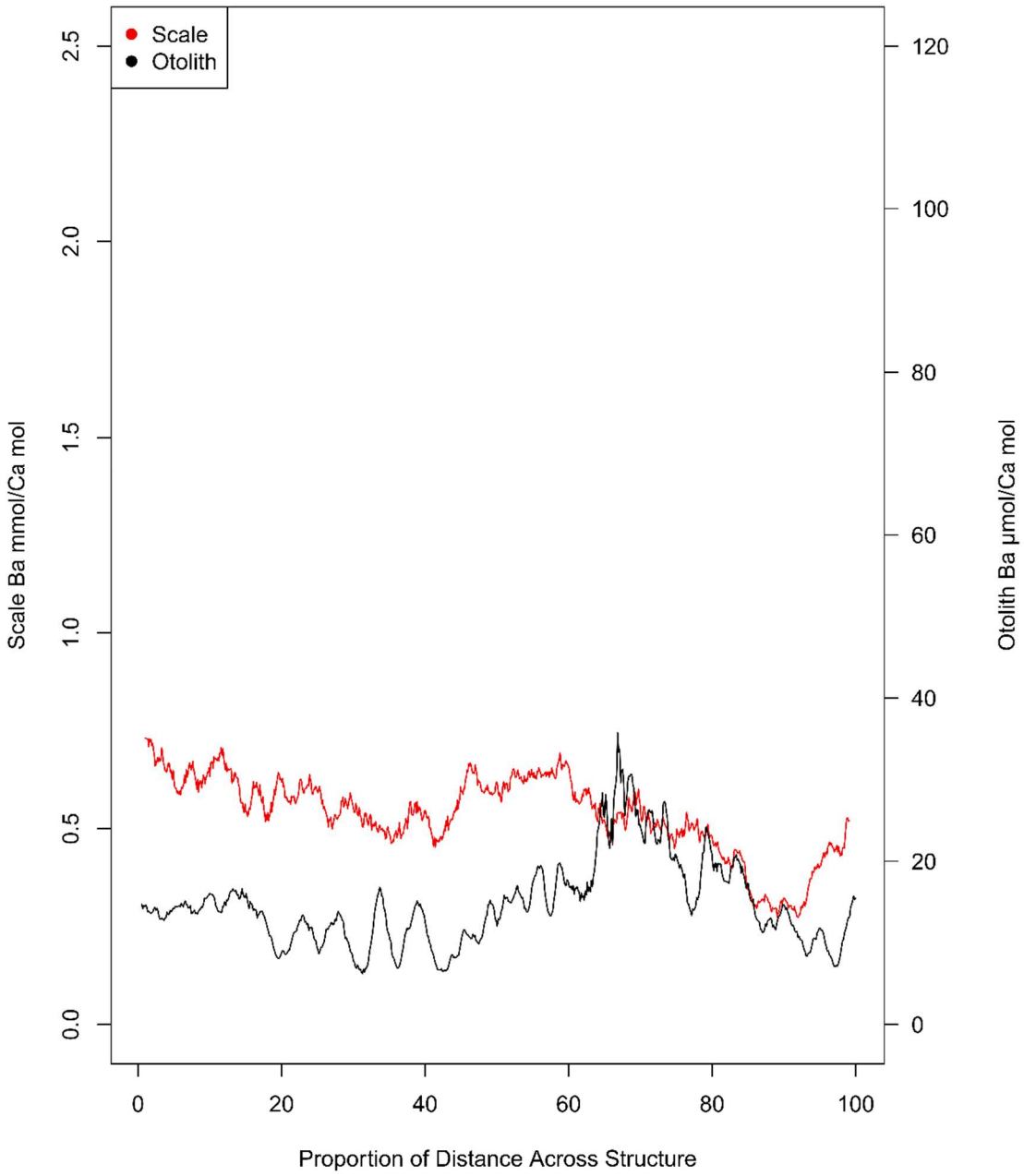
Scale
Otolith
Scale Ba mmol/Ca mol
Otolith Ba µmol/Ca mol
Proportion of Distance Across Structure
0.0
0.5
1.0
1.5
2.0
2.5
0
20
40
60
80
100
120

RD-038

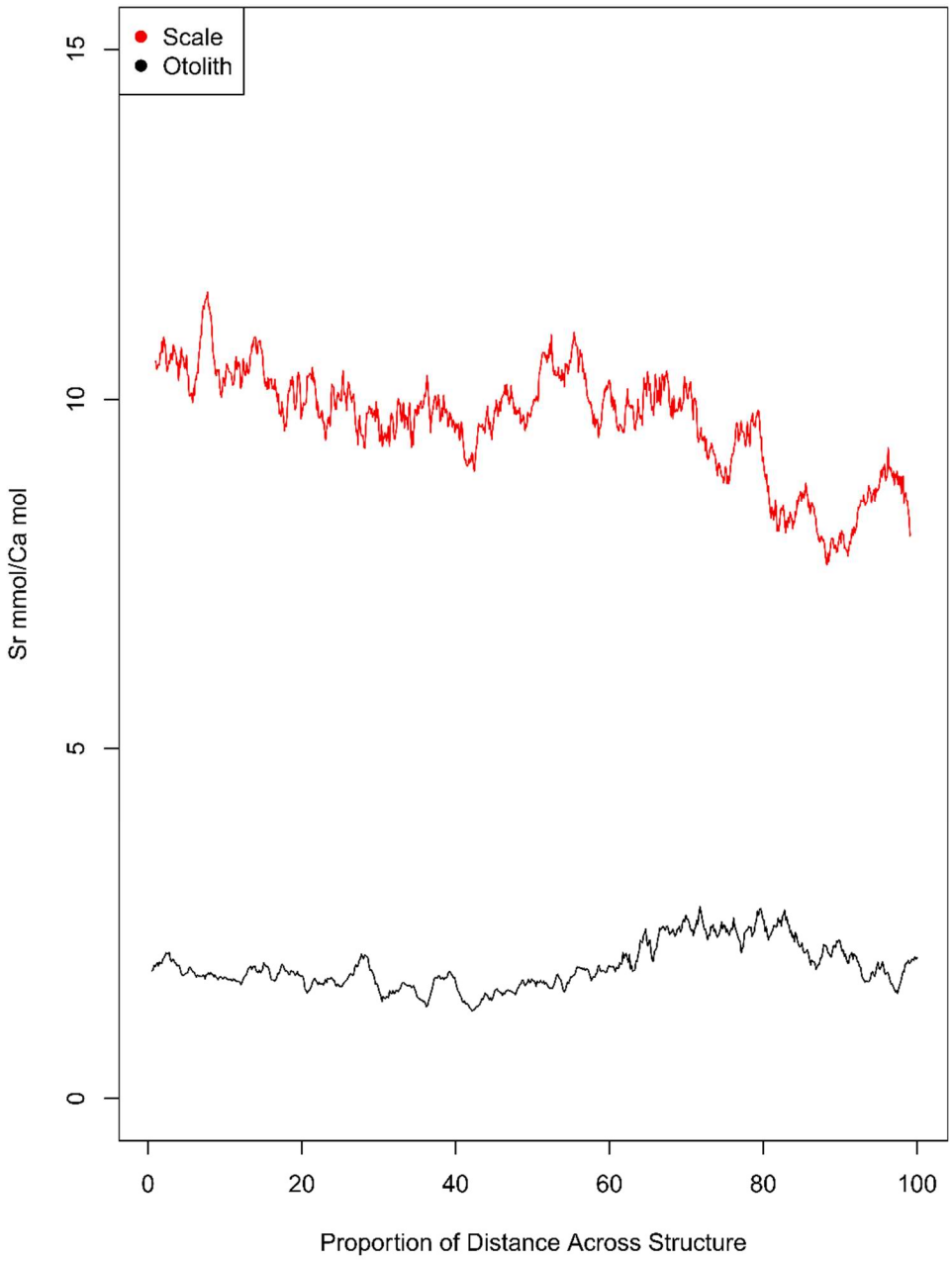
Scale
Otolith
Sr mmol/Ca mol
0
5
10
15
0
20
40
60
80
100
Proportion of Distance Across Structure

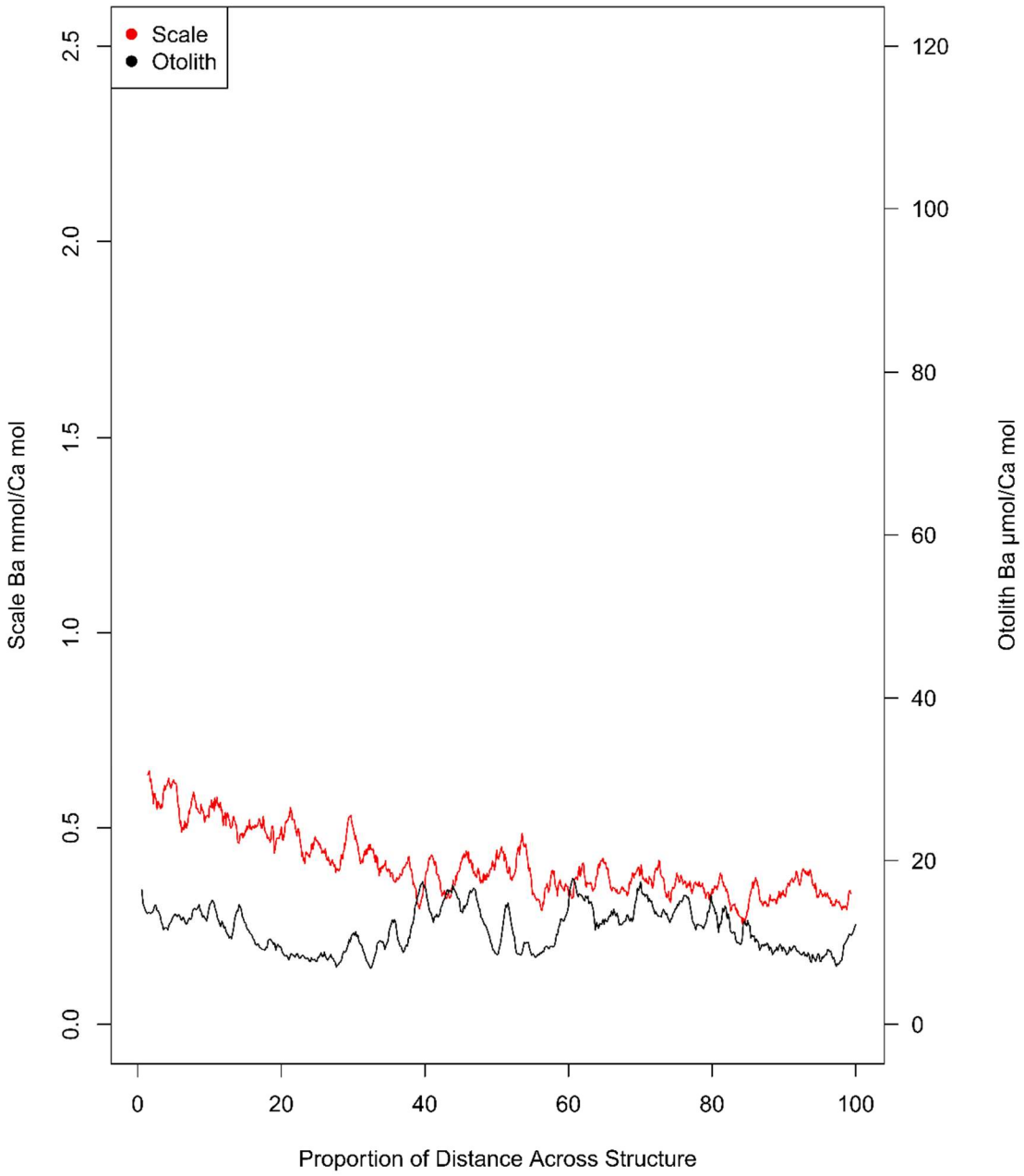
RD−039
Scale
Otolith
Scale Ba mmol/Ca mol
Otolith Ba µmol/Ca mol
Proportion of Distance Across Structure
0.0
0.5
1.0
1.5
2.0
2.5
0
20
40
60
80
100
120

RD-039

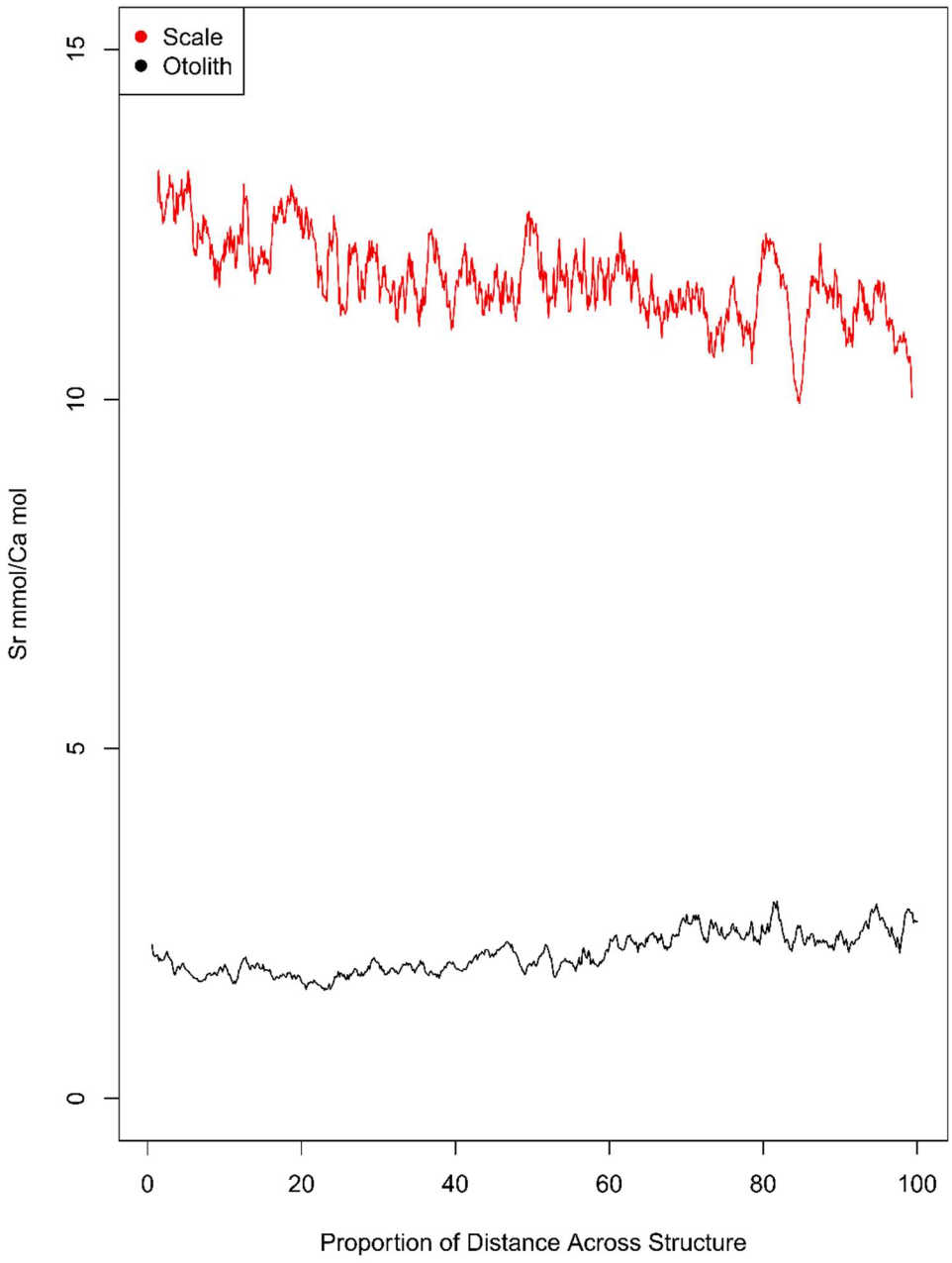
Scale
Otolith
Sr mmol/Ca mol
0
5
10
15
0
20
40
60
80
100
Proportion of Distance Across Structure

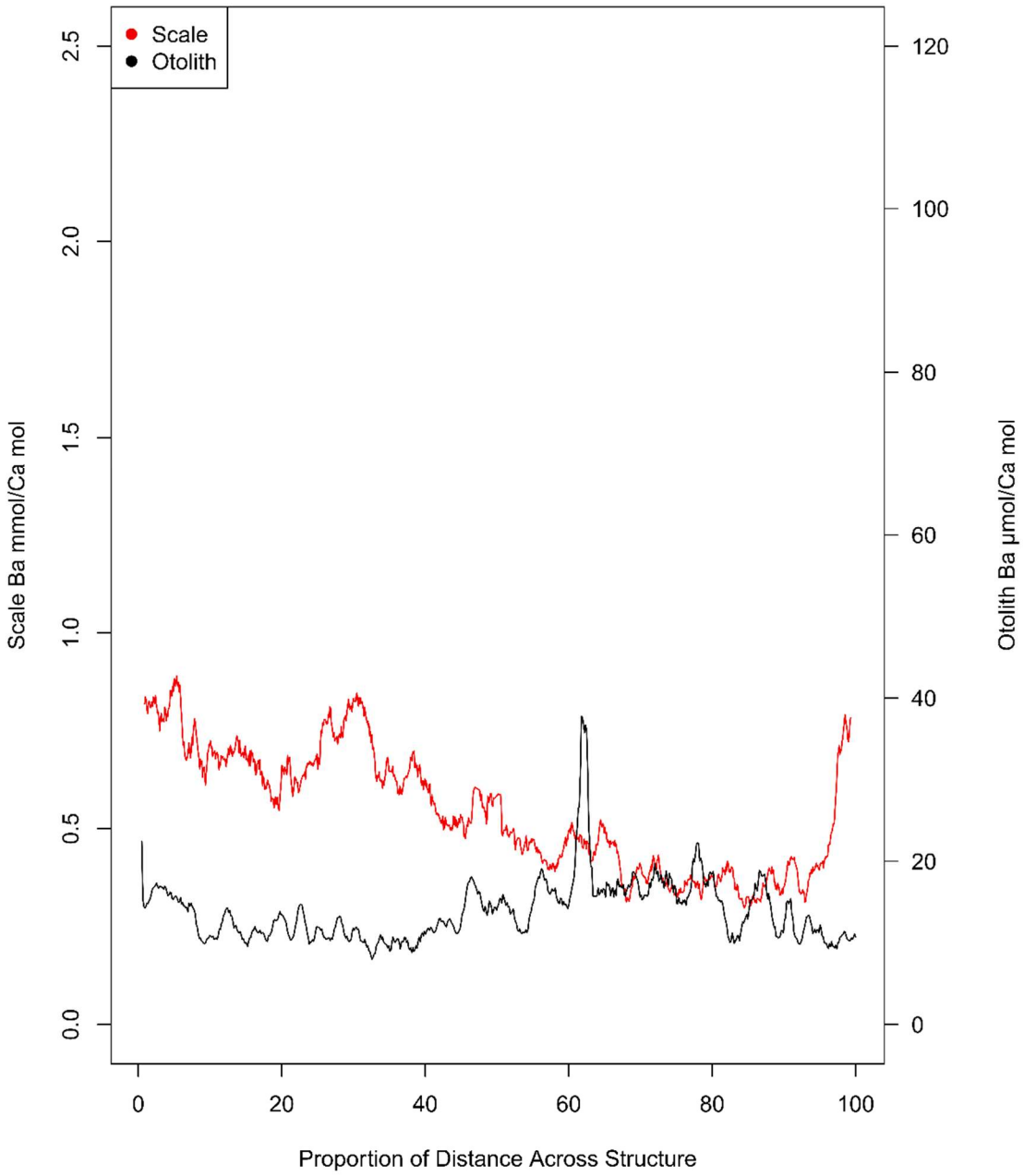
RD−040
Scale
Otolith
Scale Ba mmol/Ca mol
Otolith Ba µmol/Ca mol
Proportion of Distance Across Structure
0.0
0.5
1.0
1.5
2.0
2.5
0
20
40
60
80
100
120

RD-040

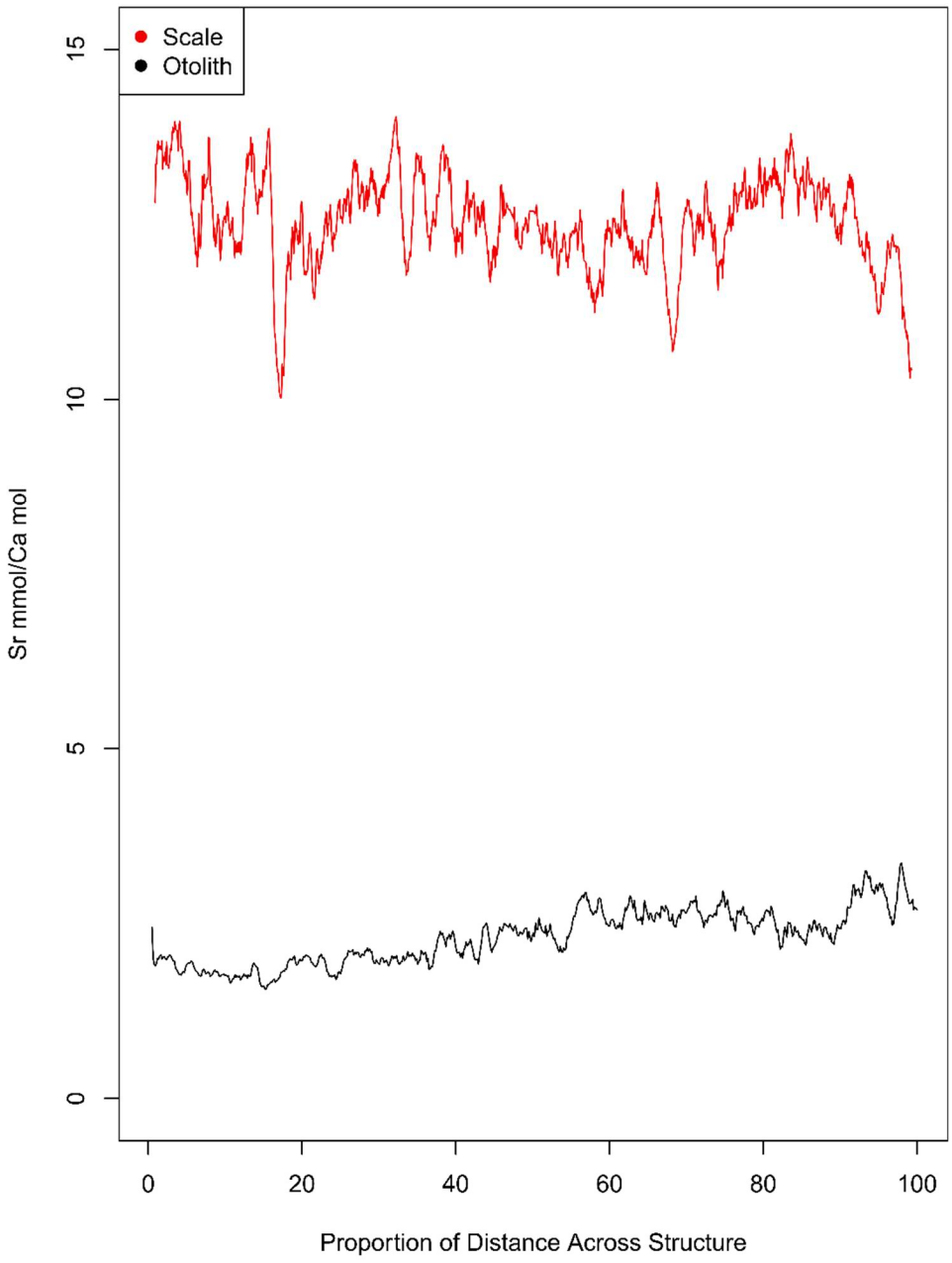
Scale
Otolith
Sr mmol/Ca mol
0
5
10
15
0
20
40
60
80
100
Proportion of Distance Across Structure

RD-041

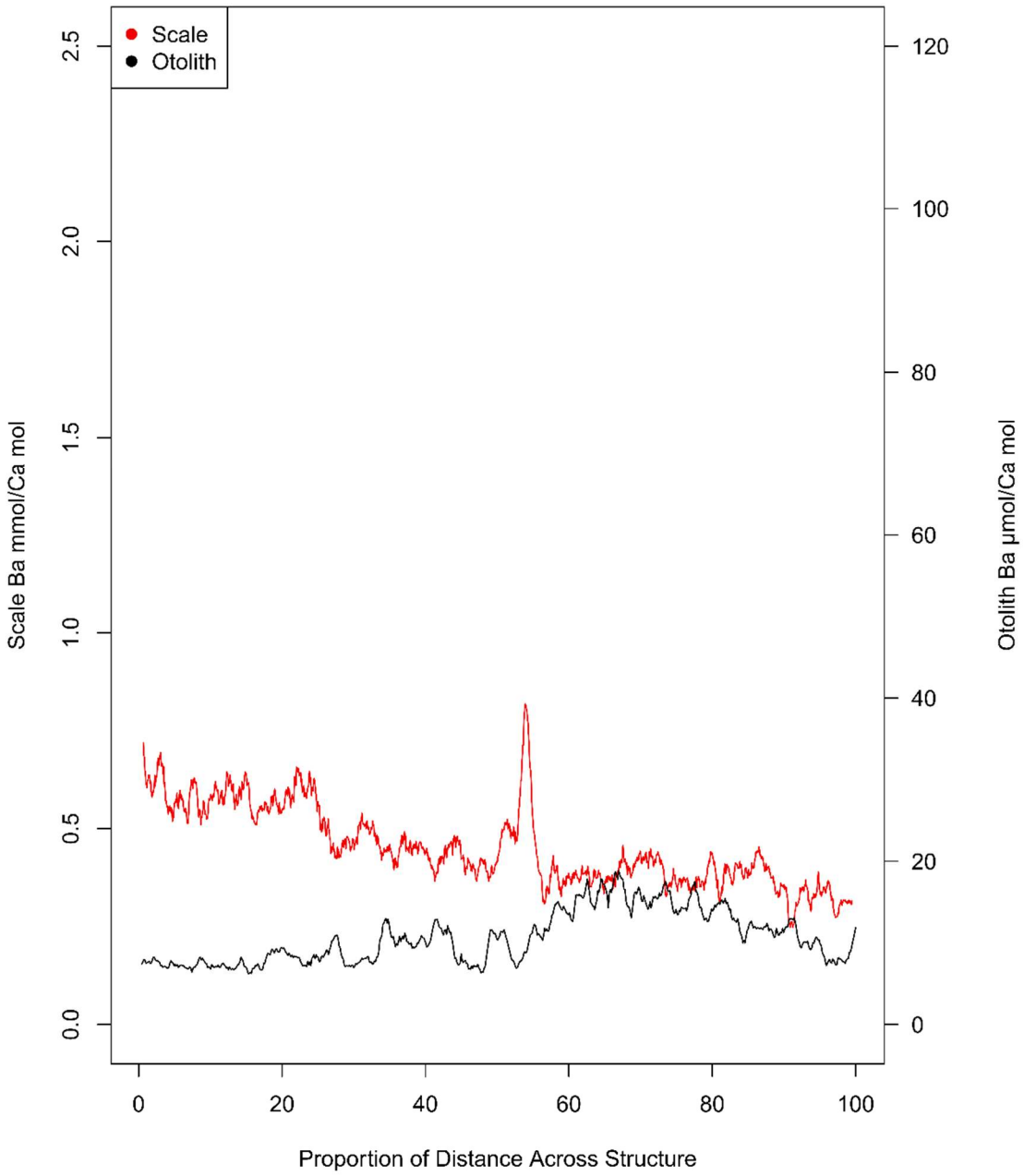
Scale
Otolith
Scale Ba mmol/Ca mol
Otolith Ba µmol/Ca mol
Proportion of Distance Across Structure
0.0
0.5
1.0
1.5
2.0
2.5
0
20
40
60
80
100
120

RD-041

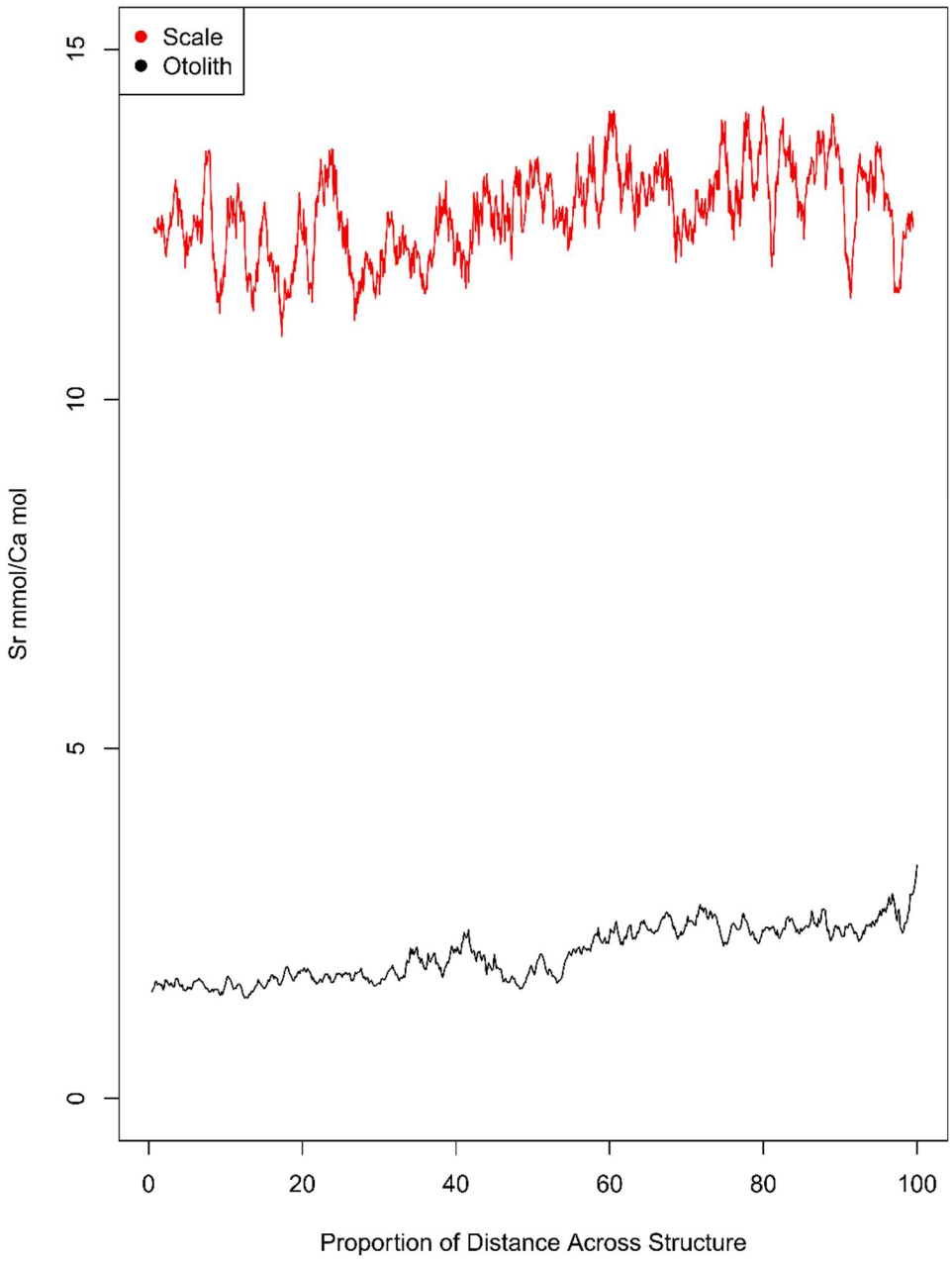
Scale
Otolith
Sr mmol/Ca mol
0
5
10
15
0
20
40
60
80
100
Proportion of Distance Across Structure

RD-042

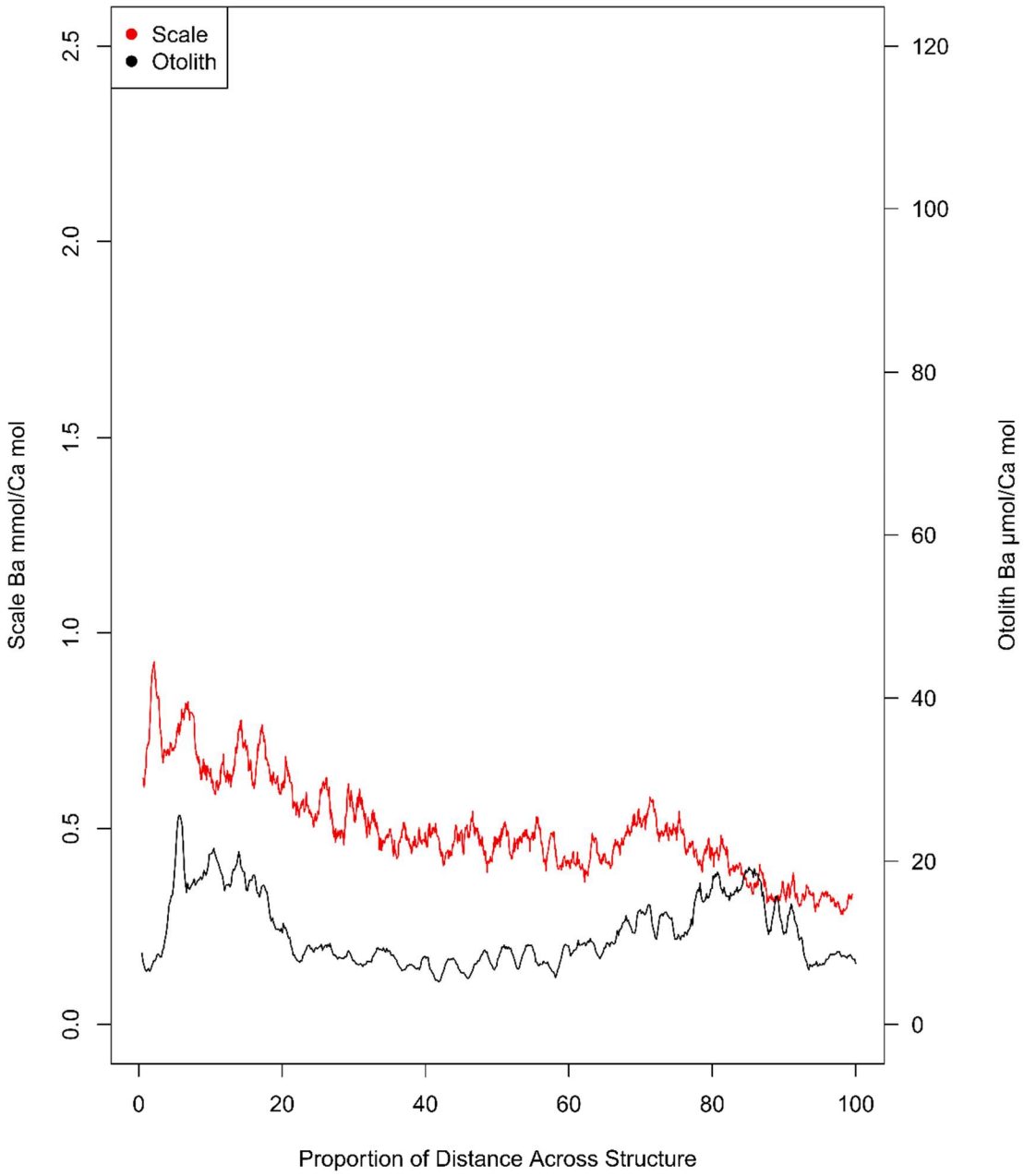
Scale
Otolith
Scale Ba mmol/Ca mol
Otolith Ba µmol/Ca mol
Proportion of Distance Across Structure
0.0
0.5
1.0
1.5
2.0
2.5
0
20
40
60
80
100
120

RD-042

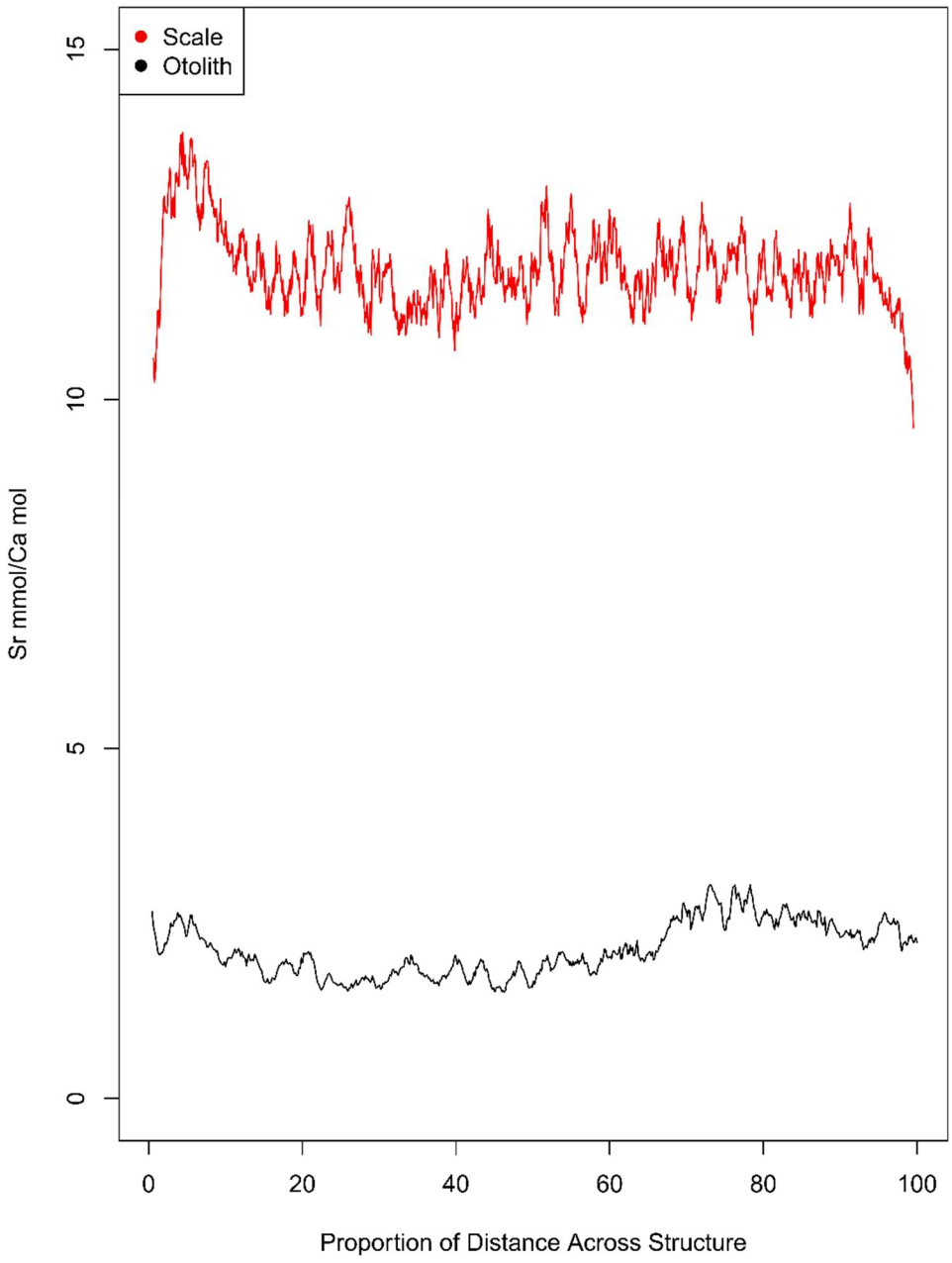
Scale
Otolith
Sr mmol/Ca mol
0
5
10
15
0
20
40
60
80
100
Proportion of Distance Across Structure

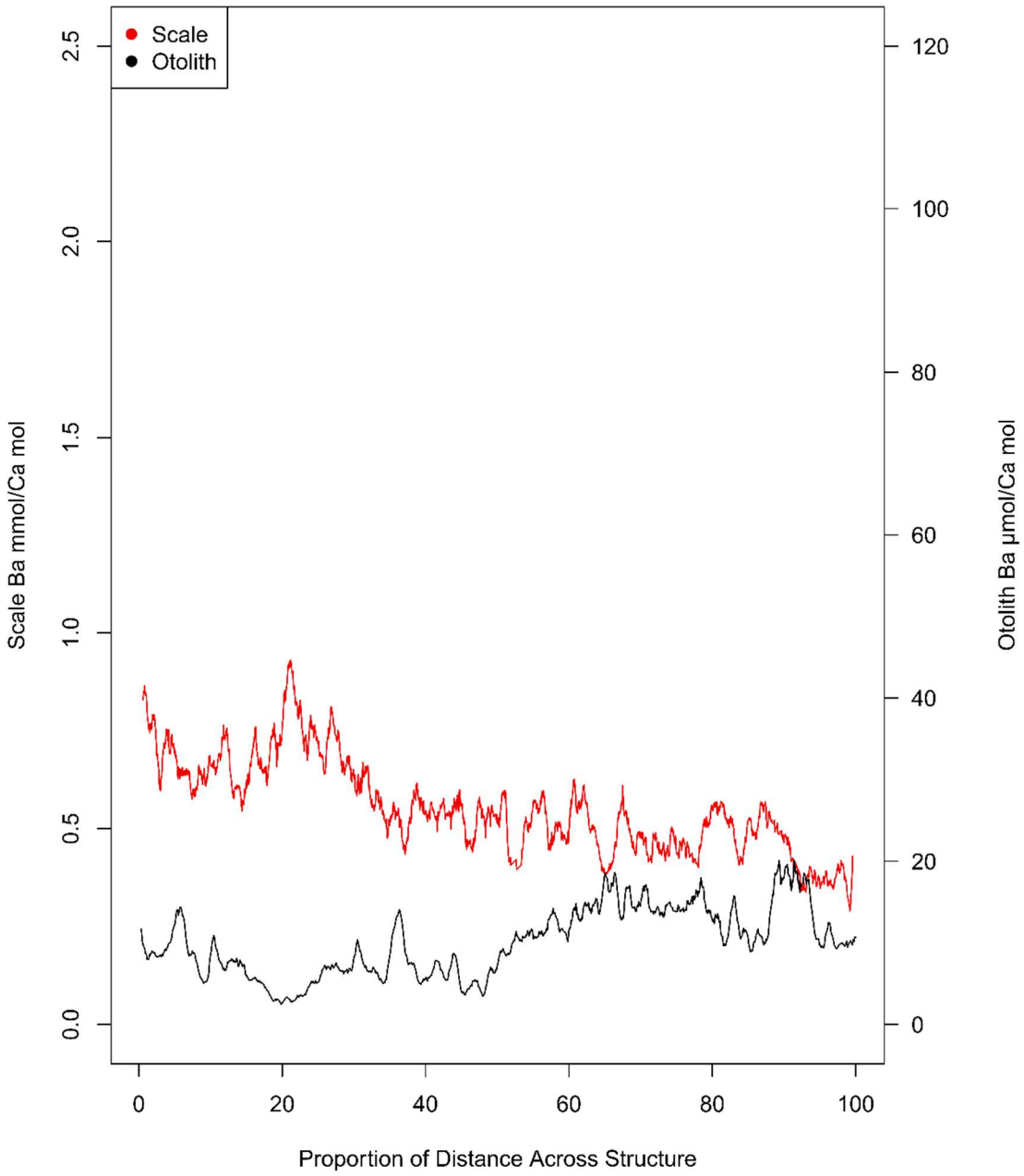
RD−043
Scale
Otolith
Scale Ba mmol/Ca mol
Otolith Ba µmol/Ca mol
Proportion of Distance Across Structure
0.0
0.5
1.0
1.5
2.0
2.5
0
20
40
60
80
100
120

RD-043

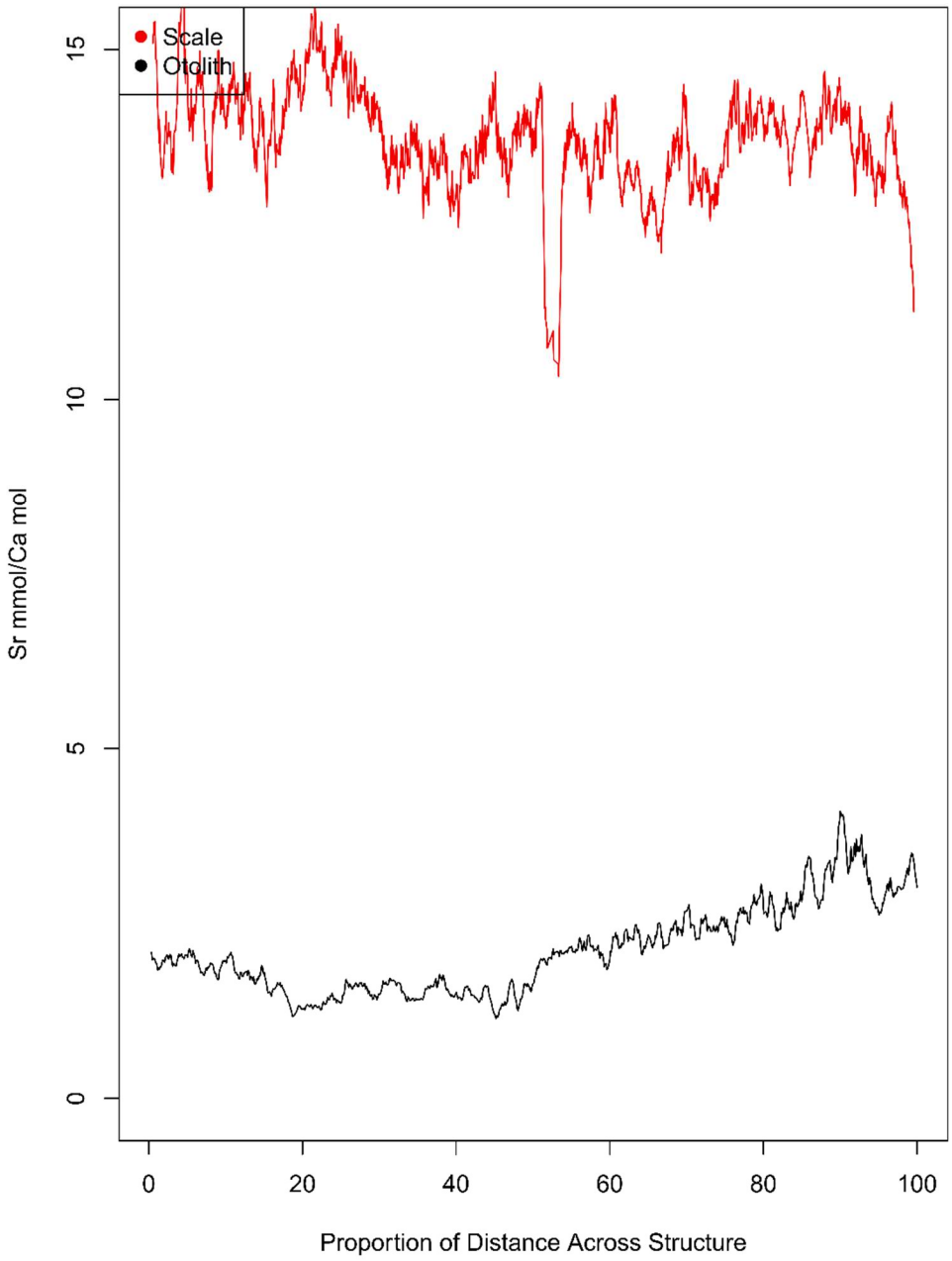
Scale
Otolith
Sr mmol/Ca mol
0
5
10
15
0
20
40
60
80
100
Proportion of Distance Across Structure

RD-044

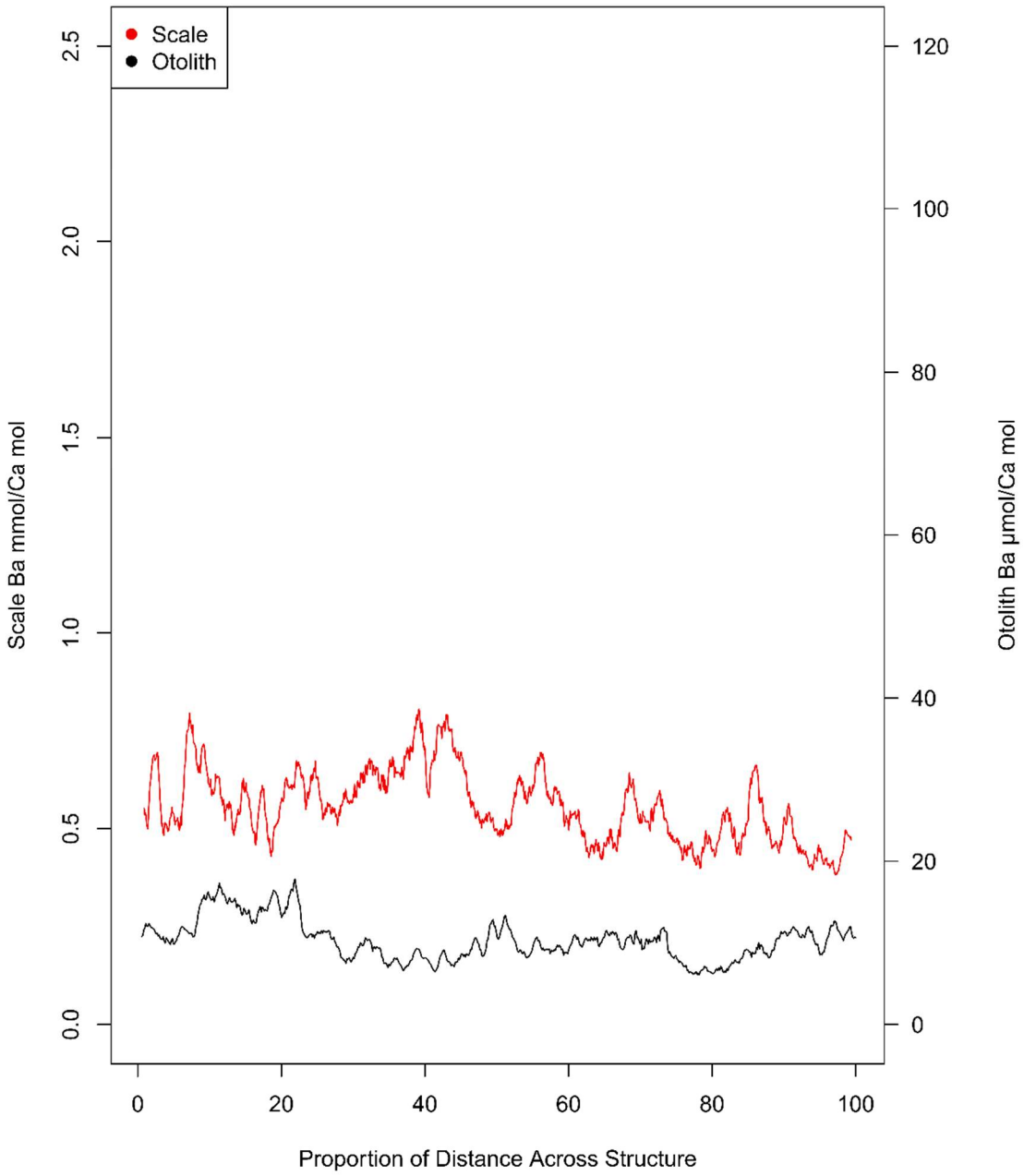
Scale
Otolith
Scale Ba mmol/Ca mol
Otolith Ba µmol/Ca mol
Proportion of Distance Across Structure
0.0
0.5
1.0
1.5
2.0
2.5
0
20
40
60
80
100
120

RD-044

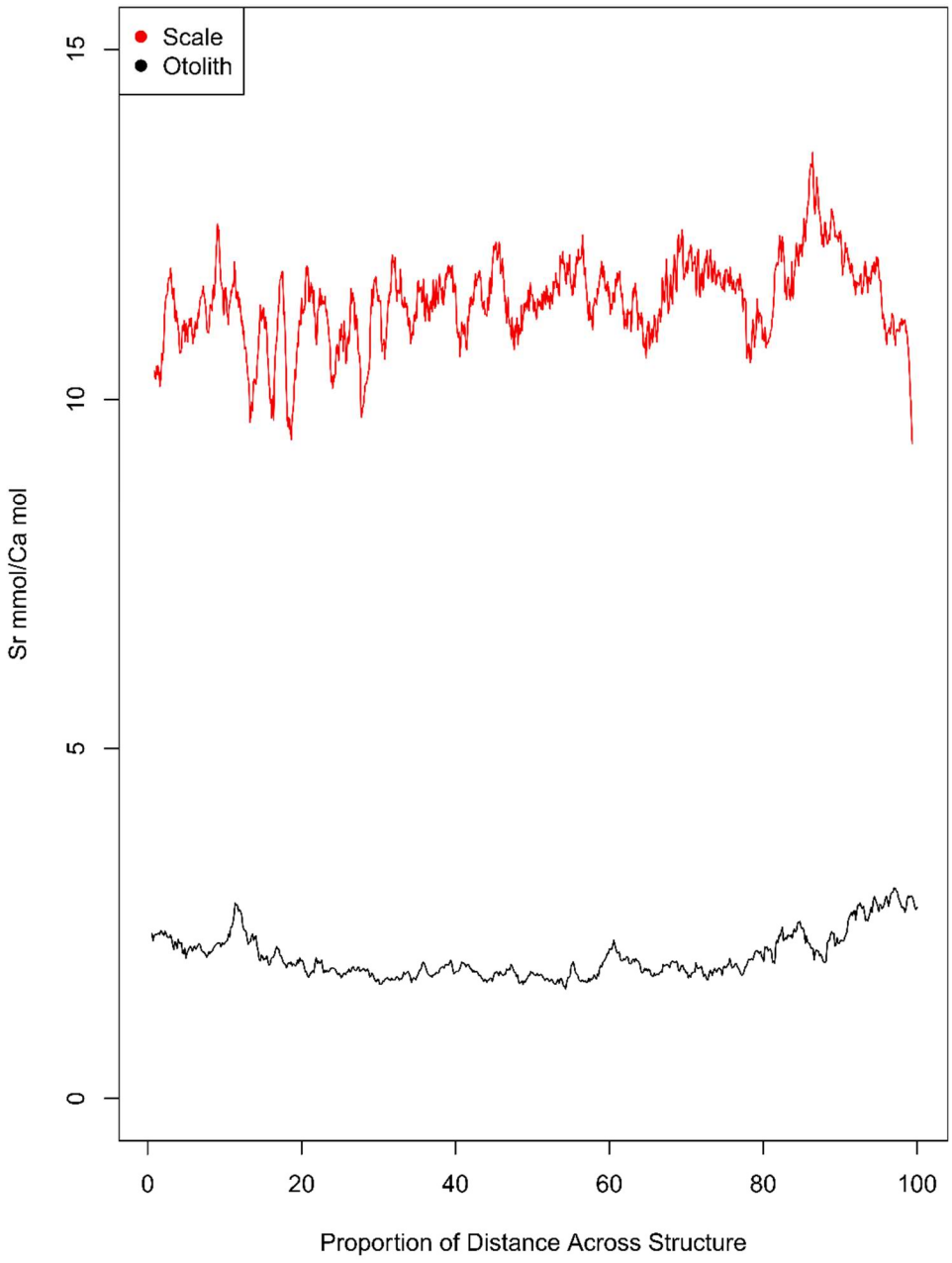
Scale
Otolith
Sr mmol/Ca mol
0
5
10
15
0
20
40
60
80
100
Proportion of Distance Across Structure

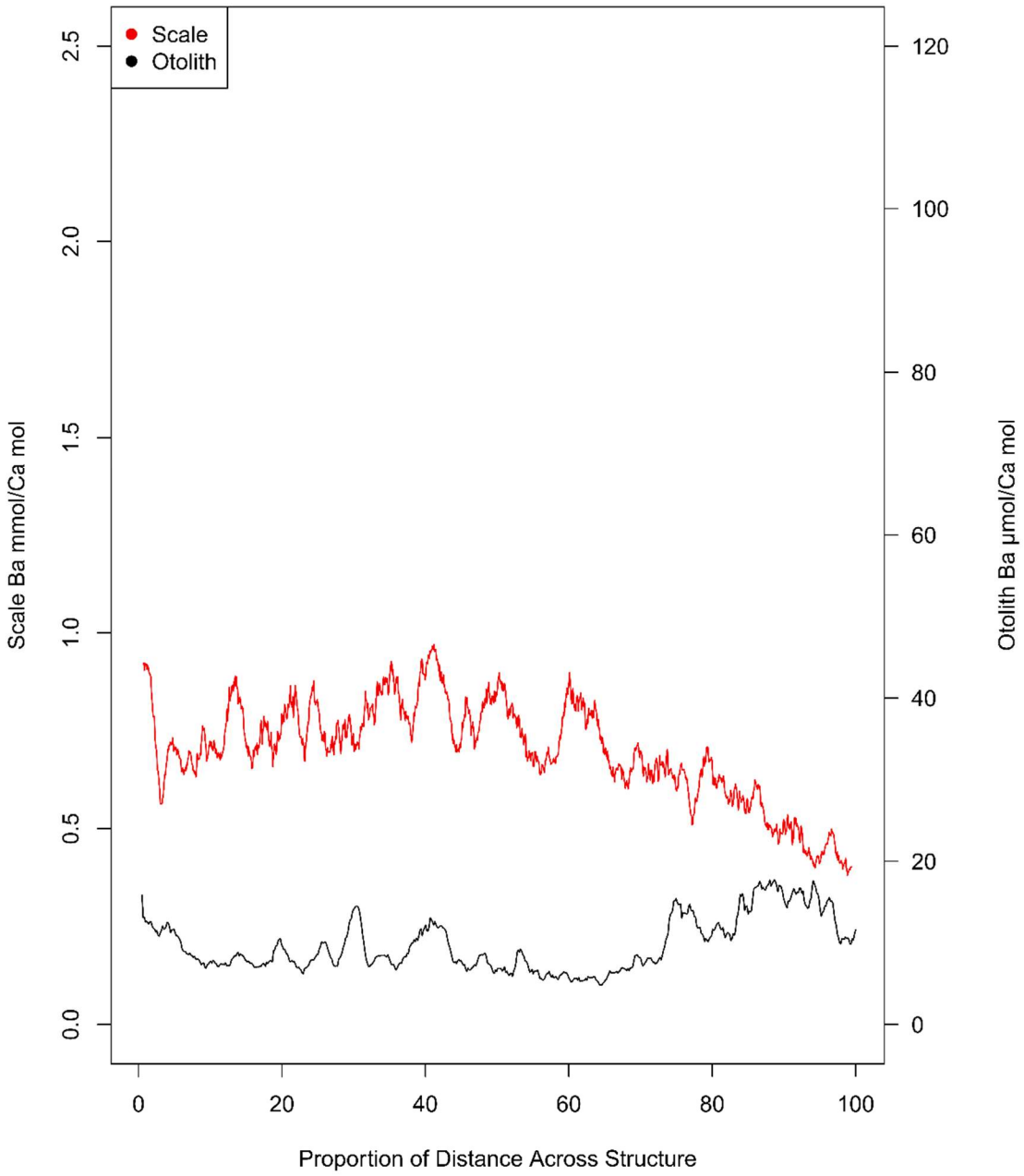
RD-045
Scale
Otolith
Scale Ba mmol/Ca mol
Otolith Ba µmol/Ca mol
Proportion of Distance Across Structure
0.0
0.5
1.0
1.5
2.0
2.5
0
20
40
60
80
100
120

RD-045

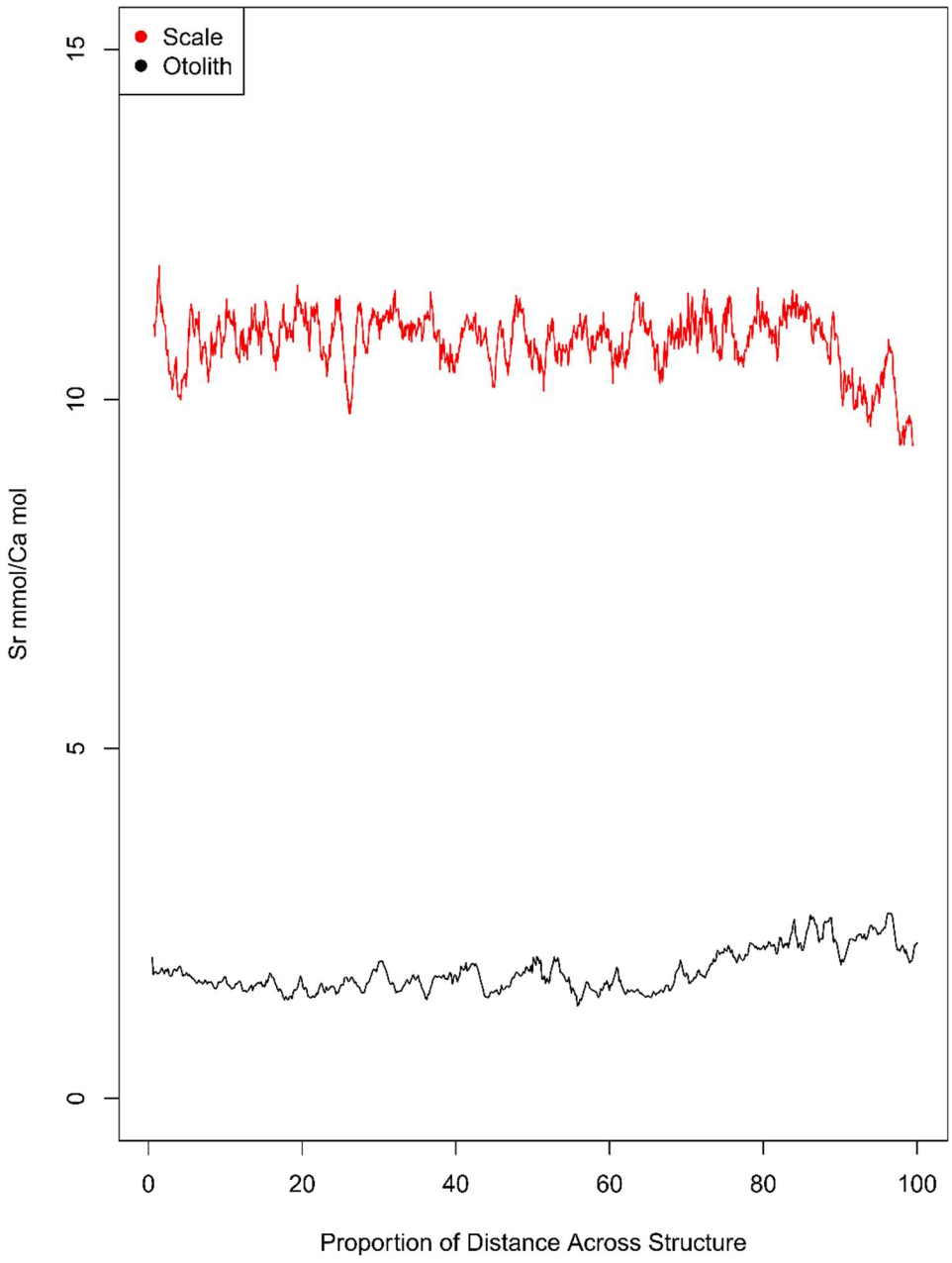
Scale
Otolith
Sr mmol/Ca mol
0
5
10
15
0
20
40
60
80
100
Proportion of Distance Across Structure

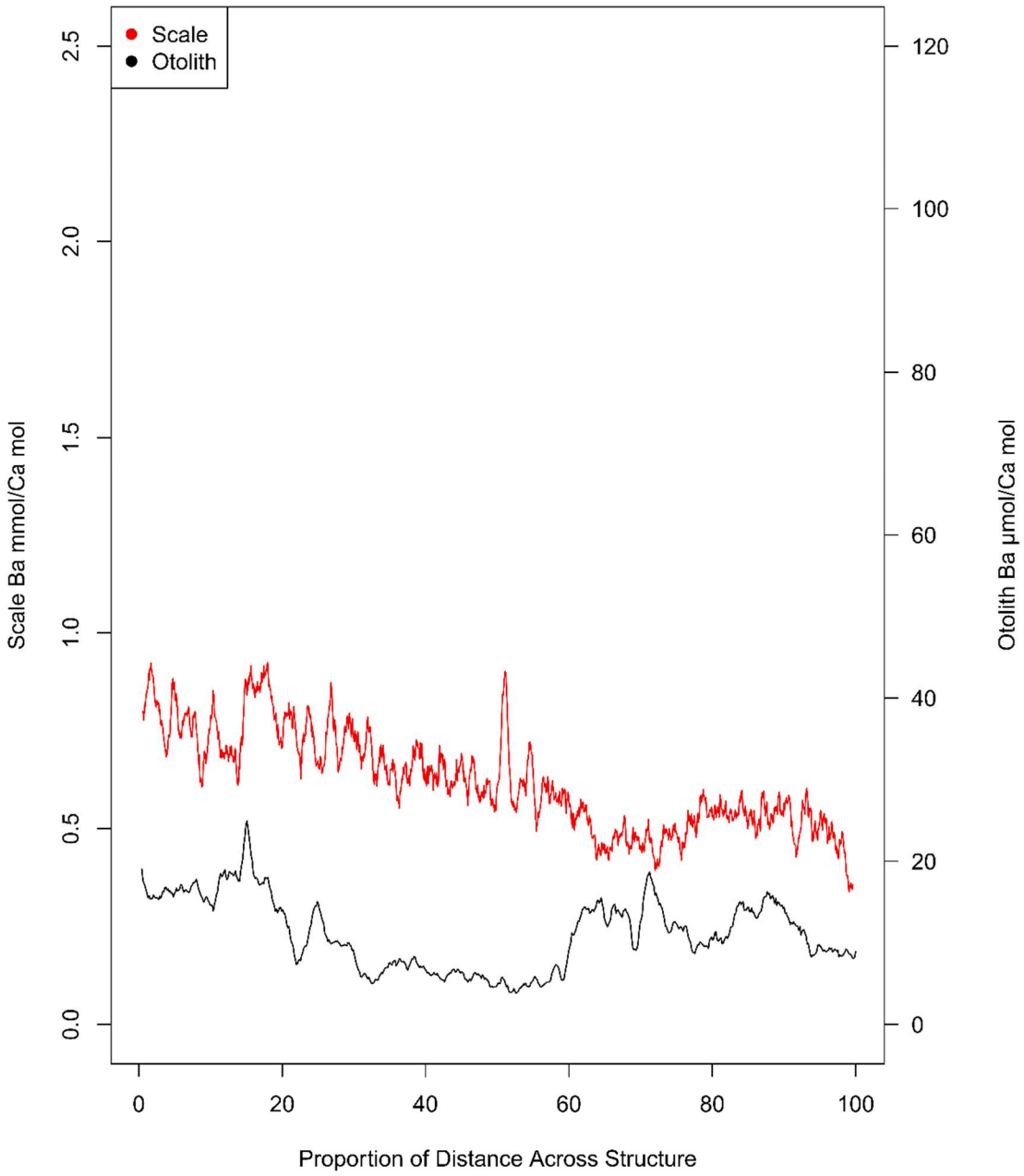
RD−046
Scale
Otolith
Scale Ba mmol/Ca mol
Otolith Ba µmol/Ca mol
Proportion of Distance Across Structure
0.0
0.5
1.0
1.5
2.0
2.5
0
20
40
60
80
100
120

RD-046

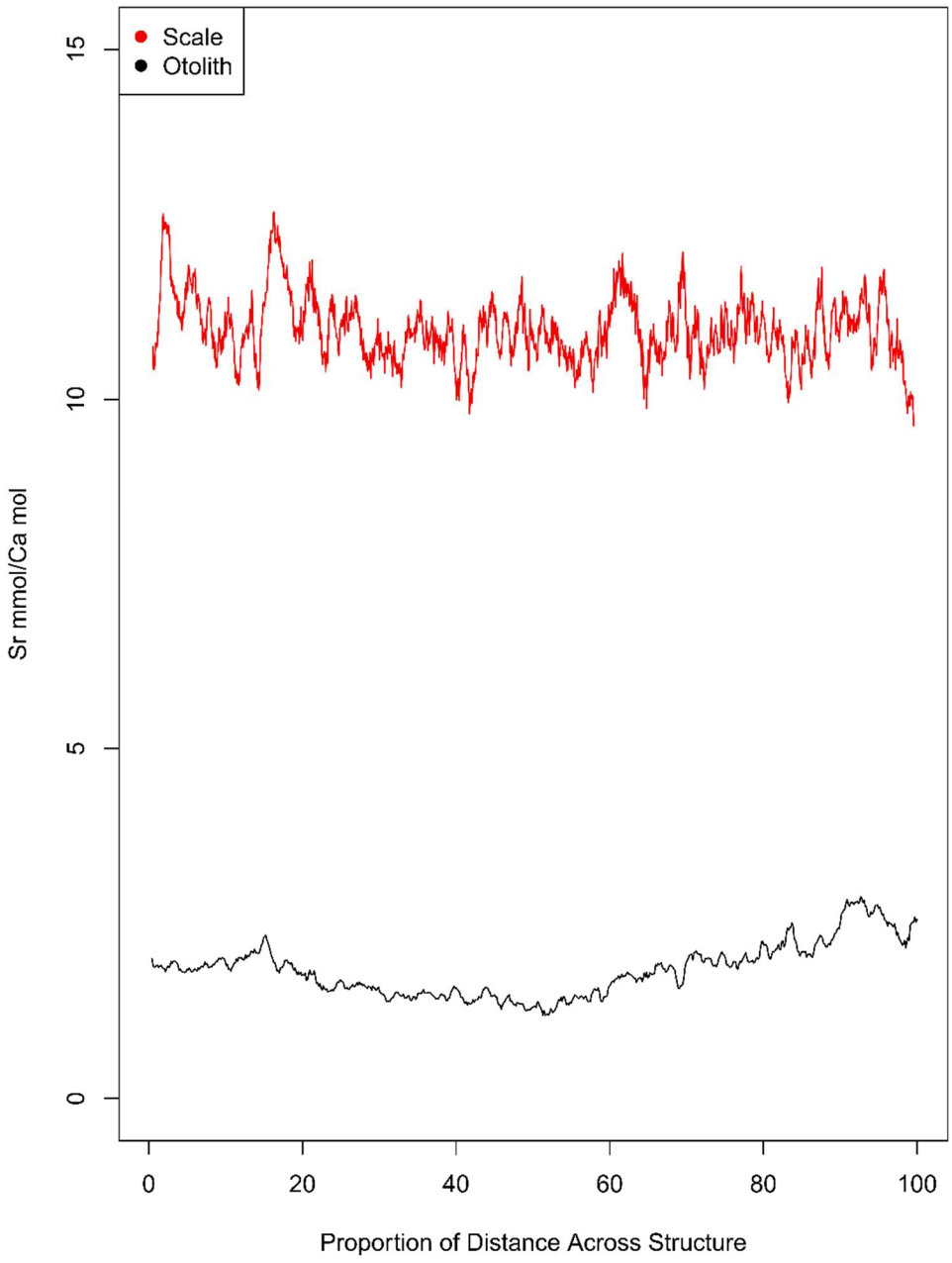
Scale
Otolith
Sr mmol/Ca mol
0
5
10
15
0
20
40
60
80
100
Proportion of Distance Across Structure

RD-047

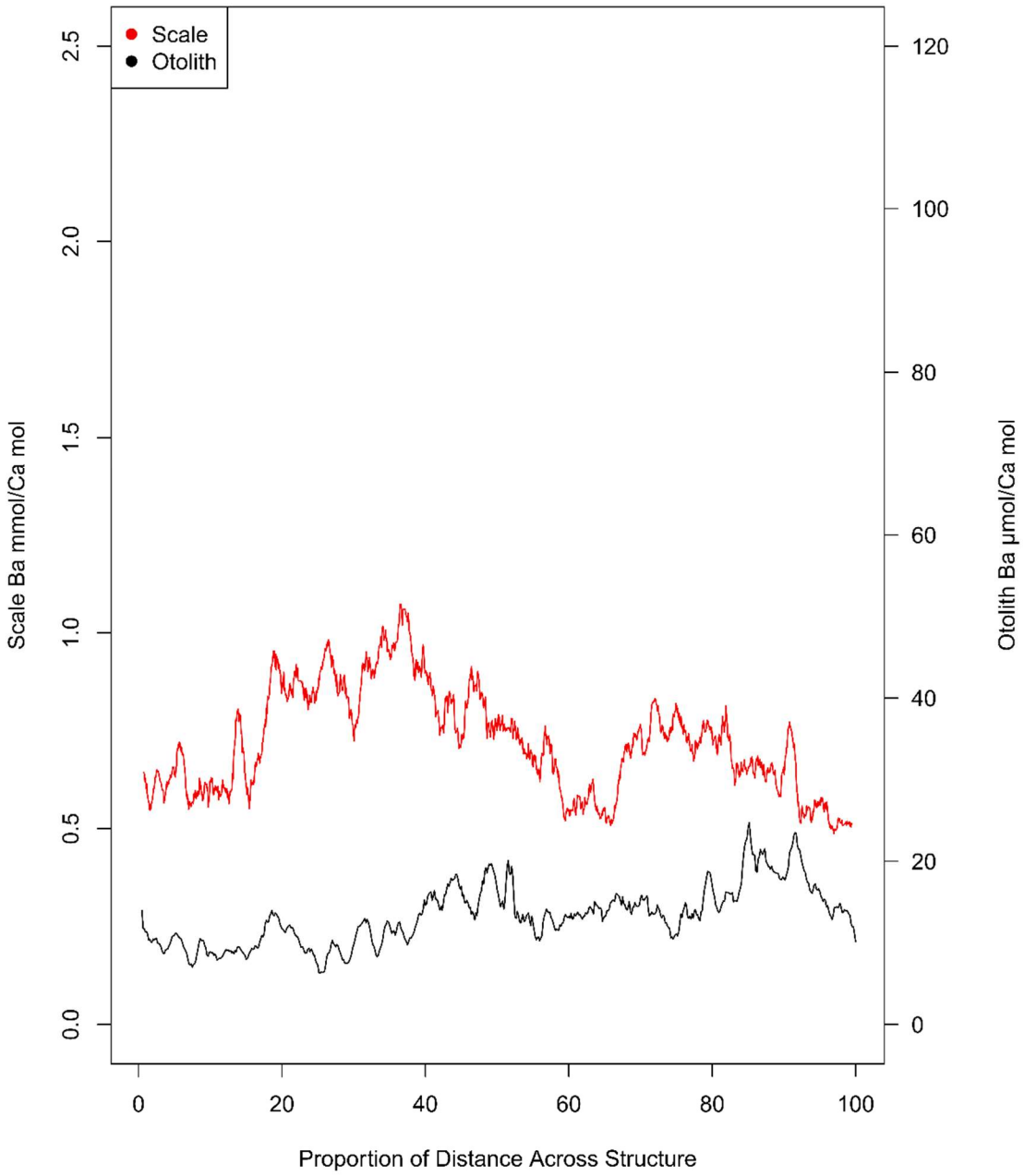
Scale
Otolith
Scale Ba mmol/Ca mol
Otolith Ba µmol/Ca mol
Proportion of Distance Across Structure
0.0
0.5
1.0
1.5
2.0
2.5
0
20
40
60
80
100
120

RD-047

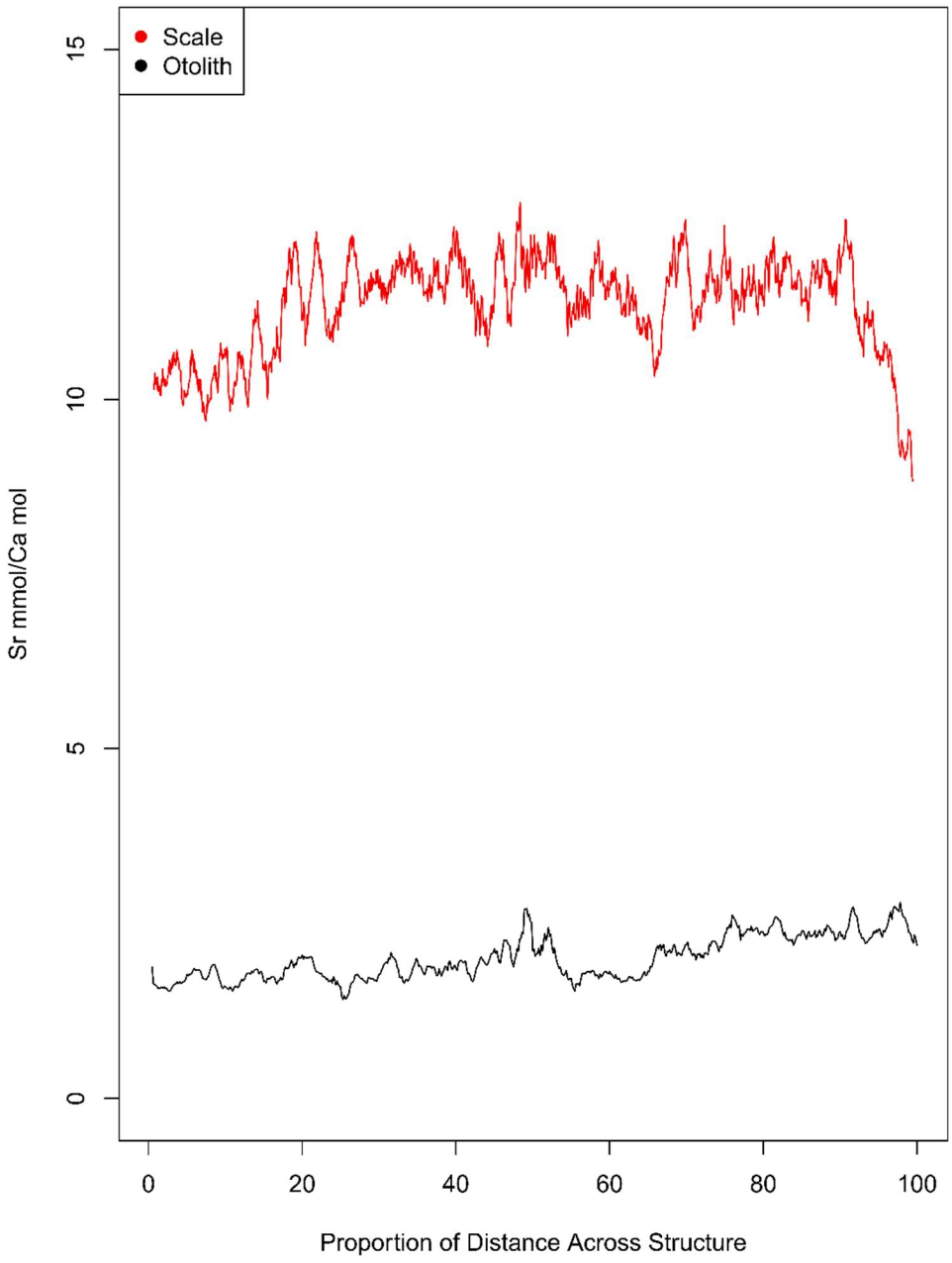
Scale
Otolith
Sr mmol/Ca mol
0
5
10
15
0
20
40
60
80
100
Proportion of Distance Across Structure

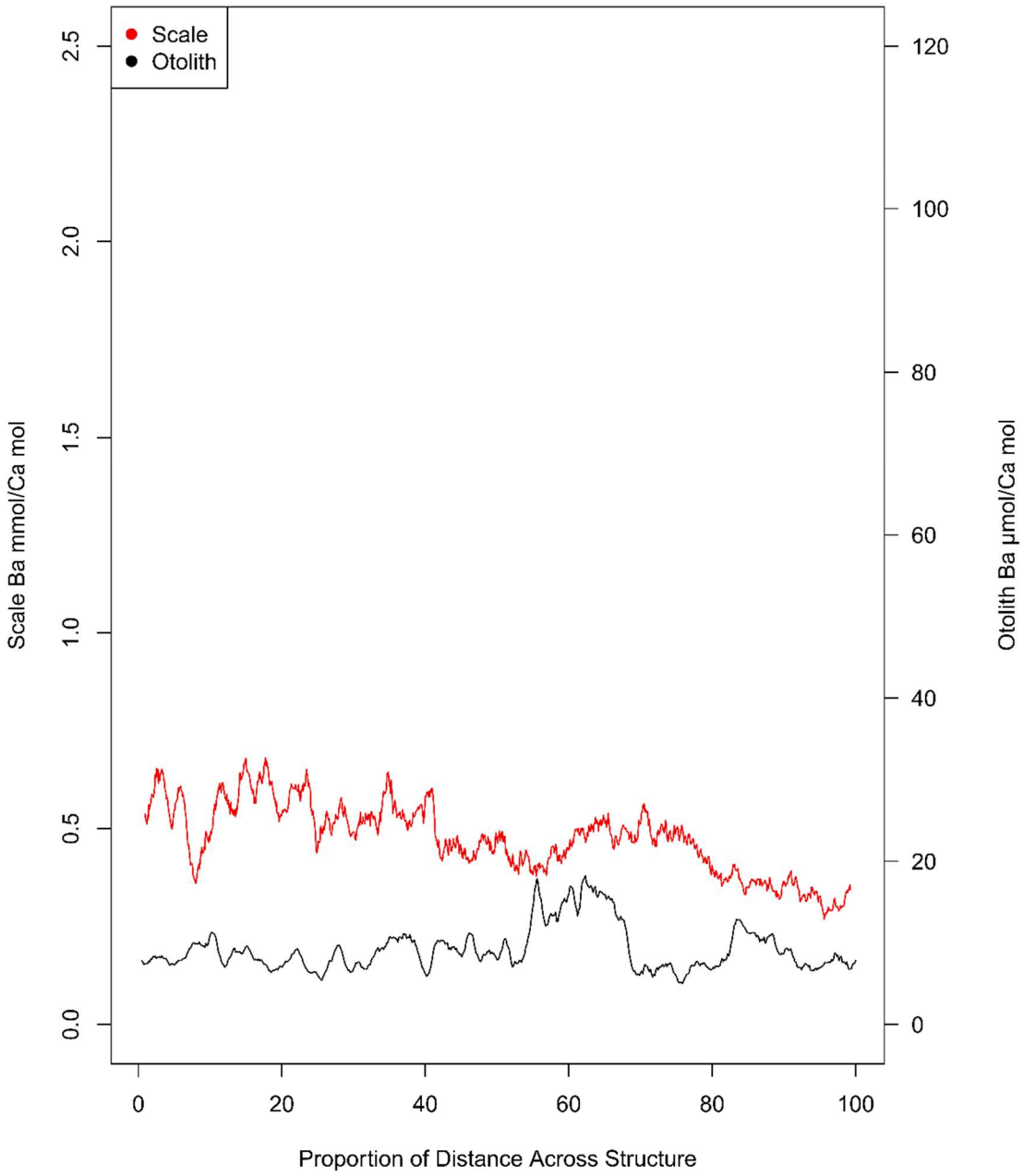
RD−048
Scale
Otolith
Scale Ba mmol/Ca mol
Otolith Ba µmol/Ca mol
Proportion of Distance Across Structure
0.0
0.5
1.0
1.5
2.0
2.5
0
20
40
60
80
100
120

RD-048

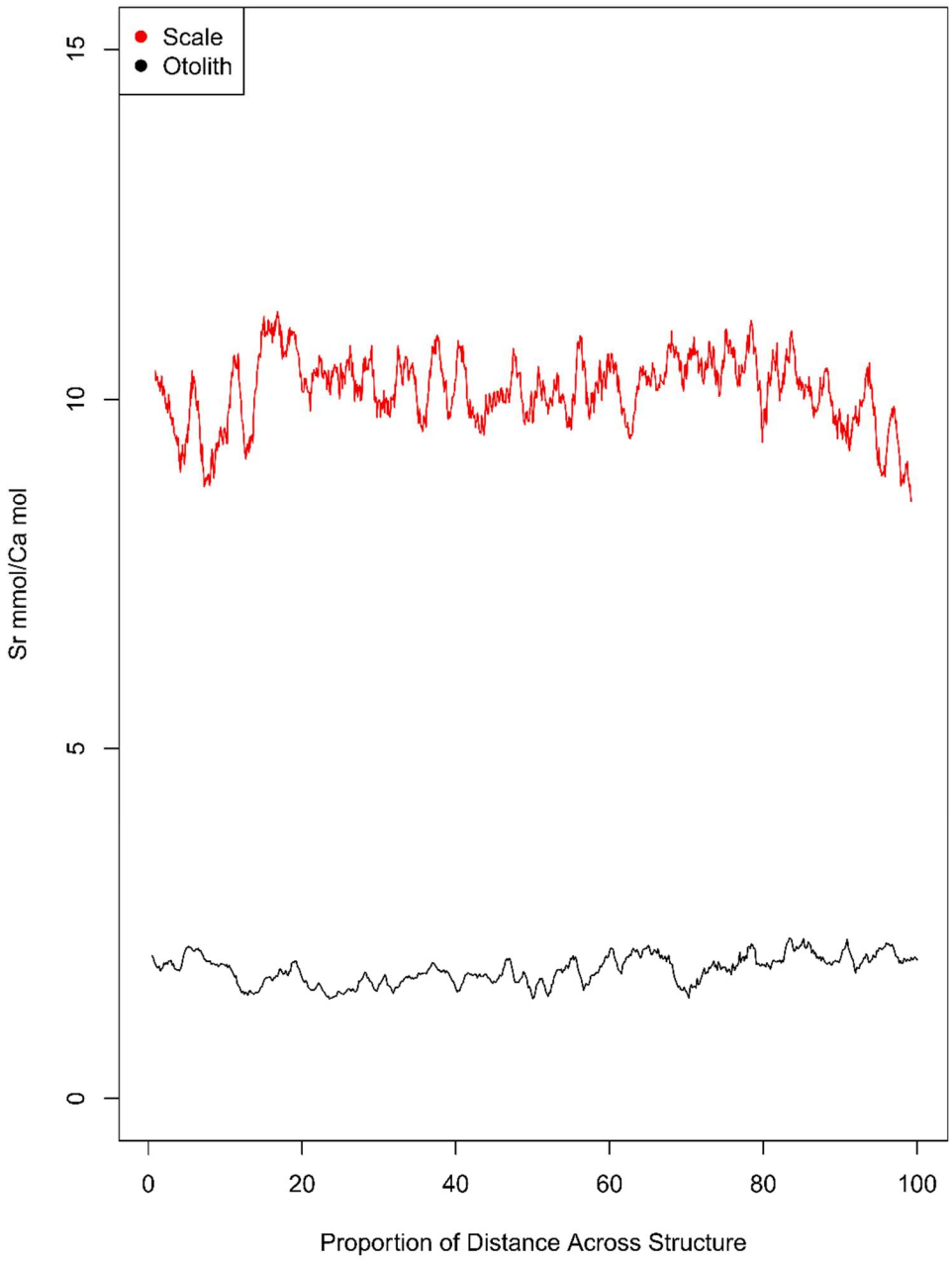
Scale
Otolith
Sr mmol/Ca mol
0
5
10
15
0
20
40
60
80
100
Proportion of Distance Across Structure

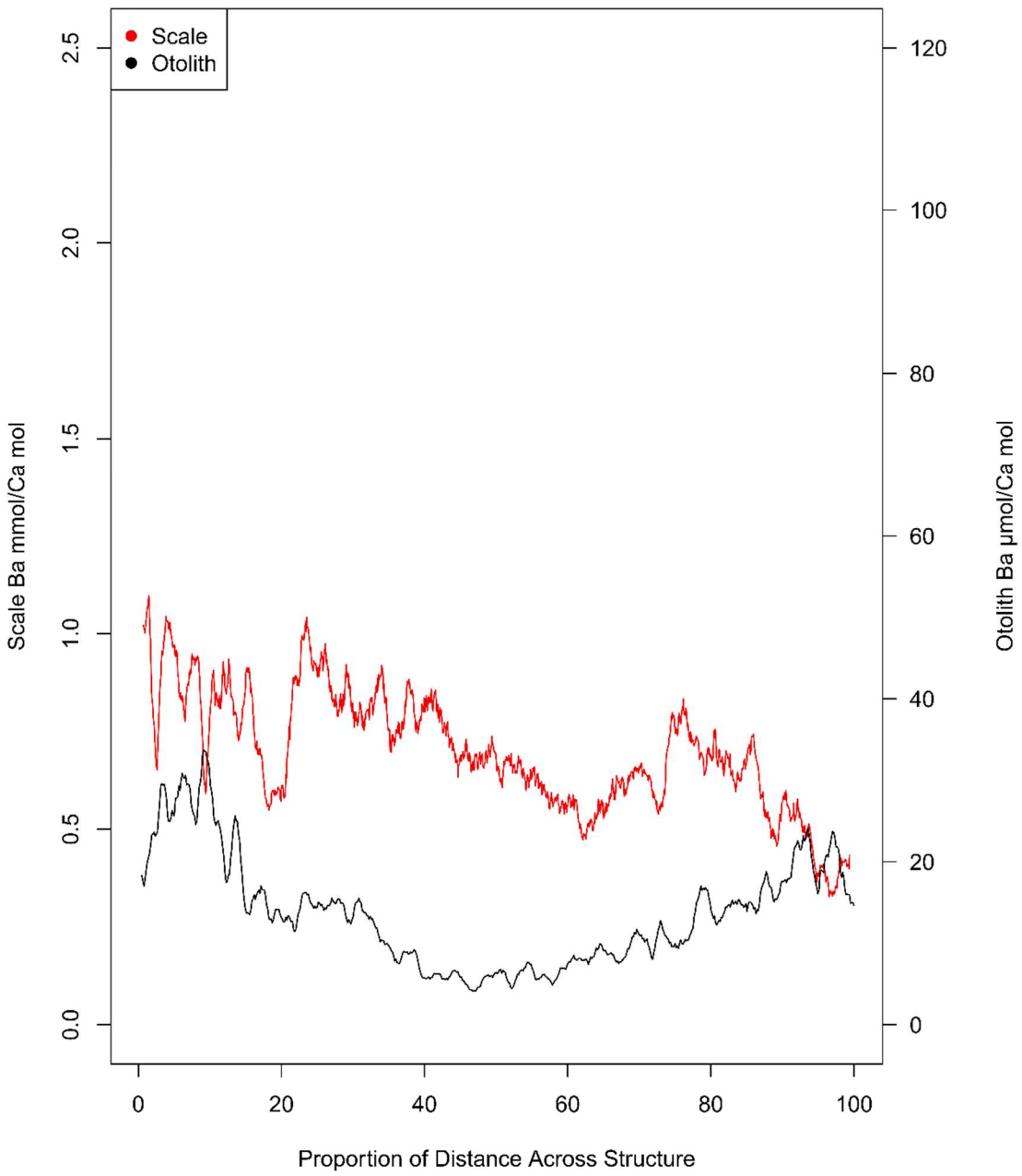
RD−049
Scale
Otolith
Scale Ba mmol/Ca mol
Otolith Ba µmol/Ca mol
Proportion of Distance Across Structure
0.0
0.5
1.0
1.5
2.0
2.5
0
20
40
60
80
100
120

RD-049

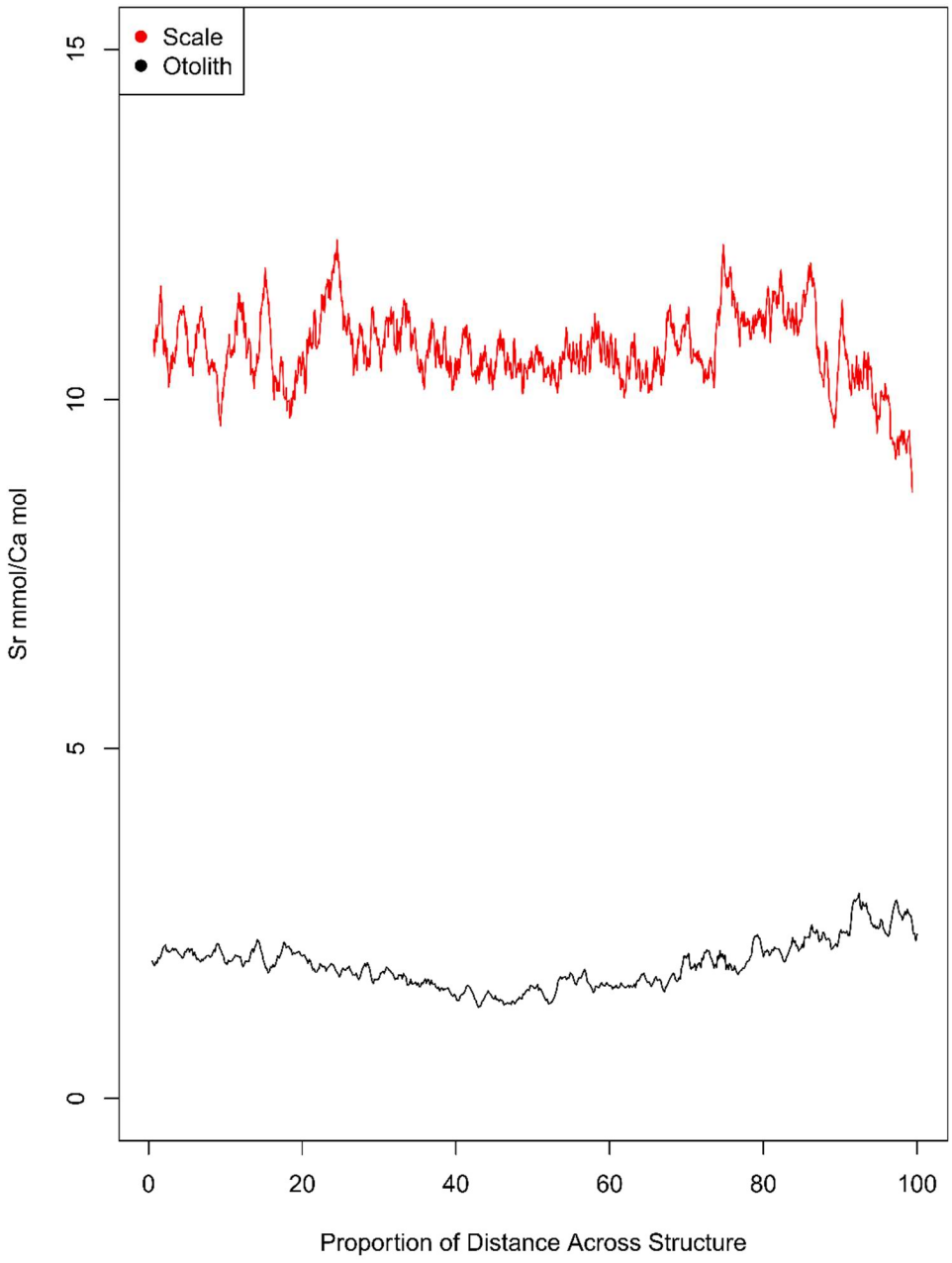
Scale
Otolith
Sr mmol/Ca mol
0
5
10
15
0
20
40
60
80
100
Proportion of Distance Across Structure

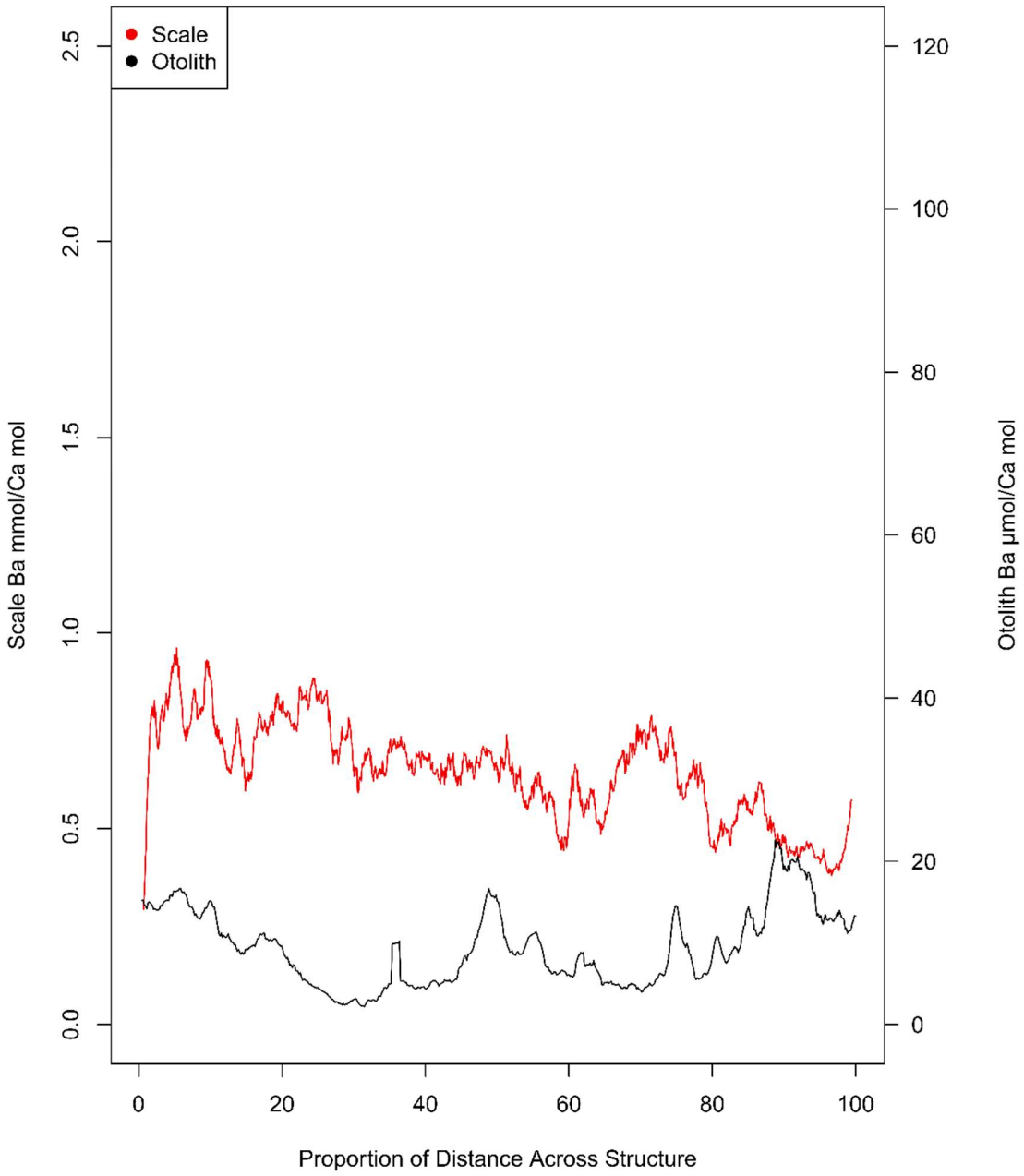
RD-050
Scale
Otolith
Scale Ba mmol/Ca mol
Otolith Ba µmol/Ca mol
Proportion of Distance Across Structure
0.0
0.5
1.0
1.5
2.0
2.5
0
20
40
60
80
100
120

RD-050

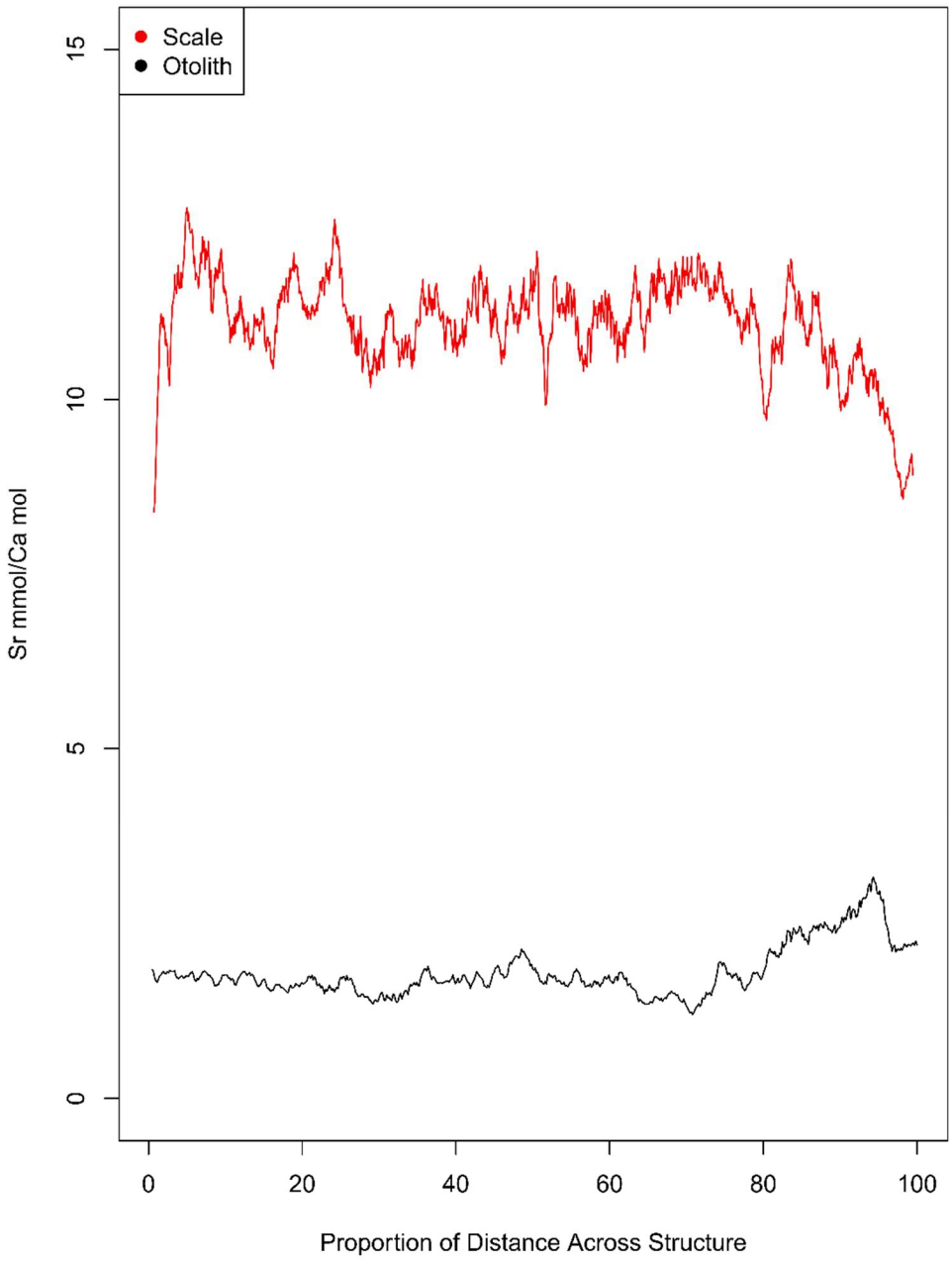
Scale
Otolith
Sr mmol/Ca mol
0
5
10
15
0
20
40
60
80
100
Proportion of Distance Across Structure

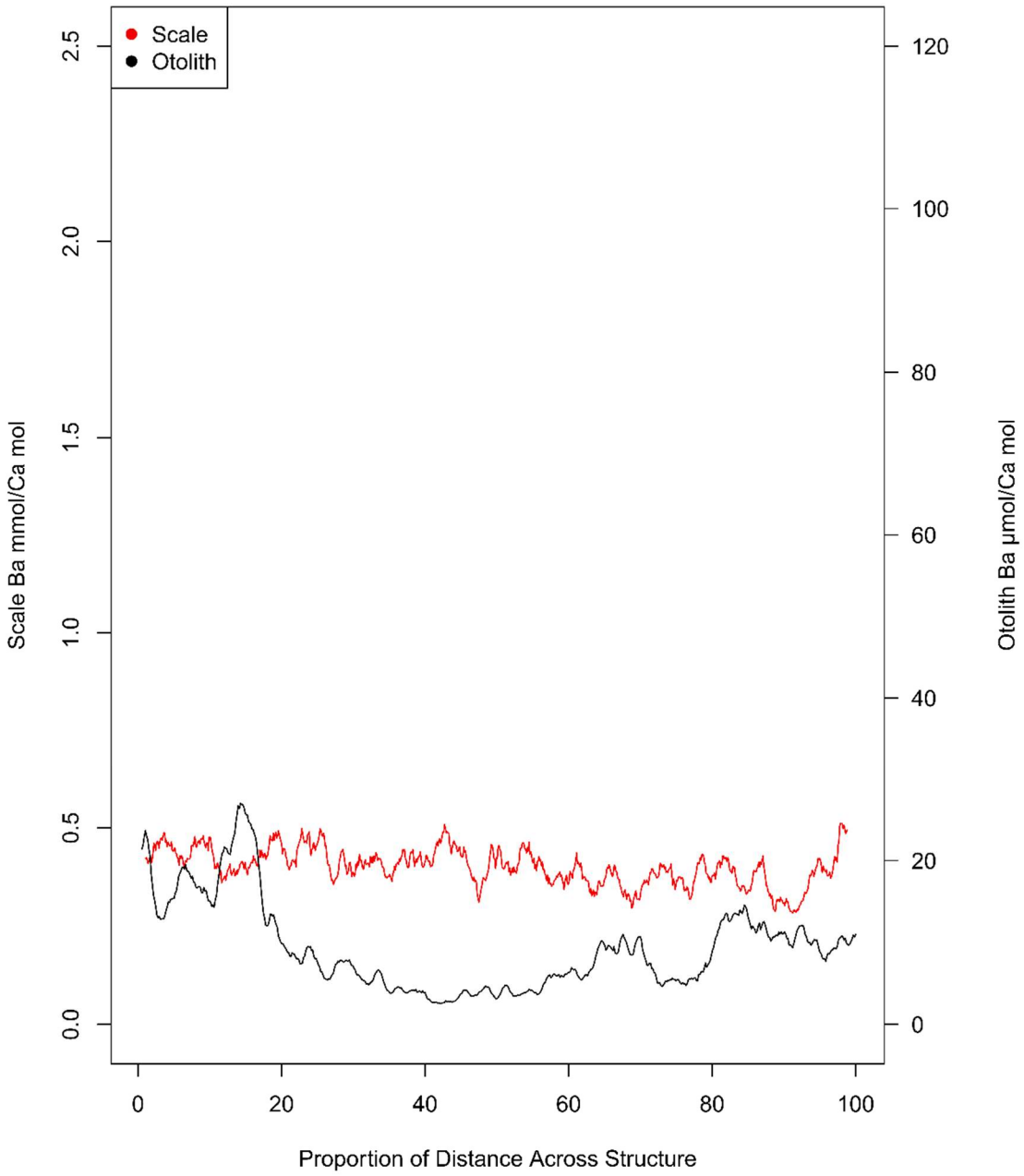
RD-051
Scale
Otolith
Scale Ba mmol/Ca mol
Otolith Ba µmol/Ca mol
Proportion of Distance Across Structure
0.0
0.5
1.0
1.5
2.0
2.5
0
20
40
60
80
100
120

RD-051

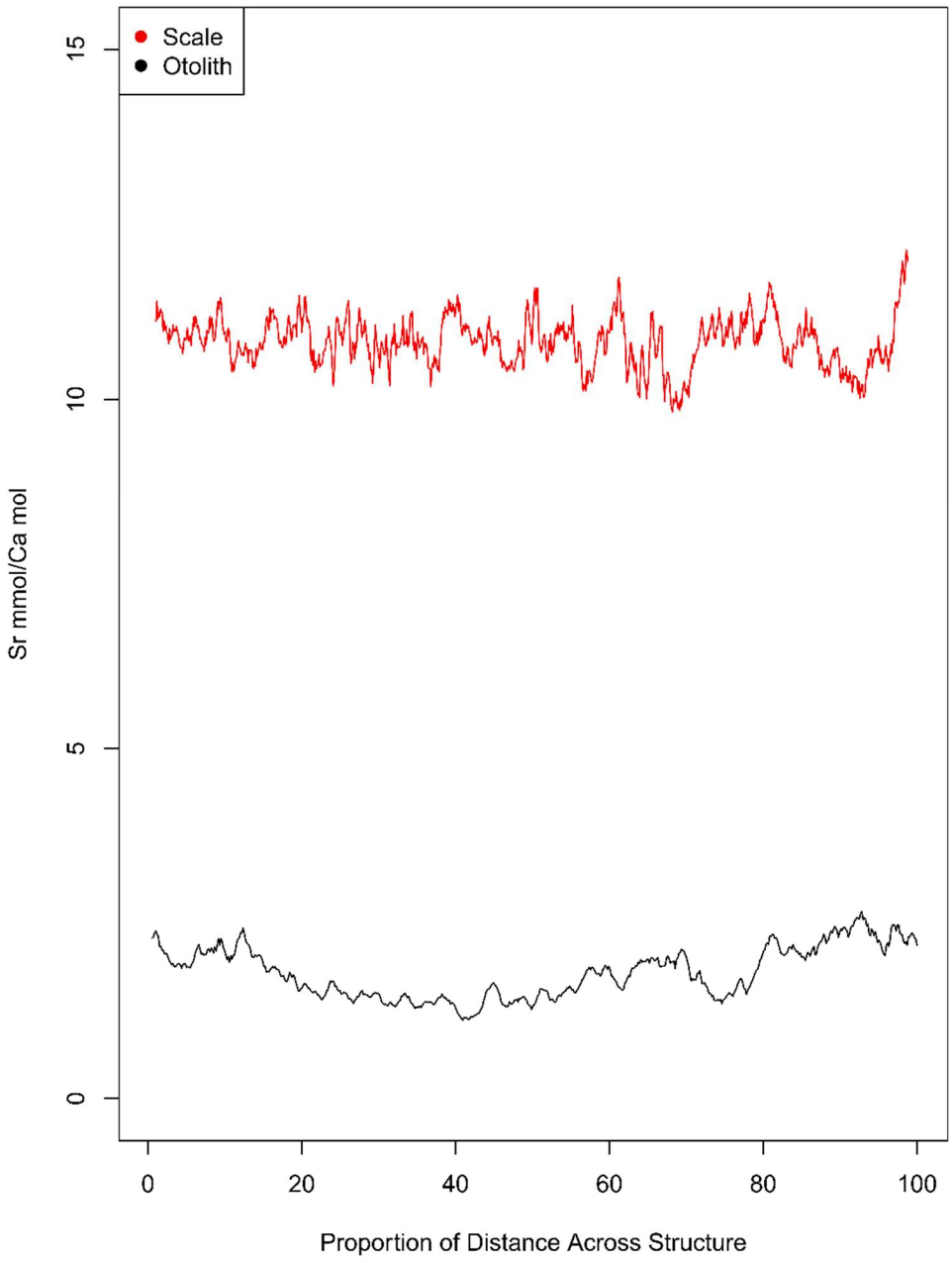
Scale
Otolith
Sr mmol/Ca mol
0
5
10
15
0
20
40
60
80
100
Proportion of Distance Across Structure

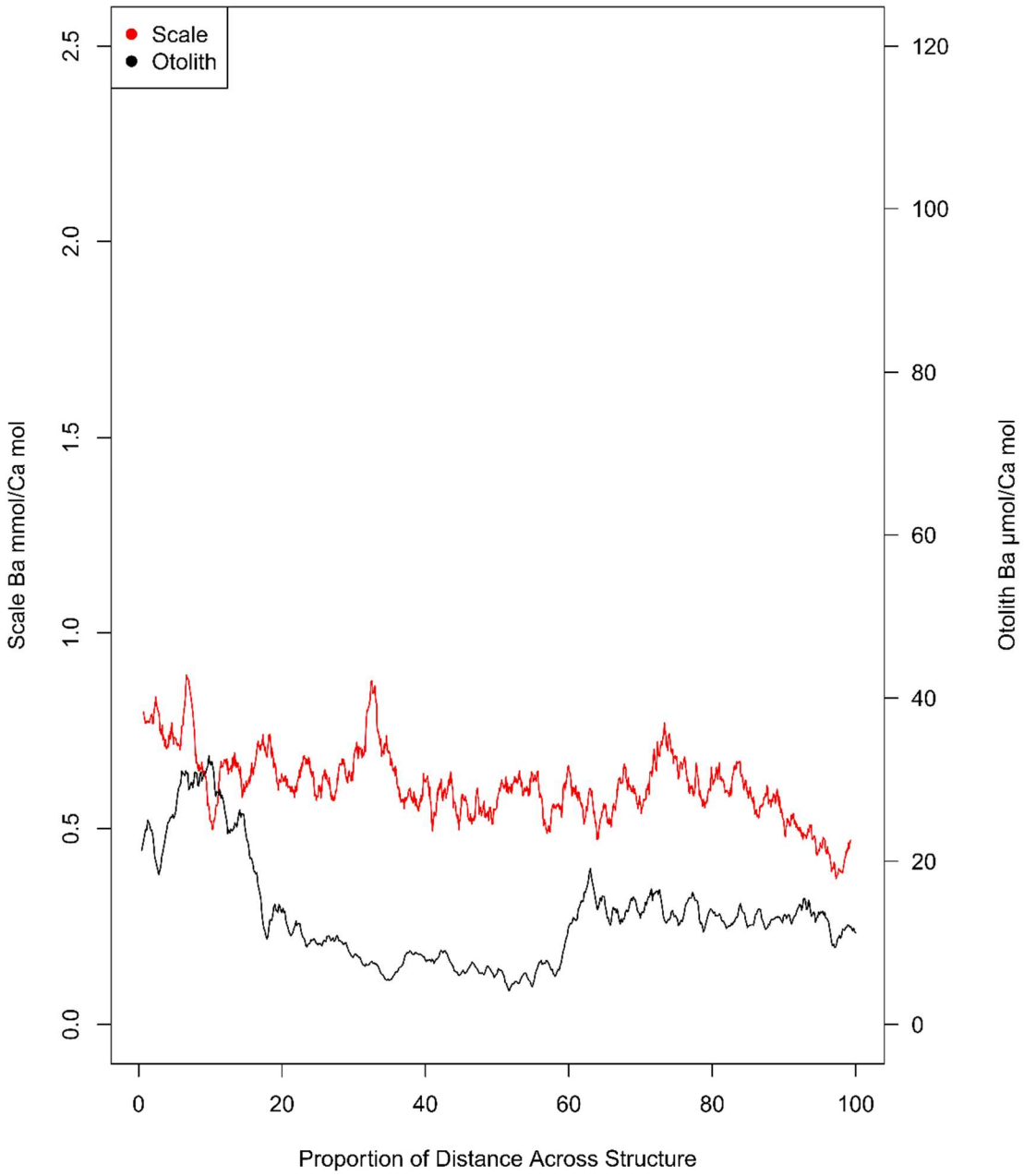
RD−052
Scale
Otolith
Scale Ba mmol/Ca mol
Otolith Ba µmol/Ca mol
Proportion of Distance Across Structure
0.0
0.5
1.0
1.5
2.0
2.5
0
20
40
60
80
100
120

RD-052

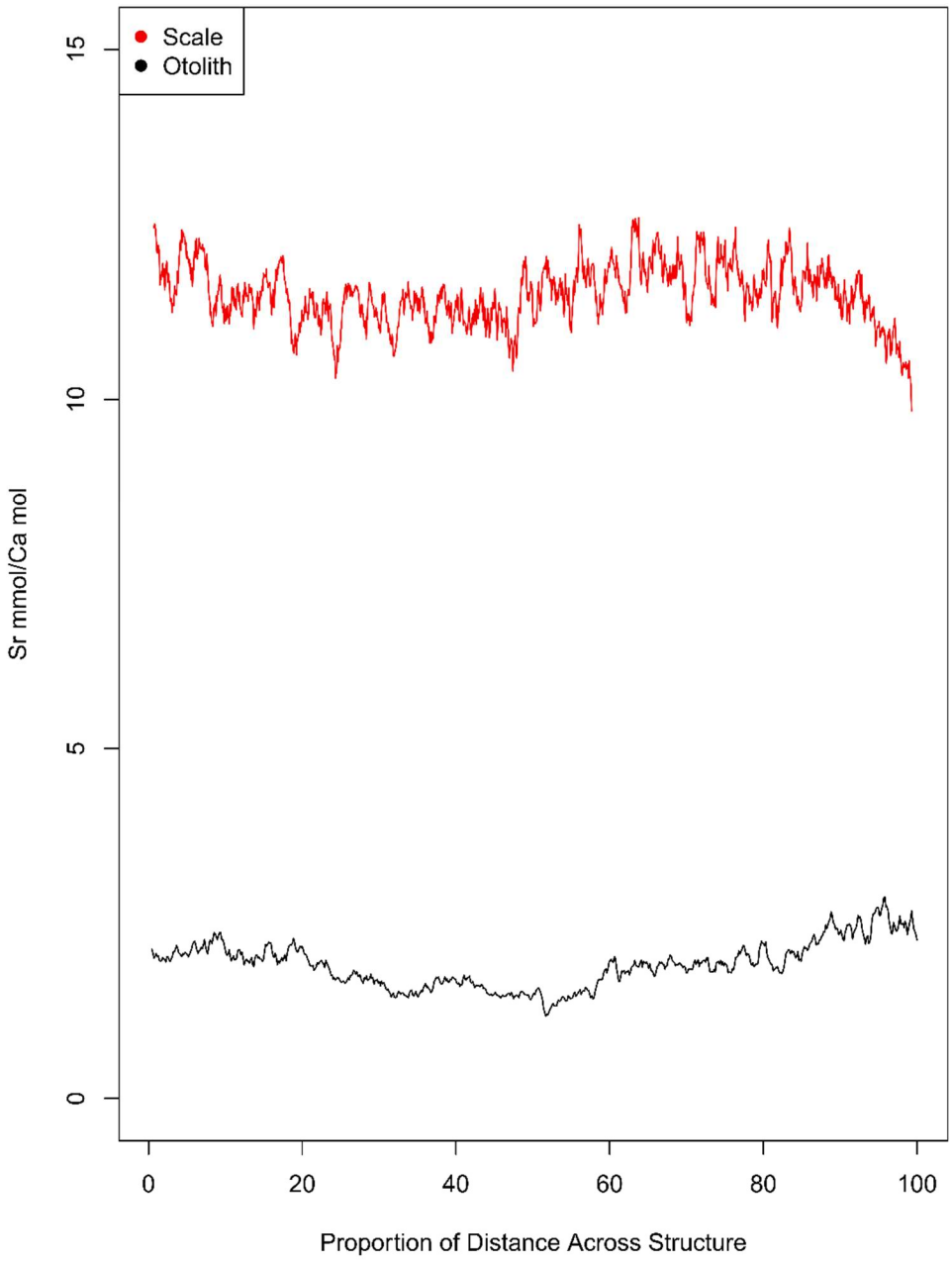
Scale
Otolith
Sr mmol/Ca mol
0
5
10
15
0
20
40
60
80
100
Proportion of Distance Across Structure

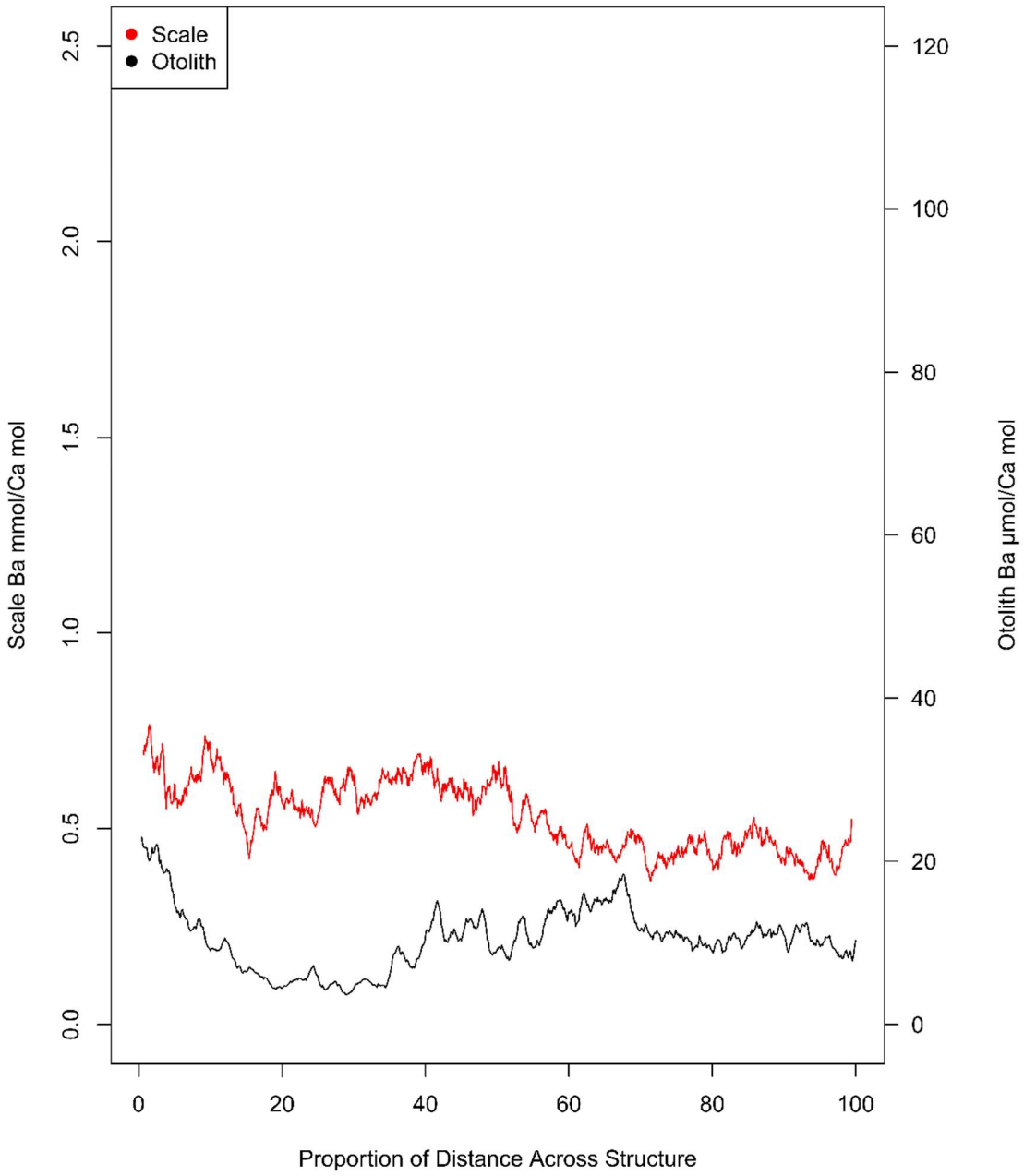
RD−053
Scale
Otolith
Scale Ba mmol/Ca mol
Otolith Ba µmol/Ca mol
Proportion of Distance Across Structure
0.0
0.5
1.0
1.5
2.0
2.5
0
20
40
60
80
100
120

RD-053

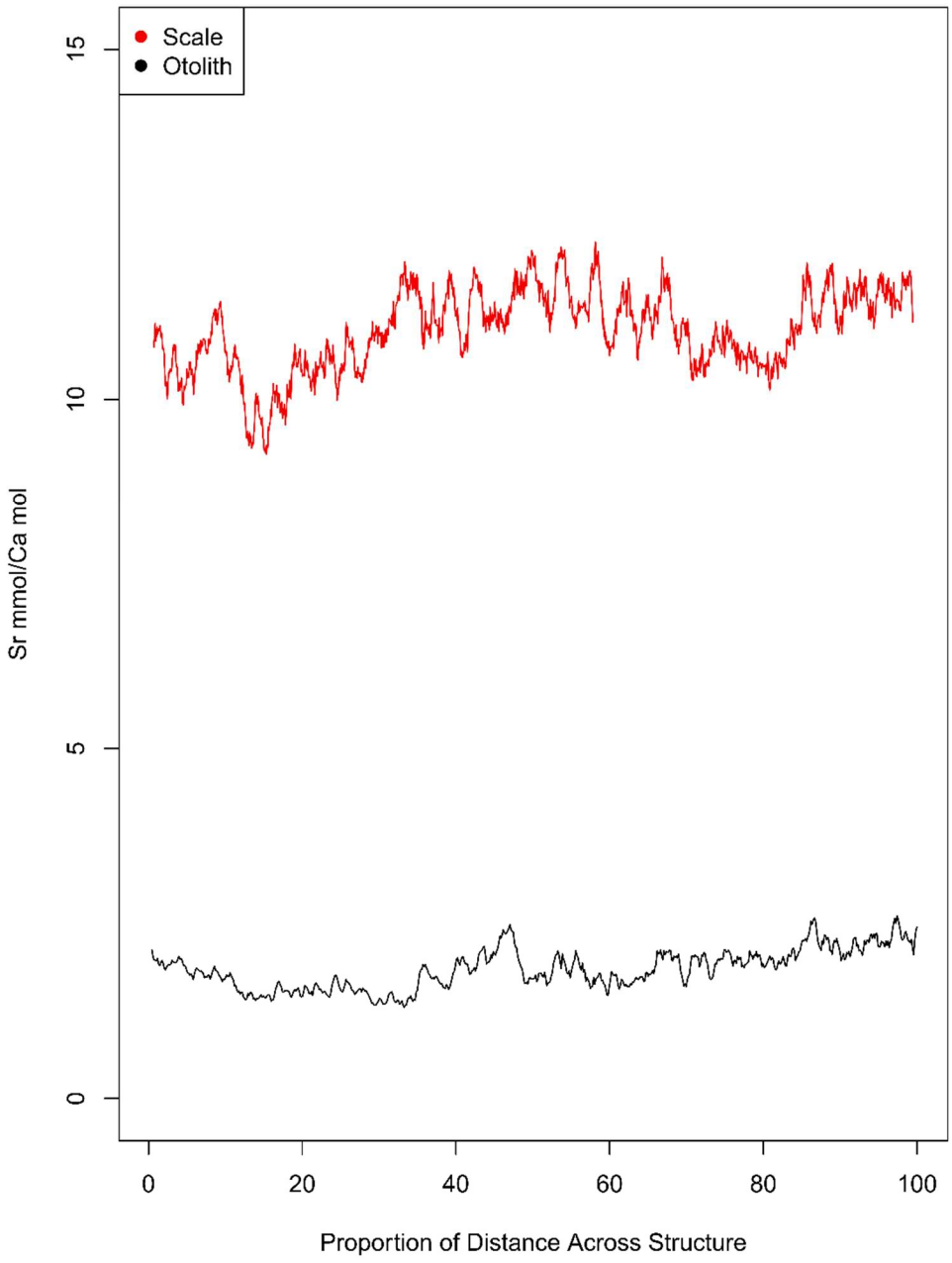
Scale
Otolith
Sr mmol/Ca mol
0
5
10
15
0
20
40
60
80
100
Proportion of Distance Across Structure

RD-054

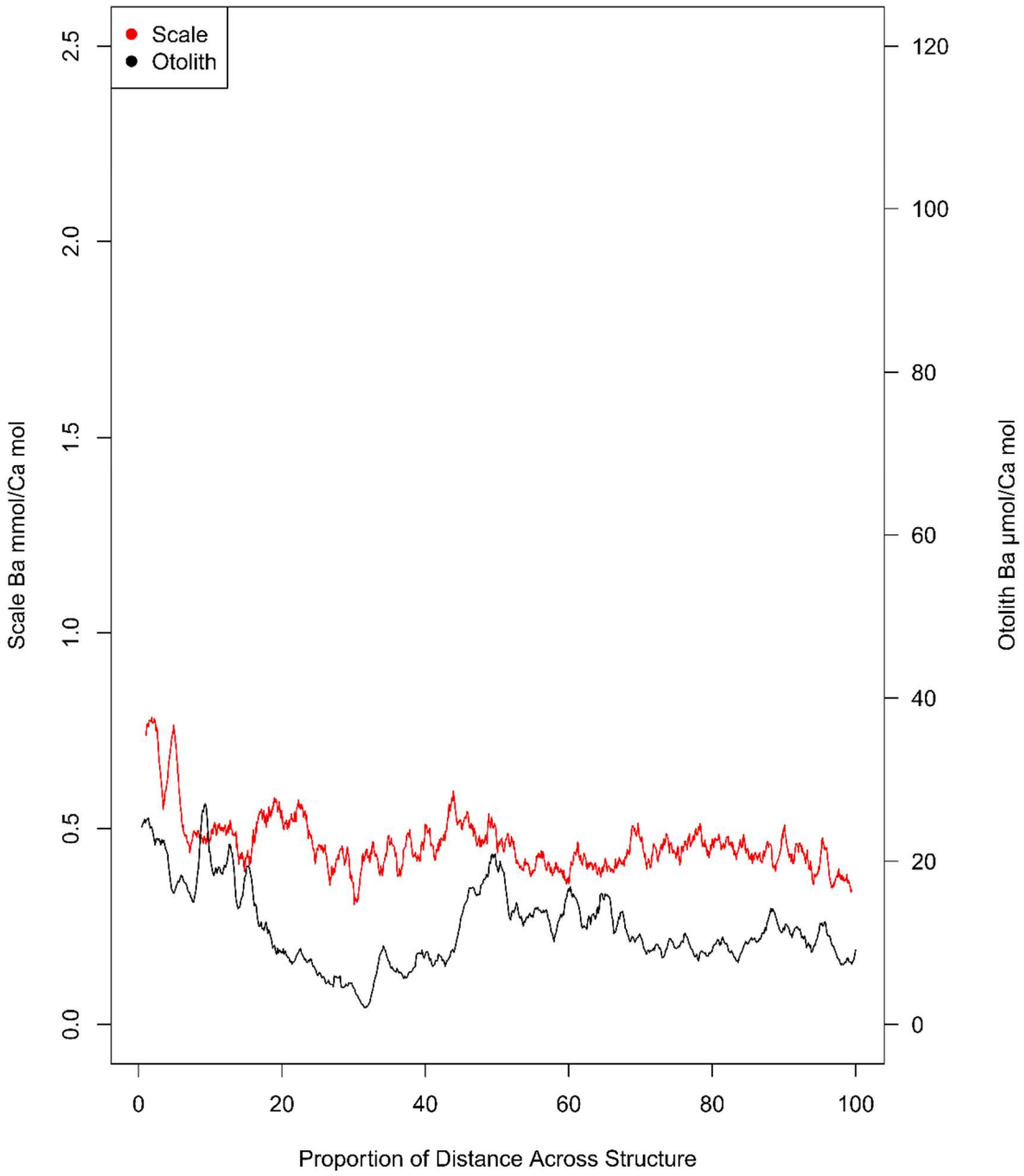
Scale
Otolith
Scale Ba mmol/Ca mol
Otolith Ba µmol/Ca mol
Proportion of Distance Across Structure
0.0
0.5
1.0
1.5
2.0
2.5
0
20
40
60
80
100
120

RD-054

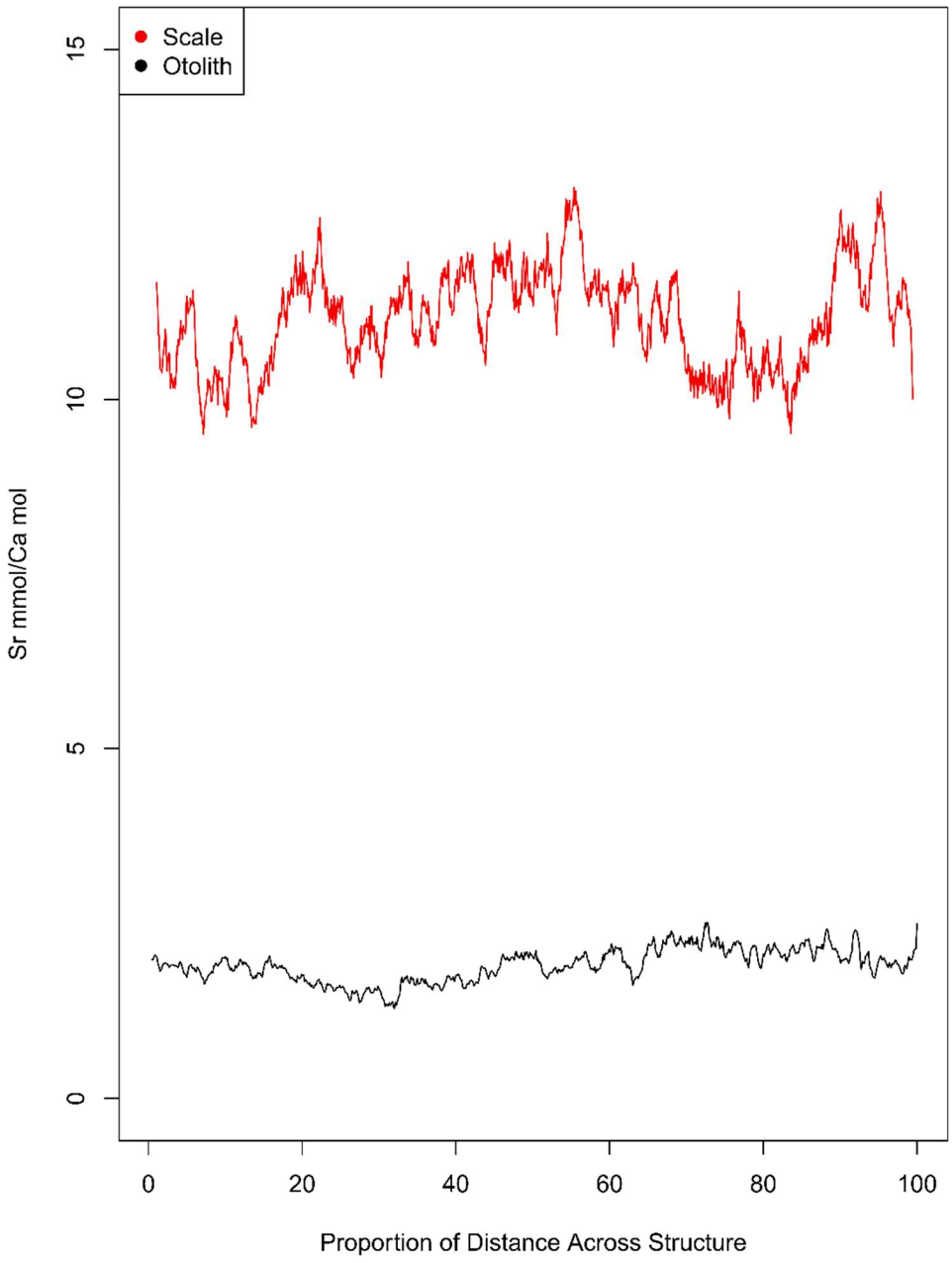
Scale
Otolith
Sr mmol/Ca mol
0
5
10
15
0
20
40
60
80
100
Proportion of Distance Across Structure

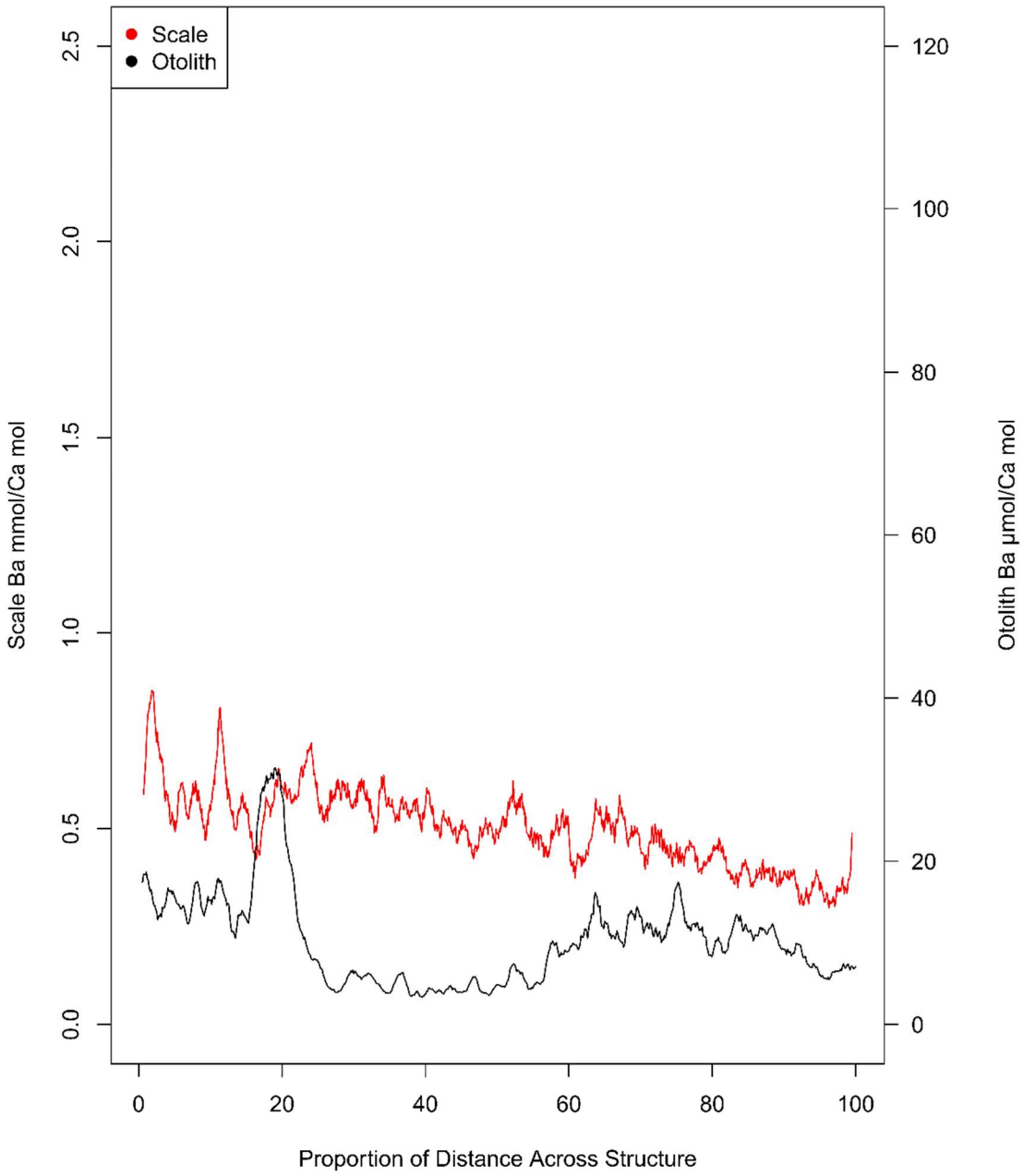
RD-055
Scale
Otolith
Scale Ba mmol/Ca mol
Otolith Ba µmol/Ca mol
Proportion of Distance Across Structure
0.0
0.5
1.0
1.5
2.0
2.5
0
20
40
60
80
100
120

RD-055

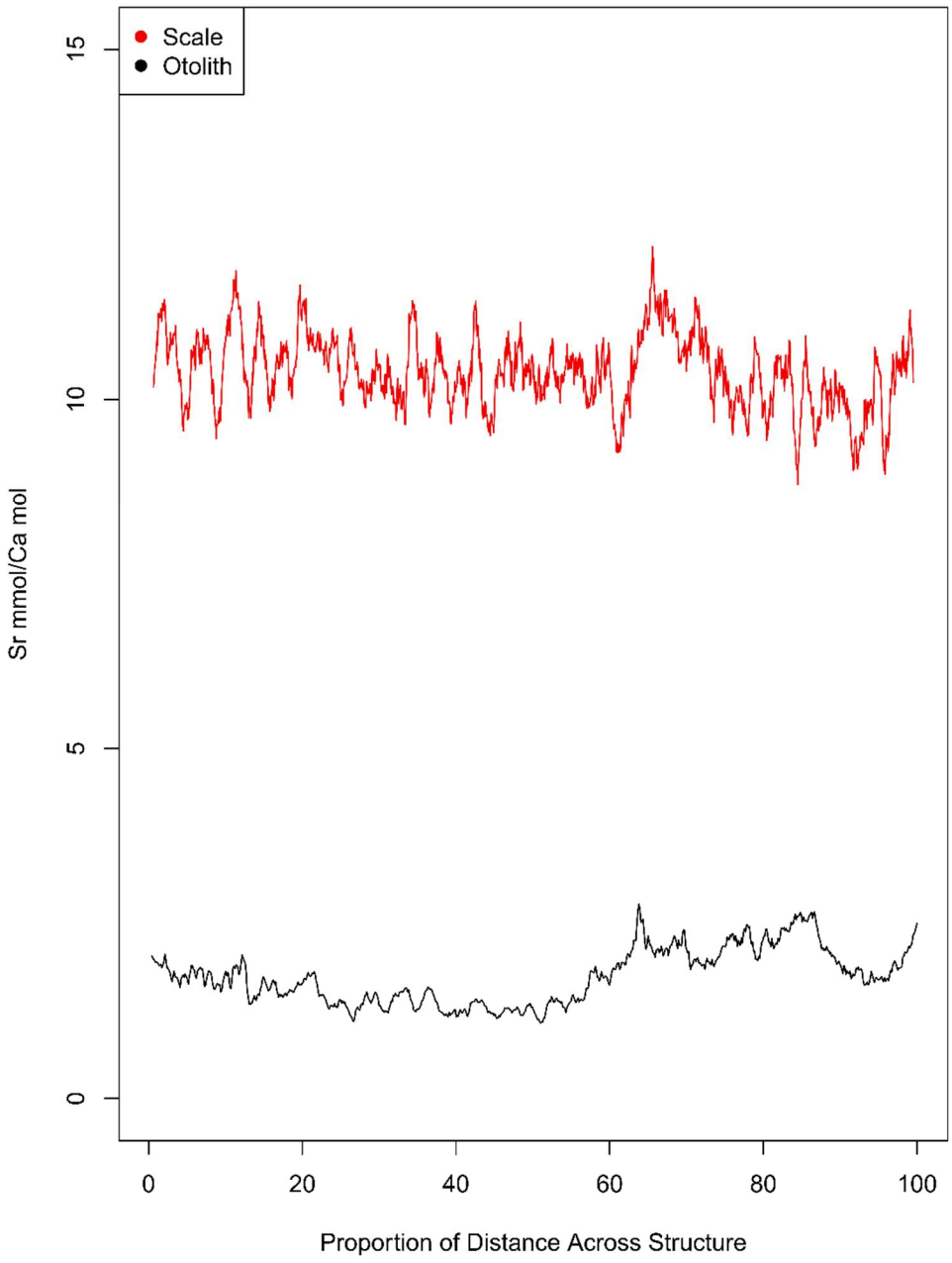
Scale
Otolith
Sr mmol/Ca mol
0
5
10
15
0
20
40
60
80
100
Proportion of Distance Across Structure

RD-056

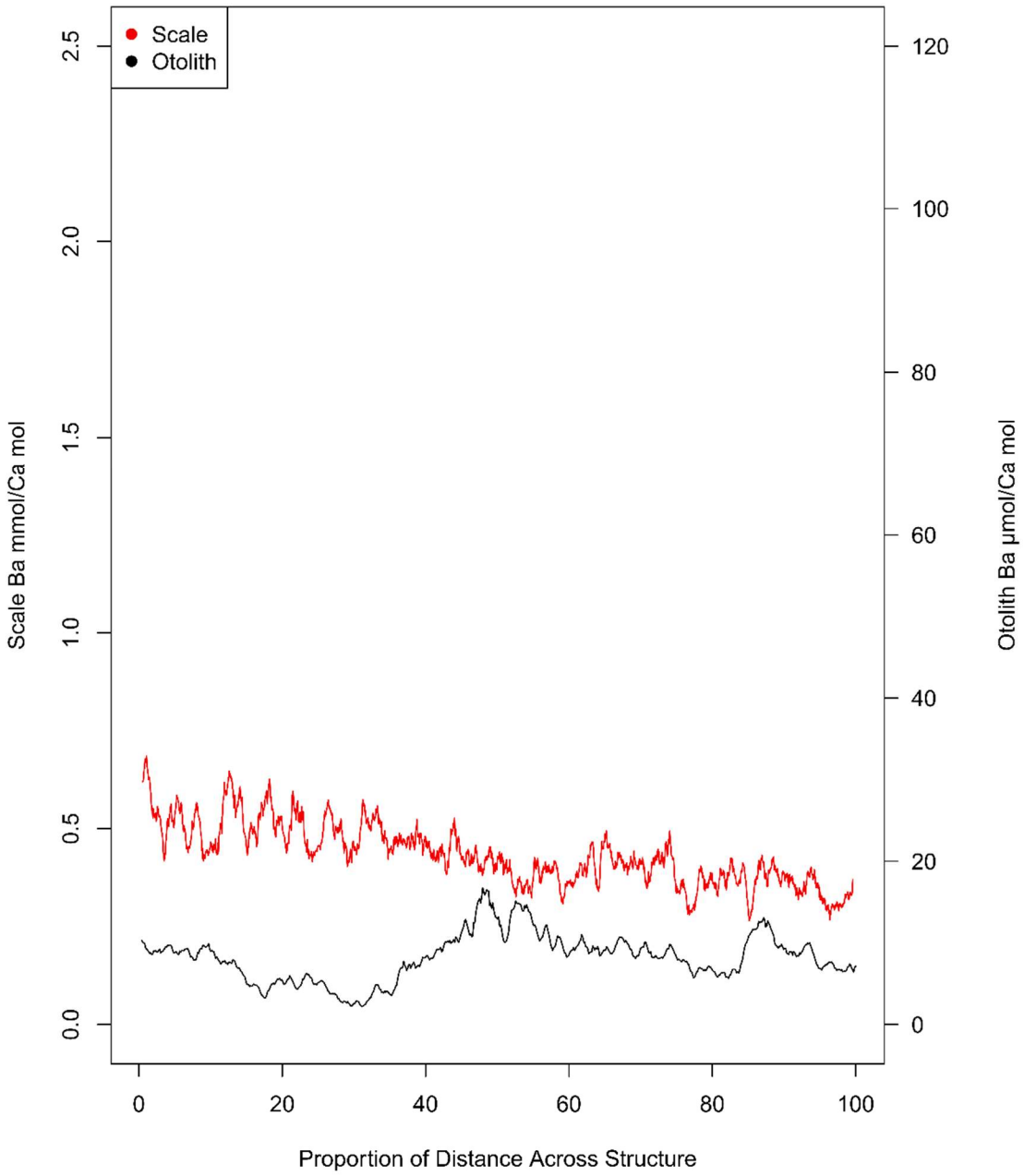
Scale
Otolith
Scale Ba mmol/Ca mol
Otolith Ba µmol/Ca mol
Proportion of Distance Across Structure
0.0
0.5
1.0
1.5
2.0
2.5
0
20
40
60
80
100
120

RD-056

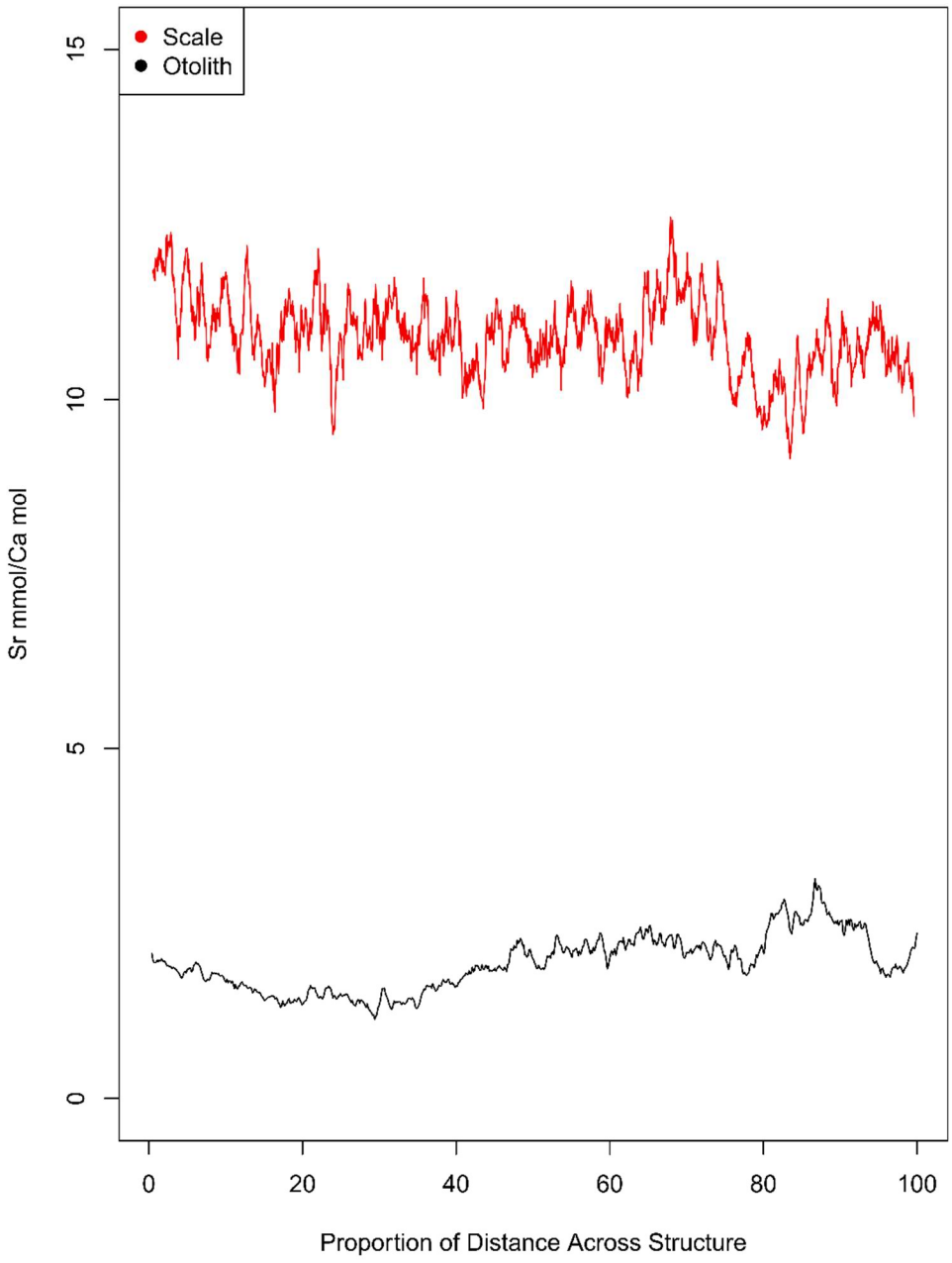
Scale
Otolith
Sr mmol/Ca mol
0
5
10
15
0
20
40
60
80
100
Proportion of Distance Across Structure

RD-057

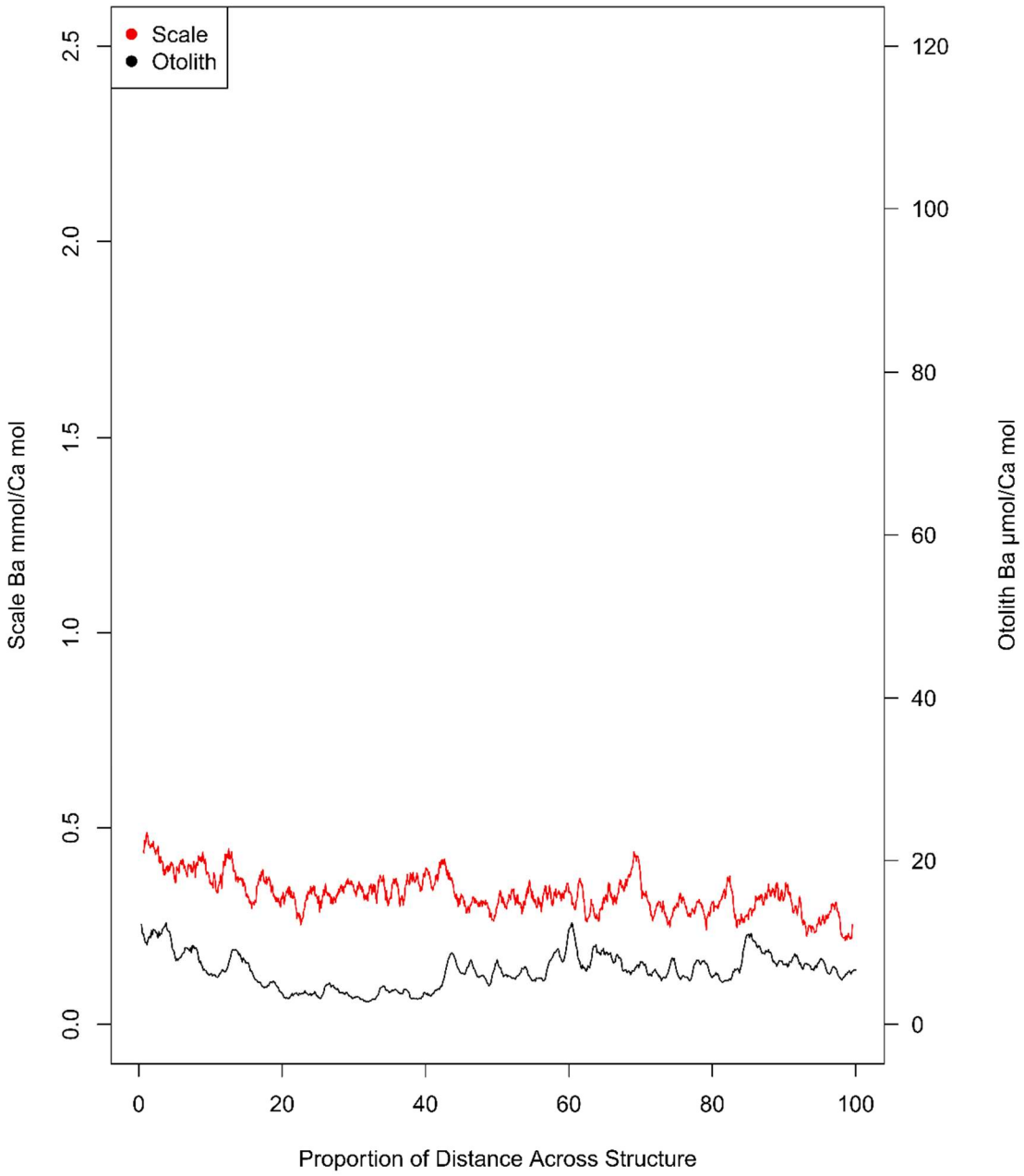
Scale
Otolith
Scale Ba mmol/Ca mol
Otolith Ba µmol/Ca mol
Proportion of Distance Across Structure
0.0
0.5
1.0
1.5
2.0
2.5
0
20
40
60
80
100
120

RD-057

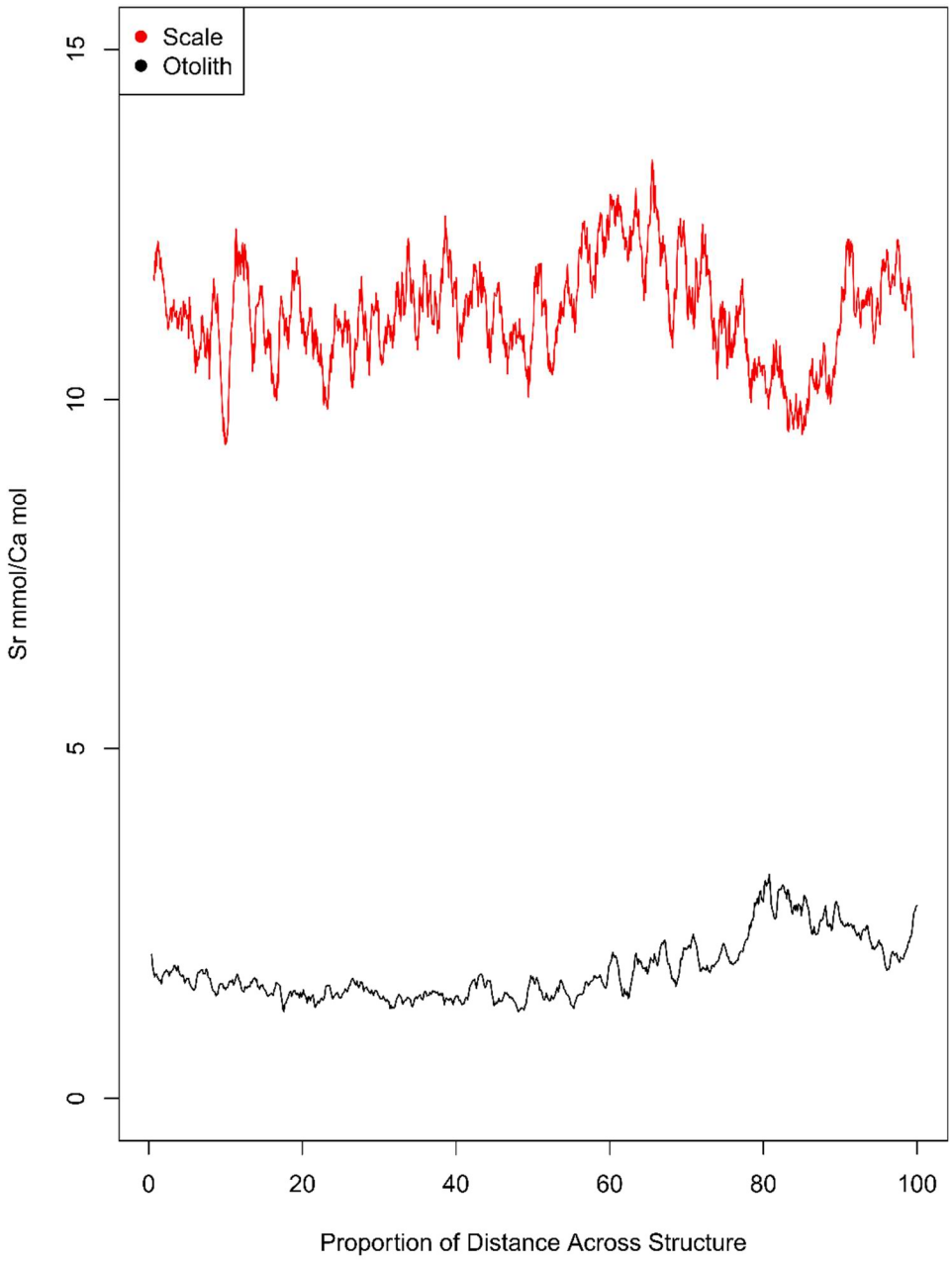
Scale
Otolith
Sr mmol/Ca mol
0
5
10
15
0
20
40
60
80
100
Proportion of Distance Across Structure

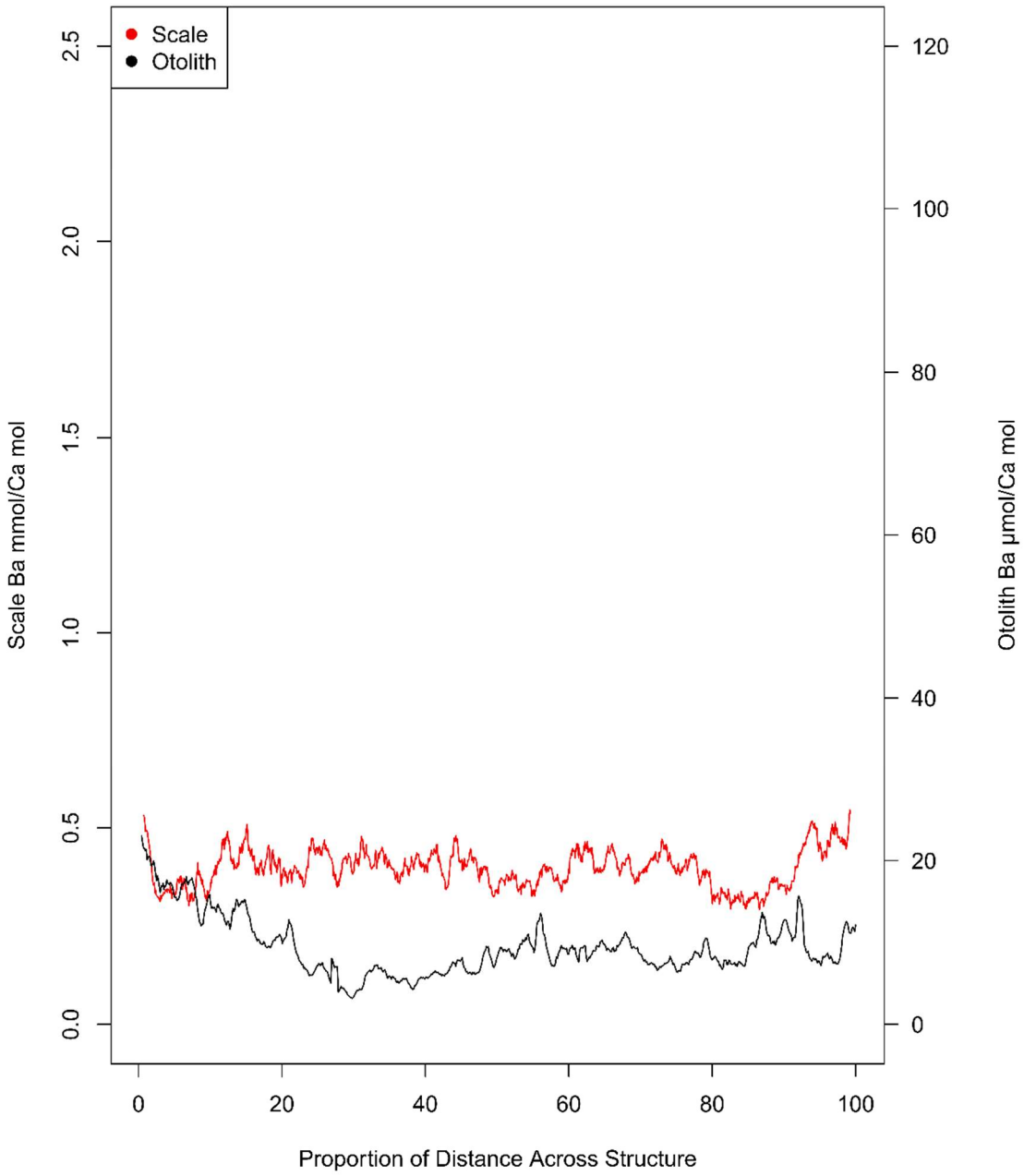
RD-058
Scale
Otolith
Scale Ba mmol/Ca mol
Otolith Ba µmol/Ca mol
Proportion of Distance Across Structure
0.0
0.5
1.0
1.5
2.0
2.5
0
20
40
60
80
100
120

RD-058

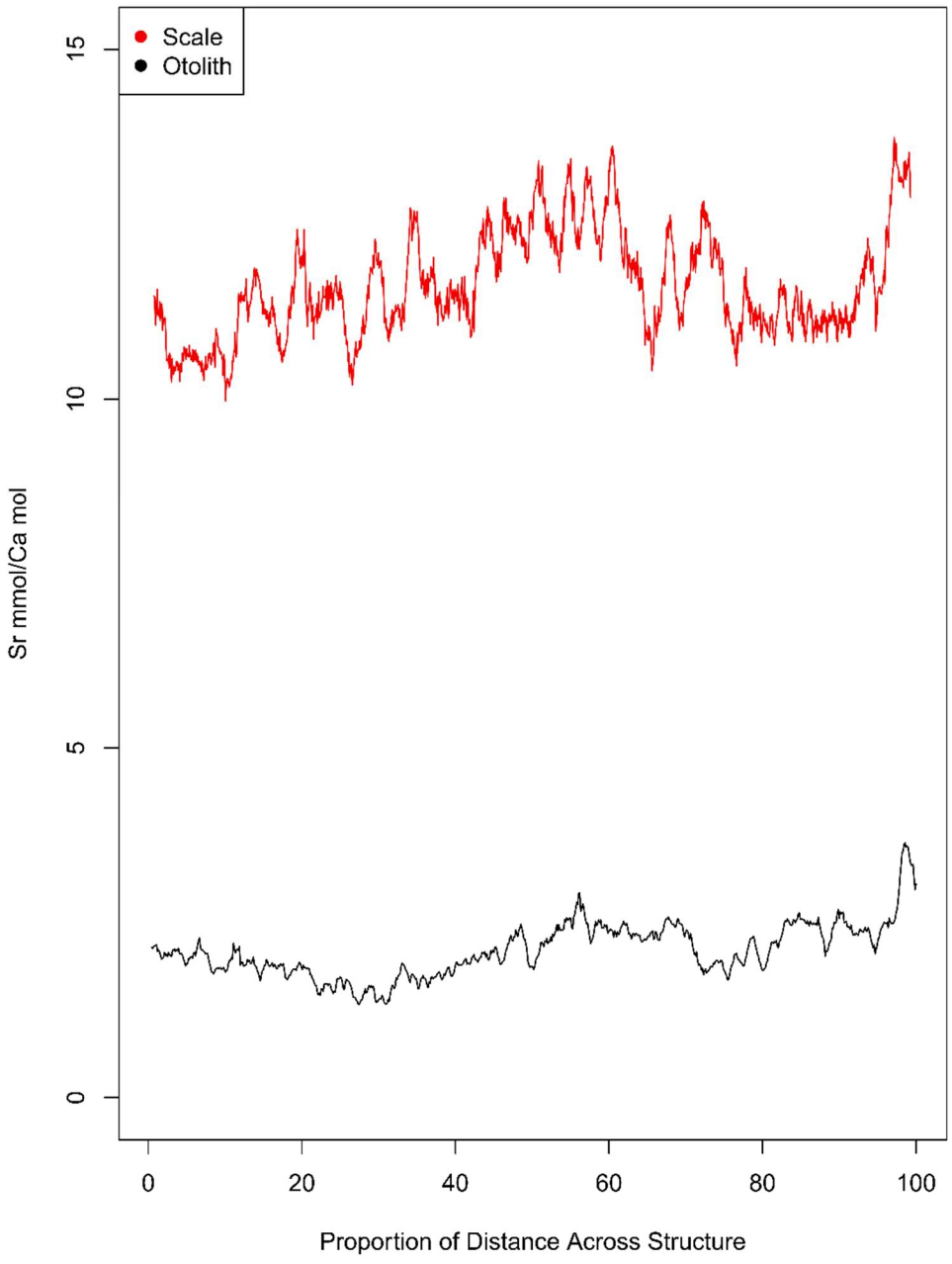
Scale
Otolith
Sr mmol/Ca mol
0
5
10
15
0
20
40
60
80
100
Proportion of Distance Across Structure

RD-059

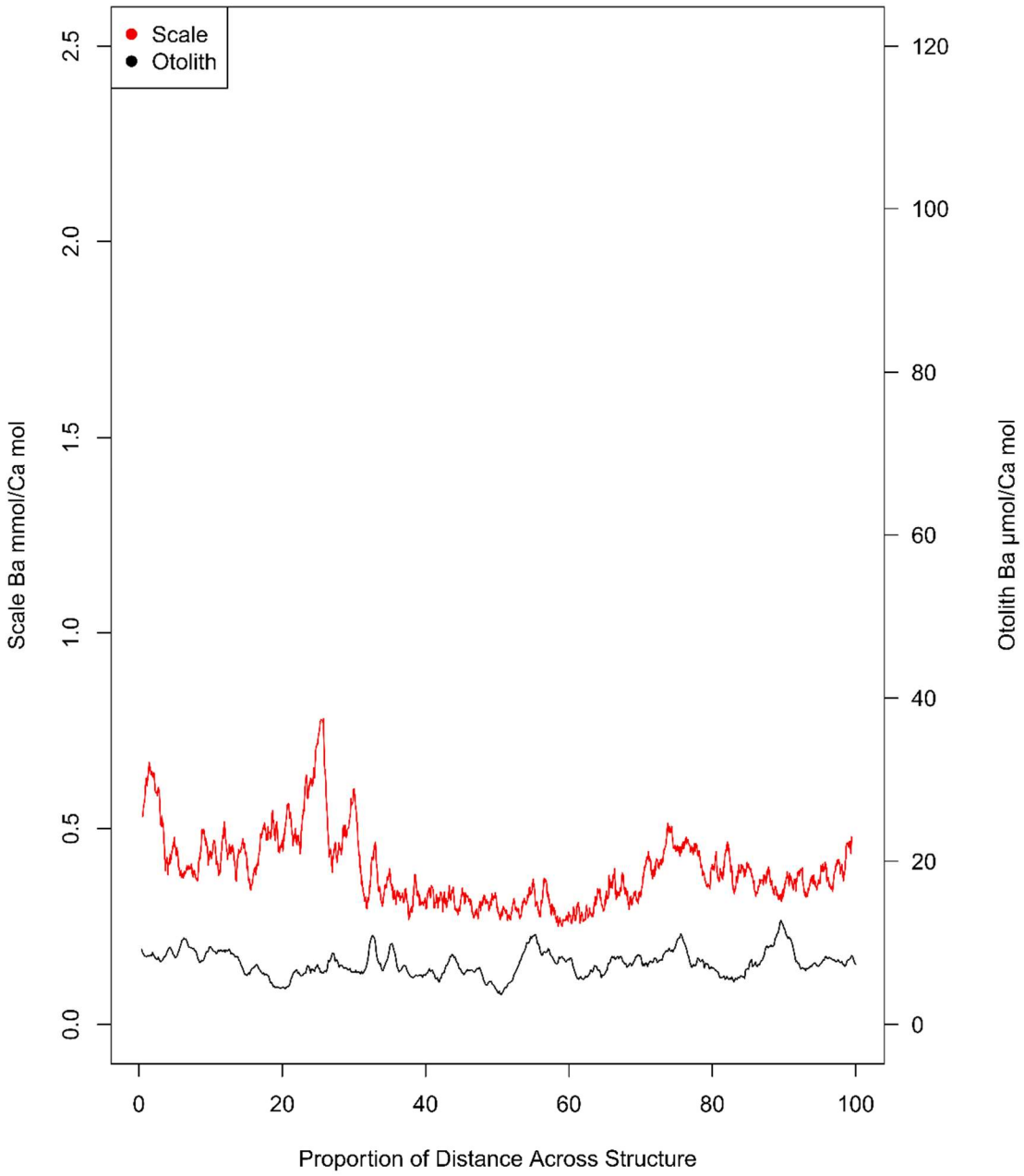
Scale
Otolith
Scale Ba mmol/Ca mol
Otolith Ba µmol/Ca mol
Proportion of Distance Across Structure
0.0
0.5
1.0
1.5
2.0
2.5
0
20
40
60
80
100
120

RD-059

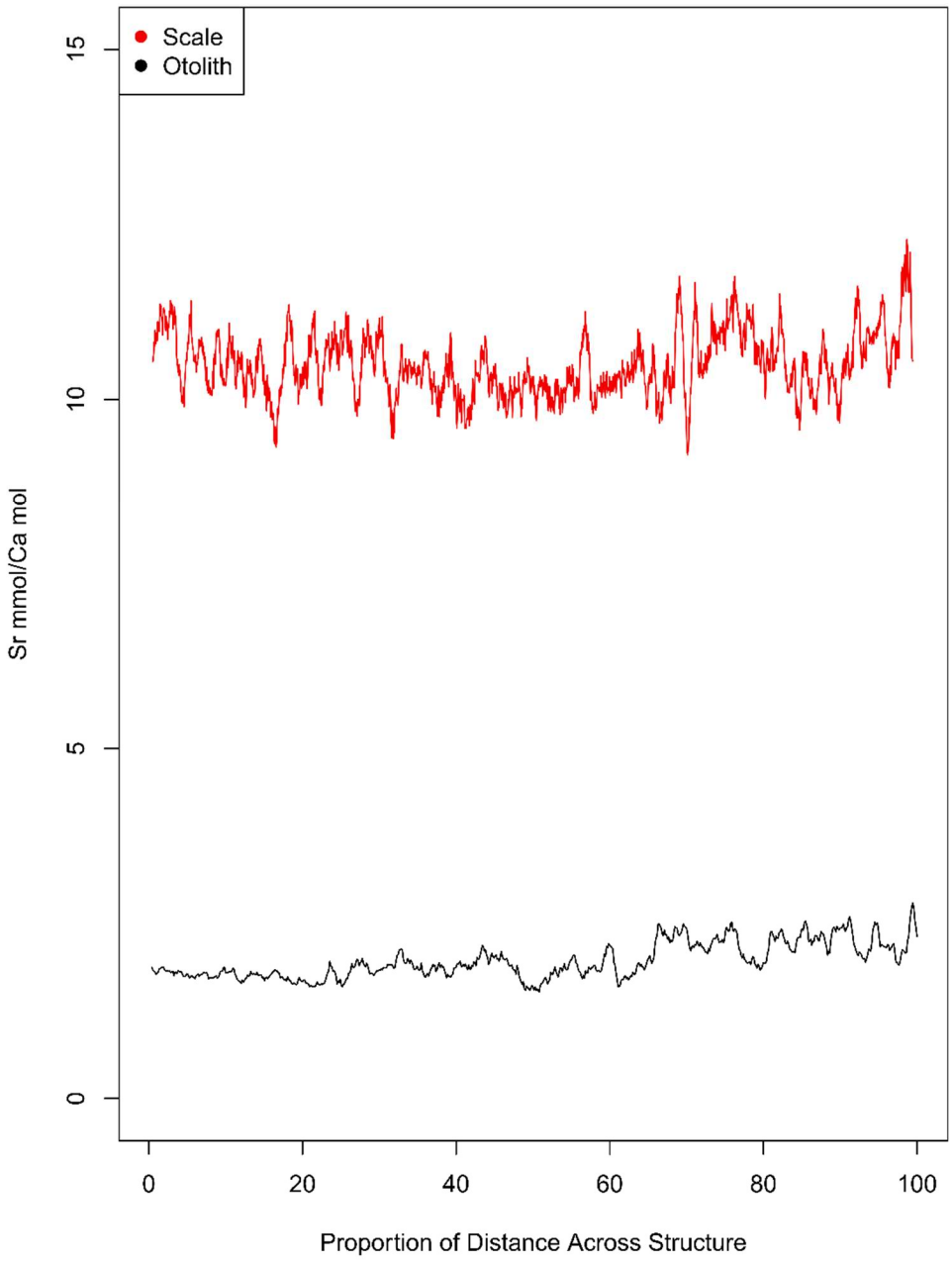
Scale
Otolith
Sr mmol/Ca mol
0
5
10
15
0
20
40
60
80
100
Proportion of Distance Across Structure

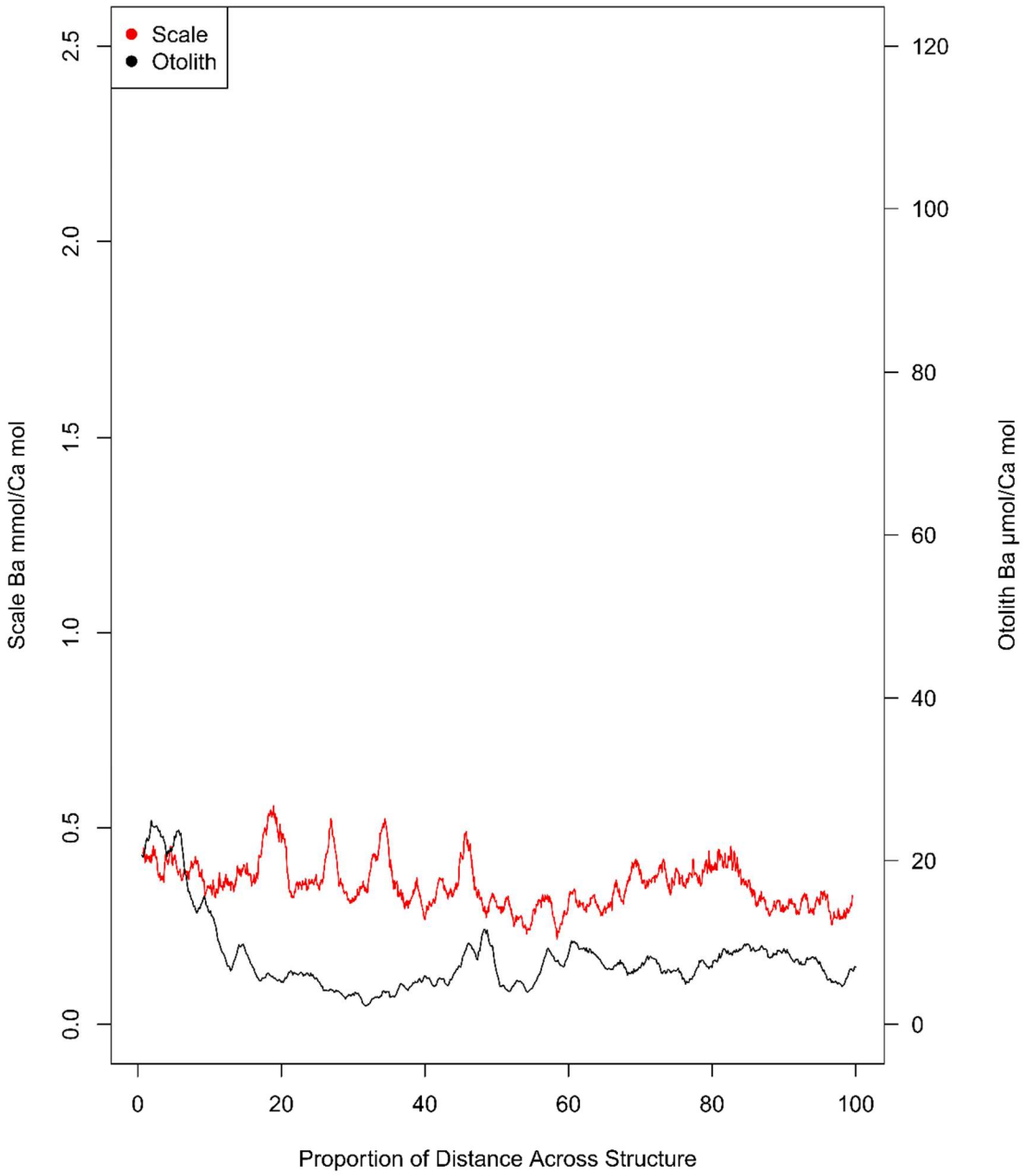
RD-060
Scale
Otolith
Scale Ba mmol/Ca mol
Otolith Ba µmol/Ca mol
Proportion of Distance Across Structure
0.0
0.5
1.0
1.5
2.0
2.5
0
20
40
60
80
100
120

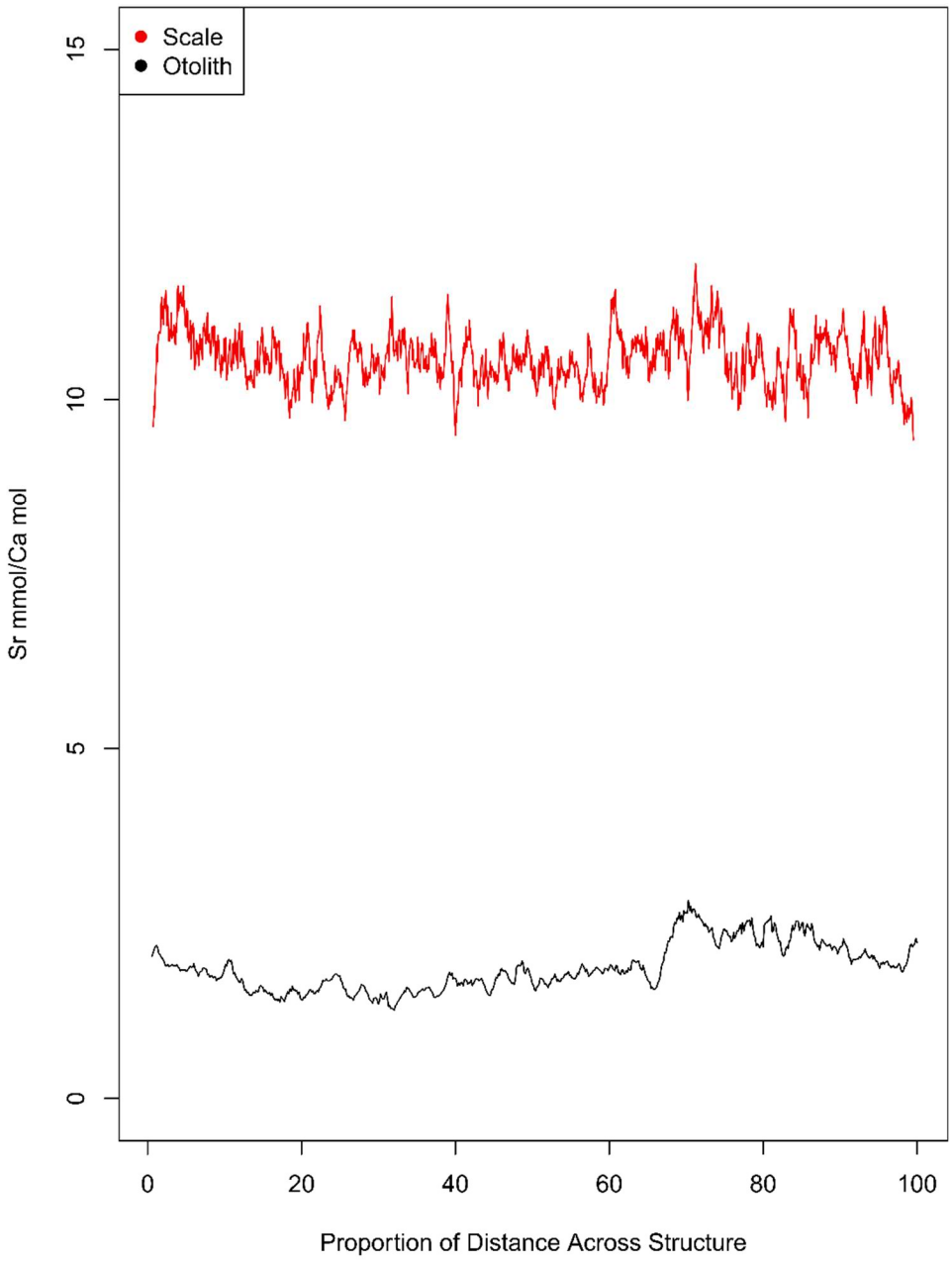
RD-060
Scale
Otolith
Sr mmol/Ca mol
0
5
10
15
0
20
40
60
80
100
Proportion of Distance Across Structure

RD-061

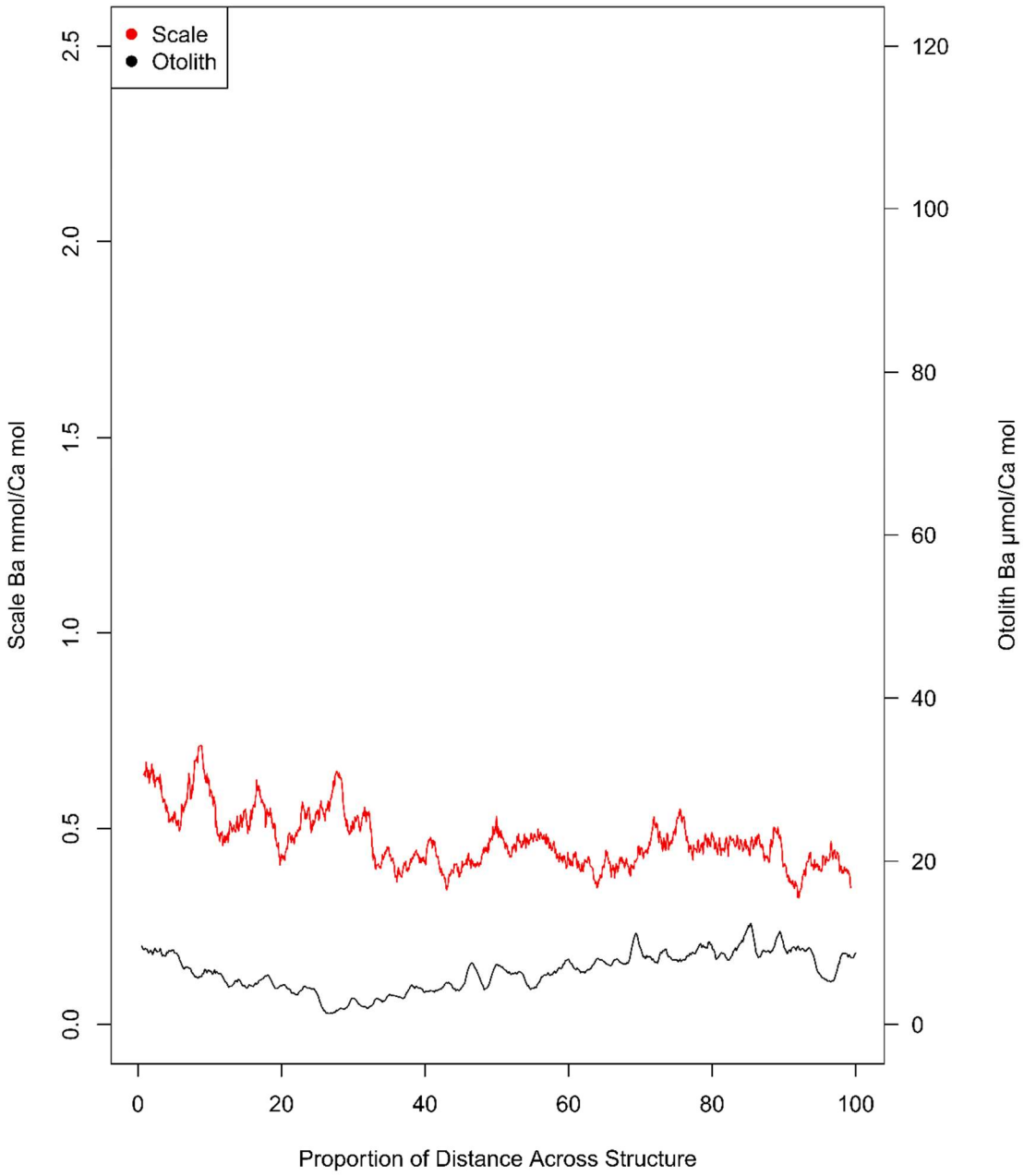
Scale
Otolith
Scale Ba mmol/Ca mol
Otolith Ba µmol/Ca mol
Proportion of Distance Across Structure
0.0
0.5
1.0
1.5
2.0
2.5
0
20
40
60
80
100
120

RD-061

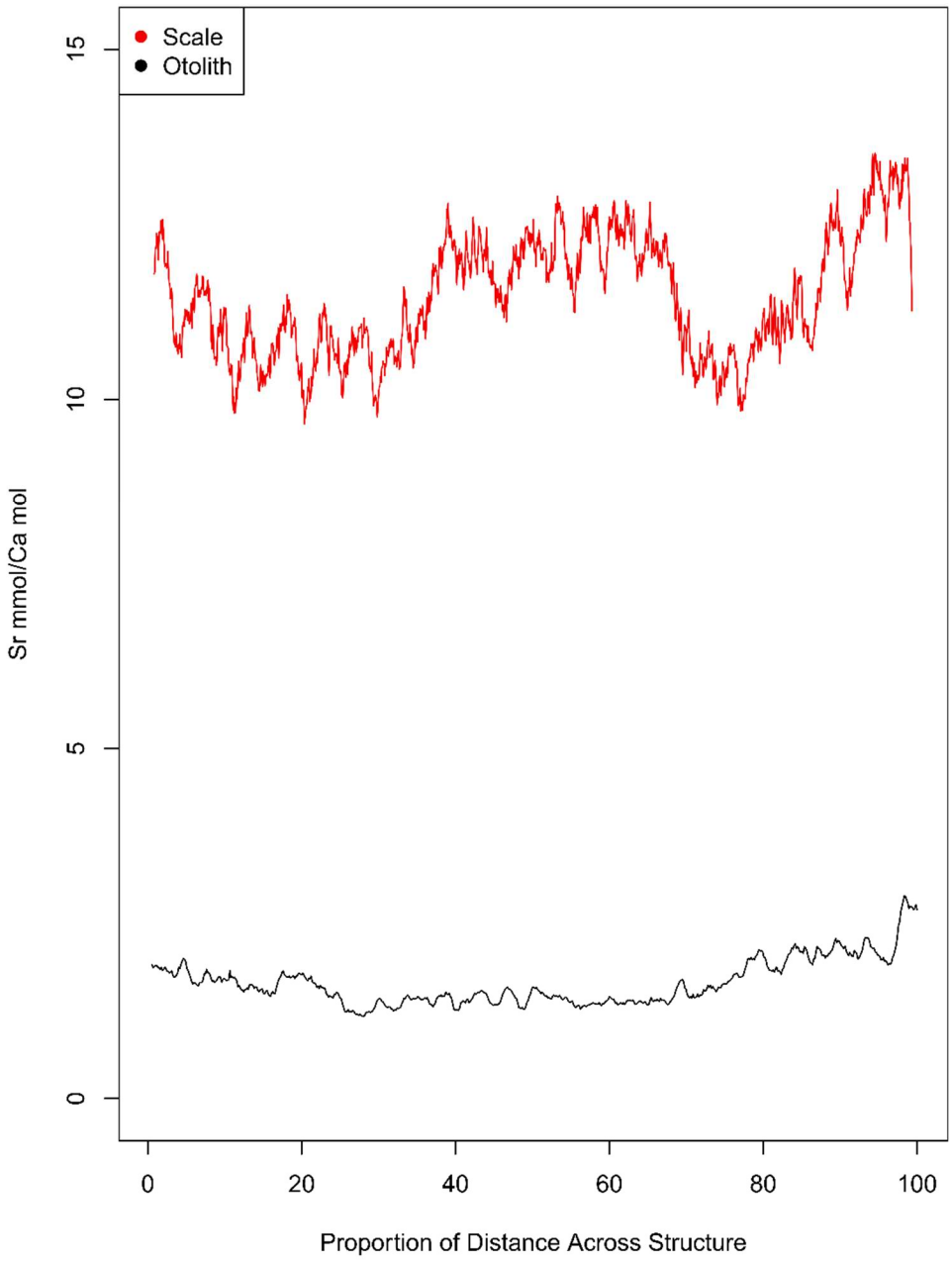
Scale
Otolith
Sr mmol/Ca mol
0
5
10
15
0
20
40
60
80
100
Proportion of Distance Across Structure

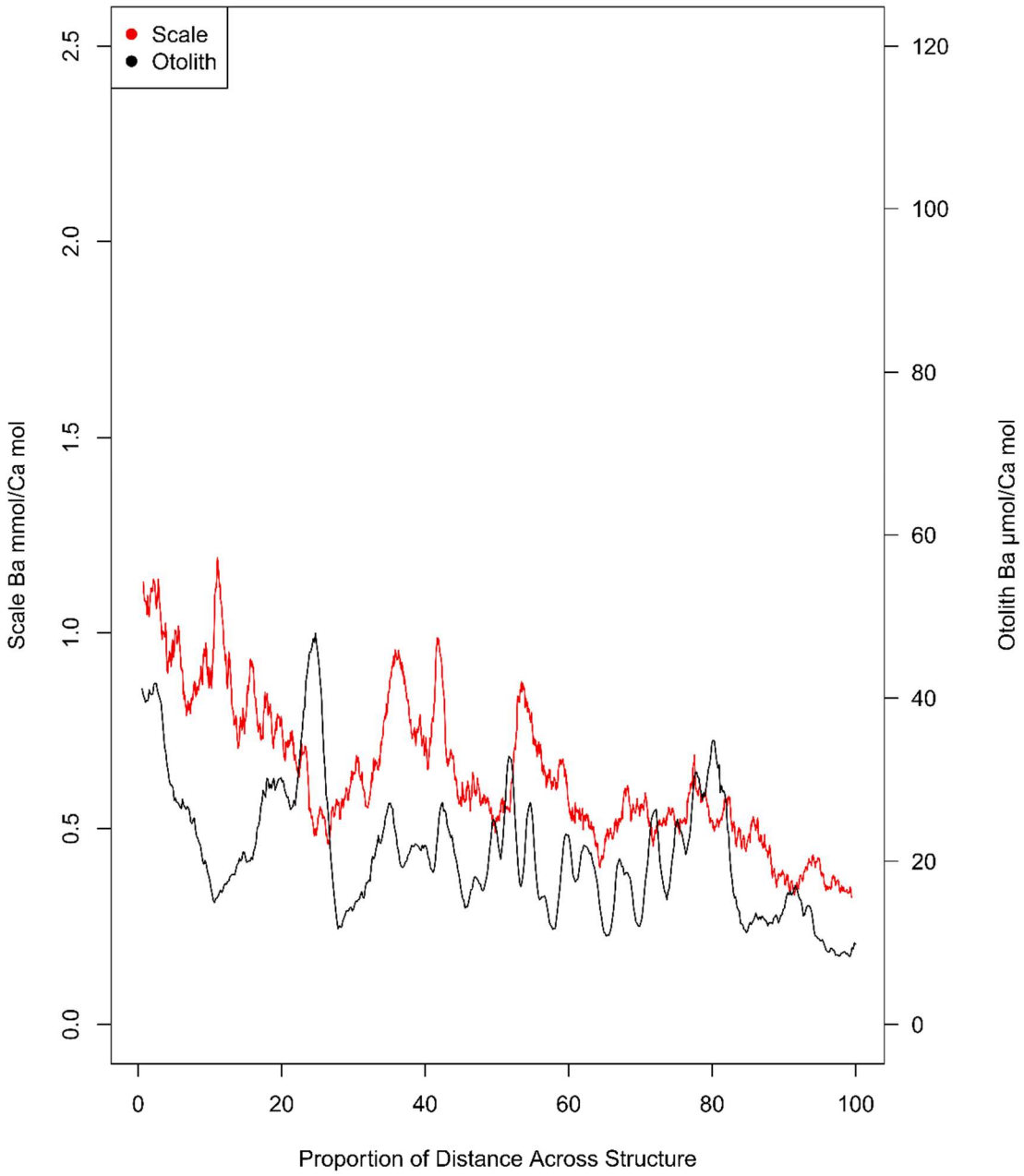
RD-062
Scale
Otolith
Scale Ba mmol/Ca mol
Otolith Ba µmol/Ca mol
Proportion of Distance Across Structure
0.0
0.5
1.0
1.5
2.0
2.5
0
20
40
60
80
100
120

RD-062

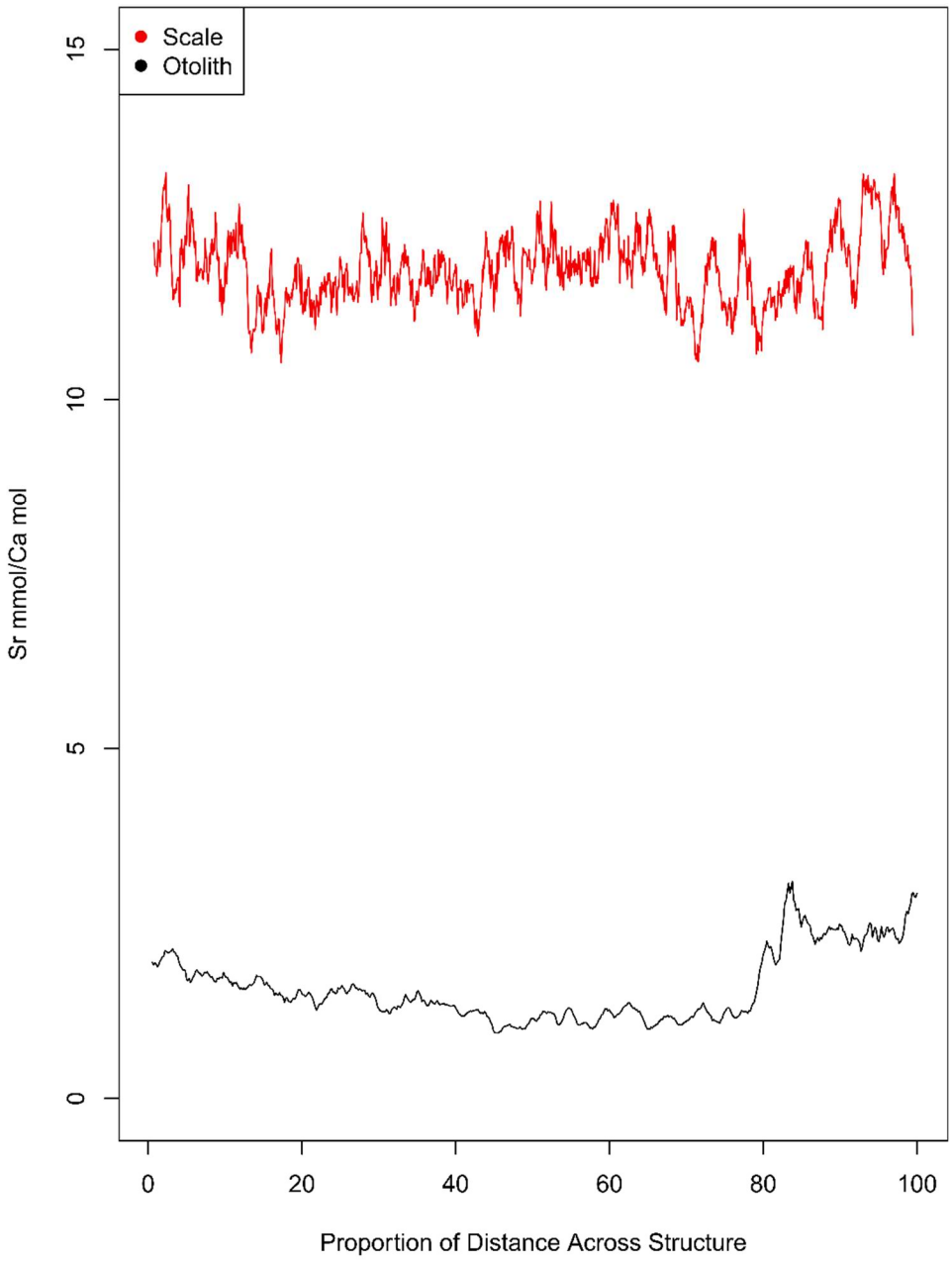
Scale
Otolith
Sr mmol/Ca mol
0
5
10
15
0
20
40
60
80
100
Proportion of Distance Across Structure

RD-063

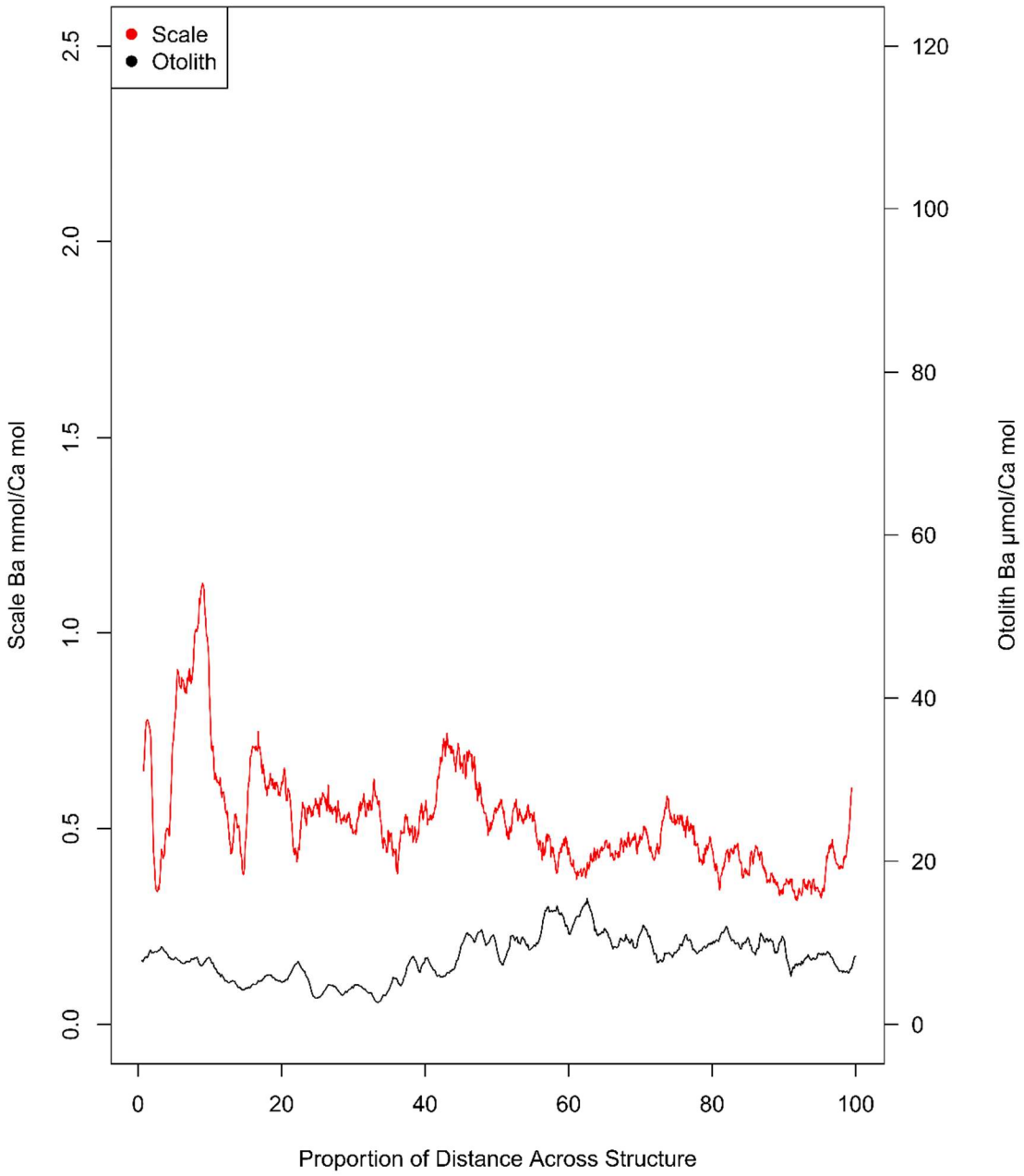
Scale
Otolith
Scale Ba mmol/Ca mol
Otolith Ba µmol/Ca mol
Proportion of Distance Across Structure
0.0
0.5
1.0
1.5
2.0
2.5
0
20
40
60
80
100
120

RD-063

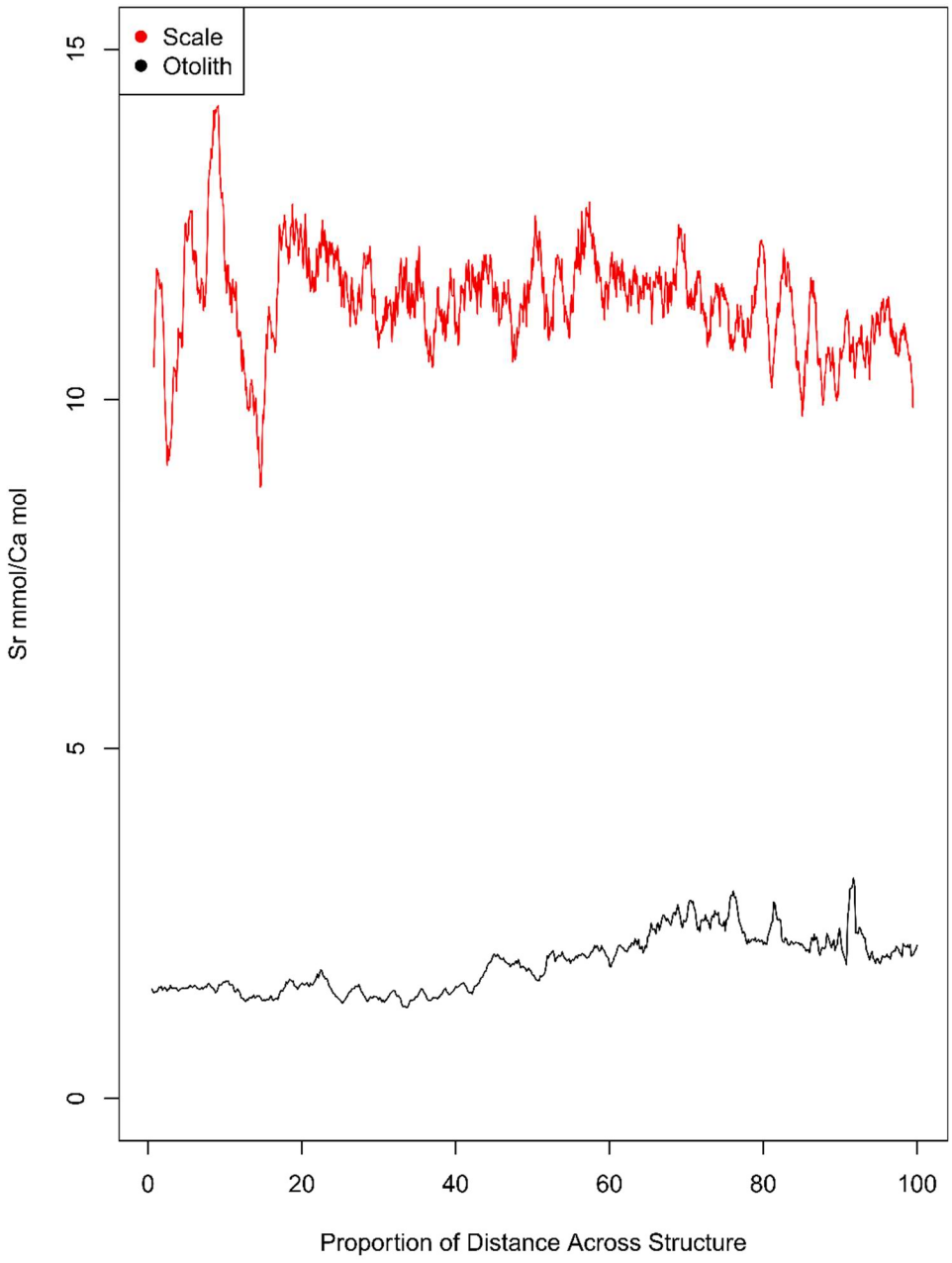
Scale
Otolith
Sr mmol/Ca mol
0
5
10
15
0
20
40
60
80
100
Proportion of Distance Across Structure

RD-064

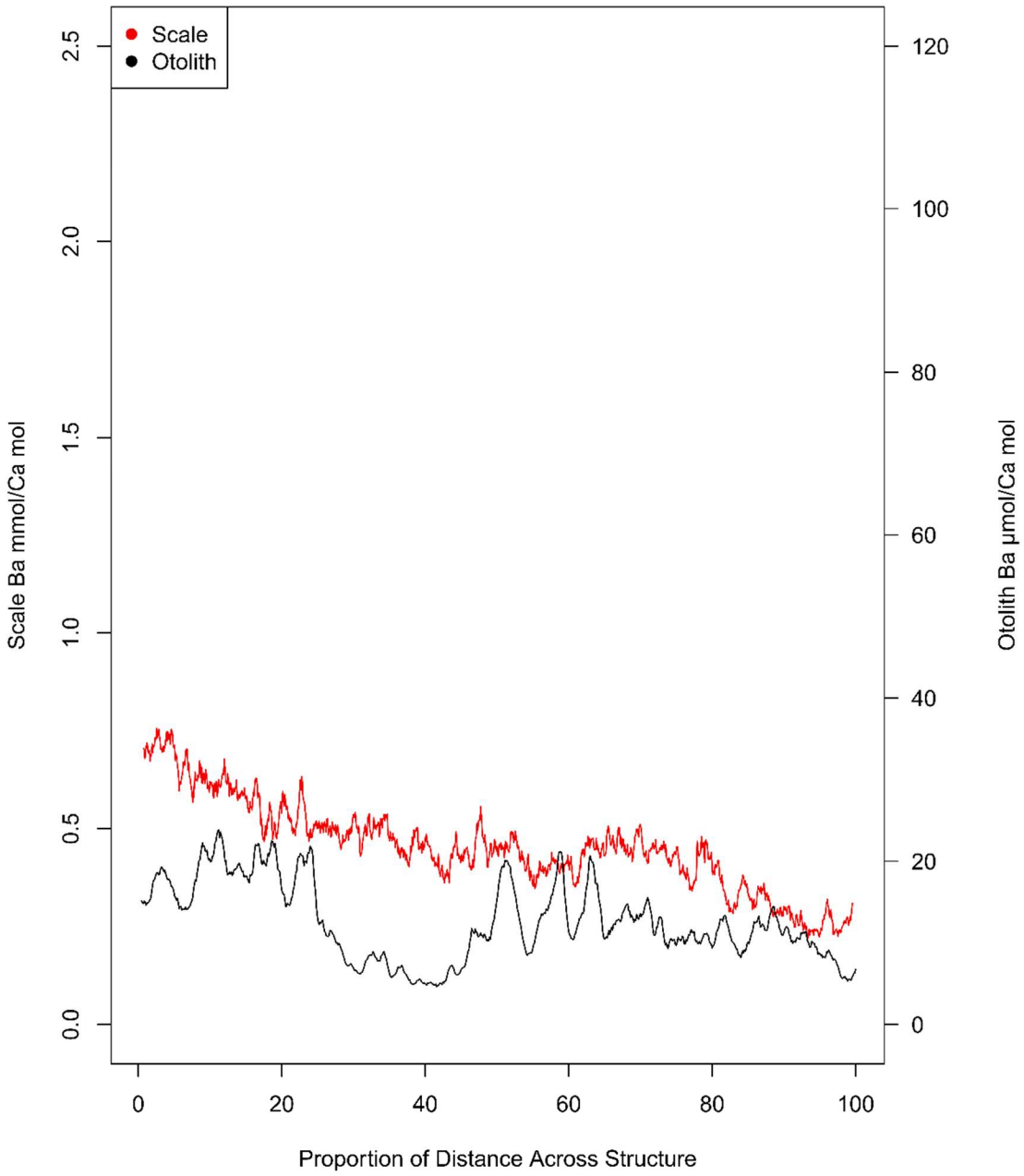
Scale
Otolith
Scale Ba mmol/Ca mol
Otolith Ba µmol/Ca mol
Proportion of Distance Across Structure
0.0
0.5
1.0
1.5
2.0
2.5
0
20
40
60
80
100
120

RD-064

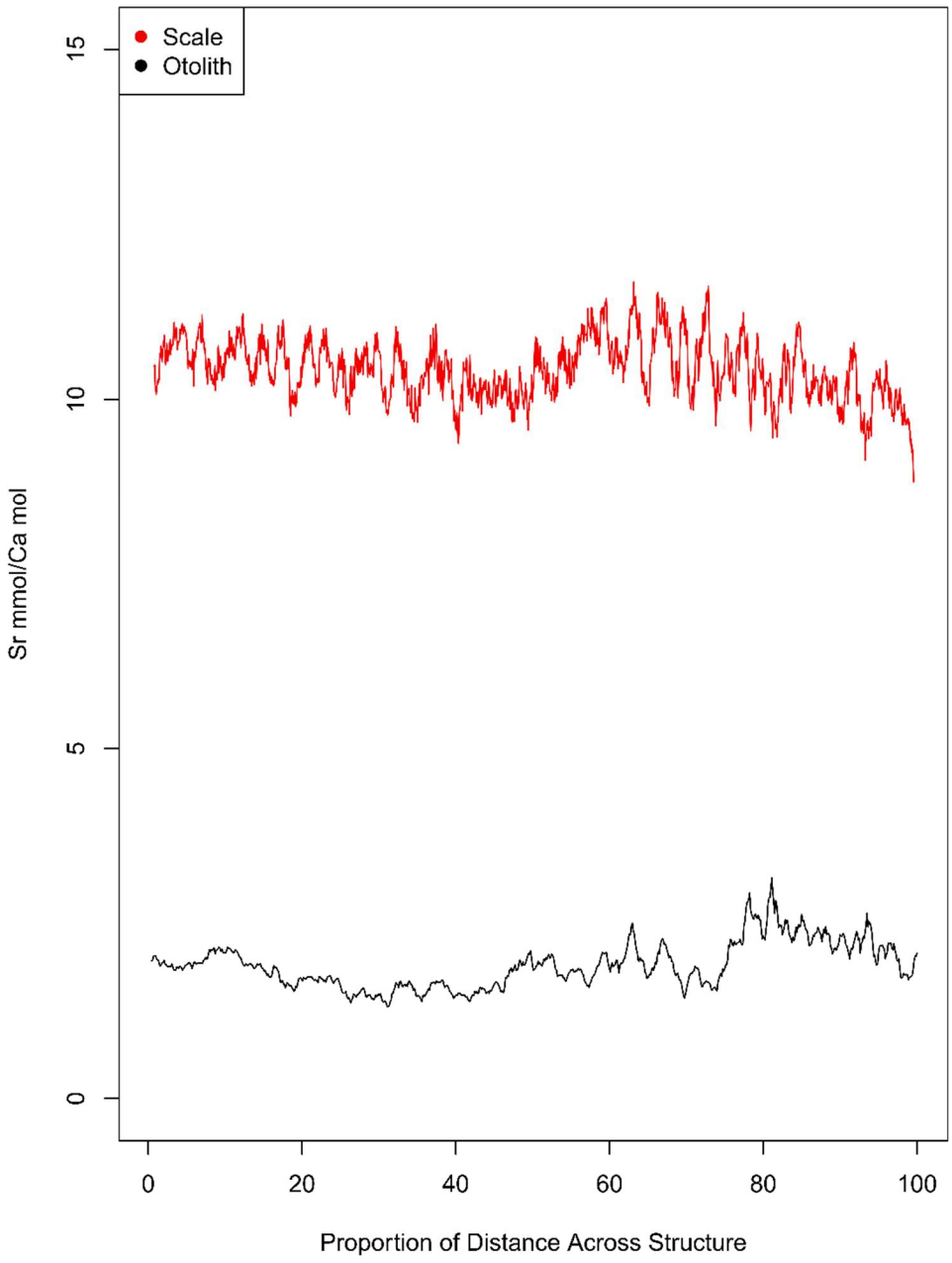
Scale
Otolith
Sr mmol/Ca mol
0
5
10
15
0
20
40
60
80
100
Proportion of Distance Across Structure

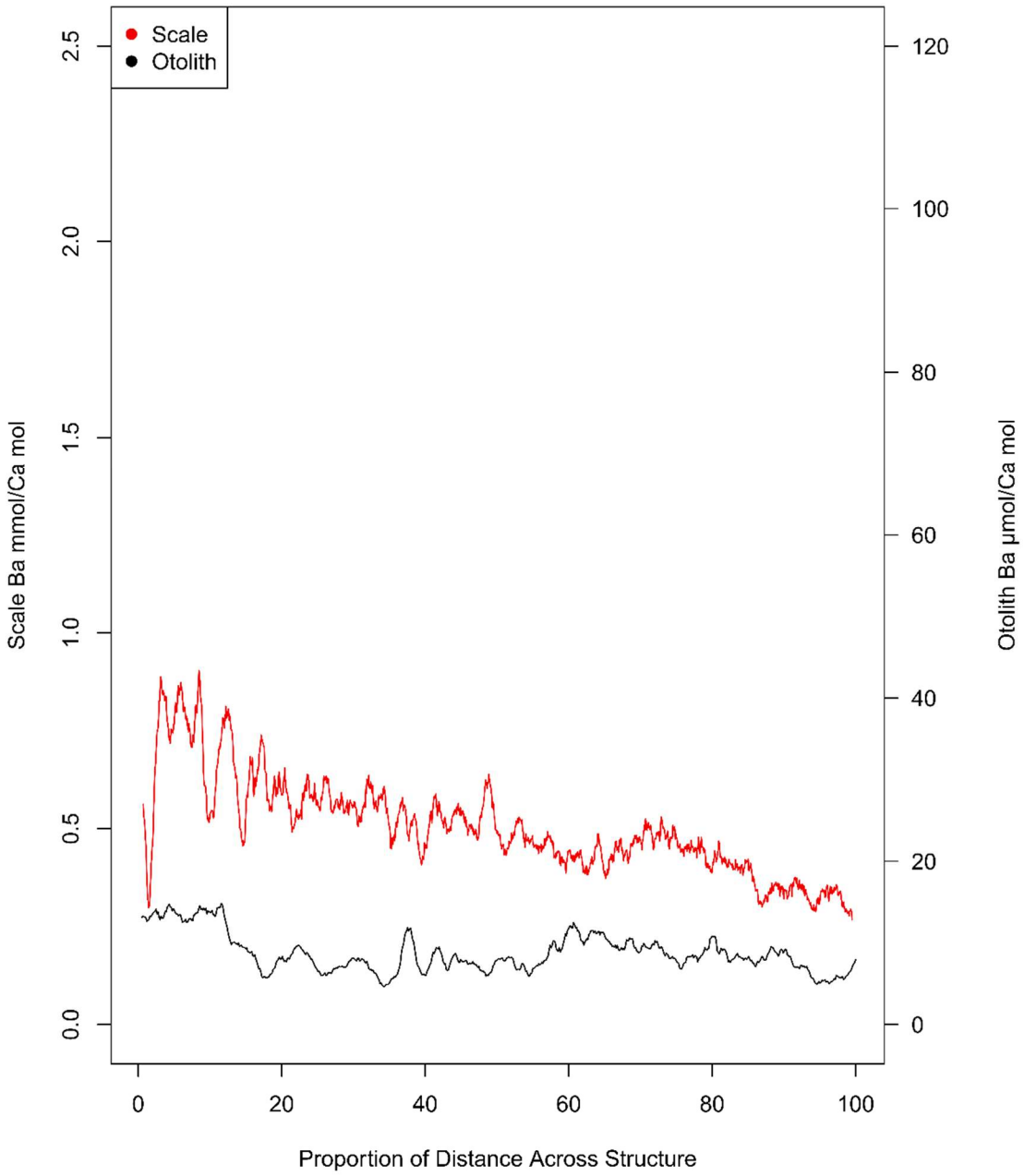
RD-065
Scale
Otolith
Scale Ba mmol/Ca mol
Otolith Ba µmol/Ca mol
Proportion of Distance Across Structure
0.0
0.5
1.0
1.5
2.0
2.5
0
20
40
60
80
100
120

RD-065

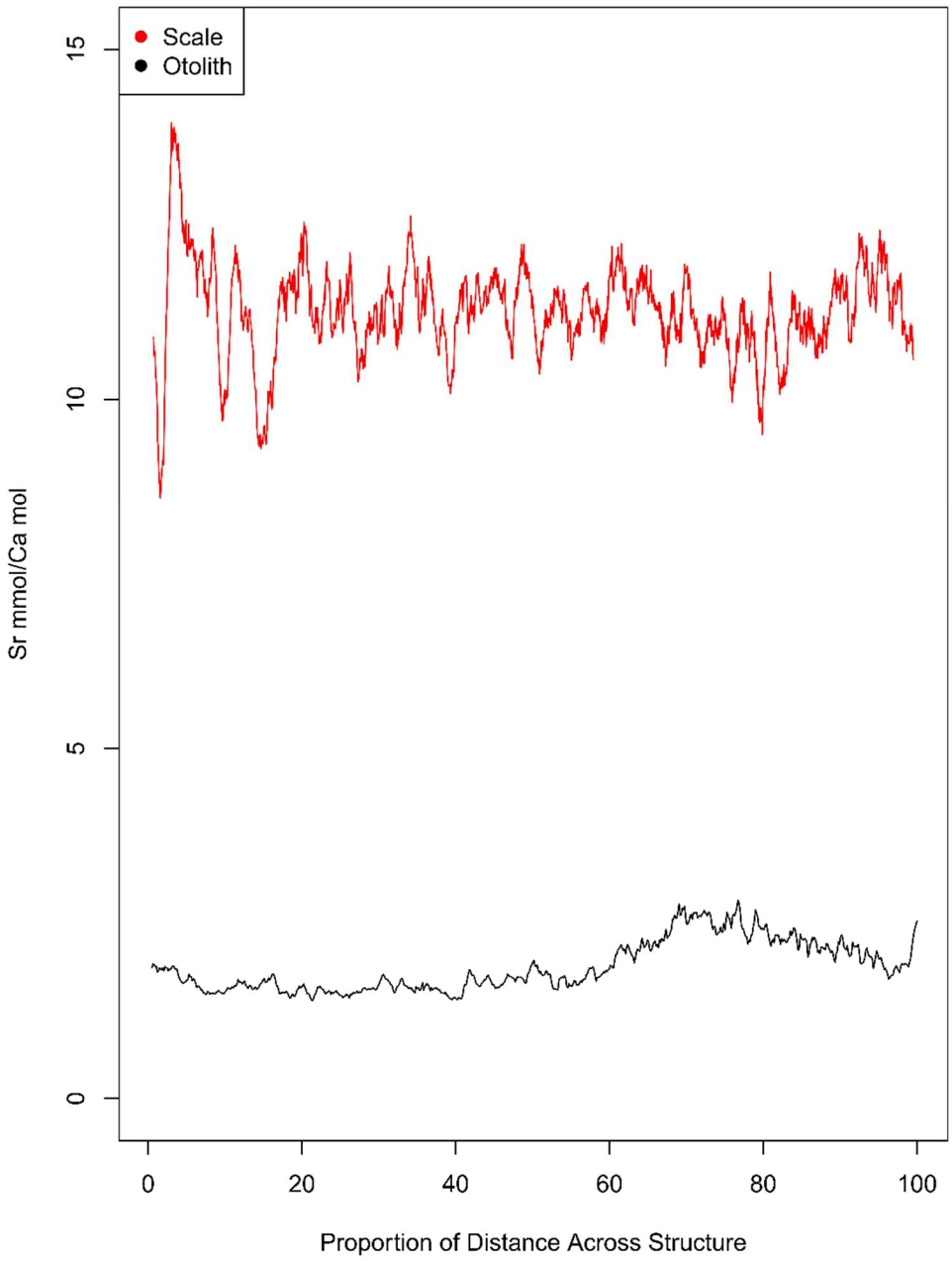
Scale
Otolith
Sr mmol/Ca mol
0
5
10
15
0
20
40
60
80
100
Proportion of Distance Across Structure

RD−066

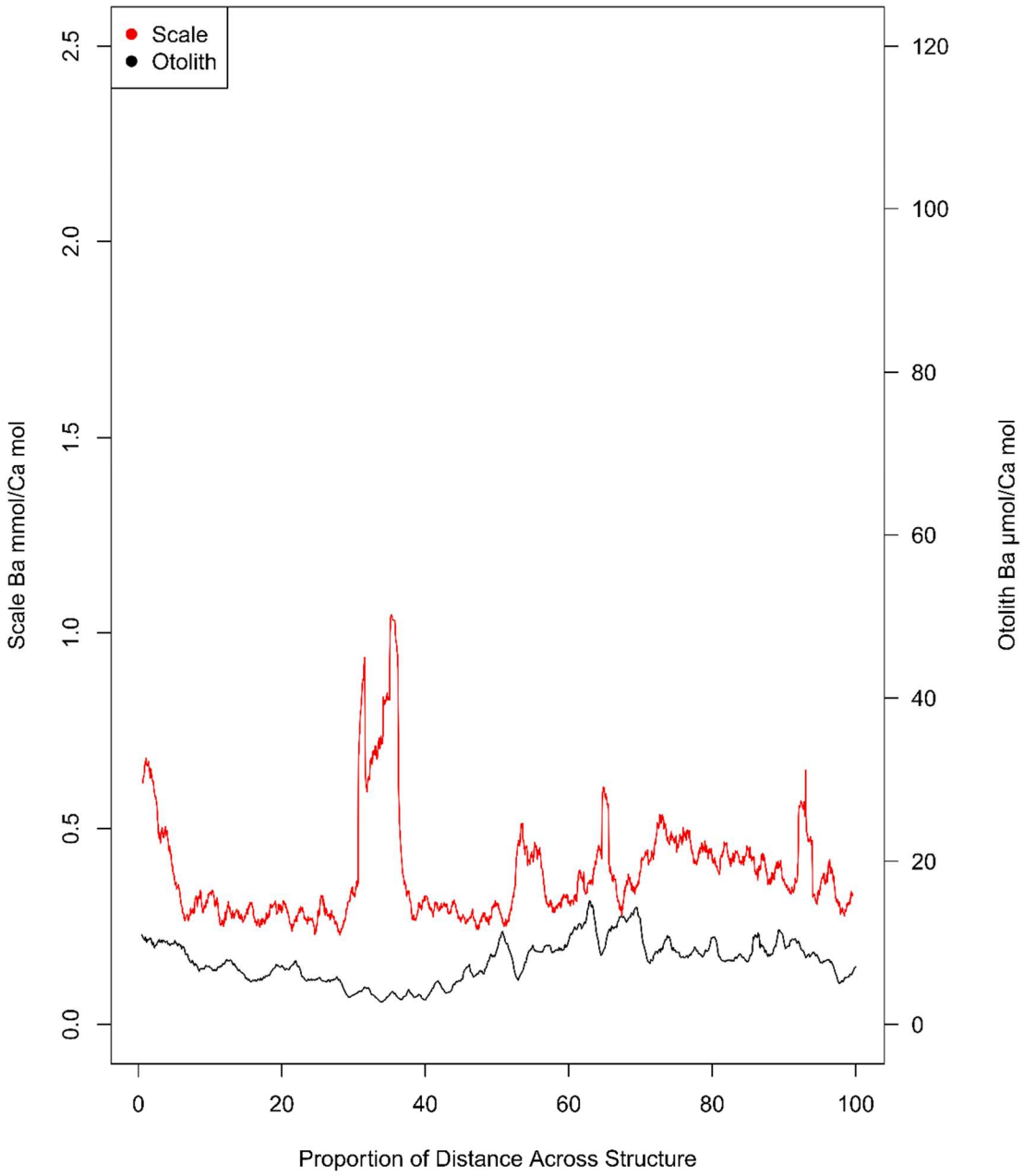
Scale
Otolith
Scale Ba mmol/Ca mol
Otolith Ba µmol/Ca mol
Proportion of Distance Across Structure
0.0
0.5
1.0
1.5
2.0
2.5
0
20
40
60
80
100
120

RD-066

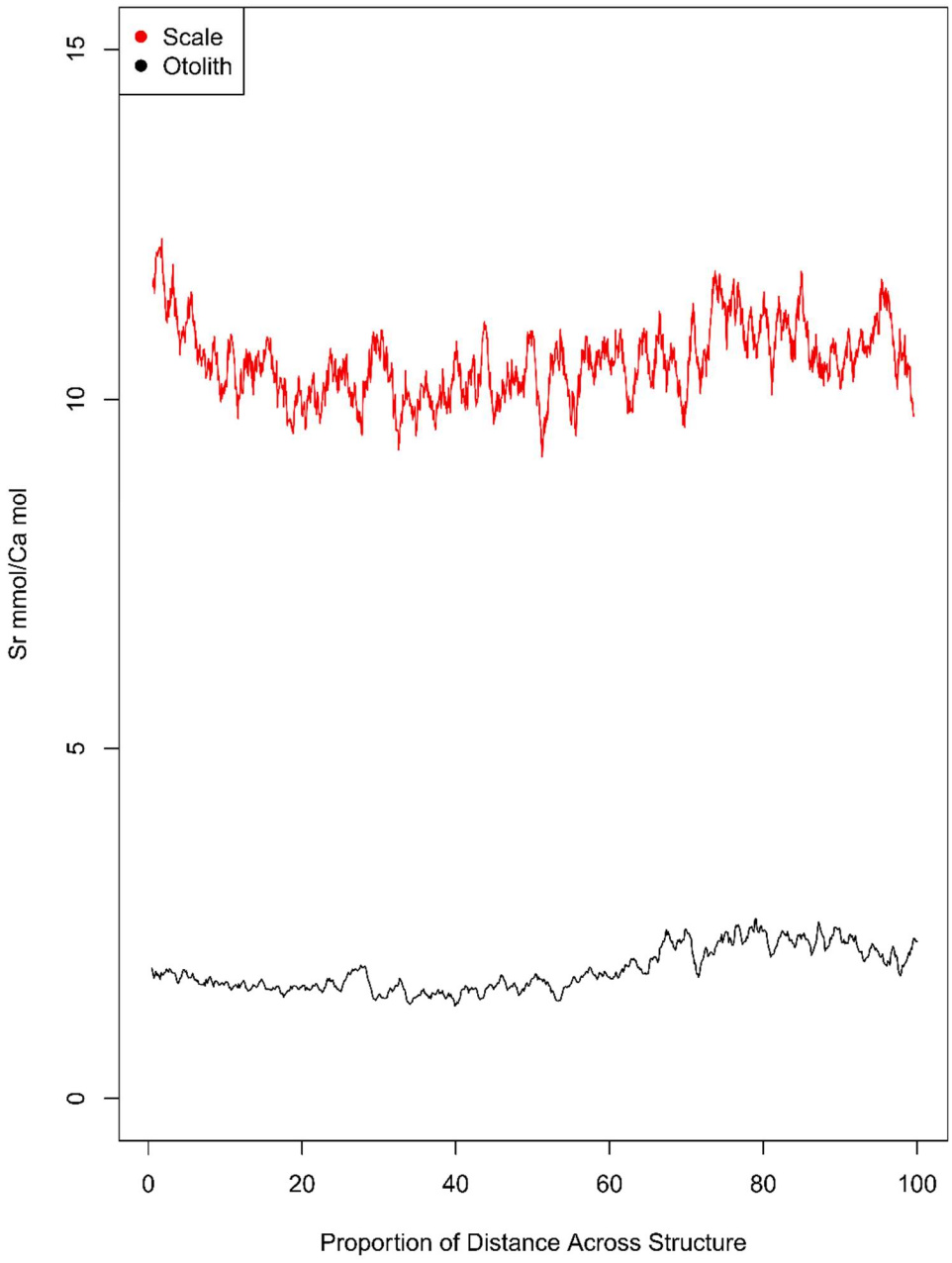
Scale
Otolith
Sr mmol/Ca mol
0
5
10
15
0
20
40
60
80
100
Proportion of Distance Across Structure

RD−067

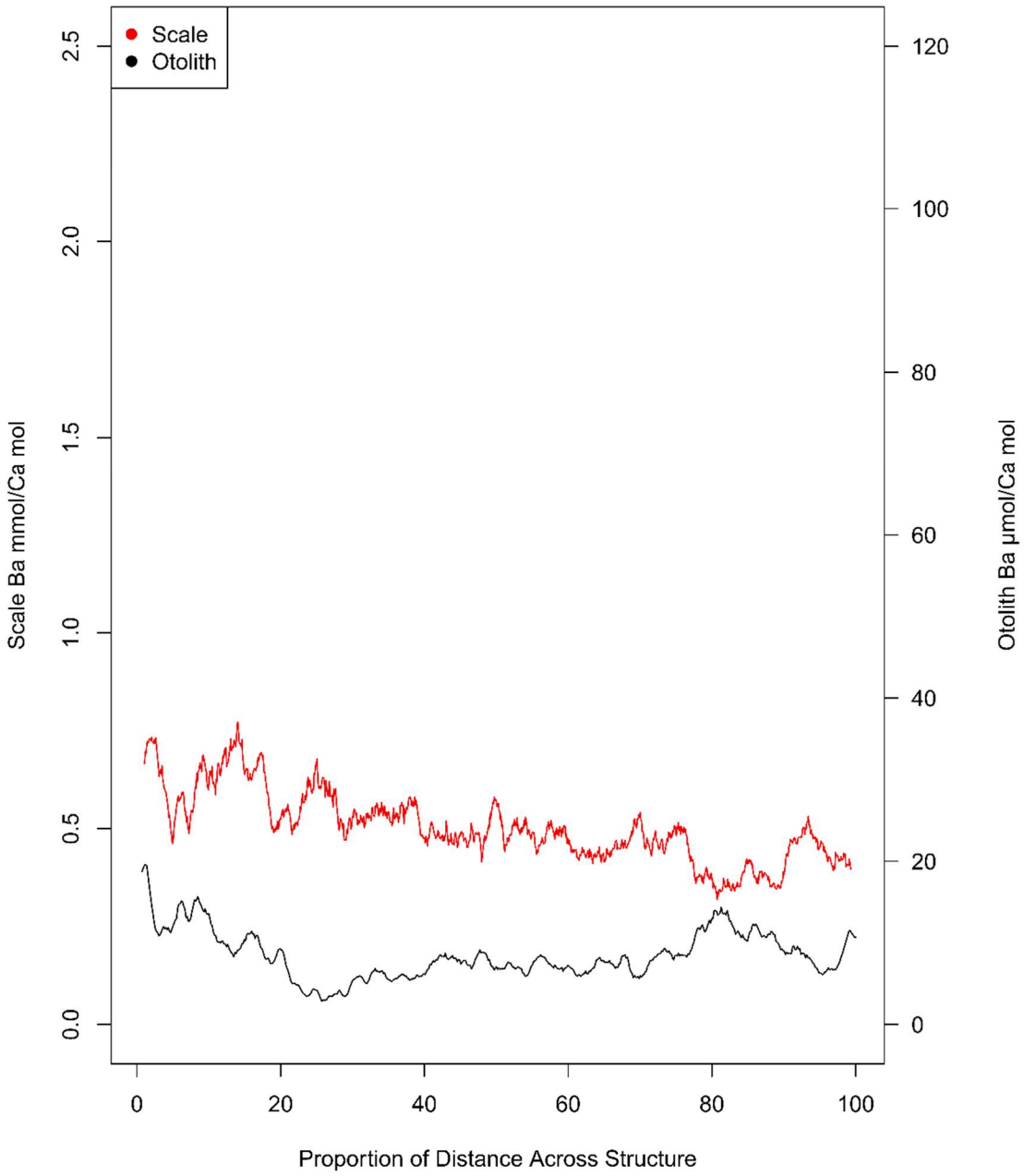
Scale
Otolith
Scale Ba mmol/Ca mol
Otolith Ba µmol/Ca mol
Proportion of Distance Across Structure
0.0
0.5
1.0
1.5
2.0
2.5
0
20
40
60
80
100
120

RD-067

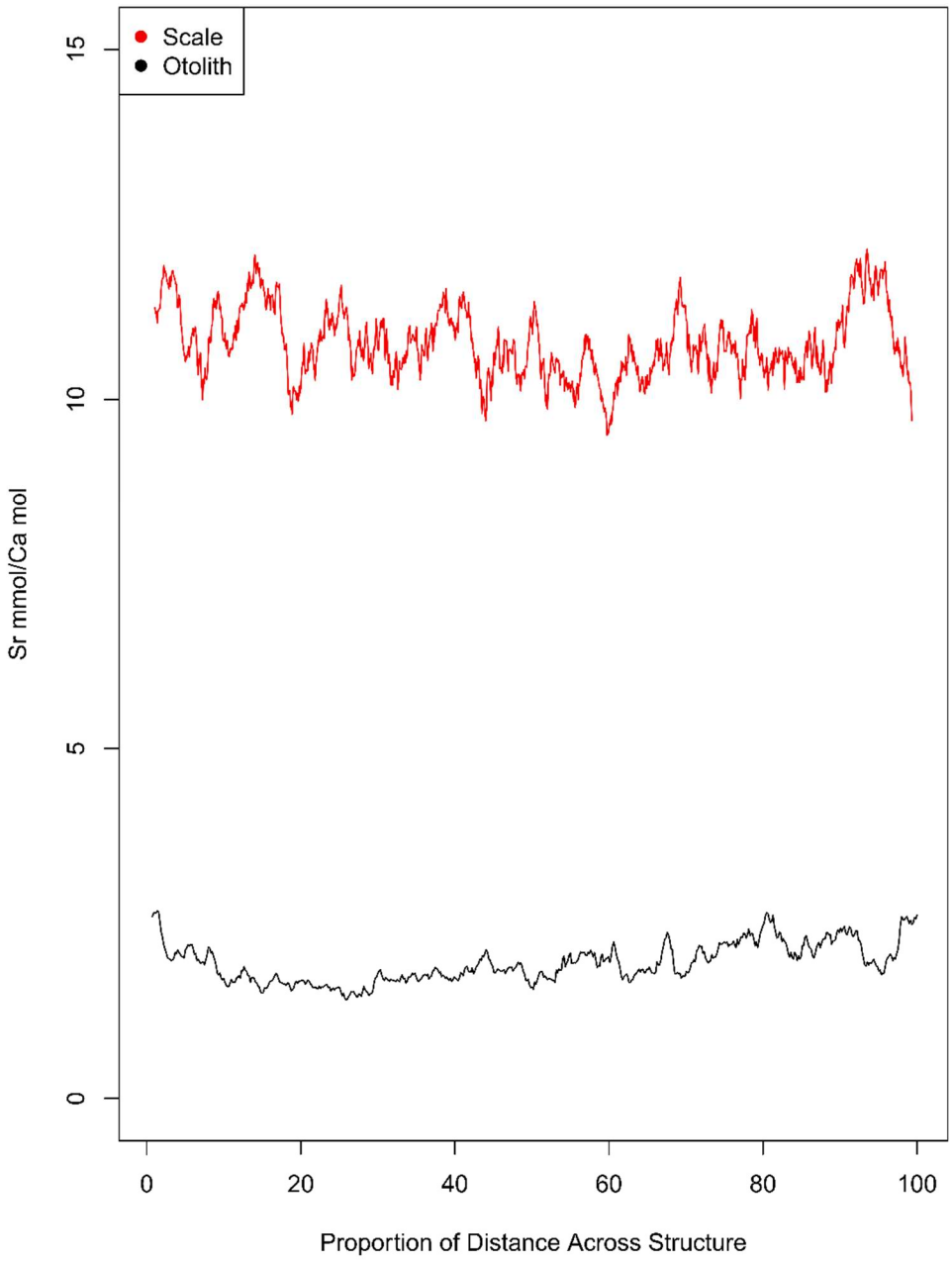
Scale
Otolith
Sr mmol/Ca mol
0
5
10
15
0
20
40
60
80
100
Proportion of Distance Across Structure

RD-068

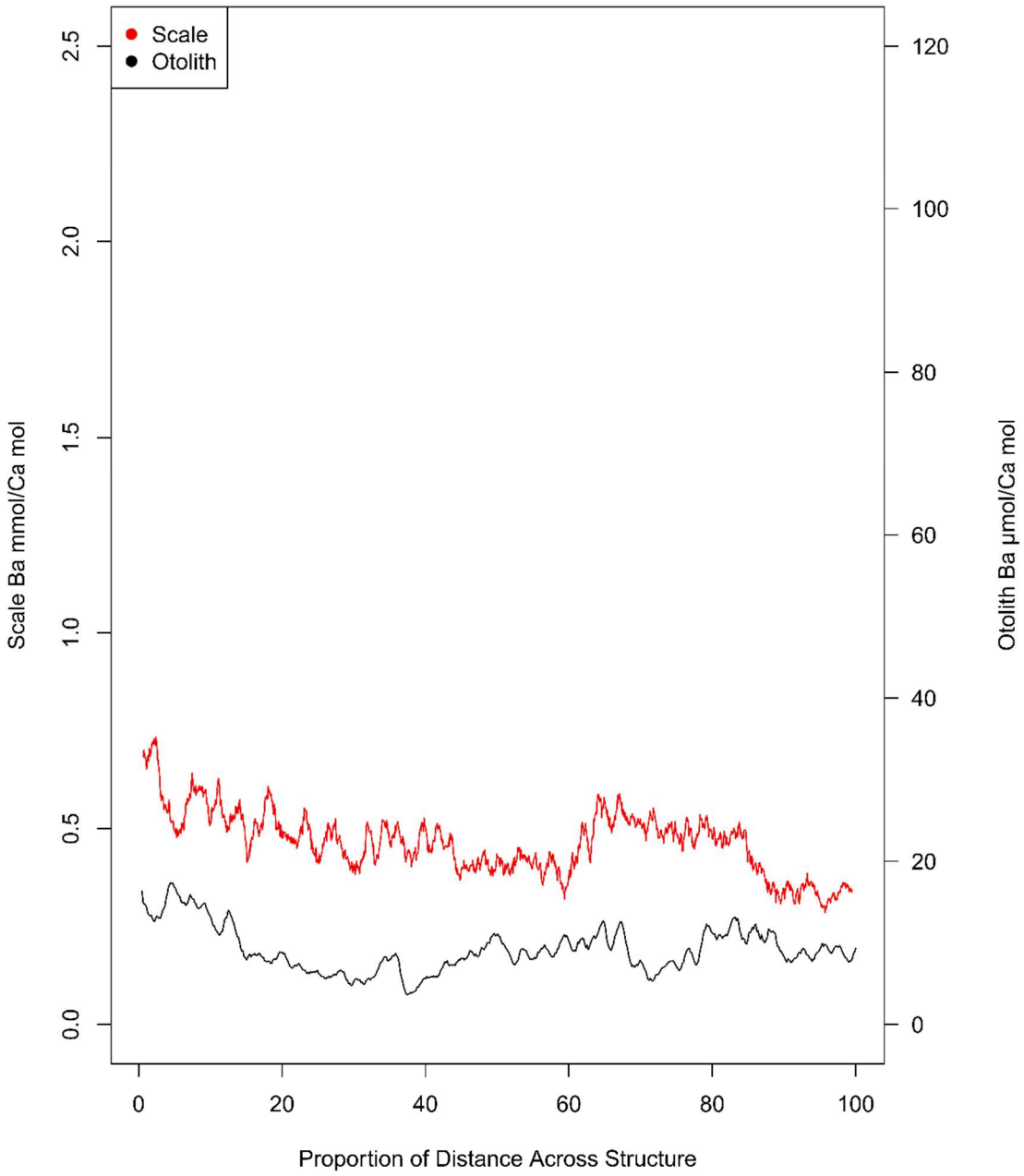
Scale
Otolith
Scale Ba mmol/Ca mol
Otolith Ba µmol/Ca mol
Proportion of Distance Across Structure
0.0
0.5
1.0
1.5
2.0
2.5
0
20
40
60
80
100
120

RD-068

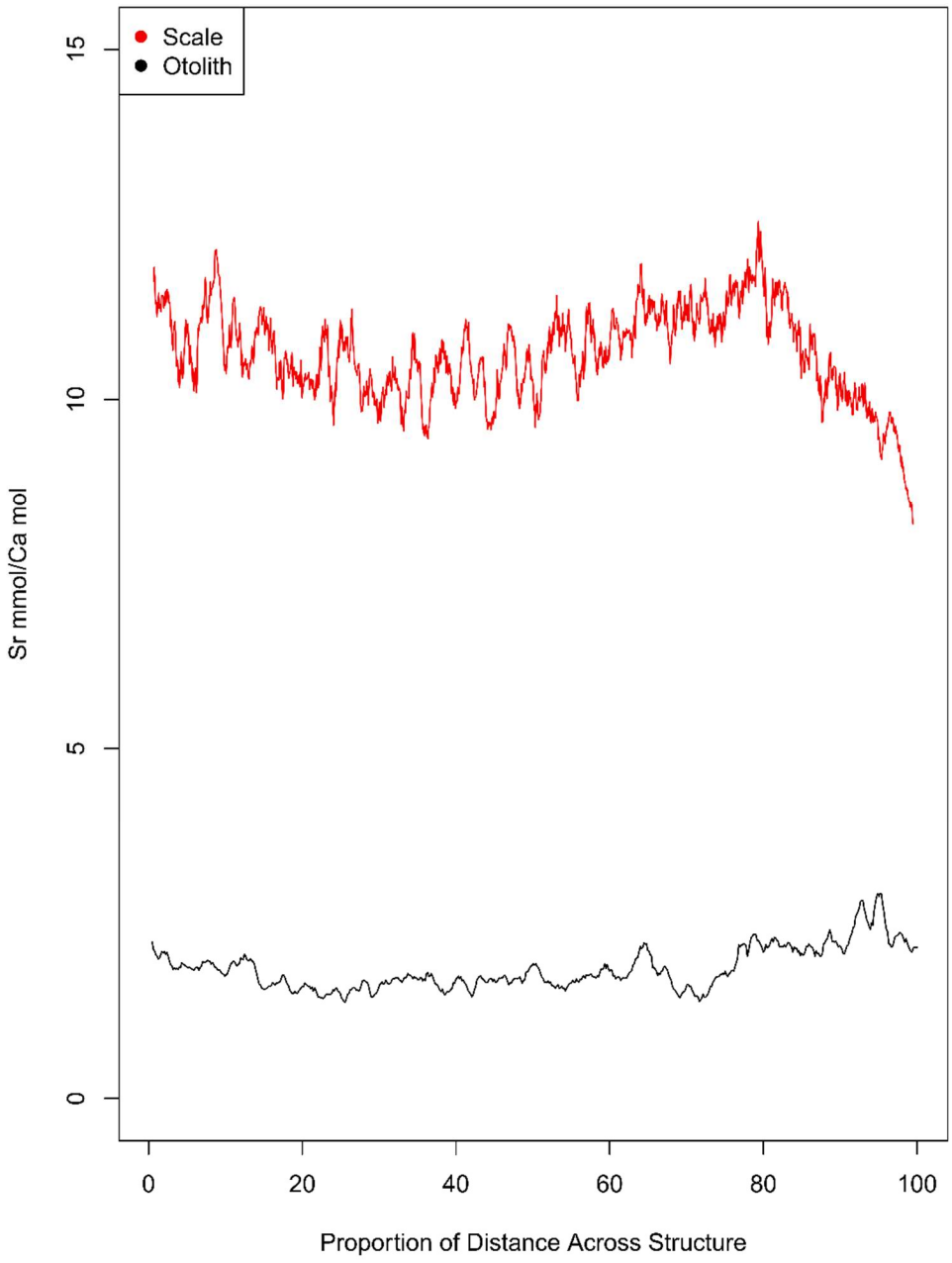
Scale
Otolith
Sr mmol/Ca mol
0
5
10
15
0
20
40
60
80
100
Proportion of Distance Across Structure

RD−069

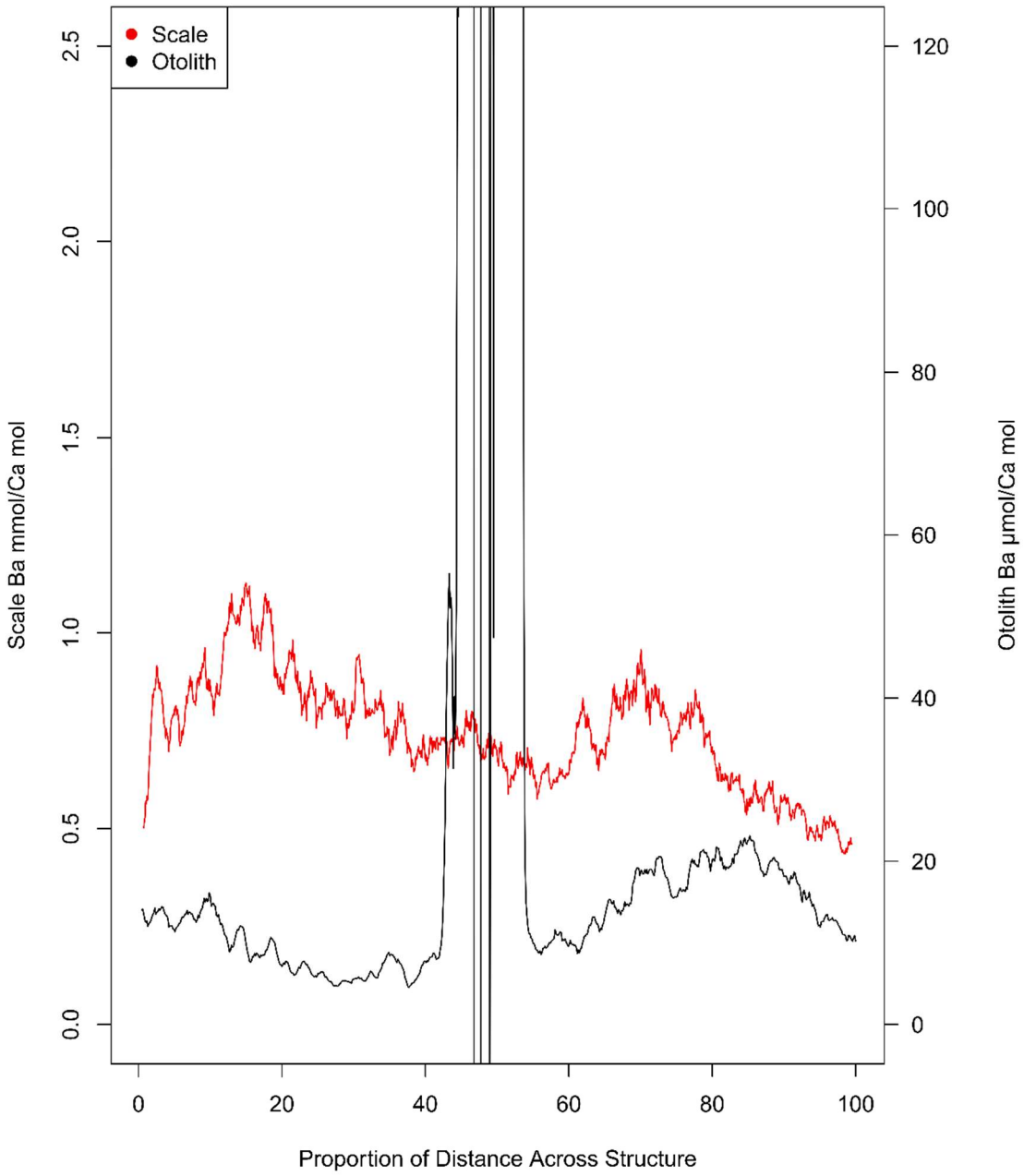
Scale
Otolith
Scale Ba mmol/Ca mol
Otolith Ba µmol/Ca mol
Proportion of Distance Across Structure
0.0
0.5
1.0
1.5
2.0
2.5
0
20
40
60
80
100
120

RD-069

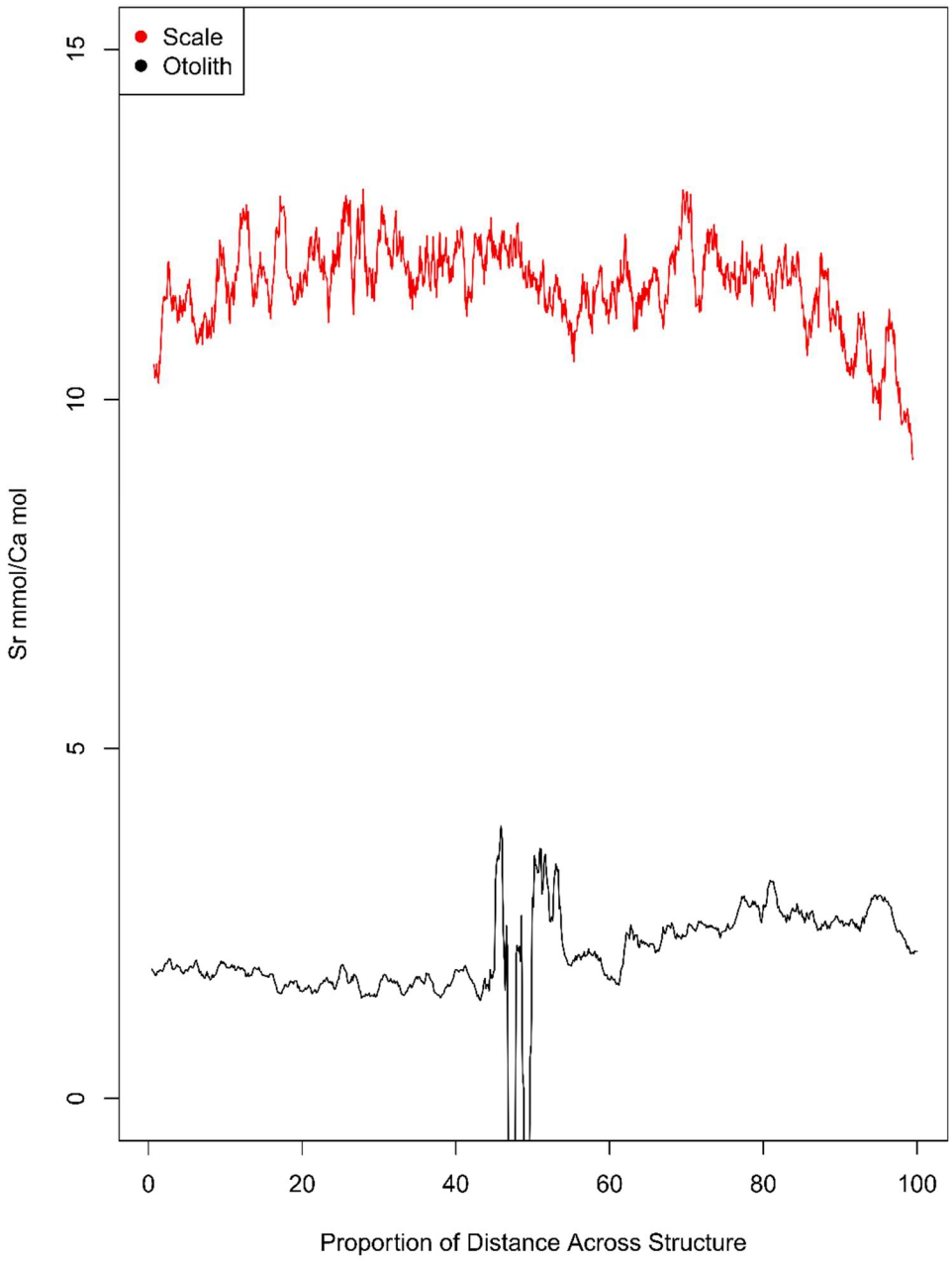
Scale
Otolith
15
10
5
0
Sr mmol/Ca mol
0
20
40
60
80
100
Proportion of Distance Across Structure

RD−070

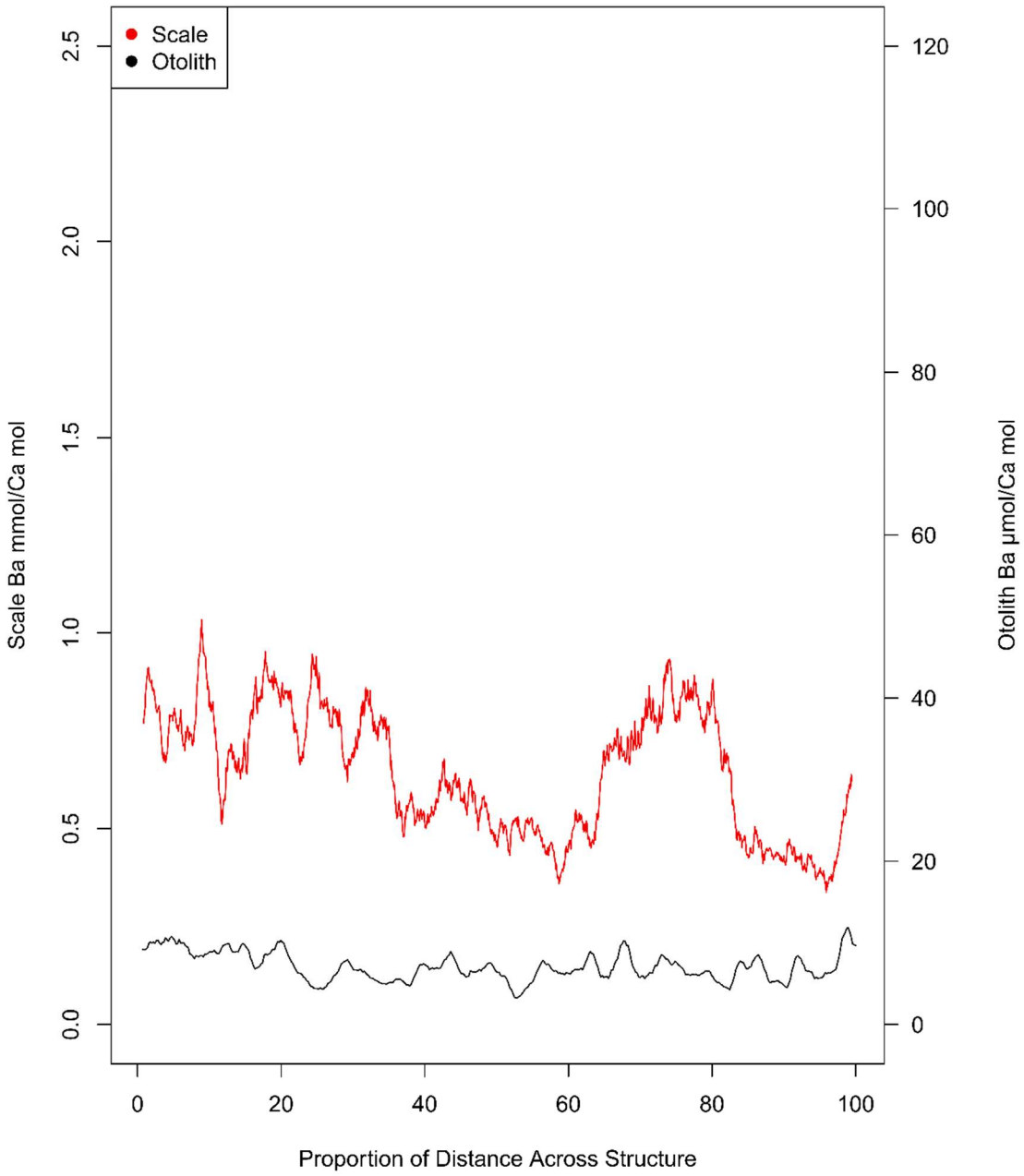
Scale
Otolith
Scale Ba mmol/Ca mol
Otolith Ba µmol/Ca mol
Proportion of Distance Across Structure
0.0
0.5
1.0
1.5
2.0
2.5
0
20
40
60
80
100
120

RD-070

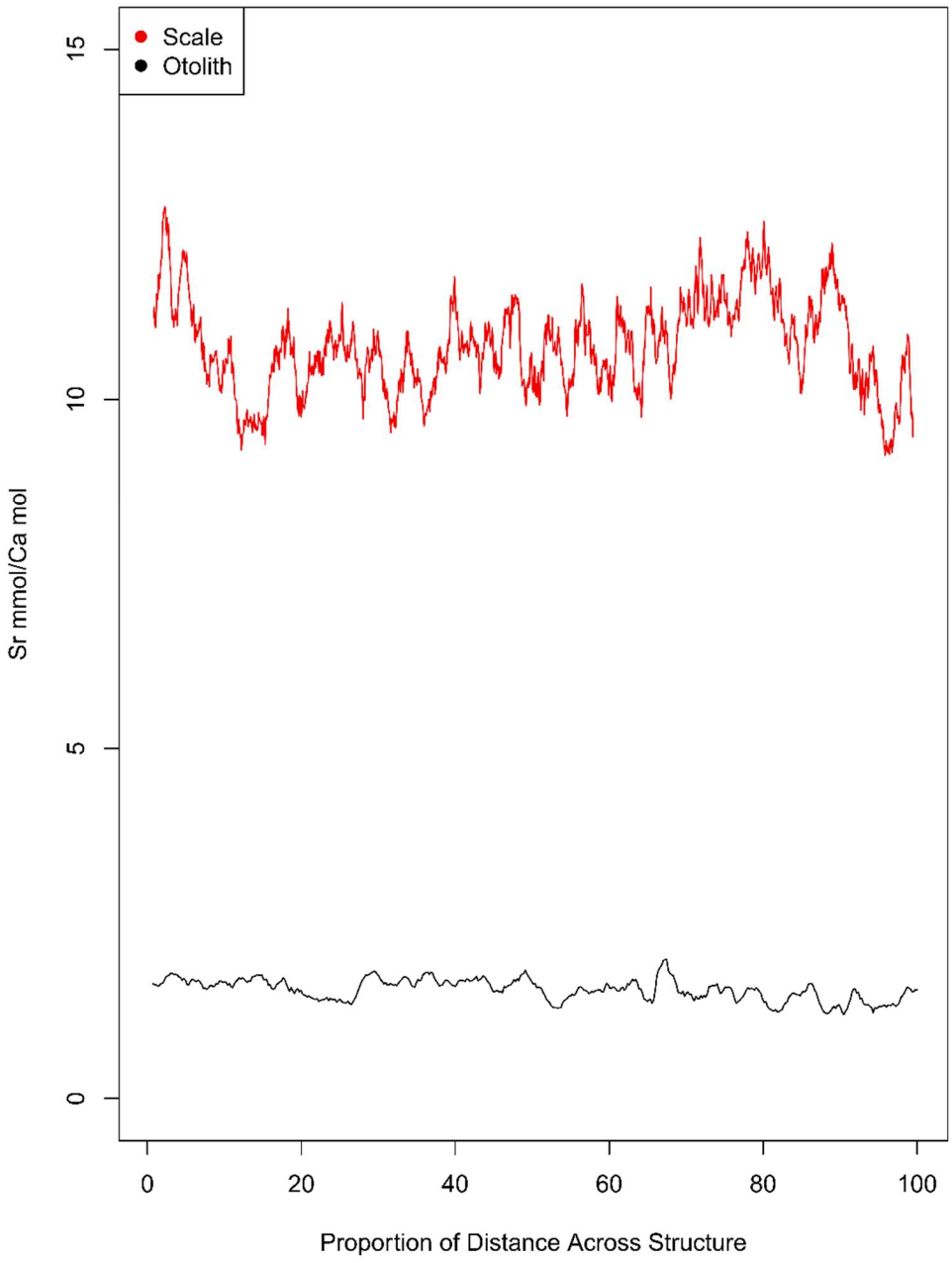
Scale
Otolith
Sr mmol/Ca mol
0
5
10
15
0
20
40
60
80
100
Proportion of Distance Across Structure

RD-071

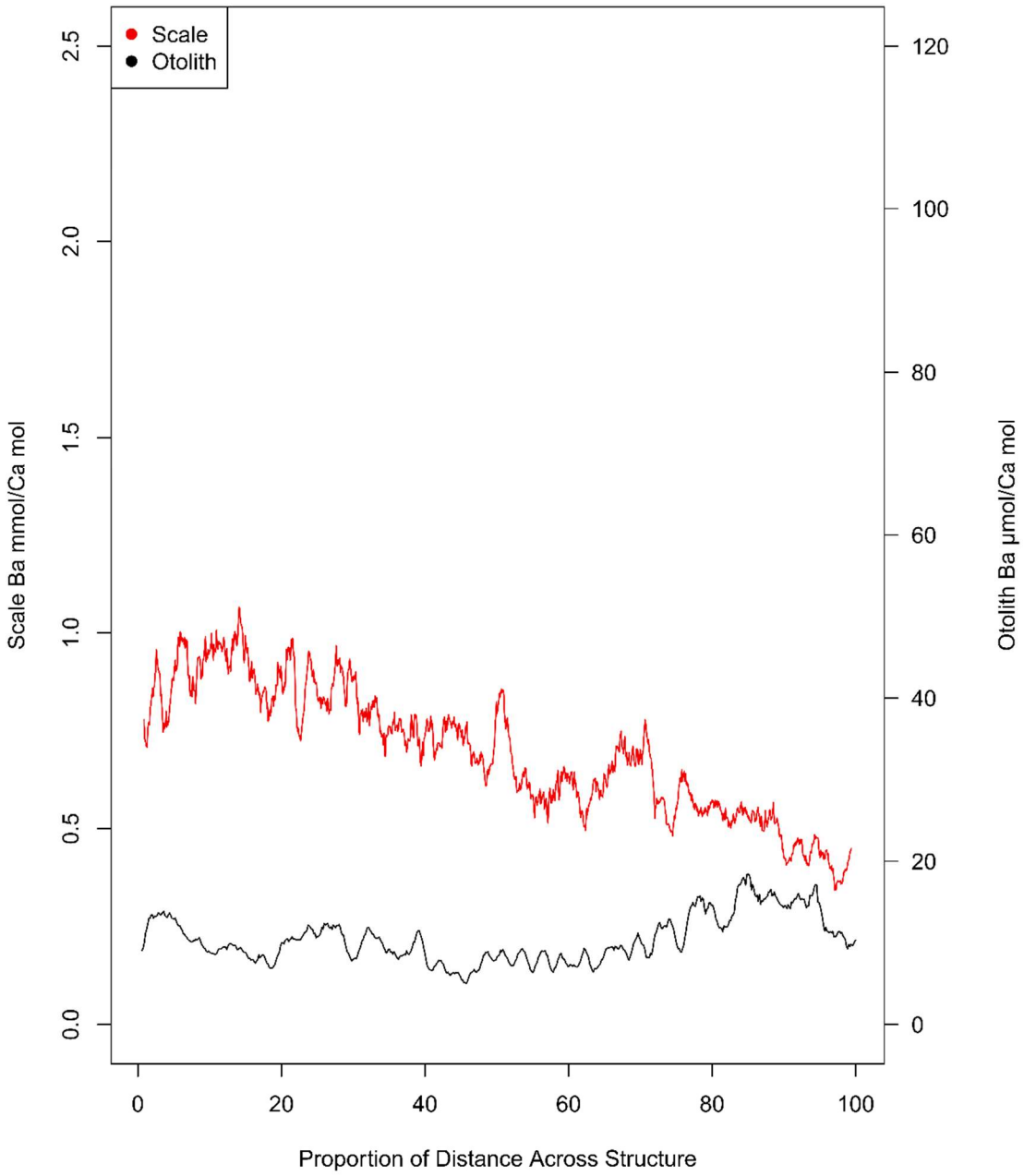
Scale
Otolith
Scale Ba mmol/Ca mol
Otolith Ba µmol/Ca mol
Proportion of Distance Across Structure
0.0
0.5
1.0
1.5
2.0
2.5
0
20
40
60
80
100
120

RD-071

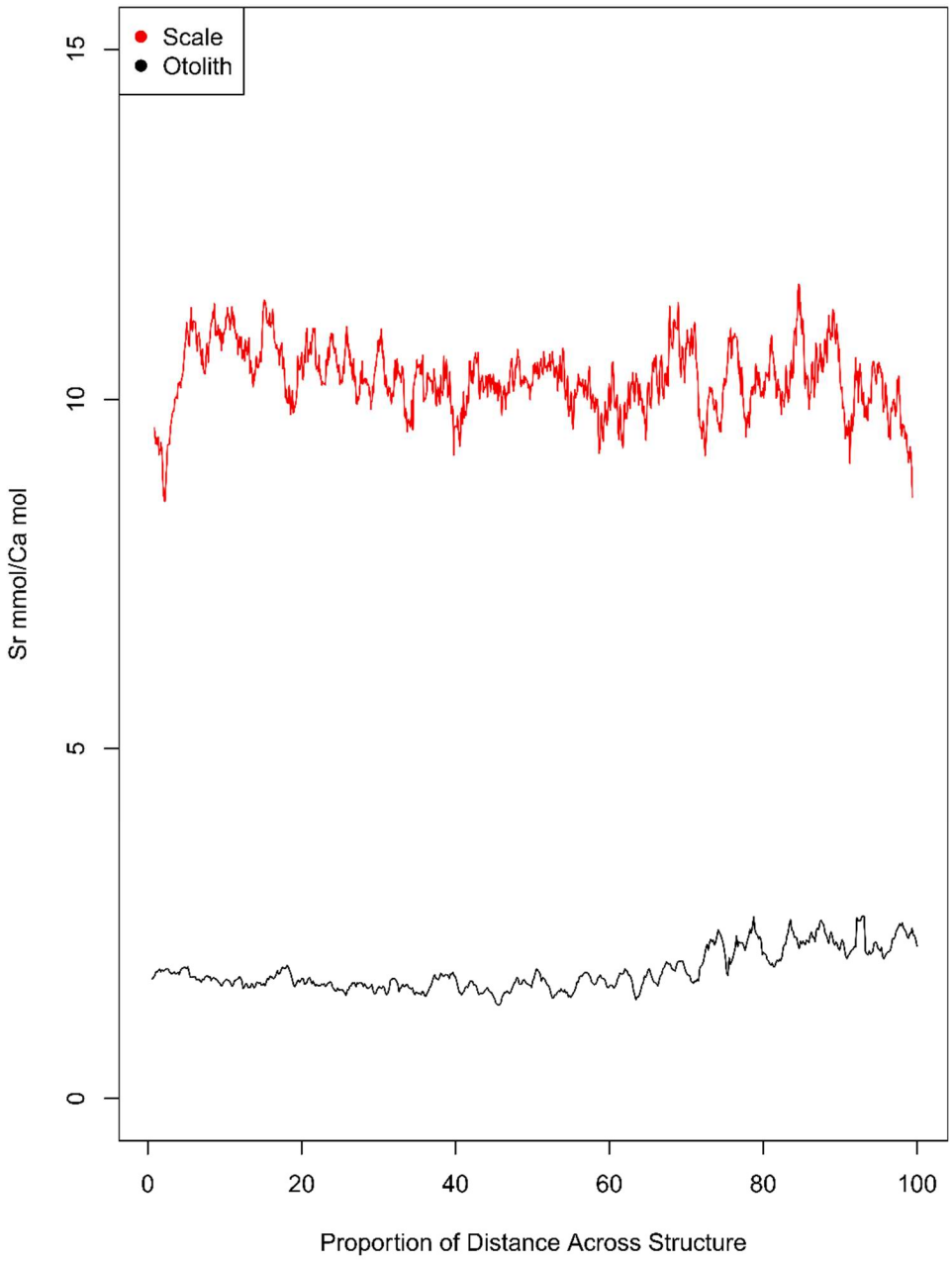
Scale
Otolith
Sr mmol/Ca mol
0
5
10
15
0
20
40
60
80
100
Proportion of Distance Across Structure

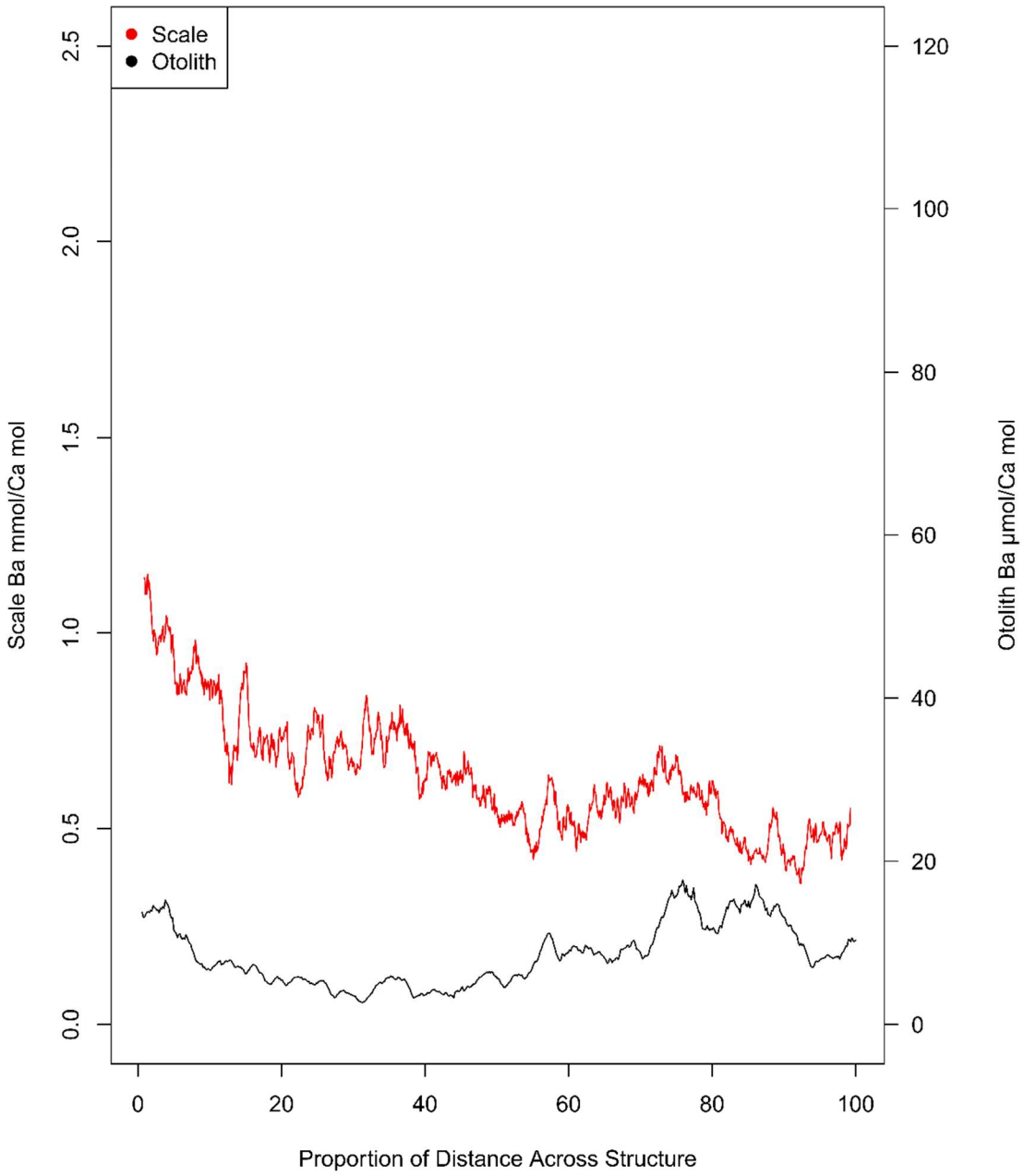
RD−072
Scale
Otolith
Scale Ba mmol/Ca mol
Otolith Ba µmol/Ca mol
Proportion of Distance Across Structure
0.0
0.5
1.0
1.5
2.0
2.5
0
20
40
60
80
100
120

RD-072

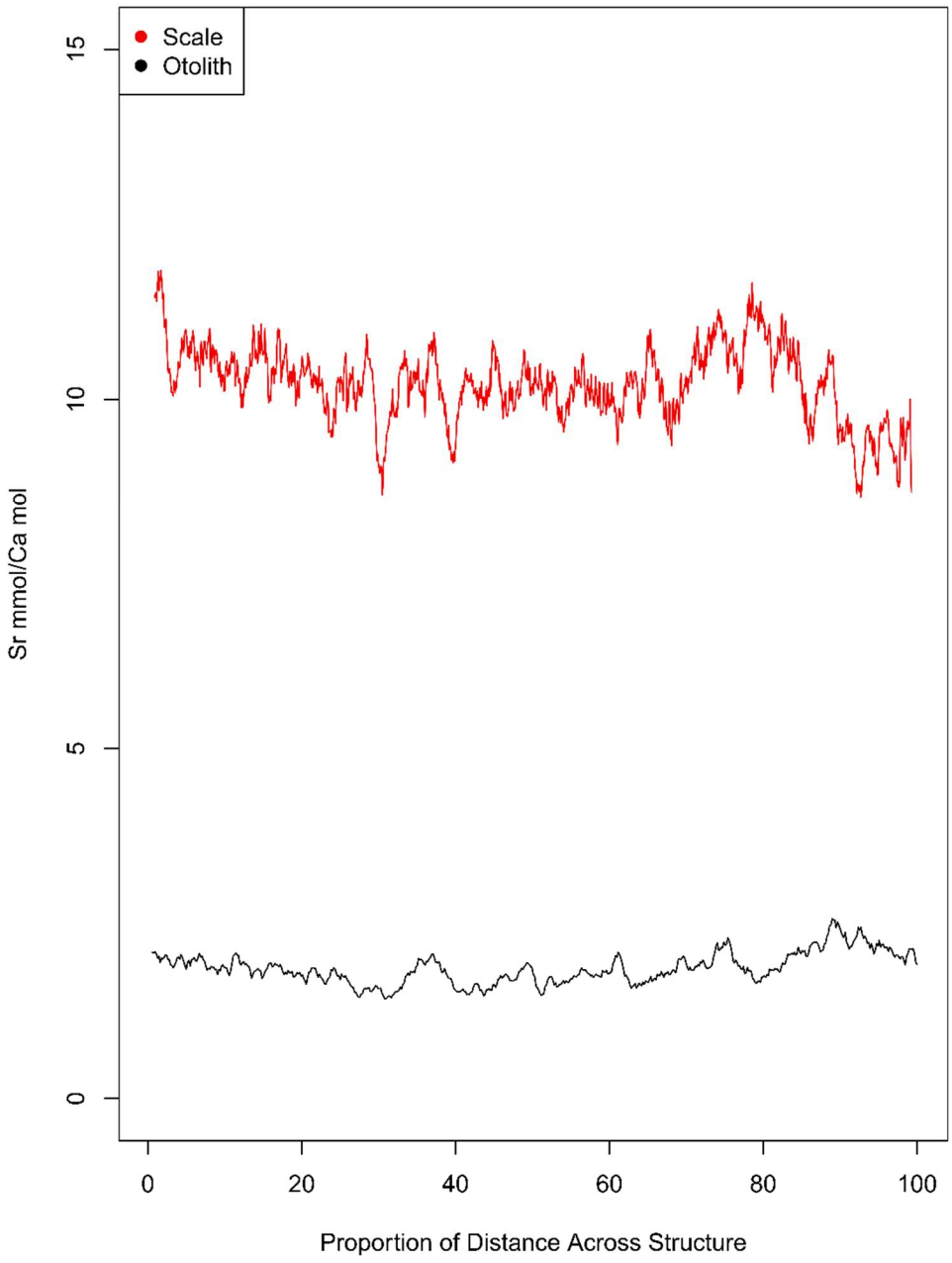
Scale
Otolith
Sr mmol/Ca mol
0
5
10
15
0
20
40
60
80
100
Proportion of Distance Across Structure

RD−073

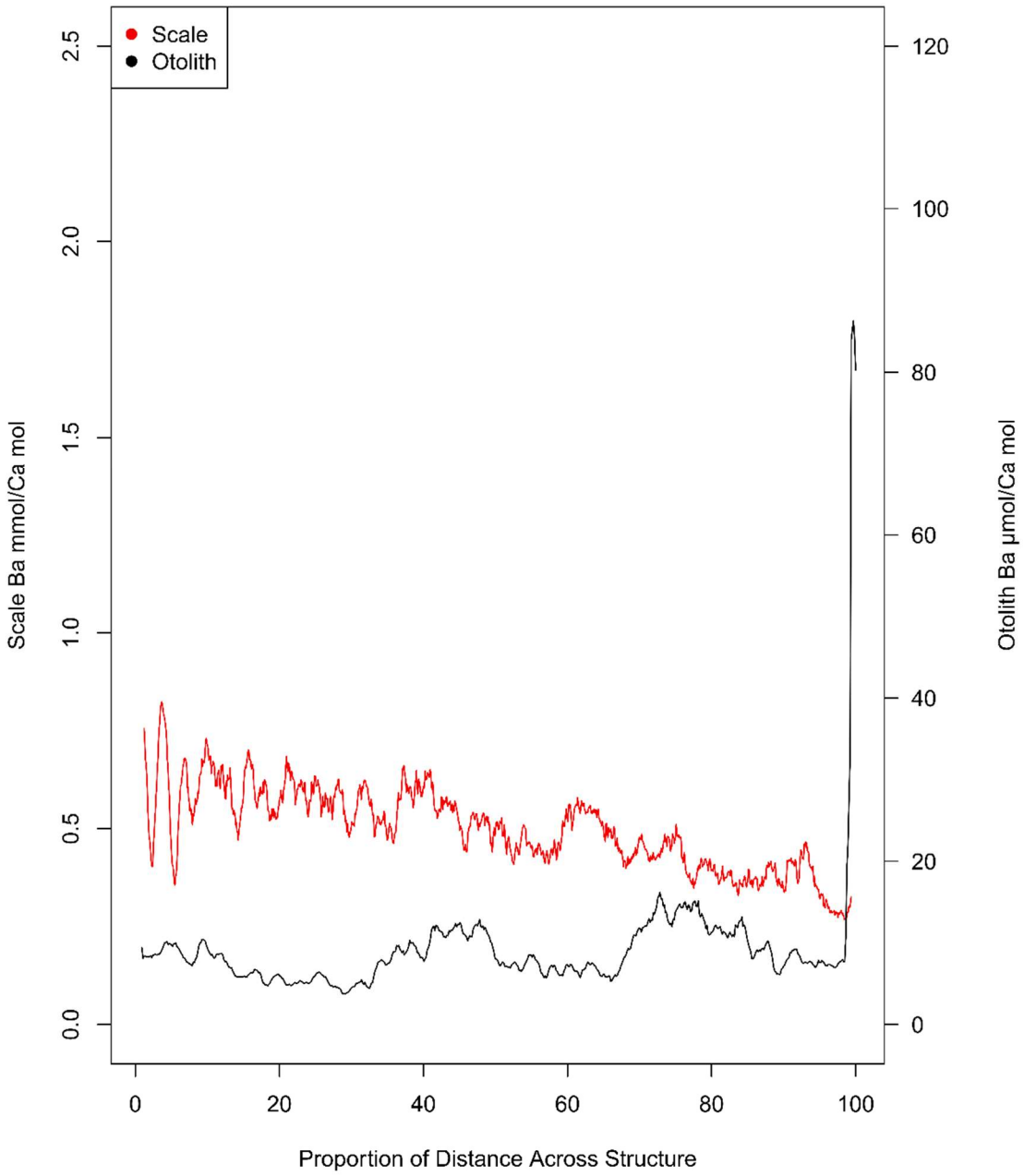
Scale
Otolith
Scale Ba mmol/Ca mol
Otolith Ba µmol/Ca mol
Proportion of Distance Across Structure
0.0
0.5
1.0
1.5
2.0
2.5
0
20
40
60
80
100
120

RD-073

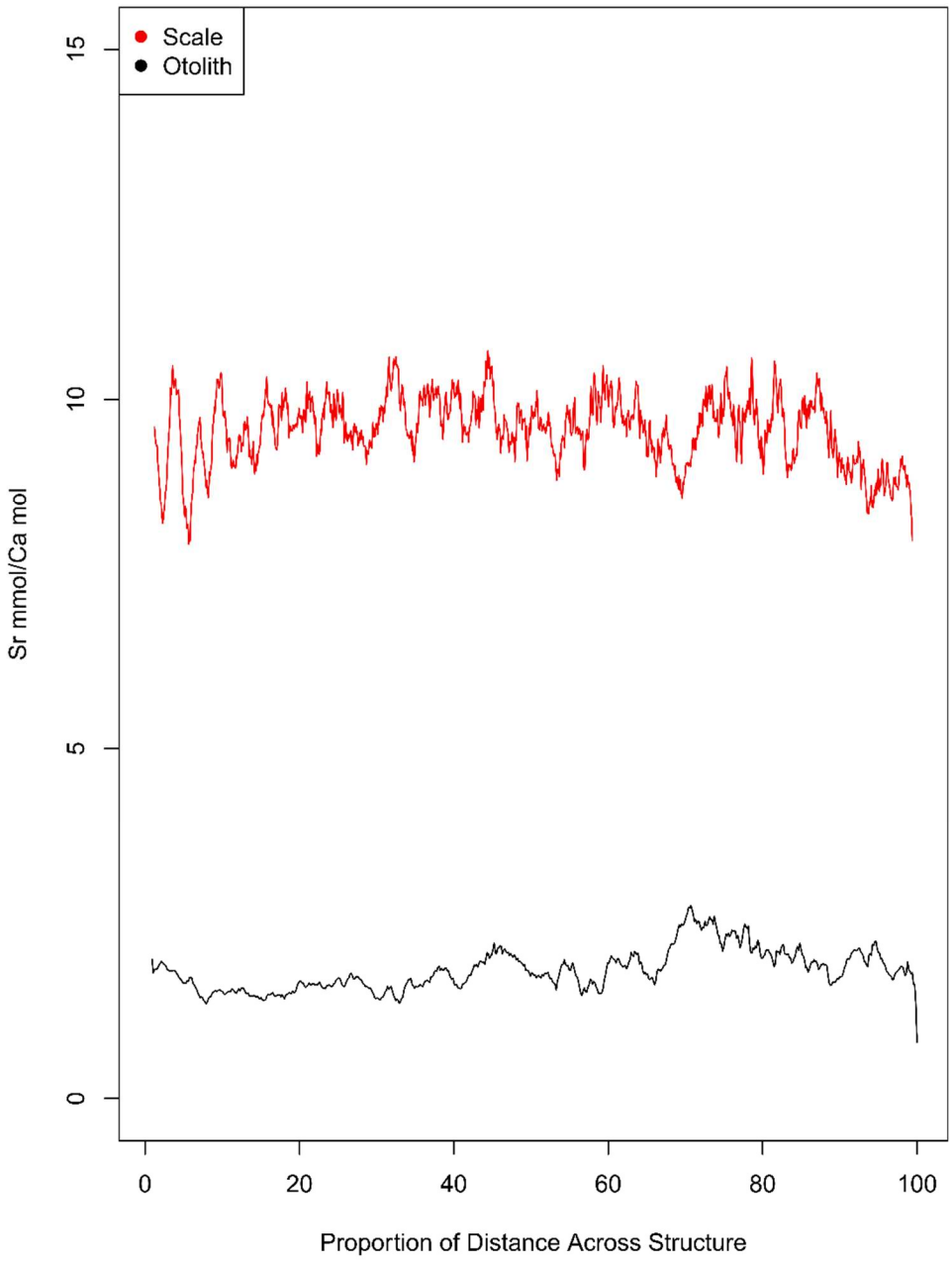
Scale
Otolith
Sr mmol/Ca mol
0
5
10
15
0
20
40
60
80
100
Proportion of Distance Across Structure

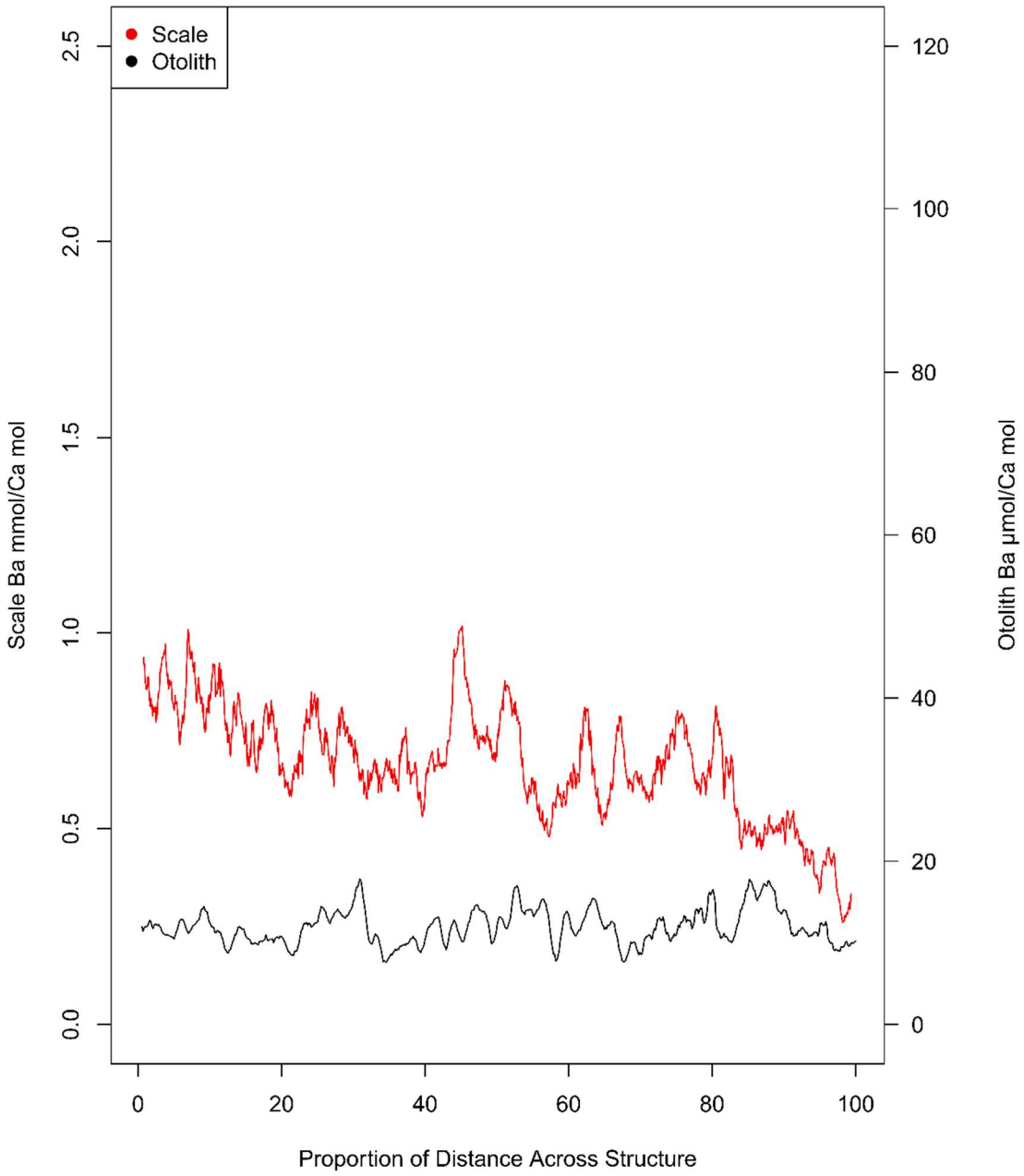
RD−074
Scale
Otolith
Scale Ba mmol/Ca mol
Otolith Ba µmol/Ca mol
Proportion of Distance Across Structure
0.0
0.5
1.0
1.5
2.0
2.5
0
20
40
60
80
100
120

RD-074

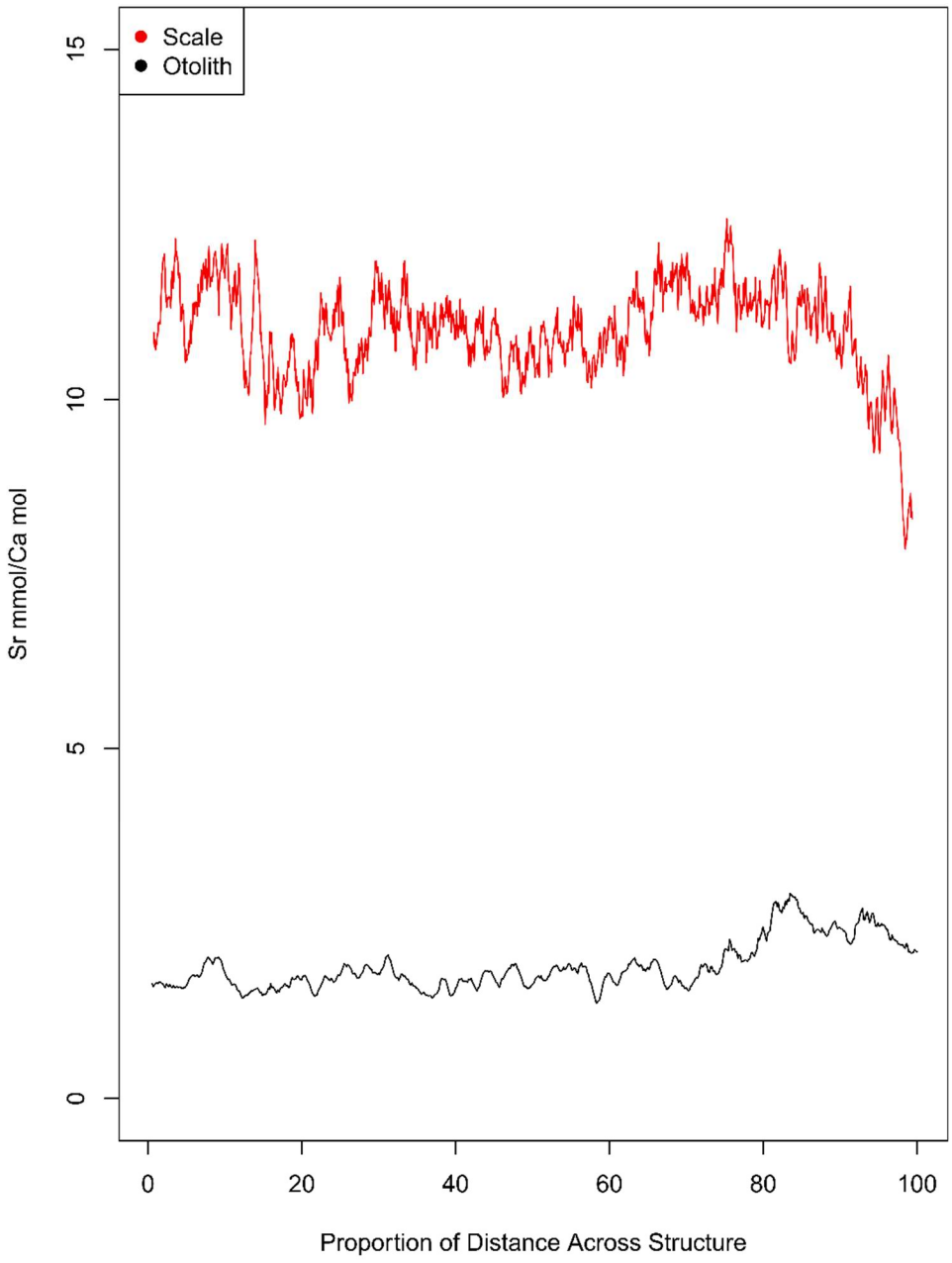
Scale
Otolith
Sr mmol/Ca mol
0
5
10
15
0
20
40
60
80
100
Proportion of Distance Across Structure

RD-075

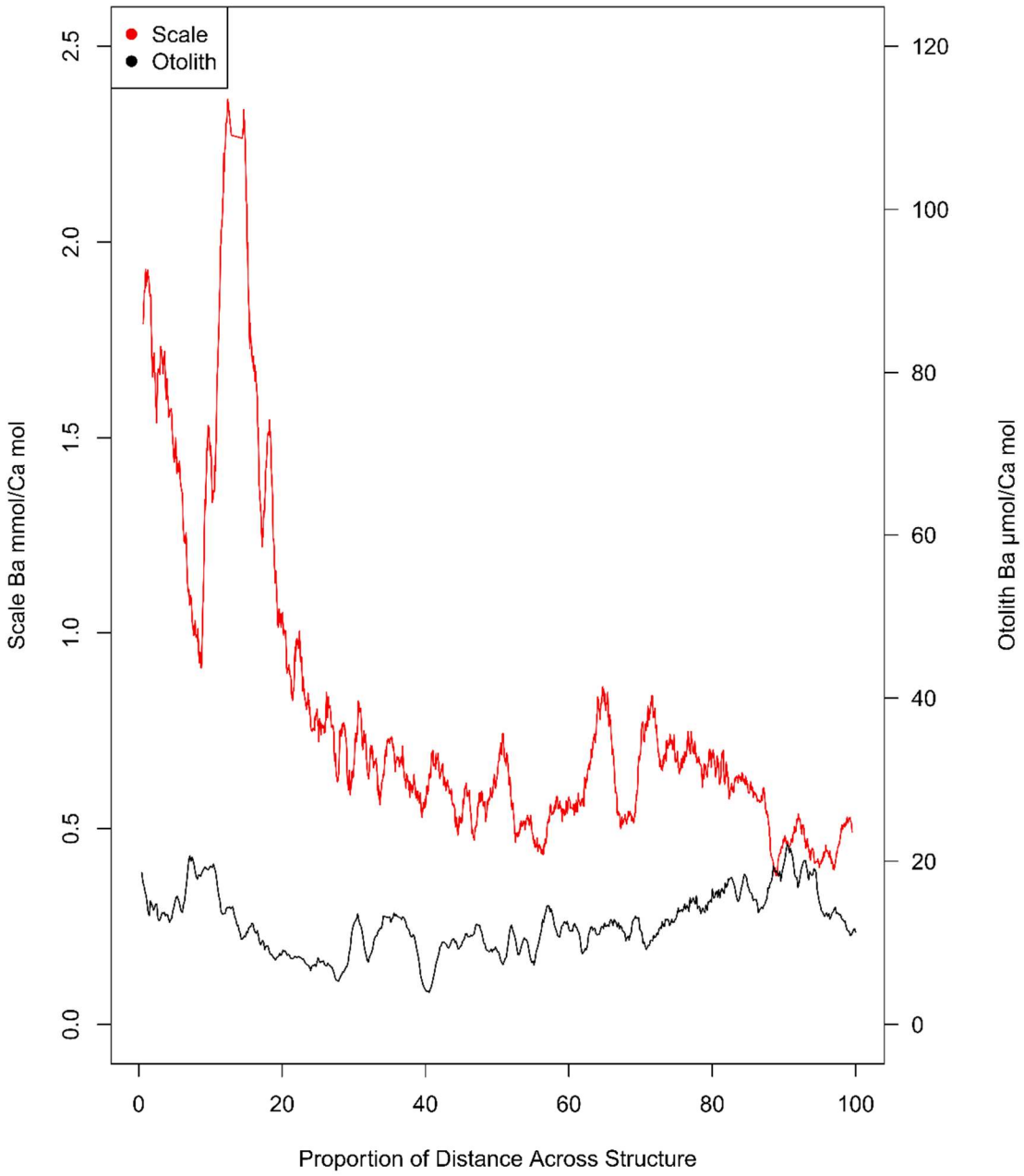
Scale
Otolith
Scale Ba mmol/Ca mol
Otolith Ba µmol/Ca mol
Proportion of Distance Across Structure
0.0
0.5
1.0
1.5
2.0
2.5
0
20
40
60
80
100
120

RD-075

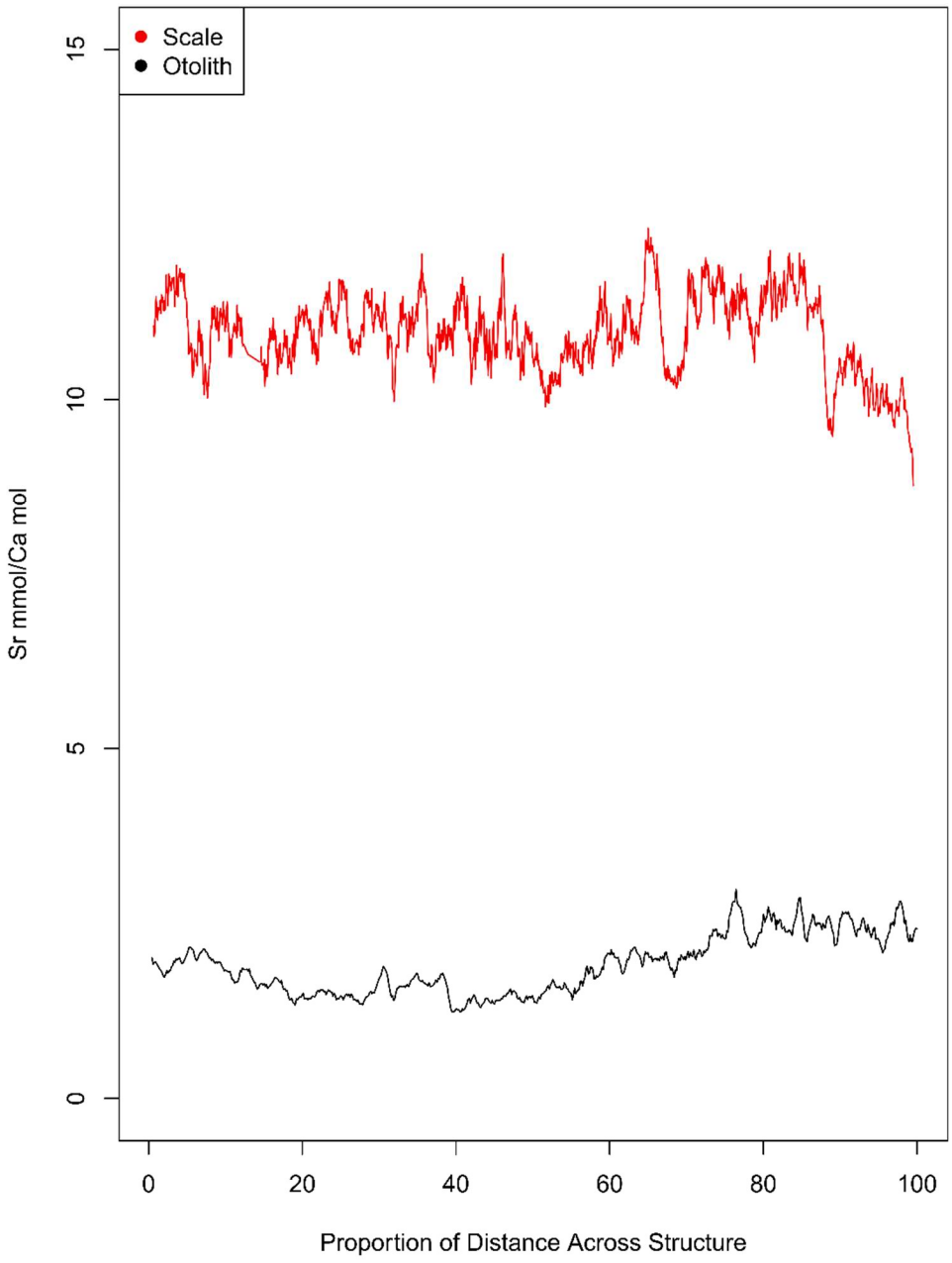
Scale
Otolith
Sr mmol/Ca mol
0
5
10
15
0
20
40
60
80
100
Proportion of Distance Across Structure

RD−076

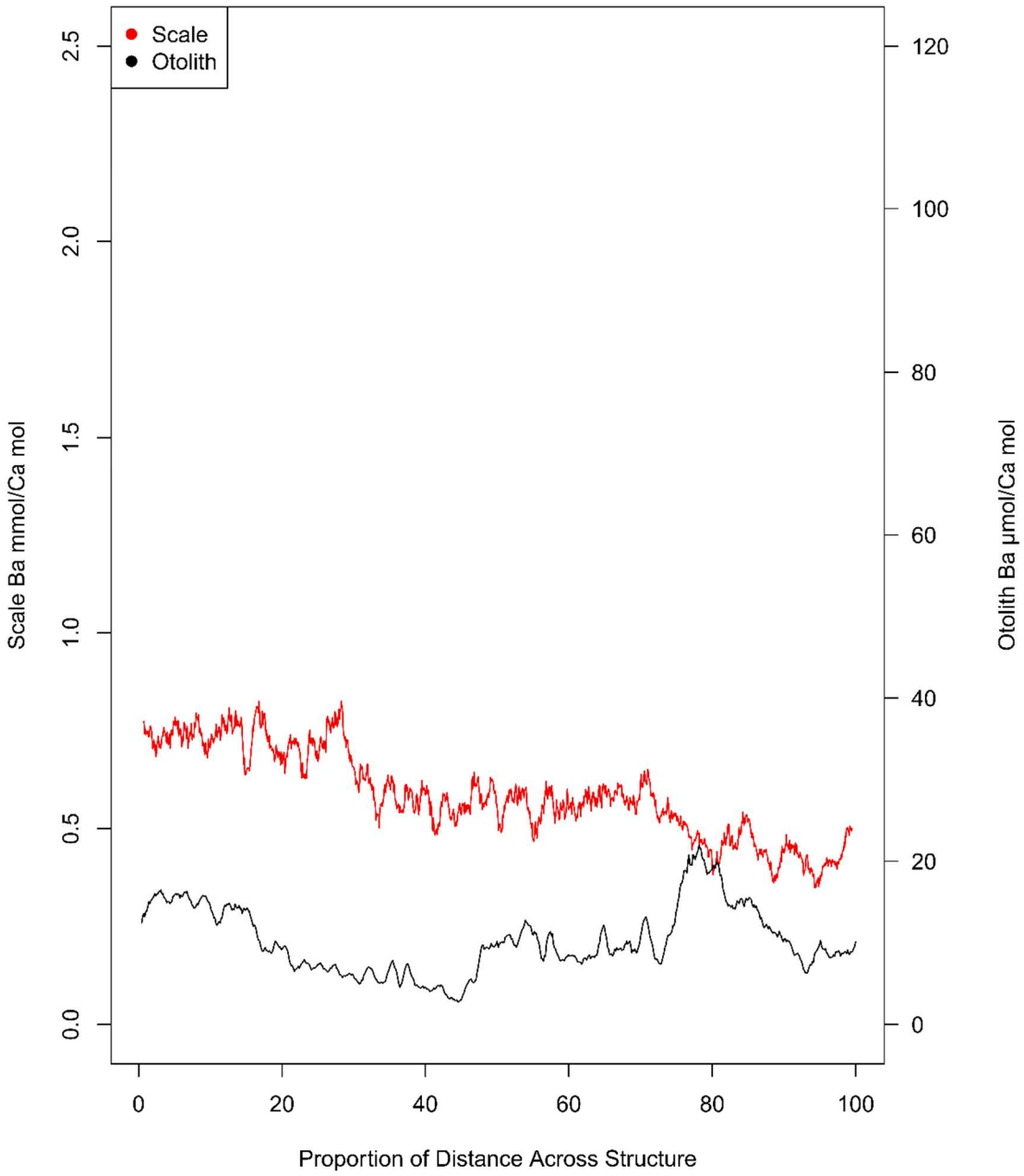
Scale
Otolith
Scale Ba mmol/Ca mol
Otolith Ba µmol/Ca mol
Proportion of Distance Across Structure
0.0
0.5
1.0
1.5
2.0
2.5
0
20
40
60
80
100
120

RD-076

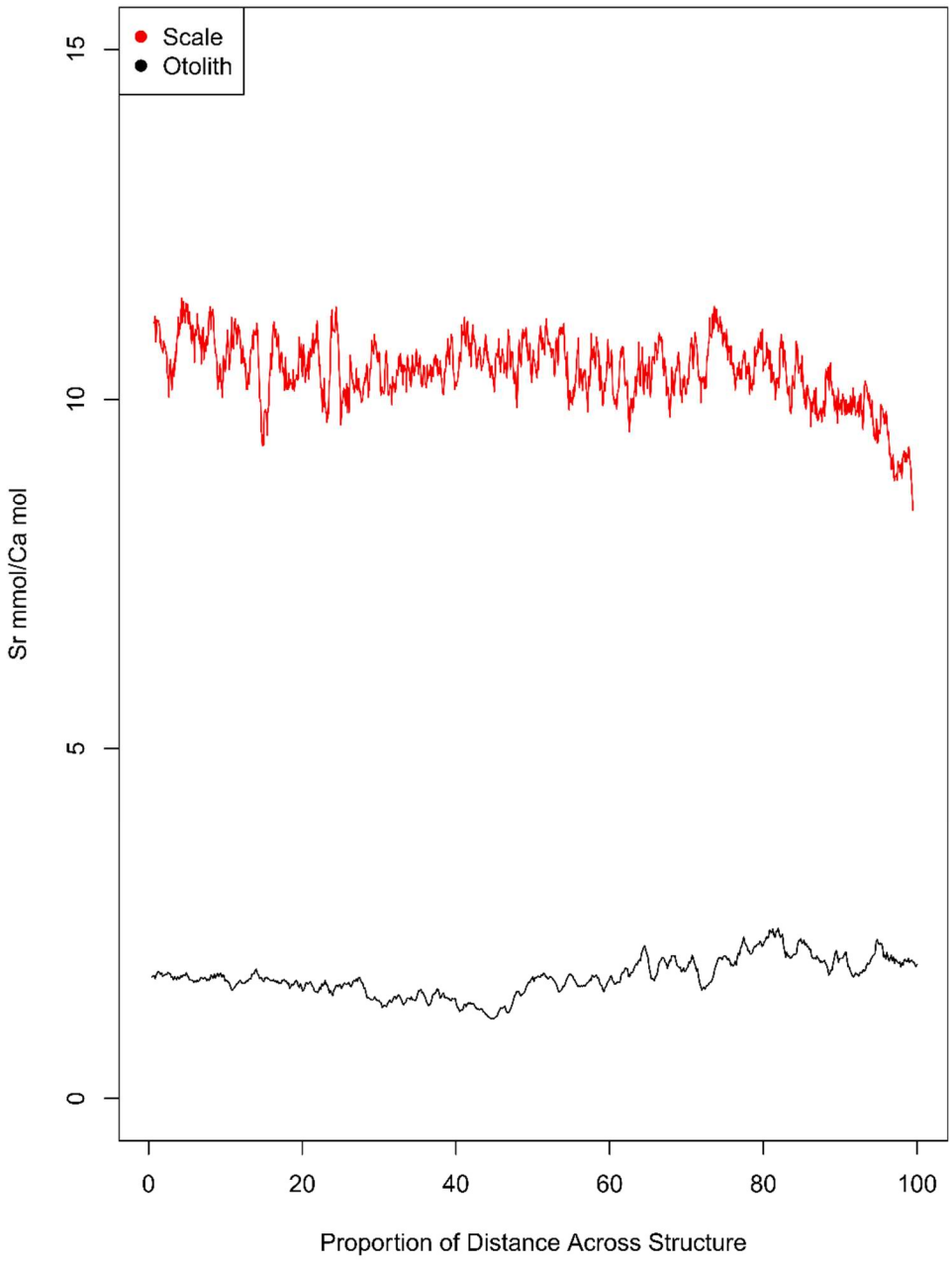
Scale
Otolith
Sr mmol/Ca mol
0
5
10
15
0
20
40
60
80
100
Proportion of Distance Across Structure

RD-077

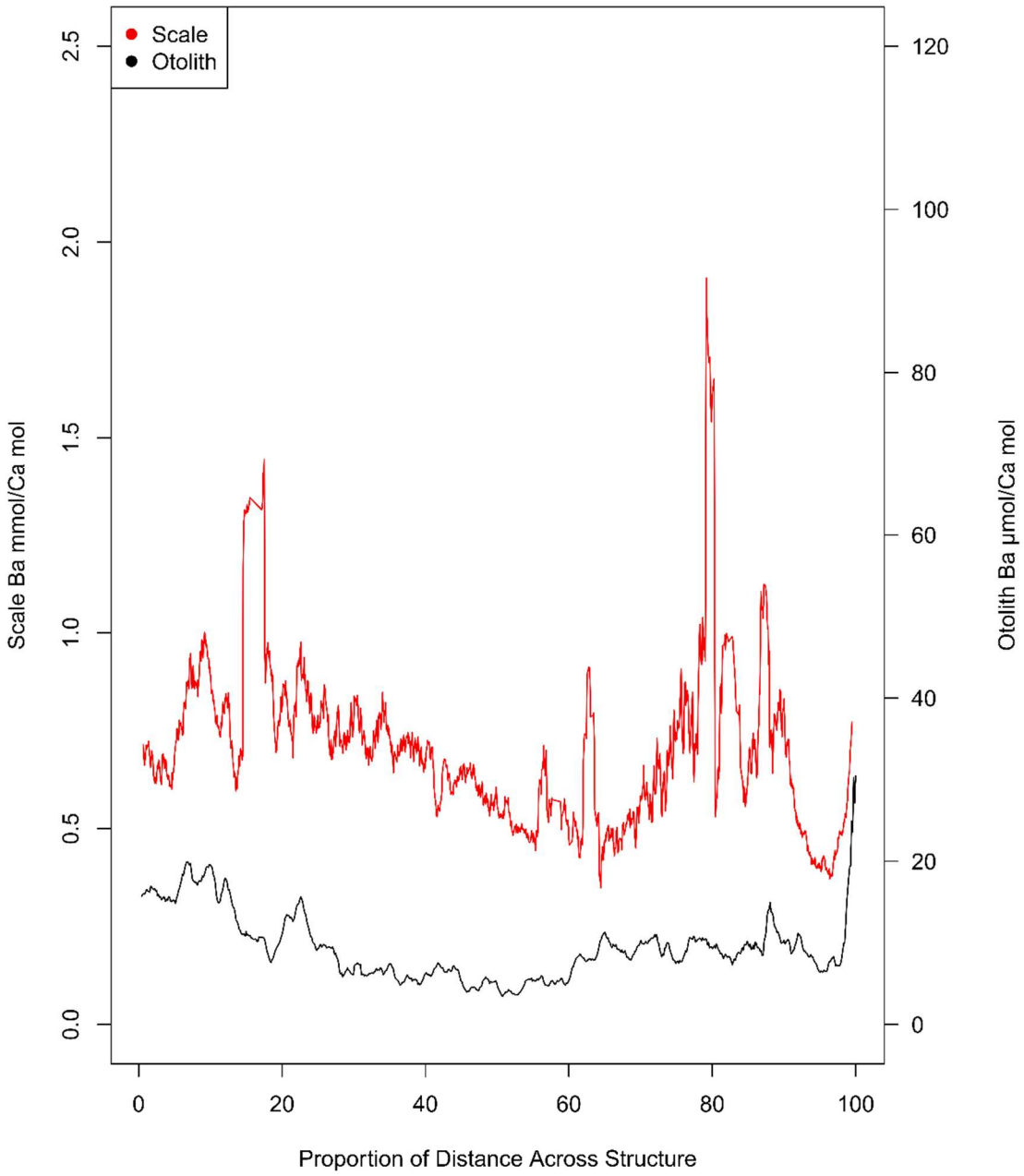
Scale
Otolith
Scale Ba mmol/Ca mol
Otolith Ba µmol/Ca mol
Proportion of Distance Across Structure
0.0
0.5
1.0
1.5
2.0
2.5
0
20
40
60
80
100
120

RD-077

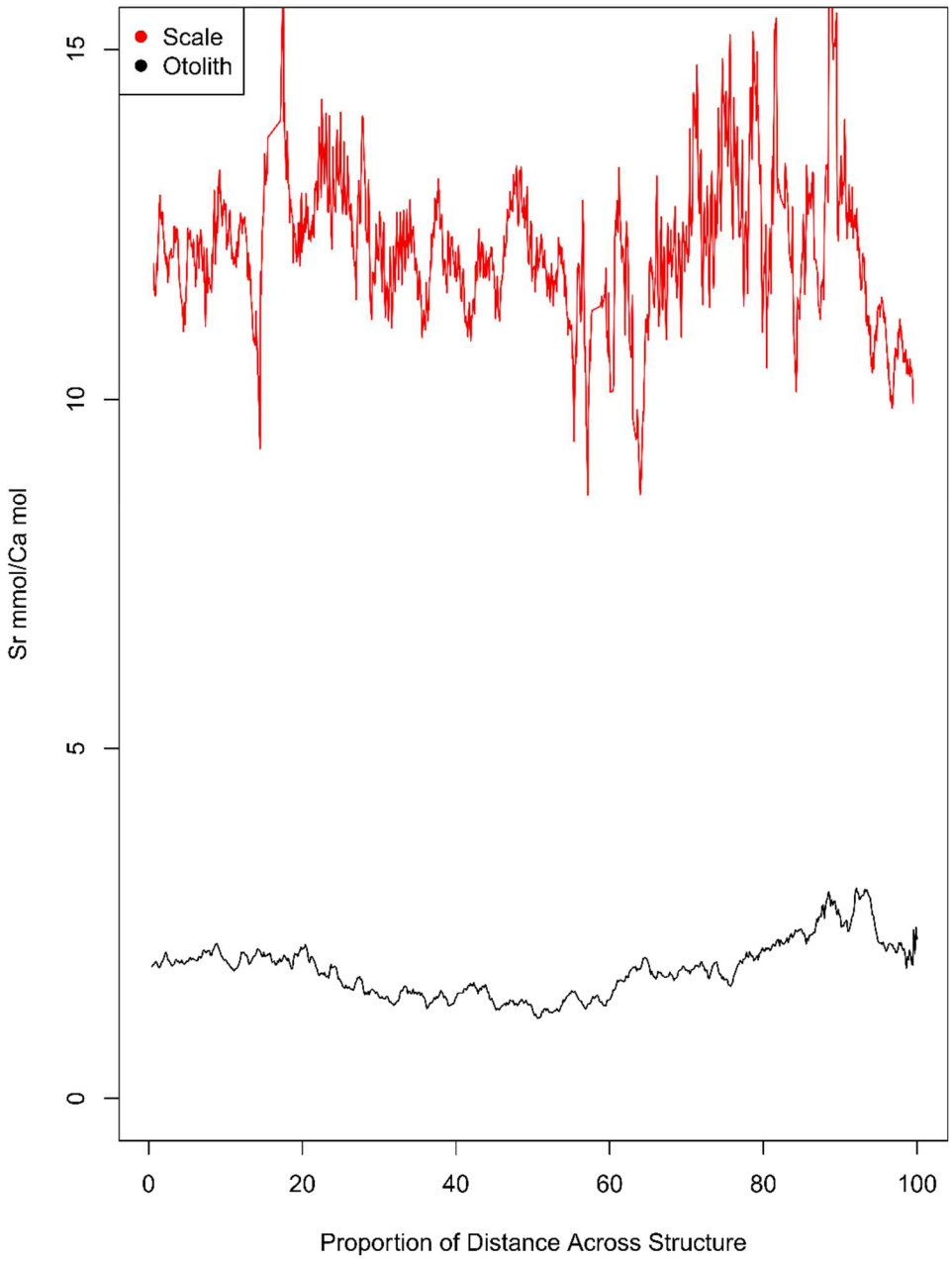
Scale
Otolith
Sr mmol/Ca mol
0
5
10
15
0
20
40
60
80
100
Proportion of Distance Across Structure

RD−078

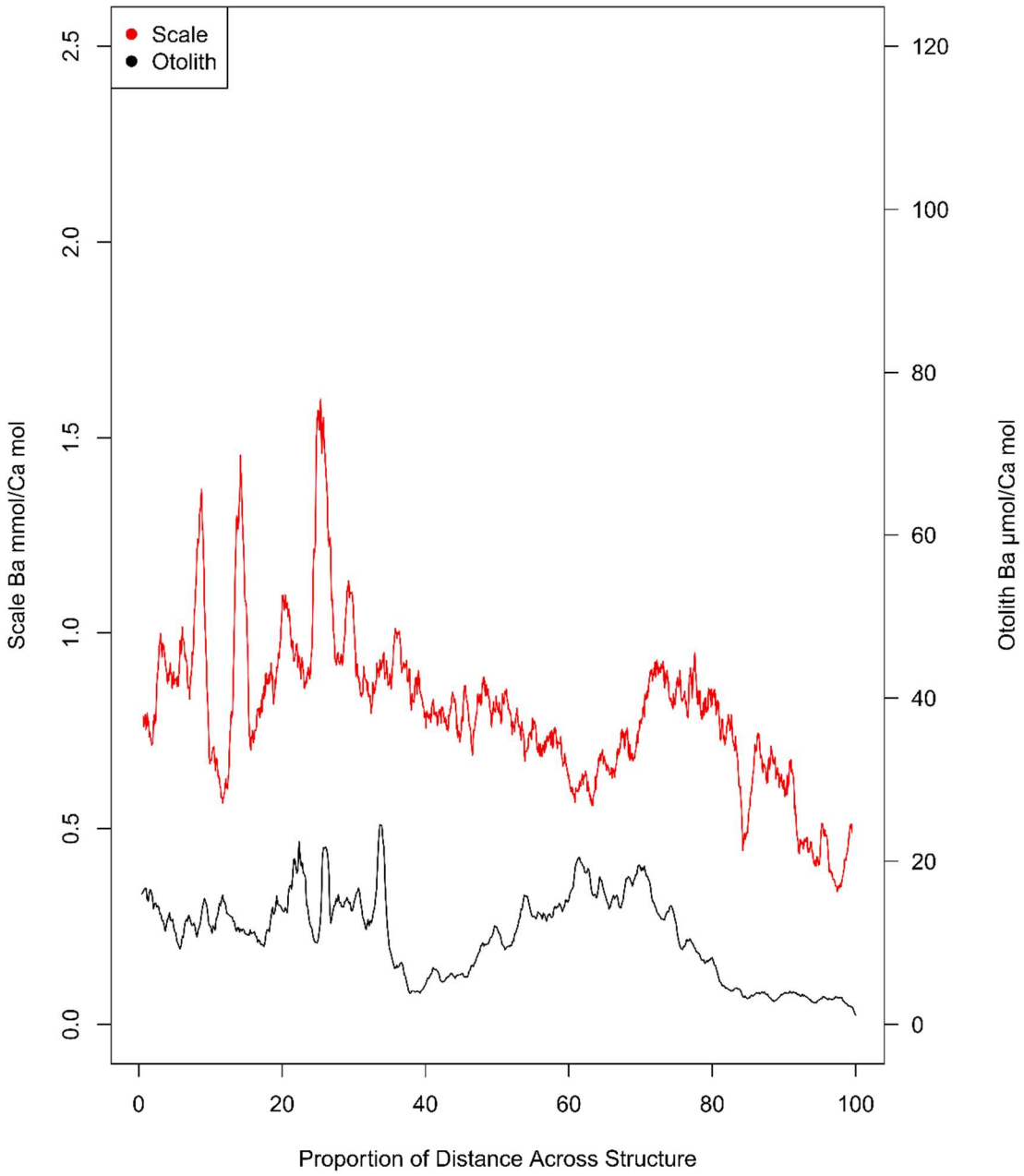
Scale
Otolith
Scale Ba mmol/Ca mol
Otolith Ba µmol/Ca mol
Proportion of Distance Across Structure
0.0
0.5
1.0
1.5
2.0
2.5
0
20
40
60
80
100
120

RD-078

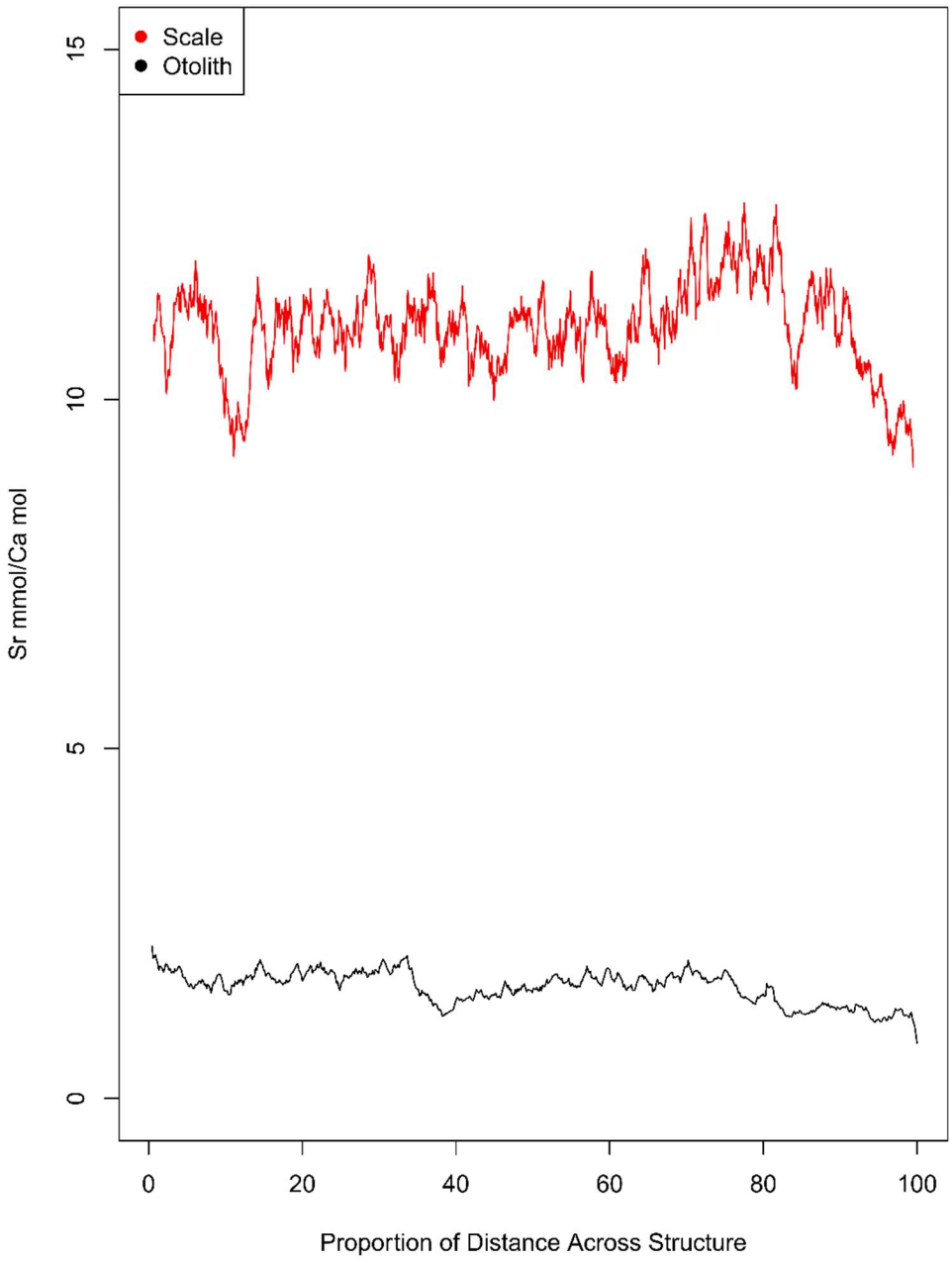
Scale
Otolith
Sr mmol/Ca mol
0
5
10
15
0
20
40
60
80
100
Proportion of Distance Across Structure

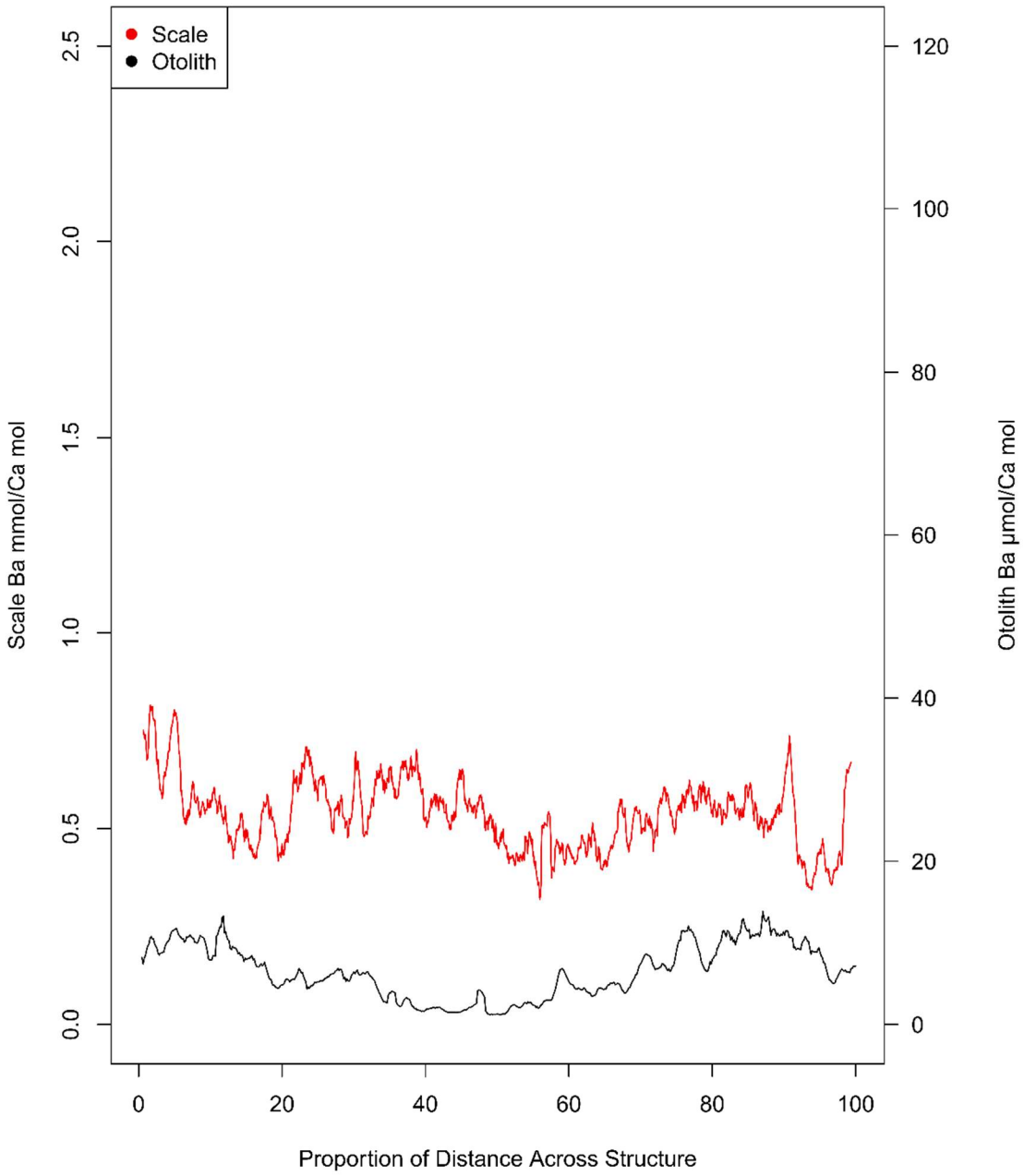
RD−079
Scale
Otolith
Scale Ba mmol/Ca mol
Otolith Ba µmol/Ca mol
Proportion of Distance Across Structure
0.0
0.5
1.0
1.5
2.0
2.5
0
20
40
60
80
100
120

RD-079

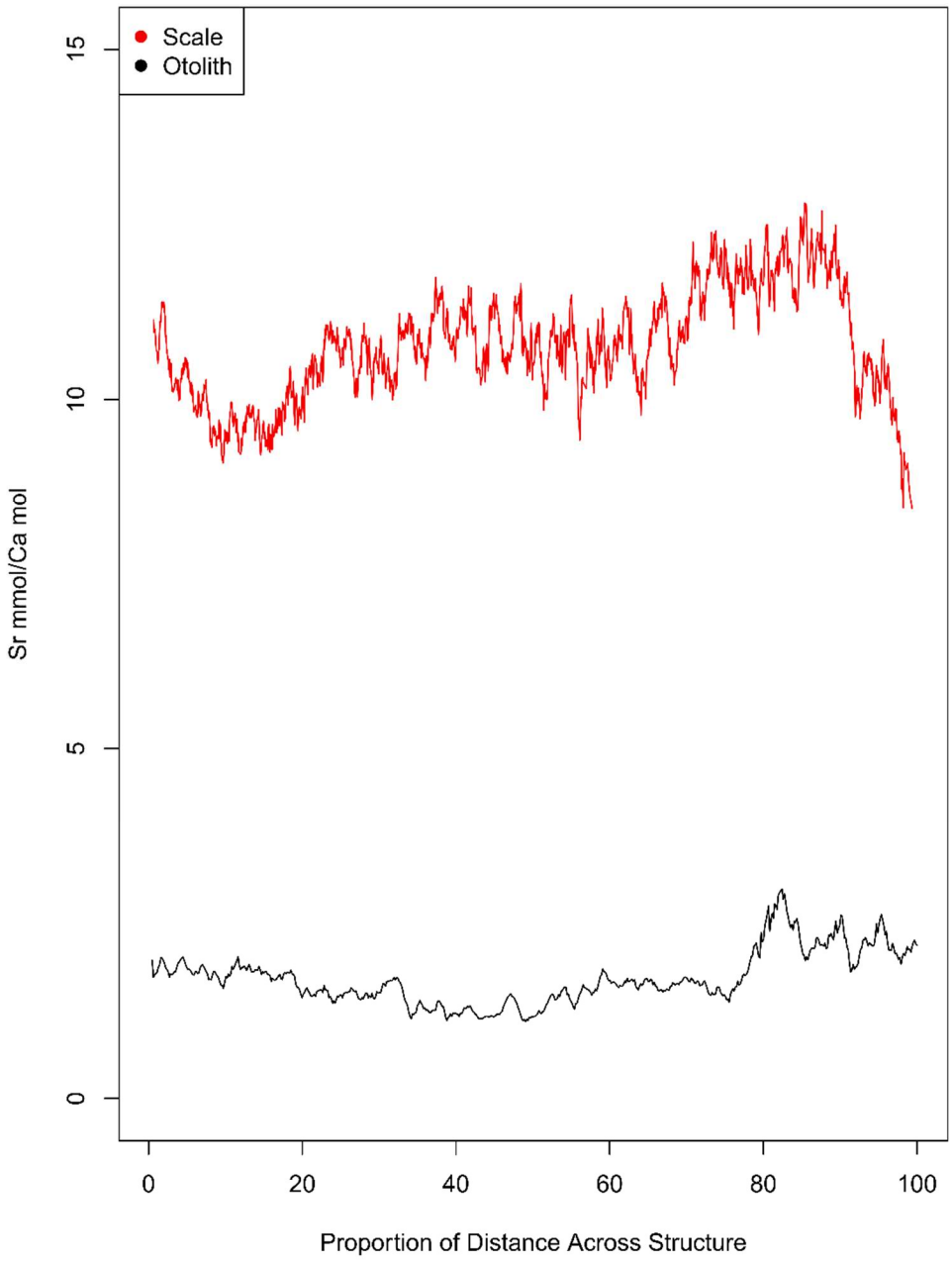
Scale
Otolith
Sr mmol/Ca mol
0
5
10
15
0
20
40
60
80
100
Proportion of Distance Across Structure

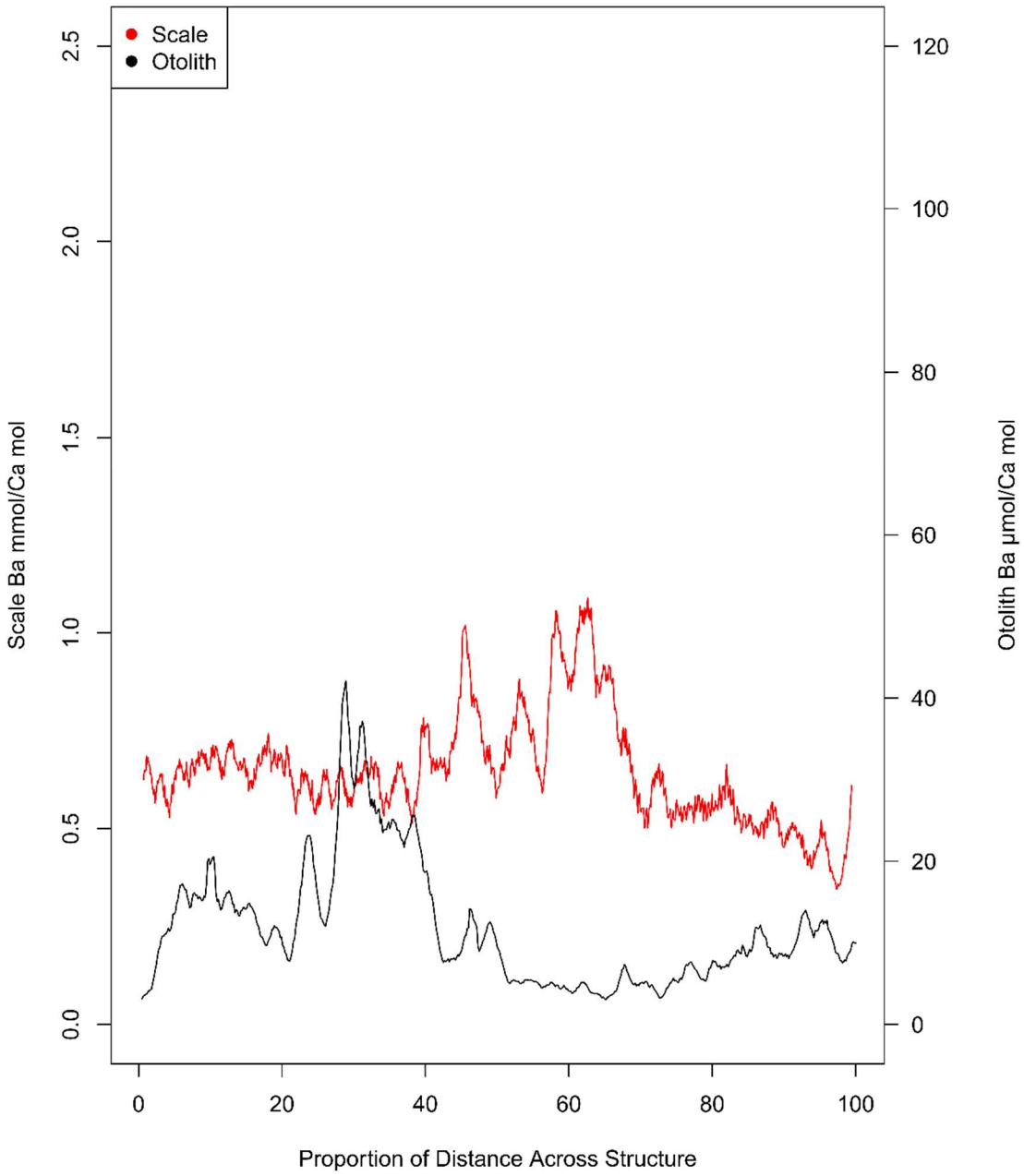
RD−080
Scale
Otolith
Scale Ba mmol/Ca mol
Otolith Ba µmol/Ca mol
Proportion of Distance Across Structure
0.0
0.5
1.0
1.5
2.0
2.5
0
20
40
60
80
100
120

RD-080

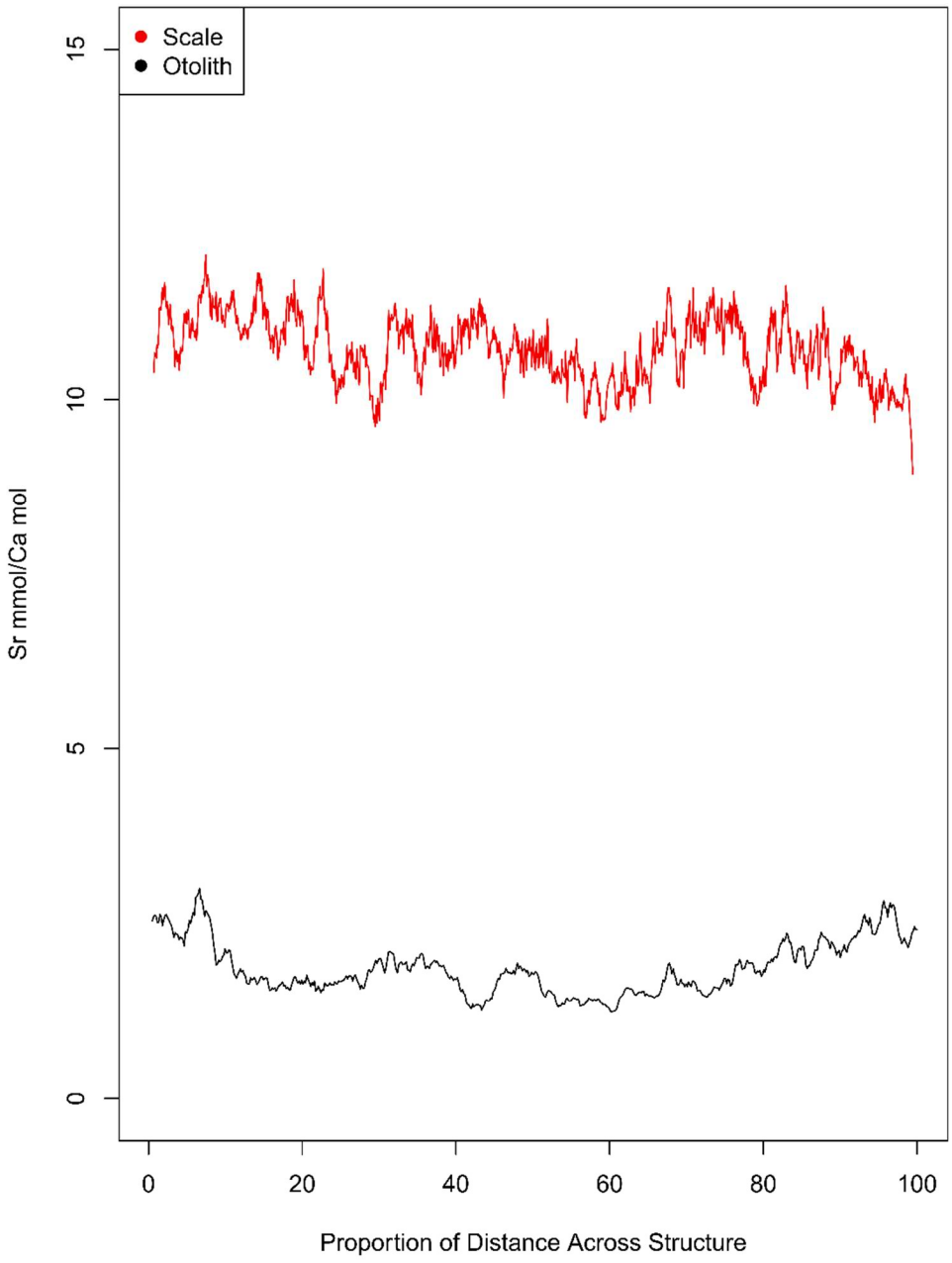
Scale
Otolith
Sr mmol/Ca mol
0
5
10
15
0
20
40
60
80
100
Proportion of Distance Across Structure

RD−081

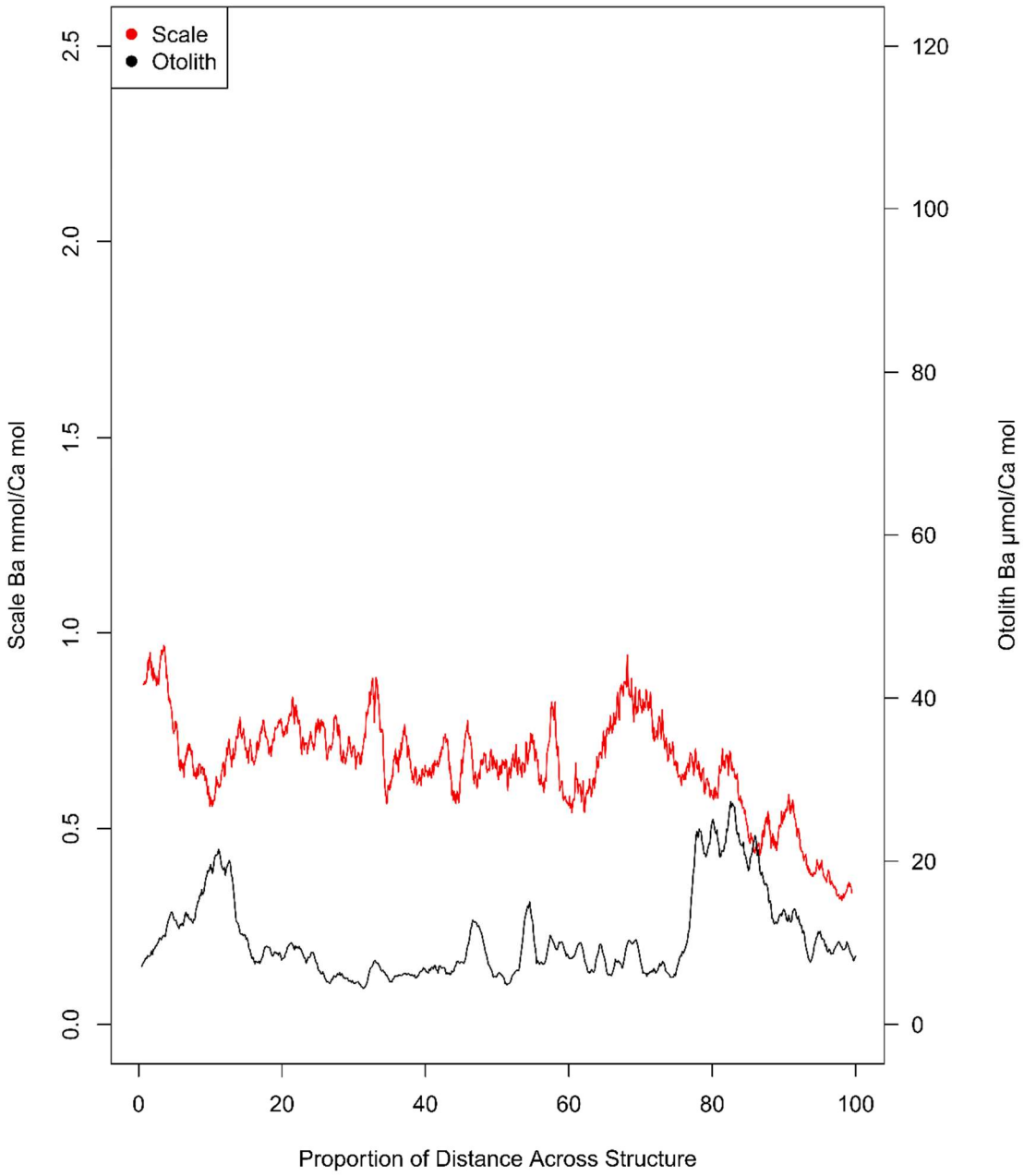
Scale
Otolith
Scale Ba mmol/Ca mol
Otolith Ba µmol/Ca mol
Proportion of Distance Across Structure
0.0
0.5
1.0
1.5
2.0
2.5
0
20
40
60
80
100
120

RD-081

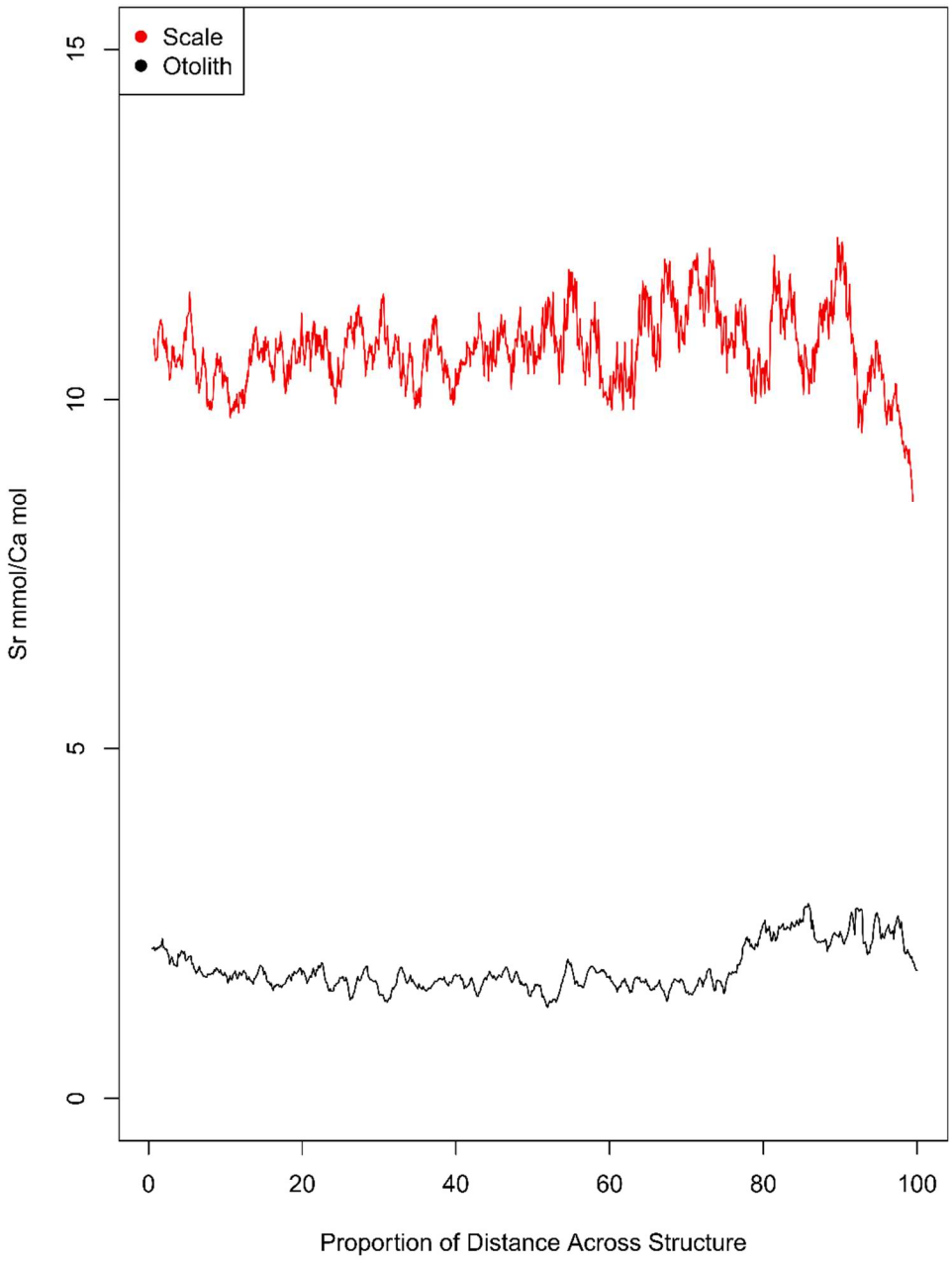
Scale
Otolith
Sr mmol/Ca mol
0
5
10
15
0
20
40
60
80
100
Proportion of Distance Across Structure

RD-082

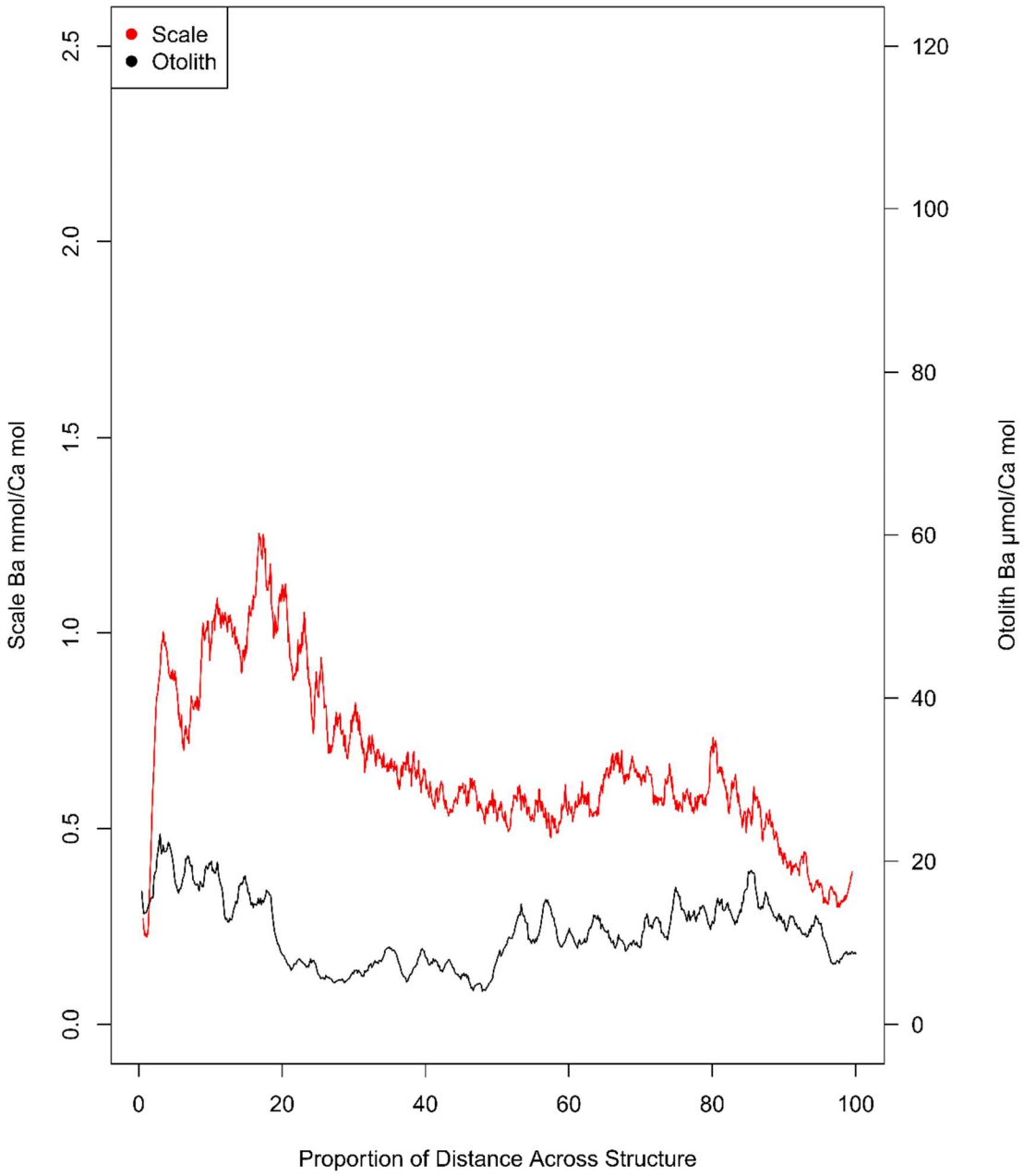
Scale
Otolith
Scale Ba mmol/Ca mol
Otolith Ba µmol/Ca mol
Proportion of Distance Across Structure
0.0
0.5
1.0
1.5
2.0
2.5
0
20
40
60
80
100
120

RD-082

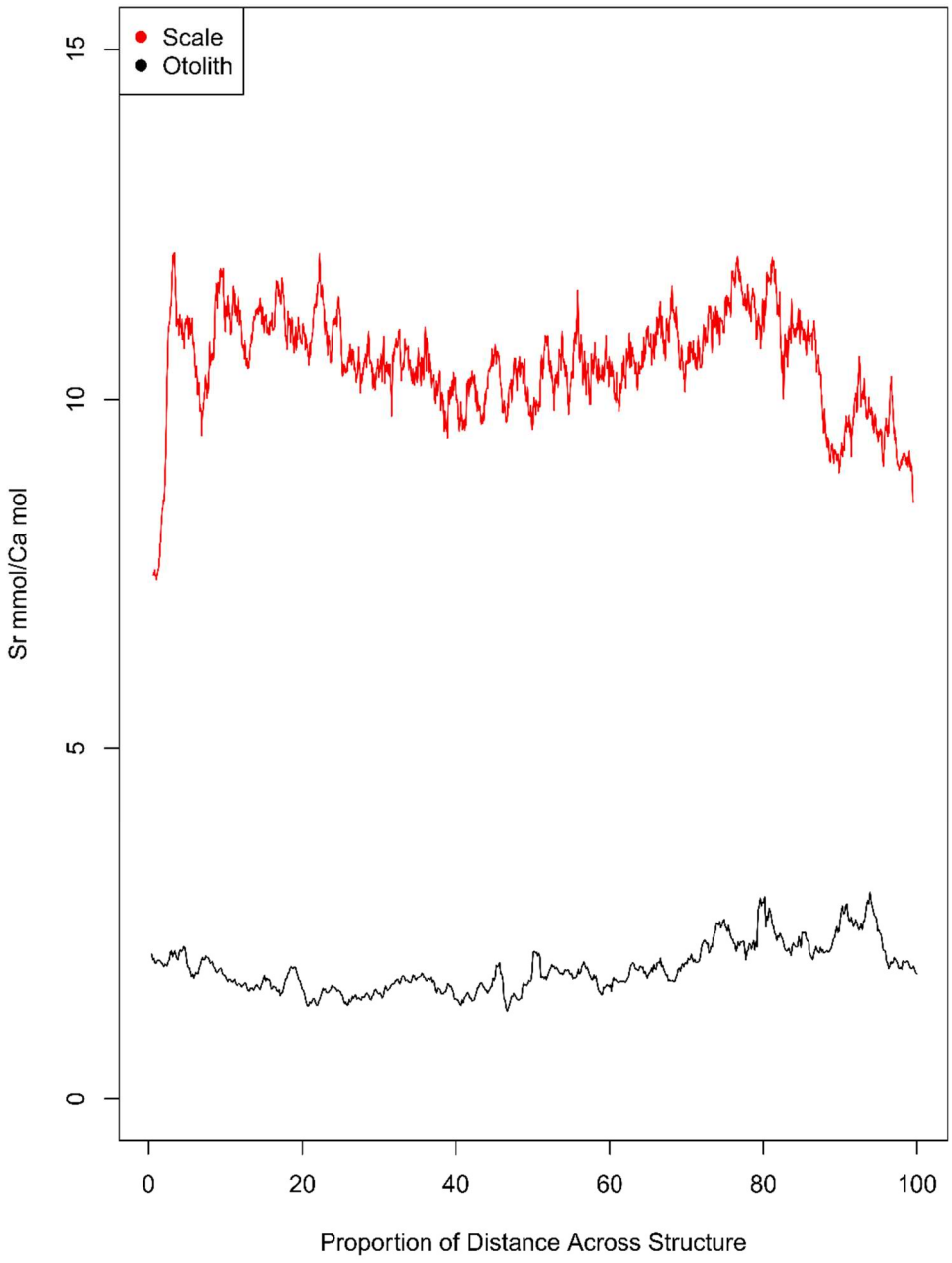
Scale
Otolith
Sr mmol/Ca mol
0
5
10
15
0
20
40
60
80
100
Proportion of Distance Across Structure

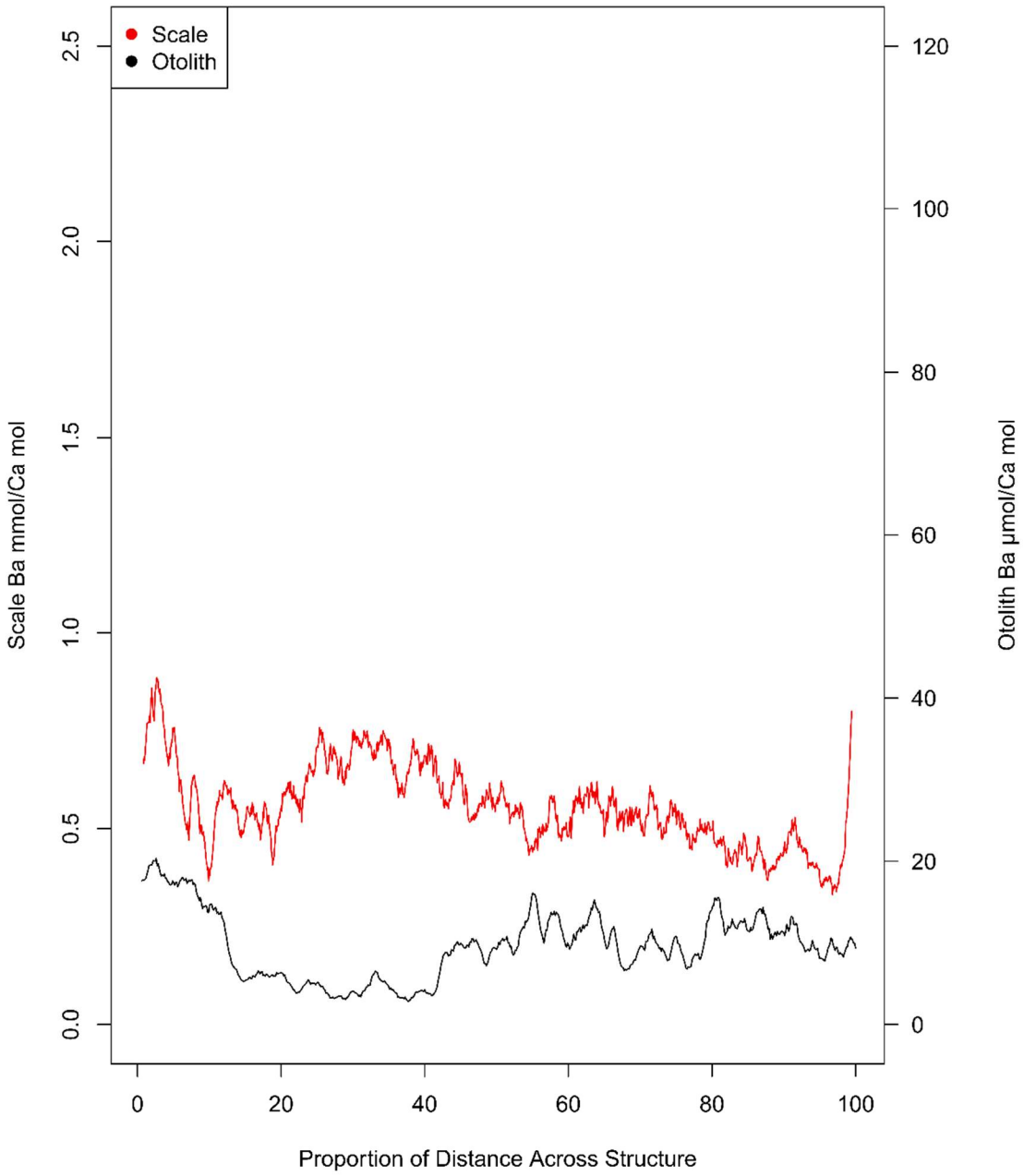
RD−083
Scale
Otolith
Scale Ba mmol/Ca mol
Otolith Ba µmol/Ca mol
Proportion of Distance Across Structure
0.0
0.5
1.0
1.5
2.0
2.5
0
20
40
60
80
100
120

RD-083

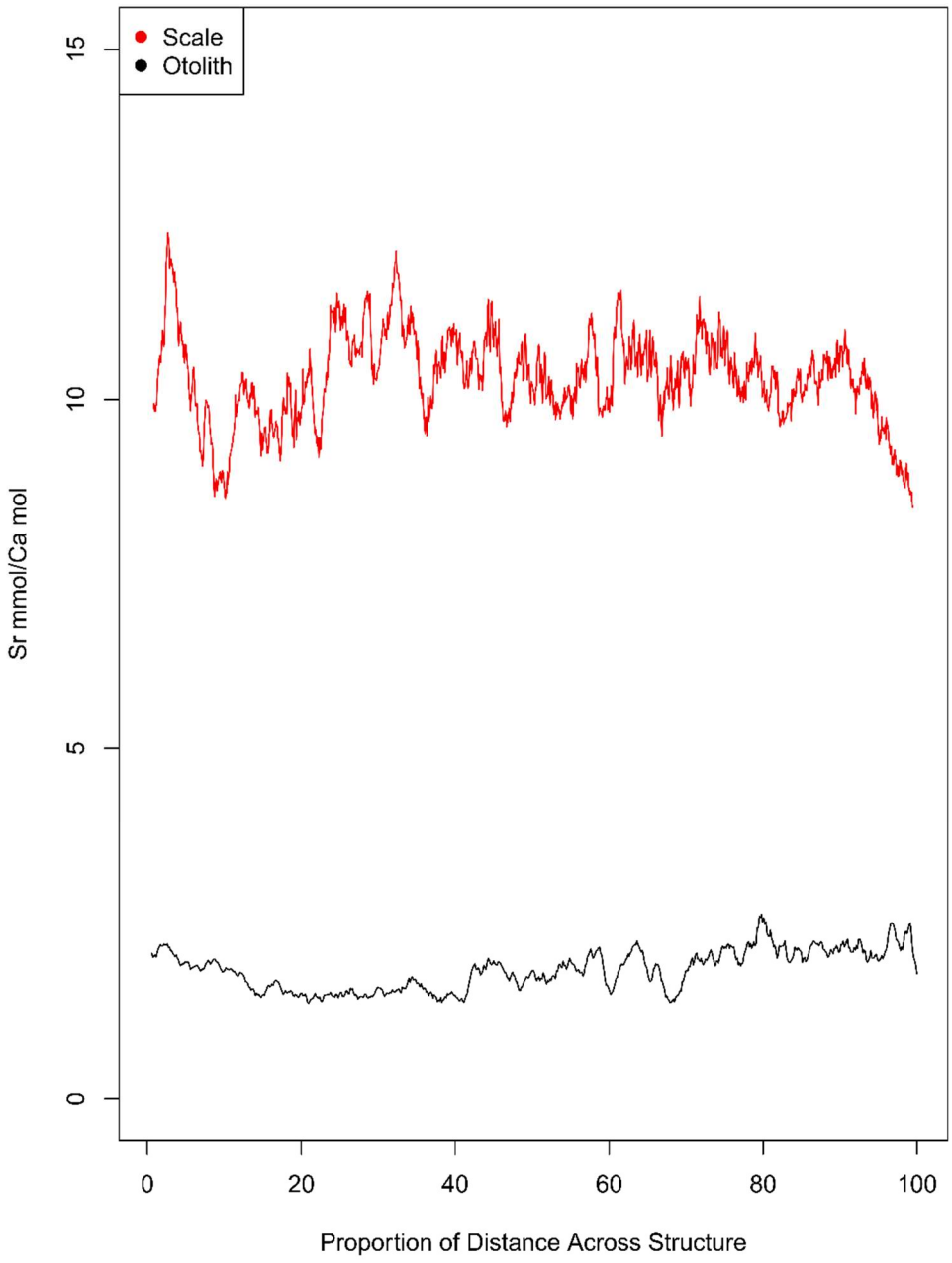
Scale
Otolith
Sr mmol/Ca mol
0
5
10
15
0
20
40
60
80
100
Proportion of Distance Across Structure

RD-084

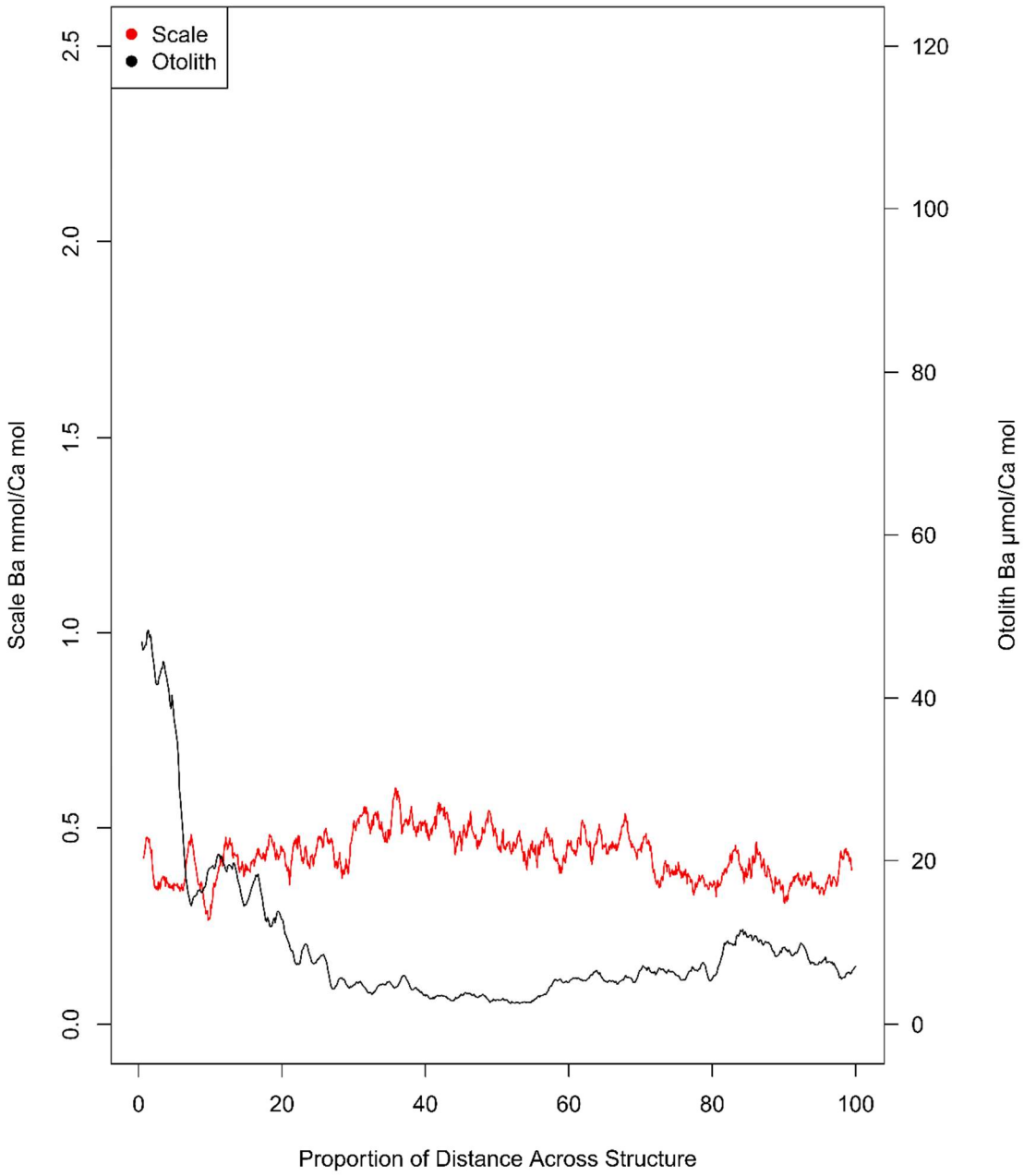
Scale
Otolith
Scale Ba mmol/Ca mol
Otolith Ba µmol/Ca mol
Proportion of Distance Across Structure
0.0
0.5
1.0
1.5
2.0
2.5
0
20
40
60
80
100
120

RD-084

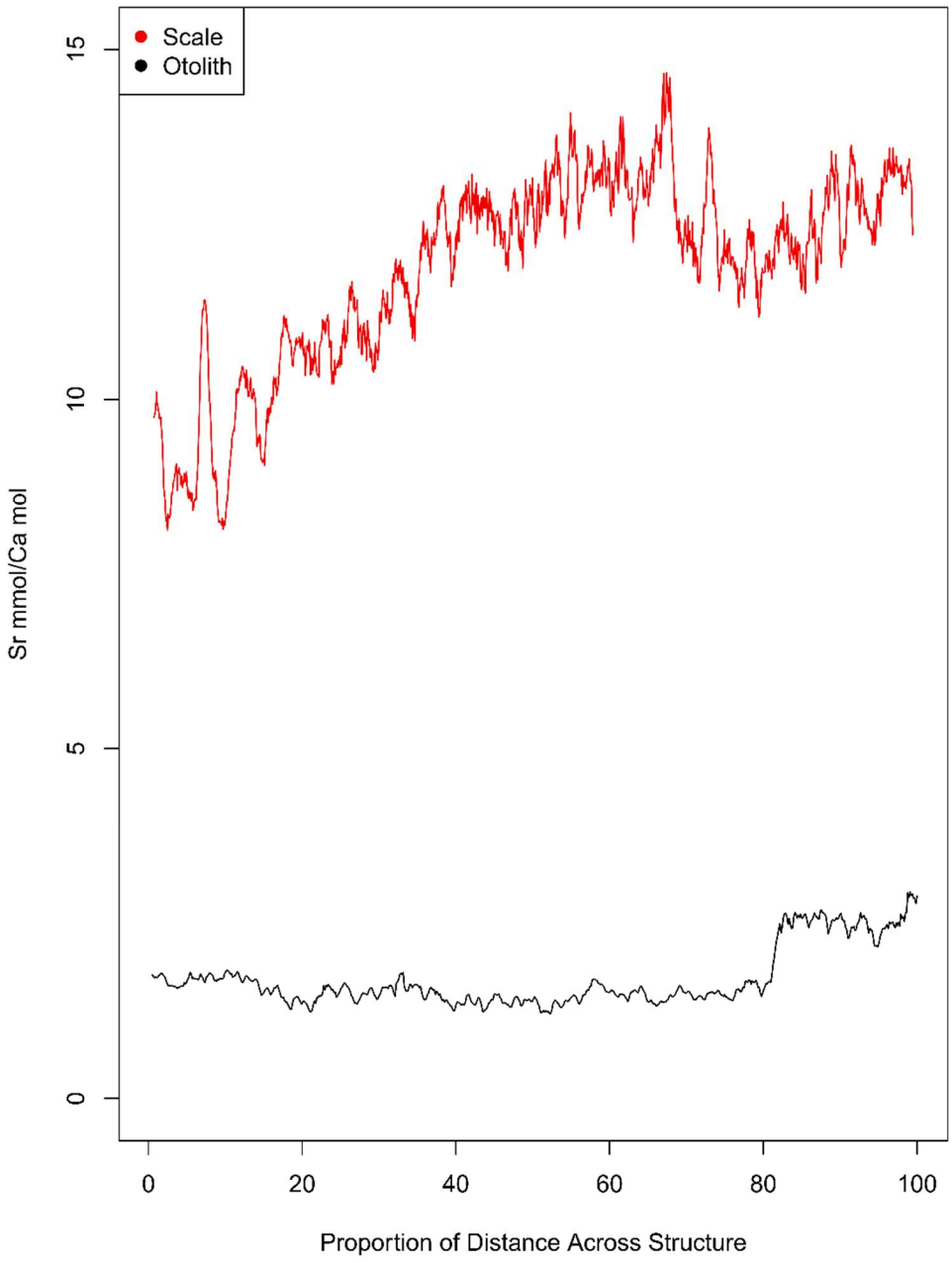
Scale
Otolith
Sr mmol/Ca mol
0
5
10
15
0
20
40
60
80
100
Proportion of Distance Across Structure

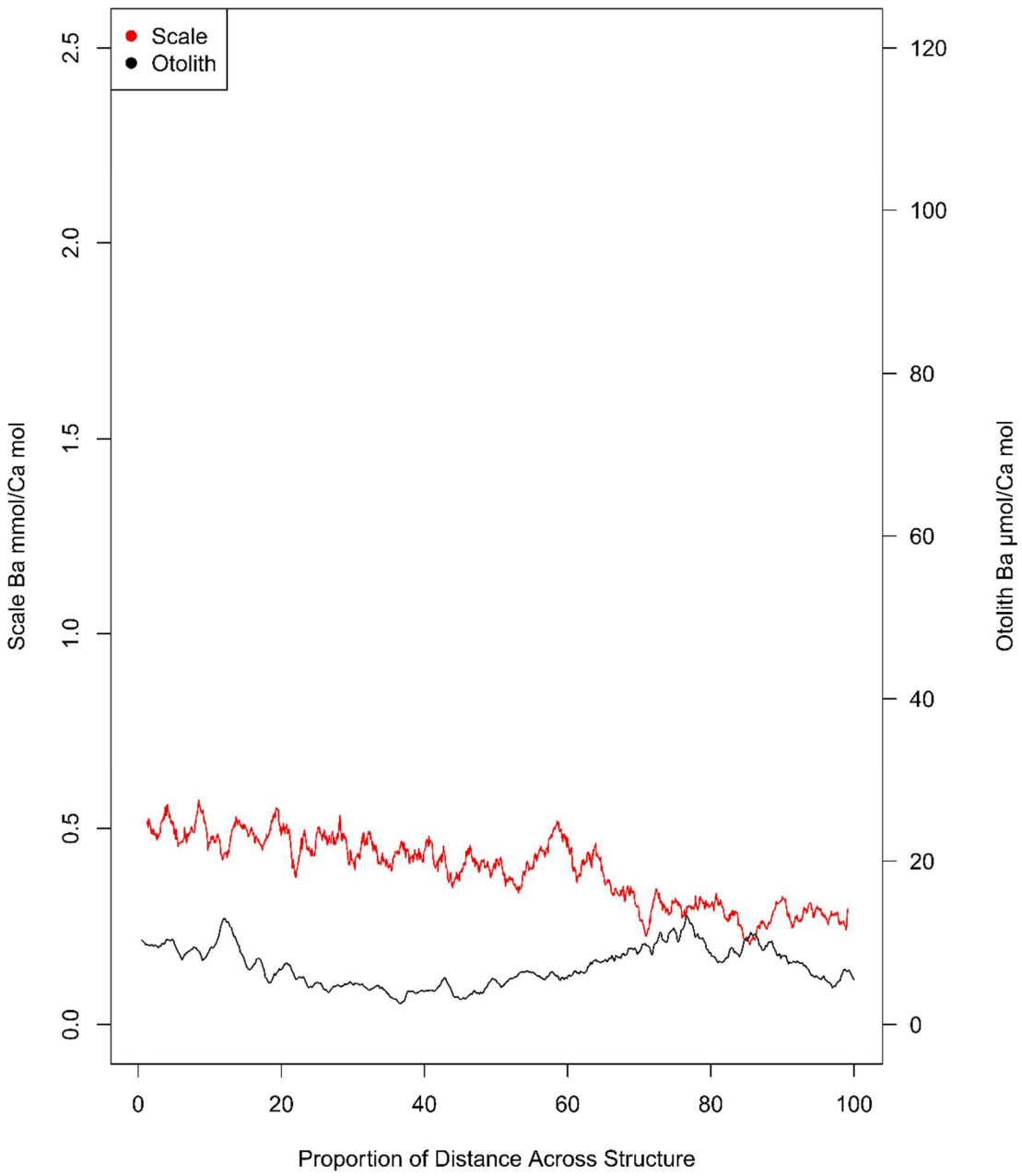
RD−085
Scale
Otolith
Scale Ba mmol/Ca mol
Otolith Ba µmol/Ca mol
Proportion of Distance Across Structure
0.0
0.5
1.0
1.5
2.0
2.5
0
20
40
60
80
100
120

RD-085

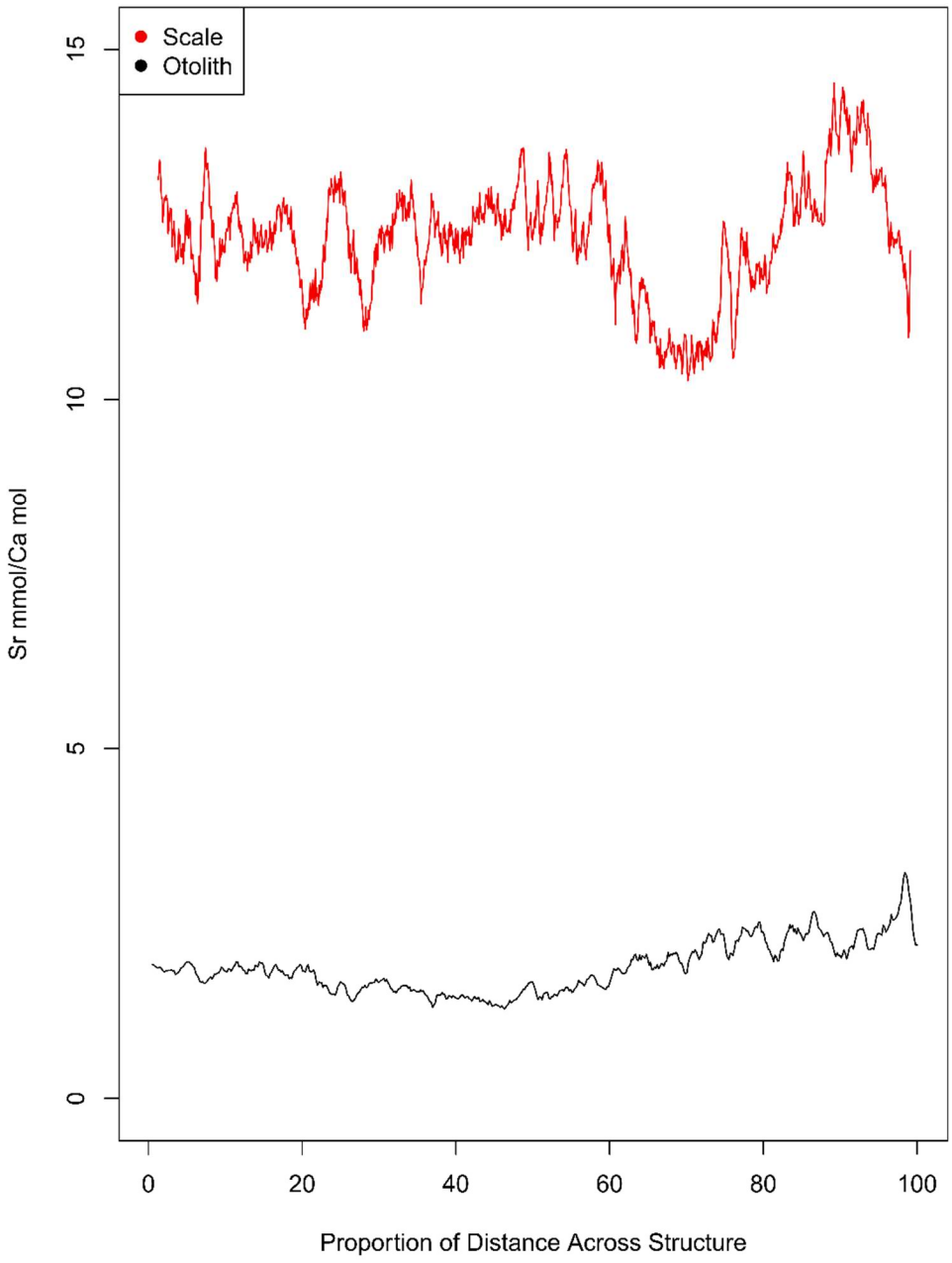
Scale
Otolith
Sr mmol/Ca mol
0
5
10
15
0
20
40
60
80
100
Proportion of Distance Across Structure

RD-086

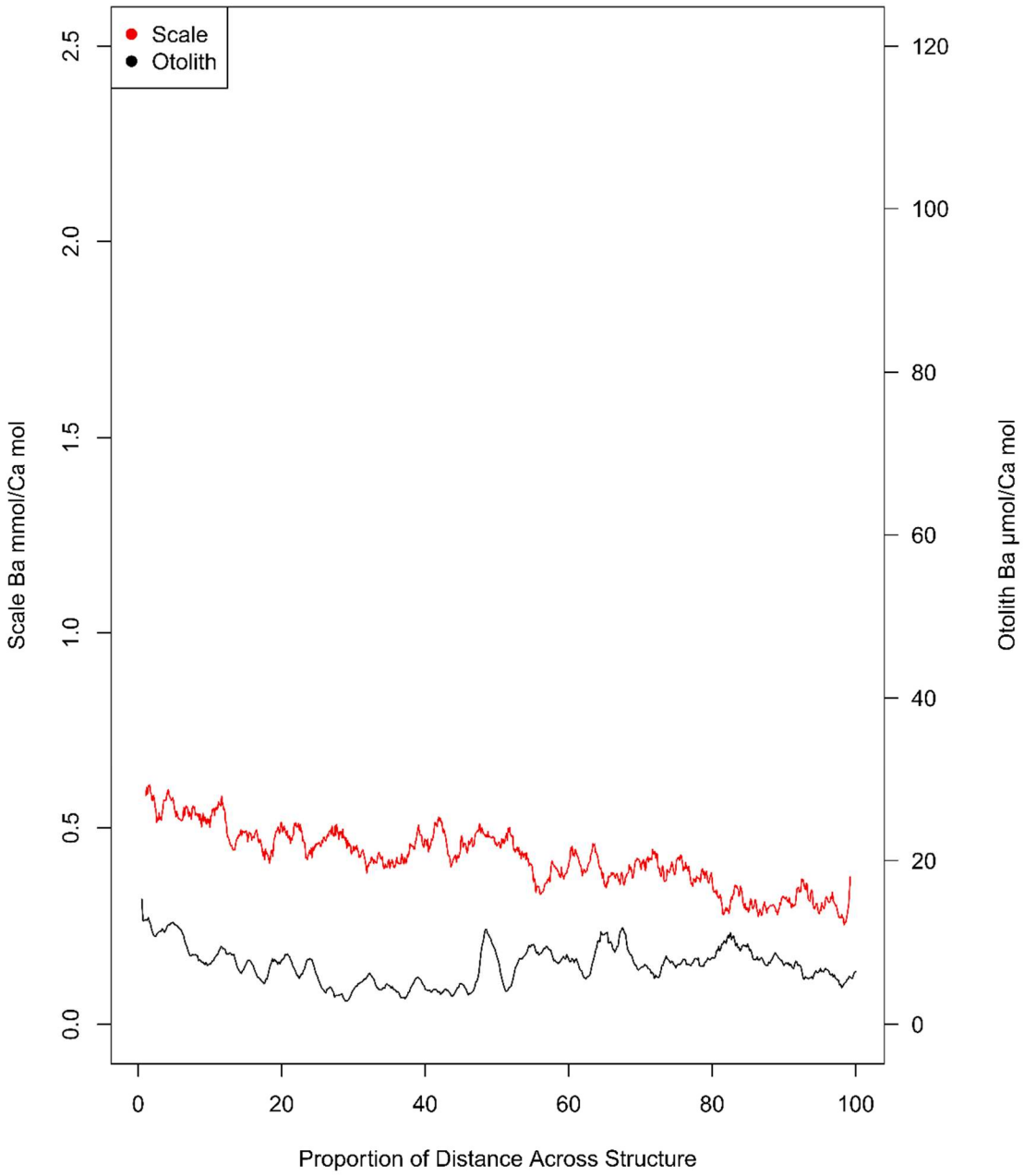
Scale
Otolith
Scale Ba mmol/Ca mol
Otolith Ba µmol/Ca mol
Proportion of Distance Across Structure
0.0
0.5
1.0
1.5
2.0
2.5
0
20
40
60
80
100
120

RD-086

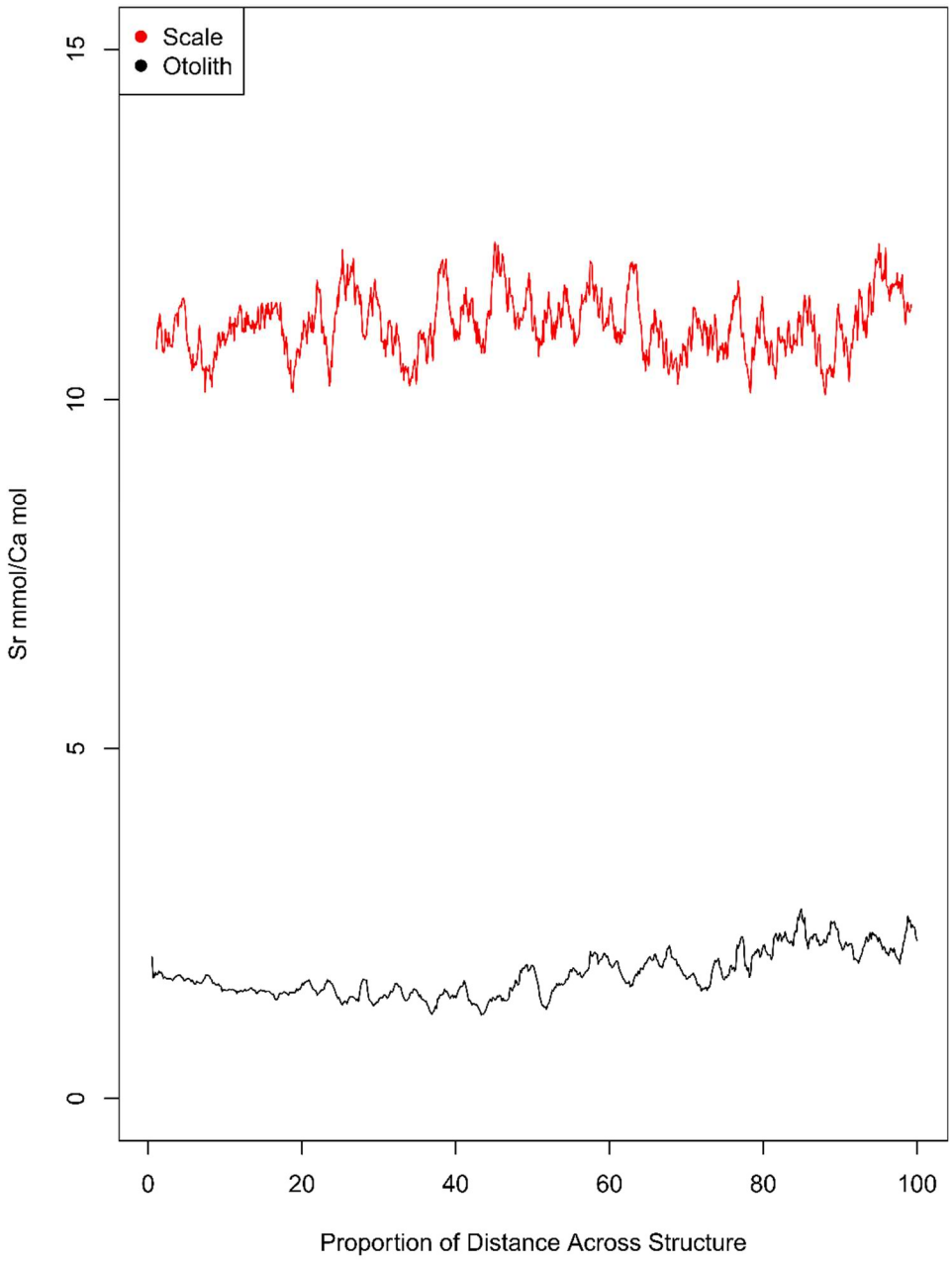
Scale
Otolith
Sr mmol/Ca mol
0
5
10
15
0
20
40
60
80
100
Proportion of Distance Across Structure

RD−087

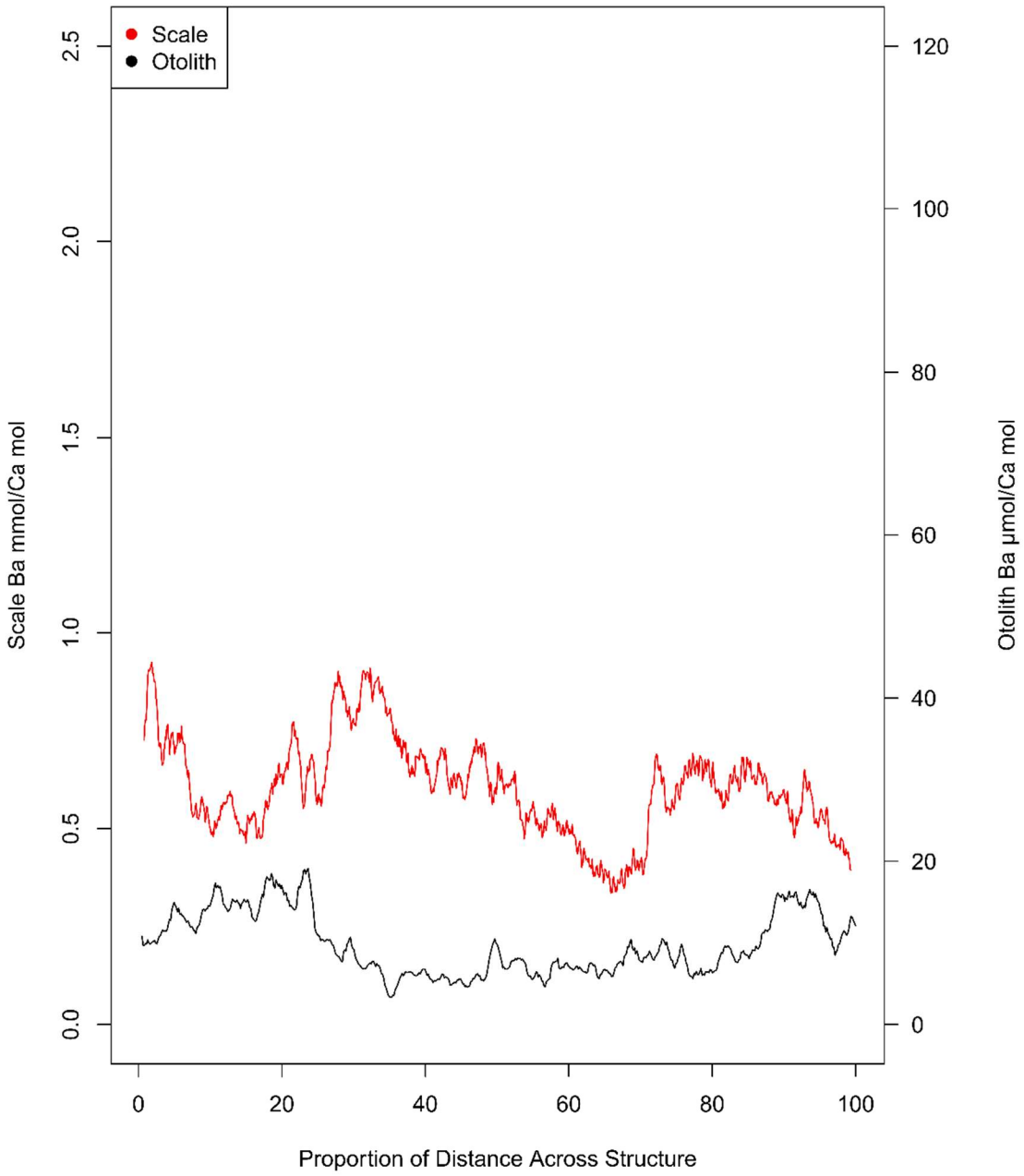
Scale
Otolith
Scale Ba mmol/Ca mol
Otolith Ba µmol/Ca mol
Proportion of Distance Across Structure
0.0
0.5
1.0
1.5
2.0
2.5
0
20
40
60
80
100
120

RD-087

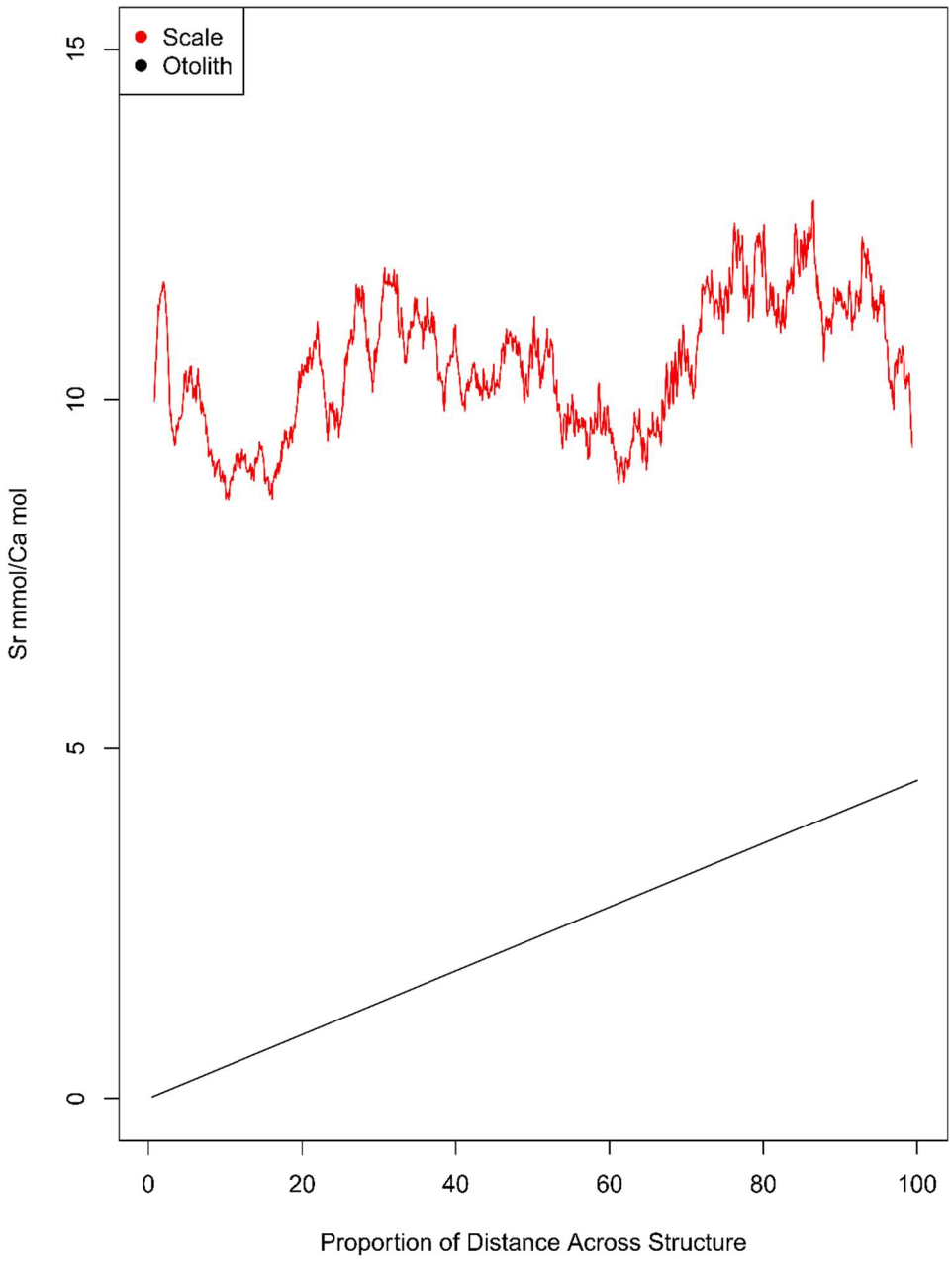
Scale
Otolith
Sr mmol/Ca mol
0
5
10
15
0
20
40
60
80
100
Proportion of Distance Across Structure

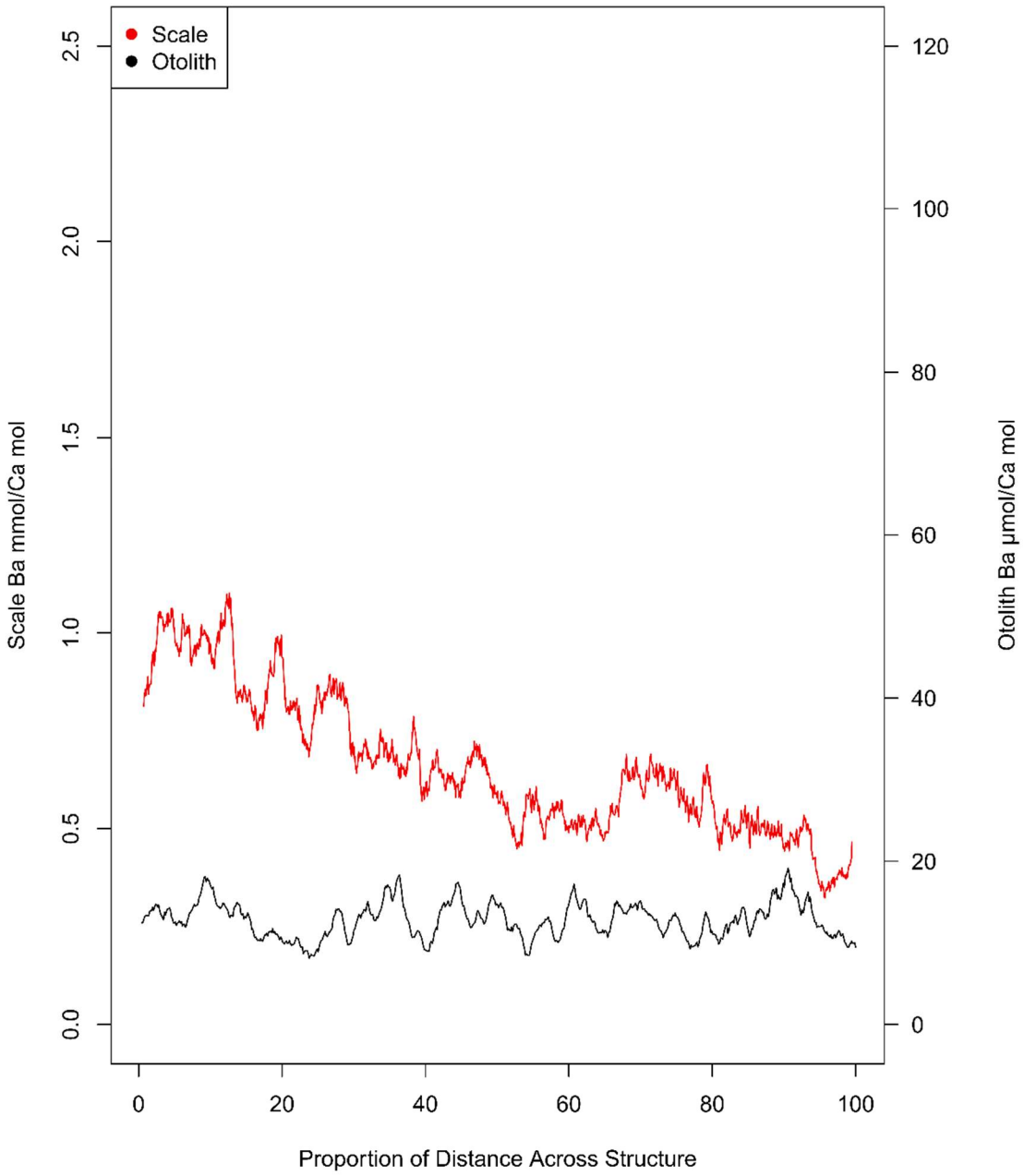
RD−088
Scale
Otolith
Scale Ba mmol/Ca mol
Otolith Ba µmol/Ca mol
Proportion of Distance Across Structure
0.0
0.5
1.0
1.5
2.0
2.5
0
20
40
60
80
100
120

RD-088

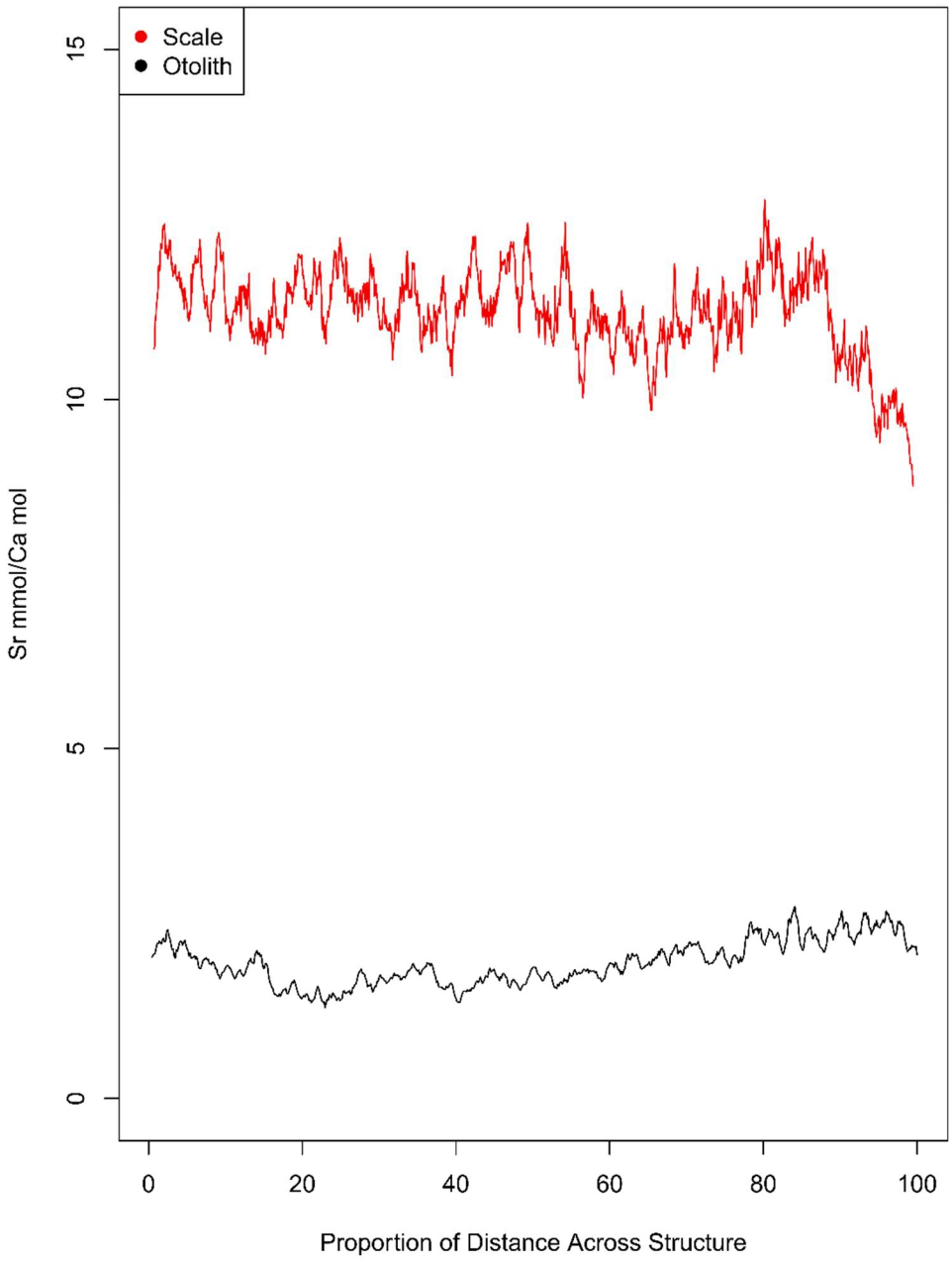
Scale
Otolith
Sr mmol/Ca mol
0
5
10
15
0
20
40
60
80
100
Proportion of Distance Across Structure

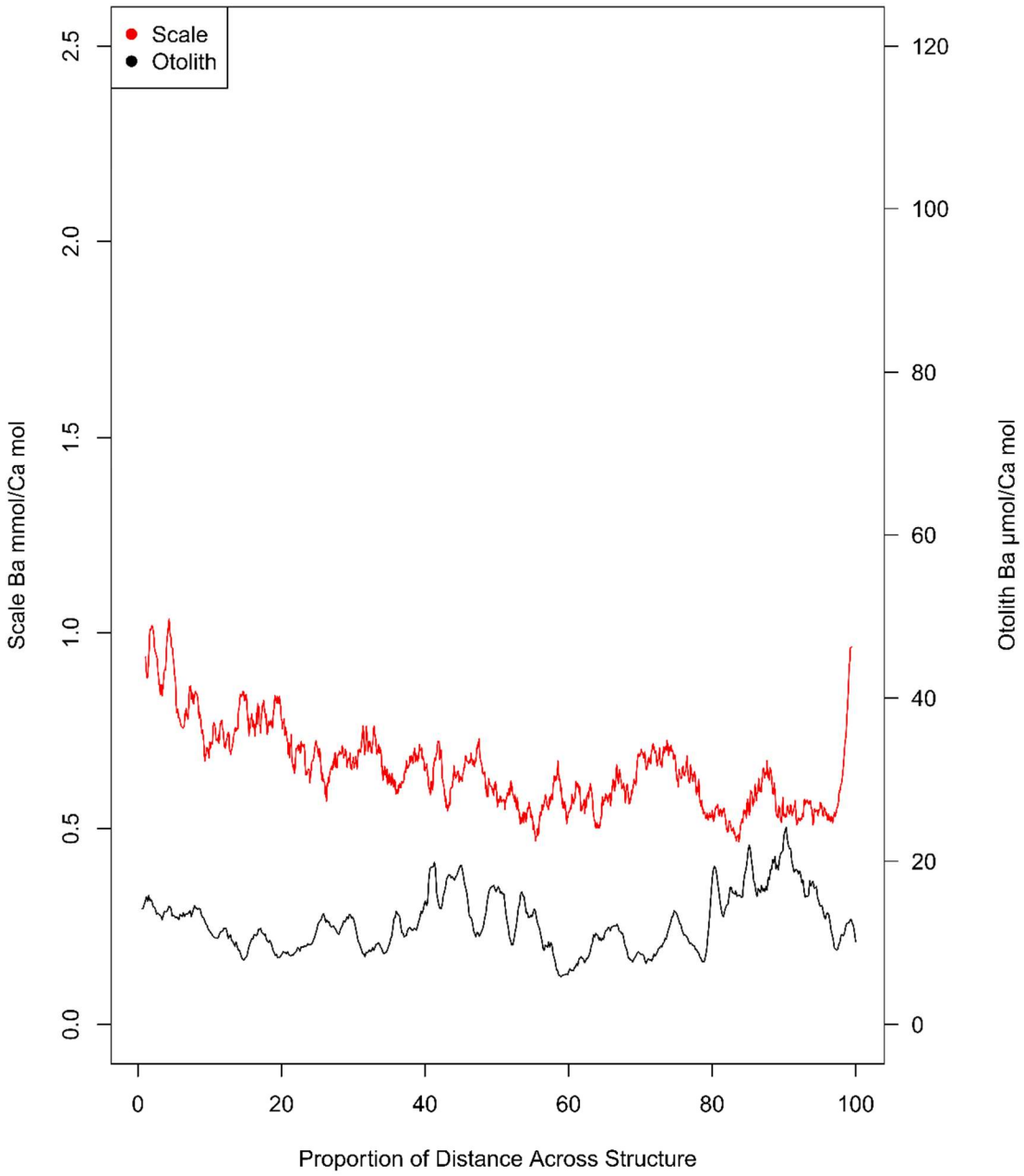
RD−089
Scale
Otolith
Scale Ba mmol/Ca mol
Otolith Ba µmol/Ca mol
Proportion of Distance Across Structure
0.0
0.5
1.0
1.5
2.0
2.5
0
20
40
60
80
100
120

RD-089

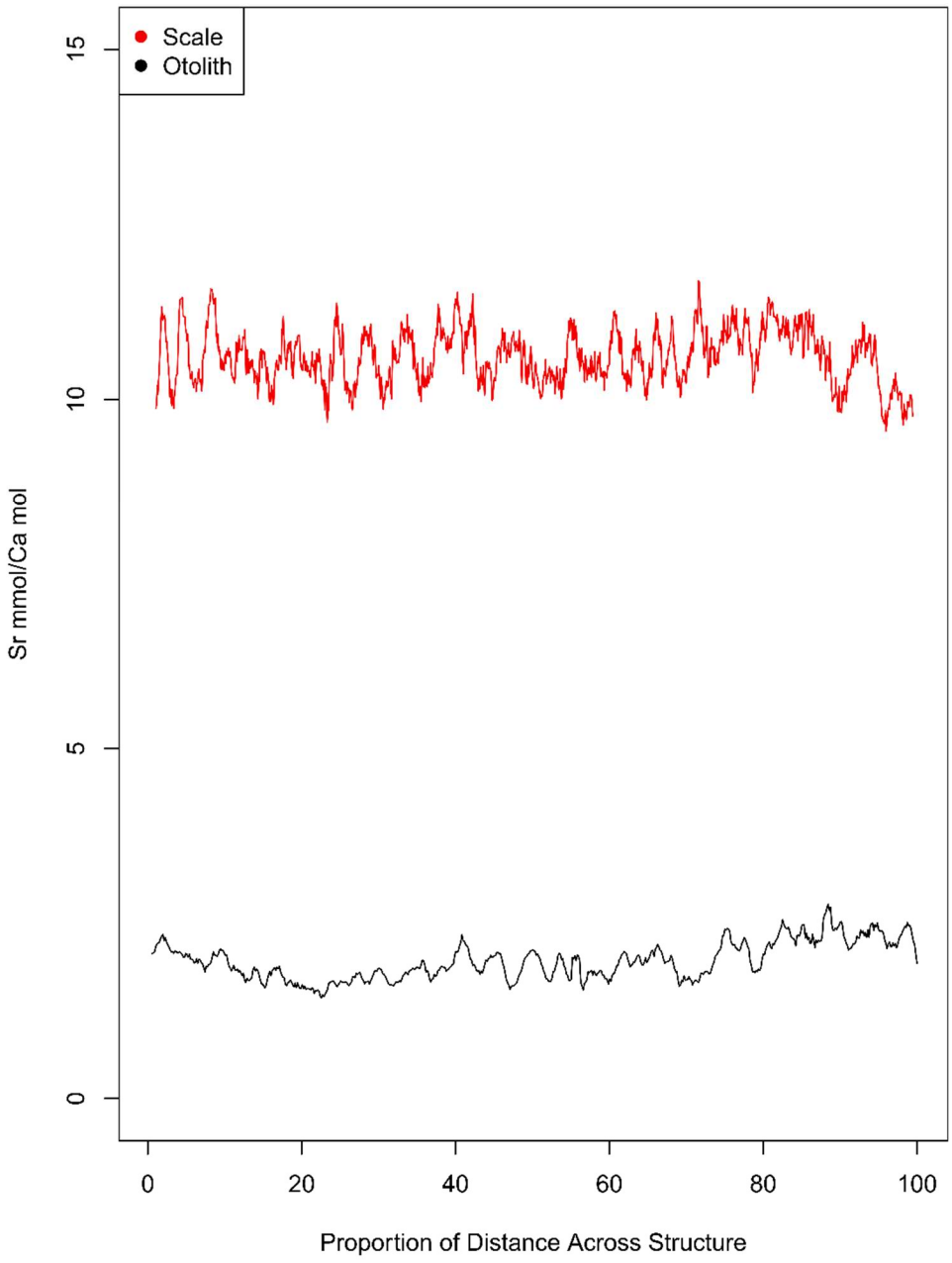
Scale
Otolith
15
10
5
0
Sr mmol/Ca mol
0
20
40
60
80
100
Proportion of Distance Across Structure

RD−090

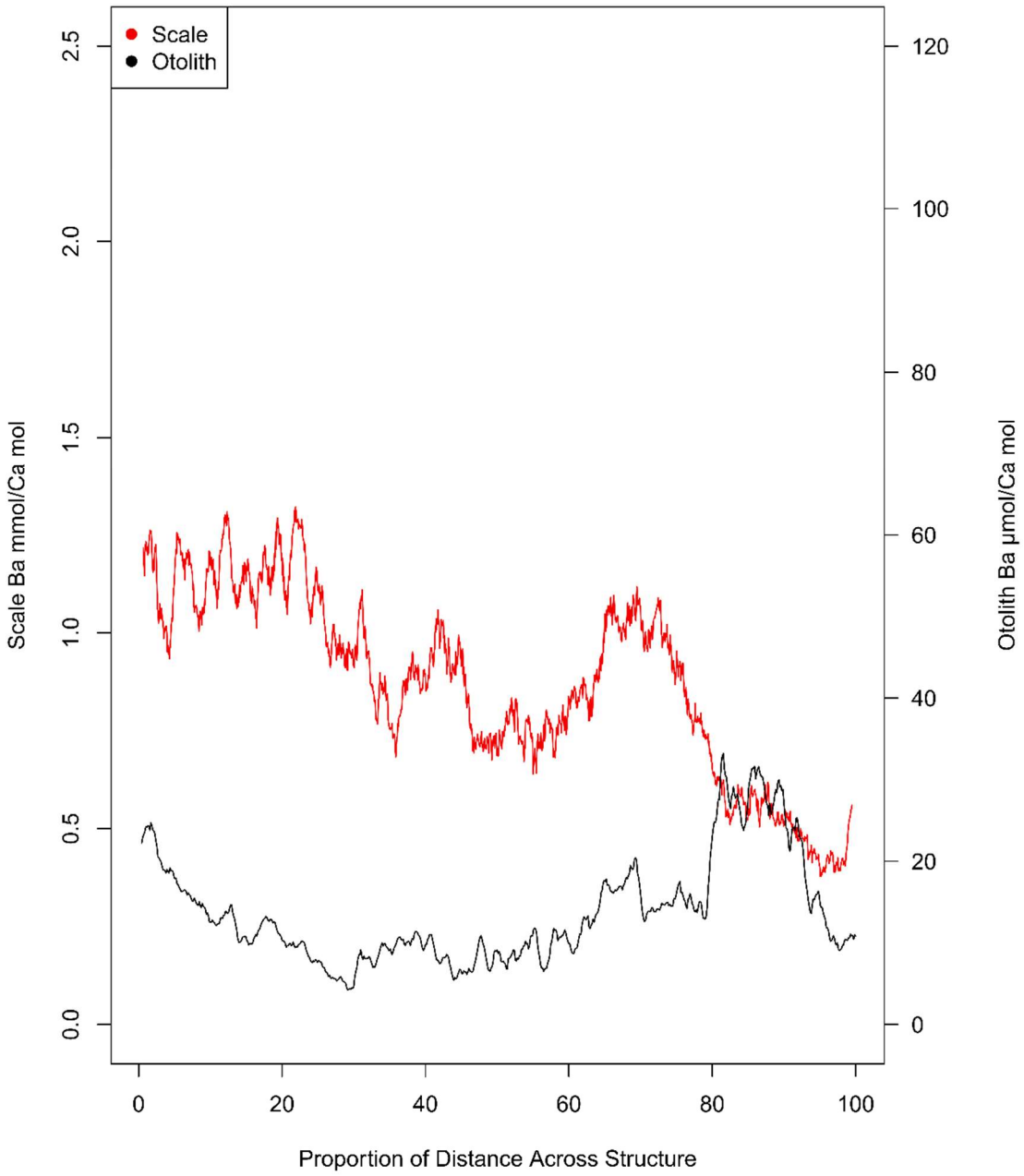
Scale
Otolith
Scale Ba mmol/Ca mol
Otolith Ba µmol/Ca mol
Proportion of Distance Across Structure
0.0
0.5
1.0
1.5
2.0
2.5
0
20
40
60
80
100
120

RD−090

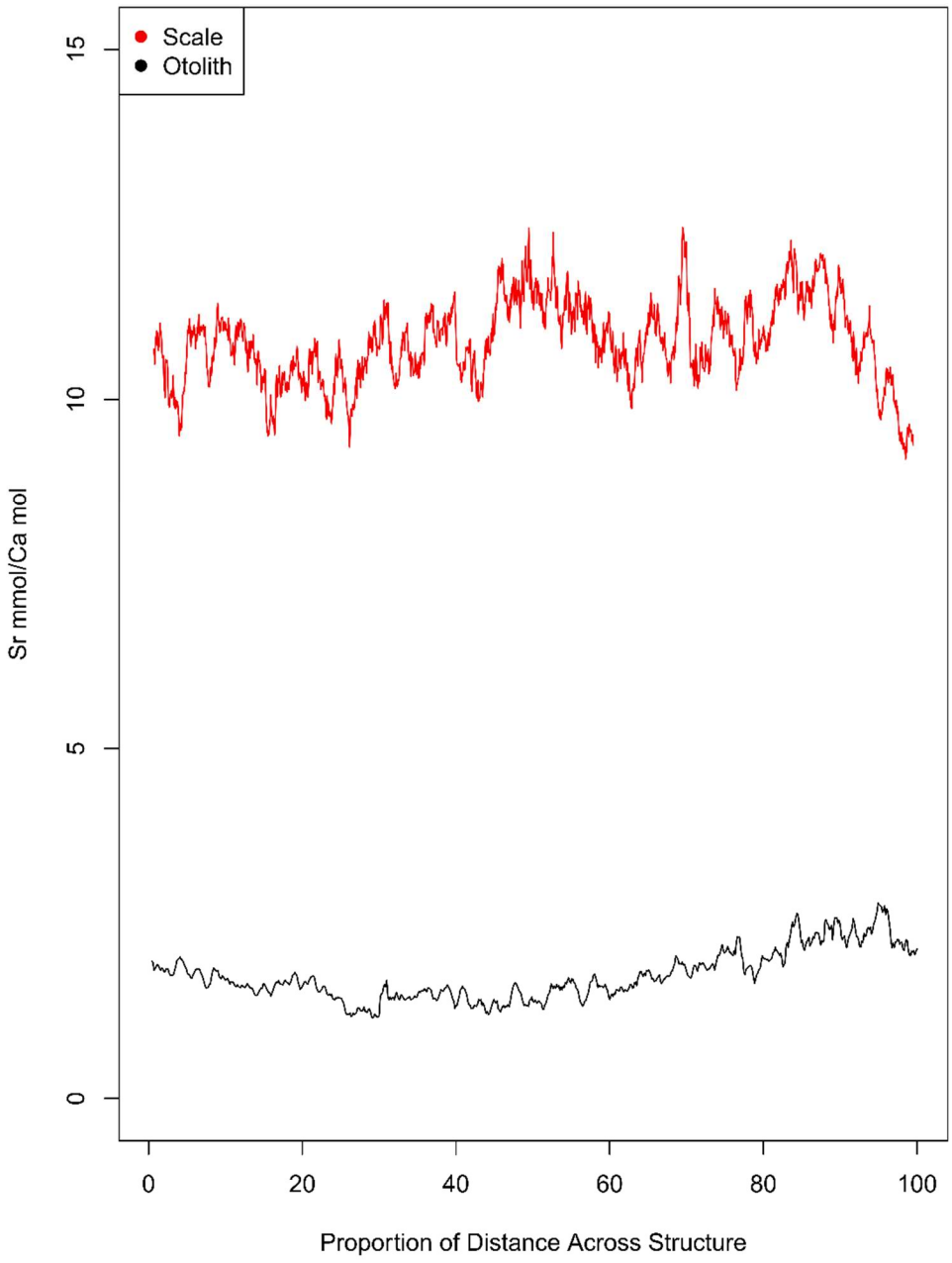
Scale
Otolith
Sr mmol/Ca mol
0
5
10
15
0
20
40
60
80
100
Proportion of Distance Across Structure

RD−091

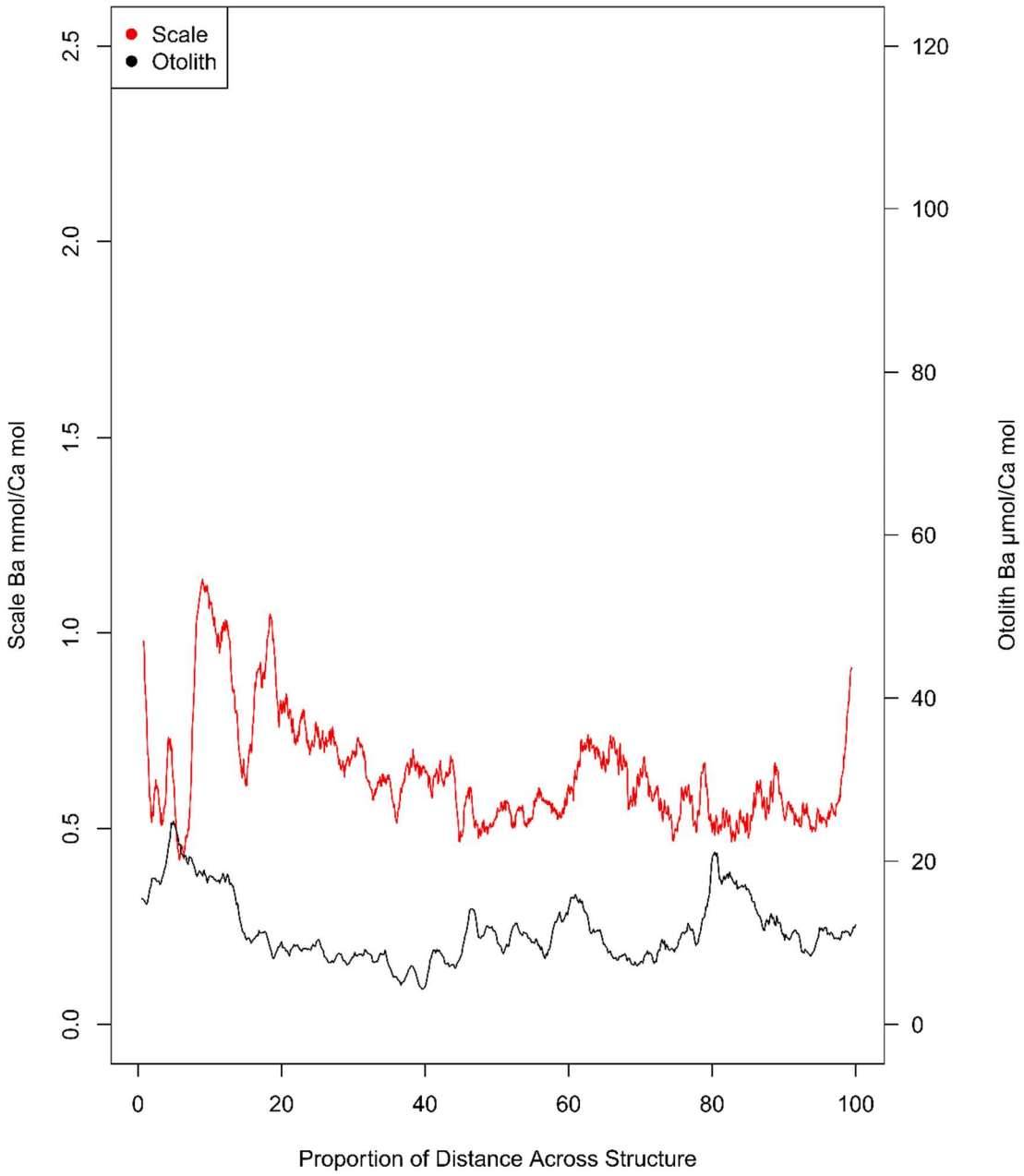
Scale
Otolith
Scale Ba mmol/Ca mol
Otolith Ba µmol/Ca mol
Proportion of Distance Across Structure
0.0
0.5
1.0
1.5
2.0
2.5
0
20
40
60
80
100
120

RD−091

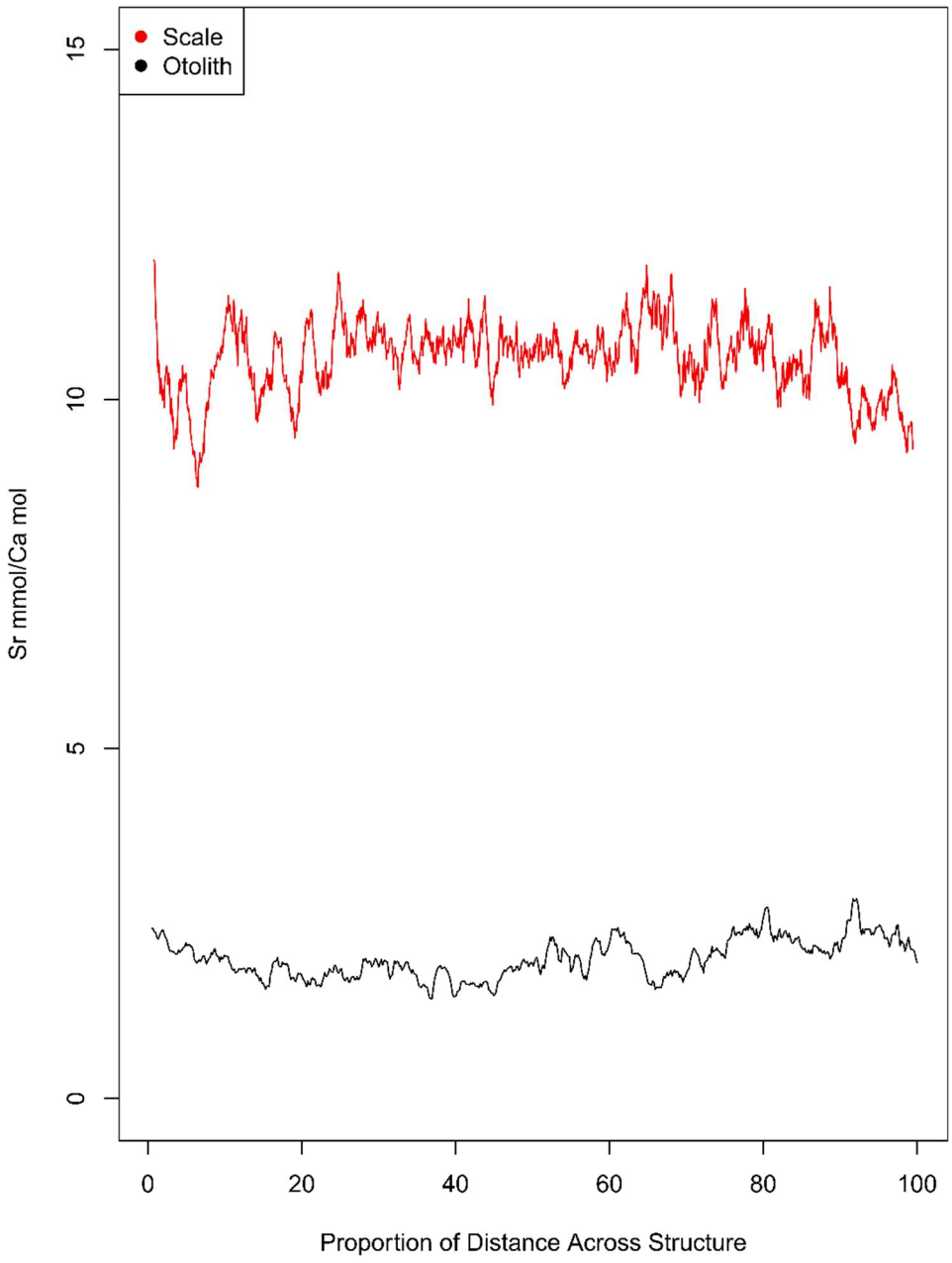
Scale
Otolith
Sr mmol/Ca mol
0
5
10
15
0
20
40
60
80
100
Proportion of Distance Across Structure

RD−092

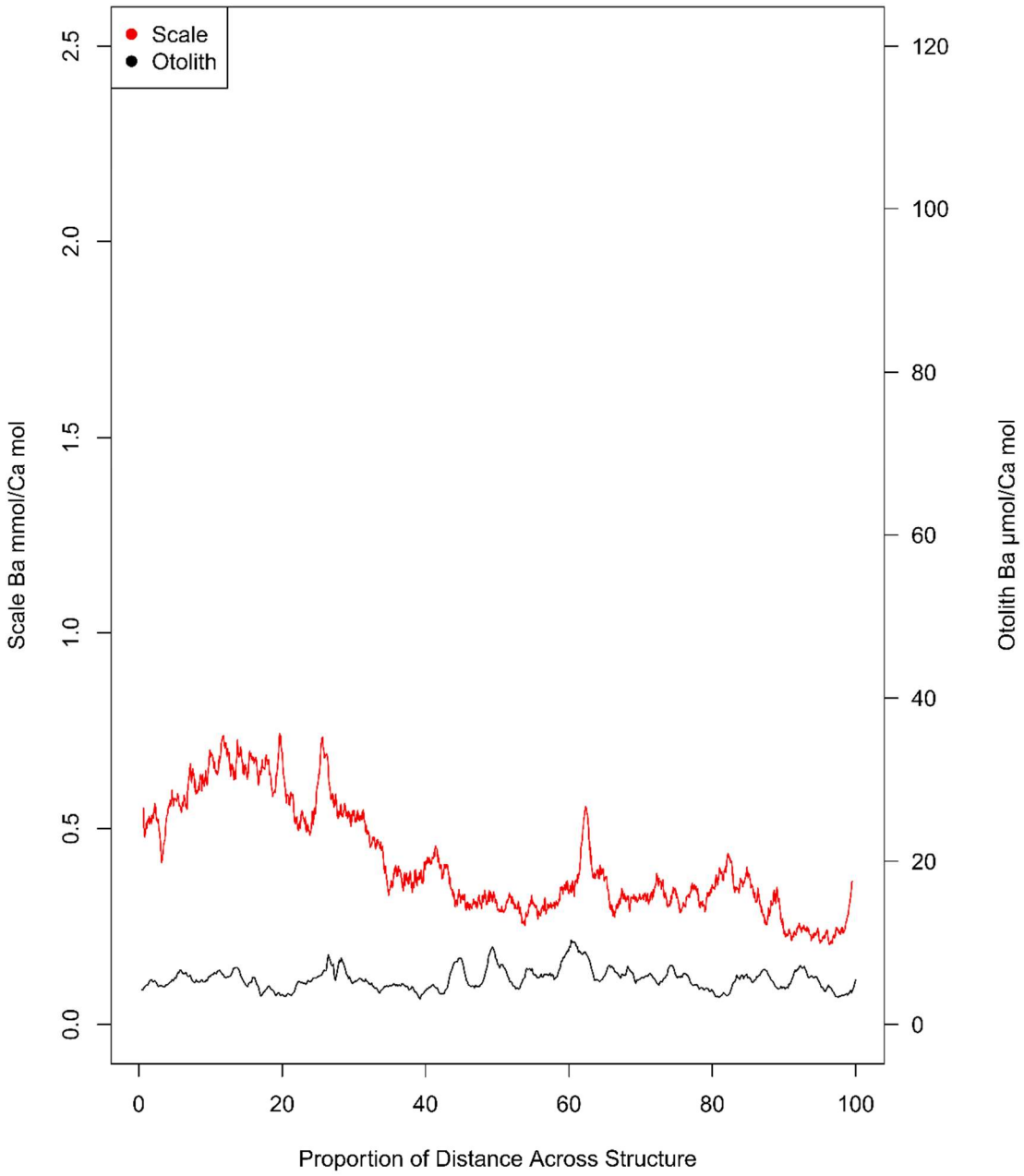
Scale
Otolith
Scale Ba mmol/Ca mol
Otolith Ba µmol/Ca mol
0.0
0.5
1.0
1.5
2.0
2.5
0
20
40
60
80
100
120
0
20
40
60
80
100
Proportion of Distance Across Structure

RD-092

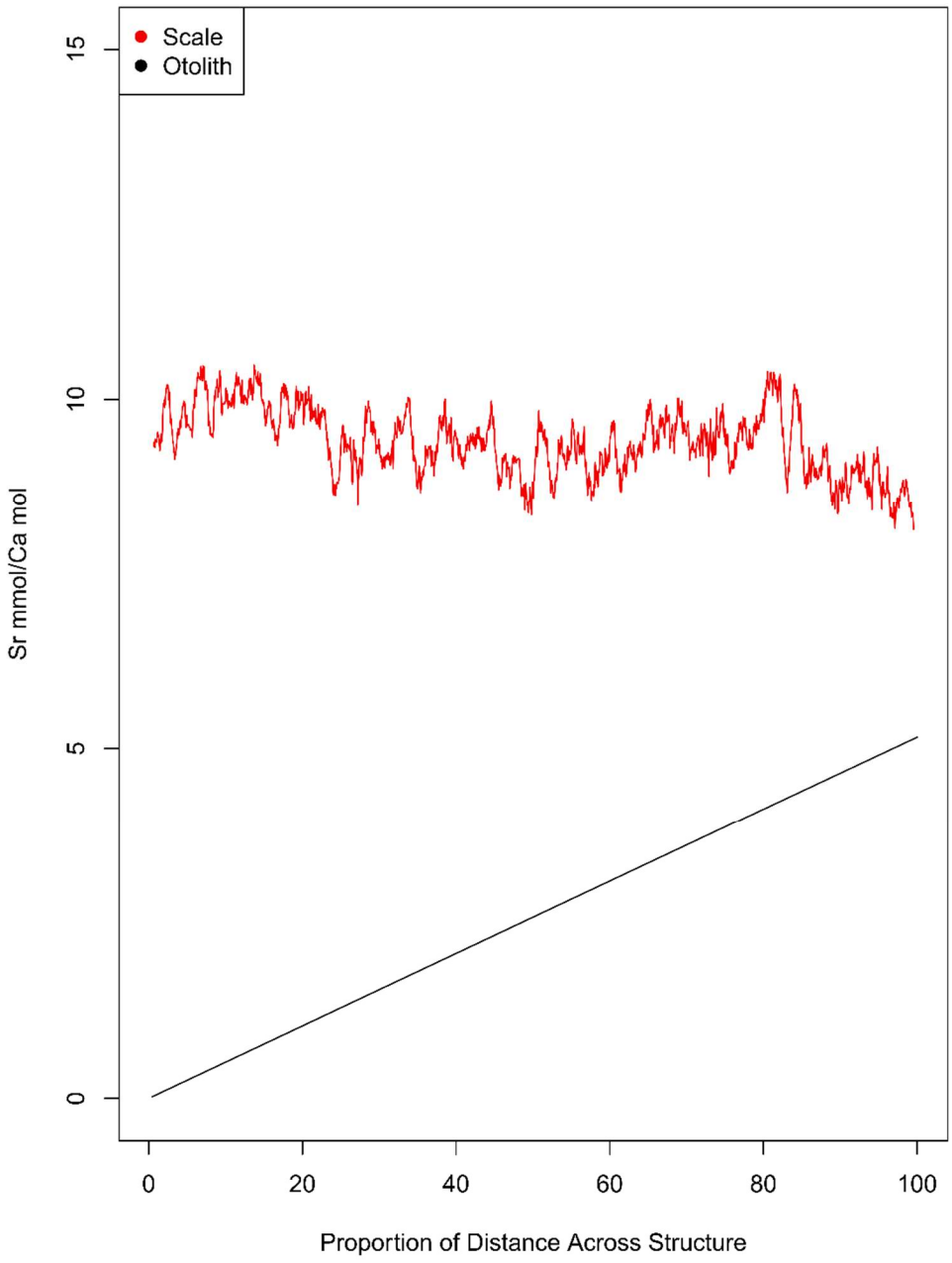
Scale
Otolith
Sr mmol/Ca mol
0
5
10
15
0
20
40
60
80
100
Proportion of Distance Across Structure

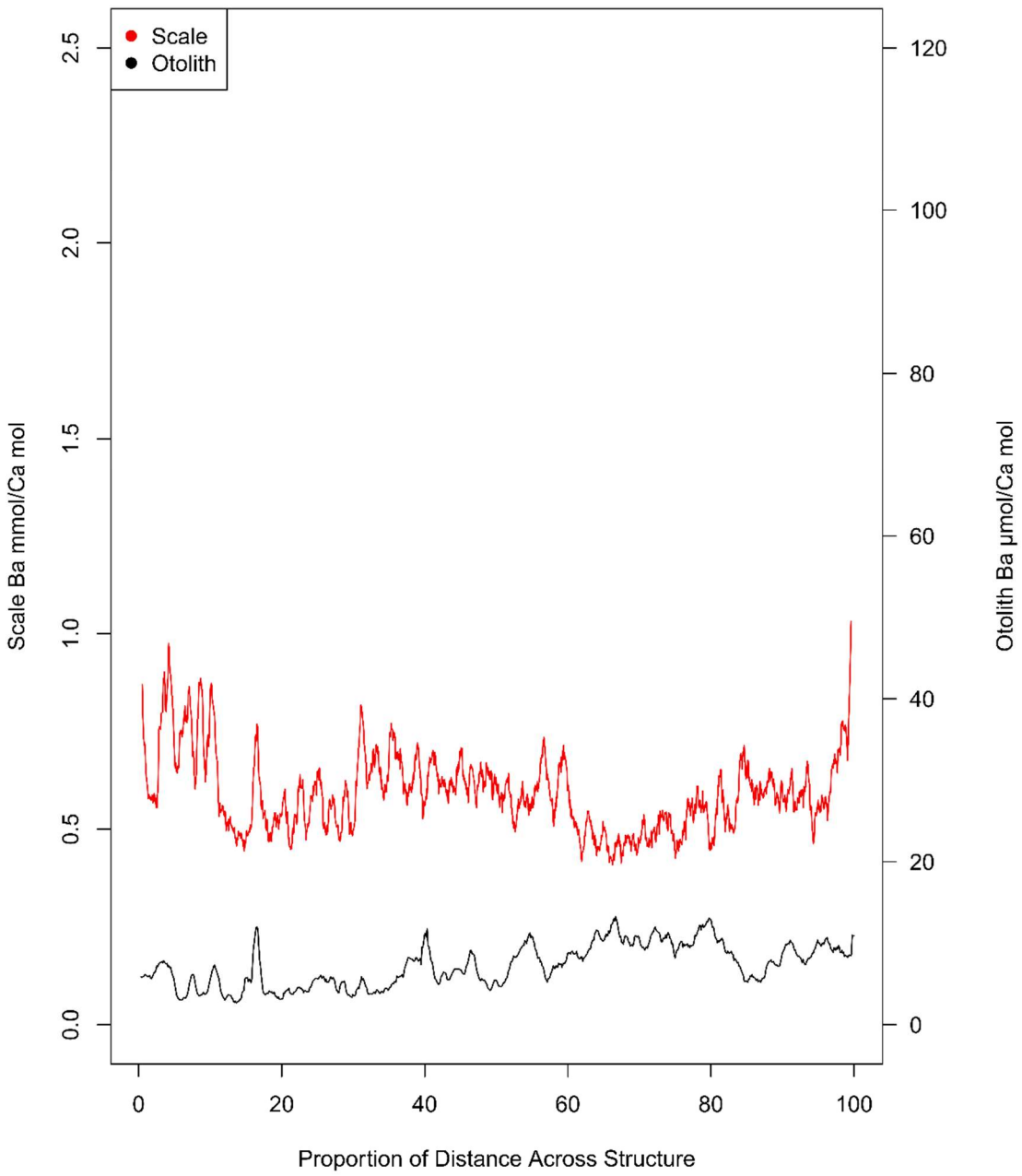
RD−093
Scale
Otolith
Scale Ba mmol/Ca mol
Otolith Ba µmol/Ca mol
Proportion of Distance Across Structure
0.0
0.5
1.0
1.5
2.0
2.5
0
20
40
60
80
100
120

RD-093

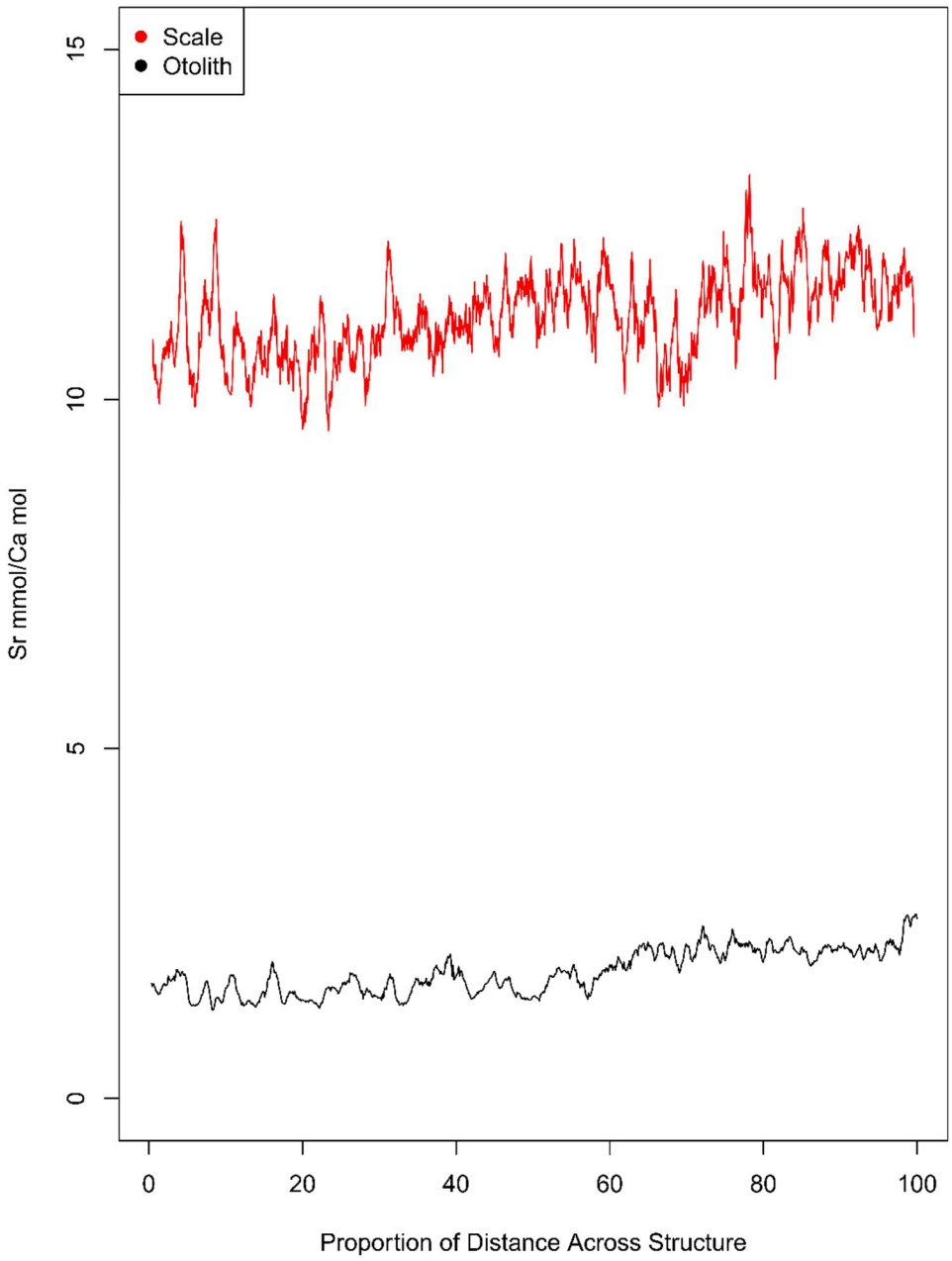
Scale
Otolith
Sr mmol/Ca mol
0
5
10
15
0
20
40
60
80
100
Proportion of Distance Across Structure

RD−094

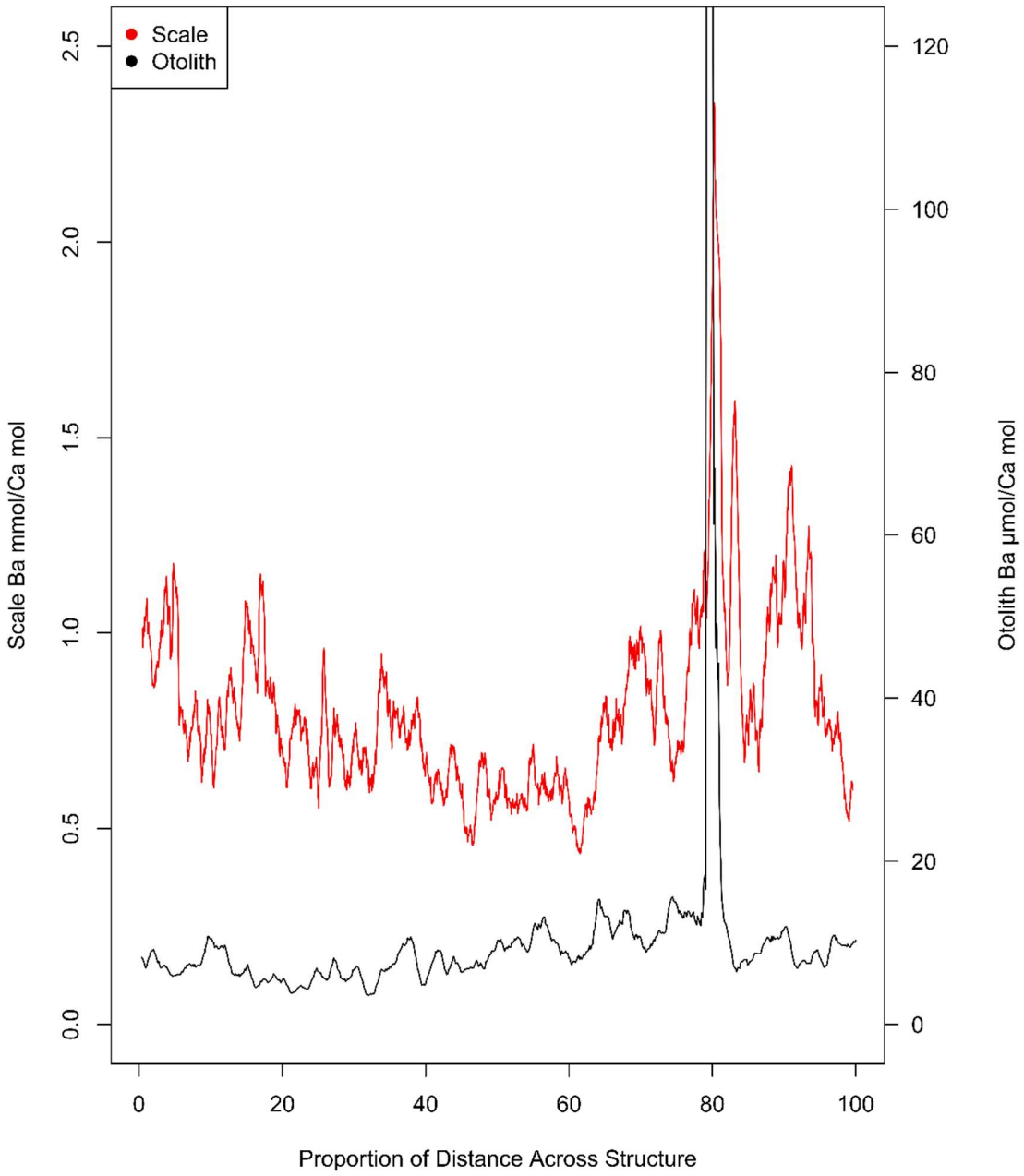
Scale
Otolith
Scale Ba mmol/Ca mol
Otolith Ba µmol/Ca mol
Proportion of Distance Across Structure
0.0
0.5
1.0
1.5
2.0
2.5
0
20
40
60
80
100
120

RD−094

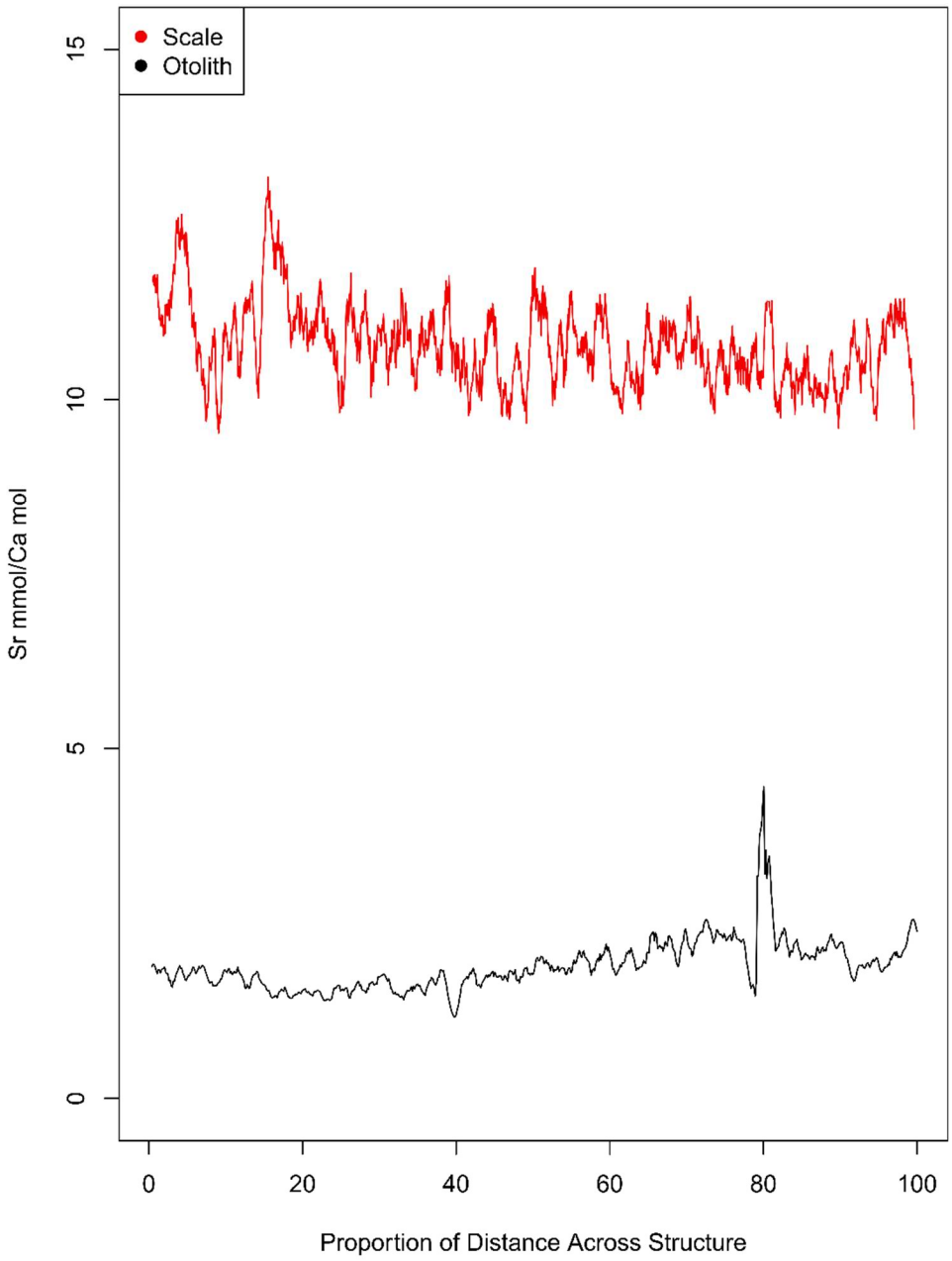
Scale
Otolith
Sr mmol/Ca mol
0
5
10
15
0
20
40
60
80
100
Proportion of Distance Across Structure

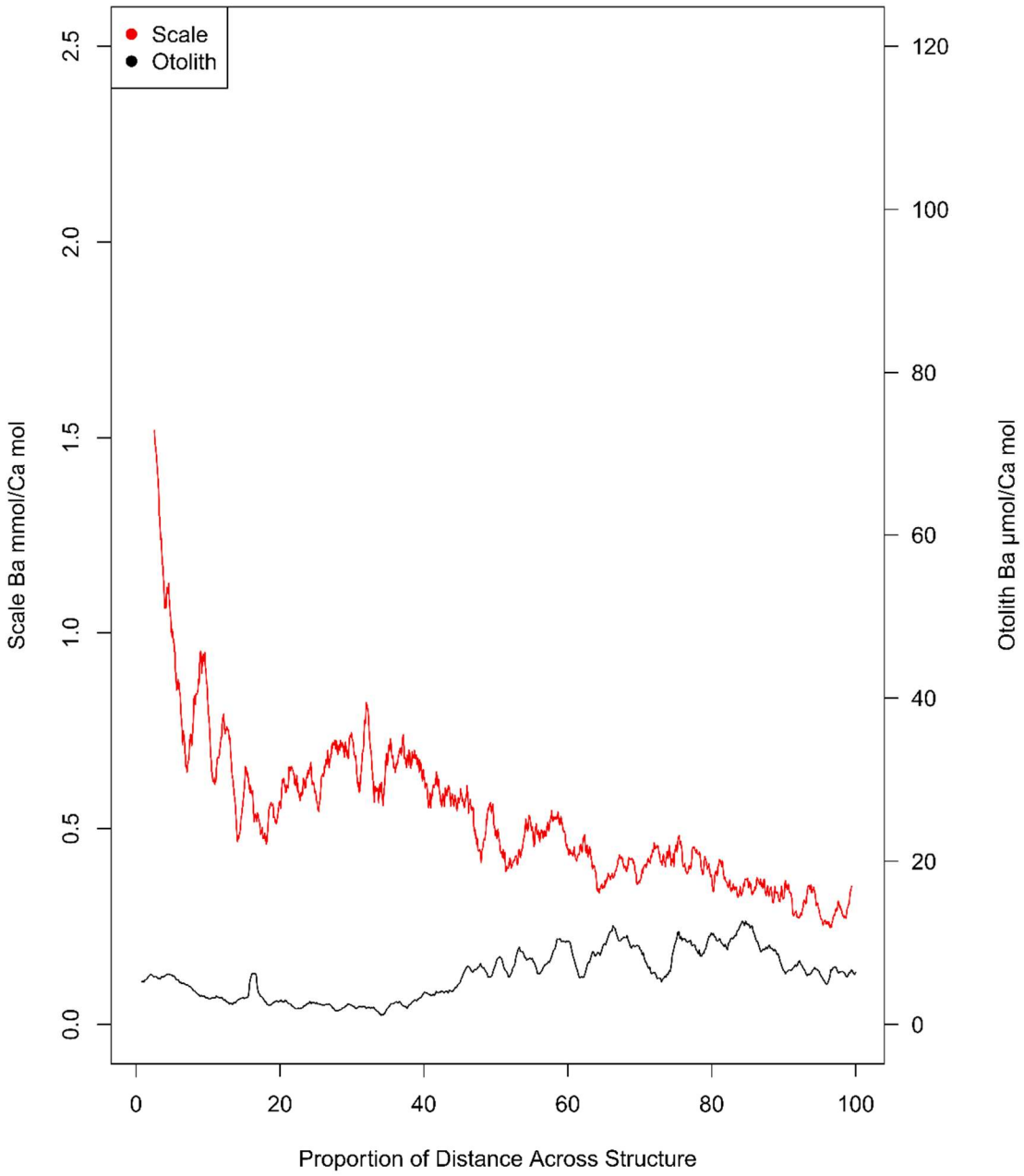
RD−095
Scale
Otolith
Scale Ba mmol/Ca mol
Otolith Ba µmol/Ca mol
Proportion of Distance Across Structure
0.0
0.5
1.0
1.5
2.0
2.5
0
20
40
60
80
100
120

RD-095

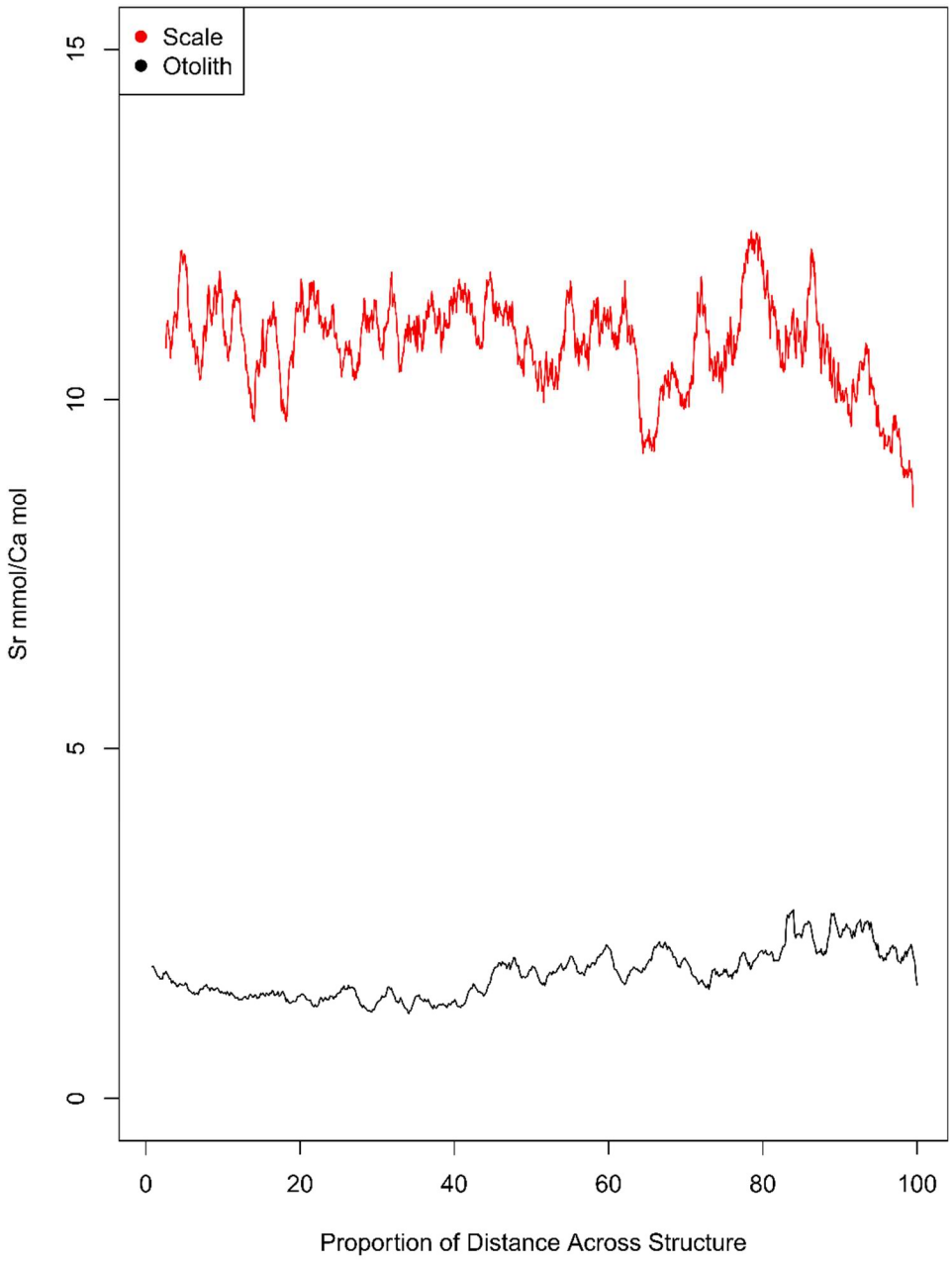
Scale
Otolith
Sr mmol/Ca mol
0
5
10
15
0
20
40
60
80
100
Proportion of Distance Across Structure

RD-096

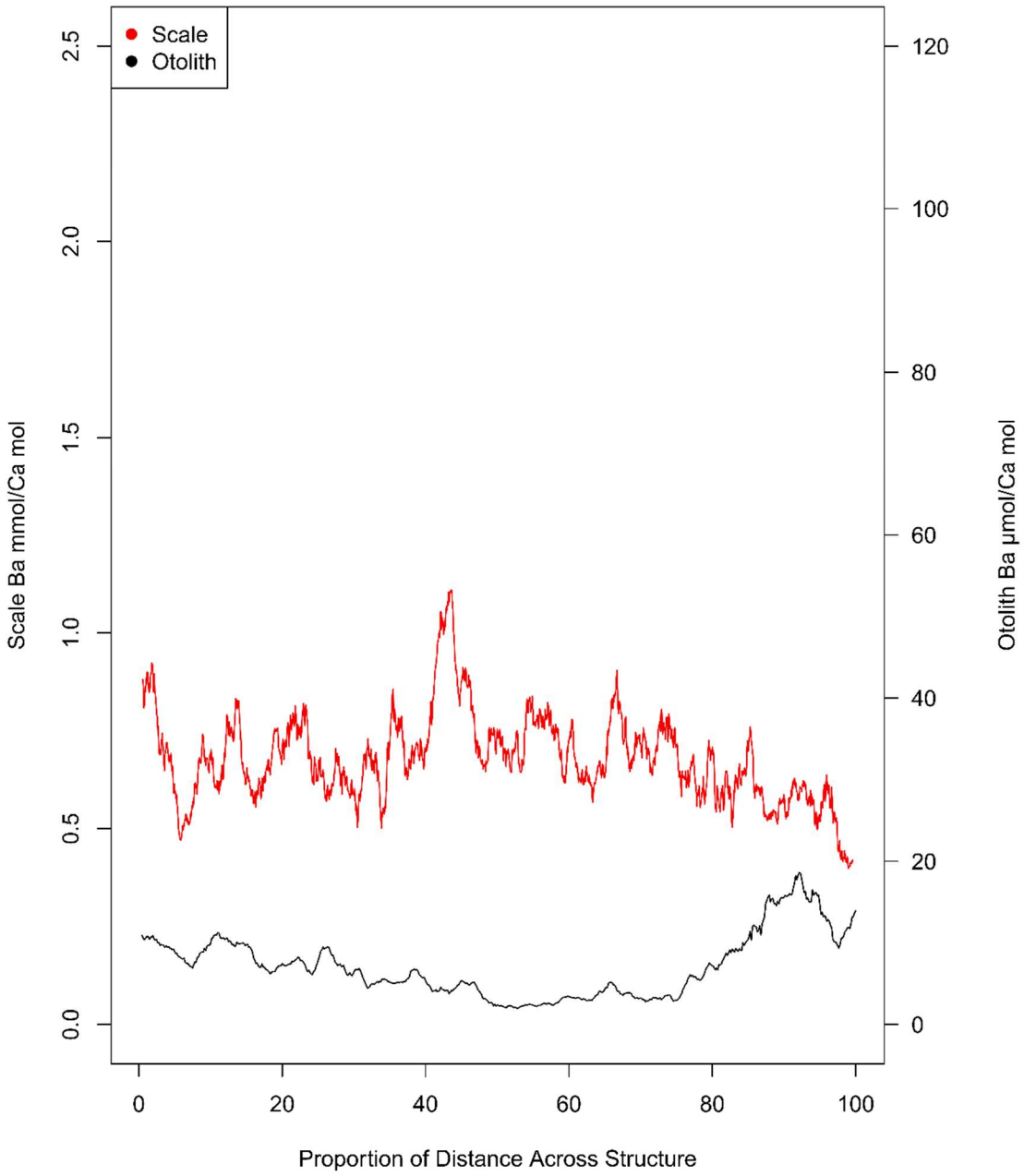
Scale
Otolith
Scale Ba mmol/Ca mol
Otolith Ba µmol/Ca mol
Proportion of Distance Across Structure
0.0
0.5
1.0
1.5
2.0
2.5
0
20
40
60
80
100
120

RD-096

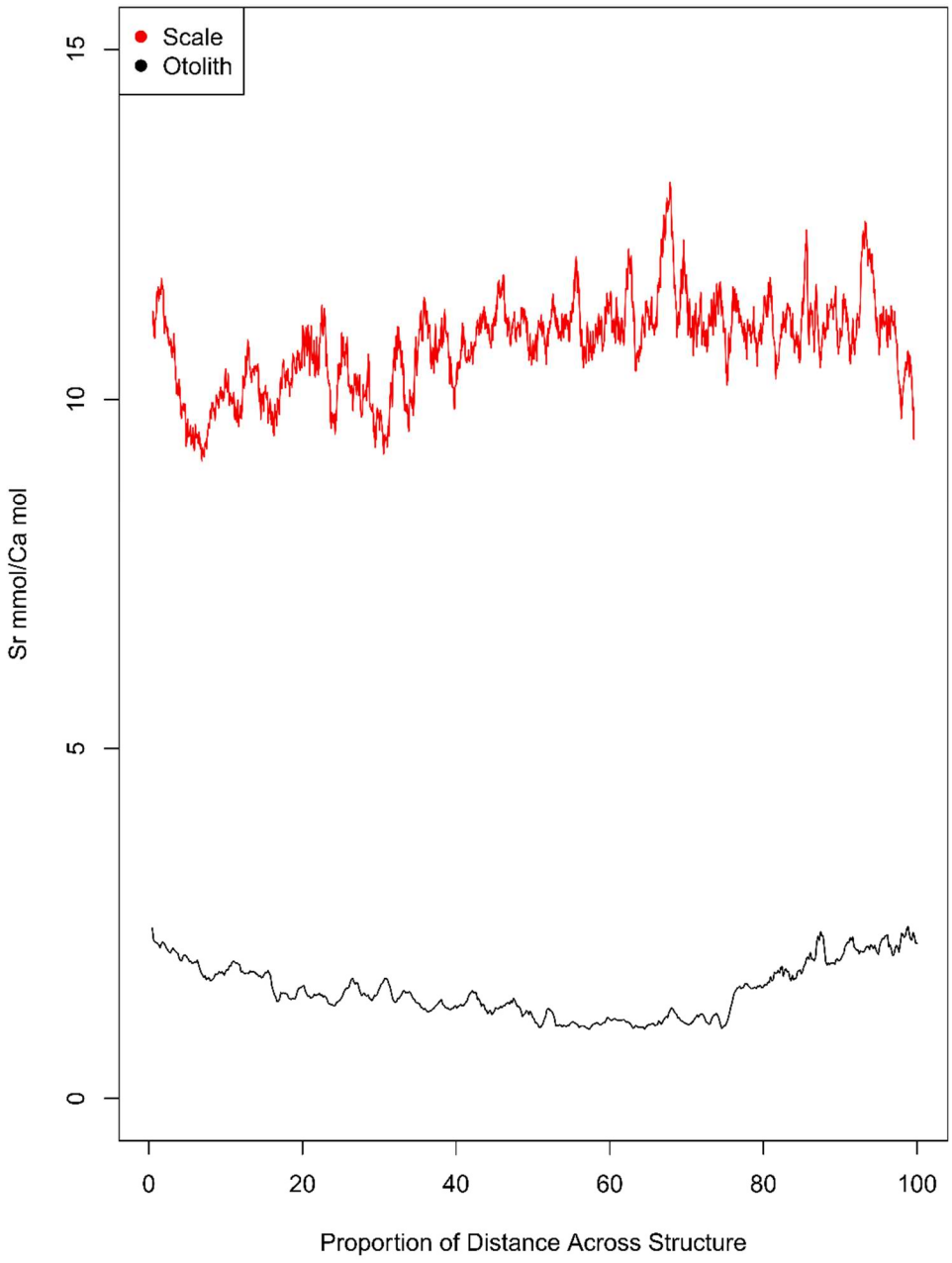
Scale
Otolith
Sr mmol/Ca mol
0
5
10
15
0
20
40
60
80
100
Proportion of Distance Across Structure

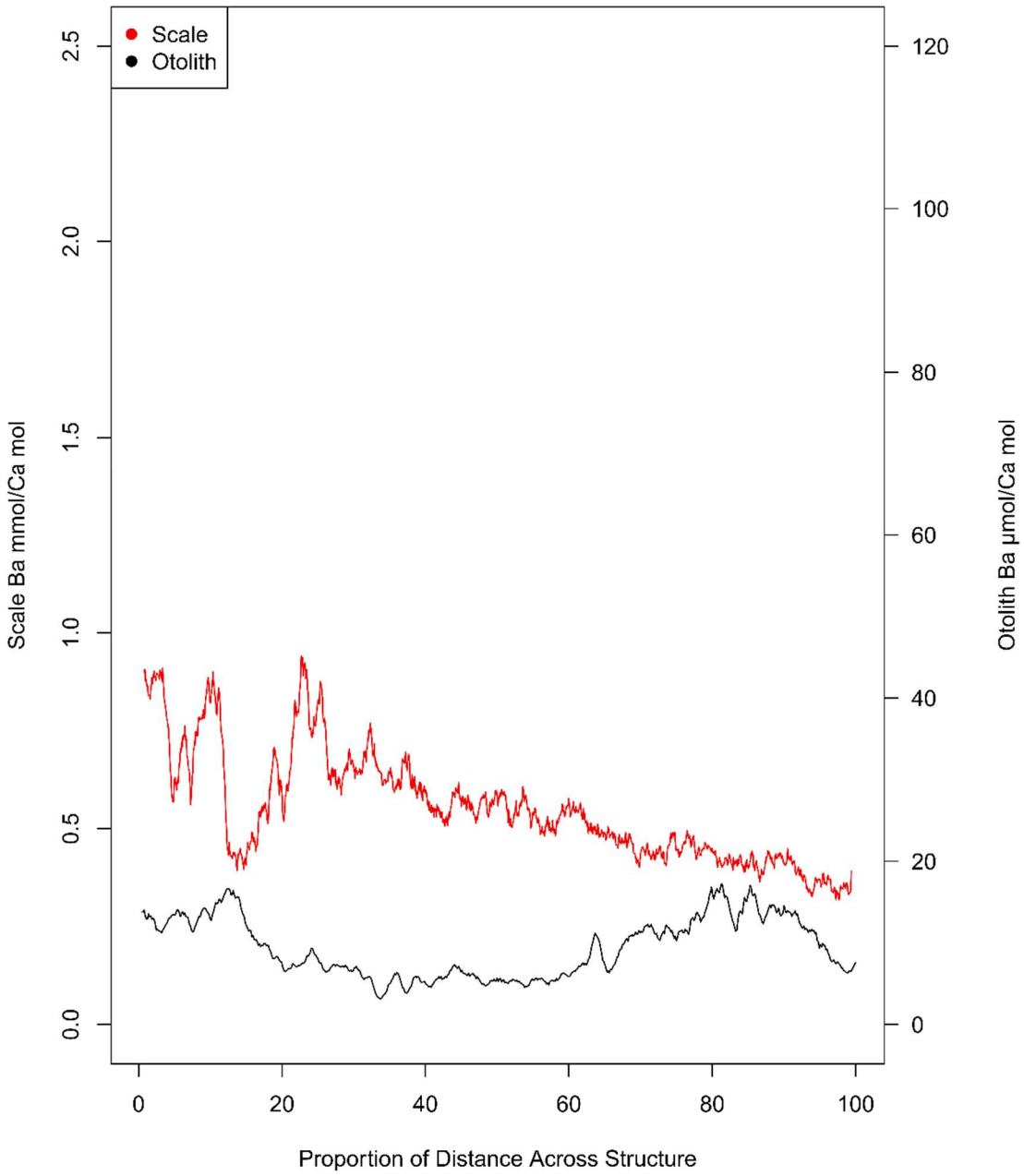
RD−097
Scale
Otolith
Scale Ba mmol/Ca mol
Otolith Ba µmol/Ca mol
Proportion of Distance Across Structure
0.0
0.5
1.0
1.5
2.0
2.5
0
20
40
60
80
100
120

RD-097

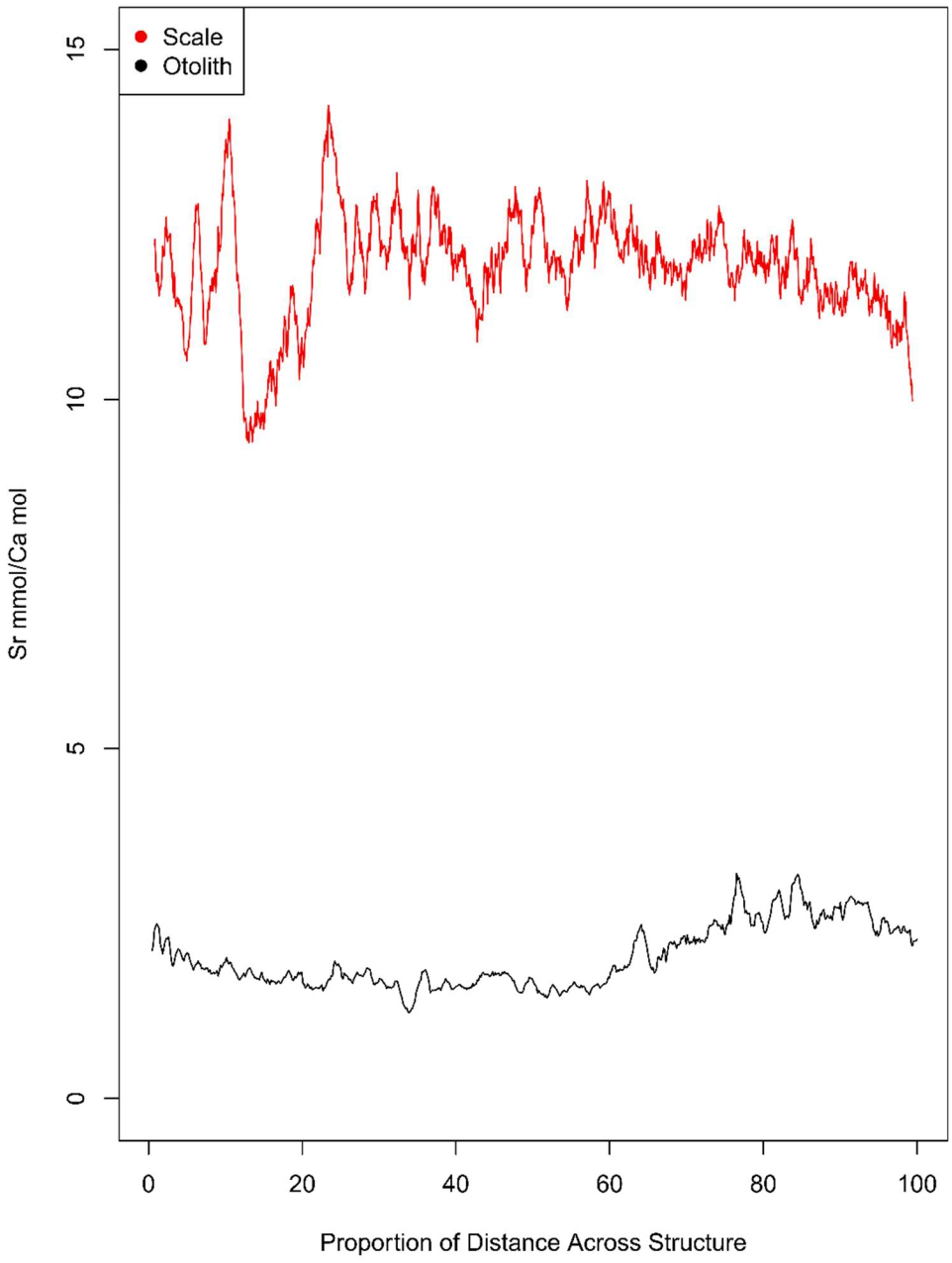
Scale
Otolith
Sr mmol/Ca mol
0
5
10
15
0
20
40
60
80
100
Proportion of Distance Across Structure

RD−098

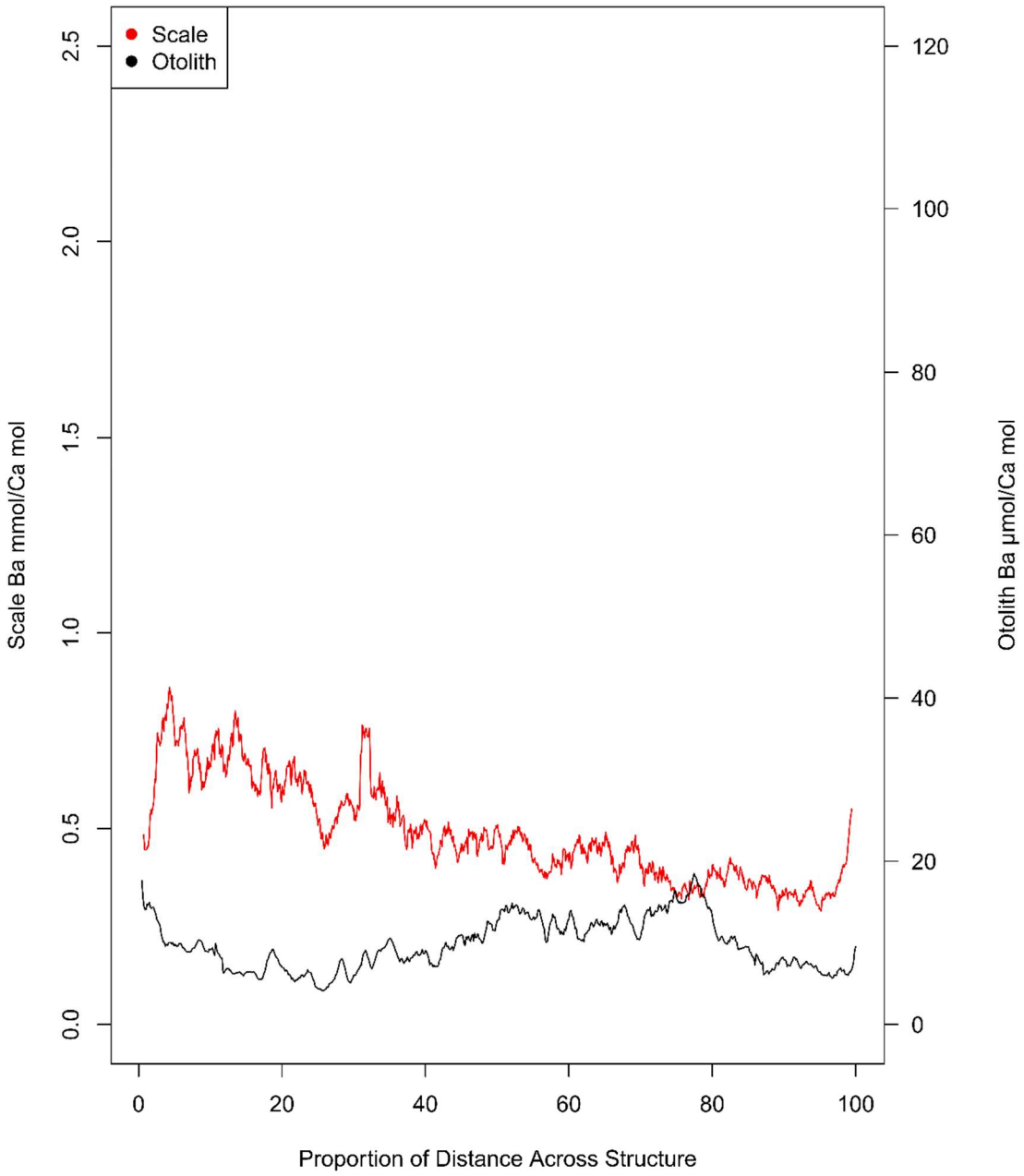
Scale
Otolith
Scale Ba mmol/Ca mol
Otolith Ba µmol/Ca mol
Proportion of Distance Across Structure
0.0
0.5
1.0
1.5
2.0
2.5
0
20
40
60
80
100
120

RD-098

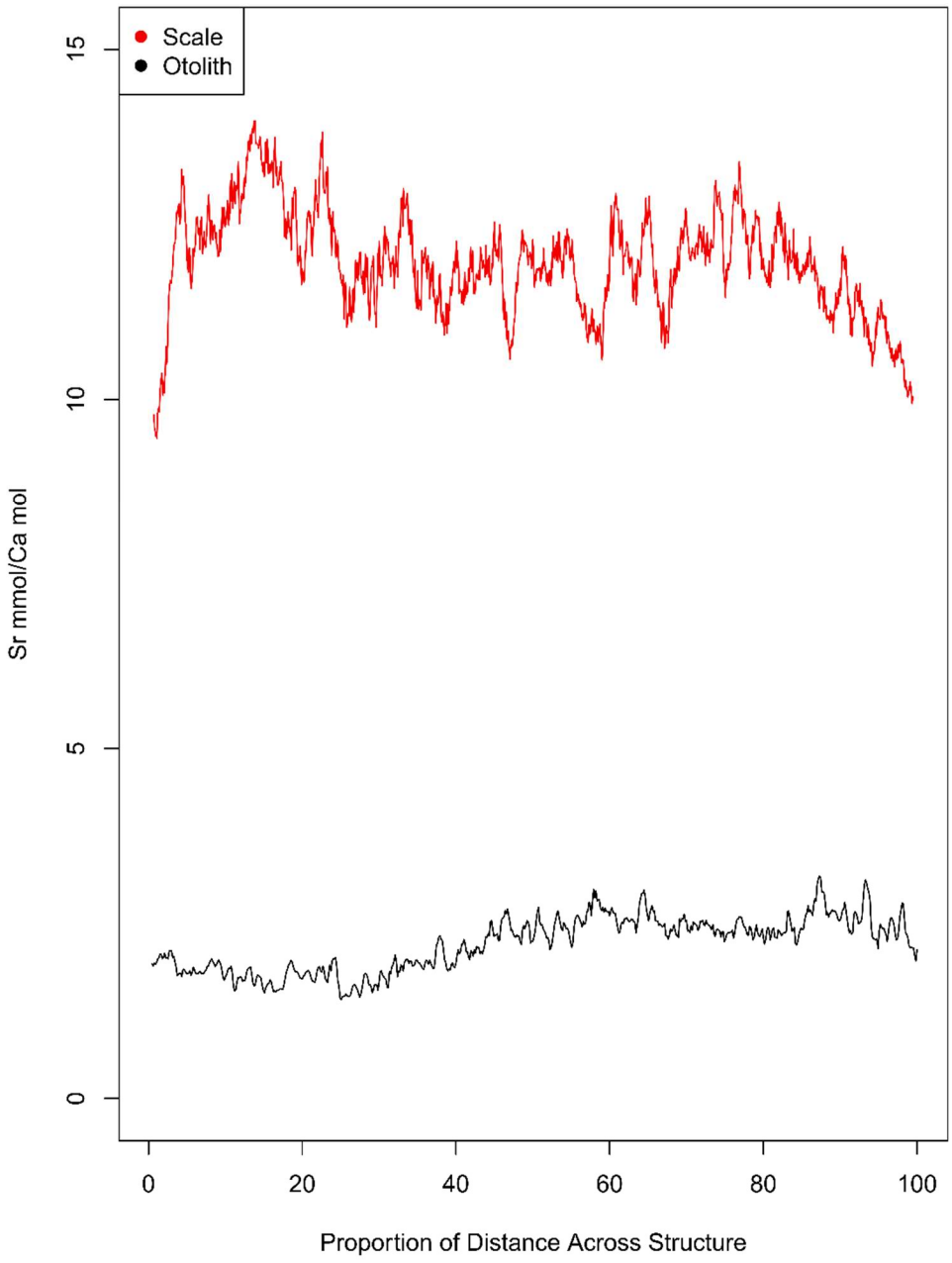
Scale
Otolith
Sr mmol/Ca mol
0
5
10
15
0
20
40
60
80
100
Proportion of Distance Across Structure

RD−099

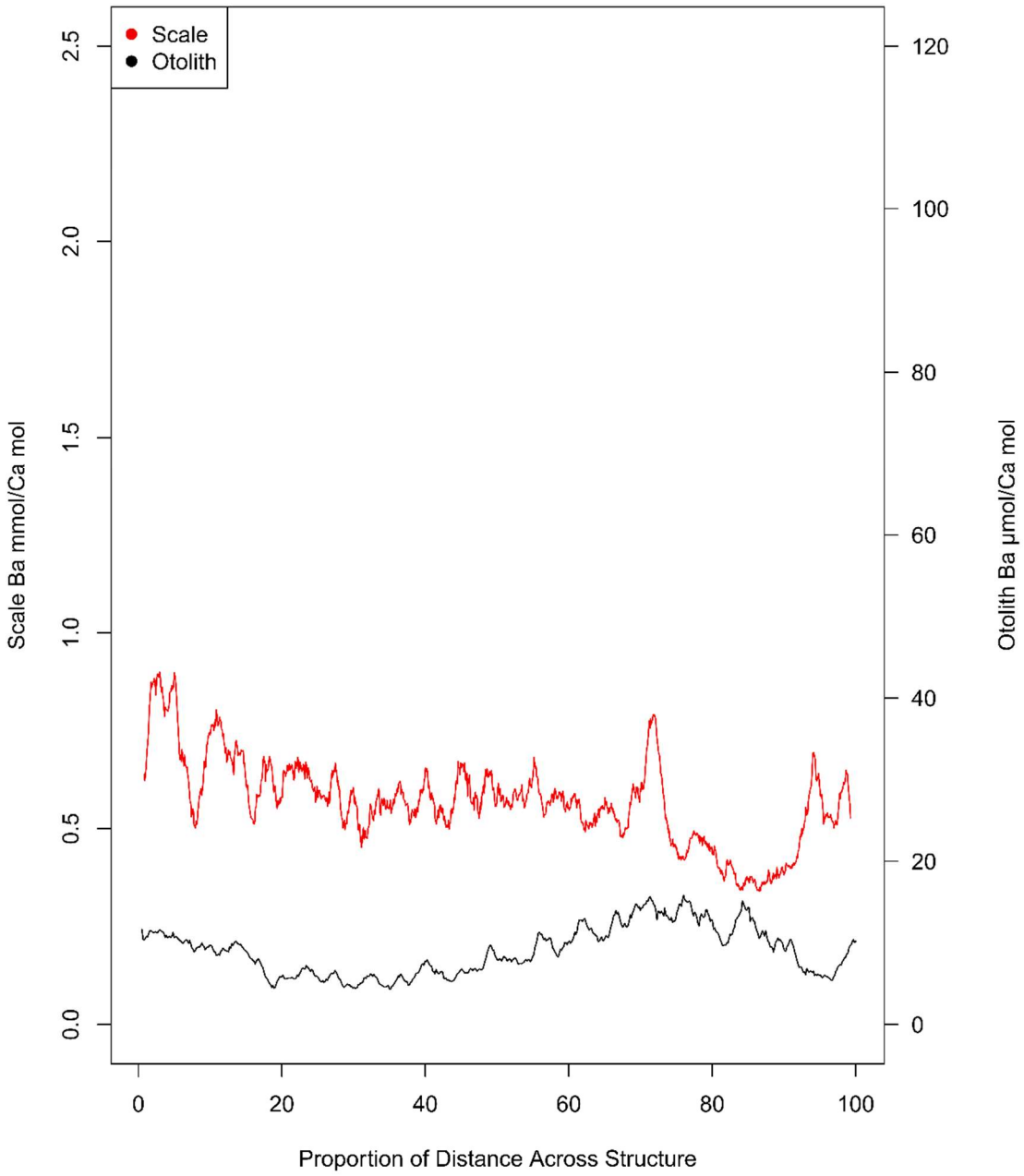
Scale
Otolith
Scale Ba mmol/Ca mol
Otolith Ba µmol/Ca mol
Proportion of Distance Across Structure
0.0
0.5
1.0
1.5
2.0
2.5
0
20
40
60
80
100
120

RD-099

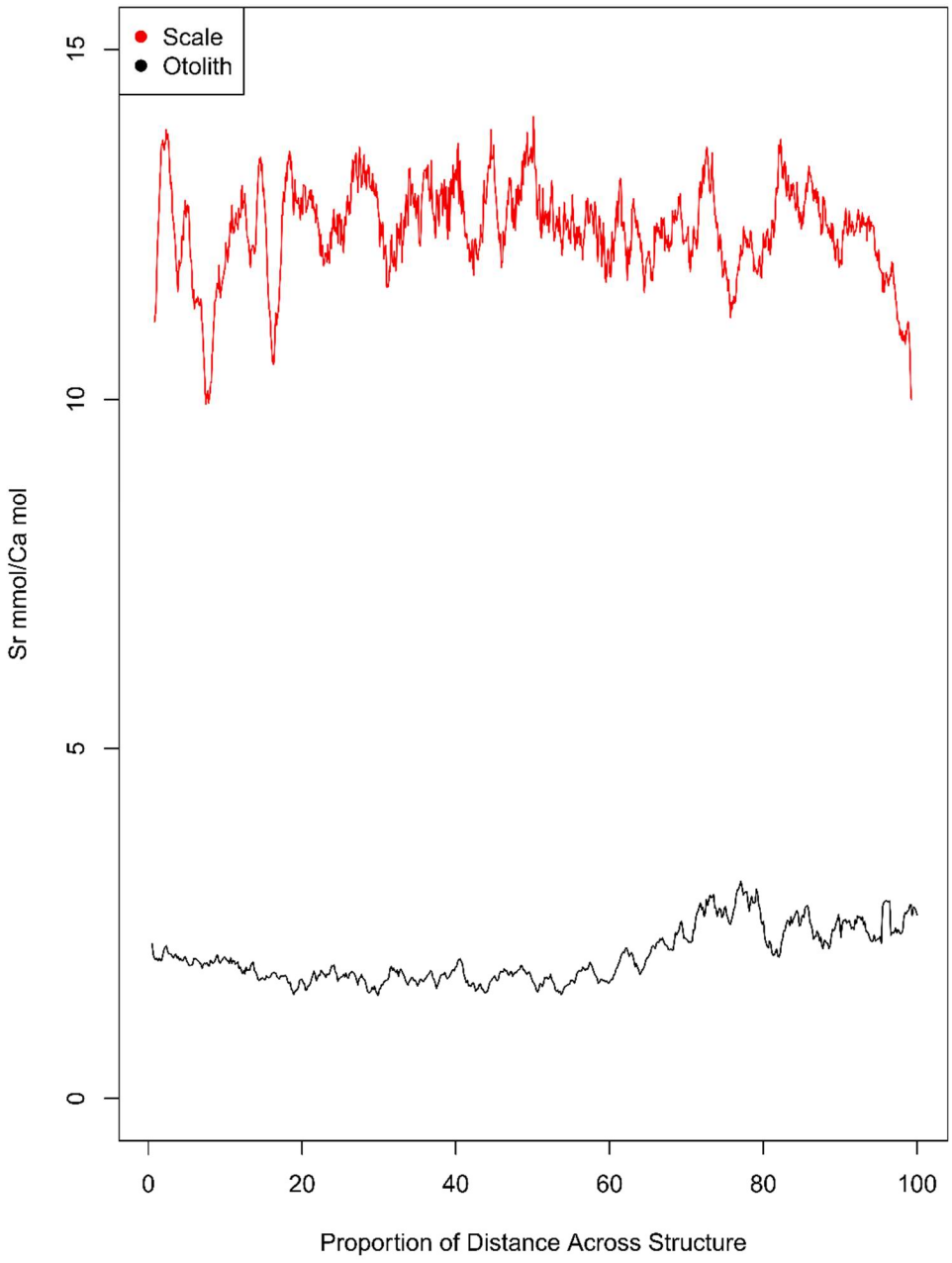
Scale
Otolith
Sr mmol/Ca mol
0
5
10
15
0
20
40
60
80
100
Proportion of Distance Across Structure

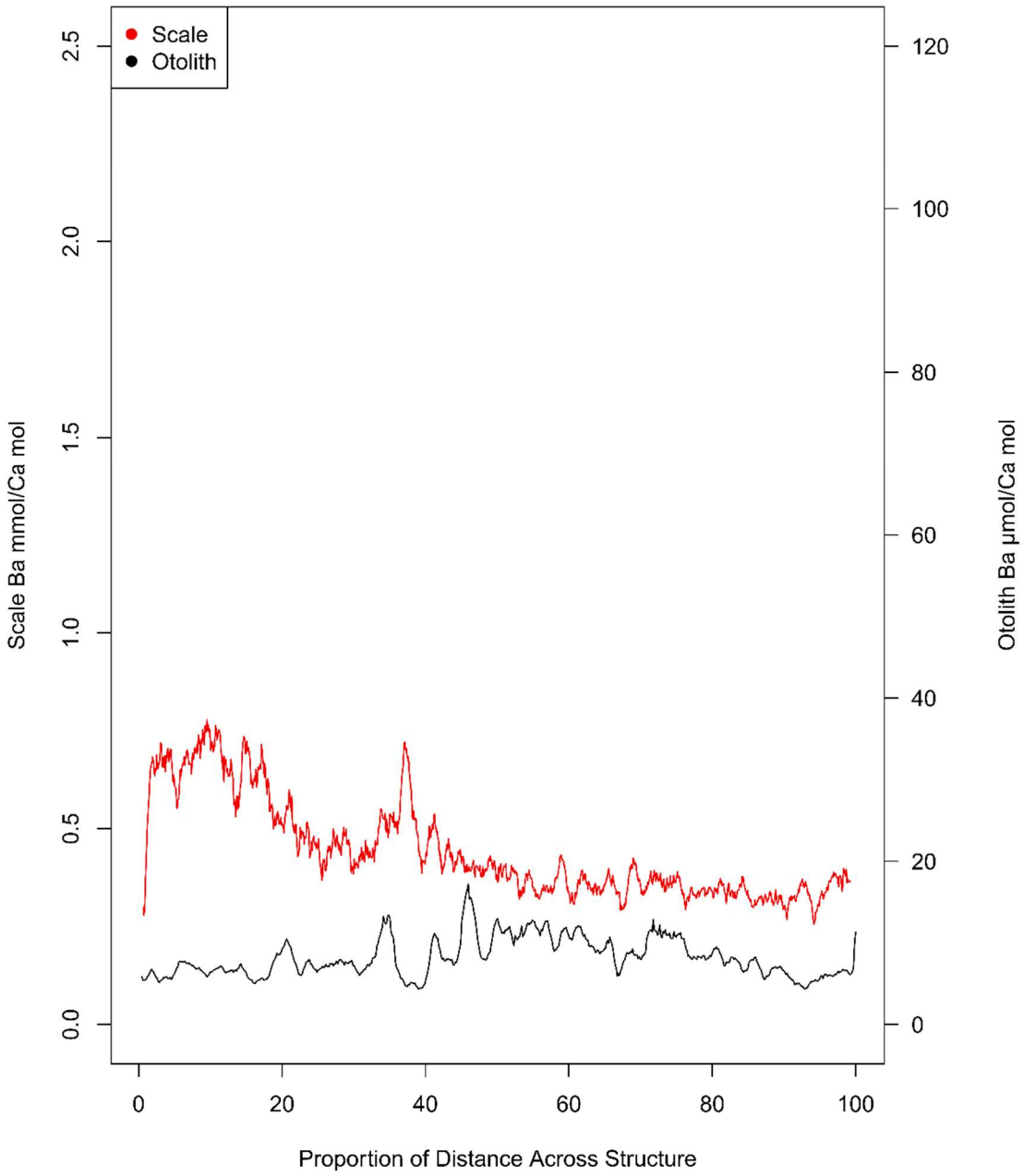
RD−100
Scale
Otolith
Scale Ba mmol/Ca mol
Otolith Ba µmol/Ca mol
Proportion of Distance Across Structure
0.0
0.5
1.0
1.5
2.0
2.5
0
20
40
60
80
100
120

RD−100

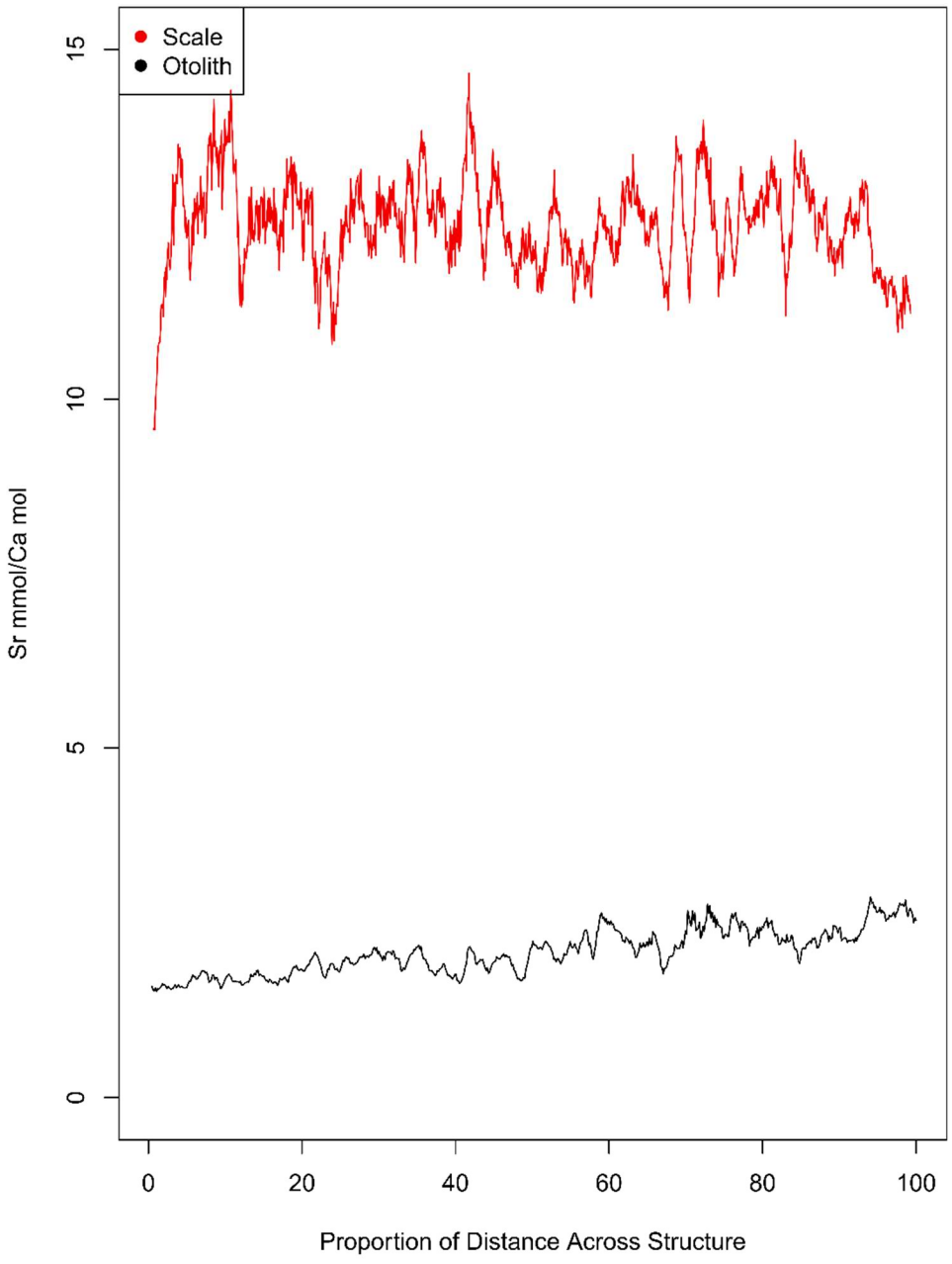
Scale
Otolith
Sr mmol/Ca mol
0
5
10
15
0
20
40
60
80
100
Proportion of Distance Across Structure